

NOVEL TARGETS AND BIOMARKERS IN SOLID TUMORS, 2nd Edition

EDITED BY: Dong-Hua Yang, Zhi Shi, Pascale Cohen and Huiqin Guo
PUBLISHED IN: Frontiers in Pharmacology





frontiers

Frontiers eBook Copyright Statement

The copyright in the text of individual articles in this eBook is the property of their respective authors or their respective institutions or funders. The copyright in graphics and images within each article may be subject to copyright of other parties. In both cases this is subject to a license granted to Frontiers.

The compilation of articles constituting this eBook is the property of Frontiers.

Each article within this eBook, and the eBook itself, are published under the most recent version of the Creative Commons CC-BY licence.

The version current at the date of publication of this eBook is CC-BY 4.0. If the CC-BY licence is updated, the licence granted by Frontiers is automatically updated to the new version.

When exercising any right under the CC-BY licence, Frontiers must be attributed as the original publisher of the article or eBook, as applicable.

Authors have the responsibility of ensuring that any graphics or other materials which are the property of others may be included in the CC-BY licence, but this should be checked before relying on the CC-BY licence to reproduce those materials. Any copyright notices relating to those materials must be complied with.

Copyright and source acknowledgement notices may not be removed and must be displayed in any copy, derivative work or partial copy which includes the elements in question.

All copyright, and all rights therein, are protected by national and international copyright laws. The above represents a summary only. For further information please read Frontiers' Conditions for Website Use and Copyright Statement, and the applicable CC-BY licence.

ISSN 1664-8714

ISBN 978-2-88963-879-6

DOI 10.3389/978-2-88963-879-6

About Frontiers

Frontiers is more than just an open-access publisher of scholarly articles: it is a pioneering approach to the world of academia, radically improving the way scholarly research is managed. The grand vision of Frontiers is a world where all people have an equal opportunity to seek, share and generate knowledge. Frontiers provides immediate and permanent online open access to all its publications, but this alone is not enough to realize our grand goals.

Frontiers Journal Series

The Frontiers Journal Series is a multi-tier and interdisciplinary set of open-access, online journals, promising a paradigm shift from the current review, selection and dissemination processes in academic publishing. All Frontiers journals are driven by researchers for researchers; therefore, they constitute a service to the scholarly community. At the same time, the Frontiers Journal Series operates on a revolutionary invention, the tiered publishing system, initially addressing specific communities of scholars, and gradually climbing up to broader public understanding, thus serving the interests of the lay society, too.

Dedication to Quality

Each Frontiers article is a landmark of the highest quality, thanks to genuinely collaborative interactions between authors and review editors, who include some of the world's best academicians. Research must be certified by peers before entering a stream of knowledge that may eventually reach the public - and shape society; therefore, Frontiers only applies the most rigorous and unbiased reviews.

Frontiers revolutionizes research publishing by freely delivering the most outstanding research, evaluated with no bias from both the academic and social point of view. By applying the most advanced information technologies, Frontiers is catapulting scholarly publishing into a new generation.

What are Frontiers Research Topics?

Frontiers Research Topics are very popular trademarks of the Frontiers Journals Series: they are collections of at least ten articles, all centered on a particular subject. With their unique mix of varied contributions from Original Research to Review Articles, Frontiers Research Topics unify the most influential researchers, the latest key findings and historical advances in a hot research area! Find out more on how to host your own Frontiers Research Topic or contribute to one as an author by contacting the Frontiers Editorial Office: researchtopics@frontiersin.org

NOVEL TARGETS AND BIOMARKERS IN SOLID TUMORS, 2nd Edition

Topic Editors:

Dong-Hua Yang, St. John's University, United States

Zhi Shi, Jinan University, China

Pascale Cohen, Université Claude Bernard Lyon 1, France

Huiqin Guo, Peking Union Medical College Hospital (CAMS), China

Publisher's note: In this 2nd edition, the following article has been updated: Wang Z, Wang Y, Zhu S, Liu Y, Peng X, Zhang S, Zhang Z, Qiu Y, Jin M, Wang R, Zhong Y and Kong D (2018) DT-13 Inhibits Proliferation and Metastasis of Human Prostate Cancer Cells Through Blocking PI3K/Akt Pathway. *Front. Pharmacol.* 9:1450. doi: 10.3389/fphar.2018.01450

Citation: Yang, D.-H., Shi, Z., Cohen, P., Guo, H., eds. (2020). Novel Targets and Biomarkers in Solid Tumors, 2nd Edition. Lausanne: Frontiers Media SA.
doi: 10.3389/978-2-88963-879-6

Table of Contents

- 06 Editorial: Novel Targets and Biomarkers in Solid Tumors**
Zhi Shi, Hui-Qin Guo, Pascale A. Cohen and Dong-Hua Yang
- 08 Targeted Next-Generation Sequencing Identifies Actionable Targets in Estrogen Receptor Positive and Estrogen Receptor Negative Endometrioid Endometrial Cancer**
Siti Syazani Suhaimi, Nurul-Syakima Ab Mutalib, Sheau S. Khor, Reena Rahayu Md Zain, Saiful Effendi Syafruddin, Nadiah Abu, Ahmad Zailani Hatta Mohd Dali and Rahman Jamal
- 24 UBE2C is a Potential Biomarker of Intestinal-Type Gastric Cancer With Chromosomal Instability**
Jun Zhang, Xinyu Liu, Guanzhen Yu, Lei Liu, Jiejun Wang, Xiaoyu Chen, Yuhai Bian, Yuan Ji, Xiaoyan Zhou, Yinan Chen, Jun Ji, Zhen Xiang, Lei Guo, Jingyuan Fang, Yihong Sun, Hui Cao, Zhenggang Zhu and Yingyan Yu
- 36 Cross-Database Analysis Reveals Sensitive Biomarkers for Combined Therapy for ERBB2+ Gastric Cancer**
Zhen Xiang, Xia Huang, Jiexuan Wang, Jun Zhang, Jun Ji, Ranlin Yan, Zhenggang Zhu, Wei Cai and Yingyan Yu
- 47 Preoperative Changes in Hematological Markers and Predictors of Glioma Grade and Survival**
Peng-Fei Wang, Zhe Meng, Hong-Wang Song, Kun Yao, Ze-Jun Duan, Chun-Jiang Yu, Shou-Wei Li and Chang-Xiang Yan
- 54 MMP-9 as a Candidate Marker of Response to BRAF Inhibitors in Melanoma Patients With BRAF^{V600E} Mutation Detected in Circulating-Free DNA**
Rossella Salemi, Luca Falzone, Gabriele Madonna, Jerry Polesel, Diana Cinà, Domenico Mallardo, Paolo A. Ascierto, Massimo Libra and Saverio Candido
- 65 SOX2 Promotes Cell Proliferation and Metastasis in Triple Negative Breast Cancer**
Peng Liu, Hailin Tang, Cailu Song, Jin Wang, Bo Chen, Xiaojia Huang, Xiaoqing Pei and Longzhong Liu
- 73 Current Standards and Recent Advances in Biomarkers of Major Endocrine Tumors**
Yanhong Luo, Hua Zhu, Tao Tan and Jianfeng He
- 83 Inhibition of WEE1 Suppresses the Tumor Growth in Laryngeal Squamous Cell Carcinoma**
Meng-Ling Yuan, Pei Li, Zi-Hao Xing, Jin-Ming Di, Hui Liu, An-Kui Yang, Xi-Jun Lin, Qi-Wei Jiang, Yang Yang, Jia-Rong Huang, Kun Wang, Meng-Ning Wei, Yao Li, Jin Ye and Zhi Shi
- 93 Olmutinib (BI1482694/HM61713), a Novel Epidermal Growth Factor Receptor Tyrosine Kinase Inhibitor, Reverses ABCG2-Mediated Multidrug Resistance in Cancer Cells**
Wei Zhang, Ying-Fang Fan, Chao-Yun Cai, Jing-Quan Wang, Qiu-Xu Teng, Zi-Ning Lei, Leli Zeng, Pranav Gupta and Zhe-Sheng Chen

- 106 ***VS-4718 Antagonizes Multidrug Resistance in ABCB1- and ABCG2-Overexpressing Cancer Cells by Inhibiting the Efflux Function of ABC Transporters***
Ning Ji, Yuqi Yang, Chao-Yun Cai, Zi-Ning Lei, Jing-Quan Wang, Pranav Gupta, Qiu-Xu Teng, Zhe-Sheng Chen, Dexin Kong and Dong-Hua Yang
- 118 ***Peptides/Proteins Encoded by Non-coding RNA: A Novel Resource Bank for Drug Targets and Biomarkers***
Song Zhu, Jizhong Wang, Yutian He, Nan Meng and Guang-Rong Yan
- 124 ***ORY-1001 Suppresses Cell Growth and Induces Apoptosis in Lung Cancer Through Triggering HK2 Mediated Warburg Effect***
Zhaoliang Lu, Yanke Guo, Xiaoya Zhang, Jing Li, Leilei Li, Shuai Zhang and Changliang Shan
- 133 ***CDH1 Gene and Hereditary Diffuse Gastric Cancer Syndrome: Molecular and Histological Alterations and Implications for Diagnosis and Treatment***
Wenyi Luo, Faysal Fedda, Patrick Lynch and Dongfeng Tan
- 142 ***DT-13 Inhibits Proliferation and Metastasis of Human Prostate Cancer Cells Through Blocking PI3K/Akt Pathway***
Zhengming Wang, Yingying Wang, Shan Zhu, Yao Liu, Xin Peng, Shaolu Zhang, Zhe Zhang, Yuling Qiu, Meihua Jin, Ran Wang, Yuxu Zhong and Dexin Kong
- 156 ***MiR-3188 Inhibits Non-small Cell Lung Cancer Cell Proliferation Through FOXO1-Mediated mTOR-p-PI3K/AKT-c-JUN Signaling Pathway***
Chunyan Wang, Enqi Liu, Wen Li, Jue Cui and Tongxiang Li
- 164 ***Correlation Between C-MYC, BCL-2, and BCL-6 Protein Expression and Gene Translocation as Biomarkers in Diagnosis and Prognosis of Diffuse Large B-cell Lymphoma***
YunXiang Zhang, Hui Wang, Cuiai Ren, Hai Yu, Wenjia Fang, Na Zhang, Sumei Gao and Qian Hou
- 175 ***Mutations Defining Patient Cohorts With Elevated PD-L1 Expression in Gastric Cancer***
Otilia Menyhárt, Lőrinc Sándor Pongor and Balázs Györffy
- 181 ***miR-26 Induces Apoptosis and Inhibits Autophagy in Non-small Cell Lung Cancer Cells by Suppressing TGF- β 1-JNK Signaling Pathway***
Yi He, Hao Liu, Lianyong Jiang, Bi Rui, Ju Mei and Haibo Xiao
- 192 ***The Prognostic and Therapeutic Value of PD-L1 in Glioma***
Ruo Qiao Chen, Feng Liu, Xin Yao Qiu and Xiao Qian Chen
- 205 ***Y₆, an Epigallocatechin Gallate Derivative, Reverses ABCG2-Mediated Mitoxantrone Resistance***
Rui-Qiang Zhao, Yan Wen, Pranav Gupta, Zi-Ning Lei, Chao-Yun Cai, Gang Liang, Dong-Hua Yang, Zhe-Sheng Chen and Yu-An Xie
- 216 ***MicroRNA-181a Functions as an Oncogene in Gastric Cancer by Targeting Caprin-1***
Qiang Lu, Yanchun Chen, Dan Sun, Shukun Wang, Kang Ding, Meiyi Liu, Yan Zhang, Yujuan Miao, Huancai Liu and Fenghua Zhou
- 226 ***Evaluating ZNF217 mRNA Expression Levels as a Predictor of Response to Endocrine Therapy in ER+ Breast Cancer***
Julie A. Vendrell, Jérôme Solassol, Balázs Györffy, Paul Vilquin, Marta Jarlier, Caterina F. Donini, Laurent Gamba, Thierry Maudelonde, Philippe Rouanet and Pascale A. Cohen

- 232 Upregulation of lncRNA NR_046683 Serves as a Prognostic Biomarker and Potential Drug Target for Multiple Myeloma**
Hang Dong, Siyi Jiang, Yunfeng Fu, Yanwei Luo, Rong Gui and Jing Liu
- 240 Research Progress on PARP14 as a Drug Target**
Wei Qin, Hong-Jie Wu, Lu-Qi Cao, Hui-Jin Li, Chun-Xia He, Dong Zhao, Lu Xing, Peng-Quan Li, Xi Jin and Hui-Ling Cao
- 252 Sphingomyelin Synthase 1 (SMS1) Downregulation is Associated With Sphingolipid Reprogramming and a Worse Prognosis in Melanoma**
Fatima Bilal, Anne Montfort, Julia Gilhodes, Virginie Garcia, Joëlle Riond, Stéphane Carpentier, Thomas Filleron, Céline Colacios, Thierry Levade, Ahmad Daher, Nicolas Meyer, Nathalie Andrieu-Abadie and Bruno Ségui
- 259 DDR1 and MT1-MMP Expression Levels are Determinant for Triggering BIK-Mediated Apoptosis by 3D Type I Collagen Matrix in Invasive Basal-Like Breast Carcinoma Cells**
Charles Saby, Guillaume Collin, Maha Sinane, Emilie Buache, Laurence Van Gulick, Frédéric Saltel, Erik Maquoi and Hamid Morjani
- 274 The ZNF217 Biomarker Predicts Low- and High-Risk Oncotype DX® Recurrence Score in ER-Positive Invasive Breast Cancers**
Pascale A. Cohen, Olivier Loudig, Christina Liu, Joseph Albanese and Susan Fineberg
- 277 The Bone Morphogenetic Protein Signaling Inhibitor LDN-193189 Enhances Metastasis Development in Mice**
Julien Voltaire, Irma Machuca-Gayet, Jonathan Lavaud, Aurélie Bellanger, Lamia Bouazza, Soumaya El Moghrabi, Isabelle Treilleux, Jean-Luc Coll, Olivier Peyruchaud, Véronique Josserand and Pascale A. Cohen



Editorial: Novel Targets and Biomarkers in Solid Tumors

Zhi Shi^{1*}, Hui-Qin Guo², Pascale A. Cohen³ and Dong-Hua Yang^{4*}

¹ Department of Cell Biology & Institute of Biomedicine, National Engineering Research Center of Genetic Medicine, Guangdong Provincial Key Laboratory of Bioengineering Medicine, College of Life Science and Technology, Jinan University, Guangzhou, China, ² Department of Thoracic Surgery, Beijing Sijitan Hospital, Capital Medical University, Beijing, China, ³ Univ Lyon, Université Claude Bernard Lyon 1, INSERM U1052, CNRS 5286, Centre de Recherche en Cancérologie de Lyon, Lyon, France, ⁴ Department of Pharmaceutical Sciences, College of Pharmacy and Health Sciences, St. John's University, Queens, NY, United States

Keywords: solid tumor, target, biomarker, drug development, therapeutics

Editorial on the Research Topic

Novel Targets and Biomarkers in Solid Tumors

This research topic “Novel Targets and Biomarkers in Solid Tumors” consists of 29 articles contributed by more than 245 authors in the fields of cancer pharmacology and therapeutics. The topic collects the most relevant research in fast emerging areas of clinical molecular diagnostics, drug development, and targeting diverse signaling pathways involved in tumorigenesis and development. Our aim was to generate a collaborative discussion contributing to the future direction of pharmaceutical drug development and therapeutic options.

Transcription factors, tyrosine kinase receptors, and enzymes are closely related to tumor cell growth, proliferation, apoptosis, invasion, and metastasis. Vendrell et al. indicated that overexpression of the ZNF217 transcription factor was predictive of clinical response to neoadjuvant endocrine therapy (ET) in postmenopausal ER-positive (ER+) breast cancer patients. Supporting Vendrell's group observations, Cohen et al. found that the expression of ZNF217 was predictive of the Oncotype DX® (ODX) Recurrence Score in ER+ breast cancers. Liu et al. provided evidence that high expression of the transcription factor SOX2 was associated with shorter overall survival and disease-free survival in patients with triple-negative breast cancer (TNBC), and inhibition of SOX2 could be a potential therapeutic strategy for TNBC. Saby et al. highlighted the relevance of low expression of DDR1, a tyrosine kinase receptor activated by collagen in the aggressiveness and the prognosis of breast carcinoma. Bilal et al. clarified that SMS1 downregulation is associated with sphingolipid metabolism reprogramming, occurs frequently in melanoma, and constitutes a poor prognosis biomarker in metastatic melanoma. Salemi et al. examined the level of MMP-9 and circulating-free DNA BRAFV600E mutations and found that they were associated with poor prognosis. Furthermore, MMP-9 might represent a promising indicator of response to BRAF inhibitors in combination with the detection of BRAFV600E mutation. Wang et al. investigated the hematological biomarkers with regard to tumor grades, IDH, age, and sex in 706 patients with gliomas. Luo et al. provided a review focusing on molecular and histological findings in hereditary diffuse gastric cancer (HDGC) syndrome and their implications for the management of CDH1 mutation carriers and the diagnosis and treatment of HDGC. Taken together, these mechanistic-based biomarkers in tumor samples might be able to predict clinical outcome, holding great promise in clinical application.

The discovery of miRNAs and lncRNAs is propelling the future advancement of biomarker development, and they also play critical roles in tumorigenesis. Lu et al. found that miR-181a is overexpressed in gastric cancer tissues and directly inhibits caprin-1 and promotes gastric cancer development. He et al. explored the miR-26-induced apoptosis and inhibited autophagy in human

OPEN ACCESS

Edited and reviewed by:

Salvatore Salomone,
University of Catania, Italy

*Correspondence:

Zhi Shi
tshizhi@jnu.edu.cn
Dong-Hua Yang
yangd1@stjohns.edu

Specialty section:

This article was submitted to
Experimental Pharmacology
and Drug Discovery,
a section of the journal
Frontiers in Pharmacology

Received: 22 June 2019

Accepted: 27 June 2019

Published: 26 July 2019

Citation:

Shi Z, Guo H-Q, Cohen PA and
Yang D-H (2019) Editorial: Novel
Targets and Biomarkers in Solid
Tumors.
Front. Pharmacol. 10:828.
doi: 10.3389/fphar.2019.00828

non-small cell lung cancer (NSCLC) cells through the TGF- β 1-JNK signaling pathway, suggesting that miR-26 could be a potential novel target for the treatment of NSCLC. Wang et al. demonstrated that miR-3188 interacted with mTOR and FOXO1 to inhibit NSCLC cell proliferation through the mTOR-p-PI3K/AKT-c-JUN signaling pathway. Therefore, miR-3188 might be a potential target for the treatment of NSCLC. Dong et al. confirmed that upregulation of lncRNA NR-046683 serves as a prognostic biomarker and potential drug target for multiple myeloma. Zhu et al. elegantly summarized the characteristics of peptides/proteins that have recently been identified as putative ncRNA translation products and their outlook for small-molecule peptide drugs, drug targets, and biomarkers. Moreover, Luo et al. summarized currently utilized biomarkers in some of the commonly known endocrine tumors, as well as future research directions.

Novel targets and biomarkers are essential components in drug developments and treatments, particularly in this era of targeted therapies. Tremendous efforts are being made to interpret the mechanisms of cancer development with the aim of discovery of novel drugs. Zhao et al. confirmed that Y6, a new epigallocatechin gallate derivative synthesized by their group, inhibited the transport activity of ABCG2. Their results showed that Y6 may potentially be a novel reversal agent in ABCG2-positive drug-resistant cancers. Ji et al. showed that VS-4718, a tyrosine kinase inhibitor targeting focal adhesion kinase (FAK), interacted with the substrate-binding sites of both ABCB1 and ABCG2 through docking study, suggesting that VS-4718 may affect the activity of ABCB1 and ABCG2 competitively. Additionally, Zhang et al. illustrated the reversal effect of olmutinib on ABCG2-mediated MDR cells. Collectively, these findings provided a novel insight into multi-drug resistance in cancer treatment. Next, Wang et al. investigated the anti-tumor effect of DT-13 on human prostate cancer cells and the underlying mechanism. Lu et al. reported the anti-tumor effect and internal molecular mechanism of ORY-1001 in KDM1A-positive lung cancer cells. Vollaie et al. demonstrated the LDN-193189 compound, a potent inhibitor of the BMP type I receptor, might affect the interaction between breast cancer cells and the bone environment, favoring the emergence and development of multiple metastases *in vivo*. Yuan et al. proved that inhibition of WEE1 by MK-1775 could exert the anti-tumor effects on laryngeal squamous cell carcinoma cells *in vivo* and *in vitro*. Finally, the review by Qin et al. presented a brief introduction on the molecular mechanisms of PARP14 as a novel drug target for several cancers, and potential PARP inhibitor-associated adverse effects are discussed.

The rapid emerging high-throughput sequencing and bioinformatics analysis technologies in gene, as well as the openness of a variety of tumor-related databases, facilitate the rapid elucidation of the intrinsic molecular mechanisms of cancer, and the screening of targets for the development of clinically effective anti-tumor drugs and biomarkers offers great opportunities. Suhaimi et al. investigated the gene mutation profile in ER-positive and -negative endometrioid endometrial cancer (EEC) through next-generation sequencing (NGS) and further elucidate the role of WHSC1 mutations in this cancer. The research method of NGS could lead to a better understanding of the biological mechanisms

of cancer and may ultimately result in improvement of treatment options and patient prognosis. Menyhárt et al. identified mutations associated with elevated PD-L1 expression that facilitate the development of better prognostic biomarkers for gastric cancer, and might offer insight into the underlying tumor biology. Chen et al. commendably summarized the expression and prognostic value of PD-L1, as well as the relationships between PD-L1 and immune cell infiltration in glioma. The mechanisms regulating PD-L1 expression and the oncogenic roles of endogenous PD-L1 were discussed. Zhang et al. investigated the protein expression of C-MYC, BCL-2, and BCL-6 in diffuse large B-cell lymphoma and their relationship with genetic abnormalities. Overexpression of those proteins suggested the possibility of translocation. Therefore, immunohistochemical detection of C-MYC, BCL-2, and BCL-6 was useful in diagnosis and prognosis of diffuse large B-cell lymphoma. Xiang et al. performed a cross-database study to analyze the data of ERBB2⁺ gastric cancer deposited in the cancer genome atlas (TCGA), gene expression omnibus (GEO), InBio MapTM, cancer cell line encyclopedia (CCLE), and cancer therapeutics response portal (CTRP), and found that a combination of ERBB2 antagonist or RARA agonist might be effective synergistic regimens for ERBB2⁺ gastric cancer. Zhang et al. explored potential biomarkers associated with the Lauren classification of gastric cancer through screening microarray datasets with information of Lauren classification in the GEO database and comparing differentially expressing genes between intestinal-type or diffuse-type gastric cancer. Chen et al. demonstrated that DEAD-Box helicase 5 interacted with transcription factor 12 and promoted the progression of osteosarcoma by stimulating cell cycle progression.

In conclusion, the “Novel Targets and Biomarkers in Solid Tumors” research topic highlights the importance of developing novel targets and biomarkers for cancer diagnosis and therapy.

AUTHOR CONTRIBUTIONS

All authors listed have made a substantial, direct, and intellectual contribution to the work, and approved it for publication.

FUNDING

ZS was supported by funds from the National Key Research and Development Program of China No. 2017YFA0505104 (ZS) and the National Natural Science Foundation of China No. 81772540. PC was supported by grants from by the French Ligue Contre le Cancer (committees 42 and 71) and Agence Nationale de la Recherche, France (2011 ANR-CESA-018-01).

Conflict of Interest Statement: The authors declare that the research was conducted in the absence of any commercial or financial relationships that could be construed as a potential conflict of interest.

Copyright © 2019 Shi, Guo, Cohen and Yang. This is an open-access article distributed under the terms of the Creative Commons Attribution License (CC BY). The use, distribution or reproduction in other forums is permitted, provided the original author(s) and the copyright owner(s) are credited and that the original publication in this journal is cited, in accordance with accepted academic practice. No use, distribution or reproduction is permitted which does not comply with these terms.



Targeted Next-Generation Sequencing Identifies Actionable Targets in Estrogen Receptor Positive and Estrogen Receptor Negative Endometrioid Endometrial Cancer

OPEN ACCESS

Edited by:

Dong-Hua Yang,
St. John's University, United States

Reviewed by:

Kaijian Hou,
American Diabetes Association,
United States
Zuodong Qin,
Hunan University of Science
and Engineering, China

*Correspondence:

Nurul-Syakima Ab Mutalib
syakima@ppukm.ukm.edu.my;
nurulsyakima@gmail.com
Rahman Jamal
rahmanj@ppukm.ukm.edu.my

[†]Shared first authorship.

Specialty section:

This article was submitted to
Experimental Pharmacology
and Drug Discovery,
a section of the journal
Frontiers in Pharmacology

Received: 26 April 2018

Accepted: 20 June 2018

Published: 13 July 2018

Citation:

Suhaimi SS, Ab Mutalib N-S,
Khor SS, Md Zain RR, Syafruddin SE,
Abu N, Mohd Dali AZH and Jamal R
(2018) Targeted Next-Generation
Sequencing Identifies Actionable
Targets in Estrogen Receptor Positive
and Estrogen Receptor Negative
Endometrioid Endometrial Cancer.
Front. Pharmacol. 9:750.
doi: 10.3389/fphar.2018.00750

Siti Syazani Suhaimi^{1†}, Nurul-Syakima Ab Mutalib^{1*†}, Sheau S. Khor²,
Reena Rahayu Md Zain³, Saiful Effendi Syafruddin¹, Nadiah Abu¹,
Ahmad Zailani Hatta Mohd Dali^{3,4} and Rahman Jamal^{1*}

¹ UKM Medical Molecular Biology Institute, Universiti Kebangsaan Malaysia, UKM Medical Center, Kuala Lumpur, Malaysia,

² Thermo Fisher Scientific, Shah Alam, Malaysia, ³ Department of Pathology, Faculty of Medicine, Universiti Kebangsaan Malaysia, Kuala Lumpur, Malaysia, ⁴ Department of Obstetrics and Gynaecology, Faculty of Medicine, Universiti Kebangsaan Malaysia, Kuala Lumpur, Malaysia

Endometrioid endometrial cancer (EEC) is the commonest form of endometrial cancer and can be divided into estrogen receptor (ER) positive and negative subtypes. The mutational profiles of EEC have been shown to aid in tailoring treatment; however, little is known about the differences between the gene mutation profiles between these two subtypes. This study aims to investigate the gene mutation profile in ER positive and negative EEC, and to further elucidate the role of *WHSC1* mutations in this cancer. EEC and normal endometrial tissues were obtained from 29 patients and subjected to next-generation sequencing (NGS) using Ion Ampliseq Comprehensive Cancer Panel™ targeting 409 cancer related. A total of 741 non-synonymous alterations were identified from 272 genes in ER positive subtype while 448 non-synonymous variants were identified from 221 genes in ER negative subtype. PTEN is the most frequently altered gene in ER positive subtype (64%, 7/11) while ARID1A is the most frequently altered gene in ER negative subtype (50%, 4/8). We also identified alterations in ERBB3 (36%, 4/11), GNAS (36%, 4/11), and WHSC1 (27%, 3/11) in the ER positive subtype. *WHSC1* R1126H and L1268P were shown to significantly increase cell viability, proliferation, migration, and survival. In addition, reduction in ER expression sensitized EEC-1 cell with *WHSC1* L1268P mutant to Fulvestrant treatment. We revealed the mutational spectra of ER positive and ER negative EEC that could lead to better understanding of the biological mechanisms of endometrial cancer and may ultimately result in improvement of treatment options and patient prognosis.

Keywords: endometrial cancer, endometrioid subtype, next-generation sequencing, estrogen receptor, *WHSC1*, Fulvestrant

INTRODUCTION

Endometrial cancer is the sixth most common cancer diagnosed among women with approximately 320,000 new cases and 76,000 deaths worldwide each year (Ferlay et al., 2013). Early detection is common as the disease is symptomatic even at an early stage and therefore is often diagnosed at Stage I (Morice et al., 2016). Despite the fact that most cases are diagnosed early, the incidence and mortality rates for endometrial cancer have been rising in both developed as well as developing countries and are expected to rise further with the increasing aging population and high prevalence of obesity (Ferlay et al., 2015; Morice et al., 2016). Furthermore, although endometrial cancer is generally thought to be a cancer of the postmenopausal women, 14% of cases are diagnosed during premenopausal period with 5% of the patients younger than 40-year old (Duska et al., 2001).

In the past three decades, endometrial cancer has been broadly divided into two subtypes based on histological characteristics, expression of estrogen receptor (ER) and grade (Bokhman, 1983). Majority of endometrial cancer which are designated as Type I endometrioid endometrial cancer (EEC) account for more than 75% of all cases (Carlson et al., 2012), follow the estrogen-related pathway, and arise from hyperplastic endometrium background (Bansal et al., 2009). Frequently diagnosed in premenopausal and young postmenopausal women, Type I EEC is often low grade and well-differentiated thus carrying a favorable outcome (Garg and Soslow, 2014). The less common Type II non-endometrioid endometrial cancer (NEEC), which accounts for 10–20% of all cases, follows the estrogen unrelated pathway and arise in background of atrophic endometrium (Doll et al., 2008). This type has a poorer prognosis and usually presents at the advanced stage, especially in older postmenopausal women (Amant et al., 2005). NEEC is also associated with a high mortality, reduced survival rates, and tendency to recur. This dualistic categorization has been incorporated into clinical decision-making algorithms to define high-risk patients, yet its prognostic value remains limited because one-fifth of EEC (i.e., Type I) will eventually relapse, whereas half of NEEC (i.e., Type II) do not (Bokhman, 1983). Furthermore, 15–20% of EEC are high-grade lesions, and it is unclear where they fit into the dualistic model (Zannoni et al., 2013).

This dualistic model has also been supported by molecular studies where Type I EEC has been symbolized by frequent alterations in *PTEN*, *PIK3CA*, *KRAS*, *CTNNB1*, and *ARID1A* as well as defects in DNA mismatch repair (MMR) resulting in the microsatellite instability (MSI) phenotype (O'Hara and Bell, 2012). In contrast, mutations in *TP53* and *PP2R1A* as well as a high expression of oncogene *Her2/ERBB2* are the major genetic changes among Type II NEEC (Lax et al., 2000; O'Hara and Bell, 2012). However, this classification is controversial due to existence of a minority of endometrial cancer cases with overlapping clinical features, morphological and molecular characterization which represents a major obstacle to effective cancer treatment (Talhouk and McAlpine, 2016). For example, Type I EEC is not completely ER positive and loss of ER expression is correlated with aggressive behavior, high grade histology, and poor survival rate

(Maniketh et al., 2014; Backes et al., 2016). In contrast to breast cancer, where the ER status (in addition to progesterone) is a pillar for its molecular and clinicopathological classification (Nadji et al., 2005), a comprehensive view of the mutation spectrum between ER positive and ER negative in the same molecular subtype (i.e., endometrioid) has not been fully elucidated. Therefore, the aim of this study is to characterize somatic gene alterations in ER positive and ER negative EEC using targeted deep sequencing of 409 cancer-related genes.

MATERIALS AND METHODS

Clinical Specimen, DNA Extraction, and Quality Assessment

Fresh frozen tissues of EECs ($n = 19$) were obtained after hysterectomy from the patients admitted to the Universiti Kebangsaan Malaysia Medical Centre (UKMMC). The cancers were classified according to the World Health Organization (WHO) classification of tumors of the female reproductive system (Pecorelli, 2009). In addition, fresh frozen normal endometrium ($n = 10$) were obtained from patients surgically treated for non-malignant endometrial diseases. This study was approved by the Universiti Kebangsaan Malaysia Research Ethics Committee (UKM 1.5.3.5/244/AP-2012-011) and carried out in accordance with the approved guidelines. All patients provided written informed consent for their tissue samples to be used for research. Immunohistochemical staining for ER (antibody clone 1D5, DAKO, Carpinteria, CA, United States) and Hematoxylin and Eosin (H&E) staining was performed on the frozen sections and then reviewed by a pathologist. Immunohistochemical staining for ER was scored as positive if 1% or more of tumor nuclei were immunoreactive and negative if less than 1% of tumor cell nuclei were immunoreactive. Only cancer specimens containing more than 80% cancer cells and normal tissues with less than 20% necrosis were subjected to DNA isolation using the QIAamp® DNA Mini Kit (Qiagen, Valencia, CA, United States) following the manufacturer's protocol.

Next-Generation Sequencing

The Ion Ampliseq™ Comprehensive Cancer Panel V2 (Life Technologies, Guilford, CT, United States), which covers 409 oncogenes and tumor suppressor genes, was used for library preparation (**Supplementary Table S1**) according to manufacturer's instruction. The libraries were then normalized to 12–25 pM for template preparation on the Ion One Touch (Life Technologies, Guilford, CT, United States). The clonal amplification of the DNA libraries on the Ion Sphere Particles (ISPs) was carried out using emulsion PCR and the subsequent isolation of templated ISPs was performed using Ion OneTouch ES (Life Technologies, Guilford, CT, United States). Subsequently, next-generation sequencing (NGS) was performed on the Ion Torrent Personal Genome Machine (PGM™) using 318™ chip and Ion Torrent PGM Sequencing 200 kit V2 (Life Technologies, Guilford, CT, United States).

Bioinformatics Analyses

Read Mapping and Variant Calling

Data from the sequencing runs were automatically transferred to the Torrent Server hosting the Torrent Suite Software v4.0.3. The readings were mapped to the reference genome (hg19) using the Torrent Mapping Alignment program (TMAP). Variant calling was generated using Torrent Variant Caller v 4.0 with low stringency settings (Life Technologies, Guilford, CT, United States).

Variant Annotation and Prioritization

The functional effects of the variants were further annotated using ANNOVAR (Wang et al., 2010) with respect to gene regions and filter-based annotations. Prediction on protein impact of variants was performed using SIFT, PolyPhen2 HDIV, PolyPhen2 HVAR, LRT, MutationTaster, MutationAssessor, FATHMM, GERP++, PhyloP, and SiPhy databases that are available in ANNOVAR. We classified SNVs as pathogenic if they were observed to be deleterious by three or more than three SNV protein prediction algorithms.

To evaluate which mutations could be actionable and to prioritize for the true somatic mutations, several additional filtering steps were performed. Details on filtrations steps are illustrated in **Supplementary Figure S1**. The alignment of each candidate variant was manually inspected to check for sequencing artifacts and alignment errors using the Integrated Genomic Viewer (IGV) (Thorvaldsdóttir et al., 2013). Oncoprint diagram and lollipop plot were created using Oncoprinter and Mutation Mapper tools, respectively (Cerami et al., 2012; Gao et al., 2013). The detected mutations were compared to those in available cancer databases from the COSMIC v82 (Forbes et al., 2017), MyCancerGenome (Van Allen et al., 2013), and International Cancer Genome Consortium (ICGC) database (Zhang et al., 2011). Cancer Genome Interpreter was used to classify driver mutation among the somatic alterations (Tamborero et al., 2018).

To identify relevant genes for further characterization, we prioritized the genes involved in endometrial cancer carcinogenesis using following strategies: (1) genes associated with EEC carcinogenesis and (2) genes relevant to ER signaling pathways [based on Kyoto Encyclopedia of Genes and Genomic (KEGG) estrogen signaling pathway (hsa04915)] (Kanehisa et al., 2016).

Sanger Sequencing for Validation

Identified variants were selected randomly for validation by Sanger sequencing. Primers for Sanger sequencing validation were designed using the IDT-DNA Primer Quest (Coralville, IA, United States). The PCR primers were described in **Supplementary Table S2**. PCR amplifications were performed using Applied Biosystem AmpliTaq® Gold 360 master Mix (Applied Biosystems, Foster City, CA, United States) following manufacturer's instructions. Sanger sequencing was performed using BigDye Terminator v.3.1 Cycle Sequencing kits (Applied Biosystems, Foster City, CA, United States) on an ABI 3500 Genetic Analyzer platform (Life Technologies, Guilford, CT, United States).

Site-Directed Mutagenesis and Constructs

The wild-type plasmid construct of *WHSC1* (RC212404) was obtained from OriGene Technologies (Rockville, MD, United States). Site-directed mutagenesis was performed using the Quick-Change™ Site-Directed Mutagenesis Kit (Stratagene, La Jolla, CA, United States), according to the manufacturer's instructions. The mutagenic primers were designed using QuickChange Primer Design Program and the sequences were provided in **Supplementary Table S3**.

Cell Lines and Transient Transfection

Endometrioid endometrial cancer-1 (ATCC® CRL-2923™) and 293T (ATCC® CRL-3216™) cells were maintained in RPMI 1640 and DMEM: F12 (both from Gibco, United States) supplemented with heat inactivated 10% fetal bovine serum (FBS; Gibco, United States). Twenty-four hours prior to transfection, cells were seeded in a 6-well plate with a density of 4×10^5 (EEC-1) and 6×10^5 (293T). Four micrograms of each construct was transfected using 8 μ l Lipofectamine 2000 (Invitrogen, Carlsbad, CA, United States) according to the manufacturer's instructions. Control cells were cells transfected with the empty vector pCMV6.

Gene Expression and Protein Analysis

Total RNA was isolated from the cell lines using the RNeasy Kit (Qiagen, Valencia, CA, United States) according to the manufacturer's directions and cDNA was synthesized using High Capacity RNA to cDNA Kit (Applied Biosystem, Foster City, CA, United States). Quantitative real-time PCR was performed using TaqMan Fast Advanced Master Mix on the ABI 7500 Fast Real-Time PCR system (Applied Biosystem, Foster City, CA, United States). Relative expression was calculated using the $\Delta\Delta C_t$ method (Livak and Schmittgen, 2001) with GAPDH as the housekeeping gene.

Protein lysate was resolved on a mini-protean TGX precast gel of 4–20% polyacrylamide (BioRad Laboratories, Hercules, CA, United States) and analyzed against the following primary antibodies; anti-DDK (Clone OTI4C5) (OriGene Technologies, Rockville, MD, United States), NSD2 (G12), ER α (HC-20), and anti- β -actin (sc-47778) (Santa Cruz Biotechnology Inc., Santa Cruz, CA, United States).

Cell-Based Assays

Cell viability was assessed using PrestoBlue® cell viability reagent (Invitrogen, Carlsbad, CA, United States), wound healing assay was performed using IBIDI Culture-Inserts (IBIDI GmbH, Martinsried, Germany), migration ability of the cells was assessed using QCM™ 24-well cell migration assay (Millipore, Billerica, MA, United States), and colony formation assay was performed by seeding 500 transfected cells in six-well plates followed by incubation at 37°C for 14 days and crystal violet staining. All assays were performed in triplicate.

BrdU Proliferation Assay

Endometrioid endometrial cancer-1 cell lines were seeded at 2×10^4 cells per well in 96-well plate and transfected

with mutants or wild type of *WHSC1* expression constructs before BrdU incorporation using BrdU Cell Proliferation Assay (Millipore, Temecula, CA, United States).

Luciferase Assay

To substantiate the importance of *WHSC1* as a potential coactivator, dual luciferase assay was performed. We used Cignal ERE Reporter Assay kit from SABiosciences (Valencia, CA, United States). 293T cells were plated at a density of 3×10^5 cells per well (96-well plates) in phenol red-free DMEM: F12 with 10% v/v charcoal–dextran-treated FBS. The cells were then transfected with 100 ng of reporter plasmid, wild-type *WHSC1* plasmid, and Renilla. Each sample was done in triplicate. The *WHSC1* mutants were transfected in the same manner. After transfection for 24 h, the cells were stimulated with 10 nM E2 or vehicle (DMEM). The Dual-Glo Luciferase Assay System (Promega) was used according to the manufacturer's instructions using VARIOLUX luminometer. Values were normalized to Renilla luciferase activity.

RESULTS

Patient Demographic Data and Tumor Characteristic

Clinical specimens used in this study were collected from patients who were treated at the UKMMC. The information on the patient's age, degree of differentiation, FIGO staging of tumor, metastasis, and ER status is summarized in **Table 1**. The majority of EEC in both groups were stage 1B 64% (7/11) in ER positive, 50% (4/8) in ER negative. While there are three cases of metastasis in ER negative = 37.5%, (3/8) has shown patients with advance disease.

TABLE 1 | Patient demographics and tumor characteristics.

Characteristics	Classification	ER positive, <i>n</i> = 11	ER negative, <i>n</i> = 8
Age	Average	52	57
FIGO staging	IA	0 (0)	0 (0)
	IB	7 (64)	4 (50)
	IC	2 (18)	2 (25)
	IIA	1 (9)	0 (0)
	IIB	0 (0)	1 (12.5)
	IIIA	0 (0)	0 (0)
	IIIB	0 (0)	1 (12.5)
	N/A	1 (9)	0 (0)
Degree of differentiation	Grade 1	5 (45)	4 (50)
	Grade 2	4 (36)	2 (25)
	Grade 3	1 (9)	1 (12.5)
	N/A	1 (9)	1 (12.5)
Metastasis lymph nodes	Yes	0 (0)	3 (37.5)
	No	11 (100)	5 (62.5)

Mutations Analysis of Endometrial Cancer With Ion Ampliseq™ Cancer Panel

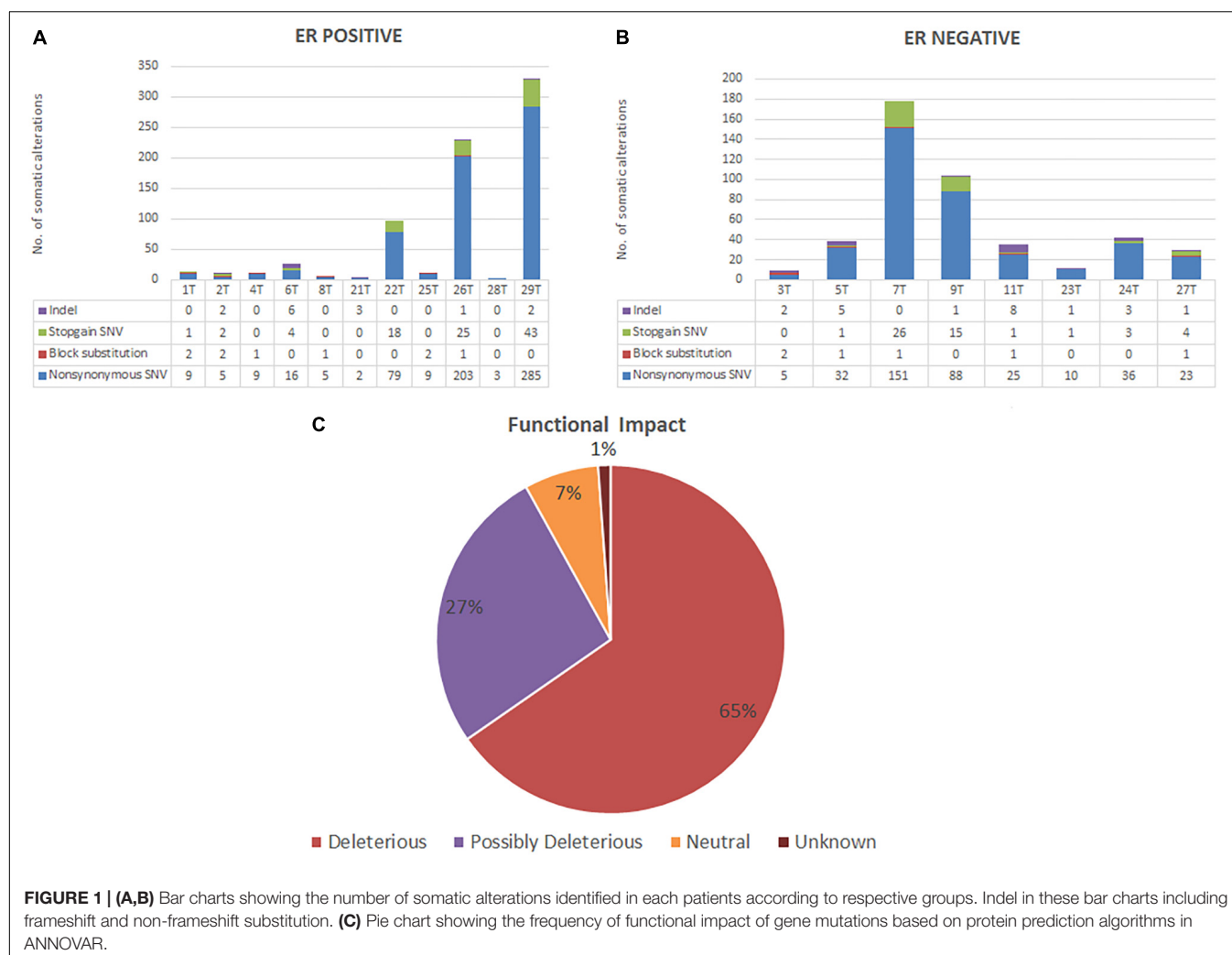
All patients from both groups have at least three alterations among the 409 genes screened. A total of 741 variants were identified in 272 genes in ER positive subtype [718 single-nucleotide variations (SNVs), 14 insertions/deletions (INDELs), and 9 block substitutions] (**Figure 1A**). While in ER negative subtype, a total of 448 variants altered in 221 different genes, including 421 SNVs, 21 INDELs, and 6 block substitutions (**Figure 1B**). We noted that mutations distribution of EECs in both subtypes were genomically heterogeneous. There were five highly mutated patients (median 178 per tumor, range from 97 to 330) and another 14 patients were non-highly mutated (median 11 mutations per tumor; range 3–42). We further investigated and found that hypermutated phenotype group could have a perturbed DNA repair system due to frequently altered DNA repair genes especially in MMR genes such as (i.e., *MSH2*, *MSH6*, and *PMS1*) (**Supplementary Table S4**).

Based on protein prediction algorithms among identified 1139 SNVs in both subtypes, 739 variants (65%) were predicted to have deleterious effects, 301 variants (27%) have possibly deleterious effects, while the other 78 variants (7%) has neutral or low protein impact (**Figure 1C**). We identified 134 out of 371 (36%) genes predicted as tumor driver which included a total of 295 alterations. From this 295 alteration, 178 (60%) were identified in ER positive whereby 9 out of 11 ER positive patients have at least two candidate driver alteration. Meanwhile in ER negative subtype, 117 (40%) alterations were identified in ER negative patients where all ER negative patients have at least three candidate driver alterations (**Supplementary Table S5**).

PTEN is the most frequently altered gene in ER positive subtype (64%, 7/11) while *ARID1A* is the most frequently altered gene in ER negative group (50%, 4/8) as shown in **Figure 2A** (**Supplementary Tables S6, S7**). Majority of *PTEN* alterations were missense and in-frame mutations. On the other hand, *ARID1A* mutations were truncating alterations including nonsense mutations and INDELs. Mutations in the ER signaling pathway is known to be important in endometrial cancer; therefore, we further examined the prevalence of mutations in the genes involved in ER signaling pathway. Overall, there are 38 genes out of 409 genes panel list of CCP known to be involved in ER signaling pathway (**Supplementary Table S1**). As shown in **Figure 2B** (**Supplementary Tables S8, S9**), *ERBB3*, *GNAS*, *PIK3R1*, and *WHSC1* are the most frequently altered genes in ER positive subtype (36%, 4/11); (36%, 4/11); (27%, 3/11); and (27%, 3/11) while *PIK3CA* is the most frequently altered gene in ER negative group (50%, 4/8). **Table 2** showed classification based on protein impact prediction and candidate driver mutations for each alteration in *PTEN*, *ARID1A*, *PIK3CA*, *ERBB3*, *GNAS*, *PIK3R1*, and *WHSC1*.

Mutations Distribution in the Functional Domains of *PTEN*, *ARID1A*, *ERBB3*, and *WHSC1*

Mutations distribution in the functional domains of *PTEN*, *ARID1A*, and *WHSC1* was illustrated in



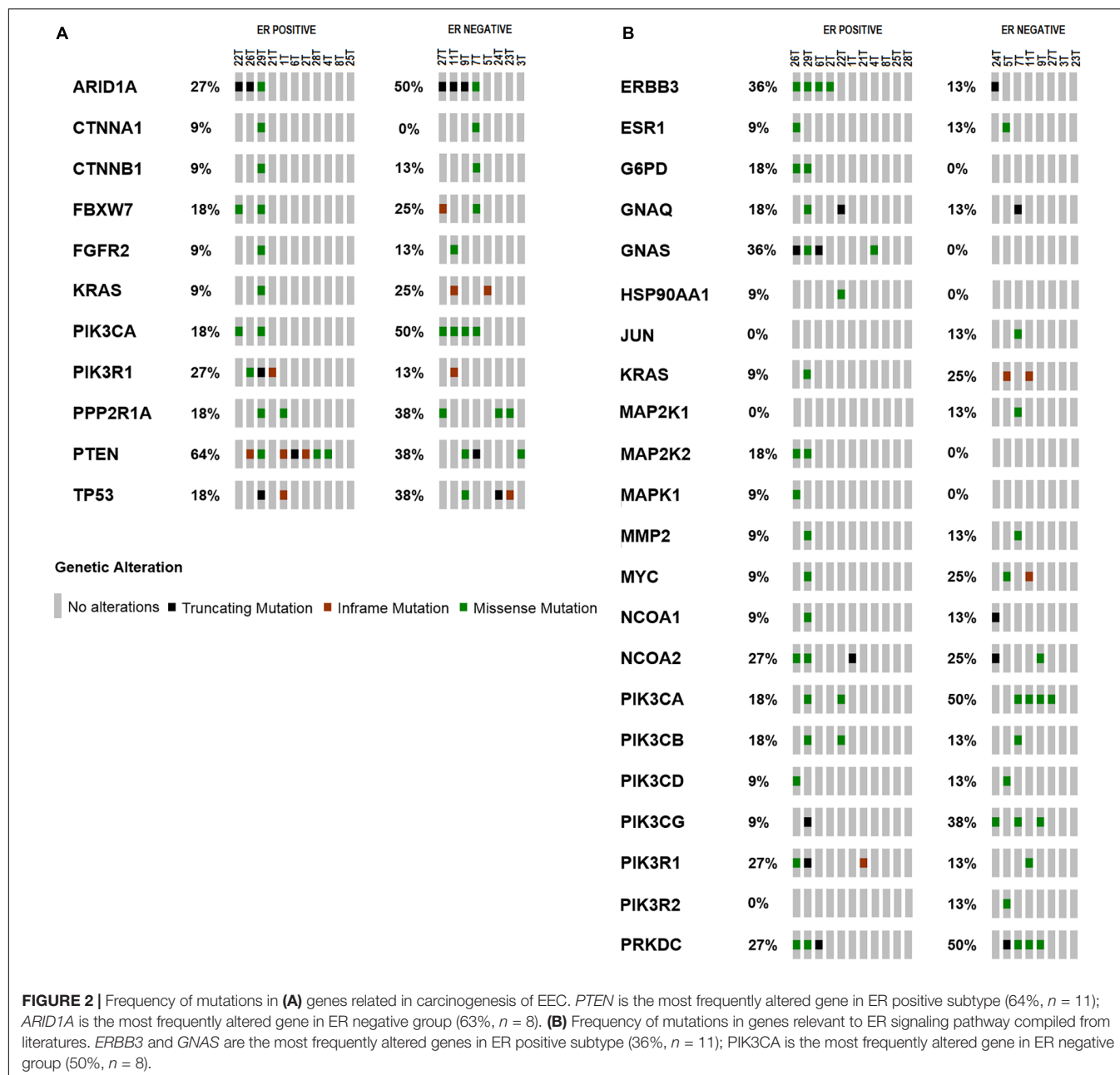
Supplementary Figure S2. Mutations in *PTEN* were localized to the catalytic phosphatase domain, with majority of mutants belongs to ER positive subtype group including the recurrent hotspot R130 residue, D92E, K128T (**Supplementary Figure S2a**). In addition, a frameshift deletion (R11fs) and two missense mutations (P190L and F341V) in C2 domain were also found in ER positive subtype. While in ER negative subtype group, two nonsense mutations (E7X and S59X) and two missense alterations (I122N and F145V) located on phosphatase domain have been identified. Most of these mutations have been reported via COSMIC v82, with the exception to R11fs, which was identified in our study.

Out of the 19 EECs sequenced, seven patients had nine *ARID1A* mutations (four mutations were identified in ER positive and five in ER negative EEC patients). Interestingly, recurrent hotspot mutation (R1989X) was observed in both ER positive and ER negative subtype group as shown in **Supplementary Figure S2b**. More *ARID1A* mutations were identified among ER negative subtype group, with mainly truncating type of mutations (nonsense and frameshift deletion) (G324fs, R1335X, R1989X, and G2040fs) and a missense

mutation (S1985P). However, two nonsense mutations (R1989X and S2269X) and two missense mutations (P1576L and R1636W) which were located on non-functional domain of *ARID1A* have been identified in ER positive subtype. This study is the first to report the somatic G2040fs variant in EEC.

Higher mutation frequency of *ERBB3* was observed in ER positive subtype (36%, 4/11) compared to ER negative subtype (18%, 1/8). As shown in **Supplementary Figure S2c**, the missense mutations in ER positive sample were mapped at functional domain of *ERBB3* gene including two in extracellular domain (L143M and P558S) and one in tyrosine kinase domain (L924V), while the others mapped on non-functional domain (R488Q), (R670Q), and (G1073V). Nevertheless, the single frameshift deletion mutation (E560fs) reported in ER negative subtype was located at the extracellular domain IV of *ERBB3*. To date, most of the mutations we discovered in *ERBB3* gene are novel, except for L143M, R488Q, and R670Q that have been recorded in Cosmic v82 and ICGC database, respectively.

WHSC1 was found to be altered in three ER positive patients and one ER negative patient. Majority of these somatic variations



were distributed along the functional domain of *WHSC1* as shown in **Supplementary Figure S2d**. All of the variants identified in this study are novel, with the exception of a mutation on the catalytic SET domain (R1126H) that has been identified in several cancers (**Supplementary Table S10**). One missense mutation K547E was identified in an area without a defined domain, while two missense mutations (P748L and L1268P) were located within the plant homeodomain (PHD) domains II and V, respectively. A nonsense mutation (R824X) was identified which was predicted to cause premature truncation of WHSC1 protein with a deletion of C terminal functional domains including PHD IV, proline-tryptophan-tryptophan-proline-2 (PWWP2), SET, and PHD V-CH5CH domain. The frequency and location

of alterations in *WHSC1* suggest that these cancer-associated mutations may have functional consequences.

Expression Analysis of Wild-Type and Mutant Constructs

The level of *WHSC1* expression was firstly screened in several cell lines (**Figure 3A**) in order to gauge its expression. Upon transfection, *WHSC1* mRNA levels were significantly reduced in the transfected cells with the mutant constructs K547E, R824X, and R1126H compared to the wild type indicating that these mutations affected the stability of the mRNA levels. However, the wild type and mutant L1268P were equally expressed in

TABLE 2 | Classification of somatic alterations in PTEN, PIK3CA, ARID1A, ERBB3, GNAS, PIK3R1, and WHSC1 genes.

Patient	ER subtype	Gene	Exonic function	Protein change	Exon	Protein impact prediction	Driver prediction
IT	ER + VE	PTEN	Nonframeshift substitution	R130P	5	NA	Driver
2T	ER + VE	PTEN	Nonframeshift substitution	R130G	5	NA	Driver
4T	ER + VE	PTEN	Nonsynonymous SNV	K128T	5	Deleterious	Driver
6T	ER + VE	PTEN	Frameshift deletion	R11fs	1	NA	Driver
26T	ER + VE	PTEN	Nonframeshift substitution	R130Q	5	NA	Driver
28T	ER + VE	PTEN	Nonsynonymous SNV	P190L	6	Deleterious	Passenger
29T	ER + VE	PTEN	Nonsynonymous SNV	F341V	8	Deleterious	Driver
29T	ER + VE	PTEN	Nonsynonymous SNV	D92E	5	Deleterious	Driver
7T	ER – VE	PTEN	Stopgain SNV	S59X	3	Deleterious	Driver
7T	ER – VE	PTEN	Stopgain SNV	E7X	1	NA	Driver
9T	ER – VE	PTEN	Nonsynonymous SNV	F145V	5	Deleterious	Driver
24T	ER – VE	PTEN	Nonsynonymous SNV	I122N	5	Deleterious	Driver
22T	ER + VE	PIK3CA	Nonsynonymous SNV	T1025A	21	Possibly deleterious	Driver
22T	ER + VE	PIK3CA	Nonsynonymous SNV	P449T	8	Deleterious	Driver
29T	ER + VE	PIK3CA	Nonsynonymous SNV	E453K	8	Possibly deleterious	Driver
29T	ER + VE	PIK3CA	Nonsynonymous SNV	E365K	6	Possibly deleterious	Driver
7T	ER – VE	PIK3CA	Nonsynonymous SNV	E81K	2	Deleterious	Driver
7T	ER – VE	PIK3CA	Nonsynonymous SNV	Q879K	18	Possibly deleterious	Passenger
7T	ER – VE	PIK3CA	Nonsynonymous SNV	I816T	17	Deleterious	Passenger
7T	ER – VE	PIK3CA	Nonsynonymous SNV	R54K	2	Possibly deleterious	Passenger
9T	ER – VE	PIK3CA	Nonsynonymous SNV	G118D	3	Deleterious	Driver
11T	ER – VE	PIK3CA	Nonsynonymous SNV	Q60H	2	Possibly deleterious	Passenger
27T	ER – VE	PIK3CA	Nonsynonymous SNV	M1043V	21	Deleterious	Driver
22T	ER + VE	ARID1A	Stopgain SNV	S2269X	20	Deleterious	Passenger
26T	ER + VE	ARID1A	Stopgain SNV	R1989X	20	Deleterious	Driver
26T	ER + VE	ARID1A	Nonsynonymous SNV	R1636W	18	Deleterious	Driver
29T	ER + VE	ARID1A	Nonsynonymous SNV	P1576L	18	Deleterious	Passenger
7T,9T	ER – VE	ARID1A	Stopgain SNV	R1989X	20	Deleterious	Driver
7T	ER – VE	ARID1A	Nonsynonymous SNV	S1985P	20	Deleterious	Passenger
9T	ER – VE	ARID1A	Frameshift deletion	G2040fs	20	NA	Driver
11T	ER – VE	ARID1A	Frameshift deletion	G324fs	1	NA	Driver
27T	ER – VE	ARID1A	Stopgain SNV	R1335X	16	Deleterious	Driver
2T	ER + VE	ERBB3	Nonsynonymous SNV	P558S	14	Deleterious	Passenger
2T	ER + VE	ERBB3	Nonsynonymous SNV	R488Q	12	Deleterious	Passenger
6T	ER + VE	ERBB3	Nonsynonymous SNV	L924V	23	Deleterious	Driver
26T	ER + VE	ERBB3	Nonsynonymous SNV	L143M	4	Deleterious	Driver
29T	ER + VE	ERBB3	Nonsynonymous SNV	G1073V	27	Possibly deleterious	Passenger
29T	ER + VE	ERBB3	Nonsynonymous SNV	R670Q	17	Neutral/Benign	Passenger
4T	ER – VE	ERBB3	Frameshift deletion	E560fs	14	NA	Passenger
6T	ER + VE	GNAS	Stopgain SNV	S192X	1	Possibly deleterious	NA
26T	ER + VE	GNAS	Stopgain SNV	R327X	11	Possibly deleterious	Passenger
29T	ER + VE	GNAS	Nonsynonymous SNV	I39T	1	Deleterious	NA
29T	ER + VE	GNAS	Nonsynonymous SNV	P338L	1	Neutral/benign	NA
4T	ER + VE	GNAS	Nonsynonymous SNV	R194P	1	Neutral/benign	NA
21T	ER + VE	PIK3R1	Nonframeshift deletion	578_580del	13	NA	Passenger
26T	ER + VE	PIK3R1	Nonsynonymous SNV	M525I	13	Possibly deleterious	Passenger
29T	ER + VE	PIK3R1	Stopgain SNV	R348X	9	Deleterious	Driver
29T	ER + VE	PIK3R1	Stopgain SNV	R162X	4	Deleterious	Driver
11T	ER – VE	PIK3R1	Nonframeshift deletion	404_405del	10	NA	Passenger
22T	ER + VE	WHSC1	Nonsynonymous SNV	K547E	7	Deleterious	Driver
22T	ER + VE	WHSC1	Stopgain SNV	R824X	13	Deleterious	Passenger
26T	ER + VE	WHSC1	Nonsynonymous SNV	R1126H	19	Deleterious	Driver
29T	ER + VE	WHSC1	Nonsynonymous SNV	L1268P	21	Deleterious	Driver
9T	ER – VE	WHSC1	Nonsynonymous SNV	P748L	12	Deleterious	Driver

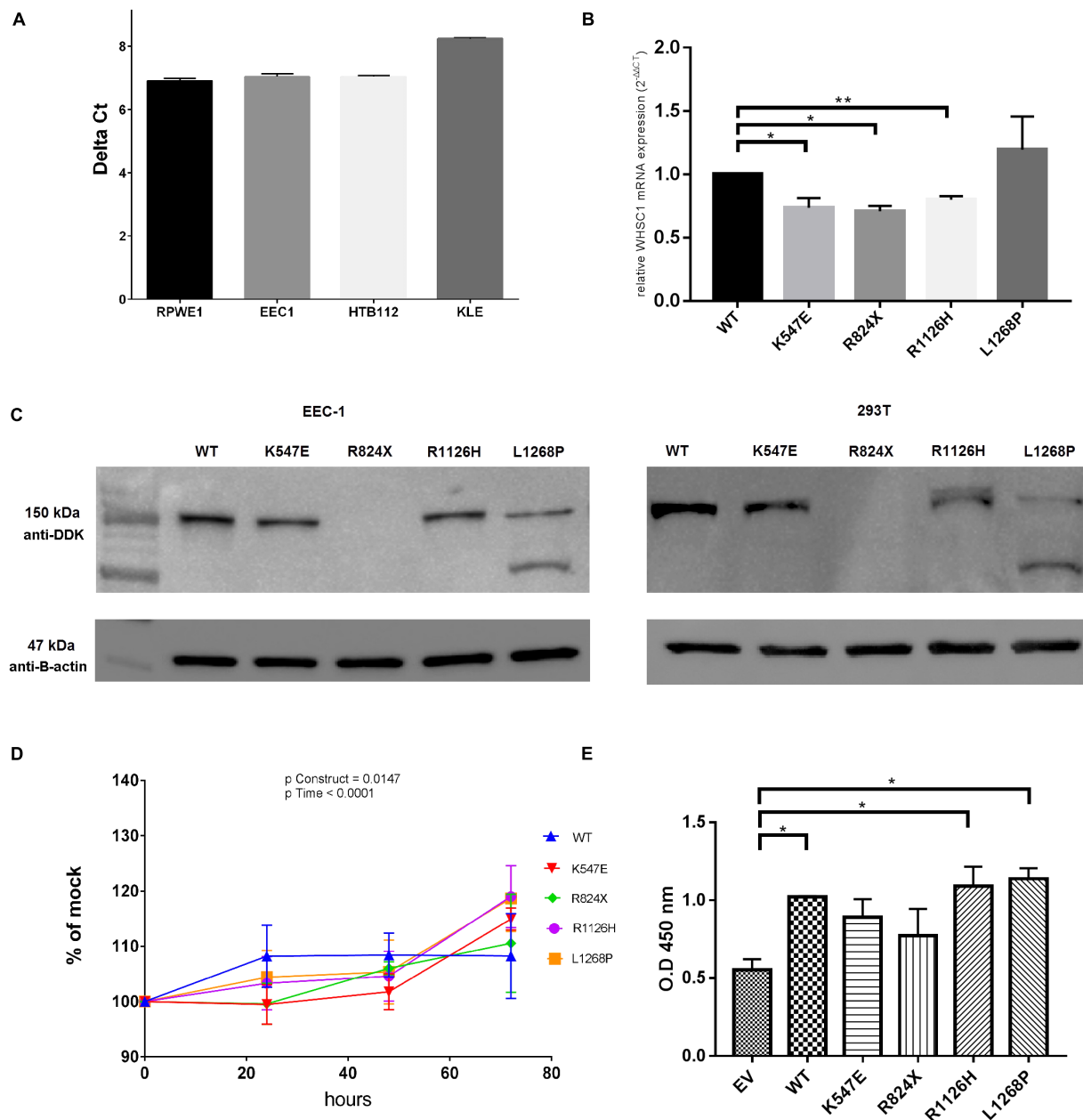


FIGURE 3 | WHSC1 gene and protein analysis. **(A)** Quantification of mRNA from nuclear extract of normal prostate cell lines (RPWE1) and endometrial cancer cell lines (EEC-1, HTB-112, KLE). **(B)** Quantification of mRNA expression of mutant *WHSC1* in EEC-1 cell line. Relative *WHSC1* mutants were calculated in comparison to WT *WHSC1* 48 h post-transfection by real-time PCR and normalized to GAPDH mRNA expression. Negative control (no template) was included in each experiment (mean \pm SD, $n = 2$, $*p < 0.05$). The mRNA expression of WT was assigned as 1. **(C)** Western blot analysis shows protein expression of wild type and *WHSC1* mutants in EEC-1 and 293T cell lines after 48 h post-transfection. Total protein harvested from EEC-1 cells and 293T cells solubilized in cell lysis buffer were analyzed using precast SDS 4–12% gels. The WT and mutants of *WHSC1* (152.1 kDa) were detected using Anti-DDK Clone OT14C5 (mouse origin). While β -actin (47 kDa) was detected using anti- β -actin (mouse origin) for positive control. Mutants *WHSC1* promote cell growth. **(D)** Mutants *WHSC1* promote cell viability. At 72 h, the mutants K547E, R1126H, and L1268P resulted in 15, 19, and 18% increase significantly in motility, respectively, over EV in EEC-1. Statistical significance in all cases was measured by Student's *t*-test ($*p < 0.05$), $n = 3$. Error bars represent average \pm SD. Overall *p*-values were calculated by two-way ANOVA for time. **(E)** Mutants *WHSC1* promote cell proliferation. BrdU colorimetric incorporation assay shows that *wild type* of *WHSC1*, R1126H, and L1268P significantly increased cell proliferation in EEC-1. Statistical significance in all cases was measured by Student's *t*-test ($*p < 0.05$), $n = 2$. Error bars represent average \pm SD.

the transfected EEC-1 cell line (Figure 3B). This result was confirmed by the Western blot in EEC-1 and 293T cell lines (Figure 3C). Of note however, there is a second migrating band

seen in L1268P in Western blot assay, which might explain the differences of mRNA of transcription level of L1268P and other mutant constructs.

Assessment of Oncogenic Properties of *WHSC1* Mutants

At 72 h, the mutants K547E, R1126H, and L1268P showed a 15 ($p = 0.0002$), 19 ($p = 0.0043$), and 18% ($p = 0.0056$) significant increase in cell proliferation, respectively, over the empty vector control in EEC-1 cell line (Figure 3D). The effect of the *WHSC1* mutants on cell proliferation was further assessed by quantifying the activity of proliferating cells within 24 h after BrdU labeling. BrdU incorporation assay revealed significant increase in DNA synthesis in *WHSC1* wild type ($p = 0.0190$), R1126H ($p = 0.0341$), and L1268P ($p = 0.0136$) mutants, relative to empty vector. In contrast, no significant effect on DNA synthesis was caused by the K547E and R824X mutants (Figure 3E).

To further address the role of constitutive activation of *WHSC1* mutants on cell migration, we employed both the wound-healing and transwell migration assays. As shown in Figure 4A, the open area was rapidly covered by the mutant R1126H and L1268P in comparison with control ($p = 0.0049$ and $p = 0.0040$, respectively). The quantified open area in vector control cells reduced from 100 to only 76%, while R1126H mutant cells reduced from 100 to 95%, whereas L1268P mutant caused reduction from 100 to 94%. The wild type *WHSC1* also showed significant wound closure from 100 to 85% ($p = 0.0233$). To further confirm migration ability of the mutants, we employed the transwell migration assay. Similarly, EEC-1 transfected with *WHSC1* mutants R1126H and L1268P displayed a significant increase in number of migrated cells (Figure 4B) ($p = 0.0102$ and $p = 0.0086$, respectively). In this transwell migration assay, the wild-type *WHSC1* also showed potential migration ability compared with vector alone control cells ($p = 0.0233$). In addition, only mutants R1126H and L1268P showed a significant increase in colony number compared to empty vector (Figure 4C) ($p = 0.00416$ and $p = 0.0232$, respectively).

WHSC1 Regulates ER α Gene Expression

Both R1126H and L1268P led to a significant increase of the coactivation potential in *WHSC1* (Figure 5) albeit lower than the wild type *WHSC1* when compared with empty vector. However, the truncated R824X mutant showed reduction of the coactivation potential of *WHSC1* suggesting that the catalytic SET activity is required for its ability to stimulate estrogen-dependent gene transcription. When compared all mutants with the wild type, only L1268P signaling did not differ significantly.

Activating *WHSC1* L1268P Is Sensitive to Fulvestrant

Fulvestrant acts as an antagonist to inhibit ER activity; therefore, we examine the effect of *WHSC1* R1126H and L1268P on the dose-dependent inhibition of proliferation in EEC-1 cells. Fulvestrant was able to inhibit the activity of wild type and *WHSC1* mutants. As shown in Figures 6A,B, L1268H had significantly greater antiproliferative effect only when compared with the empty vector with a 60% growth inhibition ($p = 0.0281$) compared to the wild type (54%) which was not significant ($p = 0.362$). The estrogen responsiveness was assayed as shown

in Figure 6C, where we compared the ability of Fulvestrant to reduce ER protein levels in wild-type and mutants *WHSC1*, in the presence and absence of estrogen. We observed that Fulvestrant was able to downregulate the ER proteins of both wild type and mutants, with more reduction seen in the L1268P mutant's ER proteins level. Upon treatment with estradiol and Fulvestrant, a clear reduction of steady-state L1268P *WHSC1* mutant's exogenous protein can be seen in the Western blot assay.

DISCUSSION

Over the past few years emergence of novel technologies based on NGS have led to a new paradigm in understanding the mutational landscape of endometrial cancers. However, most studies were limited to either characterization of endometrial cancer without stratification based on grade and histological subtypes, or were focused on aggressive serous carcinoma subtype of endometrial cancer only (Kuhn et al., 2012; Le Gallo et al., 2012; Liang et al., 2012; Chang et al., 2017). Our study is not only the first report on the mutational landscape in ER positive and ER negative EEC, but also on the functional analysis of a potential gene candidate, *WHSC1*, involved in ER positive endometrioid tumorigenesis. Of the 11 ER positive and 8 ER negative EEC patients sequenced in our study, the mutation spectrum notably diverges among both subtypes.

Among known genes that have been reported to be altered in endometrial cancer in earlier studies, *PTEN* mutations occur frequently in ER positive subtype compared to ER negative subtype. In the TCGA study on EEC, *PTEN* mutations have also been associated with ER expression in endometrial cancer (The Cancer Genome Atlas Research Network et al., 2013). However, our study showed that *PIK3CA* mutations were comparable between both ER subtypes with more events occurring in the ER negative subtype compared to ER positive subtype. This is inconsistent with results from TCGA on breast cancer, which suggested the association between *PIK3CA* with ER positive expression (The Cancer Genome Atlas Network, 2012). From the 10 patients with *PTEN* mutation in our study, only 3 patients had mutation in *PIK3CA*, which is consistent with other investigators that claimed *PIK3CA* mutations are mutually exclusive with *PTEN* mutations, suggesting that carcinogenic signaling through phosphatidylinositol 3-kinase (PI3K) pathway is mediated either through inactivation of *PTEN* or activation of *PIK3CA* (Prat et al., 2007). *ARID1A* mutations were identified in both endometrial cancer subtypes but more commonly seen in the ER negative subtype. Almost all *ARID1A* mutants in our analysis coexist with *PTEN* and *PIK3CA* mutations, and it is postulated that these mutations together induce aberrant activation of PI3K and protein kinase B (AKT) phosphorylation that result in inhibition of cell survival and apoptosis (Liang et al., 2012).

PTEN is a 200-kb gene located on chromosome 10q23.3 that consists of nine exons coding for 403 amino acids yielding a 47 kDa protein (Li, 1997). This tumor suppressor gene plays an important role in the tumorigenesis of endometrial cancer, particularly in EEC (Djordjevic et al., 2012; O'Hara and Bell, 2012; The Cancer Genome Atlas Research Network et al., 2013).

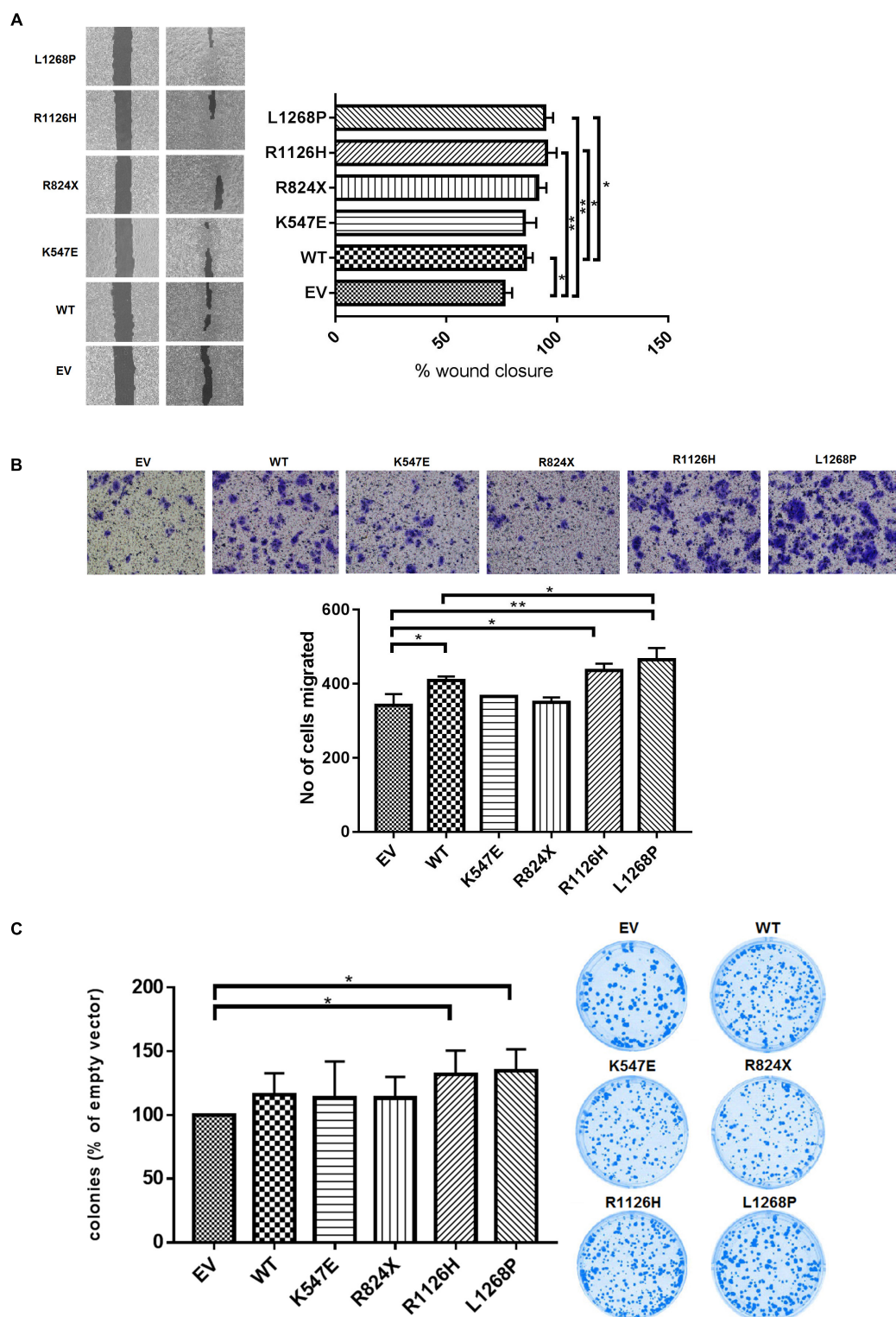


FIGURE 4 | Effect of *WHSC1* mutants on cell migration and clonogenic potential. **(A)** Wound healing assay displayed significant increase in average rate of wound closure at 72 h shown in R1126H and L1268P compared with EV and WT. **(B)** Transwell migration assay showed the numbers of migrated mutants R1126H and L1268P were significantly higher than EV. **(C)** Clonogenic survival was assessed by colony formation assay at day 14. The numbers of colonies were counted after crystal violet staining, and are expressed as percentage of cells expressing empty vector. There is significance of colony formation in R1126H and L1268P when compared with empty vector. No obvious effects were observed on the colony formation ability of EEC-1 cells after transfection with WT and mutants K547E and R824X. Statistical significance was measured by Student's *t*-test (* $p < 0.05$), $n = 3$. Error bars represent average \pm SD.

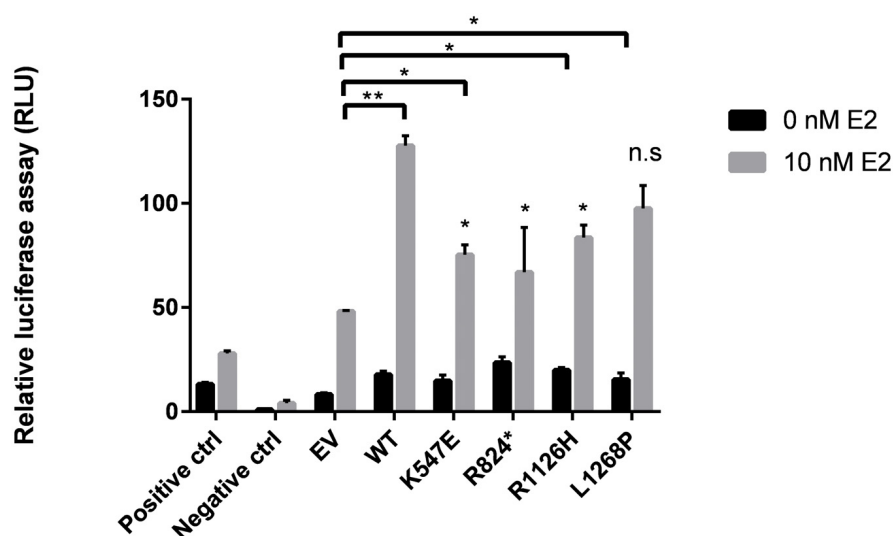


FIGURE 5 | Effects of *WHSC1* mutations on transcriptional activation of Estrogen Receptor Gene (*ERα*). WT *WHSC1* showed increase in ERE-mediated luciferase activity relative to EV. K547E, R824X, and R1126H were associated with reduced ability to activate ER activity, compared to WT. Whereas L1268P activated ER activity comparable to WT (n.s.). Data are presented as mean values \pm SD, $n = 2$.

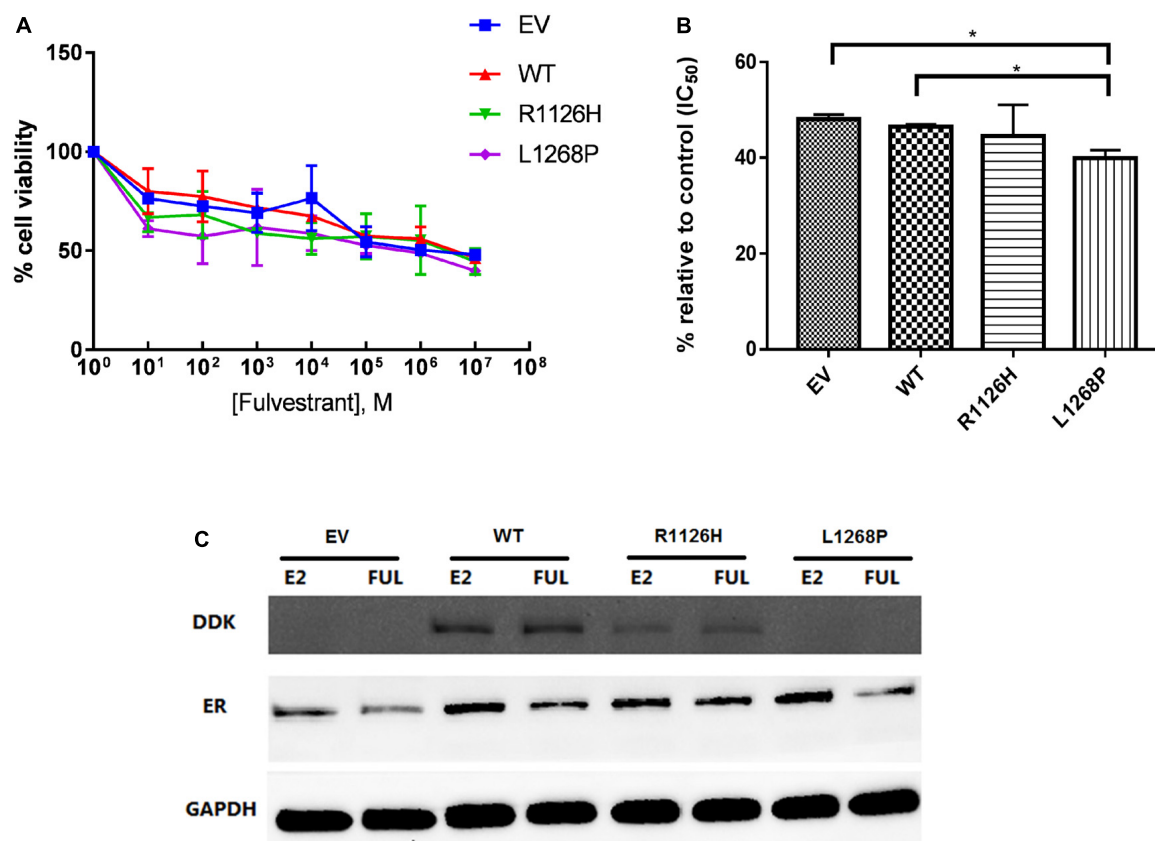


FIGURE 6 | Effect of Fulvestrant on cell proliferation in mutants *WHSC1* expressing EEC1 cells. **(A)** Treatment was performed with 10 nM E2 and various dosage of Fulvestrant for 24 h. **(B)** Quantification of proliferation after exposure to 10 nM E2 and 10⁻³ M Fulvestrant. The values represent the percentage of growing cells compared to the normalized control (100%). Results represent mean values \pm SD, $n = 2$ performed in triplicate. *WHSC1* mutants counteract the effect of ER inhibitor. **(C)** EEC-1 cells were transiently transfected with WT, R1126H, and L1268P mutant constructs and treated with 10 nM E2 or 100 nM of Fulvestrant for 24 h. Protein lysates were prepared and analyzed by Western Blot with indicated antibodies.

PTEN functions primarily as a lipid phosphatase via a dual specificity protein phosphatase dualistic domain (Maehama and Dixon, 1998). Remarkably, most reported mutations (R130, I122N, K128T) are clustered within the phosphatase signature motif between codon 122–132 that has been considered as the mutation hotspot site (Prasad et al., 2005; Bansal et al., 2009). In addition, mutations on the phosphatase binding loop D92E on this domain play critical roles as well (Giudice and Squarize, 2013). These mutants may abolish the phosphatase activity of the substrate phosphoinositide lipid, a key signaling component of PI3K pathway that regulate cell growth, proliferation, migration, and apoptosis (Fayard et al., 2010). In comparison, mutants located on C2 domain (P190L and F341V) could impair the phosphoinositide lipid binding function, ultimately its growth-suppressing activity despite retaining the catalytic phosphatase activity (Naguib et al., 2015). Other truncating mutations including nonsense and frameshift deletion (E7X, S59X, and R11fs) may result in functional inactivation of *PTEN* protein function, which leads to tumorigenesis (Xu et al., 2014). A number of *PTEN* missense mutations have been screened for its phosphatase activity which is important for its tumor suppression function, and majority of the mutants were shown to eliminate or reduce phosphatase activity (Han et al., 2000).

ARID1A mutations have been increasingly reported upon the emergence of NGS technology especially among various malignancies (Jones et al., 2012) including endometrial cancer (Liang et al., 2012). *ARID1A* is located on chromosome 1p36.11 and it contains 20 coding exons. The gene encodes a 24-kDa chromatin remodeling protein consisting of 2285 amino acids and a member of SWI/SNF family which plays a significant role in regulating the transcription of genes via ATP hydrolysis (Wilson and Roberts, 2011). Therefore, it is critical in regulating diverse cellular processes including DNA repair, differentiation, and development as well as tumor suppression (Lu and Allis, 2017). The *ARID1A* mutations identified in our study are consistent with others regardless of the type of cancers, where most were truncating mutations that would result in loss of function, supporting its tumor suppressor role (Guan et al., 2012; Chang et al., 2015). Both nonsense and frameshift mutants (R1335X, R1989X, S2269X, G324fs, and G2040fs) would result in loss of function *ARID1A* protein by nonsense-mediated mRNA decay and degradation of misfolded truncated proteins. Thus, its tumor suppression activity is abolished due to disruption in CDKN1A and SMAD3 pathway which is related to cell cycle regulation and aberrant activation of PI3K/AKT pathway (Bosse et al., 2013). Missense mutations occur less frequently in *ARID1A*; hence, the functional manifestations are poorly understood (Bateman et al., 2016). Our study showed that the mutations commonly occurred in the ER negative subtype group, suggesting that inactivation of *ARID1A* might play important role in ER-mediated transcription in endometrial cancer. Moreover, the SWI/SNF complex has been reported to be vital for the transcriptional activation of ER (Belandia et al., 2002). Mutation in *ARID1A* is not that frequent in breast cancer (only ~5%) (Jones et al., 2012) and there has been no reported association with ER status. However, low *ARID1A* expression has been found to associate with ER negativity of breast cancer (Zhang et al., 2012).

By focusing on genes involved in the ER signaling pathway, we identified relatively frequent mutations in *ERBB3*, *GNAS*, *PI3KR1*, and *WHSC1* in ER positive subtype. Previous data by TCGA reported that 5.2% (16/373) of EEC have *ERBB3* mutations (Cerami et al., 2012). This gene is located on 12q13.2 chromosome, consists of 28 exons, and encodes a protein composed of 1342 amino acids (Sithanandam and Anderson, 2008). *ERBB3* encodes a member of EGFR family receptor tyrosine kinase, which is a well-known gene to be amplified and overexpressed in various cancers (Olayioye et al., 2000). With emergence of NGS, more somatic mutations in *ERBB3* have gained attention. *ERBB3* has been uncovered as a driver cancer gene in endometrial cancer through whole exome sequencing and loss of function screening by Liang et al. (2012). Using whole exome sequencing, *ERBB3* mutations have been reported in colon, gastric, and gallbladder cancers (Jaiswal et al., 2013; Li et al., 2014). *ERBB3* comprises of extracellular ligand-binding domains (I–IV), a tyrosine kinase domain, and a regulatory domain (Olayioye et al., 2000). In concordance with previous studies, the majority of mutations detected in our patients are located in the extracellular domain (L143M, P558S, E560fs) of the gene which are predicted to induce conformational changes, dysregulate ligand binding, or heterodimerization of *ERBB3* with kinase-active *ERBB2* (Jaiswal et al., 2013). Distinct from other EGFR members, *ERBB3* has impaired tyrosine kinase activity; hence, it could be hypothesized that mutations mapped on this domain (L924V) could activate and stimulate protein tyrosine kinase (Jeong et al., 2006). These oncogenic mutations might promote tumorigenesis through aberrant activation of PI3K/AKT pathway, eliciting various biological responses including cell cycle progression, stimulation of cell migration, and invasion (Sithanandam and Anderson, 2008).

Perhaps the most promising gene from our study, based on mutation frequency and function, is *WHSC1*. It was more frequently mutated in the ER positive subtype. The *WHSC1* gene encodes a histone methyltransferase, is classified as chromatin modification group, and plays an important role in regulating gene transcription (Li et al., 2009). A previous study showed that *WHSC1* interacts with and regulate gene transcription activity of androgen receptors in prostate cancer (Kang et al., 2009) and ER in breast cancer (Feng et al., 2014), which provide a new basis for tumorigenesis in endocrine-related cancers. Hence, there is high possibility that *WHSC1* is involved in development of endometrial cancer. *WHSC1* is shown to be essential for ER α -dependent transcription induction in tamoxifen-resistant breast cancers, one of the potent coactivators in the ER pathway (Feng et al., 2014). They postulated that *WHSC1* is recruited to the ER promoter by the bromodomain protein (BRD4) and direct H3K36 methylation that is responsible for promoting transcription initiation and elongation. Moreover, genetic alterations in the transcriptional coregulators of ER genes are likely to be the key players in the development of estrogen-dependent tumors through deregulation in the estrogen signaling pathway (Girault et al., 2006), further supporting our hypothesis for *WHSC1* as the likely target gene in endometrial cancer.

WHSC1 (MMSET/NSD2) spans 120 kb, consists of 24 exons that encode a 1360 amino acid protein containing catalytic SET domain, and several chromatin-associated domains comprising a high mobility group (HMG) box which often representing a DNA-binding domain, two PWWP domains, five PHD zinc fingers defined as binding modules for methylated lysines, and C5HCH domain (Cys–His–Rich). Previous studies have almost exclusively focused on translocation and overexpression of *WHSC1* while mutations in this gene have not yet been extensively characterized (Jaffe et al., 2013), even though the occurrence in a variety of cancers is increasingly reported (Huether et al., 2014; García-Carpizo et al., 2016). Based on our analysis, *WHSC1* is frequently mutated in the ER positive subtype where four mutations (K574E, R1126H, R824X, and L1268P) were identified in three patients. We went on to study the role of these mutations in cell transformation by performing transient transfection in EEC-1 cell lines (endometrial cancer cell line expressing ER), followed by luciferase-based assay. Of the four mutations, we observed that only two *WHSC1* mutations (R1126H and L1268P) resulted in increased cell proliferation, increased ability of the cells to migrate, and survive in clonogenic growth which represents gain of function phenotype. Both mutants are likely to exhibit increased level of methyltransferase activity of H3K36, which is generally thought to drive tumorigenesis, through activation of key genes (Rao et al., 2005). We postulate that the mutant R1126H which is located in the histone binding groove on SET domain, which is in proximity to the established hotspot mutants E1099K and D1125N, lead to a hyperactive *WHSC1*, causing an increase in methyltransferases activity and hence progression of malignancies (Jaffe et al., 2013). Since the mutant R1126H exhibited independent ER pathway activation, it may be involved in endometrial carcinogenesis through other pathways. Endometrial cancer may also be triggered through the transcriptional regulation of *CCND1*, the target gene of the β -catenin/Tcf-4 complex, through H3K36 methylation and activation of the WNT signaling pathway (Toyokawa et al., 2011). This was supported by the discovery of recurrent R1126H mutants in colorectal cancer (**Supplementary Table S10**), where WNT signaling is the hallmark among the many genetic events. The other pathway that this mutation might be involved in is the RAS pathway by altering the oncogenic RAS transcriptional responses resulting in increased methyltransferase activity (García-Carpizo et al., 2016). However, there is still the need to elucidate which one is the key event since epigenetic alterations usually mediate the transcription of a plethora of genes (Huang et al., 2013).

Hormonal therapy and chemotherapy are frequently used for advanced endometrial cancer, and there is no approved molecular targeted therapy so far (Temkin and Fleming, 2009). However, in one clinical trial, the use of Fulvestrant has resulted in positive response in some patients with advanced or recurrent endometrial cancer (Emons et al., 2013). Fulvestrant is a selective ER downregulator (SERD) which competitively inhibits the binding of estradiol to the ER and it degrades ER via the ubiquitin-proteasome (Berry et al., 2008). Our study also provides evidence that Fulvestrant has the ability to induce ER degradation and that it inhibits the proliferation of the transforming mutant

L1268P cells, which is associated with increased sensitivity to this treatment. Hence, we propose that Fulvestrant the potential to inhibit the activity of ER signaling pathway in this particular mutant.

CONCLUSION

Using NGS, we have characterized the mutational landscape of different ER subtypes of EEC. We further demonstrated the role of the *WHSC1* L1268P mutation in endometrial cancer carcinogenesis by activating the ER signaling pathway and its pivotal role in promoting cell proliferation, migration, and survival. The ER signaling pathway activation by *WHSC1* LP1268H provides new evidence which is important for the future applications of targeted therapies for endometrial cancer carrying the *WHSC1* L1268P mutations. A major limitation of our study is the small sample size, therefore further studies are warranted to explore the diagnostic and therapeutic potential of our discovery.

ETHICS STATEMENT

This study was carried out in accordance with the recommendations of Guidelines for ethical review of clinical research or research involving human subjects. The protocol was approved by the Universiti Kebangsaan Malaysia Research Ethics Committee (UKM 1.5.3.5/244/AP-2012-011). All subjects gave written informed consent in accordance with the Declaration of Helsinki.

AUTHOR CONTRIBUTIONS

SSS performed the experiments and data analysis. N-SAM was involved in data interpretation, drafting the manuscript, and overseeing the experiments. SKS was heavily involved in data analysis. SES was involved in optimization of library preparation and sequencing. NA gave insight for the functional analyses. AMD is an endometrial surgeon involved in specimen collection and RMZ is a pathologist. RJ was involved in critical review of the manuscript. All authors read and approved the final manuscript.

FUNDING

This research was funded by a grant under the Projek Arus Perdana (UKM-AP-2012-011).

SUPPLEMENTARY MATERIAL

The Supplementary Material for this article can be found online at: <https://www.frontiersin.org/articles/10.3389/fphar.2018.00750/full#supplementary-material>

FIGURE S1 | Variant analysis and prioritization workflow. Summary of our variant evaluation process for identifying candidate mutations.

FIGURE S2 | Mutations distribution across exon and functional domain of (a) *PTEN*, (b) *ARID1A*, (c) *ERBB3*, and (d) *WHSC1*. Any position with a mutation obtains a circle; the length of the line depends on the number of mutations detected at that codon. The gray bar represents the entire protein with the different amino acid positions (aa). The colored boxes are specific functional domains. On top of the lollipops variants are annotated as the amino-acid change at that specific site. Blue letter indicates mutation occur in ER positive subtype while green letter indicate mutation occur in ER negative subtype of our analysis.

TABLE S1 | Ion Ampliseq™ comprehensive cancer panel.

TABLE S2 | Primer's sequence used for Sanger validation.

TABLE S3 | WHSC1 mutant primer for site-directed mutagenesis.

TABLE S4 | Somatic alterations among DNA repair gene in hypermutated patient sample.

TABLE S5 | Somatic alteration identified as driver mutations by Cancer Genome Interpreter.

TABLE S6 | Somatic alterations of ER positive subtypes in endometrioid endometrial cancer-related genes.

TABLE S7 | Somatic alteration of ER negative subtypes in endometrioid endometrial cancer-related genes.

TABLE S8 | Somatic alterations of ER positive subtype in genes relevant to estrogen signaling pathway.

TABLE S9 | Somatic alterations of ER negative subtype in genes relevant to estrogen signaling pathway.

TABLE S10 | Recurrent mutation site of WHSC1 in different cancers.

REFERENCES

- Amant, F., Moerman, P., Neven, P., Timmerman, D., Van Limbergen, E., and Vergote, I. (2005). Endometrial cancer. *Lancet* 366, 491–505. doi: 10.1016/S0140-6736(05)67063-8
- Backes, F. J., Walker, C. J., Goodfellow, P. J., Hade, E. M., Agarwal, G., Mutch, D., et al. (2016). Estrogen receptor- α as a predictive biomarker in endometrioid endometrial cancer. *Gynecol. Oncol.* 141, 312–317. doi: 10.1016/j.ygyno.2016.03.006
- Bansal, N., Yendluri, V., and Wenham, R. M. (2009). The molecular biology of endometrial cancers and the implications for pathogenesis, classification, and targeted therapies. *Cancer Control* 16, 8–13. doi: 10.1177/107327480901600102
- Bateman, N. W., Shoji, Y., Conrads, K. A., Stroop, K. D., Hamilton, C. A., Darcy, K. M., et al. (2016). Identification and functional characterization of a novel bipartite nuclear localization sequence in ARID1A. *Biochem. Biophys. Res. Commun.* 469, 114–119. doi: 10.1016/j.bbrc.2015.11.080
- Belandia, B., Orford, R. L., Hurst, H. C., and Parker, M. G. (2002). Targeting of SWI/SNF chromatin remodelling complexes to estrogen-responsive genes. *EMBO J.* 21, 4094–4103. doi: 10.1093/emboj/cdf412
- Berry, N. B., Fan, M., and Nephew, K. P. (2008). Estrogen receptor- α hinge-region lysines 302 and 303 regulate receptor degradation by the proteasome. *Mol. Endocrinol.* 22, 1535–1551. doi: 10.1210/me.2007-0449
- Bokhman, J. V. (1983). Two pathogenetic types of endometrial carcinoma. *Gynecol. Oncol.* 15, 10–17. doi: 10.1016/0090-8258(83)90111-7
- Bosse, T., Haar, N. T., Seiber, L. M., Diest, P. J., Hes, F. J., Vasen, H. F. A., et al. (2013). Loss of ARID1A expression and its relationship with PI3K-Akt pathway alterations, TP53 and microsatellite instability in endometrial cancer. *Mod. Pathol.* 26, 1525–1535. doi: 10.1038/modpathol.2013.96
- Carlson, M. J., Thiel, K. W., Yang, S., and Leslie, K. K. (2012). Catch it before it kills: progesterone, obesity, and the prevention of endometrial cancer. *Discov. Med.* 14, 215–222. doi: 10.1016/j.biotechadv.2011.08.021.Secretd
- Cerami, E., Gao, J., Dogrusoz, U., Gross, B. E., Sumer, S. O., Aksoy, B. A., et al. (2012). The cBio cancer genomics portal: an open platform for exploring multidimensional cancer genomics data. *Cancer Discov.* 2, 401–404. doi: 10.1158/2159-8290.CD-12-0095
- Chang, M. T., Asthana, S., Gao, S. P., Lee, B. H., Chapman, J. S., Kandath, C., et al. (2015). Identifying recurrent mutations in cancer reveals widespread lineage diversity and mutational specificity. *Nat. Biotechnol.* 34, 155–163. doi: 10.1038/nbt.3391
- Chang, Y. S., Huang, H., Da, Yeh, K. T., and Chang, J. G. (2017). Identification of novel mutations in endometrial cancer patients by whole-exome sequencing. *Int. J. Oncol.* 50, 1778–1784. doi: 10.3892/ijo.2017.3919
- Djordjevic, B., Hennessy, B. T., Li, J., Barkoh, B. A., Luthra, R., Mills, G. B., et al. (2012). Clinical assessment of PTEN loss in endometrial carcinoma: immunohistochemistry outperforms gene sequencing. *Mod. Pathol.* 25, 699–708. doi: 10.1038/modpathol.2011.208
- Doll, M., Abal, M., Monge, M., Gonzalez, S., Demajo, E., Colás, M., et al. (2008). Novel molecular profiles of endometrial cancer-new light through old windows. *J. Steroid Biochem. Mol. Biol.* 108, 221–229. doi: 10.1016/j.jsbmb.2007.09.020
- Duska, L. R., Garrett, A., Rueda, B. R., Haas, J., Chang, Y., and Fuller, A. F. (2001). Endometrial cancer in women 40 years old or younger. *Gynecol. Oncol.* 83, 388–393. doi: 10.1006/gyno.2001.6434
- Emons, G., Günthert, A., Thiel, F. C., Camara, O., Strauss, H. G., Breitbach, G. P., et al. (2013). Phase II study of fulvestrant 250 mg/month in patients with recurrent or metastatic endometrial cancer: a study of the Arbeitsgemeinschaft Gynäkologische Onkologie. *Gynecol. Oncol.* 129, 495–499. doi: 10.1016/j.ygyno.2013.02.039
- Fayard, E., Xue, G., Parcellier, A., Bozulic, L., and Hemmings, B. A. (2010). Protein kinase B (PKB/Akt), a key mediator of the PI3K signaling pathway. *Curr. Top. Microbiol. Immunol.* 346, 31–56. doi: 10.1007/82-2010-58
- Feng, Q., Zhang, Z., Shea, M. J., Creighton, C. J., Coarfa, C., Hilsenbeck, S. G., et al. (2014). An epigenomic approach to therapy for tamoxifen-resistant breast cancer. *Cell Res.* 24, 809–819. doi: 10.1038/cr.2014.71
- Ferlay, J., Soerjomataram, I., Dikshit, R., Eser, S., Mathers, C., Rebelo, M., et al. (2015). Cancer incidence and mortality worldwide: Sources, methods and major patterns in GLOBOCAN 2012. *Int. J. Cancer* 136, E359–E386. doi: 10.1002/ijc.29210
- Ferlay, J., Soerjomataram, I., Ervik, M., Dikshit, R., Eser, S., Mathers, C., et al. (2013). GLOBOCAN 2012 v1.0. *Cancer Incidence and Mortality Worldwide: IARC CancerBase. No. 11 [Internet]*. Available at: <http://globocan.iarc.fr>
- Forbes, S. A., Beare, D., Boutselakis, H., Bamford, S., Bindal, N., Tate, J., et al. (2017). COSMIC: Somatic cancer genetics at high-resolution. *Nucleic Acids Res.* 45, D777–D783. doi: 10.1093/nar/gkw1121
- Gao, J., Aksoy, B. A., Dogrusoz, U., Dresdner, G., Gross, B., Sumer, S. O., et al. (2013). Integrative analysis of complex cancer genomics and clinical profiles using the cBioPortal. *Sci. Signal.* 6:p11. doi: 10.1126/scisignal.2004088
- García-Carpizo, V., Sarmentero, J., Han, B., Graña, O., Ruiz-Llorente, S., Pisano, D. G., et al. (2016). NSD2 contributes to oncogenic RAS-driven transcription in lung cancer cells through long-range epigenetic activation. *Sci. Rep.* 6:32952. doi: 10.1038/srep32952
- Garg, K., and Soslow, R. A. (2014). Endometrial carcinoma in women aged 40 years and younger. *Arch. Pathol. Lab. Med.* 138, 335–342. doi: 10.5858/arpa.2012-0654-RA
- Girault, I., Bièche, I., and Lidereau, R. (2006). Role of estrogen receptor α transcriptional coregulators in tamoxifen resistance in breast cancer. *Maturitas* 54, 342–351. doi: 10.1016/j.maturitas.2006.06.003
- Giudice, F. S., and Squarize, C. H. (2013). The determinants of head and neck cancer: unmasking the PI3K pathway mutations. *J. Carcinog. Mutagen. Suppl* 5, 432–435. doi: 10.4172/2157-2518.S5-003
- Guan, B., Gao, M., Wu, C.-H., Wang, T.-L., and Shih, I.-M. (2012). Functional analysis of In-frame Indel ARID1A mutations reveals new regulatory mechanisms of its tumor suppressor functions. *Neoplasia* 14, 986–993. doi: 10.1593/neo.121218
- Han, S. Y., Kato, H., Kato, S., Suzuki, T., Shibata, H., Ishii, S., et al. (2000). Functional evaluation of PTEN missense mutations using in vitro phosphoinositide phosphatase assay. *Cancer Res.* 60, 3147–3151.
- Huang, Z., Wu, H., Chuai, S., Xu, F., Yan, F., Englund, N., et al. (2013). NSD2 Is recruited through Its PHD domain to oncogenic gene loci to drive multiple

- myeloma. *Cancer Res.* 73, 6277–6288. doi: 10.1158/0008-5472.CAN-13-1000
- Huether, R., Dong, L., Chen, X., Wu, G., Parker, M., Wei, L., et al. (2014). The landscape of somatic mutations in epigenetic regulators across 1,000 pediatric cancer genomes. *Nat. Commun.* 5:3630.
- Jaffe, J. D., Wang, Y., Chan, H. M., Zhang, J., Huether, R., Kryukov, G. V., et al. (2013). Global chromatin profiling reveals NSD2 mutations in pediatric acute lymphoblastic leukemia. *Nat. Genet.* 45, 1386–1393. doi: 10.1038/ng.2777
- Jaiswal, B. S., Kljavin, N. M., Stawiski, E. W., Chan, E., Parikh, C., Durinck, S., et al. (2013). Oncogenic ERBB3 mutations in human cancers. *Cancer Cell* 23, 603–617. doi: 10.1016/j.ccr.2013.04.012
- Jeong, E. G., Soung, Y. H., Woo, L. J., Hak, L. S., Woo, N. S., Lee, J. Y., et al. (2006). ERBB3 kinase domain mutations are rare in lung, breast and colon carcinomas. *Int. J. Cancer* 119, 2986–2987. doi: 10.1002/ijc.22257
- Jones, S., Li, M., Williams Parsons, D., Zhang, X., Wesseling, J., Kristel, P., et al. (2012). Somatic mutations in the chromatin remodeling gene ARID1A occur in several tumor types. *Hum. Mutat.* 33, 100–103. doi: 10.1002/humu.21633
- Kanehisa, M., Sato, Y., Kawashima, M., Furumichi, M., and Tanabe, M. (2016). KEGG as a reference resource for gene and protein annotation. *Nucleic Acids Res.* 44, D457–D462. doi: 10.1093/nar/gkv1070
- Kang, H. B., Choi, Y., Lee, J. M., Choi, K. C., Kim, H. C., Yoo, J. Y., et al. (2009). The histone methyltransferase, NSD2, enhances androgen receptor-mediated transcription. *FEBS Lett.* 583, 1880–1886. doi: 10.1016/j.febslet.2009.05.038
- Kuhn, E., Wu, R. C., Guan, B., Wu, G., Zhang, J., Wang, Y., et al. (2012). Identification of molecular pathway aberrations in uterine serous carcinoma by genome-wide analyses. *J. Natl. Cancer Inst.* 104, 1503–1513. doi: 10.1093/jnci/djs345
- Lax, S. F., Kendall, B., Tashiro, H., Slebos, R. J., and Hedrick, L. (2000). The frequency of p53, K- mutations, and microsatellite instability differs in uterine ras evidence endometrioid and serous carcinoma of distinct molecular genetic pathways. *Cancer* 88, 814–824. doi: 10.1002/(SICI)1097-0142(20000215)88:4<814::AID-CNCR12>3.0.CO;2-U
- Le Gallo, M., O'Hara, A. J., Rudd, M. L., Urlick, M. E., Hansen, N. F., O'Neil, N. J., et al. (2012). Exome sequencing of serous endometrial tumors identifies recurrent somatic mutations in chromatin-remodeling and ubiquitin ligase complex genes. *Nat. Genet.* 44, 1310–1315. doi: 10.1038/ng.2455
- Li, J. (1997). PTEN, a putative protein tyrosine phosphatase gene mutated in human brain, breast, and prostate cancer. *Science* 275, 1943–1947. doi: 10.1126/science.275.5308.1943
- Li, M., Zhang, Z., Li, X., Ye, J., Wu, X., Tan, Z., et al. (2014). Whole-exome and targeted gene sequencing of gallbladder carcinoma identifies recurrent mutations in the ErbB pathway. *Nat. Genet.* 46, 872–876. doi: 10.1038/ng.3030
- Li, Y., Trojer, P., Xu, C. F., Cheung, P., Kuo, A., Drury, W. J., et al. (2009). The target of the NSD family of histone lysine methyltransferases depends on the nature of the substrate. *J. Biol. Chem.* 284, 34283–34295. doi: 10.1074/jbc.M109.034462
- Liang, H., Cheung, L. W. T., Li, J., Ju, Z., Yu, S., Stemke-Hale, K., et al. (2012). Whole-exome sequencing combined with functional genomics reveals novel candidate driver cancer genes in endometrial cancer. *Genome Res.* 22, 2120–2129. doi: 10.1101/gr.137596.112
- Livak, K. J., and Schmittgen, T. D. (2001). Analysis of relative gene expression data using real-time quantitative PCR and the 2^{-ΔΔCT} method. *Methods* 25, 402–408. doi: 10.1006/meth.2001.1262
- Lu, C., and Allis, C. D. (2017). SWI/SNF complex in cancer. *Nat. Genet.* 49, 178–179. doi: 10.1038/ng.3779
- Maehama, T., and Dixon, J. E. (1998). The tumor suppressor, PTEN/ MMAC1, dephosphorylates the lipid second messenger, phosphatidylinositol 3,4,5-trisphosphate. *J. Biol. Chem.* 273, 13375–13379. doi: 10.1074/jbc.273.22.13375
- Maniketh, I., Ravikumar, G., Crasta, J. A., Prabhu, R., and Vallikad, E. (2014). Estrogen and progesterone receptor expression in endometrioid endometrial carcinomas: a clinicopathological study. *Middle East J. Cancer* 5, 67–73.
- Morice, P., Leary, A., Creutzberg, C., Abu-Rustum, N., and Darai, E. (2016). Endometrial cancer. *Gynecol. Obstet. Fertil.* 44, 239–243. doi: 10.1016/S0140-6736(15)00130-0
- Nadji, M., Gomez-Fernandez, C., Ganjei-Azar, P., and Morales, A. R. (2005). Immunohistochemistry of estrogen and progesterone receptors reconsidered: experience with 5,993 breast cancers. *Am. J. Clin. Pathol.* 123, 21–27. doi: 10.1309/4WV7-9N2G-HJ3X-1841
- Naguib, A., Bencze, G., Cho, H., Zheng, W., Tocilj, A., Elkayam, E., et al. (2015). PTEN functions by recruitment to cytoplasmic vesicles. *Mol. Cell* 58, 255–268. doi: 10.1016/j.molcel.2015.03.011
- O'Hara, A. J., and Bell, D. W. (2012). The genomics and genetics of endometrial cancer. *Adv. Genomics Genet.* 2012, 33–47. doi: 10.2147/AGG.S28953
- Olayioye, M. A., Neve, R. M., Lane, H. A., and Hynes, N. E. (2000). The ErbB signaling network: receptor heterodimerization in development and cancer. *EMBO J.* 19, 3159–3167. doi: 10.1093/emboj/19.13.3159
- Pecorelli, S. (2009). FIGO committee on gynecology oncology revised FIGO staging for carcinoma of the vulva, cervix, and endometrium. *Int. J. Gynecol. Obstet.* 105, 103–104. doi: 10.1016/j.ijgo.2009.02.012
- Prasad, M., Wang, H., Douglas, W., Barakat, R. R., and Ellenson, L. H. (2005). Molecular genetic characterization of tamoxifen-associated endometrial cancer. *Gynecol. Oncol.* 96, 25–31. doi: 10.1016/j.ygyno.2004.08.046
- Prat, J., Gallardo, A., Cuatrecasas, M., and Catasús, L. (2007). Endometrial carcinoma: pathology and genetics. *Pathology* 39, 72–87. doi: 10.1080/00313020601136153
- Rao, B., Shibata, Y., Strahl, B. D., and Lieb, J. D. (2005). Dimethylation of histone H3 at Lysine 36 demarcates regulatory and nonregulatory chromatin genome-wide. *Mol. Cell Biol.* 25, 9447–9459. doi: 10.1128/MCB.25.21.9447-9459.2005
- Sithanandam, G., and Anderson, L. M. (2008). The ERBB3 receptor in cancer and cancer gene therapy. *Cancer Gene Ther.* 15, 413–448. doi: 10.1038/cgt.2008.15
- Talhok, A., and McAlpine, J. N. (2016). New classification of endometrial cancers: the development and potential applications of genomic-based classification in research and clinical care. *Gynecol. Oncol. Res. Pract.* 3:14. doi: 10.1186/s40661-016-0035-4
- Tamborero, D., Rubio-Perez, C., Deu-Pons, J., Schroeder, M. P., Vivancos, A., Rovira, A., et al. (2018). Cancer genome interpreter annotates the biological and clinical relevance of tumor alterations. *Genome Med.* 10:25. doi: 10.1186/s13073-018-0531-8
- Temkin, S. M., and Fleming, G. (2009). Current treatment of metastatic endometrial cancer. *Cancer Control* 16, 38–45. doi: 10.1177/107327480901600106
- The Cancer Genome Atlas Network (2012). Comprehensive molecular portraits of human breast tumours. *Nature* 490, 61–70. doi: 10.1038/nature11412
- The Cancer Genome Atlas Research Network, Kandoth, C., Schultz, N., Cherniack, A. D., Akbani, R., Liu, Y., et al. (2013). Integrated genomic characterization of endometrial carcinoma. *Nature* 497, 67–73. doi: 10.1038/nature12113
- Thorvaldsdóttir, H., Robinson, J. T., and Mesirov, J. P. (2013). Integrative Genomics Viewer (IGV): high-performance genomics data visualization and exploration. *Brief. Bioinform.* 14, 178–192. doi: 10.1093/bib/bbs017
- Toyokawa, G., Cho, H. S., Masuda, K., Yamane, Y., Yoshimatsu, M., Hayami, S., et al. (2011). Histone lysine methyltransferase Wolf-hirschhorn syndrome candidate 1 is involved in human carcinogenesis through regulation of the Wnt pathway. *Neoplasia* 13, 887–898. doi: 10.1593/neo.11048
- Van Allen, E. M., Wagle, N., and Levy, M. A. (2013). Clinical analysis and interpretation of cancer genome data. *J. Clin. Oncol.* 31, 1825–1833. doi: 10.1200/JCO.2013.48.7215
- Wang, K., Li, M., and Hakonarson, H. (2010). ANNOVAR: functional annotation of genetic variants from high-throughput sequencing data. *Nucleic Acids Res.* 38:e164. doi: 10.1093/nar/gkq603
- Wilson, B. G., and Roberts, C. W. M. (2011). SWI/SNF nucleosome remodellers and cancer. *Nat. Rev. Cancer* 11, 481–492. doi: 10.1038/nrc3068
- Xu, J., Li, Z., Wang, J., Chen, H., and Fang, J. Y. (2014). Combined PTEN mutation and protein expression associate with overall and disease-free survival of glioblastoma patients. *Transl. Oncol.* 7, 196–205. doi: 10.1016/j.tranon.2014.02.004
- Zannoni, G. F., Monterossi, G., De Stefano, I., Gargini, A., Salerno, M. G., Farulla, I., et al. (2013). The expression ratios of estrogen receptor alpha

- (ERalpha) to estrogen receptor beta1 (ERbeta1) and ERalpha to ERbeta2 identify poor clinical outcome in endometrioid endometrial cancer. *Hum. Pathol.* 44, 1047–1054. doi: 10.1016/j.humpath.2012.09.007
- Zhang, J., Baran, J., Cros, A., Guberman, J. M., Haider, S., Hsu, J., et al. (2011). International cancer genome consortium data portal-a one-stop shop for cancer genomics data. *Database* 2011:bar026. doi: 10.1093/database/bar026
- Zhang, X., Zhang, Y., Yang, Y., Niu, M., Sun, S., Ji, H., et al. (2012). Frequent low expression of chromatin remodeling gene ARID1A in breast cancer and its clinical significance. *Cancer Epidemiol.* 36, 288–293. doi: 10.1016/j.canep.2011.07.006

Conflict of Interest Statement: The authors declare that the research was conducted in the absence of any commercial or financial relationships that could be construed as a potential conflict of interest.

Copyright © 2018 Suhaimi, Ab Mutalib, Khor, Md Zain, Syafruddin, Abu, Mohd Dali and Jamal. This is an open-access article distributed under the terms of the Creative Commons Attribution License (CC BY). The use, distribution or reproduction in other forums is permitted, provided the original author(s) and the copyright owner(s) are credited and that the original publication in this journal is cited, in accordance with accepted academic practice. No use, distribution or reproduction is permitted which does not comply with these terms.



UBE2C Is a Potential Biomarker of Intestinal-Type Gastric Cancer With Chromosomal Instability

Jun Zhang^{1†}, Xinyu Liu^{1†}, Guanzhen Yu^{2,3†}, Lei Liu¹, Jiejun Wang², Xiaoyu Chen⁴, Yuhai Bian⁴, Yuan Ji⁵, Xiaoyan Zhou⁶, Yinan Chen¹, Jun Ji¹, Zhen Xiang¹, Lei Guo¹, Jingyuan Fang⁴, Yihong Sun⁵, Hui Cao⁴, Zhenggang Zhu^{1*} and Yingyan Yu^{1*}

¹ Department of Surgery, Ruijin Hospital, Shanghai Key Laboratory for Gastric Neoplasms, Shanghai Institute of Digestive Surgery, Shanghai Jiao Tong University School of Medicine, Shanghai, China, ² Changzheng Hospital, Affiliated to Second Military Medical University, Shanghai, China, ³ Department of Oncology, Longhua Hospital of Shanghai University of Traditional Chinese Medicine, Shanghai, China, ⁴ Renji Hospital, Affiliated to Shanghai Jiao Tong University School of Medicine, Shanghai, China, ⁵ Zhongshan Hospital, Affiliated to Fudan University, School of Medicine, Shanghai, China, ⁶ Cancer Hospital, Affiliated to Fudan University School of Medicine, Shanghai, China

OPEN ACCESS

Edited by:

Dong-Hua Yang,
St. John's University, United States

Reviewed by:

Ru Wen,
Stanford University, United States
Yan Chang,
University of Texas at Arlington,
United States

*Correspondence:

Zhenggang Zhu
zzg1954@hotmail.com
Yingyan Yu
yingyan3y@sjtu.edu.cn

[†]These authors have contributed
equally to this work.

Specialty section:

This article was submitted to
Experimental Pharmacology and Drug
Discovery,
a section of the journal
Frontiers in Pharmacology

Received: 10 May 2018

Accepted: 13 July 2018

Published: 02 August 2018

Citation:

Zhang J, Liu X, Yu G, Liu L, Wang J, Chen X, Bian Y, Ji Y, Zhou X, Chen Y, Ji J, Xiang Z, Guo L, Fang J, Sun Y, Cao H, Zhu Z and Yu Y (2018) UBE2C Is a Potential Biomarker of Intestinal-Type Gastric Cancer With Chromosomal Instability. *Front. Pharmacol.* 9:847. doi: 10.3389/fphar.2018.00847

This study explored potential biomarkers associated with Lauren classification of gastric cancer. We screened microarray datasets on gastric cancer with information of Lauren classification in gene expression omnibus (GEO) database, and compared differentially expressing genes between intestinal-type or diffuse-type gastric cancer. Four sets of microarray data (GSE2669, GSE2680, GDS3438, and GDS4007) were enrolled into analysis. By differential gene analysis, UBE2C, CDH1, CENPF, ERO1L, SCD, SOX9, CKS1B, SPP1, MMP11, and ANLN were identified as the top genes related to intestinal-type gastric cancer, and MGP, FXD1, FAT4, SIPA1L2, MUC5AC, MMP15, RAB23, FBLN1, ANXA10, and ADH1B were genes related to diffuse-type gastric cancer. We comprehensively validated the biological functions of the intestinal-type gastric cancer related gene UBE2C and evaluated its clinical significance on 1,868 cases of gastric cancer tissues from multiple medical centers of Shanghai, China. The gain of copy number on 20q was found in 4 out of 5 intestinal-type cancer cell lines, and no similar copy number variation (CNV) was found in any diffuse-type cancer cell line. Interfering UBE2C expression inhibited cell proliferation, migration and invasion *in vitro*, and tumorigenesis *in vivo*. Knockdown of UBE2C resulted in G2/M blockage in intestinal-type gastric cancer cells. Overexpression of UBE2C activated ERK signal pathway and promoted cancer cell proliferation. U0126, an inhibitor of ERK signaling pathway reversed the oncogenic phenotypes caused by UBE2C. Moreover, overexpression of UBE2C was identified in human intestinal-type gastric cancer. Overexpression of UBE2C protein predicted poor clinical outcome. Taken together, we characterized a group of Lauren classification-associated biomarkers, and clarified biological functions of UBE2C, an intestinal-type gastric cancer associated gene. Overexpression of UBE2C resulted in chromosomal instability that disturbed cell cycle and led to poor prognosis of intestinal-type gastric cancer.

Keywords: gastric cancer, Lauren classification, data mining, biomarkers, UBE2C

INTRODUCTION

Gastric cancer is one of the most common digestive malignancies, which threatens public health worldwide, especially in Asia (Torre et al., 2015). Lauren classification is a standard histopathological classification which divides gastric cancer into two subtypes: intestinal-type and diffuse-type (Lauren, 1965). This histological classification was established based on histological observation by a Nordic pathologist half a century ago when there was no evidence at molecular level. Multiple reports including our previous study had demonstrated that there are different biological behaviors between intestinal-type and diffuse-type gastric cancers (Liu et al., 2013; Qiu et al., 2013; Chen et al., 2016). However, there is no systematic study on biomarkers that associated with Lauren classification in gastric cancer.

With the application of high-throughput gene analysis, many gene expression profiles of gastric cancer have been accumulated and deposited in open accessible database. DNA microarray or gene chip is the first one of the high-throughput technologies applied on molecular classification for cancers (Tusher et al., 2001). HER2/Neu positive breast cancer was successfully identified according to microarray analysis (Slamon and Pegram, 2001; van 't Veer et al., 2002). Utilization of high-throughput technologies also promoted changing gastric cancer research from histologic level to molecular level (Ji et al., 2002; Kim et al., 2003). Currently, a number of datasets come from separated institutes and there is no comparable analysis.

In this study, microarray datasets of gastric cancer deposited in NCBI database were extracted, and microarray data with clear Lauren classification information were enrolled into data mining. We found a set of Lauren classification-associated differential genes. UBE2C is one of the genes that highly expressed in intestinal-type gastric cancer. We validated the expression of UBE2C on a separated cohort of gastric cancer from Shanghai, China. To clarify the underlying molecular mechanisms of UBE2C, we explored the variation of UBE2C gene copy number in gastric cancer cells originated from intestinal-type or diffuse-type gastric cancers. We further analyzed biological function and related signaling pathway of UBE2C gene both *in vitro* and *in vivo*. This study established a link between up-regulation of UBE2C with chromosome instability and disturbed ERK signaling pathway in intestinal-type gastric cancer.

MATERIALS AND METHODS

DNA Microarray Data Analysis

We searched gene expression omnibus (GEO) database of NCBI (<http://www.ncbi.nlm.nih.gov/geo/>) using keywords of "Gastric Cancer," "Gastric Carcinoma" or "Stomach cancer," and obtained four sets of microarray datasets (GEO serial numbers: GSE2669, GSE2680, GSE3438, and GSE4007) that included detail information of Lauren classification. Significance Analysis of Microarray (SAM) was used for differential genes selection of intestinal-type gastric cancer and diffuse-type gastric cancer through an open-accessible tool, MultiExperiment Viewer (MEV) which supported by Stanford University (Tusher et al., 2001; Saeed et al., 2003). By adjusting permutation,

false discovery rate (FDR) and delta value, we obtained sets of differential genes between intestinal-type gastric cancer and normal mucosa, diffuse-type gastric cancer and normal mucosa, as well as differential genes between intestinal-type and diffuse-type gastric cancers.

Tissue Microarray Construction and Immunohistochemistry

This study was approved by the institutional review board of hospital, and a written informed consent was obtained from the participants of this study. A total of 1,868 cases of gastric cancer were included in this study. All cancer tissues came from gastrectomy in the following 4 medical centers of Ruijin hospital, Renji hospital, Zhongshan hospital, and Changzheng hospital, Shanghai, China from 2002 to 2015. Including criteria were: patients with histological slides and paraffin blocks. Excluding criteria were: patients who have stump gastric cancer, neoadjuvant chemotherapy, incomplete information, multiple lesions, and combined with other malignancies. Finally, 109 cases were excluded and only 1,759 cases were included in the final analysis. Among them, 1,224 cases (69.6%) were male, and 535 (30.4%) cases were female. The median age was 61-year old (22–88 year-old). All samples were fixed in neutral buffered formalin and embedded in paraffin. Patients were followed up every 6 months for the first 3 years and annually after 3 years. The last followed up was December 30, 2015, with the longest follow-up time of 142 months. The average follow-up time was 48.73 months. Tumor stage was determined based on the 7th edition of TNM staging system by AJCC/UICC organizations.

Tissue microarray blocks were constructed from these 1,759 cases using a tissue microarrayer (Beecher Instruments, Silver Spring, MD, USA). Two tissue cores (2 mm diameter) from each cancer or normal mucosa block were taken and transferred to a recipient paraffin block. Subsequently, 4-mm-thick sections were cut from each tissue microarray block, de-waxed, and dehydrated.

A standard peroxidase-conjugated streptavidin-biotin method was used for immunohistochemical staining with UBE2C (mouse-anti human UBE2C monoclonal antibody, 1:50, SC-100611, Santa Cruz, SC-100611, USA). The immunohistochemical staining results were evaluated by two independent pathologists and scored according to the percentage of positive cells and staining intensity. The graded percentage of positive cells 0 (<10%), 1 (10–30%), 2 (31–50%), and 3 (51–100%) was recorded. The staining intensity was graded as 0 (negative), 1 (weak), 2 (moderate), and 3 (strong). A cumulative score ranging from 0 to 9 was obtained by multiplying the staining intensity and percentage. The total score graded as weakly positive (scores <3) and moderately or strongly positive (scores ≥4).

Analysis of Chromosomal Copy Number in Gastric Cancer Cells

The global copy number variation (CNV) of chromosomes was analyzed in 6 different cancer cell lines: SGC-7901, BGC-823, MKN-45, MKN-28, AGS, and HTB-103 by Affymetrix®

Genome-Wide Human SNP Array 6.0 chip. The peripheral blood samples from 2 healthy individuals were used as controls. The information of gain or loss of copy number of each sample was analyzed by Genotyping Console software, which was calculated based on comparison of Hapmap project.

Cell Culture

Cancer cells were seeded in 6-well plates (3.0×10^5 cells) and cultured in RPMI-1640 medium with 10% fetal bovine serum (Gibco, Invitrogen, USA) in 5% CO₂ cell culture incubator at 37°C. Transfection of siRNAs or eukaryotic expression vectors was carried out using Lipofectamine 2000 (Invitrogen, Carlsbad, CA) according to protocol provided with the product. The cells were harvested 3–5 days following transfection.

Western Blot

The protein concentration was determined using a BCA Kit (Pierce Biotechnology, Rockford, IL, USA). Each protein extract (100 µg) was electrophoresed on a 12.5% SDS-polyacrylamide gel, transferred to PVDF membranes in a buffer containing 25 mM Tris-HCl (pH 8.3), 192 mM glycine and 20% (v/v) methanol, and blocked in 5% (w/v) skimmed milk in Tris buffered saline-Tween 20 (0.1% by volume, TBST) for 2 h at room temperature, and probed with specific primary antibodies overnight at 4°C. Blots were reacted with secondary antibodies coupled to horseradish peroxidase in TBST. The primary antibodies were mouse anti-UBE2C (1:1,000; Cat. AM1831a, ABGENT, San Diego, CA, USA), anti-ERK (Cat. 4695S, Cell Signaling Biotechnology), p-ERK (1:1,000; Cat. 9284, Cell Signaling Biotechnology) and mouse anti-glyceraldehyde-3-phosphate dehydrogenase (1:5,000, Sigma) antibody. The horseradish peroxidase-conjugated secondary antibodies were goat anti-rabbit IgG (1:2,000; Cat. 7,074, Cell Signaling Biotechnology) or horse anti-mouse IgG (1:2,000; Cat. 7,074, Cell Signaling Biotechnology). Signals were detected by a SuperSignal West Pico Chemiluminescent Substrate kit (Pierce, Rockford, IL, USA) according to the manufacturer's instructions.

Cell Proliferation Assay

CCK8 assay was performed to assess the effect of UBE2C on cell proliferation. Cells were transfected with siRNAs or UBE2C overexpressing vector for approximately 12 h. Following transfection, cells were transferred to 96-well microplates and seeded at a density of approximately 1.0×10^3 cells per well. Then each batch of cells were stained with 10 µl of CCK8 reagent (Dojindo, Kumamoto, Japan) at 37°C for 2 h every 24 h for 4 days. The coloring reaction was quantified by an automatic plate reader (Tecan, Swiss) at 450 nm. All experiments were performed in triplicate.

For clonogenicity assay, cells were transfected with siRNAs or UBE2C overexpressing vector for approximately 12 h. Following transfection, cells were transferred into 6-well plates and seeded at a density of approximately 1.0×10^3 cells per well. Culture medium was changed every 3 days. Clonogenicity was analyzed 12 days following transfection by staining cells with 0.05% crystal violet solution for 1 h. Visible colonies were manually counted.

A group of cells >50 was counted as a colony. The data were reported as means \pm SD by counting 10 fields randomly.

Cell Migration and Invasion

For migration and invasion assays, cell culture was performed in 24-well Transwell chambers (Corning, USA). For the invasion assay, the insert membranes were coated with diluted Matrigel (BD Biosciences, USA). Cells (1×10^5) were added to the upper chamber and cultured for 48 h. For the migration assay, cells were cultured under the same conditions except that the insert membranes were not coated with Matrigel. Finally, the insert membranes were cut and stained with 0.1% crystal violet for 2 min. The penetrating cells were counted under an inverted microscope and photographed in five random fields and the average number of cells per field was counted. These experiments were performed in triplicate.

Construction of shRNA and shUBE2C Plasmids

The full-length cDNA of UBE2C (NM_000690.3) was purchased (GENECHEM, Shanghai, China). The full-length cDNA of human UBE2C was cloned and inserted into pBABE-puro vector (Clontech Laboratories, Mountain View, CA, USA). Two pairs of complementary short hairpin RNA (shRNA) expression vectors targeting UBE2C (UBE2C-shRNA1 and UBE2C-shRNA2) and a pair of scrambled negative control shRNA oligonucleotides were constructed using RNAi-Ready pSIREN-RetroQ vector (Clontech Laboratories). The retroviral packaging process was performed in a plate of 293T cells. After 12 h, 15 mL viral collection medium was added into the transfected cells. Infection of BGC-823 or SGC-7901 cancer cells was performed in the presence of 5 µg/mL of polybrene (Sigma, MO, USA) in each well of a 6-well plate. Stable retroviral transduction was achieved by infection for 48 h and followed by puromycin (1 µg/mL) selection.

Assay of ERK Signaling Pathway

The ERK1/2 inhibitor U0126 was purchased from Selleckchem (Cat. 9903S). The final concentration of U0126 used in culture medium was 10 µmol/L. Cells were harvested for protein extraction and Western blotting analysis.

Tumorigenesis of UBE2C in Nude Mice

Cancer cells ($1 \times 10^6/100$ µl) transfected with UBE2C or sh-UBE2C were collected and inoculated subcutaneously into 4-week-old BALB/c nude mice (Institute of Zoology, Chinese Academy of Sciences, Shanghai). Each experimental and control groups consisted of four mice. Tumor nodules were measured every 4 days with a caliper. Mice were sacrificed after 1 month. Tumor growth curves and inhibiting rates were calculated. After tumor excision, the tissues were fixed in 10% buffered formalin. All formalin-fixed and paraffin-embedded samples were carefully examined after staining with hematoxylin-eosin (HE) and photographed. The animal experiment was approved by the Institutional Animal Care and Use Committee of Shanghai Jiao Tong University School of Medicine.

TABLE 1 | The details of four microarray datasets from GEO database.

GEO ID	Controls	Case No.	Samples	Submitter
GSE2669	Mixture of normal samples	124	64 cancer 26 gastritis 22 metaplasia 10 normal 2 other	Boussioutas A, National Cancer Centre of Singapore
GSE2680	Mixture of normal samples	90	68 intestinal- 13 diffuse- 9 mixed-	Aggarwa A, National Cancer Centre of Singapore
GSE3438	Exchange of marked staining reagents	100	50 cancer 50 normal	Kim S, Korea Research Institute of Bioscience and Biotechnology
GSE4007	Mixture of normal samples	126	90 cancer 22 normal 14 lymph node	Chen X, Stanford University

Statistical Analysis

Statistical analysis was performed using SPSS 17.0 statistical software (SPSS Inc., Chicago, IL, USA.). Associations between expression of UBE2C and clinicopathological variables were analyzed using the Chi square test. The continuous variables were expressed as mean values \pm standard deviation. The differences between groups were analyzed using the Student's *t*-test when there were only two groups, or assessed by one-way ANOVA when there were more than two groups. Two-way ANOVA was used for the analysis of multiple comparisons. Cox regression method was used to analyze multivariate survival. Kaplan-Meier method and Log-Rank test were used to analyze non-parametric survival. A *P*-value of <0.05 was considered statistically significant.

RESULTS

Data Mining Revealed Genes Related to Lauren Classification

By searching GEO database, datasets GSE2669, GSE2680, GSE3438, and GSE4007 were selected because they contain large sample size with detail clinical information including Lauren classification of gastric cancer (Table 1). We extracted differential expression genes between intestinal-type vs. control or diffuse-type vs. control by SAM method. The permutation value was set at 1,000 and FDR $<5\%$ on 1.5-fold-change. A total of 263 feature genes were characterized. Among them, 40 genes were highly expressed in intestinal-type gastric cancer, and 223 genes were highly expressed in diffuse-type gastric cancer. We listed the top 10 genes with >1.5 -fold-change in two types of gastric cancers (Table 2).

Up-Regulation of UBE2C Related to Amplification of Chromosomal Copy Number

Gastric cancer cell lines SGC-7901, BGC-823, MKN-45, MKN-28, HTB-103, and AGS were used to analyze chromosomal CNV.

Four out of 5 intestinal-type gastric cancer cell lines BGC-823, MKN-45, MKN-28, and AGS revealed amplification of chromosome 20q which contains the gene locus of UBE2C. No 20q amplification was observed in diffuse-type gastric cancer cell line HTB-103 (Figure 1).

Interfering or Enforcing UBE2C Expression Affected Cell Growth and Invasion

Two intestinal-type gastric cancer cell lines, BGC-823 which has high expression of UBE2C and SGC-7901 which has low expression of UBE2C, were used to investigate the function of UBE2C on cell growth and invasion. The expression of UBE2C was monitored by qRT-PCR and Western blot. Cell proliferation was determined by CCK-8 assay and colony formation. The migration and invasion of cancer cells were determined by transwell assay. The UBE2C knockdown using si01 and si02 sequences achieved over 50% down-regulation of UBE2C. UBE2C-si02 was used for subsequent experiments because it down-regulated UBE2C expression by up to $57.24 \pm 7.54\%$ (Figure 2A). The siRNA was transfected into BGC-823 cells, and the light absorbance of 0, 24, 48, 72, and 96 h at 450 nm wavelength was determined. Compared to the siNC, the light absorbance of 72 and 96 h of siUBE2C was 0.62 ± 0.08 vs. 1.15 ± 0.14 ($P = 0.001$) and 0.88 ± 0.16 vs. 1.96 ± 0.19 ($P = 0.001$; Figure 2B). As for colony formation assay, colony numbers were evaluated at the 21st day after siUBE2C transfection. The colony numbers were significantly reduced in siUBE2C group, compared to siNC group (85 ± 12 vs. 219 ± 12 , $P = 0.001$; Figure 2B). These results indicated that down-regulation of UBE2C inhibited cancer cell growth *in vitro*.

To examine the effect of UBE2C on cell migration and invasion abilities, transwell chambers were used. Migrated cells were counted after 48 h transfection of siUBE2C. The number of migrated cells decreased in siUBE2C group compared with the siNC group (71 ± 7 vs. 160 ± 16 , $P = 0.004$; Figure 2C, upper panel). Similarly, the number of invasive cells decreased in siUBE2C group compared with the siNC group (21 ± 4 vs. 116 ± 7 , $P = 0.001$, Figure 2C).

We reversely verified the functions of UBE2C by enforcing UBE2C expression in gastric cancer cells. The transfection efficacy of UBE2C eukaryotic expression vector was confirmed at 48 h after UBE2C transfection in SGC-7901 cells by Western blot. Compared to control, transfection of UBE2C increased protein level of UBE2C by 3.72 ± 0.75 -folds (Figure 2D, $P = 0.025$). CCK-8 assay was used to examine cell proliferation. The 450 nm absorbance at 72 and 96 h for UBE2C and control group was 1.66 ± 0.22 vs. 1.07 ± 0.17 and 2.66 ± 0.29 vs. 1.56 ± 0.22 (Figure 2E), respectively. The ability of colony formation was evaluated in the UBE2C transfected and control cells after 21 days of UBE2C transfection. The colony numbers were significantly increased in UBE2C group, compared to the control group (106 ± 16 vs. 71 ± 11 , $P = 0.043$, Figure 2E). These results supported that up-regulation of UBE2C promoted cell growth of cancer cells *in vitro*.

In addition, we analyzed the ability of cell migration and invasion at 48 h after enforcing UBE2C expression. There were

TABLE 2 | The top 10 related genes in intestinal- or diffuse-type gastric cancer.

Gene symbol	Gene names	Chromosome loci
INTESTINAL-TYPE		
UBE2C	Ubiquitin-conjugating enzyme E2C	20q13.12
CDH1	Cadherin 1, type 1, E-cadherin (epithelial)	16q22.1
ERO1L	ERO1-like (<i>S. cerevisiae</i>)	14q22.1
SCD	Stearoyl-CoA desaturase (delta-9-desaturase)	10q24.31
SOX9	SRX (sex determining region Y)-box 9	17q24.3-q25.1
CKS1B	CDC28 protein kinase regulatory subunit 1A pseudogene	8q21.13
SPP1	Osteopontin	4q21-q25
MMP11	Matrix metalloproteinase 11 (stromelysin 3)	22q11.2 22q11.23
CENPF	Centromere protein F, 350/400 ka (mitosin)	1q32-q41
ANLN	Anillin, actin binding protein	7p15-p14
DIFFUSE-TYPE		
FAT4	FAT tumor suppressor homolog 4 (<i>Drosophila</i>)	4q28.1
SIPA1L2	Signal-induced proliferation-associated 1 like 2	1q42.2
RAB23	RAB23, member RAS oncogene family	6p11
FBLN1	Fibulin 1	22q13.31
ADH1B	Alcohol dehydrogenase 1B (class I), beta polypeptide	4q21-q23
ANXA10	Annexin A10	4q33
MGP	Matrix Gla protein	12p13.1-p12.3
MUC5AC	Mucin 5AC, oligomeric mucus/gel-forming	11p15.5
FXD1	FXD domain containing ion transport regulator 1	19q13.1
MMP15	Matrix metalloproteinase 15 (membrane-inserted)	16q13-q21

increased migrated cells and increased invasive cells in the UBE2C group compared with control group (342 ± 18 vs. 204 ± 25 , $P = 0.002$; **Figure 2F**, upper panels) and (218 ± 16 vs. 103 ± 17 , $P = 0.001$), (**Figure 2F**, lower panels). These results further confirmed that overexpression of UBE2C promoted invasive ability of gastric cancer cells *in vitro*.

Down-Regulation of UBE2C Caused Cell Cycle Arrest and Inhibited ERK1/2 Signaling Pathway

Cell cycle was analyzed by synchronize cells using dual blockage of thymidine for 16 h. Flow cytometry analysis found that the G2/M fraction of BGC-823/shUBE2C group was significantly higher than those in control group (25.79 ± 0.72 vs. $0.03 \pm 0.02\%$, $P = 0.001$), while the G1 fraction (74.39 ± 0.72 vs. $80.59 \pm 2.32\%$, $P = 0.034$) and S fraction (0.01 ± 0.01 vs. $19.37 \pm 2.32\%$, $P = 0.005$) were less than those in controls (**Figure 3A**). This result suggested that about one-fourth of the cells was blocked in G2/M phase by down-regulation of UBE2C in gastric cancer cells.

The phosphorylation of extracellular signal-regulated kinase1/2 (ERK1/2) was analyzed by Western blotting. The results revealed that UBE2C silencing down-regulated the phosphorylation of the ERK1/2 in BGC-823 cancer cells, while UBE2C overexpression up-regulated phosphorylation of the ERK1/2 in SGC-7901 cancer cells (**Figure 3B**). Additionally, the ERK1/2 inhibitor U0126 was used to confirm the signaling pathway involved in UBE2C-mediated cancer progression. ERK1/2 inhibitor U0126 ($10 \mu\text{mol/L}$) decreased the phosphorylation of the ERK1/2 caused by UBE2C overexpressing

SGC7901 cells. The ratio of phosphorylated ERK1/2 to ERK1/2 was 0.55 ± 0.03 vs. 0.92 ± 0.01 , $P = 0.001$ (**Figure 3C**). On the contrary, the ratio of phosphorylated ERK1/2 to ERK1/2 increased, compared with control by UBE2C overexpression in SGC-7901 cells (0.95 ± 0.02 vs. 0.51 ± 0.02 , $P = 0.001$).

ERK1/2 inhibitor U0126 ($10 \mu\text{mol/L}$) was added in culture medium and CCK-8 assay was used to examine cell proliferation. We found that the 450 nm absorbance decreased at 72 h (0.69 ± 0.14 vs. 1.61 ± 0.19 , $P = 0.003$) and 96 h (0.82 ± 0.16 vs. 2.6 ± 0.32 , $P = 0.003$) in UBE2C-U0126 group compared to UBE2C-DMSO group, respectively. This result suggested that reduced ERK1/2 phosphorylation could reverse cell proliferation induced by UBE2C.

We analyzed the ability of cell migration and invasion at 48 h after SGC-7901 cancer cells were incubated with U0126. Compared with control group, the migrated cells in UBE2C-U0126 group were significantly less than those in UBE2C-DMSO group (286 ± 17.52 vs. 84.33 ± 17.24 , $P = 0.001$; **Figure 3D**, upper panel), while the invasive cells was also less in UBE2C-U0126 group than that in UBE2C-DMSO group (136.67 ± 12.5 vs. 51.67 ± 9.61 , $P = 0.001$, **Figure 3D**, lower panel). These results confirmed that reduced ERK1/2 phosphorylation could reverse cell invasive ability *in vitro*.

Intervening UBE2C Affected Tumorigenesis *in Vivo*

Short hairpin RNA (shUBE2C) expression vectors were constructed to silence UBE2C. Lentiviral vector was used to infect BGC-823 cells and the transfection efficacy reached 100%

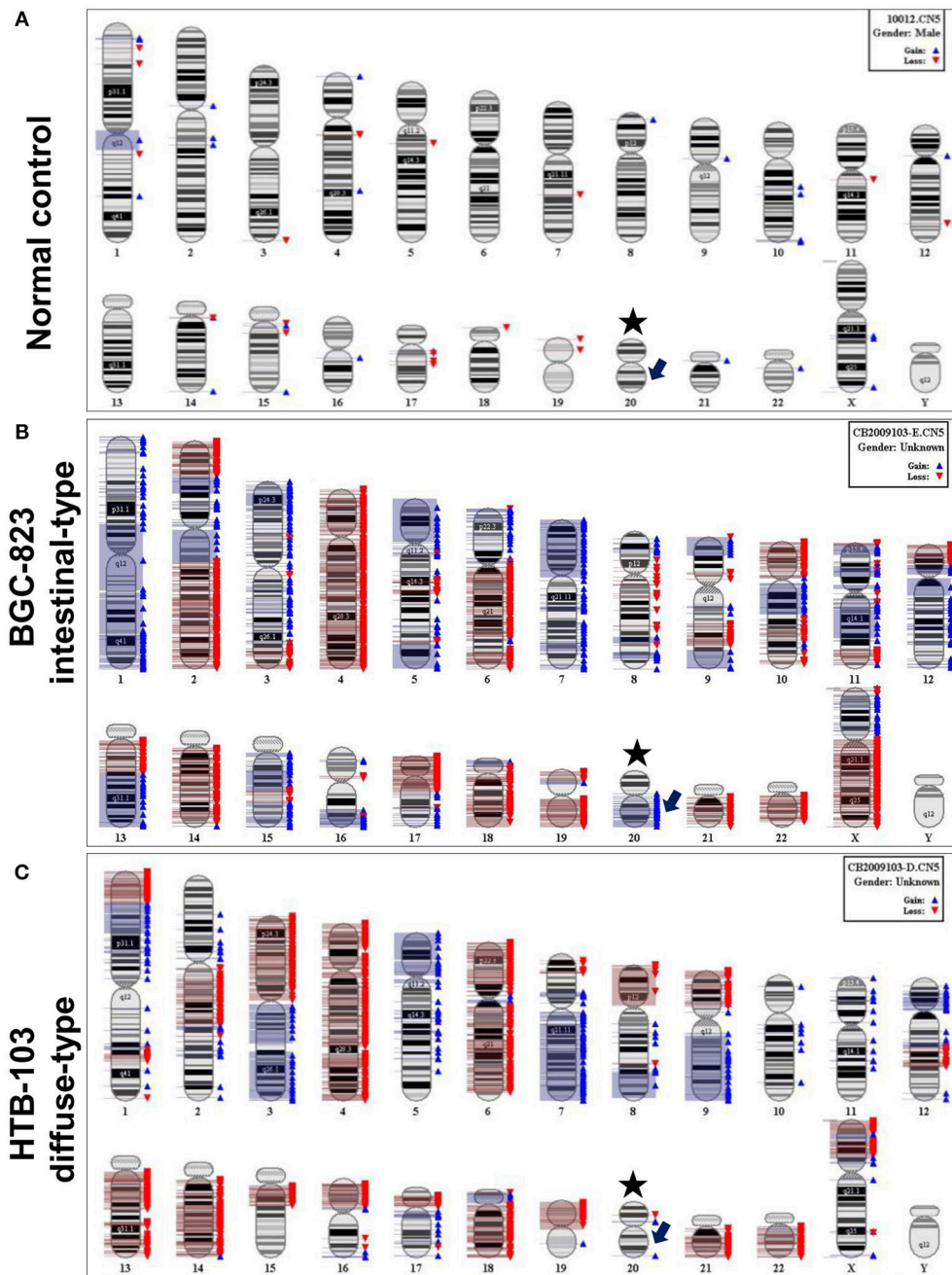


FIGURE 1 | Representative chromosomal CNV features by SNP 6.0 microarray analysis. **(A)** Normal control from healthy peripheral blood. Asterisk indicates chromosome 20, and arrow indicates gene locus of UBE2C. **(B)** CNV feature of intestinal-type gastric cancer cell line BGC-823. The blue bar on the right of chromosome represents copy number amplification, and red bar means copy number loss. The arrow indicates copy number amplification in gene locus of UBE2C. **(C)** CNV feature of diffuse-type gastric cancer cell line HTB-103. There is no copy number amplification in gene locus of UBE2C.

observed under a fluorescence microscope. The expression of UBE2C was monitored by Western blot analysis. Compared with control group, the UBE2C expression in Lv-shUBE2C cells declined $77.00 \pm 8.81\%$ ($P = 0.004$; **Figure 4A**). The effect of UBE2C in tumorigenesis was evaluated in BALB/c nude mice. BGC-823/Lv-shUBE2C cells ($1.5 \times$

10^6) and control cells were inoculated subcutaneously ($n = 4$). The tumor volumes were measured every week. Mice were sacrificed at the 35th day of tumor formation. It was found that the tumor volume was smaller in BGC-823/Lv-shUBE2C group compared with the BGC-823/Lv-shNC group. Under microscope, tumor cells were reduced in

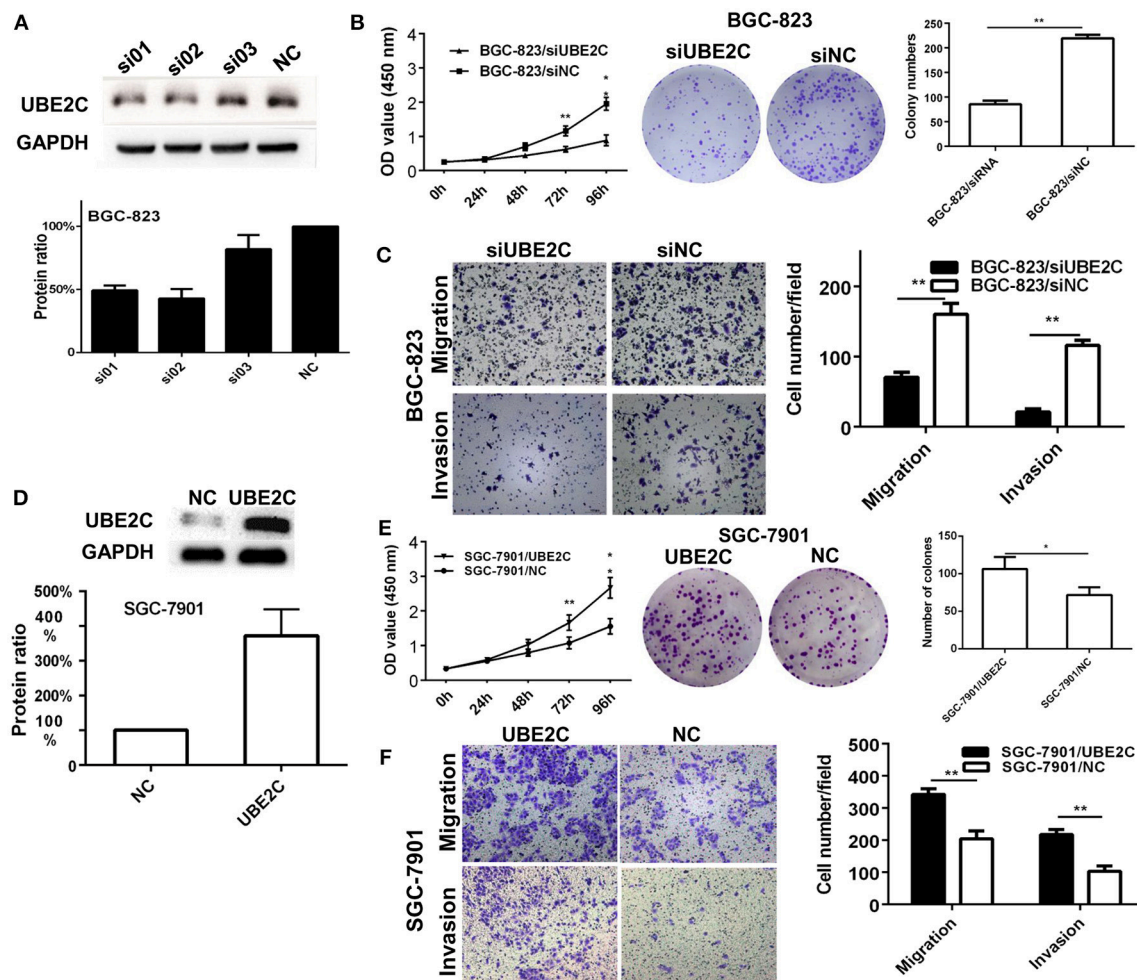


FIGURE 2 | Interfering or enforcing UBE2C expression affected cancer cell proliferation and invasion. **(A)** Protein level of UBE2C detected after siRNA transfection in BGC-823 cells. Among three siRNA sequences, si02 showed the best knockdown efficacy. **(B)** Knockdown of UBE2C decreased cell growth and colony formation in BGC-823 cells. **(C)** Knockdown of UBE2C decreased migration and invasion of BGC-823 cells. **(D)** Protein level of UBE2C detected after enforcing UBE2C expression in SGC-7901 cells. **(E)** Overexpression of UBE2C increased cell growth and colony formation in SGC-7901 cells. **(F)** Overexpression of UBE2C increased migration (upper) and invasion (lower) of SGC-7901 cells. Experiments were performed in triplicates. * $p < 0.05$; ** $p < 0.01$.

experimental group, compared to control (Figure 4B), while both tumor volume (2136.99 ± 827.98 vs. 4304.33 ± 958.75 mm³, $P = 0.015$) and tumor weight (1.8 ± 0.18 vs. 3.6 ± 1.07 g, $P = 0.04$) of BGC-823/Lv-shUBE2C group were decreased compared to those in BGC-823/Lv-shNC group (Figures 4C,D).

In addition, lentiviral vector of UBE2C was used to infect SGC-7901 cells which inoculated to nude mice ($n = 4$) subcutaneously. The tumor volumes were measured every week. Mice were sacrificed at the 35th day. Compared with the SGC-7901/Lv-NC group, the tumor volume was larger in SGC-7901/Lv-UBE2C group (2096.85 ± 944.66 vs. 3986.48 ± 1306.44 mm³, $P = 0.033$), while the tumor weight of SGC-7901/Lv-UBE2C group was heavier than that in SGC-7901/Lv-NC group (3.9 ± 0.62 vs. 2.7 ± 0.52 g, $P = 0.026$, data not shown).

Up-Regulation of UBE2C Expression in Gastric Cancer Was Validated in a Clinical Cohort

The protein expression of UBE2C was examined on tissue microarrays from a large cohort of gastric cancer by immunohistochemistry. The microarray set included 1,759 cases of cancer tissues and 1,710 cases were enrolled into final analysis because 49 cases was dropped during staining process. UBE2C was negative or weakly positive in normal gastric mucosa, while increased UBE2C expression was seen in gastric cancer, especially the intestinal-type gastric cancer (Figure 5A). The total staining score was higher in gastric cancer than that in normal mucosa (2.735 ± 2.709 vs. 0.743 ± 1.288 , $P = 0.001$, Figure 5B) by semi-quantitative analysis. The staining score of intestinal-type gastric cancer was significantly higher than that of diffuse-type gastric cancer (3.241 ± 2.839 vs. $1.951 \pm$

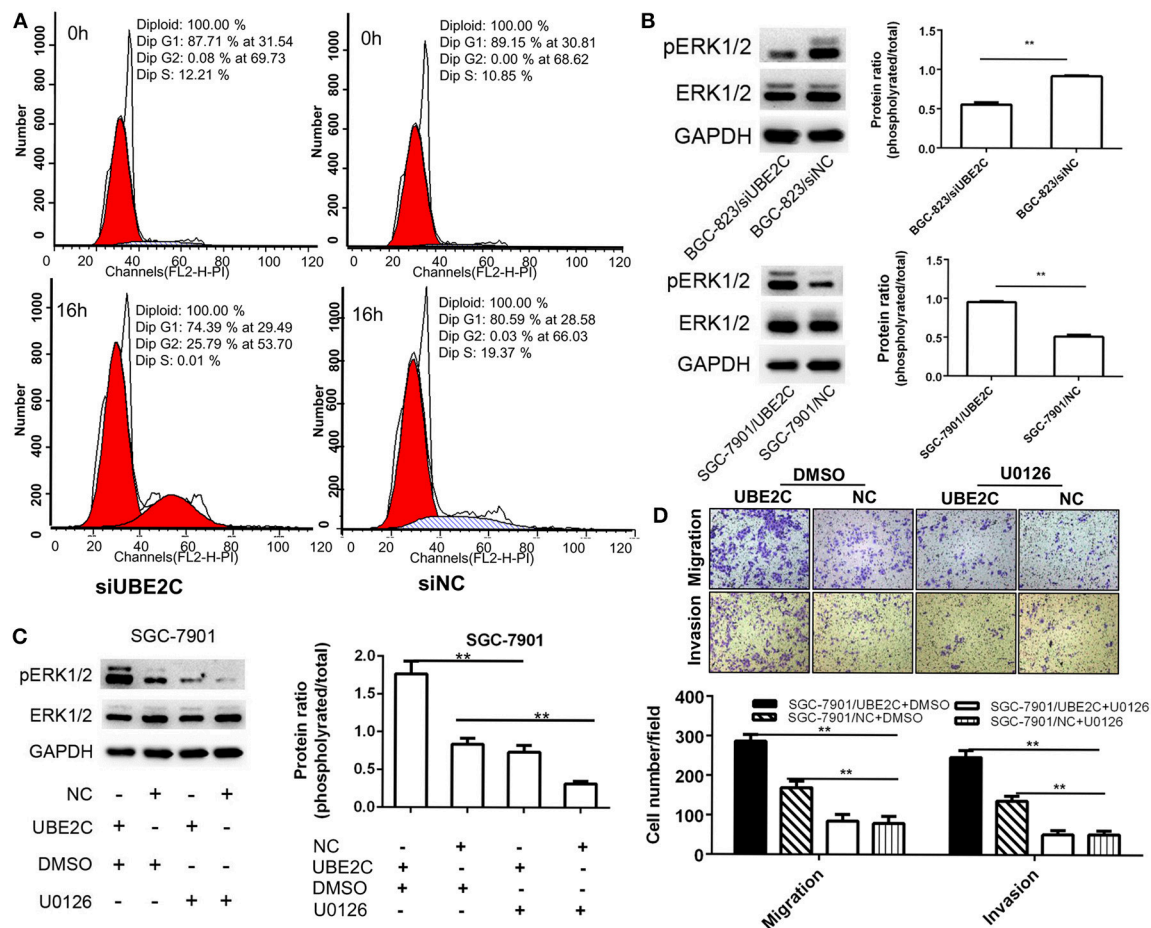


FIGURE 3 | Cell cycle and ERK1/2 signaling pathway affected by interfering or enforcing UBE2C expression. **(A)** Cell cycle detected after release of thymidine blockage at 0 and 16 h. The percentage of cells in G₂/M phase was significantly higher (25.79%) in siUBE2C group than that in siNC group (0.03%). **(B)** Knockdown of UBE2C decreased ERK1/2 phosphorylation and overexpression of UBE2C promoted ERK1/2 phosphorylation. **(C)** U0126 reversed phosphorylated ERK1/2 level caused by UBE2C overexpression. **(D)** Migration (upper) and invasion (lower) inhibited by U0126 treatment in SGC-7901 cells. Experiments were performed in triplicates. ** $p < 0.01$.

2.409, $P = 0.001$, **Figure 5C**). The diagnostic value of UBE2C expression was evaluated by ROC curve analysis. The overall AUC was 0.711 (CI: 0.693–0.730, **Figure 5D**). The AUC of intestinal-type of gastric cancer was 0.755 (CI: 0.734–0.776, **Figure 5D**), and AUC for diffuse-type of gastric cancer was 0.676 (CI: 0.647–0.704, **Figure 5D**). It suggested that UBE2C could be a potential biomarker for intestinal-type gastric cancer.

Among 1,710 cases of gastric cancer, 1,417 cases were used for survival analysis after a long-term follow-up. We divided cases into UBE2C-high group (staining score ≥ 4) and UBE2C-low group (staining score ≤ 3). There was no significant difference of overall survival between these two groups ($P = 0.361$, **Figure 6A**). However, when we separately analyzed intestinal-type and diffuse-type gastric cancer, the overall survival was significantly different between the two groups. In intestinal-type cancer, the UBE2C-high expression correlated with shorter survival than that in UBE2C-low expression group ($P = 0.037$, **Figure 6B**). In diffuse-type gastric cancer, the overall survival was slightly shortened in UBE2C-high group compared with

the UBE2C-low expression group, but there was no statistical significance ($P = 0.07$, **Figure 6C**). These results indicated that UBE2C could be an oncogene related to intestinal-type gastric cancer.

DISCUSSION

Molecular classification of cancers has been achieved based on clusters of differential expressed genes using high through-put technologies. UBE2C is one of the genes used in molecular classification in several types of cancers. Studies revealed that overexpression of UBE2C is related to some kinds of solid tumors, such as stomach cancer (Zhang H. Q. et al., 2018), colorectal cancer (Cacciola et al., 2016; Zhang Y. et al., 2018), esophageal cancer (Matsumoto et al., 2014; Li et al., 2018), pancreatic cancer (Zhao et al., 2013), breast cancer (Mo et al., 2017; Qin et al., 2017), ovarian cancer (Martínez-Canales et al., 2018), hepatocellular cancer (Ieta et al., 2007), lung cancer (Tang

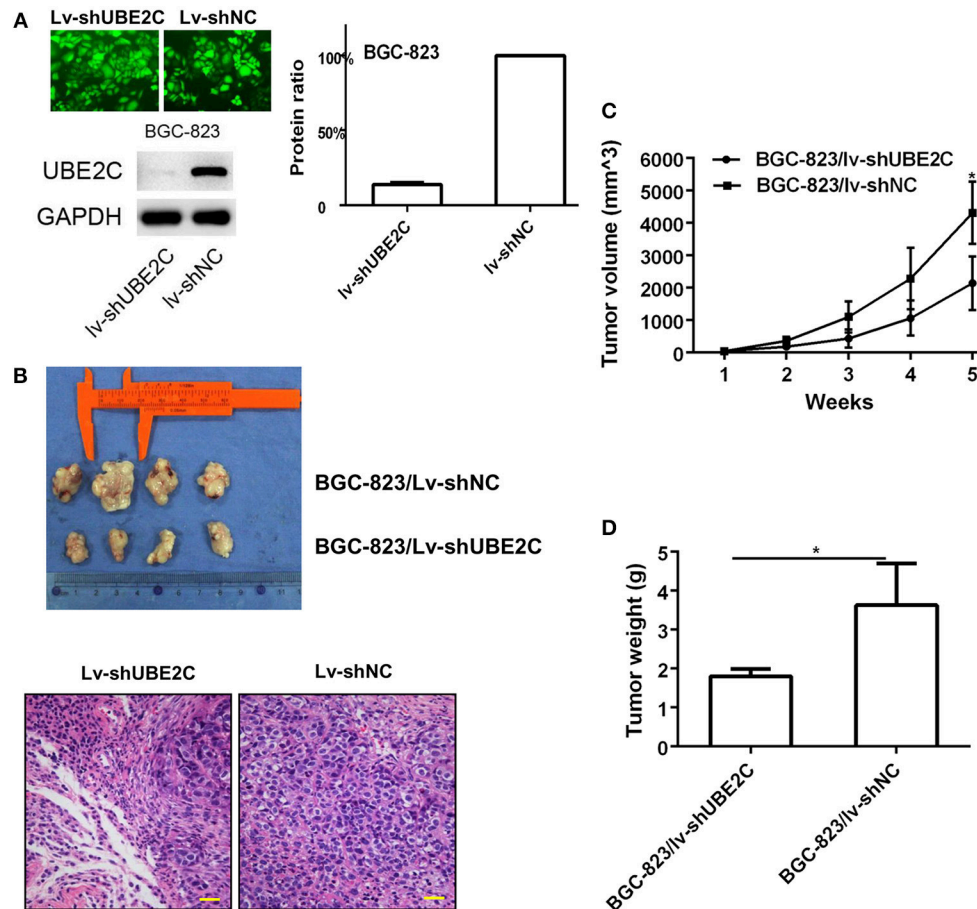


FIGURE 4 | Effect of UBE2C in *in vivo* tumorigenesis. **(A)** Fluorescent images of stably transfected BGC-823 cells (200 ×). All cells were transfected. Knockdown of Lv-shUBE2C was documented by Western blot analysis. **(B)** Knockdown of UBE2C inhibited tumorigenesis in nude mice at day 35 after tumor cell inoculation. The tumor volumes were obviously larger in experimental group than that in control group (upper). Under microscope, tumor cells were reduced in experimental group, compared to control (down). Scale bar indicates 25 μ m. **(C)** Tumor volume curves of xenografts in different groups of BGC-823 cancer cells. **(D)** Tumor weight of xenografts in different groups of BGC-823 cancer cells. * $p < 0.05$.

et al., 2014; Zhang et al., 2015), prostate cancer (Shuliang et al., 2013), and other cancers (Wagner et al., 2004; Shen et al., 2013; Kraft et al., 2017). Therefore, UBE2C has been considered as an important functional gene in cancer development.

Lauren classification has been used over half a century. This classification was proposed by a Nordic pathologist based on microscopic observation (Lauren, 1965). Since there were no supporting technologies such as immunohistochemistry, molecular biology and gene sequencing, Lauren classification was a pure experience-based cancer classification. With the development of novel technologies, especially high-throughput methods, molecular classification has become possible. However, global genomic study is high-cost and there is always a limited case number in a single study. The experimental error was inevitable in studies from small sample size. In high-throughput community, submitting data was required for international file sharing. In this case, a large number of research data were uploaded in public database. Data mining of cancer-related data in public database could greatly reduce the cost

and neutralize experimental error. Currently, huge amount of data were accumulated in GEO database of NCBI website and ArrayExpress database of EBI website (Barrett and Edgar, 2006; Parkinson et al., 2007). In this study, we focused on expressing profiles of microarray dataset of gastric cancer containing Lauren classification information, and found a set of Lauren classification-related genes. UBE2C is the gene we found that highly expressed in intestinal-type gastric cancer.

UBE2C gene is located on chromosome 20q13.12, which encodes one of the ubiquitin-binding enzyme families. Ubiquitin-binding enzymes are essential for activation of ubiquitin and binding to substrate proteins. UBE2C is a member of the anaphase promoting complex/cyclosome, and facilitates the degradation of target proteins with cell cycle progression (Nicolau-Neto et al., 2018). Therefore, UBE2C is an important regulatory factor of cell cycle. The imbalance of UBE2C expression could promote CIN and accumulated CNV of eukaryotic cells (van Ree et al., 2010; Heng et al., 2013; Sansregret et al., 2017).

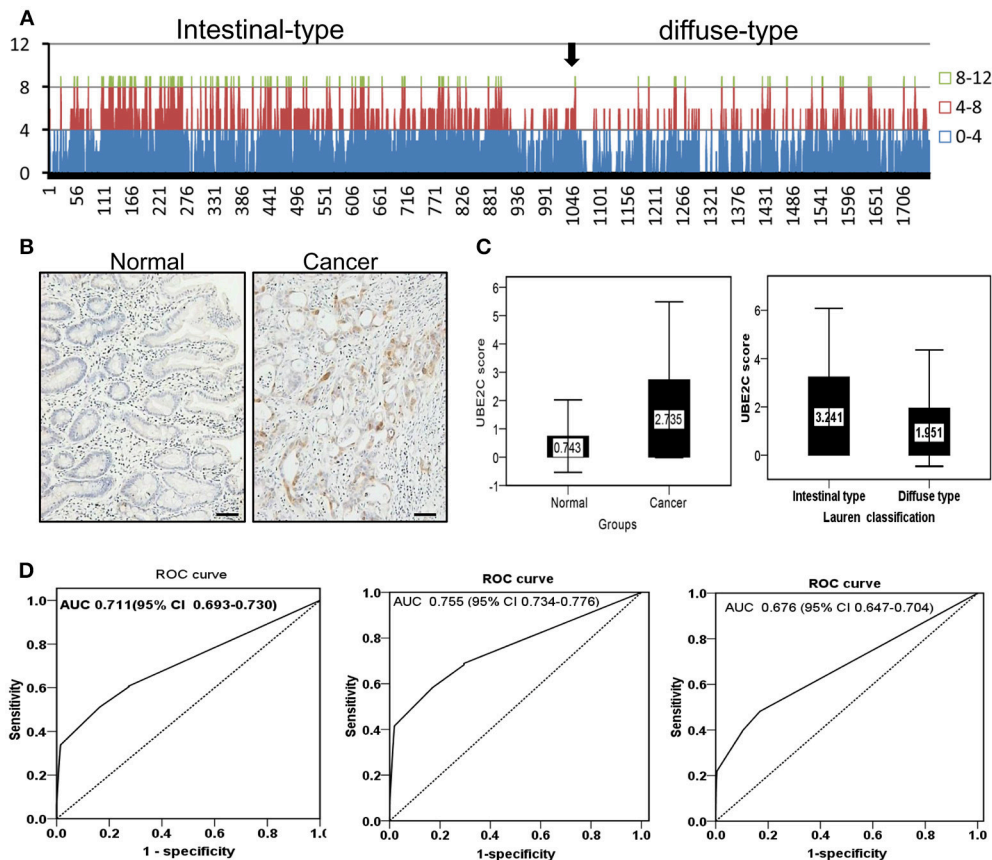


FIGURE 5 | Protein expression and diagnostic value of UBE2C analyzed in a large cohort of gastric cancer. **(A)** Overall tendency of UBE2C expression in gastric cancer. Arrow indicates the borderline between intestinal-type and diffuse-type gastric cancer. The staining score ≥ 4 is dominantly observed in intestinal-type gastric cancer. **(B)** Immunohistochemistry. UBE2C protein is expressed in cytoplasm of intestinal-type gastric cancer, but negative in the corresponding normal mucosa. Scale bar indicates 25 μm . **(C)** The staining score of UBE2C is higher in gastric cancer tissues than in normal mucosa (left); the staining score of UBE2C is higher in intestinal-type gastric cancer than that in diffuse-type gastric cancer (right). **(D)** ROC curve of UBE2C in all gastric cancers (AUC = 0.711, left), in intestinal-type gastric cancer (AUC = 0.755, middle), and in diffuse-type gastric cancer (AUC = 0.676, right).

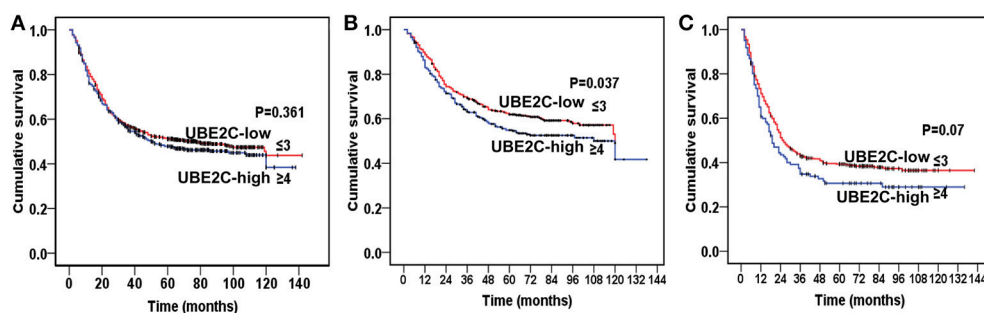


FIGURE 6 | Kaplan-Meier analysis on prognostic significance of UBE2C expression. **(A)** All gastric cancers. There is no significant difference between UBE2C-high and UBE2C-low groups. **(B)** Intestinal-type gastric cancer by Lauren classification. The overall survival is significantly shorter in UBE2C-high expression group than that of UBE2C-low group. **(C)** Diffuse-type gastric cancer. The overall survival of UBE2C-high expression group is shorter than that in UBE2C-low expression group.

In 2014, TCGA group reported a comprehensive molecular evaluation of 295 gastric cancers. They divided gastric cancer into four subtypes: tumors positive for Epstein-Barr virus, microsatellite unstable tumors, genomically stable tumors,

and tumors with CIN. The latter shows marked aneuploidy and focal amplification of receptor tyrosine kinases (Cancer Genome Atlas Research Network, 2014). We recently reviewed histopathological images of those 295 cases of gastric cancer

deposited in public database, and found that about 50% of gastric cancer in TCGA group belongs to CIN molecular subtype, which covered several phenotypes of intestinal-type gastric cancer with different degree of differentiation (Yu, 2018). In general, the overall survival of intestinal-type gastric cancer is better than that of diffuse-type gastric cancer (Liu et al., 2013). Molecular heterogeneity of cancer might explain the difference of biological behaviors of intestinal-type gastric cancer. Our study provided evidence that intestinal-type gastric cancer could be biologically heterogeneous.

ERK1/2 signaling pathway is an important signaling pathway in tumor cells, which is closely related to immortality, growth factor-independent proliferation, apoptosis escape, cell cycle acceleration and cell invasiveness (Liu et al., 2010; Chen et al., 2013). It is generally believed that the degree of activation of ERK1/2 is positively correlated with the malignancy, and is related to the innate or acquired drug resistance to chemotherapy (Zhao et al., 2015). In our study, interfering UBE2C expression led to G2/M arrest. It was known that G2/M checkpoint is an important factor for cell cycle progression and drug resistance (Yang et al., 2016). Sarin and coworkers found that efficacy of cisplatin-based chemotherapy is limited by the occurrence of innate and acquired drug resistance. They examined lung cancer cell line A549 and its cisplatin-resistant sub-line A549rCDDP2000. Compared to A549 cells, the cisplatin-resistant cell line A549rCDDP2000 lacked cisplatin-induced G2/M cell cycle arrest, and led to reduced apoptosis (Sarin et al., 2017). Actually, many anti-tumor drugs act on cell cycle, most of them are strongly dependent on G2/M checkpoint, which suggests that G2/M checkpoint is a potential target for cancer therapy (Kawabe, 2004). Several years ago, Sabitha and Rajkuma have noticed the value of UBE2C as therapeutic target. They successfully predicted two small molecular inhibitors *in silico* (Sabitha and Rajkumar, 2012). It is our hope to carry out some preclinical experiments for those small molecule inhibitors, which may provide a new strategy for targeted therapy of intestinal-type, a predominant subtype of gastric cancer.

In summary, this study identified a group of genes related to Lauren classification on the basis of data mining of public

databases. UBE2C is one of the genes overexpressed in intestinal-type gastric cancer. We explored the biological function of UBE2C gene *in vitro*, and found that the overexpression of UBE2C is related to gain of DNA copy number caused by CIN of intestinal-type carcinoma. Overexpression of UBE2C accelerates cell cycle progression and promotes cell growth and invasiveness of gastric cancer cells by activating ERK1/2 signaling pathway. The increased expression of UBE2C of intestinal-type gastric cancer is verified in a large cohort of gastric cancer tissues from Shanghai, China. It was found that overexpression of UBE2C could be the underlying molecular mechanism of biological heterogeneity of intestinal-type gastric cancer and overexpression of UBE2C correlated with poor overall survival of intestinal-type cancer.

AUTHOR CONTRIBUTIONS

JZ, XL, GY, ZZ, and YY conceived the original idea and designed the study. GY, JW, XC, YB, YJ, XZ, JF, YS, and HC provided samples from multiple medical centers. LL, YC, JJ, ZX, and LG performed experiments. JZ and YY performed data analysis and manuscript writing. All authors contributed to data interpretation.

FUNDING

This project was supported by National Key R&D Program of China (2017YFC0908303, 2016YFC1303202), the National Natural Science Foundation of China (81772505 and 81372644), Shanghai Science and Technology Committee (18411953100), the Cross-Institutes Research Fund of Shanghai Jiao Tong University (YG2017ZD01, YG2015MS62), the Innovation Foundation of Translational Medicine of Shanghai Jiao Tong University School of Medicine (15ZH4001, TM201617, and TM201702), and Technology Transfer Project of Science & Technology Dept. Shanghai Jiao Tong University School of Medicine.

REFERENCES

- Barrett, T., and Edgar, R. (2006). Mining microarray data at NCBI's Gene Expression Omnibus (GEO)*. *Methods Mol. Biol.* 338, 175–190. doi: 10.1385/1-59745-097-9:175
- Cacciola, N. A., Calabrese, C., Malapelle, U., Pellino, G., De Stefano, A., Sepe, R., et al. (2016). UbcH10 expression can predict prognosis and sensitivity to the antineoplastic treatment for colorectal cancer patients. *Mol. Carcinog.* 55, 793–807. doi: 10.1002/mc.22322
- Cancer Genome Atlas Research Network. (2014). Comprehensive molecular characterization of gastric adenocarcinoma. *Nature* 513, 202–209. doi: 10.1038/nature13480
- Chen, L., Pan, Y., Gu, L., Nie, Z., He, B., Song, G., et al. (2013). ERK1/2 signalling pathway is involved in CD147-mediated gastric cancer cell line SGC7901 proliferation and invasion. *Exp. Biol. Med.* 238, 903–912. doi: 10.1177/1535370213493706
- Chen, Y. C., Fang, W. L., Wang, R. F., Liu, C. A., Yang, M. H., Lo, S. S., et al. (2016). Clinicopathological variation of Lauren classification in gastric cancer. *Pathol. Oncol. Res.* 22, 197–202. doi: 10.1007/s12253-015-9996-6
- Heng, H. H., Bremer, S. W., Stevens, J. B., Horne, S. D., Liu, G., Abdallah, B. Y., et al. (2013). Chromosomal instability (CIN): what it is and why it is crucial to cancer evolution. *Cancer Metastasis Rev.* 32, 325–340. doi: 10.1007/s10555-013-9427-7
- Ieta, K., Ojima, E., Tanaka, F., Nakamura, Y., Haraguchi, N., Mimori, K., et al. (2007). Identification of overexpressed genes in hepatocellular carcinoma, with special reference to ubiquitin-conjugating enzyme E2C gene expression. *Int. J. Cancer* 121, 33–38. doi: 10.1002/ijc.22605
- Ji, J., Chen, X., Leung, S. Y., Chi, J. T., Chu, K. M., Yuen, S. T., et al. (2002). Comprehensive analysis of the gene expression profiles in human gastric cancer cell lines. *Oncogene* 21, 6549–6556. doi: 10.1038/sj.onc.1205829
- Kawabe, T. (2004). G2 checkpoint abrogators as anticancer drugs. *Mol. Cancer Ther.* 3, 513–519.
- Kim, B., Bang, S., Lee, S., Kim, S., Jung, Y., Lee, C., et al. (2003). Expression profiling and subtype-specific expression of stomach cancer. *Cancer Res.* 63, 8248–8255.

- Kraft, S., Moore, J. B., Muzikansky, A., Scott, K. L., and Duncan, L. M. (2017). Differential UBE2C and HOXA1 expression in melanocytic nevi and melanoma. *J. Cutan. Pathol.* 44, 843–850. doi: 10.1111/cup.12997
- Lauren, P. (1965). The two histological main types of gastric carcinoma: diffuse and so-called intestinal-type carcinoma. An attempt at a histo-clinical classification. *Acta Pathol. Microbiol. Scand.* 64, 31–49. doi: 10.1111/apm.1965.64.1.31
- Li, L., Li, X., Wang, W., Gao, T., and Shi, Z. (2018). UBE2C is involved in the functions of ECRG4 on esophageal squamous cell carcinoma. *Biomed. Pharmacother.* 98, 201–206. doi: 10.1016/j.biopha.2017.12.066
- Liu, L., Wang, Z. W., Ji, J., Zhang, J. N., Yan, M., Zhang, J., et al. (2013). A cohort study and meta-analysis between histopathological classification and prognosis of gastric carcinoma. *Anticancer. Agents Med. Chem.* 13, 227–234. doi: 10.2174/1871520611313020007
- Liu, L., Zhang, H., Sun, L., Gao, Y., Jin, H., Liang, S., et al. (2010). ERK/MAPK activation involves hypoxia-induced MGr1-Ag/37LRP expression and contributes to apoptosis resistance in gastric cancer. *Int. J. Cancer* 127, 820–829. doi: 10.1002/ijc.25098
- Martínez-Canales, S., Lopez de Rodas, M., Nuncia-Cantarero, M., Paez, R., Amir, E., Gyorffy, B., et al. (2018). Functional transcriptomic annotation and protein-protein interaction analysis identify EZH2 and UBE2C as key upregulated proteins in ovarian cancer. *Cancer Med.* 7, 1896–1907. doi: 10.1002/cam4.1406
- Matsumoto, A., Ishibashi, Y., Urashima, M., Omura, N., Nakada, K., Nishikawa, K., et al. (2014). High UBE2C protein expression as a marker of poor prognosis in esophageal squamous cell carcinoma. *Anticancer Res.* 34, 955–962.
- Mo, C. H., Gao, L., Zhu, X. F., Wei, K. L., Zeng, J. J., Chen, G., et al. (2017). The clinicopathological significance of UBE2C in breast cancer: a study based on immunohistochemistry, microarray and RNA-sequencing data. *Cancer Cell Int.* 17:83. doi: 10.1186/s12935-017-0455-1
- Nicolau-Neto, P., Palumbo, A., De Martino, M., Esposito, F., de Almeida Simao, T., Fusco, A., et al. (2018). UBE2C is a transcriptional target of the cell cycle regulator FOXM1. *Genes* 9:E188. doi: 10.3390/genes9040188
- Parkinson, H., Kapushesky, M., Shojatalab, M., Abeygunawardena, N., Coulson, R., Farne, A., et al. (2007). ArrayExpress—a public database of microarray experiments and gene expression profiles. *Nucleic Acids Res.* 35, D747–D750. doi: 10.1093/nar/gkl995
- Qin, T., Huang, G., Chi, L., Sui, S., Song, C., Li, N., et al. (2017). Exceptionally high UBE2C expression is a unique phenomenon in basal-like type breast cancer and is regulated by BRCA1. *Biomed. Pharmacother.* 95, 649–655. doi: 10.1016/j.biopha.2017.08.095
- Qiu, M. Z., Cai, M. Y., Zhang, D. S., Wang, Z. Q., Wang, D. S., Li, Y. H., et al. (2013). Clinicopathological characteristics and prognostic analysis of Lauren classification in gastric adenocarcinoma in China. *J. Transl. Med.* 11:58. doi: 10.1186/1479-5876-11-58
- Sabitha, K., and Rajkumar, T. (2012). Identification of small molecule inhibitors against UBE2C by using docking studies. *Bioinformation* 8, 1047–1058. doi: 10.6026/97320630081047
- Saeed, A. I., Sharov, V., White, J., Li, J., Liang, W., Bhagabati, N., et al. (2003). TM4: a free, open-source system for microarray data management and analysis. *Biotechniques* 34, 374–378.
- Sansregret, L., Patterson, J. O., Dewhurst, S., Lopez-Garcia, C., Koch, A., McGranahan, N., et al. (2017). APC/C dysfunction limits excessive cancer chromosomal instability. *Cancer Discov.* 7, 218–233. doi: 10.1158/2159-8290.CD-16-0645
- Sarin, N., Engel, F., Kalayda, G. V., Mannewitz, M., Cinatl, J. Jr., Rothweiler, F., et al. (2017). Cisplatin resistance in non-small cell lung cancer cells is associated with an abrogation of cisplatin-induced G2/M cell cycle arrest. *PLoS ONE* 12:e0181081. doi: 10.1371/journal.pone.0181081
- Shen, Z., Jiang, X., Zeng, C., Zheng, S., Luo, B., Zeng, Y., et al. (2013). High expression of ubiquitin-conjugating enzyme 2C (UBE2C) correlates with nasopharyngeal carcinoma progression. *BMC Cancer* 13:192. doi: 10.1186/1471-2407-13-192
- Shuliang, S., Lei, C., Guangwu, J., and Changjie, L. (2013). Involvement of ubiquitin-conjugating enzyme E2C in proliferation and invasion of prostate carcinoma cells. *Oncol. Res.* 21, 121–127. doi: 10.3727/096504013X13832473329953
- Slamon, D., and Pegram, M. (2001). Rationale for trastuzumab (Herceptin) in adjuvant breast cancer trials. *Semin. Oncol.* 28(1 Suppl. 3), 13–19. doi: 10.1016/S0093-7754(01)90188-5
- Tang, X. K., Wang, K. J., Tang, Y. K., and Chen, L. (2014). Effects of ubiquitin-conjugating enzyme 2C on invasion, proliferation and cell cycling of lung cancer cells. *Asian Pac. J. Cancer Prev.* 15, 3005–3009. doi: 10.7314/APJCP.2014.15.7.3005
- Torre, L. A., Bray, F., Siegel, R. L., Ferlay, J., Lortet-Tieulent, J., and Jemal, A. (2015). Global cancer statistics, (2012). *CA Cancer J. Clin.* 65, 87–108. doi: 10.3322/caac.21262
- Tusher, V. G., Tibshirani, R., and Chu, G. (2001). Significance analysis of microarrays applied to the ionizing radiation response. *Proc. Natl. Acad. Sci. U.S.A.* 98, 5116–5121. doi: 10.1073/pnas.091062498
- van Ree, J. H., Jeganathan, K. B., Malureanu, L., and van Deursen, J. M. (2010). Overexpression of the E2 ubiquitin-conjugating enzyme UbcH10 causes chromosome missegregation and tumor formation. *J. Cell Biol.* 188, 83–100. doi: 10.1083/jcb.200906147
- van't Veer, L. J., Dai, H., van de Vijver, M. J., He, Y. D., Hart, A. A., Mao, M., et al. (2002). Gene expression profiling predicts clinical outcome of breast cancer. *Nature* 415, 530–536. doi: 10.1038/415530a
- Wagner, K. W., Sapinoso, L. M., El-Rifai, W., Frierson, H. F., Butz, N., Mestan, J., et al. (2004). Overexpression, genomic amplification and therapeutic potential of inhibiting the UbcH10 ubiquitin conjugase in human carcinomas of diverse anatomic origin. *Oncogene* 23, 6621–6629. doi: 10.1038/sj.onc.1207861
- Yang, M., Qu, Y., Shi, R., Wu, X., Su, C., Hu, Z., et al. (2016). Ubiquitin-conjugating enzyme UbcH10 promotes gastric cancer growth and is a potential biomarker for gastric cancer. *Oncol. Rep.* 36, 779–786. doi: 10.3892/or.2016.4906
- Yu, Y. (2018). Molecular classification and precision therapy of cancer: immune checkpoint inhibitors. *Front. Med.* 12, 229–235. doi: 10.1007/s11684-017-0581-0
- Zhang, H. Q., Zhao, G., Ke, B., Ma, G., Liu, G. L., Liang, H., et al. (2018). Overexpression of UBE2C correlates with poor prognosis in gastric cancer patients. *Eur. Rev. Med. Pharmacol. Sci.* 22, 1665–1671. doi: 10.26355/eurrev_201803_14578
- Zhang, Y., Tian, S., Li, X., Ji, Y., Wang, Z., and Liu, C. (2018). UBE2C promotes rectal carcinoma via miR-381. *Cancer Biol. Ther.* 19, 230–238. doi: 10.1080/15384047.2017.1416939
- Zhang, Z., Liu, P., Wang, J., Gong, T., Zhang, F., Ma, J., et al. (2015). Ubiquitin-conjugating enzyme E2C regulates apoptosis-dependent tumor progression of non-small cell lung cancer via ERK pathway. *Med. Oncol.* 32:149. doi: 10.1007/s12032-015-0609-8
- Zhao, Y. Y., Yu, L., Liu, B. L., He, X. J., and Zhang, B. Y. (2015). Downregulation of P-gp, Ras and p-ERK1/2 contributes to the arsenic trioxide-induced reduction in drug resistance towards doxorubicin in gastric cancer cell lines. *Mol. Med. Rep.* 12, 7335–7343. doi: 10.3892/mmr.2015.4367
- Zhao, Z. K., Wu, W. G., Chen, L., Dong, P., Gu, J., Mu, J. S., et al. (2013). Expression of UbcH10 in pancreatic ductal adenocarcinoma and its correlation with prognosis. *Tumour Biol.* 34, 1473–1477. doi: 10.1007/s13277-013-0671-9

Conflict of Interest Statement: The authors declare that the research was conducted in the absence of any commercial or financial relationships that could be construed as a potential conflict of interest.

Copyright © 2018 Zhang, Liu, Yu, Liu, Wang, Chen, Bian, Ji, Zhou, Chen, Ji, Xiang, Guo, Fang, Sun, Cao, Zhu and Yu. This is an open-access article distributed under the terms of the Creative Commons Attribution License (CC BY). The use, distribution or reproduction in other forums is permitted, provided the original author(s) and the copyright owner(s) are credited and that the original publication in this journal is cited, in accordance with accepted academic practice. No use, distribution or reproduction is permitted which does not comply with these terms.



Cross-Database Analysis Reveals Sensitive Biomarkers for Combined Therapy for ERBB2+ Gastric Cancer

Zhen Xiang^{1†}, Xia Huang^{2†}, Jiexuan Wang¹, Jun Zhang¹, Jun Ji¹, Ranlin Yan¹, Zhenggang Zhu¹, Wei Cai^{1*} and Yingyan Yu^{1*}

¹ Department of Surgery, Ruijin Hospital, Shanghai Institute of Digestive Surgery, Shanghai Key Laboratory of Gastric Neoplasms, Shanghai, China, ² Department of Disease Prevention and Control, Ruijin Hospital, Shanghai Jiao Tong University School of Medicine, Shanghai, China

OPEN ACCESS

Edited by:

Dong-Hua Yang,
St. John's University, United States

Reviewed by:

Qi Liu,
Tongji University, China
Ru Wen,
Stanford University, United States
Zhi Shi,
Jinan University, China

*Correspondence:

Wei Cai
cw11109@rjh.com.cn
Yingyan Yu
yingyan3y@sjtu.edu.cn;
ruijinhospitalyyy@163.com

[†]These authors have contributed
equally to this work.

Specialty section:

This article was submitted to
Experimental Pharmacology
and Drug Discovery,
a section of the journal
Frontiers in Pharmacology

Received: 21 May 2018

Accepted: 17 July 2018

Published: 03 August 2018

Citation:

Xiang Z, Huang X, Wang J, Zhang J,
Ji J, Yan R, Zhu Z, Cai W and Yu Y
(2018) Cross-Database Analysis
Reveals Sensitive Biomarkers for
Combined Therapy for ERBB2+
Gastric Cancer.
Front. Pharmacol. 9:861.
doi: 10.3389/fphar.2018.00861

Exploring ERBB2-related pathways will help us finding sensitive molecules and potential combined therapeutic targets of ERBB2-targeted therapy for ERBB2+ gastric cancer (GC). In this study, we performed a cross-databases study focused on ERBB2+ GC. The data of ERBB2+ GC deposited in the cancer genome atlas (TCGA), gene expression omnibus (GEO), InBio MapTM, cancer cell line encyclopedia (CCLE), and cancer therapeutics response portal (CTRP) were analyzed. The correlation of expression levels of candidate and IC50 of candidate genes-targeted drugs were verified on NCI-N87 and MKN-45 GC cell lines. We found that RARA, THRA, CACNB1, and TOP2A are drug sensitive biomarkers of ERBB2-targeted treatment with FDA-approved drugs. All these genes act through Myc signaling pathway. Myc is the downstream hub gene of both ERBB2 and RARA. The expression of RARA, THRA, and CACNB1 were negatively correlated with Myc activation, while ERBB2 and TOP2A positively correlated with Myc activation. SH3BGRL3, SH3BGRL, and NRG2 were identified as potential ligands of ERBB2. The ERBB2+ GC with RARA amplification demonstrated better prognosis than those without RARA amplification, while overexpression of NRG2 and SH3BGRL correlated with poor prognosis in ERBB2+ GC. About 90% of ERBB2+ GC was compatible with chromosome instability (CIN) subtype of TCGA, which overlaps with intestinal-type GC in Lauren classification. In validating experiments, combination of Lapatinib and all-trans retinoic acid (ATRA) synergistically suppresses cell growth, and accompanied by decreased expression of MYC. In conclusions, we identified several predicting biomarkers for ERBB2-targeted therapy and corresponding histological features of ERBB2+ GC. Combination of ERBB2 antagonist or RARA agonist may be effective synergistic regimens for ERBB2+ GC.

Keywords: gastric cancer, HER2, RARA, lapatinib, ATRA

INTRODUCTION

Gastric cancer (GC) is one of the most common cancers and the third leading cause of mortality worldwide (Ferlay et al., 2015). In China, both of the morbidity and mortality of GC rank the second (Chen et al., 2016). The major therapeutic approaches for GC are surgery, adjuvant chemotherapy and targeted therapy. The targeted drugs approved by FDA are trastuzumab

(for ERBB2), cetuximab (for EGFR), and ramucirumab (for VEGF2) (Van Cutsem et al., 2012; Wilke et al., 2014). Lapatinib, a small-molecule inhibitor of ERBB2, plus paclitaxel demonstrated activity in the second-line treatment of ERBB2+ GC (Hecht et al., 2016). In clinics, ERBB2+ GC is defined by scoring 3⁺ by immunohistochemistry or copy number amplification by FISH (He et al., 2013). In general, ERBB2+ GC accounts for about 13% of all GC cases (Bass et al., 2014). A phase III ToGA study showed that the incidence of ERBB2+ GC is up to 22% (Bang et al., 2010). Because the prognosis of ERBB2+ GC is poor, clarifying the mechanisms of drug sensitivity of ERBB2+ GC will be of clinical significance in ERBB2-targeted therapy (Wang et al., 2017). Currently, trastuzumab plus fluorouracil and platinum can effectively improve overall survival of ERBB2+ GC patients, but the response rate was only 32–68% (Ock et al., 2015). Finding additional therapeutic targets for combined therapy will benefit more ERBB2+ GC patients.

ERBB2 is located in chromosome 17q21.2, where some common oncogenes or tumor suppressor genes, such as TOP2A, TAU, p53, and HIC-1 are located (Zhang and Yu, 2011). Our previous studies confirmed that re-activation of tumor suppressor HIC-1 by small-activating RNAs inhibits cell division, growth and invasion (Zhao et al., 2014, 2015). Retinoic acid receptor alpha (RARA) is another gene located on chromosome 17q21.2. Paroni et al. (2012) reported that combination of RARA agonist and ERBB2-targeted drug demonstrated a synergistic anticancer activity in breast cancer. It suggested that some novel therapeutic targets for ERBB2+ GC may harbor on chromosome 17. In this study, we analyzed ERBB2-related pathways and explored potential drug sensitivity biomarkers that could be used as reference for targeted therapy of ERBB2+ GC.

MATERIALS AND METHODS

Data Extraction and Data Mining

The data of gene expression, copy number variation, tissue images and clinical information of 413 GC cases was extracted from The Cancer Genome Atlas database (TCGA¹) and cBioPortal database² (Cerami et al., 2012; Gao et al., 2013; Bass et al., 2014). The data of gene expression and copy number variation of GC was also extracted from GSE62717 and GSE57302 in gene expression omnibus (GEO) database³ (Qian et al., 2014; Cristescu et al., 2015). The data of protein-protein interaction was used in InBio MapTM database⁴ (Li et al., 2017). The information of Lapatinib IC50 of 17 GC cell lines were extracted from database of Cancer Cell Line Encyclopedia (CCLE⁵) (Barretina et al., 2012). The information of Afatinib IC50 of 16 GC cell lines was extracted from database of Cancer Therapeutics Response Portal (CTRP⁶) (Basu et al., 2013). Kyoto Encyclopedia of Genes

and Genomes (KEGG) pathway database is used for explaining functions and biology of genes⁷. The analytic results were confirmed for proteins expression using The Human Protein Atlas⁸.

Gastric Cancer Cell Lines and Cell Culture

Human GC cell lines NCI-N87 and MKN45 were purchased from the type Culture Collection of Chinese Academy of Sciences (Shanghai, China). All cell lines were cultured in RPMI-1640 containing 10% fetal bovine serum (FBS) at 37°C in a humidified incubator with 95% air and 5% CO₂.

Cell Viability Assay

Firstly, 5000/well NCI-N87 or MKN45 cells were placed in 96 well plates (100 µl/well). Cells were treated by different concentrations of Lapatinib (Selleck, Houston, TX, United States) and All-Trans Retinoic Acid (ATRA, Selleck, Houston, TX, United States), respectively. CCK-8(10 µl/well) was used and OD value was measured at 450 nm by spectrophotometry (BioTek, VT, United States) at different time points.

Western Blot

The cytoplasmic protein and nuclear protein were extracted, respectively by extraction kit (Cat. P0027, Beyotime, Shanghai, China) according to the protocols. Western blot was performed as previously described (Duan et al., 2016). The antibodies used in this study were as following: HRP-conjugated mouse monoclonal GAPDH (1: 5000, Cat. HRP-60004, Proteintech Group, Inc. Wuhan, China), rabbit monoclonal Histone H3 (1: 5000, Cat. ab1791, Abcam, Cambridge, United Kingdom), and rabbit monoclonal c-MYC (1:1000, Cat. ab32072, Abcam, Cambridge, United Kingdom). Of those, GAPDH and Histone H3 were used as internal controls for cytoplasmic protein and nuclear protein, respectively.

Statistical Analysis

EdgeR package in R language was used to screen differentially expressed genes (Robinson et al., 2010). We plotted OncoPrinter map based on gene copy number data from TCGA and cBioPortal platforms. Pheatmap package in R language was utilized to plot heatmap. Receiver operating characteristic (ROC) was plotted and an optimal cutoff value was selected for biomarkers from clinical samples. The median value was used as cutoff value for cancer cell lines. Survival rate was calculated by Kaplan-Meier method and log-rank test. GSEA software was applied to perform gene set enrichment analysis (Subramanian et al., 2005). Pearson correlation between RNA levels and IC50 was analyzed by Pearson test. CompuSyn software (ComboSyn Inc., Paramus, NJ, United States) was used to calculating combination index (CI) of drugs synergistic effects. CI < 1, =1, and >1 indicate synergistic, additive and antagonistic effects, respectively (Yu et al., 2018). Other statistical analysis was performed by using GraphPad Prism 6.0 (Inc., La Jolla, CA,

¹<https://cancergenome.nih.gov/>

²<http://www.cbioportal.org/>

³<https://www.ncbi.nlm.nih.gov/geo/>

⁴<https://www.intomics.com/inbio/map/#home>

⁵<http://www.broadinstitute.org/ccle>

⁶<http://portals.broadinstitute.org/ctrp.v2.1/>

⁷<http://www.genome.jp/kegg/pathway.html>

⁸<https://www.proteinatlas.org/>

United States). *P*-value less 0.05 was considered statistically significant.

RESULTS

ERBB2+ GC Showed Amplification of RARA, THRA, CACNB1, and TOP2A

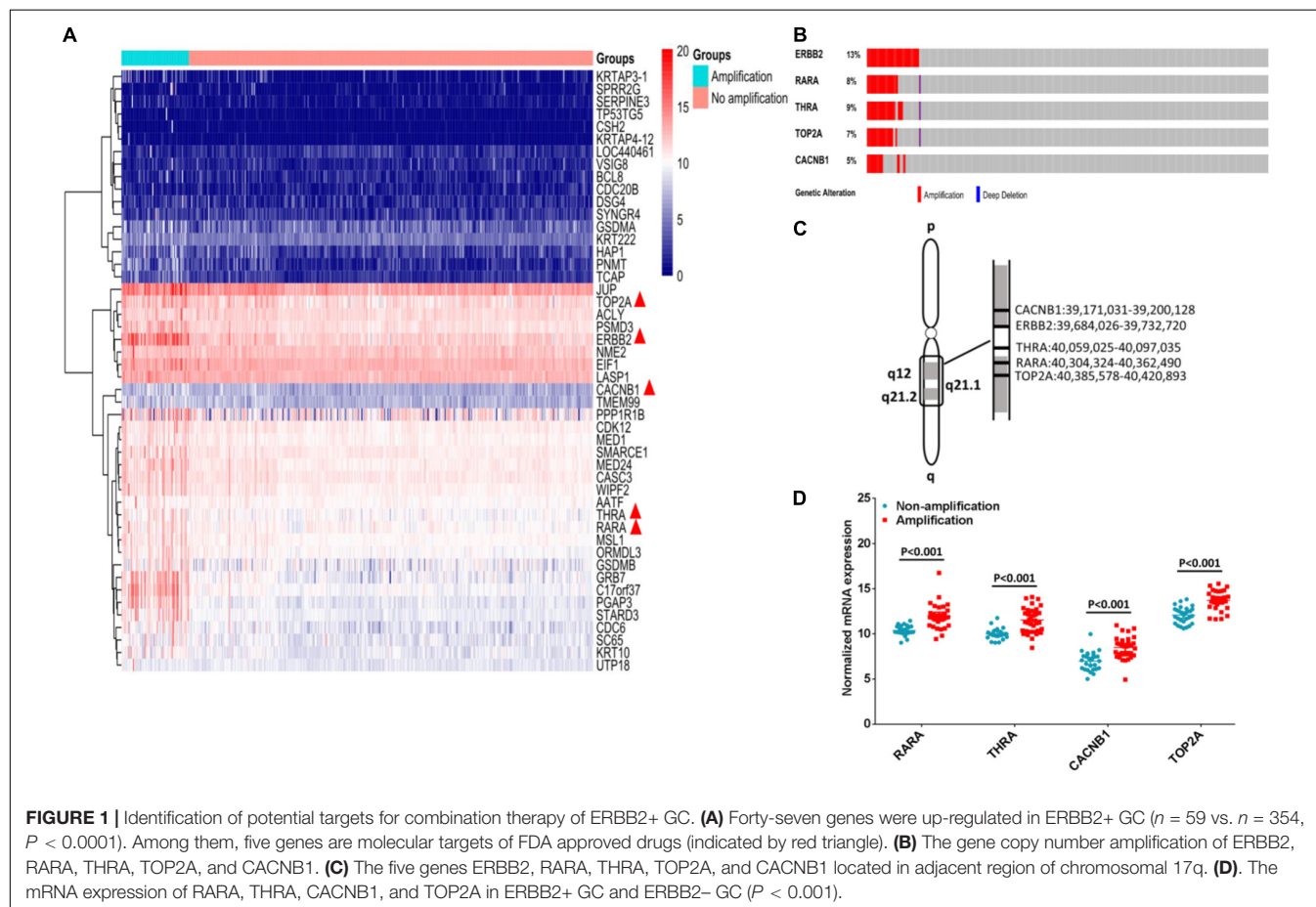
Among 413 cases of GC from TCGA dataset, ERBB2+ GC accounted for 14.29% (59/413 cases), and the others were ERBB2- GC (354/413 cases). We compared the differential expressed genes and copy number variations between ERBB2+ and ERBB2- GC groups. Forty-seven differential expressed genes were selected based on the likelihood ratio (LR) and *P*-value ($LR > 100$, $P < 0.0001$; **Figure 1A**). Four out of these 47 genes are the molecular targets of FDA-approved drugs. They are CACNB1 (calcium voltage-gated channel auxiliary subunit beta 1) for amlodipine, TOP2A (DNA topoisomerase II alpha) for etoposide, RARA for ATRA and THRA (thyroid hormone receptor, alpha) for tiratricol. These genes were selected as potential targets of combination therapy with ERBB2-targeted drugs.

Gene amplification of RARA, THRA, CACNB1, and TOP2A was often accompanied by ERBB2 amplification (**Figure 1B**). These genes were located in adjacent region of chromosomal 17q

(**Figure 1C**). In ERBB2+ GC, the rate of gene amplification was 57.63% (34 out of 59) for RARA, 62.71% (37 out of 59 (62.71%)) for THRA, 50.85% (30 out of 59) for TOP2A, and 54.24% (32 out of 59) for CACNB1. The elevated mRNAs were also identified for cases with gene amplification, compared to cases without gene amplification (**Figure 1D**, $P < 0.001$).

Amplified Genes of Chromosome 17q Were Myc Pathway-Related Genes

Gene set enrichment analysis (GSEA) is a visualized method of the gene ontology analysis, which could help researchers finding a group of functional genes in a signaling pathway. Through GSEA, we found that all amplified genes of 17q are Myc-related genes. Of those, RARA, THRA, and CACNB1 were negatively correlated with Myc activation, which revealed minus value of enrichment score (ES). For instance, the ES value of RARA is -1.93 (FDR = 0.017, $P = 0.004$, **Figure 2A**), THRA is -1.85 (FDR = 0.035, $P = 0.010$, **Figure 2B**), and CACNB1 is -1.89 (FDR = 0.028, $P = 0.004$, **Figure 2C**). TOP2A and ERBB2 were positively associated with Myc activation (ES = 2.05, FDR = 0.002, $P < 0.001$, **Figure 2D** and (ES = 1.88, FDR = 0.077, $P = 0.018$, **Figure 2E**). These results implied that agonists of RARA, THRA, and CACNB1 or inhibitors of TOP2A or ERBB2 might be combined together for the treatment of ERBB2+ GC.



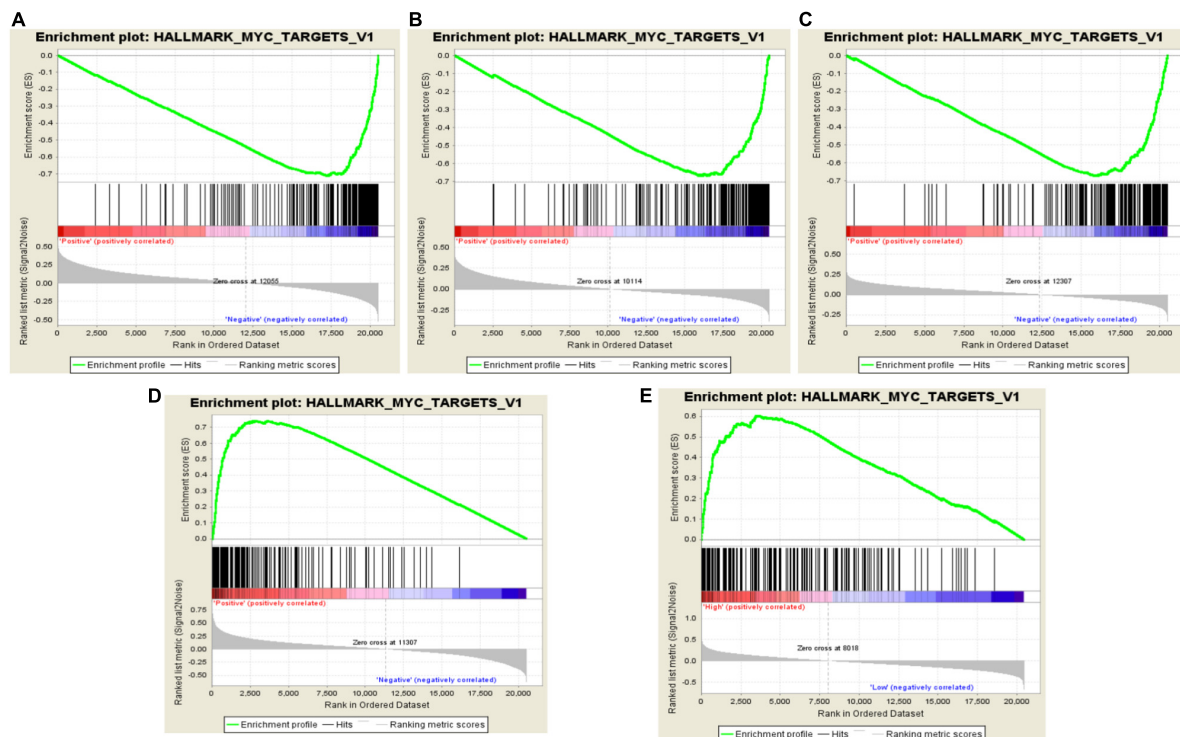


FIGURE 2 | Identification of RARA, THRA, CACNB1, and TOP2A related pathways in ERBB2+ GC. (A–C) RARA, THRA, and CACNB1 are negatively related to Myc pathway activation with minus ES value. (D,E) TOP2A and ERBB2 are positively related to Myc pathway activation with plus ES value. The green curve represents enrichment score. The highest point is the enrichment score value in Myc pathway. The ES value indicates the correlation between gene and Myc pathway. The black bar codes represent genes in pathway, which are ordered according to their expression levels. The left end or right end genes are leading edge subset strongly contributed to ES value. The bottom numbers represent order of expression levels from high to low in genome.

The Association Between Amplified Genes and Biological Significance

The association and pathway of amplified genes were analyzed by InBio Map™. SH3BGRL3, SH3BGRL, and Neuregulin 2 (NRG2) are three candidate ligands of ERBB2. Both RARA and ERBB2 are upstream genes in Myc pathway (Figure 3A). To clarify the clinical significance of amplified genes in ERBB2+ GC, these genes in two datasets from TCGA and GEO were further analyzed. The tendency of better prognosis was noted in RARA amplification group, compared to non-RARA amplification group of ERBB2+ GC in both TCGA cohort (HR = 0.628, 95% CI 0.242–1.539, $P = 0.295$, Figure 3B), and GEO cohort (HR = 0.312, 95% CI 0.104–0.942, $P = 0.04$, Figure 3C). In ERBB2+ GC of TCGA cohort, high levels of NRG2 and SH3BGRL were significantly related to poor prognosis ($P = 0.009$ and $P = 0.042$, respectively, Figures 3D,E), but not for SH3BGRL3 ($P = 0.267$, Figure 3F). These results implied the ligand function of NRG2 and SH3BGRL in cancer progression of ERBB2+ GC.

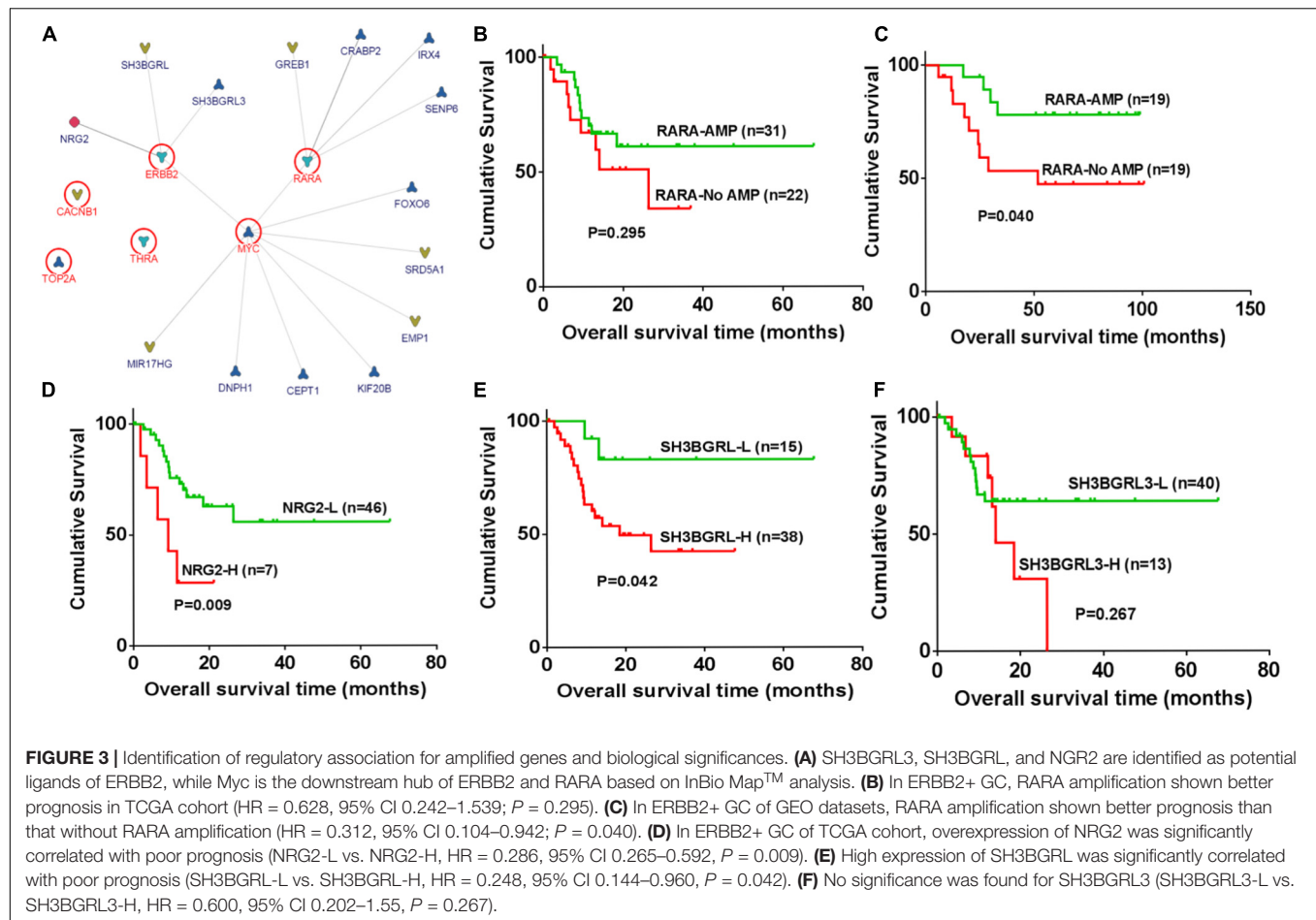
The Relationship Between Amplified Genes and Sensitivity to ERBB2-Targeted Drugs

Since the gene copy number, mRNA level and IC50 value to ERBB2-targeted drugs of multiple cancer cell lines were deposited

in CCLE database, the drug responsive status of 17 GC cell lines was analyzed. Among those, four cell lines (NCI-N87, KE39, NUGC-4, and MKN-7) were ERBB2-amplified cell lines that showed lower IC50 (μM) to drug Lapatinib than other GC cell lines ($P = 0.031$, Figure 4A, left). The ERBB2-amplified cell lines also showed lower IC50 (μM) to drug Afatinib than other cell lines ($P = 0.027$, Figure 4A, right). The CNV of ERBB2 or RARA and their responses to targeted drugs Lapatinib or Afatinib of GC cell lines were listed in Table 1. Cell line NCI-N87 were more sensitive to ERBB2-targeted drugs, which is related to dual amplification of ERBB2 and RARA, while MKN7 was not sensitive to ERBB2-targeted drugs, which is related to non-amplification of RARA.

The Relationship of Expression of ERBB2, RARA, NRG2, and SH3BGRL and Sensitivity to ERBB2-Targeted Drugs

ERBB2 mRNA overexpression was often significantly related to lower IC50 to Lapatinib ($R = -0.446$, $P = 0.073$) and Afatinib ($R = -0.515$, $P = 0.041$). Similarly, overexpression of RARA mRNA was significantly associated with lower IC50 to Lapatinib ($R = -0.494$, $P = 0.044$) and Afatinib ($R = -0.482$, $P = 0.059$). However, there was no significant correlation for NRG2 and SH3BGRL mRNA expression and drug sensitivity (Figure 4B).



Nevertheless, GC cases with overexpression of ERBB2 and NRG2 (ERBB2-H/NRG2-H) were more sensitive to Lapatinib, compared to low gene expression of ERBB2-L/NRG2-L group ($P = 0.042$, **Figure 4C**, left). However, there was no significant difference between ERBB2-H/SH3BGRL-H group and ERBB2-L/NRG2-L group for drug Afatinib (**Figure 4C**, right).

The relationship of simultaneous overexpression of NRG2, ERBB2, and RARA with Lapatinib sensitivity was listed in **Table 2**. Group 1: NRG2-L/ERBB2-L/RARA-L; Group 2: high expression of any one of NRG2, ERBB2, or RARA; Group 3: lower expression of any one of NRG2, ERBB2, or RARA; and Group 4: NRG2-H/ERBB2-H/RARA-H. The IC₅₀ to Lapatinib of Group 4 was the lowest ($P = 0.001$). Group 3 is better than that in Group 2 for sensitivity to Lapatinib (**Figure 4D**).

ERBB2+ GC Strongly Associates With CIN Subtype of TCGA and Intestinal-Type of Lauren Classification

The clinical details and histology of TCGA cohort were recorded in cBioPortal database⁹, which provided opportunity to analyze correlation between genomic information and clinicopathological characteristics. For 59 cases of ERBB2+

GC, the pathology reports and slide images of 46 cases were uploaded in database (**Figure 5A**). Fifty-three cases out of 59 ERBB2+ GC (89.83%) belong to chromosome instability (CIN) molecular subtype, and the others include three Epstein-Bar Virus-related (EBV) subtype, two genome stable (GS) subtype, and one microsatellite instability (MSI) subtype (**Figure 5B**). Based on their pathological reports of ERBB2+ GC, all of those are intestinal-type GC in traditional Lauren classification, such as tubular adenocarcinoma, papillary adenocarcinoma, and a few mucinous adenocarcinomas.

Validating Study of Lapatinib and ATRA Drugs on Different GC Cell Lines

Based on data analysis of multiple GC cell lines (**Table 2**), cell line NCI-N87 (ERBB2-H/RARA-H) and MKN-45 (ERBB2-L/RARA-L) were selected for further validating experiments. The IC₅₀s of Lapatinib (targeted to ERBB2) and ATRA (targeted to RARA) were assayed by CCK8 method on NCI-N87 and MKN-45 cell lines. As showed in **Figure 6A**, cell line NCI-N87 was more sensitive than cell line MKN-45 to drug Lapatinib (IC₅₀ 0.88 μM vs. 15.38 μM, $P < 0.001$), while there was no significant difference of IC₅₀s of ATRA in both GC cell lines (71.26 μM vs. 67.70 μM, $P = 0.281$). By further CI analysis, synergistic effect of ATRA (25 μM)

⁹http://www.cbioportal.org/study?id=~stad_tcga_pub#clinical

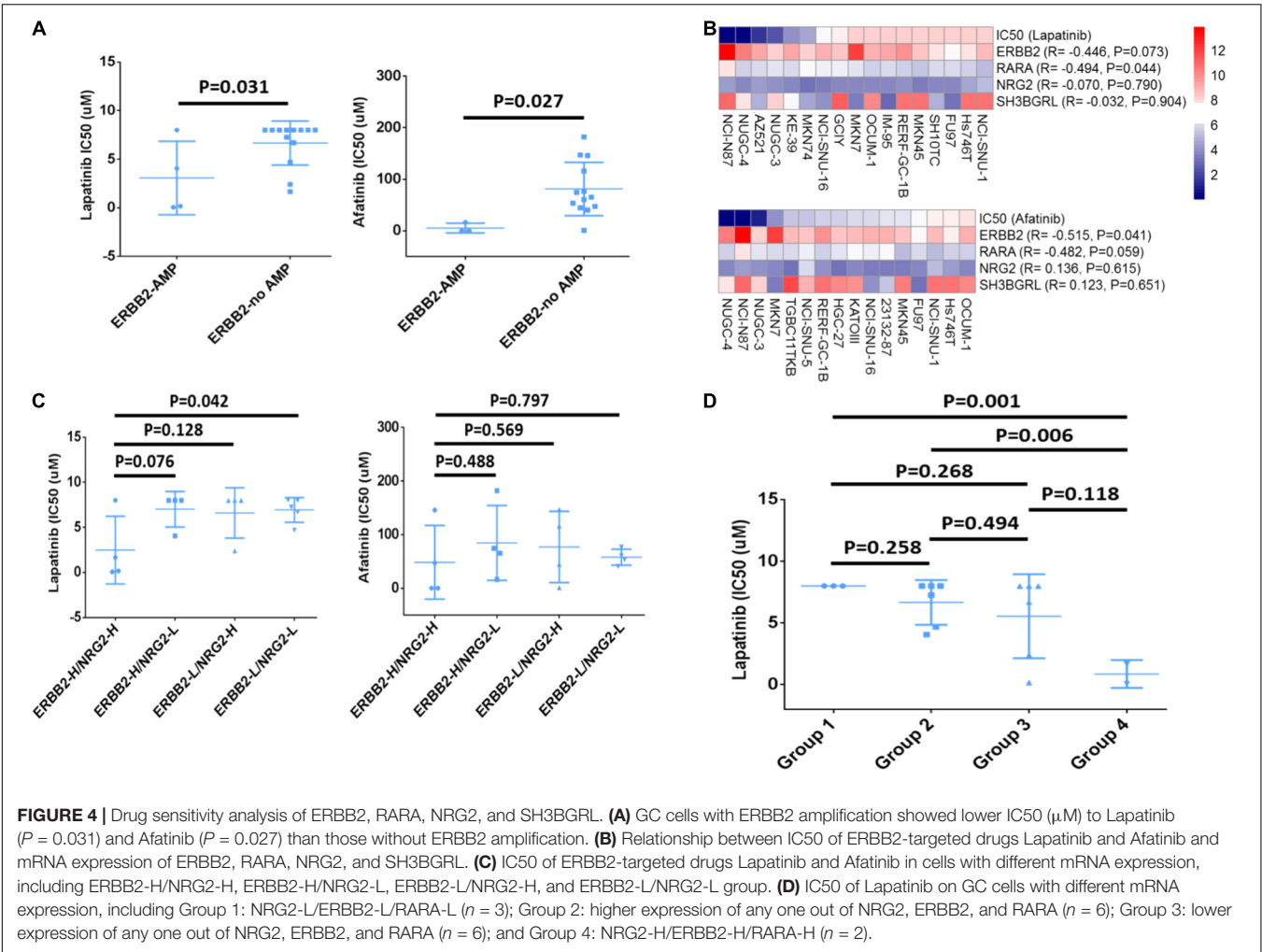


TABLE 1 | The correlation of CNV of ERBB2 or RARA with sensitivity to Lapatinib or Afatinib in ERBB2+ GC cells.

Cell lines	ERBB2 amplification	RARA amplification	Lapatinib IC50 (μM)	Afatinib IC50 (μM)
NCI-N87	Yes	Yes	0.066	0.141
NUGC-4	Yes	No	0.171	0.077
KE39	Yes	No	4.056	NA
MKN7	Yes	No	8.000	16.50

and Lapatinib (between 0.005 and 0.5 μM) was observed on NCI-N87 cell line, but not in MKN-45 cell line (Table 3). To verify the effect on Myc signaling pathway, the cytoplasmic protein and nuclear protein were extracted separately, and examined expressing levels after incubating Lapatinib, ATRA or both. As results, after 2 h incubation of Lapatinib (0.05 μM), ATRA (25 μM), or both on NCI-N87 and MKN-45 cells, obvious down-regulation of MYC protein levels of cytoplasm and nucleus was found in Lapatinib treated NCI-N87 cells, but bot ATRA did. Importantly, incubation of Lapatinib and ATRA simultaneously further reduced nuclear protein level of MYC in NCI-N87 cells

(Figure 6B, right). The similar effects were also observed on NCI-N87 cells after 48 h incubation by Lapatinib and ATRA, or both (Figure 6C, right). However, these effects were not observed in MKN-45 cells (Figures 6B,C, left).

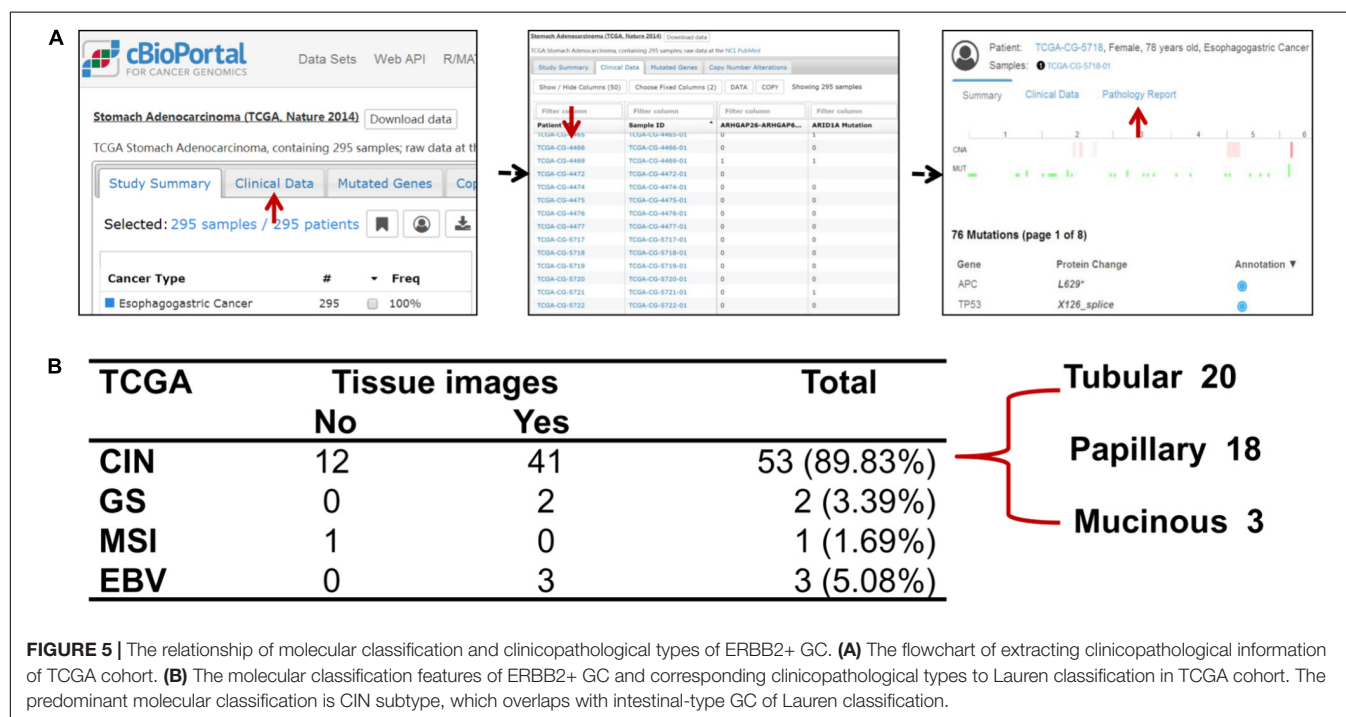
DISCUSSION

ERBB2 plays a critical role in carcinogenesis and cancer progression and has become a targeted therapeutic molecule in breast cancer and GC. Exploring ERBB2 related pathways and mechanisms of resistance will help oncologist to overcome drug resistance and enhance therapeutic effect of ERBB2-targeted therapy (Shi et al., 2016). Clinically, not all ERBB2+ GC respond well to ERBB2-targeted treatment due to innate resistance or acquired resistance (Kim et al., 2014; Piro et al., 2016). Therefore, exploring resistant mechanism of ERBB2+ GC is desirable. Han et al found that SRC inhibitor combined with trastuzumab can synergistically inhibit proliferation of ERBB2+ GC *in vitro* (Han et al., 2014).

Two decades passed since trastuzumab was used for treatment of ERBB2+ breast cancer (Goldenberg, 1999; Shak, 1999;

TABLE 2 | The association of Lapatinib sensitivity, mRNA expression and gene amplification of ERBB2, RARA, and NRG2.

GC cell lines	ERBB2 mRNA	ERBB2 Amp	RARA mRNA	RARA Amp	NRG2 mRNA	NRG2 Amp	Groups	Lapatinib IC50 (μ M)
NCIN87	13.68068	ERBB2-H	7.579796	RARA-H	4.240898	NRG2-H	Group 4	0.06610655
AZ521	9.076744	ERBB2-H	5.968132	RARA-H	4.311362	NRG2-H	Group 4	1.659918428
NUGC4	10.21848	ERBB2-H	5.721415	RARA-L	3.852881	NRG2-H	Group 3	0.171543315
MKN7	12.00612	ERBB2-H	6.058238	RARA-H	3.661981	NRG2-L	Group 3	8
RERFGC1B	9.667308	ERBB2-H	5.777195	RARA-L	3.974191	NRG2-H	Group 3	8
NUGC3	8.006484	ERBB2-L	6.300127	RARA-H	3.986192	NRG2-H	Group 3	2.410752535
SNU16	8.917765	ERBB2-H	6.59063	RARA-H	3.545393	NRG2-L	Group 3	6.697770596
FU97	6.999068	ERBB2-L	6.050557	RARA-H	3.820554	NRG2-H	Group 3	8
KE39	9.27483	ERBB2-H	5.956177	RARA-L	3.61809	NRG2-L	Group 2	4.056060314
GCIY	8.439433	ERBB2-L	6.460522	RARA-H	3.708975	NRG2-L	Group 2	7.255415916
MKN74	8.119466	ERBB2-L	6.73371	RARA-H	3.257784	NRG2-L	Group 2	4.689732791
IM95	9.108876	ERBB2-H	5.806562	RARA-L	3.74757	NRG2-L	Group 2	8
HS746T	7.43275	ERBB2-L	5.676293	RARA-L	4.431395	NRG2-H	Group 2	8
SNU1	8.776752	ERBB2-L	5.182644	RARA-L	5.151627	NRG2-H	Group 2	8
OCUM1	9.006604	ERBB2-L	5.674769	RARA-L	3.74211	NRG2-L	Group 1	8
SH10TC	7.577364	ERBB2-L	5.941876	RARA-L	3.724585	NRG2-L	Group 1	8
MKN45	8.476658	ERBB2-L	5.247703	RARA-L	3.581405	NRG2-L	Group 1	8



Sakamoto and Mitsuyama, 2000). Some ERBB family inhibitors, such as Lapatinib and Afatinib are also developed for treatment of ERBB2+ breast cancer or GC (Geuna et al., 2012; Huang and Rizzo, 2012; Lin et al., 2012; Schuler et al., 2012; Hecht et al., 2016). Large amount of clinical information as well as their corresponding genomic changes has been submitted to open databases. Cross-database analysis is a challenging work, but it helps researchers to get an overview of interested problems. In this study, we performed a cross-database data mining for factors involved in sensitivity or resistance to ERBB2-targeted therapy in ERBB2+ GC. We found that both ERBB2 and RARA are

involved in Myc signaling pathway. Myc is the important hub gene of both ERBB2 and RARA. By data mining, a total of 47 genes were outlined as potential targets of treatment for ERBB2+ GC. We noticed that RARA, THRA, CACNB1, and TOP2A are targets of FDA-approved drugs. For instance, CACNB1 is a calcium channel protein and the inhibitor amlodipine is one of the most popular medications for treatment of high blood pressure (Gregg et al., 1993; Nussberger et al., 2008). TOP2A is the target of etoposide, which has been used in cancer treatment (Slater et al., 2001; Bartlett et al., 2015). RARA, which participates in regulation of cell development, differentiation, apoptosis and

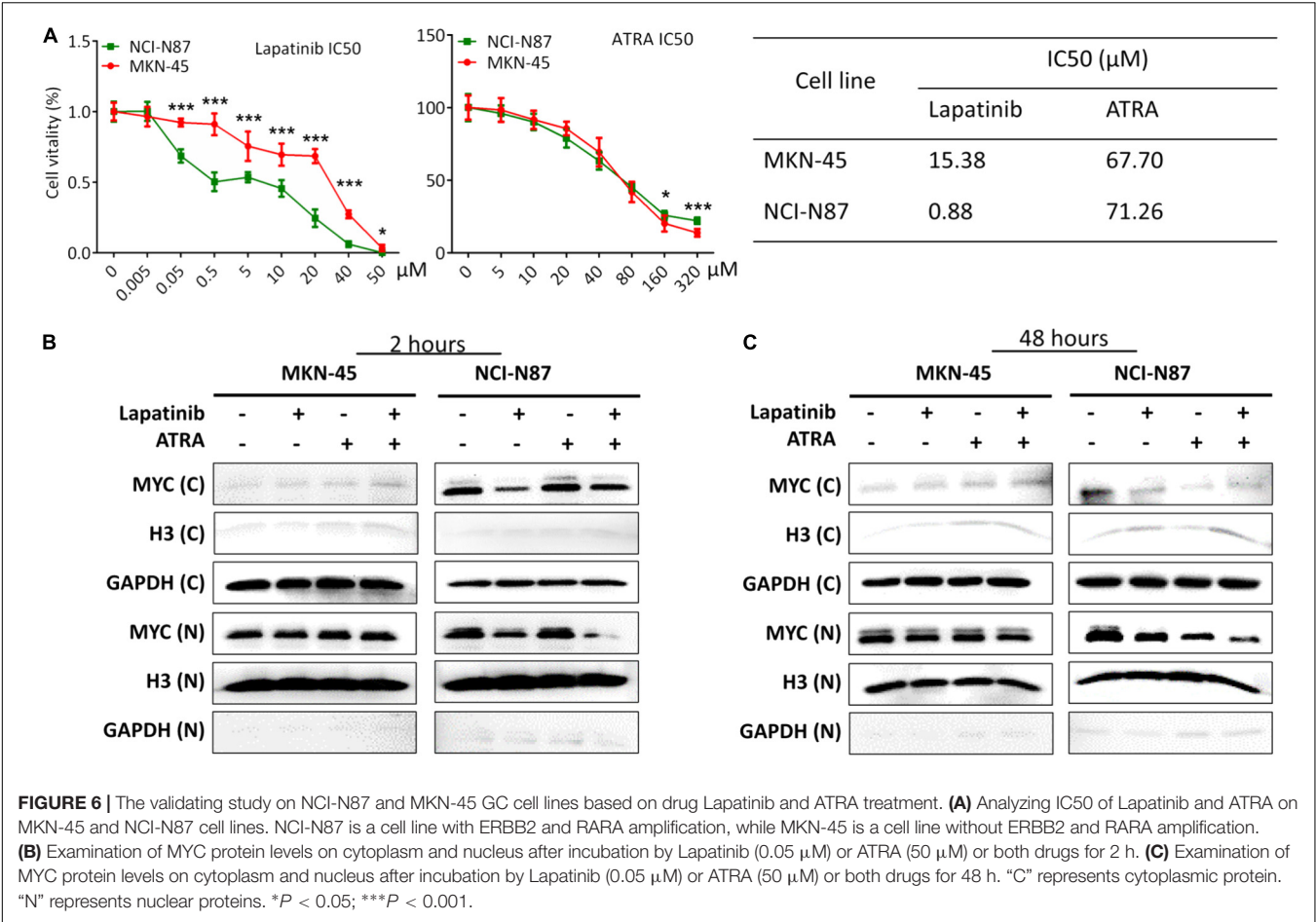


TABLE 3 | Analysis of combination index for Lapatinib and ATRA (25 μM).

Lapatinib (μM)	NCI-N78		MKN-45	
	IR	CI	IR	CI
0.005	0.31	0.70	0.08	3.28
0.05	0.64	0.24	0.20	1.35
0.5	0.77	0.41	0.26	2.18
5	0.77	3.16	0.43	8.28

CI, combination index; IR, inhibition rate.

granulopoiesis. ATRA is a RARA agonist, which revealed clinical efficacy in leukemia treatment (Degos and Wang, 2001). THRA is thyroid hormone receptor alpha, whose ligand tiratricol was used in treatment of hypothyroidism (Yazdanparast et al., 2006; Tylki-Szymanska et al., 2015). GSEA is a powerful tool to find biological pathways for associated genes. By GSEA method, all amplified genes ERBB2, RARA, THRA, CACNB1, and TOP2A are identified to be related to Myc signaling pathway. Myc plays important roles in carcinogenesis and cancer progression (Sun et al., 2011; Stine et al., 2015). In gastric carcinogenesis, pathogen infection of *H. pylori* and EBV could activate Myc pathway (Calcagno et al., 2008). Our cross-database analysis suggests that inhibitor of TOP2A and agonist of RARA, THRA,

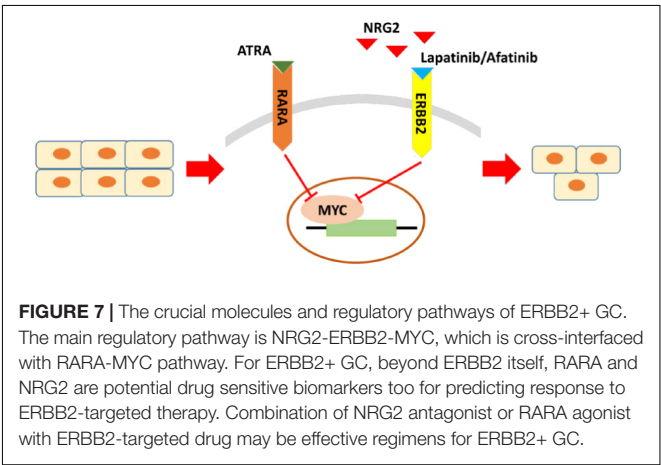


FIGURE 7 | The crucial molecules and regulatory pathways of ERBB2+ GC. The main regulatory pathway is NRG2-ERBB2-MYC, which is cross-interfaced with RARA-MYC pathway. For ERBB2+ GC, beyond ERBB2 itself, RARA and NRG2 are potential drug sensitive biomarkers too for predicting response to ERBB2-targeted therapy. Combination of NRG2 antagonist or RARA agonist with ERBB2-targeted drug may be effective regimens for ERBB2+ GC.

or CACNB1 may have synergistic efficacy in ERBB2-targeted therapy for ERBB2+ GC. Li and coworkers found that ERBB2 activated downstream Myc and promoted cells proliferation by phosphorylating AKT1 and Erk1/2 in cervical cancer (Li et al., 2018). RARA could interact with Myc and regulate RARA-dependent genes expression in leukemia cells (Uribealago et al., 2012).

In this study, three potential ligands (SH3BGRL3, SH3BGRL, and NRG2) of ERBB2 have been proposed. The latter has been reported as a ligand for ERBB3/ERBB4 (Chang et al., 1997; Schulze et al., 2005; Chiang et al., 2015). Slattery and coworkers found that NRG2 as a growth factor was involved in progression of breast cancer (Slattery et al., 2013). Sun and colleagues found that both NRG1 and NRG2 functioned as ligands of ERBB family and involved in progression of non-small cell lung cancer (Sun et al., 2009). Hitherto, the relationship of NRG2 and ERBB2 in GC is not clear yet. Our analysis disclosed that overexpression of NRG2 is significantly associated with poor prognosis of ERBB2+ GC. Some reports suggested that NRG2 can promote phosphorylation of ERBB2, ERBB3, and ERBB4 directly or indirectly (Sliwkowski et al., 1994; Chang et al., 1997; Mill et al., 2011). Therefore, NRG2 as a potential ligand of ERBB2 is worth further explored. Regarding to SH3BGRL3 and SH3BGRL, there is no any report on the relationship of these genes with ERBB2. In the present study, the simultaneous overexpression of ERBB2, NRG2, and RARA were correlated with increased sensitivity to Lapatinib. We speculate that ERBB2, NRG2, and RARA might act together as a functional network.

It has been reported that there are some histopathological features of ERBB2+ GC (Park et al., 2016). ERBB2 positivity is more often observed in intestinal-type GC (He et al., 2013; Irkkan et al., 2017). Up-to-date, there is no correlation analysis on both levels of genomics and clinical histology for ERBB2+ GC. TCGA database provides a good resource for comparative analysis on both levels because it stores perfect genomics and histological information for GC samples. In 59 cases of ERBB2+ GC, 46 cases were accompanied by whole slide tissue images. ERBB2+ GC revealed characteristic histopathology. All 46 cases were classified into intestinal-type GC using Lauren classification, mainly including tubular adenocarcinoma, papillary adenocarcinoma, and a few mucinous adenocarcinomas. The majority (near 90%) of ERBB2+ GC was classified into CIN subtype on genomic level using TCGA molecular classification (Bass et al., 2014). These findings provide an important clue for clinical selection of ERBB2-targeted therapy.

In our validating study, we confirmed that GC cell line with amplified ERBB2 and RARA (NCI-N87) was sensitive to Lapatinib relative to GC cell without amplified ERBB2 and RARA (MKN-45). The sensitivity to ATRA on both cell lines did not show significant difference, which may attribute to some alternative pathways for ATRA-mediated apoptosis (Patrad et al.,

2018). We found that Lapatinib and ATRA could synergistically inhibit cell growth in NCI-N87 cell, but not in MKN-45 cell. These biological effects were involved in interfering Myc signaling pathway. The similar effect was reported for breast cancer (Paroni et al., 2012).

In summary, by cross-database analysis, GC with increased expression of ERBB2, RARA, and NRG2 simultaneously should be taken as sensitive category to Lapatinib therapy. The current study proposed that NRG2-ERBB2-MYC is cross-interfaced with RARA-MYC pathway. Intervention of both routes will regulate hub gene Myc, and then inhibit cell growth for ERBB2+ GC (Figure 7). Moreover, combination of RARA agonist ATRA with ERBB2-targeted drug disclosed synergistic anticancer effect for ERBB2+ GC *in vitro*.

AUTHOR CONTRIBUTIONS

YY, XH, and ZZ were involved in concept and design. ZX, JW, and JZ acquired the data and performed data mining. ZX, JJ, and RY performed the experiments. WC and YY supported the analysis. All authors wrote, reviewed, and revised the manuscript.

FUNDING

This project was supported by National Key R&D Program of China (2017YFC0908303 and 2016YFC1303202), the National Natural Science Foundation of China (81772505 and 81372644), Shanghai Science and Technology Committee (18411953100), the Cross-Institutes Research Fund of Shanghai Jiao Tong University (YG2017ZD01 and YG2015MS62), Innovation Foundation of Translational Medicine of Shanghai Jiao Tong University School of Medicine (15ZH4001, TM201617, and TM 201702), and Technology Transfer Project of Science & Technology Dept. Shanghai Jiao Tong University School of Medicine.

ACKNOWLEDGMENTS

We acknowledge multiple open databases of TCGA, GEO (GSE62717 and GSE57302), InBio MapTM, CCLE, KEGG and The Human Protein Atlas.

REFERENCES

- Bang, Y. J., Van Cutsem, E., Feyereislova, A., Chung, H. C., Shen, L., Sawaki, A., et al. (2010). Trastuzumab in combination with chemotherapy versus chemotherapy alone for treatment of HER2-positive advanced gastric or gastro-oesophageal junction cancer (ToGA): a phase 3, open-label, randomised controlled trial. *Lancet* 376, 687–697. doi: 10.1016/S0140-6736(10)61121-X
- Barretina, J., Caponigro, G., Stransky, N., Venkatesan, K., Margolin, A. A., Kim, S., et al. (2012). The cancer cell line encyclopedia enables predictive modelling of anticancer drug sensitivity. *Nature* 483, 603–607. doi: 10.1038/nature11003
- Bartlett, J. M., McConkey, C. C., Munro, A. F., Desmedt, C., Dunn, J. A., Larsimont, D. P., et al. (2015). Predicting anthracycline Benefit: TOP2A and CEP17-not only but also. *J. Clin. Oncol.* 33, 1680–1687. doi: 10.1200/JCO.2013.54.7869
- Bass, A. J., Thorsson, V., Shmulevich, I., Reynolds, S. M., Miller, M., Bernard, B., et al. (2014). Comprehensive molecular characterization of gastric adenocarcinoma. *Nature* 513, 202–209. doi: 10.1038/nature13480
- Basu, A., Bodycombe, N. E., Cheah, J. H., Price, E. V., Liu, K., Schaefer, G. I., et al. (2013). An interactive resource to identify cancer genetic and lineage dependencies targeted by small molecules. *Cell* 154, 1151–1161. doi: 10.1016/j.cell.2013.08.003
- Calcagno, D. Q., Leal, M. F., Assumpcao, P. P., Smith, M. A., and Burbano, R. R. (2008). MYC and gastric adenocarcinoma carcinogenesis. *World J. Gastroenterol.* 14, 5962–5968. doi: 10.3748/wjg.14.5962
- Cerami, E., Gao, J., Dogrusoz, U., Gross, B. E., Sumer, S. O., Aksoy, B. A., et al. (2012). The cBio cancer genomics portal: an open platform for exploring

- multidimensional cancer genomics data. *Cancer Discov.* 2, 401–404. doi: 10.1158/2159-8290.CD-12-0095
- Chang, H., Riese, D. J., Gilbert, W., Stern, D. F., and McMahon, U. J. (1997). Ligands for ErbB-family receptors encoded by a neuregulin-like gene. *Nature* 387, 509–512. doi: 10.1038/387509a0
- Chen, W., Zheng, R., Baade, P. D., Zhang, S., Zeng, H., Bray, F., et al. (2016). Cancer statistics in China, 2015. *CA Cancer J. Clin.* 66, 115–132. doi: 10.3322/caac.21338
- Chiang, C. Y., Pan, C. C., Chang, H. Y., Lai, M. D., Tzai, T. S., Tsai, Y. S., et al. (2015). SH3BGR13 protein as a potential prognostic biomarker for urothelial carcinoma: a novel binding partner of epidermal growth factor receptor. *Clin. Cancer Res.* 21, 5601–5611. doi: 10.1158/1078-0432.CCR-14-3308
- Cristescu, R., Lee, J., Nebozhyn, M., Kim, K. M., Ting, J. C., Wong, S. S., et al. (2015). Molecular analysis of gastric cancer identifies subtypes associated with distinct clinical outcomes. *Nat. Med.* 21, 449–456. doi: 10.1038/nm.3850
- Degos, L., and Wang, Z. Y. (2001). All trans retinoic acid in acute promyelocytic leukemia. *Oncogene* 20, 7140–7145. doi: 10.1038/sj.onc.1204763
- Duan, Y., Gao, Y., Zhang, J., Chen, Y., Jiang, Y., Ji, J., et al. (2016). Mitochondrial aldehyde dehydrogenase 2 protects gastric mucosa cells against DNA damage caused by oxidative stress. *Free Radic. Biol. Med.* 93, 165–176. doi: 10.1016/j.freeradbiomed.2016.02.001
- Ferlay, J., Soerjomataram, I., Dikshit, R., Eser, S., Mathers, C., Rebelo, M., et al. (2015). Cancer incidence and mortality worldwide: sources, methods and major patterns in GLOBOCAN 2012. *Int. J. Cancer* 136, E359–E386. doi: 10.1002/ijc.29210
- Gao, J., Aksoy, B. A., Dogrusoz, U., Dresdner, G., Gross, B., Sumer, S. O., et al. (2013). Integrative analysis of complex cancer genomics and clinical profiles using the cBioPortal. *Sci. Signal.* 6:1. doi: 10.1126/scisignal.2004088
- Geuna, E., Montemurro, F., Aglietta, M., and Valabrega, G. (2012). Potential of afatinib in the treatment of patients with HER2-positive breast cancer. *Breast Cancer* 4, 131–137. doi: 10.2147/BCTT.S25868
- Goldenberg, M. M. (1999). Trastuzumab, a recombinant DNA-derived humanized monoclonal antibody, a novel agent for the treatment of metastatic breast cancer. *Clin. Ther.* 21, 309–318. doi: 10.1016/S0149-2918(00)88288-0
- Gregg, R. G., Powers, P. A., and Hogan, K. (1993). Assignment of the human gene for the beta subunit of the voltage-dependent calcium channel (CACNLB1) to chromosome 17 using somatic cell hybrids and linkage mapping. *Genomics* 15, 185–187. doi: 10.1006/geno.1993.1029
- Han, S., Meng, Y., Tong, Q., Li, G., Zhang, X., Chen, Y., et al. (2014). The ErbB2-targeting antibody trastuzumab and the small-molecule SRC inhibitor saracatinib synergistically inhibit ErbB2-overexpressing gastric cancer. *mAbs* 6, 403–408. doi: 10.4161/mabs.27443
- He, C., Bian, X. Y., Ni, X. Z., Shen, D. P., Shen, Y. Y., Liu, H., et al. (2013). Correlation of human epidermal growth factor receptor 2 expression with clinicopathological characteristics and prognosis in gastric cancer. *World J. Gastroenterol.* 19, 2171–2178. doi: 10.3748/wjg.v19.i14.2171
- Hecht, J. R., Bang, Y. J., Qin, S. K., Chung, H. C., Xu, J. M., Park, J. O., et al. (2016). Lapatinib in combination with capecitabine plus oxaliplatin in human epidermal growth factor receptor 2-positive advanced or metastatic gastric. *J. Clin. Oncol.* 34, 443–451. doi: 10.1200/JCO.2015.62.6598
- Huang, Y., and Rizzo, R. C. (2012). A water-based mechanism of specificity and resistance for lapatinib with ErbB family kinases. *Biochemistry* 51, 2390–2406. doi: 10.1021/bi2016553
- Irkkan, C., Balci, S., Guler Tezel, G., Akinci, B., Yalcin, B., and Guler, G. (2017). Comparison of clinicopathologic parameters and survivals between epstein-barr virus-positive and her2-positive gastric cancers. *Appl. Immunohistochem. Mol. Morphol.* 25, 609–614. doi: 10.1097/PAL.0000000000000353
- Kim, J., Fox, C., Peng, S., Pusung, M., Pectasides, E., Matthee, E., et al. (2014). Preexisting oncogenic events impact trastuzumab sensitivity in ERBB2-amplified gastroesophageal adenocarcinoma. *J. Clin. Invest.* 124, 5145–5158. doi: 10.1172/JCI75200
- Li, S., Ma, Y. M., Zheng, P. S., and Zhang, P. (2018). GDF15 promotes the proliferation of cervical cancer cells by phosphorylating AKT1 and Erk1/2 through the receptor ErbB2. *J. Exp. Clin. Cancer Res.* 37:80. doi: 10.1186/s13046-018-0744-0
- Li, T., Wernersson, R., Hansen, R. B., Horn, H., Mercer, J., Slodkiewicz, G., et al. (2017). A scored human protein-protein interaction network to catalyze genomic interpretation. *Nat. Methods* 14, 61–64. doi: 10.1038/nmeth.4083
- Lin, N. U., Winer, E. P., Wheatley, D., Carey, L. A., Houston, S., Mendelson, D., et al. (2012). A phase II study of afatinib (BIBW 2992), an irreversible ErbB family blocker, in patients with HER2-positive metastatic breast cancer progressing after trastuzumab. *Breast Cancer Res. Treat.* 133, 1057–1065. doi: 10.1007/s10549-012-2003-y
- Mill, C. P., Zordan, M. D., Rothenberg, S. M., Settleman, J., Leary, J. F., and Riese, D. J. (2011). ErbB2 Is Necessary for ErbB4 Ligands to Stimulate Oncogenic Activities in Models of Human Breast Cancer. *Genes Cancer* 2, 792–804. doi: 10.1177/1947601911431080
- Nussberger, J., Aubert, J. F., Bouzourene, K., Pellegrin, M., Hayoz, D., and Mazzolai, L. (2008). Renin inhibition by aliskiren prevents atherosclerosis progression: comparison with irbesartan, atenolol, and amlodipine. *Hypertension* 51, 1306–1311. doi: 10.1161/HYPERTENSIONAHA.108.110932
- Ock, C. Y., Lee, K. W., Kim, J. W., Kim, J. S., Kim, T. Y., Lee, K. H., et al. (2015). Optimal patient selection for trastuzumab treatment in her2-positive advanced gastric cancer. *Clin. Cancer Res.* 21, 2520–2529. doi: 10.1158/1078-0432.CCR-14-2659
- Park, C. K., Park, J. S., Kim, H. S., Rha, S. Y., Hyung, W. J., Cheong, J. H., et al. (2016). Receptor tyrosine kinase amplified gastric cancer: clinicopathologic characteristics and proposed screening algorithm. *Oncotarget* 7, 72099–72112. doi: 10.18632/oncotarget.12291
- Paroni, G., Fratelli, M., Gardini, G., Bassano, C., Flora, M., Zanetti, A., et al. (2012). Synergistic antitumor activity of lapatinib and retinoids on a novel subtype of breast cancer with coamplification of ERBB2 and RARA. *Oncogene* 31, 3431–3443. doi: 10.1038/onc.2011.506
- Patrad, E., Niapour, A., Farassati, F., and Amani, M. (2018). Combination treatment of all-trans retinoic acid (ATRA) and gamma-secretase inhibitor (DAPT) cause growth inhibition and apoptosis induction in the human gastric cancer cell line. *Cytotechnology* 70, 865–877. doi: 10.1007/s10616-018-0199-3
- Piro, G., Carbone, C., Cataldo, I., Di Nicolantonio, F., Giacomuzzi, S., Aprile, G., et al. (2016). An FGFR3 autocrine loop sustains acquired resistance to trastuzumab in gastric cancer patients. *Clin. Cancer Res.* 22, 6164–6175. doi: 10.1158/1078-0432.CCR-16-0178
- Qian, Z., Zhu, G., Tang, L., Wang, M., Zhang, L., Fu, J., et al. (2014). Whole genome gene copy number profiling of gastric cancer identifies PAK1 and KRAS gene amplification as therapy targets. *Genes Chromosomes Cancer* 53, 883–894. doi: 10.1002/gcc.22196
- Robinson, M. D., McCarthy, D. J., and Smyth, G. K. (2010). edgeR: a bioconductor package for differential expression analysis of digital gene expression data. *Bioinformatics* 26, 139–140. doi: 10.1093/bioinformatics/btp616
- Sakamoto, G., and Mitsuyama, S. (2000). New molecule-targeting therapy with herceptin (trastuzumab), an anti-HER2 (c-erbB-2) monoclonal antibody. *Breast Cancer* 7, 350–357. doi: 10.1007/BF02966404
- Schuler, M., Awada, A., Harter, P., Canon, J. L., Possinger, K., Schmidt, M., et al. (2012). A phase II trial to assess efficacy and safety of afatinib in extensively pretreated patients with HER2-negative metastatic breast cancer. *Breast Cancer Res. Treat.* 134, 1149–1159. doi: 10.1007/s10549-012-2126-1
- Schulze, W. X., Deng, L., and Mann, M. (2005). Phosphotyrosine interactome of the ErbB-receptor kinase family. *Mol. Syst. Biol.* 1:0008. doi: 10.1038/msb4100012
- Shak, S. (1999). Overview of the trastuzumab (Herceptin) anti-HER2 monoclonal antibody clinical program in HER2-overexpressing metastatic breast cancer. Herceptin Multinational Investigator Study Group. *Semin. Oncol.* 26(4 Suppl. 12), 71–77.
- Shi, H., Zhang, W., Zhi, Q., and Jiang, M. (2016). Lapatinib resistance in HER2+ cancers: latest findings and new concepts on molecular mechanisms. *Tumour Biol.* [Epub ahead of print]. doi: 10.1007/s13277-016-5467-2
- Slater, L. M., Stupecky, M., Sweet, P., Osann, K., Eklöf, A., and Arquilla, E. R. (2001). Etoposide induction of tumor immunity in Lewis lung cancer. *Cancer Chemother. Pharmacol.* 48, 327–332. doi: 10.1007/s002800100357
- Slattery, M. L., John, E. M., Stern, M. C., Herrick, J., Lundgreen, A., Giuliano, A. R., et al. (2013). Associations with growth factor genes (FGF1, FGF2, PDGFB, FGFR2, NRG2, EGF, ERBB2) with breast cancer risk and survival: the Breast Cancer Health Disparities Study. *Breast Cancer Res. Treat.* 140, 587–601. doi: 10.1007/s10549-013-2644-5
- Sliwkowski, M. X., Schaefer, G., Akita, R. W., Lofgren, J. A., Fitzpatrick, V. D., Nuijens, A., et al. (1994). Coexpression of erbB2 and erbB3 proteins reconstitutes a high affinity receptor for heregulin. *J. Biol. Chem.* 269, 14661–14665.

- Stine, Z. E., Walton, Z. E., Altman, B. J., Hsieh, A. L., and Dang, C. V. (2015). MYC, Metabolism, and Cancer. *Cancer Discov.* 5, 1024–1039. doi: 10.1158/2159-8290.CD-15-0507
- Subramanian, A., Tamayo, P., Mootha, V. K., Mukherjee, S., Ebert, B. L., Gillette, M. A., et al. (2005). Gene set enrichment analysis: a knowledge-based approach for interpreting genome-wide expression profiles. *Proc. Natl. Acad. Sci. U.S.A.* 102, 15545–15550. doi: 10.1073/pnas.0506580102
- Sun, M., Behrens, C., Feng, L., Ozburn, N., Tang, X., Yin, G., et al. (2009). HER family receptor abnormalities in lung cancer brain metastases and corresponding primary tumors. *Clin. Cancer Res.* 15, 4829–4837. doi: 10.1158/1078-0432.CCR-08-2921
- Sun, T., Wang, C., Xing, J., and Wu, D. (2011). miR-429 modulates the expression of c-myc in human gastric carcinoma cells. *Eur. J. Cancer* 47, 2552–2559. doi: 10.1016/j.ejca.2011.05.021
- Tylki-Szymanska, A., Acuna-Hidalgo, R., Krajewska-Walasek, M., Lecka-Ambroziak, A., Stehouwer, M., Gilissen, C., et al. (2015). Thyroid hormone resistance syndrome due to mutations in the thyroid hormone receptor alpha gene (THRA). *J. Med. Genet.* 52, 312–316. doi: 10.1136/jmedgenet-2014-102936
- Uribealago, I., Benitah, S. A., and Di Croce, L. (2012). From oncogene to tumor suppressor: the dual role of Myc in leukemia. *Cell Cycle* 11, 1757–1764. doi: 10.4161/cc.19883
- Van Cutsem, E., de Haas, S., Kang, Y. K., Ohtsu, A., Tebbutt, N. C., Ming, et al. (2012). Bevacizumab in combination with chemotherapy as first-line therapy in advanced gastric cancer: a biomarker evaluation from the AVAGAST randomized phase III trial. *J. Clin. Oncol.* 30, 2119–2127. doi: 10.1200/JCO.2011.39.9824
- Wang, Y., He, L., and Cheng, Y. (2017). An independent survival prognostic role for human epidermal growth factor receptor 2 in gastric cancer: evidence from a meta-analysis. *Clin. Transl. Oncol.* 20, 212–220. doi: 10.1007/s12094-017-1711-5
- Wilke, H., Muro, K., Van Cutsem, E., Oh, S. C., Bodoky, G., Shimada, Y., et al. (2014). Ramucirumab plus paclitaxel versus placebo plus paclitaxel in patients with previously treated advanced gastric or gastro-oesophageal junction adenocarcinoma (RAINBOW): a double-blind, randomised phase 3 trial. *Lancet Oncol.* 15, 1224–1235. doi: 10.1016/S1470-2045(14)70420-6
- Yazdanparast, P., Carlsson, B., Oikarinen, A., Risteli, J., Lavin, T., and Faergemann, J. (2006). Action of topical thyroid hormone analogue, triiodothyroacetic acid in reversing glucocorticoid-induced skin atrophy in humans. *Thyroid* 16, 1157–1162. doi: 10.1089/thy.2006.16.1157
- Yu, M., Liu, T., Chen, Y., Li, Y., and Li, W. (2018). Combination therapy with protein kinase inhibitor H89 and Tetrandrine elicits enhanced synergistic antitumor efficacy. *J. Exp. Clin. Cancer Res.* 37:114. doi: 10.1186/s13046-018-0779-2
- Zhang, W., and Yu, Y. (2011). The important molecular markers on chromosome 17 and their clinical impact in breast cancer. *Int. J. Mol. Sci.* 12, 5672–5683. doi: 10.3390/ijms12095672
- Zhao, F., Pan, S., Gu, Y., Guo, S., Dai, Q., Yu, Y., et al. (2014). Small activating RNA restores the activity of the tumor suppressor HIC-1 on breast cancer. *PLoS One* 9:e86486. doi: 10.1371/journal.pone.0086486
- Zhao, F., Pan, S., Gu, Y., Guo, S., Dai, Q., Yu, Y., et al. (2015). Reactivation of HIC-1 gene by saRNA inhibits clonogenicity and invasiveness in breast cancer cells. *Oncol. Lett.* 9, 159–164. doi: 10.3892/ol.2014.2633

Conflict of Interest Statement: The authors declare that the research was conducted in the absence of any commercial or financial relationships that could be construed as a potential conflict of interest.

Copyright © 2018 Xiang, Huang, Wang, Zhang, Ji, Yan, Zhu, Cai and Yu. This is an open-access article distributed under the terms of the Creative Commons Attribution License (CC BY). The use, distribution or reproduction in other forums is permitted, provided the original author(s) and the copyright owner(s) are credited and that the original publication in this journal is cited, in accordance with accepted academic practice. No use, distribution or reproduction is permitted which does not comply with these terms.



Preoperative Changes in Hematological Markers and Predictors of Glioma Grade and Survival

Peng-Fei Wang^{1†}, Zhe Meng^{1†}, Hong-Wang Song¹, Kun Yao², Ze-Jun Duan², Chun-Jiang Yu¹, Shou-Wei Li^{1*} and Chang-Xiang Yan^{1*}

¹ Department of Neurosurgery, Sanbo Brain Hospital, Capital Medical University, Beijing, China, ² Department of Pathology, Sanbo Brain Hospital, Capital Medical University, Beijing, China

OPEN ACCESS

Edited by:

Dong-Hua Yang,
St. John's University, United States

Reviewed by:

Cristiana Tanase,
Victor Babes National Institute of
Pathology, Romania
Jennifer Totonchy,
Chapman University, United States

*Correspondence:

Shou-Wei Li
15011339604@163.com
Chang-Xiang Yan
yancx65828@sina.com

[†]These authors have contributed
equally to this work

Specialty section:

This article was submitted to
Experimental Pharmacology and Drug
Discovery,
a section of the journal
Frontiers in Pharmacology

Received: 06 June 2018

Accepted: 20 July 2018

Published: 14 August 2018

Citation:

Wang P-F, Meng Z, Song H-W, Yao K,
Duan Z-J, Yu C-J, Li S-W and Yan C-X
(2018) Preoperative Changes in
Hematological Markers and Predictors
of Glioma Grade and Survival.
Front. Pharmacol. 9:886.
doi: 10.3389/fphar.2018.00886

Background: Preoperative hematological markers that indicate nutritional, coagulation, and inflammation statuses have prognostic value for gliomas. This study aimed to investigate hematological markers with regard to tumor grades, isocitrate dehydrogenase mutations (IDH), age, and sex in patients with gliomas.

Methods: From 2008 to 2017, patients with a pathological diagnosis of glioma who underwent surgery were retrospectively enrolled in this study. Information from clinical records, including age, sex, preoperative experiment tests (routine blood tests, biochemistry, and coagulation examinations), pathological results, and IDH status, was collected. A univariable survival analysis was performed. Hematological factors such as the neutrophil-to-lymphocyte ratio (NLR), platelet-to-lymphocyte-ratio (PLR), and albumin-to-globulin (AGR) were calculated. The prognostic nutrition index (PNI) was calculated as $10 \times \text{serum albumin value (g/dl)} + 0.005 \times \text{peripheral lymphocyte count (per mm}^3\text{)}$.

Results: Our study included 706 patients. The univariate analysis showed that age, IDH-1, and hematological factors were all significantly associated with overall survival (OS) in patients with gliomas. Our results showed that inflammation markers (NLR, PLR, and fibrinogen) were positively associated with age, whereas AGR was negatively associated with age. The PLR was significantly increased, whereas the AGR and PNI were decreased in women with gliomas, as compared with men. We found that inflammation markers increased and nutrition markers decreased with gliomas grade. However, these hematological markers did not significantly differ with IDH status. NLR was the best single hematological marker for distinguishing glioblastoma (GBM) [0.684 (0.645–0.723)], IDH-wt GBM [0.672 (0.631–0.71)] from other gliomas subtypes. Combinations of age with PNI and age with AGR were the best predictors of GBM [0.750 (0.713–0.786)] and IDH-wt GBM [0.759 (0.719–0.798)], respectively.

Conclusion: Preoperative hematological marker levels vary among glioma grades and have high predictive values for GBM.

Keywords: glioma, prognostic biomarkers, grades, gender, IDH mutations

INTRODUCTION

Gliomas are the most common malignant primary tumors that originate from the central nervous systems (CNS) (Ostrom et al., 2017). According to the 2016 World Health Organization (WHO) criteria, gliomas are classified as grades I-IV, with different molecular subtypes and histopathologies (Louis et al., 2016). Glioma therapies greatly vary across the different grades and molecular subtypes (Tanase et al., 2015; Nabors et al., 2017). Designing individual therapies after identifying the glioma grade and molecular subtype is very helpful. However, the traditional way to identify the glioma grade and molecular subtype is to acquire tumor tissue by surgery or biopsy, which causes significant trauma to the human body. The disadvantages of conventional invasive methods motivate us to develop a reliable method for predicting glioma grade and survival.

Recently, mounting evidence has suggested that preoperative hematological markers related to nutrition, coagulation, and

inflammation are predictive and prognostic factors of cancers (Perisanidis et al., 2015; He J. et al., 2017; Hwang et al., 2017; Ye et al., 2018; Zhao et al., 2018). In gliomas, neutrophil-to-lymphocyte ratio (NLR) (Han et al., 2015; Lopes et al., 2018), platelet-to-lymphocyte ratio (PLR) (Han et al., 2015), fibrinogen, albumin-to-globulin ratio (AGR) (Xu W. Z. et al., 2017), and prognostic nutrition index (PNI) (He Z. Q. et al., 2017; Xu W. Z. et al., 2017) have been identified as prognostic markers. Moreover, the levels of these hematological markers vary among tumor grades, providing diagnostic value for gliomas (Schwartzbaum et al., 1999; Zadora et al., 2015; Zheng et al., 2017). However, existing studies that investigated their diagnostic values have not included all markers. Little is known about the relationship between age, sex, and the hematological factors for the prognoses of patients with gliomas.

The present study aimed to identify the tumor grade, subtype, and clinical outcome in gliomas using hematological markers. We compared the levels of these hematological markers, including NLR, PLR, fibrinogen, AGR, and PNI among patients with different glioma grades and molecular subtypes. We also performed a receiver operating characteristic curve (ROC) analysis to identify the optimal combinations for glioma diagnosis.

METHODS

Study Population

We retrospectively enrolled 706 patients with gliomas at the Sanbo Brain Hospital, from 2008 to 2017. All patients underwent surgical treatment and had a pathological diagnosis of glioma (Louis et al., 2007, 2016). Routine biochemistry and coagulation blood test results were obtained preoperatively. Patients with metabolic diseases, hematological diseases, autoimmune diseases, or current infections were excluded. Patients who were treated with glucocorticoids or anti-inflammatory drugs were also not included. IDH-1R^{132H} mutations were determined by immunohistochemistry, as described in our previous report (Wang et al., 2017). Overall survival (OS) was calculated from the date of surgery to death or censored at the final follow-up, which was in December 2017. This study was approved by the

TABLE 1 | Baseline characteristics.

Age	
Mean ± SD	45.15 ± 13.39
Median (range)	45 (7–80)
Gender	
Female	299 (42.4%)
Male	407 (57.6%)
Tumor grade	
WHO II	238 (33.7%)
WHO III	154 (21.8%)
WHO IV	314 (44.5%)
IDH-1R^{132H}	
Mutation	311 (44.1%)
Wild type	395 (55.9%)
Neutrophil (10⁹/L)	
Mean ± SD	3.83 ± 1.38
Platelet (10⁹/L)	
Mean ± SD	222.64 ± 58.90
Lymphocyte (10⁹/L)	
Mean ± SD	1.87 ± 0.62
NLR	
Mean ± SD	2.39 ± 1.71
PLR	
Mean ± SD	133.26 ± 62.44
Fibrinogen (g/l)	
Mean ± SD	2.44 ± 0.61
Albumin (g/L)	
Mean ± SD	43.03 ± 3.96
AGR	
Mean ± SD	1.87 ± 0.36
PNI	
Mean ± SD	52.37 ± 5.27

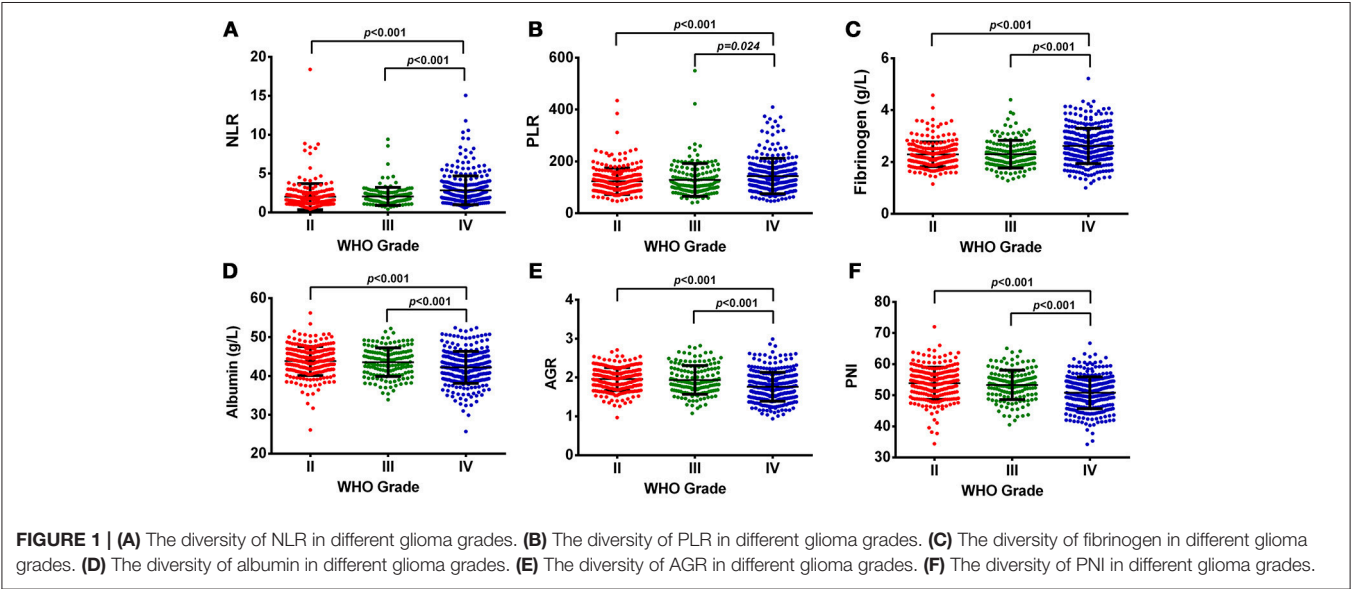
Data are n (%), unless otherwise indicated. SD, standard deviation; IDH, isocitrate dehydrogenase; NLR, neutrophil-to-lymphocyte ratio; PLR, platelet-to-lymphocyte ratio; AGR, albumin-to-globulin ratio; PNI, prognostic nutrition index.

TABLE 2 | Univariate analysis of prognostic factors.

Variable	All gliomas		GBM	
	HR (95% CI)	P	HR (95% CI)	P
Age	1.04 (1.03–1.05)	0.000	1.01 (1.00–1.03)	0.019
Gender	1.04 (0.82–1.31)	0.770	0.96 (0.72–1.28)	0.782
IDH-1R ^{132H}	3.25 (2.50–4.23)	0.000	1.75 (1.22–2.50)	0.002
NLR	0.41 (0.31–0.54)	0.000	0.57 (0.41–0.79)	0.001
PLR	0.51 (0.36–0.71)	0.000	0.69 (0.50–0.93)	0.017
Fib	0.37 (0.26–0.52)	0.000	0.59 (0.41–0.83)	0.003
Alb	1.62 (1.24–2.13)	0.000	0.46 (0.25–0.84)	0.012
AGR	2.00 (1.47–2.73)	0.000	1.51 (1.03–2.21)	0.036
PNI	1.69 (1.33–2.14)	0.000	1.73 (1.08–2.76)	0.022

TABLE 3 | The association of hematological factors with age and gender in gliomas.

Variable	All glioma					GBM				
	Age		Gender			Age		Gender		
	Correlation (<i>r</i>)	<i>P</i>	Female	Male	<i>P</i>	Correlation (<i>r</i>)	<i>P</i>	Female	Male	<i>P</i>
NLR	0.142	0.000	2.42 ± 1.88	2.37 ± 1.57	0.745	0.111	0.050	3.01 ± 2.35	2.71 ± 1.39	0.206
PLR	0.086	0.023	143.56 ± 71.23	125.70 ± 53.95	0.000	0.064	0.256	158.25 ± 81.51	133.06 ± 55.77	0.003
Fib	0.278	0.000	2.47 ± 0.61	2.41 ± 0.61	0.244	0.232	0.000	2.68 ± 0.68	2.57 ± 0.69	0.161
Alb	−0.185	0.000	42.65 ± 3.86	43.31 ± 4.02	0.029	−0.198	0.000	41.87 ± 4.13	42.39 ± 4.09	0.275
AGR	−0.264	0.000	1.79 ± 0.35	1.92 ± 0.35	0.000	−0.253	0.000	1.67 ± 0.35	1.82 ± 0.37	0.000
PNI	−0.229	0.000	51.76 ± 5.32	52.81 ± 5.19	0.009	−0.224	0.000	50.17 ± 5.51	51.19 ± 4.85	0.084



ethics committee of the Sanbo Brain Hospital, Capital Medical University.

Calculations of Hematological Markers

We calculated the hematological markers as follows: NLR = neutrophil count/lymphocyte count; PLR = platelet count/lymphocyte count; AGR = albumin/globulin; and PNI = albumin [g/L] + total lymphocyte count × 5.

Statistical Analysis

SPSS 22.0, Graph Pad Prism 6, and X-tile 3.61 were used for data analysis, drawing figures, and identifying continuous variable cutoffs, respectively. The hematological marker levels were compared across tumor grades, IDH-1 subtypes, and sexes using the student's *t*-test. The correlation of hematological markers with age was analyzed with the *spearman* test. The area under the curve (AUC) was acquired using ROC analysis, to identify the diagnostic value of prognostic factors and their combinations. A *univariate analysis* was used for the survival analysis. Statistical significance was determined as *p* < 0.05.

RESULTS

Study Characteristics

The basic clinical characteristics of the 706 patients with gliomas are shown in **Table 1**. The median patient age was 45 (7–80) years, and 42.4% (299/706) of the patients were women. There were 238 (33.7%), 154 (21.8%), and 314 (44.5%) patients with grade II, III, and IV gliomas, respectively. The IDH-1 mutation rate was 44.1% (311/706). The mean neutrophil, platelet, lymphocyte, albumin, and fibrinogen values were 3.83 ± 1.38 , 222.64 ± 58.90 , 1.87 ± 0.62 , 43.03 ± 3.96 , and 2.44 ± 0.61 , respectively. The mean NLR, PLR, AGR, and PNI were 2.39 ± 1.71 , 133.26 ± 62.44 , 1.87 ± 0.36 , and 52.37 ± 5.27 , respectively. The survival analysis showed that younger age; IDH-1 mutations; higher albumin, AGR, and PNI levels; and lower NLR, PLR, and fibrinogen levels were favorable prognostic factors of OS in all gliomas and glioblastomas (GBMs) (**Table 2**).

The Association of Hematological Markers With Age and Sex in All Gliomas and GBM

We found that nutrition-related markers, such as albumin, AGR, and PNI, were significantly negatively correlated with age in all

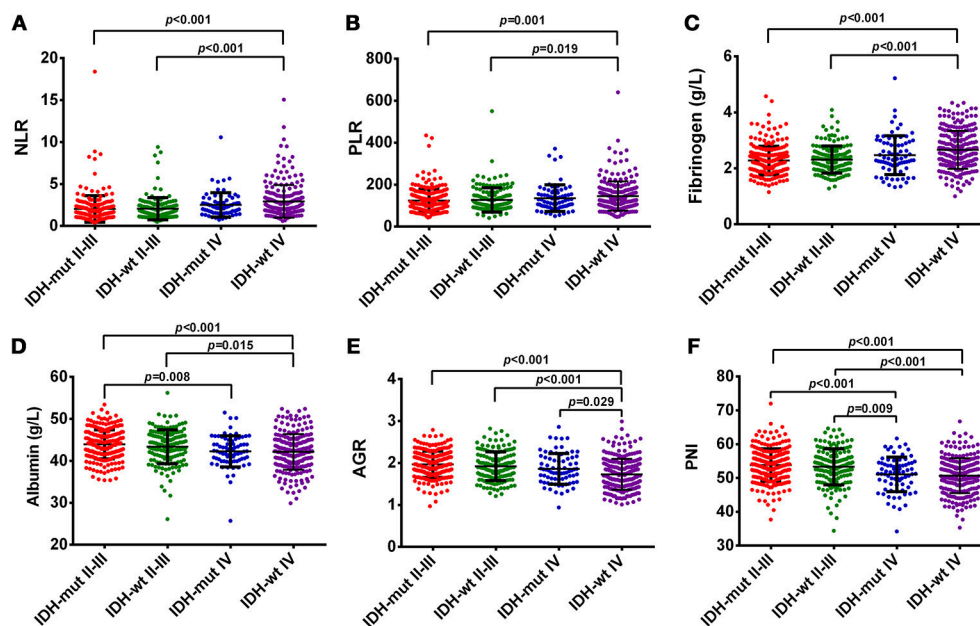


FIGURE 2 | (A) The diversity of NLR in different glioma grades and IDH-mutation status. (B) The diversity of PLR in different glioma grades and IDH-mutation status. (C) The diversity of fibrinogen in different glioma grades and IDH-mutation status. (D) The diversity of albumin in different glioma grades and IDH-mutation status. (E) The diversity of AGR in different glioma grades and IDH-mutation status. (F) The diversity of PNI in different glioma grades and IDH-mutation status.

gliomas ($p < 0.001$) and GBMs ($p < 0.001$). In contrast, a positive correlation was observed with age and NLR ($p < 0.001$), PLR ($p = 0.023$), and fibrinogens ($p < 0.001$) in all gliomas. Although fibrinogen ($p < 0.001$) positively correlated with age, a non-statistically significant association was found between age and NLR ($p = 0.050$) and PLR ($p = 0.256$) in GBMs. These results indicate generally poor nutrition and severe inflammation states in elderly patients with gliomas (Table 3).

Increased levels of albumin (43.31 ± 4.02 vs. 42.65 ± 3.86 , $p = 0.029$), AGR (1.92 ± 0.35 vs. 1.79 ± 0.35 , $p = 0.000$), and PNI (52.81 ± 5.19 vs. 51.76 ± 5.32 , $p = 0.009$) were found in men, in contrast to women with gliomas. However, only one nutrition marker, AGR, was higher in men than in women with GBMs (1.82 ± 0.37 vs. 1.67 ± 0.35 , $p = 0.000$). PLRs significantly decreased in men in both all glioma (143.56 ± 71.23 vs. 125.70 ± 53.95 , $p = 0.000$) and GBM (158.25 ± 81.51 vs. 133.06 ± 55.77 , $p = 0.003$; Table 3) cohorts.

Hematological Marker Levels Vary Among Glioma Grades and Molecular Subtypes

In our study, OS was negatively correlated with glioma grades ($p < 0.001$, Supplementary Figure 1A). Increased levels of NLR, PLR, and fibrinogen were noted in GBMs, compared with Grade II and III gliomas (Figure 1). The levels of albumin, AGR, and PNI significantly decreased in GBMs, in contrast to Grade III and II gliomas (Figure 1). Next, we classified gliomas based on IDH-1^{R132H} status as follows: IDH-mut II-III, IDH-wt II-III, IDH-mut GBM, and IDH-wt GBM. OS significantly differed among the four groups ($p < 0.001$, Supplementary Figure 1B). Inflammatory markers such as NLR, PLR, and fibrinogen were

elevated in IDH-wt GBM, compared with II-III gliomas with or without IDH mutation. However, the levels of nutrition markers varied among the four subtypes (Figure 2). The worst nutritional status was observed in IDH-wt GBM, followed by that of IDH-mut GBM (Figure 2).

The Diagnostic Value of Hematological Markers in Predicting Glioma Grade and Subtype

First, we used one marker to predict GBMs and IDH-1 wt subtype (Table 4). The ROC curve analysis showed that NLR had the highest diagnostic value for distinguishing GBM from grade II to III [0.684 (0.645–0.723), Figure 3A] and predicting the GBM IDH-1 wt molecular subtype [0.672 (0.631–0.71), Figure 3B]. Next, we investigated whether we could increase the diagnostic value by combining these hematological markers (Table 4). We found that the combination of age and PNI was best suited for predicting the diagnosis of GBMs [0.750 (0.713–0.786)] (Figure 3C). Furthermore, the combination of age and AGR had the highest AUC for distinguishing GBM IDH-1 wt from other subtypes [0.759 (0.719–0.798), Figure 3D].

DISCUSSION

Our study shows that the prognostic value of hematological markers and their levels vary among glioma grades and molecular subtypes. Moreover, patient age, sex, and hematological markers were strongly associated. These results indicate different inflammation and nutritional states, with regard to patient

TABLE 4 | The diagnostic value of hematological markers in predicting glioma grade and subtype.

Marker	AUC (95% CI)	
	GBM	IDH – wt GBM
NLR	0.684 (0.645–0.723)	0.672 (0.631–0.714)
PLR	0.590 (0.547–0.632)	0.594 (0.550–0.638)
Fib	0.652 (0.611–0.693)	0.660 (0.616–0.703)
Alb	0.618 (0.576–0.660)	0.602 (0.557–0.647)
AGR	0.659 (0.619–0.700)	0.670 (0.627–0.713)
PNI	0.661 (0.621–0.701)	0.645 (0.602–0.688)
Age + NLR	0.745 (0.708–0.782)	0.753 (0.713–0.793)
Age + PLR	0.727 (0.689–0.765)	0.742 (0.701–0.783)
Age + Fib	0.733 (0.695–0.771)	0.746 (0.705–0.786)
Age + Alb	0.733 (0.695–0.770)	0.742 (0.702–0.783)
Age + AGR	0.738 (0.701–0.776)	0.759 (0.719–0.798)
Age + PNI	0.750 (0.713–0.786)	0.753 (0.713–0.793)
NLR + PLR	0.680 (0.641–0.720)	0.666 (0.623–0.708)
NLR + Fib	0.689 (0.649–0.729)	0.688 (0.645–0.730)
NLR + Alb	0.699 (0.661–0.738)	0.688 (0.647–0.730)
NLR + AGR	0.712 (0.672–0.751)	0.711 (0.669–0.753)
NLR + PNI	0.692 (0.653–0.731)	0.683 (0.641–0.724)
PLR + Fib	0.665 (0.624–0.706)	0.673 (0.630–0.717)
PLR + Alb	0.647 (0.606–0.688)	0.639 (0.595–0.682)
PLR + AGR	0.676 (0.635–0.716)	0.685 (0.643–0.727)
PLR + PNI	0.662 (0.622–0.702)	0.650 (0.607–0.692)
Fib + Alb	0.678 (0.638–0.718)	0.670 (0.627–0.713)
Fib + AGR	0.681 (0.641–0.721)	0.694 (0.652–0.736)
Fib + PNI	0.704 (0.665–0.743)	0.693 (0.651–0.735)
Alb + AGR	0.664 (0.623–0.704)	0.671 (0.628–0.714)
Alb + PNI	0.660 (0.620–0.700)	0.646 (0.604–0.689)
AGR + PNI	0.690 (0.650–0.729)	0.689 (0.647–0.731)

age, sex, tumor grade, and genetic alternations. Furthermore, we combined these prognostic factors to predict glioma classification.

This study shows that NLR, PLR, and fibrinogens were positively correlated with glioma grade, whereas PNI and AGR were negatively correlated with glioma grade. In addition, previous studies observed higher NLRs (Zadora et al., 2015) and lower PNIs in higher grade gliomas (He Z. Q. et al., 2017). These results indicate that patients with higher grade gliomas have more severe inflammation and poorer nutritional statuses. NLR and PLR hematological markers were not associated with IDH mutations in this study, which is consistent with our previous report (Wang et al., 2017). However, immune responses in the tumor microenvironment are more significantly regulated by IDH mutations in lower grade gliomas (Qian et al., 2018). This result might be due to differences between systemic and local inflammation and immune regulation.

We found that inflammation markers were positively correlated with age in patients with gliomas or GBM. These results explain why older age is a negative prognostic factor in gliomas, as a result of inflammation status. Furthermore, we

observed different hematological marker levels between women and men, and specifically, albumin was higher in men than in women. Consistent with data from other studies (Zhou et al., 2016), we observed that PNI was higher in men than women. We found that PLR was higher in women than in men, both in gliomas and GBMs, which was contrary to Xu et al.'s report (Xu W. et al., 2017). There were no survival differences with regard to sex, and this finding might be influenced by NLR and fibrinogens, which showed no differences with respect to sex.

We observed that NLR was the best single predictive marker for distinguishing GBM and IDH-wt GBM from other types of gliomas. Our results are consistent with the finding that NLR was able to predict the diagnosis of glioma from acoustic neuroma, meningioma, and non-lesional epilepsy (Zheng et al., 2017). Our study showed that the best combinations for predicting the diagnosis of GBM or IDH-wt GBM were age + PNI and age + AGR; however, NLR + LMR had the highest diagnostic accuracy. It should be noted that grade I gliomas were included in a previous study (Zheng et al., 2017), and more studies are needed to confirm and optimize the prognostic factor combinations.

The mechanisms underlying the associations between hematological markers and glioma grades were not very clear. The tumor-infiltrating neutrophil count was positively correlated with glioma grade, by promoting the progression of glioma (Fossati et al., 1999; Liang et al., 2014). Moreover, Fossati et al. observed that circulating neutrophils were positively associated with glioma grade, which was influenced by glioma-derived factors that may impact neutrophil circulation and infiltration (Fossati et al., 1999). Neutrophil-induced immunosuppression and angiogenesis in gliomas have also been found to promote glioma progression (Massara et al., 2017). The circulating fibrinogen could activate neutrophils via integrin $\alpha_M\beta_2$ (Steinbrecher et al., 2010; Massara et al., 2017). Natural killer cell function has also been found to be negatively affected by fibrinogen, which suppresses anti-tumor immunity (Degen and Palumbo, 2012). Albumin, AGR, and PNI are all associated with nutritional status in patients with cancer. Albumin also reflects the systemic inflammation status, as it is downregulated by tumor necrosis factor alpha (TNF α) and interleukin 6 (IL-6) (Chojkier, 2005). Furthermore, TNF α and IL-6 could negatively affect the function of immune cells in GBMs (Kozłowska et al., 2016).

This study has several limitations. First, as our study had a retrospective design, some unavoidable biases may exist. Second, we did not continuously monitor various prognostic factors. Furthermore, we only investigated the changes of blood indices and did not study the differences of tumor immune microenvironments. Therefore, prospective multicenter studies, continuous perioperative monitoring, and further molecular biology experiments are needed. Furthermore, previous reports indicated that hematological markers could effectively distinguish gliomas from non-lesional epilepsy, acoustic neuroma, and meningioma (Zheng et al., 2017). However, the present study focused on the correlation between hematological markers and tumor grade, molecular subtype, and

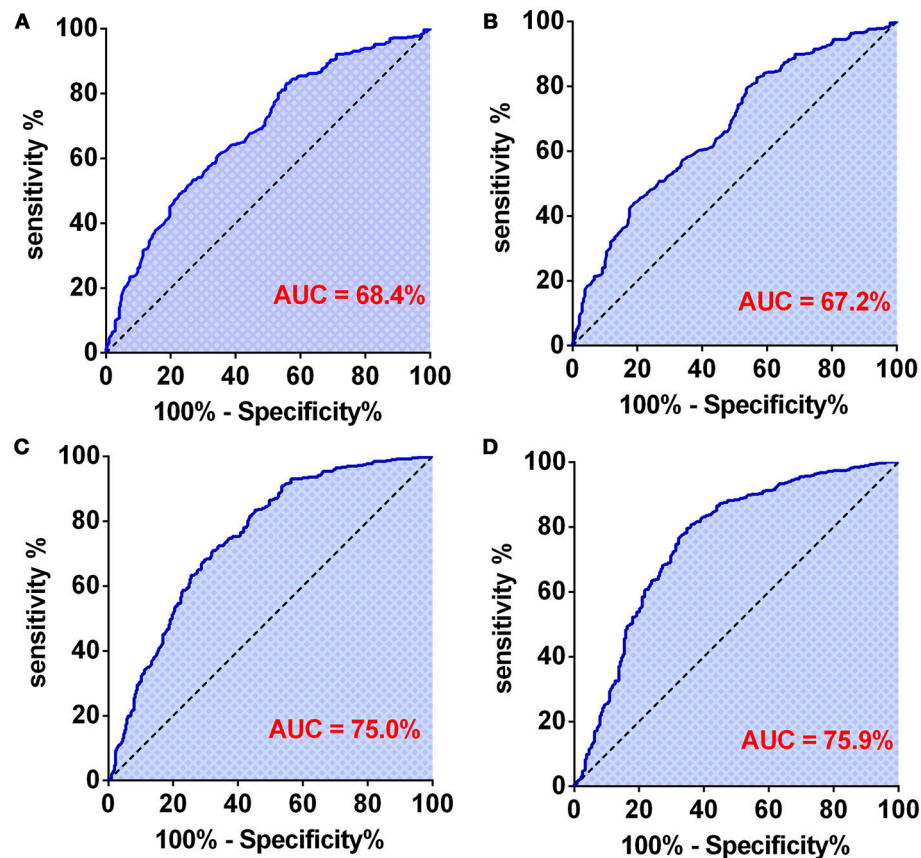


FIGURE 3 | (A) The diagnostic value of preoperative NLR in patients with GBM. (B) The diagnostic value of preoperative NLR in patients with grade IV-IDH wild type. (C) The diagnostic value of preoperative age + PNI combination in patients with GBM. (D) The diagnostic value of preoperative age + AGR combination in patients with grade IV-IDH wild type.

clinical outcomes in glioma. Therefore, we did not investigate the hematological markers in other neuropathological states.

In conclusion, our study proves that there are different prognostic factors among glioma grades and molecular subtypes, and NLR was the best single marker to distinguish GBM and IDH-wt GBM. The combinations of age with PNI and age with AGR could best diagnose IDH-wt GBM. These prognostic factors correlate with age and sex in patients with gliomas.

AUTHOR CONTRIBUTIONS

C-XY and S-WL: conception and design; P-FW, ZM, and H-WS: collection and follow-up; P-FW and ZM: data analysis and interpretation. All authors manuscript writing, final approval of manuscript, and accountable for all aspects of the work.

REFERENCES

Chojkier, M. (2005). Inhibition of albumin synthesis in chronic diseases: molecular mechanisms. *J. Clin. Gastroenterol.* 39, S143–S146. doi: 10.1097/01.mcg.0000155514.17715.39

FUNDING

This work was supported by grants from the National Key Technology Research and Development Program of the Ministry of Science and Technology of China (No. 2014BAI04B01) and the Natural Science Foundation of Beijing (No. 7182076).

SUPPLEMENTARY MATERIAL

The Supplementary Material for this article can be found online at: <https://www.frontiersin.org/articles/10.3389/fphar.2018.00886/full#supplementary-material>

Supplementary Figure 1 | (A) Kaplan-Meier survival curves of glioma patients in grade II ($n = 238$), III ($n = 154$), IV ($n = 314$), have significant value ($p < 0.001$). (B) Kaplan-Meier survival curves of glioma patients in IDH-1^{R132H}-mutant II-III ($n = 236$), IDH-1^{R132H}-wild type II-III ($n = 156$), IDH-1^{R132H}-mutant IV ($n = 75$), IDH-1^{R132H}-wild type ($n = 239$) have significant value ($p < 0.001$).

Degen, J. L., and Palumbo, J. S. (2012). Hemostatic factors, innate immunity and malignancy. *Thromb. Res.* 129(Suppl. 1), S1–S5. doi: 10.1016/S0049-3848(12)70143-3

Fossati, G., Ricevuti, G., Edwards, S. W., Walker, C., Dalton, A., and Rossi, M. L. (1999). Neutrophil infiltration into human

- gliomas. *Acta Neuropathol.* 98, 349–354. doi: 10.1007/s004010051093
- Han, S., Liu, Y., Li, Q., Li, Z., Hou, H., and Wu, A. (2015). Pre-treatment neutrophil-to-lymphocyte ratio is associated with neutrophil and T-cell infiltration and predicts clinical outcome in patients with glioblastoma. *BMC Cancer* 15:617. doi: 10.1186/s12885-015-1629-7
- He, J., Pan, H., Liang, W., Xiao, D., Chen, X., Guo, M., et al. (2017). Prognostic effect of albumin-to-globulin ratio in patients with solid tumors: a systematic review and meta-analysis. *J. Cancer* 8, 4002–4010. doi: 10.7150/jca.21141
- He, Z. Q., Ke, C., Al-Nahari, F., Duan, H., Guo, C. C., Wang, Y., et al. (2017). Low preoperative prognostic nutritional index predicts poor survival in patients with newly diagnosed high-grade gliomas. *J. Neurooncol.* 132, 239–247. doi: 10.1007/s11060-016-2361-0
- Hwang, K. T., Chung, J. K., Roh, E. Y., Kim, J., Oh, S., Kim, Y. A., et al. (2017). prognostic influence of preoperative fibrinogen to albumin ratio for breast cancer. *J. Breast Cancer* 20, 254–263. doi: 10.4048/jbc.2017.20.3.254
- Kozłowska, A. K., Tseng, H. C., Kaur, K., Topchyan, P., Inagaki, A., Bui, V. T., et al. (2016). Resistance to cytotoxicity and sustained release of interleukin-6 and interleukin-8 in the presence of decreased interferon-gamma after differentiation of glioblastoma by human natural killer cells. *Cancer Immunol. Immunother.* 65, 1085–1097. doi: 10.1007/s00262-016-1866-x
- Liang, J., Piao, Y., Holmes, L., Fuller, G. N., Henry, V., Tiao, N., et al. (2014). Neutrophils promote the malignant glioma phenotype through S100A4. *Clin. Cancer Res.* 20, 187–198. doi: 10.1158/1078-0432.CCR-13-1279
- Lopes, M., Carvalho, B., Vaz, R., and Linhares, P. (2018). Influence of neutrophil-lymphocyte ratio in prognosis of glioblastoma multiforme. *J. Neurooncol.* 136, 173–180. doi: 10.1007/s11060-017-2641-3
- Louis, D. N., Ohgaki, H., Wiestler, O. D., Cavenee, W. K., Burger, P. C., Jouvett, A., et al. (2007). The 2007 WHO classification of tumours of the central nervous system. *Acta Neuropathol.* 114, 97–109. doi: 10.1007/s00401-007-0243-4
- Louis, D. N., Perry, A., Reifenberger, G., von Deimling, A., Figarella-Branger, D., Cavenee, W. K., et al. (2016). The 2016 World Health Organization classification of tumors of the central nervous system: a summary. *Acta Neuropathol.* 131, 803–820. doi: 10.1007/s00401-016-1545-1
- Massara, M., Persico, P., Bonavita, O., Mollica Poeta, V., Locati, M., Simonelli, M., et al. (2017). Neutrophils in Gliomas. *Front. Immunol.* 8:1349. doi: 10.3389/fimmu.2017.01349
- Nabors, L. B., Portnow, J., Ammirati, M., Baehring, J., Brem, H., Butowski, N., et al. (2017). NCCN guidelines insights: central nervous system cancers, version 1.2017. *J. Natl. Compr. Canc. Netw.* 15, 1331–1345. doi: 10.6004/jnccn.2017.0166
- Ostrom, Q. T., Gittleman, H., Liao, P., Vecchione-Koval, T., Wolinsky, Y., Kruchko, C., et al. (2017). CBTRUS Statistical report: primary brain and other central nervous system tumors diagnosed in the United States in 2010–2014. *Neuro Oncol.* 19, v1–v88. doi: 10.1093/neuonc/nox158
- Perisanidis, C., Psyrri, A., Cohen, E. E., Engelmann, J., Heinze, G., Perisanidis, B., et al. (2015). Prognostic role of pretreatment plasma fibrinogen in patients with solid tumors: a systematic review and meta-analysis. *Cancer Treat. Rev.* 41, 960–970. doi: 10.1016/j.ctrv.2015.10.002
- Qian, Z., Li, Y., Fan, X., Zhang, C., Wang, Y., Jiang, T., et al. (2018). Molecular and clinical characterization of IDH associated immune signature in lower-grade gliomas. *Oncoimmunology* 7:e1434466. doi: 10.1080/2162402X.2018.1434466
- Schwartzbaum, J. A., Lal, P., Evanoff, W., Mamrak, S., Yates, A., Barnett, G. H., et al. (1999). Presurgical serum albumin levels predict survival time from glioblastoma multiforme. *J. Neurooncol.* 43, 35–41. doi: 10.1023/A:1006269413998
- Steinbrecher, K. A., Horowitz, N. A., Blevins, E. A., Barney, K. A., Shaw, M. A., Harmel-Laws, E., et al. (2010). Colitis-associated cancer is dependent on the interplay between the hemostatic and inflammatory systems and supported by integrin alpha(M)beta(2) engagement of fibrinogen. *Cancer Res.* 70, 2634–2643. doi: 10.1158/0008-5472.CAN-09-3465
- Tanase, C., Albulescu, R., Codrici, E., Popescu, I. D., Mihai, S., Enciu, A. M., et al. (2015). Circulating biomarker panels for targeted therapy in brain tumors. *Future Oncol.* 11, 511–524. doi: 10.2217/fon.14.238
- Wang, P. F., Song, H. W., Cai, H. Q., Kong, L. W., Yao, K., Jiang, T., et al. (2017). Preoperative inflammation markers and IDH mutation status predict glioblastoma patient survival. *Oncotarget* 8, 50117–50123. doi: 10.18632/oncotarget.15235
- Xu, W. Z., Li, F., Xu, Z. K., Chen, X., Sun, B., Cao, J. W., et al. (2017). Preoperative albumin-to-globulin ratio and prognostic nutrition index predict prognosis for glioblastoma. *Oncotargets Ther.* 10, 725–733. doi: 10.2147/OTT.S127441
- Xu, W., Wang, D., Zheng, X., Ou, Q., and Huang, L. (2017). Sex-dependent association of preoperative hematologic markers with glioma grade and progression. *J. Neurooncol.* 137, 279–287. doi: 10.1007/s11060-017-2714-3
- Ye, L. L., Oei, R. W., Kong, F. F., Du, C. R., Zhai, R. P., Ji, Q. H., et al. (2018). The prognostic value of preoperative prognostic nutritional index in patients with hypopharyngeal squamous cell carcinoma: a retrospective study. *J. Transl. Med.* 16:12. doi: 10.1186/s12967-018-1391-0
- Zadora, P., Dabrowski, W., Czarko, K., Smolen, A., Kotlinska-Hasic, E., Wiorkowski, K., et al. (2015). Preoperative neutrophil-lymphocyte count ratio helps predict the grade of glial tumor - a pilot study. *Neurol. Neurochir. Pol.* 49, 41–44. doi: 10.1016/j.pjnns.2014.12.006
- Zhao, Z., Zhao, X., Lu, J., Xue, J., Liu, P., and Mao, H. (2018). Prognostic roles of neutrophil to lymphocyte ratio and platelet to lymphocyte ratio in ovarian cancer: a meta-analysis of retrospective studies. *Arch. Gynecol. Obstet.* 297, 849–857. doi: 10.1007/s00404-018-4678-8
- Zheng, S. H., Huang, J. L., Chen, M., Wang, B. L., Ou, Q. S., and Huang, S. Y. (2017). Diagnostic value of preoperative inflammatory markers in patients with glioma: a multicenter cohort study. *J. Neurosurg.* 3, 1–10. doi: 10.3171/2017.3.JNS161648
- Zhou, X. W., Dong, H., Yang, Y., Luo, J. W., Wang, X., Liu, Y. H., et al. (2016). Significance of the prognostic nutritional index in patients with glioblastoma: a retrospective study. *Clin. Neurol. Neurosurg.* 151, 86–91. doi: 10.1016/j.clineuro.2016.10.014

Conflict of Interest Statement: The authors declare that the research was conducted in the absence of any commercial or financial relationships that could be construed as a potential conflict of interest.

Copyright © 2018 Wang, Meng, Song, Yao, Duan, Yu, Li and Yan. This is an open-access article distributed under the terms of the Creative Commons Attribution License (CC BY). The use, distribution or reproduction in other forums is permitted, provided the original author(s) and the copyright owner(s) are credited and that the original publication in this journal is cited, in accordance with accepted academic practice. No use, distribution or reproduction is permitted which does not comply with these terms.



MMP-9 as a Candidate Marker of Response to BRAF Inhibitors in Melanoma Patients With $BRAF^{V600E}$ Mutation Detected in Circulating-Free DNA

Rossella Salemi^{1†}, Luca Falzone^{1†}, Gabriele Madonna², Jerry Polesel³, Diana Cinà⁴, Domenico Mallardo², Paolo A. Ascierto², Massimo Libra^{1,5*} and Saverio Candido^{1,5}

OPEN ACCESS

Edited by:

Dong-Hua Yang,
St. John's University, United States

Reviewed by:

Flavio Rizzolio,
Università Ca' Foscari, Italy
Aristidis M. Tsatsakis,
University of Crete, Greece

*Correspondence:

Massimo Libra
mlibra@unict.it;
m.libra@unict.it

[†]These authors have contributed
equally to this work

[‡]These authors share first authorship

Specialty section:

This article was submitted to
Experimental Pharmacology
and Drug Discovery,
a section of the journal
Frontiers in Pharmacology

Received: 21 June 2018

Accepted: 16 July 2018

Published: 14 August 2018

Citation:

Salemi R, Falzone L, Madonna G,
Polesel J, Cinà D, Mallardo D,
Ascierto PA, Libra M and Candido S
(2018) MMP-9 as a Candidate Marker
of Response to BRAF Inhibitors
in Melanoma Patients With $BRAF^{V600E}$
Mutation Detected in Circulating-Free
DNA. *Front. Pharmacol.* 9:856.
doi: 10.3389/fphar.2018.00856

¹ Department of Biomedical and Biotechnological Sciences, University of Catania, Catania, Italy, ² Unit of Melanoma, Cancer Immunotherapy and Innovative Therapy, Istituto Nazionale Tumori "Fondazione G. Pascale", Naples, Italy, ³ Unit of Cancer Epidemiology, Aviano National Cancer Institute, IRCCS, Aviano, Italy, ⁴ Clinical Pathology Unit, Garibaldi Hospital, Catania, Italy, ⁵ Research Center for Prevention, Diagnosis and Treatment of Cancer, University of Catania, Catania, Italy

The $BRAF^{V600E}$ mutation is associated with melanoma development and its detection in circulating-free DNA cannot be observed in all melanoma patients harboring this mutation in tumor specimens. Beside the circulating-free DNA $BRAF^{V600E}$ mutation, other markers of therapeutic response should be identified. Matrix metalloproteinase-9 (MMP-9) could be one of them as its role as indicator of invasiveness in melanoma have been explored. In this study, MMP-9 was evaluated in melanoma cells after treatment with dabrafenib. *In vitro* data were validated in 26 melanoma patients, of which 14 treated with BRAF inhibitor alone and 12 treated with both BRAF and MEK inhibitors, by ELISA assay and droplet digital PCR for measuring MMP-9 serum levels and circulating-free DNA $BRAF^{V600E}$ mutation, respectively. Statistical analyses were performed to evaluate the prognostic significance of MMP-9, progression-free survival (PFS) and overall survival (OS) according to the $BRAF^{V600E}$ mutation and MMP-9 levels. The performed analyses showed that MMP-9 and pEK1-2 were statistically down-regulated in melanoma cells after treatment with dabrafenib. Circulating-free DNA $BRAF^{V600E}$ mutation was detected in 11 out of 26 melanoma patients showing higher levels of MMP-9 compared to those with undetectable $BRAF^{V600E}$ mutation. Furthermore, higher levels of MMP-9 and circulating-free DNA $BRAF^{V600E}$ mutation were associated with lower PFS and OS. Finally, the monitoring of therapy showed that MMP-9 significantly decreased at T1 and T2, but not at T-last, for the patients with detectable circulating-free DNA $BRAF^{V600E}$ mutation. In conclusion, high levels of MMP-9 and circulating-free DNA $BRAF^{V600E}$ mutation are associated with poor PFS and OS. MMP-9 may represent a promising indicator of response to BRAF inhibitors in combination with the detection of $BRAF^{V600E}$ mutation.

Keywords: $BRAF^{V600E}$, MMP-9, circulating-free DNA, biomarker, droplet digital PCR, liquid biopsy

INTRODUCTION

In the last decade, the treatment of melanoma has been revolutionized by the introduction in the therapy of several pharmacological molecules. In particular, with the recent introduction of the immune checkpoint inhibitors and the new selective tyrosine kinase inhibitors, including BRAF and MEK inhibitors, there has been a significant improvement in the progression-free survival (PFS) and overall survival (OS) of patients with melanoma (Spagnolo et al., 2016; Ugurel et al., 2017). Despite these promising results, a part of patients develops pharmacological resistance significantly reducing the effectiveness to these treatments (Sandri et al., 2016; Kalal et al., 2017). Several studies showed a very high mortality rate for cutaneous melanoma ranging from 2.17 to 2.7 per 100,000 persons (McCourt et al., 2014; Tejera-Vaquerizo et al., 2016; Brunssen et al., 2017). This high mortality rate is mainly linked to the aggressiveness of cutaneous melanomas (Mathieu et al., 2012), to the development of drug resistance (Lim et al., 2017) and to their high invasive and metastatic powers (Aladowicz et al., 2013).

It was demonstrated that CM invasiveness is mainly due to the over-expression of several proteases, including matrix

metalloproteinases (MMPs) (Hofmann et al., 2000; Saladi et al., 2010; Sandri et al., 2016). In particular, a fundamental role is played by Matrix Metalloproteinase 9 (MMP-9) that promoted melanoma invasiveness and spreading via the degradation of several components of the extracellular matrix (Lu et al., 2011; Tang et al., 2013; Shi et al., 2014; Guarneri et al., 2017). Of note, the MMP-9 expression is regulated by several molecular pathways (Gordon et al., 2009; Wu et al., 2015) and its over-expression is associated to epigenetic events (Falzone et al., 2016b) and to the aberrant activation of the Ras-Raf-MEK-ERK, MAPK and PI3K/PTEN/AKT/mTOR signaling pathways (Dange et al., 2015; Shi et al., 2015). In addition, the MMP-9 expression is also regulated by several miRNAs (Falzone et al., 2016a; Yang et al., 2017).

Several point mutations affect key genes involved in the regulation of these pathways altering the cellular homeostasis resulting in cell proliferation, apoptosis prevention and tumor invasion (Zhang et al., 2016; Liu et al., 2017). Among these point mutations, *BRAF*^{V600E} represents the most frequent alteration observed in melanoma (Forbes et al., 2017) and many scientific evidences suggest that *BRAF*^{V600E} mutation is associated with the over-expression of MMP-9 in several tumor types, including melanoma (Mesa et al., 2006; Frasca et al., 2008; Guarneri et al., 2017). Other mutations may occur in

TABLE 1 | Distribution of 28 patients with melanoma according to socio-demographic and clinical characteristics.

	All		Cancer progression				Vital status			
			No		Yes		Alive		Dead	
	<i>n</i>	(%)	<i>n</i>	(%)	<i>n</i>	(%)	<i>n</i>	(%)	<i>n</i>	(%)
Sex										
Man	14	(50.0)	2	(40.0)	12	(52.2)	4	(44.4)	10	(52.6)
Woman	14	(50.0)	3	(60.0)	11	(47.8)	5	(55.6)	9	(47.4)
Fisher test			<i>p</i> = 1.000				<i>p</i> = 1.000			
Age at treatment initiation (years)										
<45	11	(39.3)	2	(40.0)	9	(39.1)	5	(55.6)	6	(31.6)
45–59	10	(35.7)	1	(20.0)	9	(39.1)	1	(11.1)	9	(47.4)
≥60	7	(25.0)	2	(40.0)	5	(21.7)	3	(33.3)	4	(21.1)
Fisher test			<i>p</i> = 0.824				<i>p</i> = 0.195			
Melanoma type										
S.P.I.	6	(21.4)	1	(20.0)	5	(21.7)	2	(22.2)	4	(21.1)
Cutaneous	22	(78.6)	4	(80.0)	18	(78.3)	7	(77.8)	15	(79.0)
Fisher test			<i>p</i> = 1.000				<i>p</i> = 1.000			
Stage										
M1a	7	(25.9)	2	(20.0)	5	(22.7)	2	(22.2)	5	(27.8)
M1b	4	(14.8)	1	(10.0)	3	(13.6)	2	(22.2)	2	(11.1)
M1c	16	(59.3)	2	(20.0)	14	(63.6)	5	(55.6)	11	(61.1)
Fisher test			<i>p</i> = 0.502				<i>p</i> = 0.726			
Therapy										
Monotherapy	15	(57.7)	1	(20.0)	14	(60.9)	4	(44.4)	11	(57.9)
Combo	13	(42.3)	4	(80.0)	9	(39.1)	5	(55.6)	8	(42.1)
Fisher test			<i>p</i> = 0.153				<i>p</i> = 0.689			
LDH										
<480	17	(80.0)	4	(80.0)	13	(56.5)	6	(66.7)	11	(57.9)
≥480	11	(20.0)	1	(20.0)	10	(43.5)	3	(33.3)	8	(42.1)
Fisher test			<i>p</i> = 0.620				<i>p</i> = 1.000			

NRAS, TERT, PTEN and, less frequently, PIK3CA (Zhang et al., 2016).

The identification of these mutated genes allowed to develop new therapeutic approaches using selective inhibitors for such altered proteins. Promising results were achieved by the treatment with BRAF inhibitors alone or in combination with MEK inhibitors (Chen et al., 2017; Russo et al., 2017). However, the identification of effective biomarker of therapeutic response is still lacking (Masucci et al., 2017; Branca et al., 2018; Ross et al., 2018; Veenstra et al., 2018).

It has been demonstrated that circulating-free DNA analysis allows to characterize the molecular features of tumors. The analysis of circulating-free DNA may be used to identify directly in serum or plasma *BRAF*^{V600E} mutated clones and establish the efficacy of the treatments and the tumor aggressiveness (Schreuer et al., 2016; Herbreteau et al., 2017; Quéreux et al., 2017).

However, the reduction of circulating-free DNA *BRAF*^{V600E} mutated clones, followed by the treatment with BRAF inhibitors, was not directly associated with clinical efficacy (Ascierto et al., 2013; Schreuer et al., 2016). Therefore, there is a need to identify new markers that can be associated with the MAPK pathway modulation as consequence of BRAF inhibitors treatment. Among these, MMP-9 may be a right marker candidate easily detected in the peripheral blood samples from melanoma patients. Moreover, MMP-9 was demonstrated to be a marker of aggressiveness in several tumors, including melanoma (Falzone et al., 2016b; Zhang et al., 2016); while, its role as an indicator of therapeutic response was not fully investigated yet.

On these bases, in the present study functional experiments were performed using melanoma cell models to confirm the correlation between MMP-9 expression and MAPK pathway

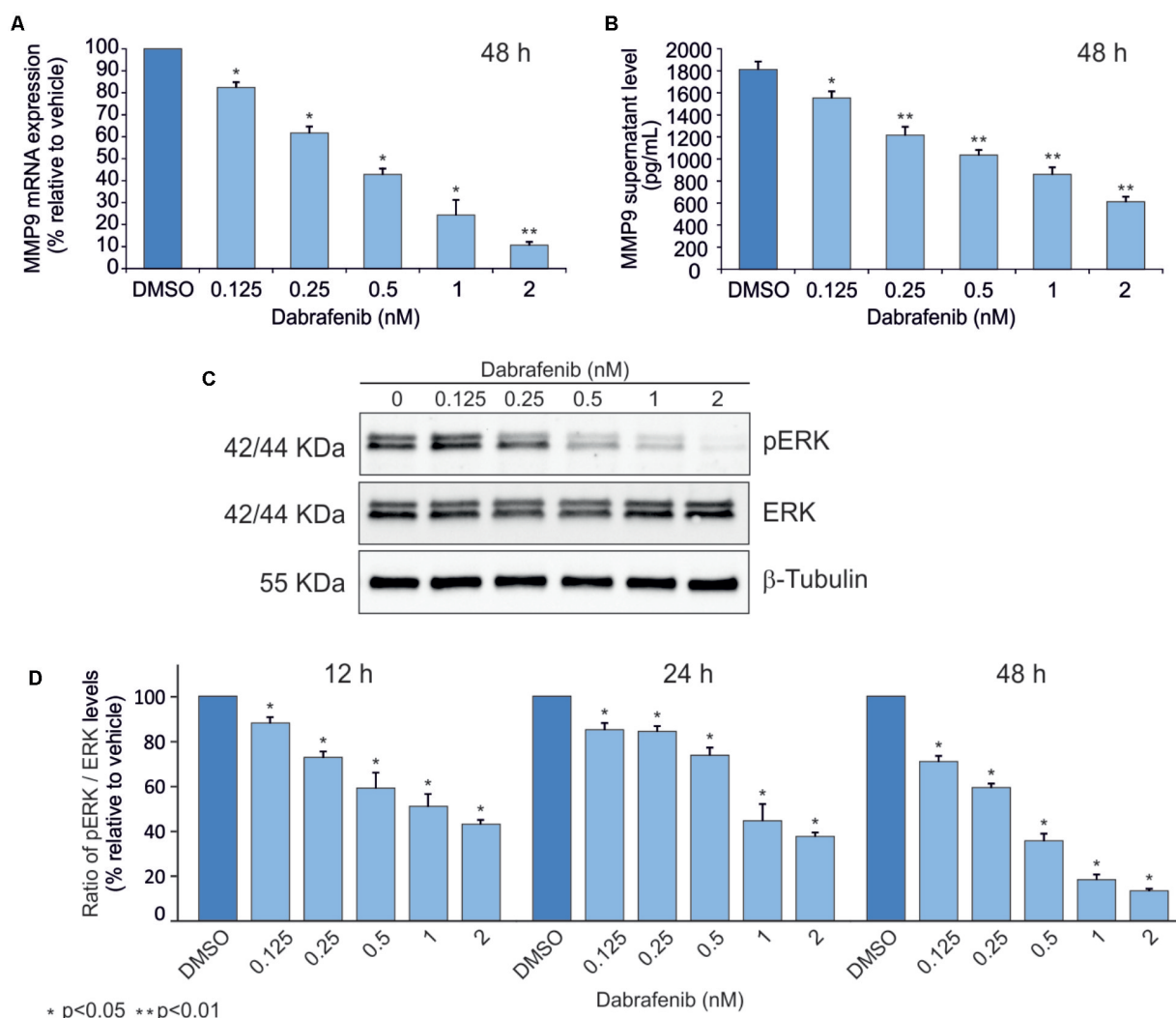


FIGURE 1 | Dabrafenib treatment of A375 cell line. MMP-9 expression levels were evaluated by qPCR (A) and ELISA Assay (B) in A375 cell line treated with increasing doses of dabrafenib (0.125, 0.25, 0.5, 1, and 2 nM) for 48 h. pERK and total ERK protein levels were evaluated by Western blot analysis after treatment with dabrafenib for 12, 24, and 48 h (C,D). The statistical significance of the two-tailed Student's *t*-test was referred to the control. * $p < 0.05$; ** $p < 0.01$.

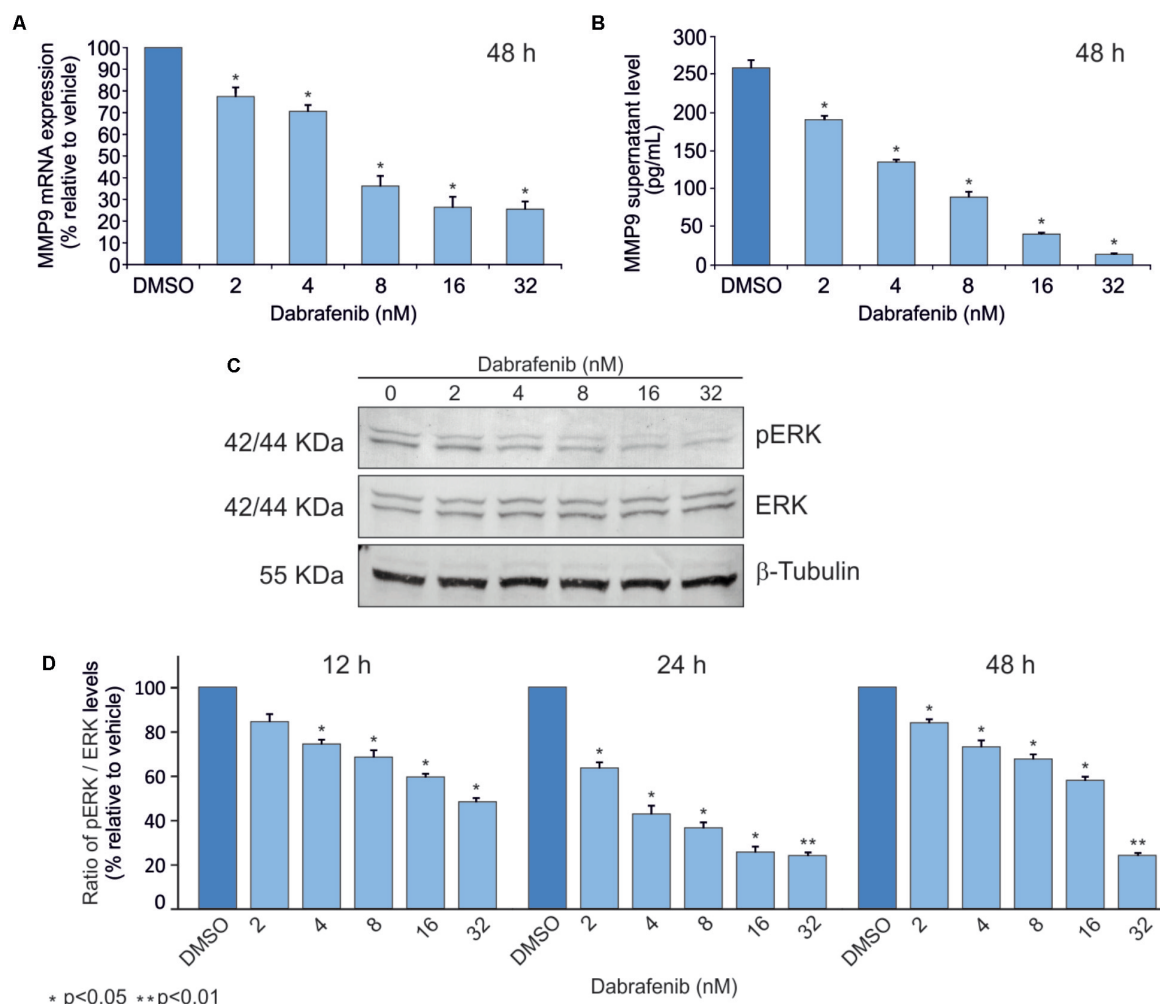


FIGURE 2 | Dabrafenib treatment of A2058 cell line. A2058 cell line was treated with different doses of dabrafenib (2, 4, 8, 16, and 32 nM) for 12, 24, and 48 h. Real-Time PCR (A) and ELISA assay (B) were performed to evaluate MMP-9 expression levels of A2058 after 48 h of treatment. pERK and total ERK protein levels in A2058 cells treated with dabrafenib at 12, 24, 48 h were evaluated by Western blot (C,D). The statistical significance of the two-tailed Student's *t*-test was referred to the control. * $p < 0.05$; ** $p < 0.01$.

modulation during the treatment with BRAF inhibitors. Validation of *in vitro* data were assessed in peripheral blood samples from melanoma patients analyzing MMP-9 levels according to the presence of circulating-free DNA *BRAF*^{V600E} mutation.

MATERIALS AND METHODS

Cell Lines and Treatment

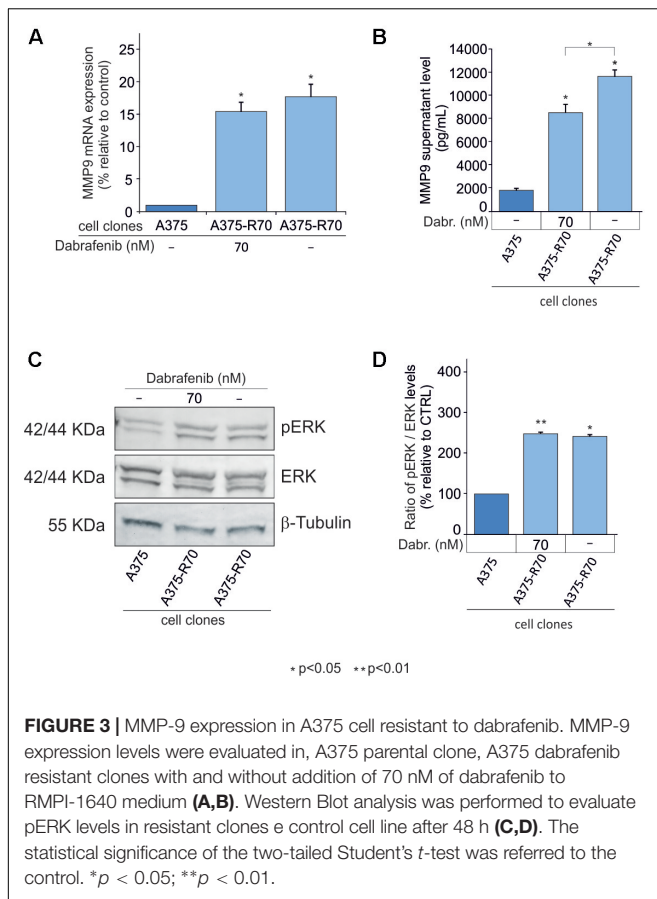
The A375 and A2058 melanoma cell lines were purchased from ATCC (Rockville, MD, United States). Both cell lines were cultured in RPMI-1640 medium supplemented with L-glutamine (2 mmol/L), penicillin (100 IU), streptomycin (100 µg/ml) and 10% fetal bovine serum (FBS) (all provided from GIBCO TM) and grown in humidified incubator (5% CO₂) at 37°C. The cell lines were seeded in 60 mm cell-culture dishes (Thermo Fisher

Scientific Inc., Waltham, MA, United States) at a density of 300,000 cells/well and 400,000 cells/well for A375 and A2058, respectively.

A375 cells were treated with dabrafenib (dissolved in DMSO) (cat. n. S2807 - Selleckchem, United States) at the concentration of 2, 1, 0.5, 0.25, 0.125 nM, whereas A2058 cells were treated with 32, 16, 8, 4, 2 nM of dabrafenib. DMSO was used as control. Both cell lines were treated for 12, 24, and 48 h.

Dabrafenib resistant A375 cells were obtained by culturing the cells with growing concentration of dabrafenib (up to 70 nM) for 2 months. Parental A375 and resistant A375 cells both untreated and treated with 70 nM dabrafenib were seeded in triplicate in 60 mm cell-culture dishes for 48 h.

For each cellular condition, conditioned supernatants were collected and cleaned up from debris by centrifugation. Adherent cells were collected by scraper after washing once in cold 1X DPBS GIBCO TM (cat. n. 14190250 - Thermo Fisher Scientific



Inc., Waltham, MA, United States). Cell pellets were collected by centrifugation and stored at -80°C . All experiments were conducted in triplicate.

ELISA

ELISA test was performed to detect MMP-9 levels in A375 and A2058 culture supernatants using MMP-9 Human ELISA Kit (cat. n. BMS2016-2 - Invitrogen Corporation, Carlsbad, CA, United States) according to the manufacturer's instructions. Whereas, Human MMP-9 Quantikine ELISA KIT (cat. n. DMP900 - R&D Systems, Minneapolis, MN, United States) was used to detect serum levels of MMP-9 in melanoma patients enrolled in this study. Optical density (OD) was measured by Tecan ELISA plate reader (Tecan, Männedorf, Switzerland). Linear regression analysis was performed to generate standard curve from average absorbance of standards. MMP-9 concentrations were calculated fitting the average of duplicate ODs of each sample with standard curve.

Real-Time PCR Quantification of MMP-9 Transcript Levels

Total RNA was extracted from cellular pellet by using the PureLink RNA mini RNA extraction kit (cat. n. 12183025 - Ambion/Life Technologies, Carlsbad, CA, United States) according to the manufacturer's instructions. For each sample,

1 μg of total RNA was reverse transcribed using SuperScript III Reverse Transcriptase kit (cat. n. 18080044 - Thermo Fisher Scientific Inc., Waltham, MA, United States). First-strand cDNA was used for quantitative PCR (qPCR) reactions performed using the AB 7300 Real-Time PCR system (Applied Biosystems, Foster City, CA, United States). Amplification was performed using Fast SYBR Green Master Mix (cat. n. 4385617 - Applied Biosystems, Foster City, CA, United States) according to the conditions reported below:

Initial denaturation at 95°C for 10 min, followed by 40 cycles at 95°C for 15 s and 60°C for 1 min. Relative expression of MMP-9 transcript was performed using the $2^{-\Delta\Delta C_t}$ method. For the detection of MMP-9 transcript the following primers were used:

Forward 5'-GAACCAATCTCACCGACAGG-3'; Reverse 5'-CCACAACCTCGTCATCGTCG-3'. The phosphoglycerate kinase 1 (PGK1) housekeeping gene was used as an internal control for result normalization.

PGK1 primer sequences were: Forward 5'-TTAAAGGGAA GCGGGTCGTT-3'; Reverse 5'-CAGGCATGGGCACACCAT-3'.

Western Blot

Cellular pellets were lysed in NP-40 cell lysis buffer (cat. n. FNN0021 - Thermo Fisher Scientific Inc., Waltham, MA, United States) supplemented with protease and phosphatase inhibitor cocktails (Sigma, St. Louis, MO, United States). Quick StartTM Bradford 1X Dye Reagent assay (cat. n. 5000205 - Bio-Rad Laboratories, Inc., Hercules, CA, United States) was used to quantify protein amount. For each sample, 30 μg of proteins were electrophoretically separated using 4–15% Mini Protean TGX Precast Gels (cat. n. 4561083 - Bio-Rad Laboratories, Inc., Hercules, CA, United States). Bio-Rad Trans-Blot Turbo was used to transfer the gel proteins into a PVDF/nitrocellulose membrane (Bio-Rad Laboratories, Inc.). Primary antibody Anti-MAP Kinase ERK1/ERK2 (pThr202/ pThr204) rabbit Ab (diluted 1:1000 - cat. n. 442685) and Anti-MAP Kinase ERK1/ERK2 rabbit Ab (diluted 1:1000 - cat. n. 442704) (Merck Millipore, Darmstadt, Germany) were used to detect phosphorylated and total ERK 1/2 proteins.

Tubulin housekeeping protein was detected by using Anti-beta Tubulin rabbit Ab (diluted 1:1000 - cat. n. 15568- Abcam, Cambridge, United Kingdom). Chemiluminescent detection was performed using Clarity Western ECL Substrate (cat. n. 1705060 - Bio-Rad Laboratories, Inc., Hercules, CA, United States). Western blot images were collected by Bio-Rad ChemiDoc Touch Imaging System and analyzed with ImageJ software (National Institutes of Health, Bethesda, MD, United States). All Western blot experiments were performed in triplicate.

Melanoma Patients

In this study 28 melanoma patients treated with BRAF inhibitors (53.5%) alone or in combination with MEK inhibitors (46.5%) were included. Informed consent forms were signed by each participant, and appropriate ethical committee approval was obtained. For each patient socio-demographics, clinical-pathological and therapeutics data were reported in **Table 1**. Peripheral blood samples were collected from patients prior each cycle of chemotherapy. Serum and plasma were obtained

by centrifugation at 2,000 *g* for 10 min and immediately frozen (−80°C) until further analysis. All patients were enrolled at National Cancer Institute "Fondazione Giovanni Pascale," Naples (Italy) and accepted the informed consent, according to the recommendations of the Board of Ethics of the study hospitals.

Circulating-Free DNA Isolation

Circulating-free DNA isolation was obtained from serum of melanoma samples enrolled in the present study according to manual protocols adapted from Hufnagl C and colleagues (Hufnagl et al., 2013). Briefly, 1 mL of serum, 100 µL of solution composed by EDTA (250 mmol/L) and NaCl (750 mmol/L), 100 µL of 100 g/L sodium dodecyl sulfate and 40 µL of proteinase K (stock solution 20 mg/mL) were added. After 2 h incubation at 56°C, the proteins were precipitated with 200 µL of saturated 6M NaCl solution (final concentration of 0.86 mol/L). The circulating-free DNA was extracted from supernatant by phenol-chloroform mixture at room-temperature (RT). After 5 min of incubation at RT, mixture was centrifuged for 15 min at 14,000 *g*. The upper phase was transferred in a new tube and mixed to an equal volume of absolute ethanol and then incubated over night at −20°C. The DNA was centrifuged for 15 min at 14,000 *g*. The precipitated pellet was first washed with 70% ethanol and finally dissolved in 20 µL of DNase and RNase free water. For two of 28 samples the extracted circulating-free DNA was found to be excessively degraded and therefore the circulating-free DNA *BRAF*^{V600E} mutation detection was not performed.

Circulating-Free DNA *BRAF*^{V600E} Mutation Detection

The *BRAF*^{V600E} mutation was detected in circulating-free DNA using Bio-Rad droplet PCR analysis system (Bio-Rad Laboratories, Inc., Hercules, CA, United States), according to the manufacturer's protocol. Briefly, a 22 µL of reaction mixture was prepared by mixing 11 µL ddPCR Supermix for probes (no dUTP – cat. n. 1863010), 1 µL of Bio-Rad *BRAF*-V600E FAM/HEX mixture (cat. n. dHsaMDV2010027), 5 µL of circulating-free DNA sample and 5 µL of PCR water. Twenty microliters of PCR reaction was loaded on the cartridge containing 70 µL of Droplet Generation Oil (cat. n. 1863005 - Bio-Rad Laboratories, Inc., Hercules, CA, United States) in appropriate wells, and then Droplet Generator QX100 was used to generate the nano-sized droplets. Droplet mixture was transferred in PCR plate and amplified by C 1000 Touch Thermal Cycler (Bio-Rad Laboratories, Inc., Hercules, CA, United States) under the following cycling conditions: 10 min at 95°C, 40 cycles of 94°C for 30 s, 55°C for 1 min, followed by 98°C for 10 min (ramp rate 2°C/s).

Fluorescent signals were detected using QX200 Droplet Reader (Bio-Rad Laboratories, Inc., Hercules, CA, United States) and analyzed using QuantaSoft software, version 1.7.4 (QuantaSoft, Prague, Czechia). Samples were considered positive when three or more FAM/HEX-positive droplets were

detected. Absolute quantification (copies/mL) were determined using the QuantaSoft software.

Statistical Analysis

MMP-9 mRNA expression, MMP-9 supernatant level and pERK/ERK ratio in treated melanoma cells and relative control were compared using two-tailed Student's *t*-test. Fisher exact test was used to determine the association between clinical characteristics and cancer progression and vital status. Mann-Whitney test was used to compare the serum concentration of MMP-9 clustered melanoma patients according to clinical-pathological parameters.

Progression-free survival was calculated from the date of treatment initiation to progression, death, or end of follow-up, whichever occurred first. OS was calculated from the date of treatment initiation to patients' death. Survival curves were estimated through Kaplan–Meier method; log-rank non-parametric test was used to compare the survival distributions of melanoma patients according to the detectability of circulating-free DNA *BRAF*^{V600E} mutation and the MMP-9 serum concentration. Statistically significant difference was considered when $p \leq 0.05$ (two-tailed).

TABLE 2 | MMP-9 concentration at baseline in serum of 28 patients with melanoma according to socio-demographic, clinical characteristics and molecular features.

	<i>n</i>	MMP-9 (ng/mL)		Mann-Whitney test
		Median	Interquartile range	
Overall		684	427–1118	
Sex				
Man	14	684	417–1108	$p = 0.927$
Woman	14	662	437–1128	
Age at treatment initiation (years)				
<45	11	601	482–1148	$p = 0.807$
45–59	10	870	352–882	
≥60	7	670	354–1108	
Melanoma type				
S.P.I.	6	1204	417–1930	$p = 0.131$
Cutaneous	22	636	437–873	
Stage				
M1a	7	601	482–723	$p = 0.624$
M1b	4	614	470–1801	
M1c	16	872	427–1159	
Therapy				
Monotherapy	15	697	437–1108	$p = 0.596$
Combo	13	670	352–1128	
LDH				
<480	17	671	482–882	$p = 0.796$
≥480	11	686	354–1238	
<i>BRAF</i>^{V600E}				
Undetectable	15	557	354–722	$p = 0.058$
Detectable	11	873	437–1238	

RESULTS

MMP-9 Expression Levels in Melanoma Cells Sensitive and Resistant to Dabrafenib

To test the hypothesis that MMP-9 expression is associated with MAPK pathway modulation, induced by the treatment with BRAF inhibitors, A375 and A2058 melanoma cells harboring *BRAF*^{V600E} mutation were used.

ELISA and Real-Time PCR analyses showed that MMP-9 was statistically down-regulated ($p < 0.05$) in A375 and A2058 melanoma cell lines after treatment with dabrafenib for 48 h (Figures 1A,B, 2A,B). No significant MMP-9 modulation was observed when the cell lines were treated for 12 and 24 h (data not shown). Similar trend was observed for pERK1-2 protein levels detected by Western Blot in both A375 and A2058 cell lines at 12, 24, and 48 h ($p < 0.05$) (Figures 1C,D, 2C,D).

To verify if MMP-9 may be involved in the mechanism of resistance to BRAF inhibitors, such as dabrafenib, resistant clones of A375 were used. Both higher mRNA and protein MMP-9 expression levels were observed in the A375 resistant clones compared to those detected in the parental cells. As expected, the increase of MMP-9 expression was independent to the treatment with dabrafenib (Figures 3A,B). To further investigate the effects of resistance to dabrafenib on MAPK pathway, pERK1-2 levels in resistant clones were measured. pERK1-2 levels were higher in resistant clones when compared with sensitive parental cells ($p < 0.05$) (Figures 3C,D).

These *in vitro* data showed that BRAF inhibitor efficiently counteracts the MAPK signal pathway in A375 cells where the concomitant decrease of pERK and MMP-9

levels was observed in a dose-dependent manner. In contrast, activation of pERK was observed in resistant cell clones with concomitant MMP-9 overexpression. These encouraging data support the notion that MMP-9 may be considered a marker of response to dabrafenib in melanoma cells.

Circulating MMP-9 Expression Levels in Peripheral Blood From Melanoma Patients Treated With BRAF Inhibitors

MMP-9 serum levels were evaluated in melanoma samples according to socio-demographic, clinical and molecular features, including the presence of circulating-free DNA *BRAF*^{V600E} mutation (Table 2). Such mutation was identified in 11 out of 26 melanoma patients (42%). Notably, MMP-9 higher levels were observed in patients with detectable circulating-free DNA *BRAF*^{V600E} mutation compared to those with undetectable *BRAF*^{V600E} mutation ($p = 0.058$). In agreement with these data, it appears speculating that higher levels of MMP-9 are associated with the spreading of tumor DNA in the bloodstream where *BRAF*^{V600E} mutation is detectable (Table 2). Accordingly, the PFS and OS are higher in melanoma patients with undetectable circulating-free DNA *BRAF*^{V600E} mutation compared with those harboring the detectable mutation ($p = 0.004$ and $p = 0.007$ respectively) (Table 3 and Figures 4A,C). These data indicate that the detectability of circulating-free DNA *BRAF*^{V600E} mutation may be considered as a negative prognostic factor. Although no statistics significance has been reached due to the low number of patients, it was observed that highest MMP-9 levels were associated with a lower PFS and OS (Table 3 and Figures 4B,D). No statistical difference was observed for both PFS and OS

TABLE 3 | Median time to progression (TTP) and progression free survival (PFS) in 28 patients with melanoma according to BRAF and MMP-9.

	Patients	Progressions	Median TTP (days)	PFS			Deaths	OS		
				6 mos	12 mos	24 mos		6 mos	12 mos	24 mos
Overall	28	23	219	67.9%	39.3%	17.9%	14	92.9%	71.4%	46.4%
<i>BRAF</i>^{V600E}										
Undetectable	15	10	280	80.0%	60.0%	33.3%	5	93.3%	93.3%	66.7%
Detectable	11	11	219	54.6%	9.1%	0.0%	9	90.9%	45.5%	18.2%
			$p = 0.398$	Log-rank test: $p = 0.004$				Log-rank test: $p = 0.007$		
MMP-9 at treatment initiation (ng/mL)										
<680	14	11	240	78.6%	42.9%	21.4%	6	100%	85.7%	57.1%
≥680	14	12	195	57.1%	35.7%	14.3%	9	85.7%	57.1%	35.7%
			$p = 0.450$	Log-rank test: $p = 0.415$				Log-rank test: $p = 0.219$		
<i>BRAF</i>^{V600E} and MMP-9 at treatment initiation (ng/mL)										
Undetectable and <680	10	7	353	90.0%	60.0%	30.0%	3	100%	100%	70.0%
Undetectable and ≥680	5	3	153	60.0%	60.0%	40.0%	2	80.0%	80.0%	60.0%
Detectable and <680	4	4	205	50.0%	0.0%	0.0%	3	100%	50.0%	25.0%
Detectable and ≥680	7	7	219	57.1%	14.3%	0.0%	6	85.7%	42.9%	14.3%
			$p = 0.153$	Log-rank test: $p = 0.037$				Log-rank test: $p = 0.056$		
Therapy										
Monotherapy	15	14	206	60.0%	26.7%	0.0%	9	100%	60.0%	40.0%
Combo	13	9	240	76.9%	53.9%	30.8%	6	84.6%	84.6%	53.9%
			$p = 0.705$	Log-rank test: $p = 0.102$				Log-rank test: $p = 0.496$		

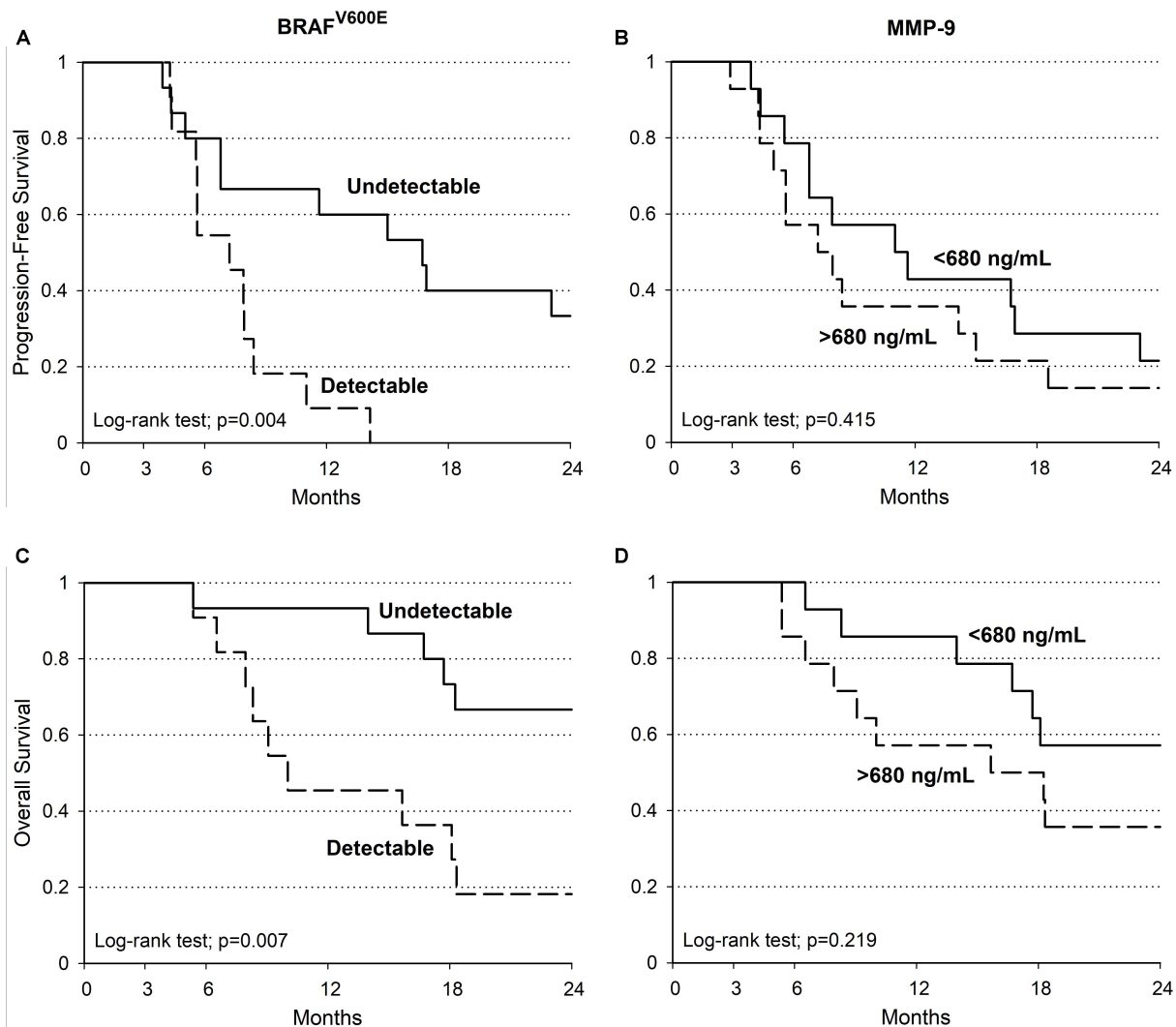


FIGURE 4 | Melanoma patients PFS and OS. Kaplan-Meier estimate of PFS and OS in patients with detectable (dotted line) and undetectable (continuous line) $BRAF^{V600E}$ (PFS log-rank test: $p = 0.004$; OS log-rank test: $p = 0.007$) (A,C). PFS and OS evaluations in patients with MMP-9 serum concentration at baseline (continuous line: < 680 ng/mL; dotted line: ≥ 680 ng/mL; PFS log-rank test: $p = 0.415$; OS log-rank test: $p = 0.219$) (B,D).

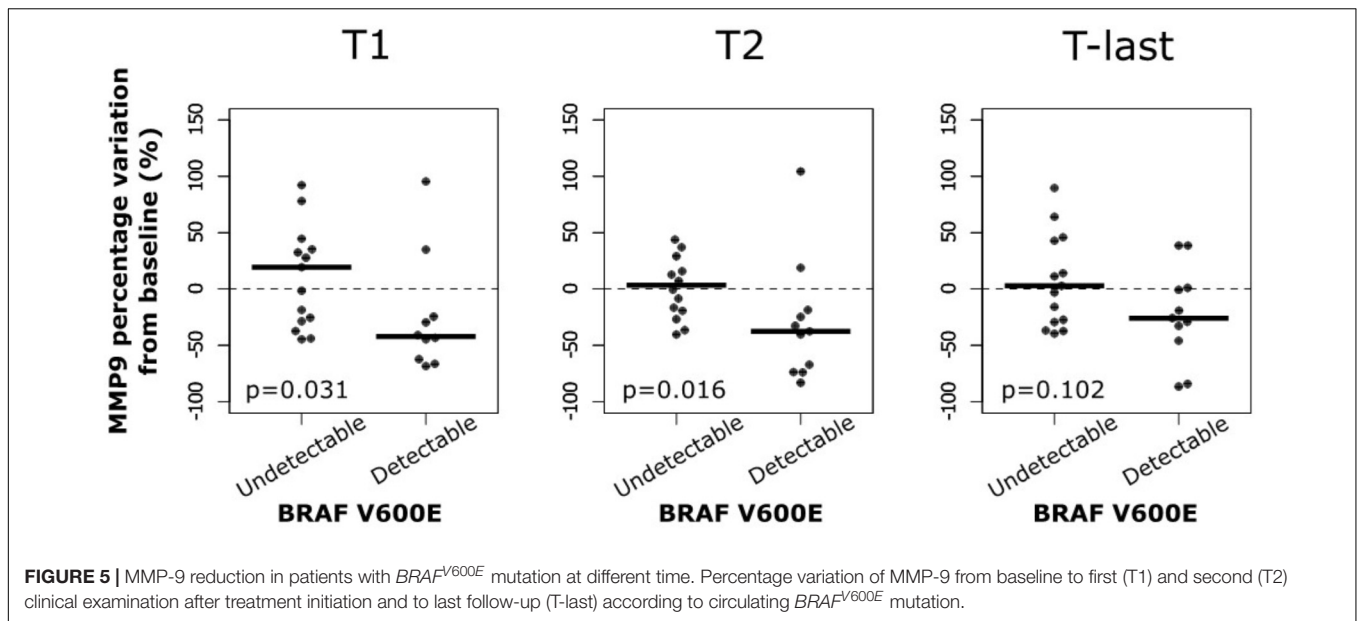
in patients treated with monotherapy or combination therapy (Table 3).

In addition, the percentage of MMP-9 serum variations at different times during the treatment with BRAF inhibitors were analyzed in melanoma patients. Such variations were also evaluated according to the detectability of circulating-free DNA $BRAF^{V600E}$ mutation. No significant percentage variations of MMP-9 serum levels were observed in melanoma patients at different times during the treatment with BRAF inhibitors (data not shown). While, a significant percentage of MMP-9 decrement in samples with circulating-free DNA $BRAF^{V600E}$ mutation compared to those with undetectable one was observed at T1 and T2 (Figure 5). Such percentage of MMP-9 decrement was not observed at T-last where novel microenvironmental factors and/or genetic alteration may occur conferring a drug resistance phenotype to the

tumor cells (Figure 5). These data indicate that the MMP-9 decrement is more evident during the first week of treatment, where the therapy is effective, in melanoma patients with detectable circulating-free DNA $BRAF^{V600E}$ mutation. However, at last follow-up MMP-9 decrement in those patients is not significant compared to patients with undetectable $BRAF^{V600E}$ mutation, suggesting that the treatment became ineffective.

DISCUSSION

In the last decade, the treatment with BRAF and MEK kinase inhibitors improved the prognosis of advanced melanoma. However, a significant fraction of these patients experiences progression disease. The identification of new biomolecular



markers of progression disease and acquired resistance may lead to change therapeutic setting and, eventually, reduce overtreatment (Fattore et al., 2016, 2017; Leonardi et al., 2018).

Improvement of liquid biopsy through the recent advances in molecular technologies, such as the development of digital polymerase chain reaction (dPCR), led to identify tumor molecular features by analyzing the circulating-free DNA harboring pathogenetic mutations (Busser et al., 2017; Gorgannezhad et al., 2018). Several studies showed that detection of circulating-free DNA $BRAF^{V600E}$ mutations is predictive of the response to MAPKs inhibitors in melanoma treatment. In particular, high basal levels of circulating-free DNA $BRAF^{V600E}$ mutation are associated with poor response to therapy and PFS and OS (Ascierto et al., 2013; Sanmamed et al., 2015; Santiago-Walker et al., 2016; Lee et al., 2018). Furthermore, it has been demonstrated that increase of circulating-free DNA $BRAF$ mutation during treatment is predictive of acquired resistance and therapeutic failure (Gray et al., 2015).

To the best of our knowledge, no previous studies have identified new markers that can be linked with the MAPK pathway modulation after treatment with BRAF inhibitors. However, MMP-9 has been associated with the aberrant activation of MAPK pathway in melanoma, suggesting its role as prognostic indicator (Guarneri et al., 2017). Therefore, in the present study, the modulation of MMP-9 in melanoma after treatment with B-RAF inhibitors was analyzed through different experimental approaches.

Our *in vitro* data showed that BRAF inhibitor efficiently counteracts the MAPK signal pathway in A375 cells where the concomitant decrease of pERK and MMP-9 levels was observed in a dose-dependent manner. Furthermore, to verify if MMP-9 may be involved in the mechanism of resistance to BRAF inhibitors A375 resistant cells were obtained and pERK protein levels showed opposite behavior

compared to sensitive cells when treated with dabrafenib. In particular, an activation of pERK was observed in resistant cell clones with concomitant MMP-9 overexpression. These encouraging data support the notion that MMP-9 may be considered a marker of response to dabrafenib in melanoma cells.

After the *in vitro* evaluations, circulating-free DNA $BRAF^{V600E}$ mutation and MMP-9 serum levels were evaluated in melanoma patients. Unexpectedly, circulating-free DNA $BRAF^{V600E}$ mutation was detected in only the 42% (11 out of 26) of melanoma patients positive to $BRAF^{V600E}$ mutation after the histopathological diagnosis. Interestingly, ELISA assay showed that MMP-9 serum levels were higher in patients with detectable circulating-free DNA $BRAF^{V600E}$ mutation compared to those with undetectable $BRAF^{V600E}$ mutation suggesting that the increase of MMP-9 in the subset of patients with detectable circulating mutation are associated with the spreading of tumor and in the release of circulating-free DNA in the bloodstream. These evidences encourage the use of MMP-9 as a prognostic marker in the subsets of patients with detectable circulating mutation, where the concomitant evaluation of circulating-free DNA status and MMP-9 serum levels may give important information about the prognosis of patients.

Indeed, the PFS and OS analyses according to the circulating-free DNA $BRAF^{V600E}$ status and the MMP-9 expression levels showed a worse prognosis for melanoma patients with detectable circulating $BRAF^{V600E}$ mutation and high MMP-9 serum levels (>680 ng/mL) compared with those with undetectable mutation and lower levels of MMP-9.

Finally, the analysis of MMP-9 during the treatment showed that MMP-9 serum protein levels significantly decreased at T1 and T2, but not at the last follow-up, for the patients with detectable circulating-free DNA $BRAF^{V600E}$ mutation.

Overall, the results of the present study confirm that the occurrence of circulating-free DNA BRAF^{V600E} mutation is a negative prognostic factor of cutaneous melanoma; furthermore, MMP-9 may be considered a prognostic indicator of response to BRAF inhibitors only in the subset of patients harboring the circulating-free DNA BRAF^{V600E} mutation supporting the notion that MMP-9 is associated with the MAPK pathway. Further studies, including a larger series of melanoma patients, are needed to better clarify the impact of MMP-9 as a marker of response to treatment with BRAF inhibitors.

ETHICS STATEMENT

This study was carried out in accordance with the recommendations of Ethics Committee of the Istituto Nazionale Tumori of Naples with written informed consent from all subjects. All subjects gave written informed consent in accordance with the Declaration of Helsinki. The protocol was

approved by the Ethics Committee of the Istituto Nazionale Tumori of Naples.

AUTHOR CONTRIBUTIONS

SC, ML, and PA conceived the study. SC and GM dealt with the study design in all its experimental phases. LE, RS, and DC performed the experiments and the quality control of data and procedures. GM, DM, LE, and RS performed the data analyses and interpretation, while, JP executed all the statistical analyses. LE and SC wrote the manuscript. ML and PA reviewed the final version of the manuscript. All authors read and approved the final version of the manuscript.

FUNDING

This study was supported by the Lega Italiana per la Lotta contro i Tumori [Ricerca Sanitaria 2016 – Programma 5 × 1000 anno 2014].

REFERENCES

- Aladowicz, E., Ferro, L., Vitali, G. C., Venditti, E., Fornasari, L., and Lanfranccone, L. (2013). Molecular networks in melanoma invasion and metastasis. *Future Oncol.* 9, 713–726. doi: 10.2217/fon.13.9
- Ascierto, P. A., Minor, D., Ribas, A., Lebbe, C., O'Hagan, A., Arya, N., et al. (2013). Phase II trial (BREAK-2) of the BRAF inhibitor dabrafenib (GSK2118436) in patients with metastatic melanoma. *J. Clin. Oncol.* 31, 3205–3211. doi: 10.1200/JCO.2013.49.8691
- Branca, M., Orso, S., Molinari, R. C., Xu, H., Guerrier, S., Zhang, Y., et al. (2018). Is nonmetastatic cutaneous melanoma predictable through genomic biomarkers? *Melanoma Res.* 28, 21–29. doi: 10.1097/CMR.0000000000000412
- Brunssen, A., Waldmann, A., Eisemann, N., and Katalinic, A. (2017). Impact of skin cancer screening and secondary prevention campaigns on skin cancer incidence and mortality: a systematic review. *J. Am. Acad. Dermatol.* 76, e10–e139. doi: 10.1016/j.jaad.2016.07.045
- Busser, B., Lupo, J., Sancey, L., Mouret, S., Faure, P., Plumas, J., et al. (2017). Plasma circulating tumor DNA levels for the monitoring of melanoma patients: landscape of available technologies and clinical applications. *Biomed. Res. Int.* 2017:5986129. doi: 10.1155/2017/5986129
- Chen, P., Chen, F., and Zhou, B. (2017). Therapeutic efficacy and safety of combined BRAF and MEK inhibition in patients with malignant melanoma: a meta-analysis. *Onco Targets Ther.* 10, 5391–5403. doi: 10.2147/OTT.S147438
- Dange, M. C., Agarwal, A. K., and Kalraiyi, R. D. (2015). Extracellular galectin-3 induces MMP-9 expression by activating p38 MAPK pathway via lysosome-associated membrane protein-1 (LAMP1). *Mol. Cell. Biochem.* 404, 79–86. doi: 10.1007/s11010-015-2367-5
- Falzone, L., Candido, S., Salemi, R., Basile, M. S., Scalisi, A., McCubrey, J. A., et al. (2016a). Computational identification of microRNAs associated to both epithelial to mesenchymal transition and NGAL/MMP-9 pathways in bladder cancer. *Oncotarget* 8, 72758–72766. doi: 10.18632/oncotarget.11805
- Falzone, L., Salemi, R., Travali, S., Scalisi, A., McCubrey, J. A., Candido, S., et al. (2016b). MMP-9 overexpression is associated with intragenic hypermethylation of MMP-9 gene in melanoma. *Aging* 8, 933–944. doi: 10.18632/aging.100951
- Fattore, L., Costantini, S., Malpicci, D., Ruggiero, C. F., Ascierto, P. A., Croce, C. M., et al. (2017). MicroRNAs in melanoma development and resistance to target therapy. *Oncotarget* 8, 22262–22278. doi: 10.18632/oncotarget.14763
- Fattore, L., Mancini, R., Acunzo, M., Romano, G., Laganà, A., Pisanu, M. E., et al. (2016). miR-579-3p controls melanoma progression and resistance to target therapy. *Proc. Natl. Acad. Sci. U.S.A.* 113, E5005–E5013. doi: 10.1073/pnas.1607753113
- Forbes, S. A., Beare, D., Boutselakis, H., Bamford, S., Bindal, N., Tate, J., et al. (2017). COSMIC: somatic cancer genetics at high-resolution. *Nucleic Acids Res.* 45, D777–D783. doi: 10.1093/nar/gkw1121
- Frasca, F., Nucera, C., Pellegri, G., Gangemi, P., Attard, M., Stella, M., et al. (2008). BRAF(V600E) mutation and the biology of papillary thyroid cancer. *Endocr. Relat. Cancer* 15, 191–205. doi: 10.1677/ERC-07-0212
- Gordon, G. M., Ledee, D. R., Feuer, W. J., and Fini, M. E. (2009). Cytokines and signaling pathways regulating matrix metalloproteinase-9 (MMP-9) expression in corneal epithelial cells. *J. Cell. Physiol.* 221, 402–411. doi: 10.1002/jcp.21869
- Gorganezhad, L., Umer, M., Islam, M. N., Nguyen, N. T., and Shiddiky, M. J. A. (2018). Circulating tumor DNA and liquid biopsy: opportunities, challenges, and recent advances in detection technologies. *Lab Chip* 18, 1174–1196. doi: 10.1039/C8LC00100F
- Gray, E. S., Rizos, H., Reid, A. L., Boyd, S. C., Pereira, M. R., Lo, J., et al. (2015). Circulating tumor DNA to monitor treatment response and detect acquired resistance in patients with metastatic melanoma. *Oncotarget* 6, 42008–42018. doi: 10.18632/oncotarget.5788
- Guarneri, C., Bevelacqua, V., Polesel, J., Falzone, L., Cannavò, P. S., Spandidos, D. A., et al. (2017). NF-κB inhibition is associated with OPN/MMP-9 downregulation in cutaneous melanoma. *Oncol. Rep.* 37, 737–746. doi: 10.3892/or.2017.5362
- Herbretau, G., Vallée, A., Knol, A. C., Théoleyre, S., Quéreux, G., Khammari, A., et al. (2017). Circulating tumour DNA: analytical aspects and clinical applications for metastatic melanoma patients. *Ann. Biol. Clin.* 75, 619–630.
- Hofmann, U. B., Westphal, J. R., Van Muijen, G. N., and Ruiter, D. J. (2000). Matrix metalloproteinases in human melanoma. *J. Invest. Dermatol.* 115, 337–344. doi: 10.1046/j.1523-1747.2000.00068.x
- Hufnagl, C., Stöcher, M., Moik, M., Geisberger, R., and Greil, R. (2013). A modified Phenol-chloroform extraction method for isolating circulating cell free DNA of tumor patients. *J. Nucleic Acids Invest.* 4, 1–3. doi: 10.4081/jnai.2013.4282
- Kalal, B. S., Upadhyay, D., and Pai, V. R. (2017). Chemotherapy resistance mechanisms in advanced skin cancer. *Oncol. Rev.* 11:326. doi: 10.4081/oncol.2017.326
- Lee, R. J., Gremel, G., Marshall, A., Myers, K. A., Fisher, N., Dunn, J. A., et al. (2018). Circulating tumor DNA predicts survival in patients with resected high-risk stage II/III melanoma. *Ann. Oncol.* 29, 490–496. doi: 10.1093/annonc/mdx717
- Leonardi, G. C., Falzone, L., Salemi, R., Zanghi, A., Spandidos, D. A., McCubrey, J. A., et al. (2018). Cutaneous melanoma: from pathogenesis to therapy. *Int. J. Oncol.* 52, 1071–1080. doi: 10.3892/ijo.2018.4287

- Lim, S. Y., Menzies, A. M., and Rizos, H. (2017). Mechanisms and strategies to overcome resistance to molecularly targeted therapy for melanoma. *Cancer* 123, 2118–2129. doi: 10.1002/cncr.30435
- Liu, S., Gao, G., Yan, D., Chen, X., Yao, X., Guo, S., et al. (2017). Effects of miR-145-5p through NRAS on the cell proliferation, apoptosis, migration, and invasion in melanoma by inhibiting MAPK and PI3K/AKT pathways. *Cancer Med.* 6, 819–833. doi: 10.1002/cam4.1030
- Lu, P., Takai, K., Weaver, V. M., and Werb, Z. (2011). Extracellular matrix degradation and remodeling in development and disease. *Cold Spring Harb. Perspect. Biol.* 3:a005058. doi: 10.1101/cshperspect.a005058
- Masucci, G. V., Cesano, A., Eggermont, A., Fox, B. A., Wang, E., Marincola, F. M., et al. (2017). The need for a network to establish and validate predictive biomarkers in cancer immunotherapy. *J. Transl. Med.* 15:223. doi: 10.1186/s12967-017-1325-2
- Mathieu, V., Pirker, C., Schmidt, W. M., Spiegel-Kreinecker, S., Lötsch, D., Heffeter, P., et al. (2012). Aggressiveness of human melanoma xenograft models is promoted by aneuploidy-driven gene expression deregulation. *Oncotarget* 3, 399–413. doi: 10.18632/oncotarget.473
- McCourt, C., Dolan, O., and Gormley, G. (2014). Malignant melanoma: a pictorial review. *Ulster Med. J.* 83, 103–110.
- Mesa, C. Jr., Mirza, M., Mitsutake, N., Sartor, M., Medvedovic, M., Tomlinson, C., et al. (2006). Conditional activation of RET/PTC3 and BRAFV600E in thyroid cells is associated with gene expression profiles that predict a preferential role of BRAF in extracellular matrix remodeling. *Cancer Res.* 66, 6521–6529. doi: 10.1158/0008-5472.CAN-06-0739
- Quéreux, G., Herbreteau, G., Knol, A. C., Vallée, A., Khammari, A., Théoleyre, S., et al. (2017). Efficient treatment of a metastatic melanoma patient with a combination of BRAF and MEK inhibitors based on circulating tumor DNA analysis: a case report. *BMC Res. Notes* 10:320. doi: 10.1186/s13104-017-2650-5
- Ross, C. L., Kaushik, S., Valdes-Rodriguez, R., and Anvekar, R. (2018). MicroRNAs in cutaneous melanoma: role as diagnostic and prognostic biomarkers. *J. Cell. Physiol.* 233, 5133–5141. doi: 10.1002/jcp.26395
- Russo, I., Zorzetto, L., Frigo, A. C., Chiarion Sileni, V., and Alaibac, M. A. (2017). comparative study of the cutaneous side effects between BRAF monotherapy and BRAF/MEK inhibitor combination therapy in patients with advanced melanoma: a single-centre experience. *Eur. J. Dermatol.* 27, 482–486.
- Saladi, S. V., Keenen, B., Marathe, H. G., Qi, H., Chin, K. V., and de la Serna, I. L. (2010). Modulation of extracellular matrix/adhesion molecule expression by BRG1 is associated with increased melanoma invasiveness. *Mol. Cancer* 9:280. doi: 10.1186/1476-4598-9-280
- Sandri, S., Faião-Flores, F., Tiago, M., Pennacchi, P. C., Massaro, R. R., Alves-Fernandes, D. K., et al. (2016). Vemurafenib resistance increases melanoma invasiveness and modulates the tumor microenvironment by MMP-2 upregulation. *Pharmacol. Res.* 111, 523–533. doi: 10.1016/j.phrs.2016.07.017
- Sanmamed, M. F., Fernández-Landázuri, S., Rodríguez, C., Zárate, R., Lozano, M. D., Zubiri, L., et al. (2015). Quantitative cell-free circulating BRAFV600E mutation analysis by use of droplet digital PCR in the follow-up of patients with melanoma being treated with BRAF inhibitors. *Clin. Chem.* 61, 297–304. doi: 10.1373/clinchem.2014.230235
- Santiago-Walker, A., Gagnon, R., Mazumdar, J., Casey, M., Long, G. V., Schadendorf, D., et al. (2016). Correlation of BRAF mutation status in circulating-free DNA and tumor and association with clinical outcome across four BRAFi and MEKi clinical trials. *Clin. Cancer Res.* 22, 567–574. doi: 10.1158/1078-0432.CCR-15-0321
- Schreuer, M., Meersseman, G., Van Den Herrewegen, S., Jansen, Y., Chevolet, I., Bott, A., et al. (2016). Quantitative assessment of BRAF V600 mutant circulating cell-free tumor DNA as a tool for therapeutic monitoring in metastatic melanoma patients treated with BRAF/MEK inhibitors. *J. Transl. Med.* 14:95. doi: 10.1186/s12967-016-0852-6
- Shi, H., Liu, L., Liu, L., Geng, J., Zhou, Y., and Chen, L. (2014). β -Elemene inhibits the metastasis of B16F10 melanoma cells by downregulation of the expression of uPA, uPAR, MMP-2, and MMP-9. *Melanoma Res.* 24, 99–107. doi: 10.1097/CMR.0000000000000043
- Shi, H., Wu, Y., Wang, Y., Zhou, M., Yan, S., Chen, Z., et al. (2015). Liquiritigenin potentiates the inhibitory effects of cisplatin on invasion and metastasis via downregulation MMP-2/9 and PI3 K/AKT signaling pathway in b16f10 melanoma cells and mice model. *Nutr. Cancer* 67, 761–770. doi: 10.1080/01635581.2015.1037962
- Spagnolo, F., Picasso, V., Lambertini, M., Ottaviano, V., Dozin, B., and Queirolo, P. (2016). Survival of patients with metastatic melanoma and brain metastases in the era of MAP-kinase inhibitors and immunologic checkpoint blockade antibodies: a systematic review. *Cancer Treat. Rev.* 45, 38–45. doi: 10.1016/j.ctrv.2016.03.003
- Tang, Z. Y., Liu, Y., Liu, L. X., Ding, X. Y., Zhang, H., and Fang, L. Q. (2013). RNAi-mediated MMP-9 silencing inhibits mouse melanoma cell invasion and migration in vitro and in vivo. *Cell Biol. Int.* 37, 849–854. doi: 10.1002/cbin.10107
- Tejera-Vaquero, A., Descalzo-Gallego, M. A., Otero-Rivas, M. M., Posada-García, C., Rodríguez-Pazos, L., Pastushenko, I., et al. (2016). Skin cancer incidence and mortality in Spain: a systematic review and meta-analysis. *Actas Dermosifiliogr.* 107, 318–328. doi: 10.1016/j.ad.2015.12.008
- Ugurel, S., Röhmel, J., Ascierto, P. A., Flaherty, K. T., Grob, J. J., Hauschild, A., et al. (2017). Survival of patients with advanced metastatic melanoma: the impact of novel therapies-update. *Eur. J. Cancer* 2017, 247–257. doi: 10.1016/j.ejca.2017.06.028
- Veenstra, R., Kostine, M., Cleton-Jansen, A. M., de Miranda, N. F., and Bovée, J. V. (2018). Immune checkpoint inhibitors in sarcomas: in quest of predictive biomarkers. *Lab. Invest.* 98, 41–50. doi: 10.1038/labinvest.2017.128
- Wu, Y. J., Neoh, C. A., Tsao, C. Y., Su, J. H., and Li, H. H. (2015). Sinulariolide suppresses human hepatocellular carcinoma cell migration and invasion by inhibiting matrix metalloproteinase-2/-9 through MAPKs and PI3K/Akt signaling pathways. *Int. J. Mol. Sci.* 16, 16469–16482. doi: 10.3390/ijms160716469
- Yang, L., Song, X., Zhu, J., Li, M., Ji, Y., Wu, F., et al. (2017). Tumor suppressor microRNA-34a inhibits cell migration and invasion by targeting MMP-2/MMP-9/FNDC3B in esophageal squamous cell carcinoma. *Int. J. Oncol.* 51, 378–388. doi: 10.3892/ijo.2017.4015
- Zhang, T., Dutton-Regester, K., Brown, K. M., and Hayward, N. K. (2016). The genomic landscape of cutaneous melanoma. *Pigment Cell Melanoma Res.* 29, 266–283. doi: 10.1111/pcmr.12459

Conflict of Interest Statement: The authors declare that the research was conducted in the absence of any commercial or financial relationships that could be construed as a potential conflict of interest.

Copyright © 2018 Salemi, Falzone, Madonna, Polesel, Cinà, Mallardo, Ascierto, Libra and Candido. This is an open-access article distributed under the terms of the Creative Commons Attribution License (CC BY). The use, distribution or reproduction in other forums is permitted, provided the original author(s) and the copyright owner(s) are credited and that the original publication in this journal is cited, in accordance with accepted academic practice. No use, distribution or reproduction is permitted which does not comply with these terms.



SOX2 Promotes Cell Proliferation and Metastasis in Triple Negative Breast Cancer

Peng Liu^{1†}, Hailin Tang^{1†}, Cailu Song^{1*†}, Jin Wang¹, Bo Chen¹, Xiaojia Huang¹, Xiaoqing Pei^{2*} and Longzhong Liu^{2*}

¹ State Key Laboratory of Oncology in South China, Collaborative Innovation Center of Cancer Medicine, Department of Breast Oncology, Sun Yat-sen University Cancer Center, Guangzhou, China, ² State Key Laboratory of Oncology in South China, Collaborative Innovation Center of Cancer Medicine, Department of Ultrasound, Sun Yat-sen University Cancer Center, Guangzhou, China

OPEN ACCESS

Edited by:

Dong-Hua Yang,
St. John's University, United States

Reviewed by:

Chun Wu,
Janssen Research and Development,
United States
Anca Maria Cimpeanu,
University of Medicine and Pharmacy,
Timisoara, Romania

*Correspondence:

Cailu Song
songcl@sysucc.org.cn
Xiaoqing Pei
peixq@sysucc.org.cn
Longzhong Liu
liulzh@sysucc.org.cn

[†] These authors have contributed
equally to this work

Specialty section:

This article was submitted to
Experimental Pharmacology
and Drug Discovery,
a section of the journal
Frontiers in Pharmacology

Received: 14 June 2018

Accepted: 02 August 2018

Published: 21 August 2018

Citation:

Liu P, Tang H, Song C, Wang J,
Chen B, Huang X, Pei X and Liu L
(2018) SOX2 Promotes Cell
Proliferation and Metastasis in Triple
Negative Breast Cancer.
Front. Pharmacol. 9:942.
doi: 10.3389/fphar.2018.00942

This study explored the expression, biological function and prognostic role of SOX2 in triple negative breast cancer (TNBC). Quantitative real-time PCR and immunohistochemistry were used to detect the expression of SOX2 in TNBC cell lines and clinical tissues. MTT assay, Transwell assay, flow cytometry and xenograft mouse model were used to assess the biological functions of SOX2. It was found that SOX2 was up-regulated in both TNBC cell lines and clinical tissues. High expression of SOX2 was associated with shorter overall survival and disease free survival. Moreover, inhibition of SOX2 suppressed cell proliferation and invasion, induced cell apoptosis *in vitro*, and suppressed tumorigenesis and metastasis *in vivo*. In addition, analysis of TNM stage and lymph nodes infiltration among the 237 TNBC patients by paired χ^2 test showed that SOX2 was inversely correlated with tumor status, our findings provided evidence that SOX2 acts as a tumor promoter in TNBC and inhibition of SOX2 could be a potential therapeutic strategy for TNBC.

Keywords: SOX2, triple negative breast cancer, proliferation, metastasis, potential target

INTRODUCTION

Triple negative breast cancer (TNBC) is defined by the lack of estrogen receptor (ER), progesterone receptor (PR) as well as the gene expression of human epidermal growth factor receptor 2 (HER2) (Denkert et al., 2016). TNBC accounts for approximately 20% of all breast cancers and is an aggressive breast cancer subtype with poor prognosis (Liedtke et al., 2010). Currently, the main strategy of therapy for TNBC is chemotherapy. However, drug resistance and tumor metastasis occurs frequently (Zhang et al., 2016). Although trastuzumab is an effective targeted therapeutic drug for HER2+ breast cancer, there is no effective specific targeted agent approved for the treatment of TNBC (Yao et al., 2017). Therefore, new targeted strategies for TNBC are urgently needed.

Triple negative breast cancer is a heterogeneous disease characterized by aberrations at genomic or molecular levels resulting in a great multitude of dysregulated signaling pathways (Jiang et al., 2014; Hon et al., 2016). SRY-related HMG box-containing transcription factor-2 (SOX2) is one of these abnormal expressed genes in many cancers including breast cancer (Zheng et al., 2015). SOX2 is a key transcription factor and plays an extremely important role in maintaining pluripotency of stem cells. SOX2 is highly expressed in embryonic tissues while rarely expressed in adult normal somatic cells (Feng and Wen, 2015). As an important cancer stem cell marker, SOX2 is involved in cell proliferation,

differentiation, invasion, metastasis, drug resistance, relapse, and others processes of tumors (Saigusa et al., 2009; Yang S. et al., 2015). Such as SOX2 can promote tumor tumorigenesis and development in tongue squamous cell carcinoma, osteosarcoma, or gastric cancer through various signaling pathways (Liu et al., 2018; Luo et al., 2018; Maurizi et al., 2018). Studies show that SOX2 is frequently abnormally expressed in a variety of malignant tumors. For example, SOX2 is not expressed in normal breast tissues but highly expressed in breast cancer tissues (Abd El-Maqsoud and Abd El-Rehim, 2014); SOX2 is highly expressed in normal gastric mucosa, but there is almost no expression of SOX2 in intestinal metaplasia of gastric mucosa (Carrasco-Garcia et al., 2016), suggesting that the expression of SOX2 is tumor specific.

A number of studies have shown that the expression of SOX2 is associated with the prognosis of metastatic or recurrence tumors. The DNA amplification and protein expression of SOX2 are associated with smoking status and histology, and is favorable for prognosis in NSCLC (Li et al., 2016). SOX2 expression is correlated with the expression of proliferation and apoptosis-related proteins and is associated with clinicopathological parameters of worse outcome in primary head and neck squamous cell carcinomas (Schröck et al., 2014). SOX2 can predict prognosis for head and neck squamous cell carcinoma (Chung et al., 2018), and its expression also can be associated with an advanced tumor stage in adenoid cystic carcinoma of the head and neck (Thierauf et al., 2018). SOX2 has also been proved to have anti-proliferative, anti-metastatic, and pro-apoptotic effects. SOX2 is associated with pathological stage and clinical outcome in gastric cancer. SOX2 is the independent prognostic marker for gastric cancer (Wang et al., 2015). The level of SOX2 expression is valuable to predict distant metastasis or the prognosis of nasopharyngeal carcinoma (Wang et al., 2012).

The prognostic value of SOX2 in TNBC is not well-documented. Therefore, it is important to explore the functions and roles of SOX2 in TNBC. Here, we explore the expression, functions and prognostic roles of SOX2 in TNBC and confirm the association of SOX2 in TNBC.

MATERIALS AND METHODS

Cell Lines and Culture

Human normal mammary epithelial cell lines (MCF-10A and 184A1) and breast cancer cell lines (MCF-7, BT474, T47D, MDA-MB-468, BT-20, MDA-MB-435, BT549, and MDA-MB-231) were obtained from the American Type Culture Collection (Manassas, VA, United States) and passaged in our laboratory for less than 6 months after thawing frozen aliquots. All the cell lines were authenticated by short-tandem repeat DNA profiling and all found to be free of mycoplasma infection before use. All cells were maintained according to the supplier's instructions.

Clinical Samples

Fresh tissue samples from 20 TNBC tissues (TNBC) and their corresponding paired normal adjacent tissues (Normal), 20

non-triple-negative breast cancer tissues (NTNBC) and their adjacent normal mammal tissues (Control) were cut during surgery and immediately stored in RNAlater (Ambion). The age range of 20 TNBC patients is between 29 and 67, with an average age of (50.7 ± 7.61). The age range of 20 NTNBC patients is between 31 and 64 years, with an average age of (51.3 ± 8.22). There was no significant difference in the basic data between the two groups of patients. These tissue samples were subjected to quantitative real-time polymerase chain reaction (qRT-PCR) analysis. Another 237 TNBC tissues were collected during surgery to be formalin-fixed and embedded in paraffin and then subjected to immunohistochemistry (IHC). All clinical samples were collected between 2006 and 2012 at the Sun Yat-sen University Cancer Center (SYSUCC). The age range of 237 TNBC patients is between 27 and 63, with an average age of (50.93 ± 9.05). This study was approved by the Ethics Committee of SYSUCC Health Authority. The collection and use of tissues followed procedures that are in accordance with the ethical standards formulated in the Declaration of Helsinki. Informed consents were obtained from all patients included in the study.

qRT-PCR Analysis

The total RNA from all cell lines and tissues were extracted with TRIzol reagent (Invitrogen, Carlsbad, CA, United States). Reverse transcription and qRT-PCR reactions were performed with qSYBR-green-containing PCR kit (Qiagen, United States). The threshold cycle value (CT, the fractional cycle number at which the fluorescence of each sample passes the fixed threshold) of SOX2 was normalized against the CT value of internal control β -actin. The fold change was determined as $2^{-\Delta\Delta C_t}$. The primers for qRT-PCR detection were synthesized by Invitrogen. SOX2 forward, 5'-TAATTAGAATTCATGTA CAACATGATGGAGACG-3', reverse, 5'-TAATTAGGTACCT CACATGTGTGAGAGGGGCGAGTGTGC-3'. The detection was performed with Bio-Rad IQTM5 Multicolour Real-Time PCR Detection System (United States).

IHC Analysis and Scoring System

After deparaffinization and rehydration, the slides were treated with 90% methanol/3% H_2O_2 solution for 10 min at room temperature to block endogenous peroxidase. Then, the slides were soaked in sodium citrate buffer (10 mM Sodium citrate, 0.05% Tween 20, pH 6.0) under $96^\circ C$ for 5 min for antigen retrieval. After blocking by BSA, antibody against SOX2 (Santa Cruz, CA, United States) was used. We added antibody to the slides for overnight storage at $4^\circ C$ and then incubated the slides at room temperature with biotinylated secondary antibody for 10 min, and finally HRP-Streptavidin for 10 min. After DAB staining, the results were graded for intensity. The intensities of SOX2 staining were scored between 0 and 4 according to the standards of 0–1 (no staining), 1–2 (weak staining), 2–3 (medium staining), and 3–4 (strong staining). The percentages of SOX2 positive cells in 3 representative high-power fields of individual samples were analyzed. Scores of intensity multiplied by the percentages of positive cells equalled

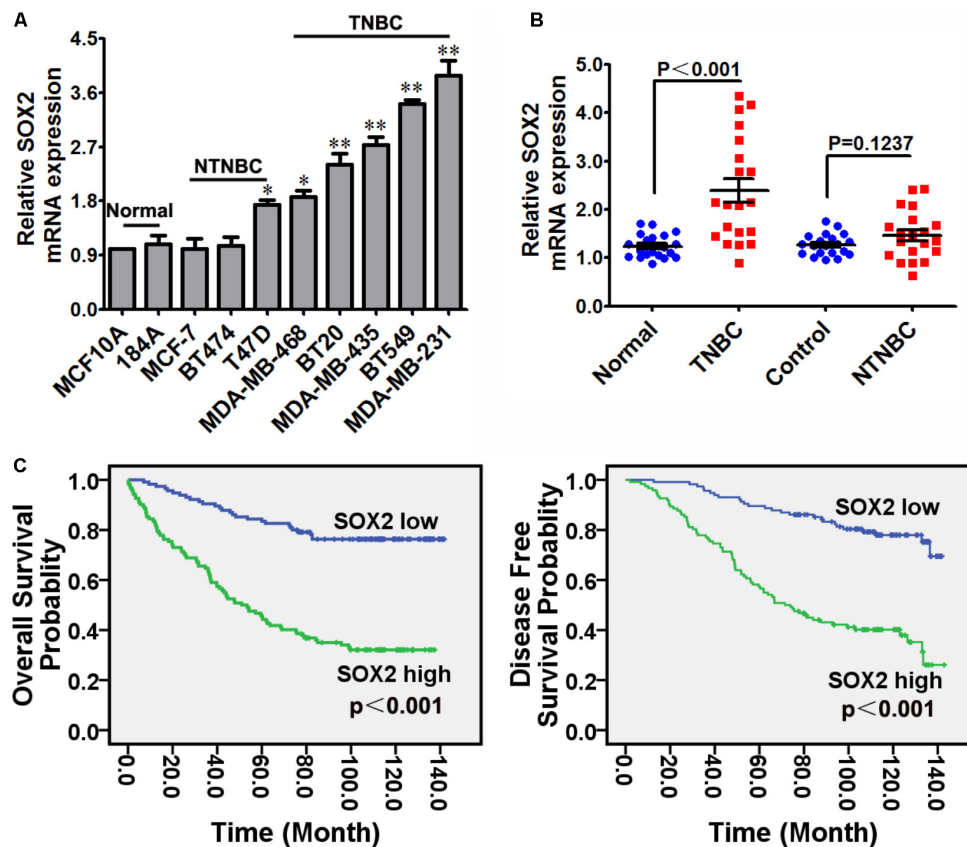


FIGURE 1 | SOX2 overexpressed in TNBC cells and tissues, and correlated with poor clinical outcomes in TNBC. **(A)** Expression of SOX2 in 4 TNBC cell lines, 4 NTNBC cell lines and 2 mammary normal cell lines detected by qRT-PCR. β -actin was used as an internal control (* $p < 0.05$, ** $p < 0.01$). **(B)** Expression of SOX2 in 20 TNBC tissues and their corresponding paired normal adjacent tissues (Normal), 20 NTNBC tissues and their corresponding paired normal adjacent tissues (Control). **(C)** OS and DFS curves for 237 cases of TNBC patients with high or low level of SOX2 expression.

to the final scores of SOX2 expression. The maximum score was 4 and the minimum score was 0. Individual samples were evaluated by three pathologists in a blinded manner, and those expression scores greater or equal to 2 were defined as high expression, less than 2 was defined as low expression.

Establishment of Stably Transfected Cell Lines

Recombinant shRNA lentiviruses containing sh-SOX2 and sh-control were purchased from Fugen (Guangzhou, Guangdong, China). Four shRNA sequences were respectively used to knock down SOX2 in MDA-MB-231 and BT549. The relative SOX2 mRNA expression after transfection was respectively showed in **Supplementary Figure S2** and **S3**. MDA-MB-231 and BT549 cells were respectively infected with sh-SOX2 or sh-control in 24-well plates with the medium changed every 24 h. Cells were selected with minimum lethal concentration of 5 mg/L puromycin (Invivogen, San Diego, CA, United States) for 10 days till drug-resistant cells were obtained. Then these stably transfected cells were used in the following *in vivo* or *in vitro* experiments.

Cell Proliferation Assay

MDA-MB-231 and BT549 cells respectively infected with sh-SOX2 or sh-control were plated in 6-well plates at a desired cell concentration. The number of cells was counted at 24, 48, 72, and 96 h after incubation by Coulter Counter (Beckman Coulter, Fullerton, CA, United States) in triplicate.

Cell Invasion Assay

MDA-MB-231 and BT549 cells infected with sh-SOX2 or sh-control were seeded in the upper chamber with Matrigel in the insert of a 24-well culture plate (BD Biosciences, Bedford, MA, United States) with serum-free medium. Then the lower chamber was added with DMEM medium with 15% fetal bovine serum as a chemoattractant. Then the invasive cells adhering to the lower membrane of the inserts were stained with Crystal Violet after 48 h of incubation. At last the invasive cells were counted and imaged with OLYMPUS IX71 Inverted Microscope (Olympus, Japan, Image-Pro Plus7.0 imaging system).

Apoptosis Assay

5×10^5 of MDA-MB-231 and BT549 cells infected with sh-SOX2 or sh-control were collected and washed twice with ice-cold PBS.

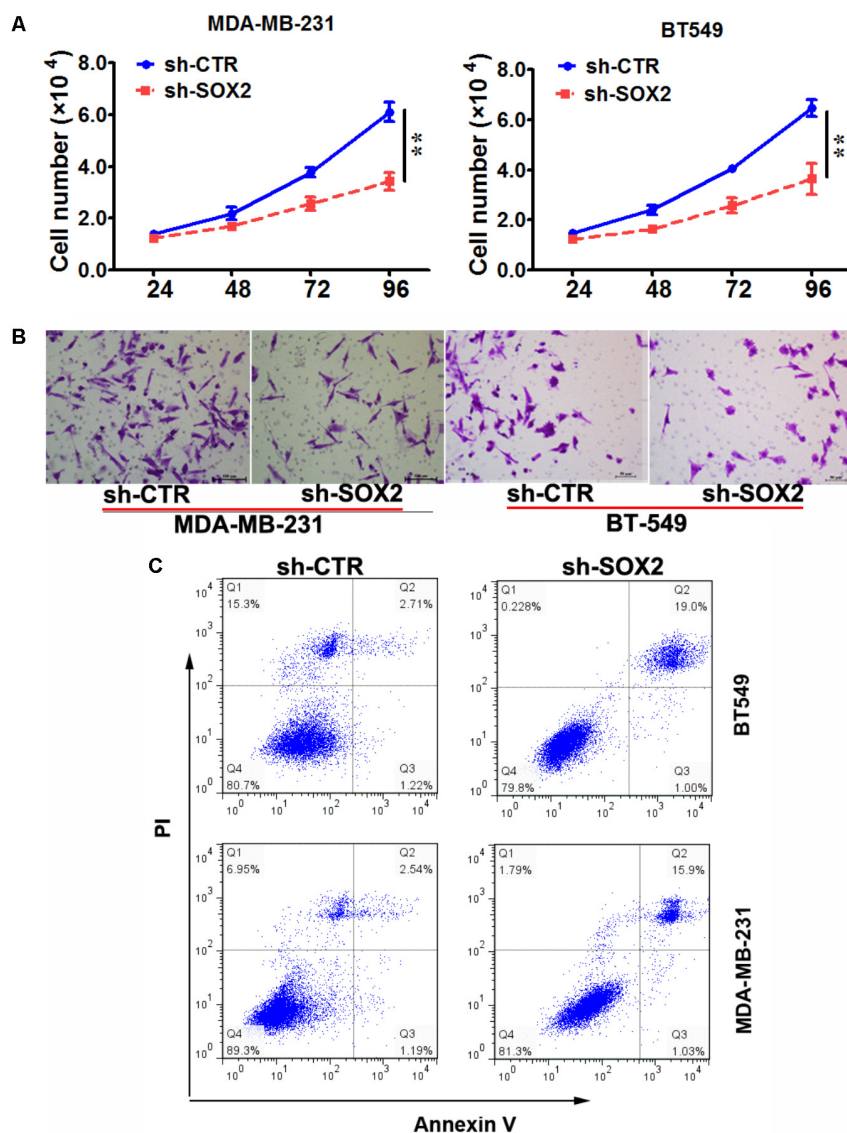


FIGURE 2 | SOX2 inhibition reduced cell proliferation and invasion, and promoted cell apoptosis in TNBC. **(A)** MDA-MB-231 and BT-549 cells were infected with sh-SOX2 or sh-control lentivirus. Cell number was counted at 24, 48, 72, 96 h after infection (** $p < 0.01$). **(B)** The invasion ability of MDA-MB-231 and BT-549 cells infected with sh-SOX2 or sh-control lentivirus detected by transwell assays. **(C)** The apoptosis ability of MDA-MB-231 and BT-549 cells infected with sh-SOX2 or sh-control lentivirus detected by apoptosis assays.

The cells were treated with Alexa Fluor®488 annexin V/Dead Cell Apoptosis Kit (Invitrogen, Carlsbad, CA, United States) for Flow Cytometry analysis according to manufacturer's instructions. The negative control for the double staining was untreated cells. The apoptosis ability of MDA-MB-231 and BT-549 were immediately detected by a FACSCalibur instrument (Becton Dickinson, San Diego, CA, United States).

Mouse Xenograft Model

5×10^6 MDA-MB-231 cells infected with sh-SOX2 or sh-control were inoculated subcutaneously into the dorsal flanks of nude mice (6 mice in each group). The mice were sacrificed after 28 days, then necropsies were performed, and the tumors

were weighed. Then IHC was used to detect the expression of SOX2 in tumor tissues of nude mice. In order to explore the effect of sh-SOX2 on tumor metastasis, 5×10^5 MDA-MB-231 cells infected with sh-SOX2 or sh-control were injected into the tail vein of nude mice (5 mice in each group). The mice were sacrificed 28 days later, and then necropsies were performed. The number of micrometastases in lung tissues per HE-stained section of every individual mice were analyzed by morphological observation with microscope. All procedures for handling animals were performed according with the institutional guidelines and all possible steps were taken to avoid animal suffering at all stages during the experiment.

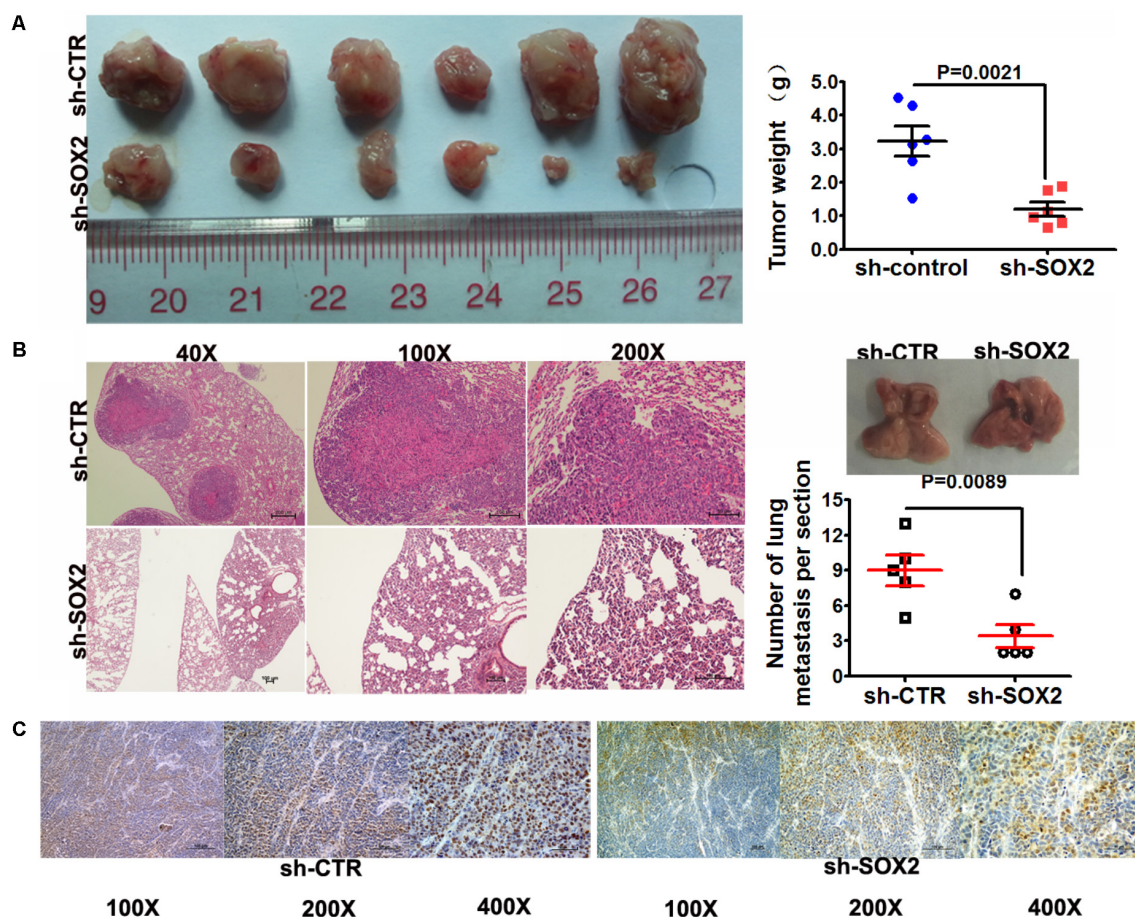


FIGURE 3 | SOX2 inhibition reduced tumorigenesis and metastasis in xenograft model. **(A)** Tumor xenografts in mice. MDA-MB-231 cells infected with sh-SOX2 or sh-control were subcutaneously injected into nude mice (6 in each group). 28 days later, the mice were sacrificed and dissected, and the tumors were weighed. **(B)** Tumor metastasis in mouse xenograft models. MDA-MB-231 cells infected with sh-SOX2 or sh-control lentivirus were injected into the tail vein of nude mice (5 in each group). 28 days later, the mice were sacrificed and micrometastases in the lung per HE-stained section from individual mice were calculated. **(C)** Expression levels of SOX2 in the mouse xenograft model. The expression level of SOX2 in the sh-SOX2 group was significantly lower than that in the sh-CTR group.

Statistical Analysis

All statistical analyses were performed by SPSS16.0 software. *t*-Test and χ^2 test were used to compare the data between groups. Kaplan–Meier method and Log-rank test were used to plot Overall survival (OS) and disease free survival (DFS) curves. Survival was counted from the day of surgery. The differences were considered statistically significant when $p < 0.05$.

RESULTS

SOX2 Was Overexpressed and Correlated With Poor Clinical Outcomes in TNBC

The expression of SOX2 in eight breast cancer cell lines (five TNBC cell lines, three NTNBC cell lines) and two mammary normal cell lines were detected by qRT-PCR. The results showed that SOX2 was strongly expressed in all 8 breast cancer cell lines, particularly in TNBC cell lines (Figure 1A and Supplementary

Figure S1): The SOX2 expression levels for some of the TNBC, NTNBC or normal mammary cell lines. The expression of SOX2 in 20 TNBC tissues and their matched adjacent normal tissues (Normal), 20 NTNBC tissues and their matched adjacent normal tissues (Control) were also detected by qRT-PCR. The results showed that approximately 95% (19/20) of the tissues in TNBC group showed notable increase in SOX2 expression compared with the average expression in Normal group ($p < 0.001$, Figure 1B). However, there was no significant increase of SOX2 expression in NTNBC tissues compared with the Control group ($p = 0.1237$, Figure 1B). These data indicated that SOX2 was mainly overexpressed in TNBC.

In order to determine the significance of SOX2 in clinical prognosis of TNBC, we performed IHC to evaluate SOX2 expression in 237 TNBC tissues. The 237 cases of tissues were divided into low or high groups based on the level of SOX2 expression. The presentative IHC images of three staining degrees (weak-medium-strong) of SOX2 expression under a microscope were showed in Supplementary Figure S4 (400X). Then OS and

DFS curves of these TNBC patients were performed by Kaplan–Meier survival analysis. The results indicated that patients with high SOX2 expression exhibited shorter time of OS ($p < 0.001$) and DFS ($p < 0.001$) than patients with low SOX2 expression (Figure 1C). These data indicated that overexpression of SOX2 was significantly associated with poor clinical outcomes of TNBC.

SOX2 Inhibition Reduced Cell Proliferation and Invasion, and Promoted Cell Apoptosis in TNBC

The above results indicated an inverse correlation between the SOX2 expression and the clinical outcomes of TNBC. We hypothesized that inhibition of SOX2 expression may improve the malignant status of TNBC. Therefore, we explore the role of SOX2 in proliferation, invasion, and apoptosis in TNBC cell lines. Two TNBC cell lines (MDA-MB-231 and BT549) were respectively infected with sh-SOX2 or sh-control lentivirus. Then the proliferation ability of these two cell lines was detected by MTT assay. We found that the cell numbers in sh-SOX2 infected group (sh-SOX2) were significantly reduced compared with sh-control infected group (sh-CTR) (Figure 2A). Meanwhile, the invasion ability of cells was detected by Transwell assay. As expected, the invasion ability of sh-SOX2 group was significantly decreased compared with sh-CTR group (Figure 2B). Furthermore, the apoptosis ability of cells was tested by Apoptosis assay. Consistent

with our hypothesis, the number of apoptosis cells of sh-SOX2 group was obviously more than those in sh-CTR group (Figure 2C).

SOX2 Inhibition Reduced Tumorigenesis and Metastasis in Xenograft Model

To further evaluate the role of SOX2 in tumor formation and growth *in vivo*, we adopted xenograft model of human TNBC cells in nude mice. MDA-MB-231 cells infected with sh-SOX2 or sh-control lentivirus were injected subcutaneously into nude mice (6 mice in each group). All mice were sacrificed to harvest the xenograft tumors after 28 days. The results showed that the mean volume and weight of tumors generated from sh-SOX2 group were both significantly lower than sh-control group (Figure 3A). Then the effect of SOX2 on tumor metastasis *in vivo* was performed by metastatic model of human TNBC cells in nude mice. MDA-MB-231 cells infected with sh-SOX2 or sh-control lentivirus were transplanted into the nude mice via tail vein injection. The mice were anesthetized after 28 days and all lungs were dissected. Hematoxylin and eosin (HE) staining was performed to evaluate the tissue morphology. The result showed that the number of macroscopic lung metastases and the SOX2 expression levels observed in sh-SOX2 group was significantly lower than sh-CTR group (Figures 3B,C). These results showed that SOX2 inhibition reduced tumorigenesis and metastasis in TNBC.

TABLE 1 | Clinicopathological variables and SOX2 expression in 237 TNBC patients.

Variables	Total (n = 237)	SOX2 low (n = 115)		SOX2 high (n = 122)		p-Value
		No.	%	No.	%	
Age (years)						0.578
< 50	142	71	50.0	71	50.0	
> = 50	95	44	46.3	51	53.7	
Menopause						0.884
Yes	98	47	48.0	51	52.0	
No	139	68	48.9	71	51.1	
Tumor size (cm)						0.117
= < 2	75	42	56.0	33	44.0	
> 2	162	73	45.1	89	54.9	
Tumor status (T)						<0.001**
T _{1–2}	202	109	54.0	93	46.0	
T _{3–4}	35	6	17.1	29	82.9	
TNM stage						<0.001**
I–II	167	99	59.3	68	40.7	
III–IV	70	16	22.9	54	77.1	
LN infiltrated						<0.001**
Yes	114	24	21.1	90	78.9	
No	123	91	74.0	32	26.0	
Histological grade						0.218
G1	3	2	66.7	1	33.3	
G2	115	60	52.2	55	47.8	
G3	119	53	44.5	66	55.5	

**Statistically significant ($p < 0.01$); % means percentage within the row. LNs, lymph nodes; G1, well-differentiated; G2, moderately differentiated; G3, poorly differentiated.

Increased SOX2 Levels Were Correlated With Tumor Status, TNM Stage, and Lymph Nodes Infiltration

We explored the potential clinicopathological implications when the expression of SOX2 altered. The expression level of SOX2 was inversely correlated with tumor status, TNM stage and lymph nodes infiltration (three *p*-values were less than 0.001), but not correlated with the patients' age, menopause, tumor size, and histological grade (four *p*-values were more than 0.05) among these 237 TNBC patients (Table 1). These results revealed that SOX2 may play a vital role in the occurrence and progression of TNBC.

DISCUSSION

Breast cancer is the most common malignancy and the second most common cause of cancer death among female malignant neoplasms (Huang et al., 2016). TNBC is a highly aggressive subcategory of breast cancer. The lack of well-defined molecular targets leads to no effective and readily available targeted therapies for treatment of TNBC (Mayer et al., 2014). In addition, tumor relapse, metastasis and drug resistance also render standard chemotherapy ineffective in the treatment of TNBC (Schröck et al., 2014). Search for specific molecular biomarkers for the treatment of TNBC has become an important area of research for both basic scientists and clinicians.

The acquisition of metastatic phenotypes of various cancers has been linked to the alterations of SOX2 expression. SOX2 is frequently up regulated in cancers and related with worse outcomes. It is reported that SOX2 promotes metastasis through the induction of the epithelial-mesenchymal transition (EMT) (Li et al., 2015). High expression of SOX2 has been correlated with tumor progression of oral squamous cell carcinoma (Fu et al., 2016), hepatocellular carcinoma (Zhao et al., 2015), colorectal cancer (Zheng et al., 2017), glioblastoma (Dong et al., 2017) and others. In this study, we found that SOX2 was up-regulated in both TNBC cell lines and clinical tissues by qRT-PCR. We also found that high expression of SOX2 was associated with shorter OS and DFS. We evaluated the immunohistochemical expression of SOX2 in 237 cases of TNBC tissues and assessed their prognostic significance. We found that SOX2 expression showed a significant association with tumor status, TNM stage and lymph nodes infiltration. All these results are consistent with the existing reports that high

expression of SOX2 is associated with poor OS in intrahepatic cholangiocarcinomas (Gu and Jang, 2014). SOX2 was reported to be a prognostic indicator of tongue squamous cell carcinoma (Huang et al., 2014). These results suggest that SOX2 could be a prognostic biomarker for TNBC as well.

Furthermore, we found that SOX2 inhibition reduced cell proliferation and invasion, induced cell apoptosis *in vitro*. SOX2 inhibition also suppressed tumorigenesis and metastasis *in vivo*. These results indicate that SOX2 can act as a tumor promoter in TNBC. Inhibition the expression of SOX2 by recombinant shRNA lentiviruses containing sh-SOX2 can improve the alleviate malignancy of TNBC. All these results are consistent with the existing studies that silencing SOX2 expression by RNA interference can inhibit the proliferation, invasion and metastasis, and induces apoptosis in human laryngeal cancer (Yang N. et al., 2015). Our results demonstrate that SOX2 has a tremendous potential to be a therapeutic target against TNBC.

CONCLUSION

In summary, inhibiting the expression of SOX2 can reduce the malignancy state of TNBC including proliferation, invasion, and metastasis. Our findings reveal the biological functions of SOX2 in TNBC. SOX2 is a valuable biomarker for TNBC prognosis and could be a potential therapeutic target of TNBC.

AUTHOR CONTRIBUTIONS

HT and CS designed and carried out the experiments. CS interpreted the data and wrote the manuscript. PL, JW, BC, XH, XP, and LL collected the human samples and clinical data.

FUNDING

This study was supported by the National Natural Science Foundation of China (81472469 to HT; 61372007 to LL).

SUPPLEMENTARY MATERIAL

The Supplementary Material for this article can be found online at: <https://www.frontiersin.org/articles/10.3389/fphar.2018.00942/full#supplementary-material>

REFERENCES

- Abd El-Maqsood, N. M., and Abd El-Rehim, D. M. (2014). Clinicopathologic implications of EpCAM and Sox2 expression in breast cancer[J]. *Clin. Breast Cancer* 14:e1-9. doi: 10.1016/j.clbc.2013.09.006
- Carrasco-Garcia, E., Santos, J. C., Garcia, I., Brianti, M., García-Puga, M., Pedrazzoli, J. Jr., et al. (2016). Paradoxical role of SOX2 in gastric cancer. *Am. J. Cancer Res.* 6, 701–713.
- Chung, J. H., Jung, H. R., Jung, A. R., Lee, Y. C., Kong, M., Lee, J. S., et al. (2018). SOX2 activation predicts prognosis in patients with head and neck squamous cell carcinoma. *Sci. Rep.* 8:1677. doi: 10.1038/s41598-018-20086-w
- Denkert, C., Liedtke, C., Tutt, A., and von, Minckwitz G (2016). Molecular alterations in triple-negative breast cancer-the road to new treatment strategies. *Lancet* 389, 2430–2442. doi: 10.1016/S0140-6736(16)32454-0
- Dong, H., Hao, X., Cui, B., and Guo, M. (2017). MiR-429 suppresses glioblastoma multiforme by targeting SOX2. *Cell Biochem. Funct.* 35, 260–268. doi: 10.1002/cbf.3271
- Feng, R., and Wen, J. (2015). Overview of the roles of Sox2 in stem cell and development. *Biol. Chem.* 396, 883–891. doi: 10.1515/hsz-2014-0317

- Fu, T. Y., Hsieh, I. C., Cheng, J. T., Tsai, M. H., Hou, Y. Y., Lee, J. H., et al. (2016). Association of OCT4, SOX2, and NANOG expression with oral squamous cell carcinoma progression. *J. Oral Pathol. Med.* 45, 89–95. doi: 10.1111/jop.12335
- Gu, M. J., and Jang, B. I. (2014). Clinicopathologic significance of Sox2, CD44 and CD44v6 expression in intrahepatic cholangiocarcinoma. *Pathol. Oncol. Res.* 20, 655–660. doi: 10.1007/s12253-014-9745-2
- Hon, J. D., Singh, B., Sahin, A., Du, G., Wang, J., Wang, V. Y., et al. (2016). Breast cancer molecular subtypes: from TNBC to QNBC. *Am. J. Cancer Res.* 6, 1864–1872.
- Huang, C. F., Xu, X. R., Wu, T. F., Sun, Z. J., and Zhang, W. F. (2014). Correlation of ALDH1, CD44, OCT4 and SOX2 in tongue squamous cell carcinoma and their association with disease progression and prognosis. *J. Oral Pathol. Med.* 43, 492–498. doi: 10.1111/jop.12159
- Huang, X., Li, X., Xie, X., Ye, F., Chen, B., Song, C., et al. (2016). High expressions of LDHA and AMPK as prognostic biomarkers for breast cancer. *Breast* 30, 39–46. doi: 10.1016/j.breast.2016.08.014
- Jiang, T., Shi, W., Natowicz, R., Ononye, S. N., Wali, V. B., Kluger, Y., et al. (2014). Statistical measures of transcriptional diversity capture genomic heterogeneity of cancer. *BMC Genomics* 15:876. doi: 10.1186/1471-2164-15-876
- Li, Q., Liu, F., Zhang, Y., Fu, L., Wang, C., Chen, X., et al. (2016). Association of SOX2 and nestin DNA amplification and protein expression with clinical features and overall survival in non-small cell lung cancer: a systematic review and meta-analysis. *Oncotarget* 7, 34520–34531. doi: 10.18632/oncotarget.9145
- Li, Y., Lv, Z., He, G., Wang, J., Zhang, X., Lu, G., et al. (2015). The SOX17/miR-371-5p/SOX2 axis inhibits EMT, stem cell properties and metastasis in colorectal cancer. *Oncotarget* 6, 9099–9112. doi: 10.18632/oncotarget.3603
- Liedtke, C., Gonzalez-Angulo, A. M., and Pusztai, L. (2010). “Definition of triple-negative breast cancer and relationship to basal-like molecular subtype,” in *DeVita, Hellman, and Rosenberg's Cancer: Principles and Practice of Oncology*, eds V. T. DeVita, T. S. Lawrence, and S. A. Rosenberg (Philadelphia, PA: Lippincott Williams & Wilkins), 1–6.
- Liu, X., Qiao, B., Zhao, T., Hu, F., Lam, A. K., and Tao, Q. (2018). Sox2 promotes tumor aggressiveness and epithelial-mesenchymal transition in tongue squamous cell carcinoma. *Int. J. Mol. Med.* 42, 1418–1426. doi: 10.3892/ijmm.2018.3742
- Luo, J., Yan, R., He, X., and He, J. (2018). SOX2 inhibits cell proliferation and metastasis, promotes apoptotic by downregulating CCND1 and PARP in gastric cancer. *Am. J. Transl. Res.* 10, 639–647.
- Maurizi, G., Verma, N., Gadi, A., Mansukhani, A., and Basilico, C. (2018). Sox2 is required for tumor development and cancer cell proliferation in osteosarcoma. *Oncogene* doi: 10.1038/s41388-018-0292-2 [Epub ahead of print].
- Mayer, I. A., Abramson, V. G., Lehmann, B. D., and Pietenpol, J. A. (2014). New strategies for triple-negative breast cancer—deciphering the heterogeneity. *Clin. Cancer Res.* 20, 782–790. doi: 10.1158/1078-0432.CCR-13-0583
- Saigusa, S., Tanaka, K., Toiyama, Y., Yokoe, T., Okugawa, Y., Ioue, Y., et al. (2009). Correlation of CD133, OCT4, and SOX2 in rectal cancer and their association with distant recurrence after chemoradiotherapy. *Ann. Surg. Oncol.* 16, 3488–3498. doi: 10.1245/s10434-009-0617-z
- Schneider, B. P., Winer, E. P., Foulkes, W. D., Garber, J., Perou, C. M., Richardson, A., et al. (2008). Triple-negative breast cancer: risk factors to potential targets. *Clin. Cancer Res.* 14, 8010–8018. doi: 10.1158/1078-0432.CCR-08-1208
- Schröck, A., Bode, M., Göke, F. J., Bareiss, P. M., Schairer, R., Wang, H., et al. (2014). Expression and role of the embryonic protein SOX2 in head and neck squamous cell carcinoma. *Carcinogenesis* 35, 1636–1642. doi: 10.1093/carcin/bgu094
- Thierauf, J., Weissinger, S. E., Veit, J. A., Affolter, A., Laureano, N. K., Beutner, D., et al. (2018). Low SOX2 expression marks a distinct subset of adenoid cystic carcinoma of the head and neck and is associated with an advanced tumor stage. *PLoS One* 13:e0194989. doi: 10.1371/journal.pone.0194989
- Wang, X., Liang, Y., Chen, Q., Xu, H. M., Ge, N., Luo, R. Z., et al. (2012). Prognostic significance of SOX2 expression in nasopharyngeal carcinoma. *Cancer Invest.* 30, 79–85. doi: 10.3109/07357907.2011.630049
- Wang, S., Tie, J., Wang, R., Hu, F., Gao, L., Wang, W., et al. (2015). SOX2, a predictor of survival in gastric cancer, inhibits cell proliferation and metastasis by regulating PTEN. *Cancer Lett.* 358, 210–219. doi: 10.1016/j.canlet.2014.12.045
- Yang, N., Wang, Y., Hui, L., Li, X., and Jiang, X. (2015). Silencing SOX2 expression by RNA interference inhibits proliferation, invasion and metastasis, and induces apoptosis through MAP4K4/JNK signaling pathway in human laryngeal cancer TU212 cells. *J. Histochem. Cytochem.* 63, 721–733. doi: 10.1369/0022155415590829
- Yang, S., Zheng, J., Xiao, X., Xu, T., Tang, W., Zhu, H., et al. (2015). SOX2 promotes tumorigenicity and inhibits the differentiation of I-type neuroblastoma cells. *Int. J. Oncol.* 46, 317–323. doi: 10.3892/ijo.2014.2713
- Yao, H., He, G., Yan, S., Chen, C., Song, L., Rosol, T. J., et al. (2017). Triple-negative breast cancer: is there a treatment on the horizon? *Oncotarget* 8, 1913–1924. doi: 10.18632/oncotarget.12284
- Zhang, J. F., Liu, J., Wang, Y., and Zhang, B. (2016). Novel therapeutic strategies for patients with triple-negative breast cancer. *Onco Targets Ther.* 9, 6519–6528. doi: 10.2147/OTT.S105716
- Zhao, X., Sun, B., Sun, D., Liu, T., Che, N., Gu, Q., et al. (2015). Slug promotes hepatocellular cancer cell progression by increasing sox2 and nanog expression. *Oncol. Rep.* 33, 149–156. doi: 10.3892/or.2014.3562
- Zheng, J., Xu, L., Pan, Y., Yu, S., Wang, H., Kennedy, D., et al. (2017). Sox2 modulates motility and enhances progression of colorectal cancer via the Rho-ROCK signaling pathway. *Oncotarget* 8, 98635–98645. doi: 10.18632/oncotarget.21709
- Zheng, Y., Qin, B., Li, F., Xu, S., Wang, S., and Li, L. (2015). Clinicopathological significance of Sox2 expression in patients with breast cancer: a meta-analysis. *Int. J. Clin. Exp. Med.* 8, 22382–22392.

Conflict of Interest Statement: The authors declare that the research was conducted in the absence of any commercial or financial relationships that could be construed as a potential conflict of interest.

Copyright © 2018 Liu, Tang, Song, Wang, Chen, Huang, Pei and Liu. This is an open-access article distributed under the terms of the Creative Commons Attribution License (CC BY). The use, distribution or reproduction in other forums is permitted, provided the original author(s) and the copyright owner(s) are credited and that the original publication in this journal is cited, in accordance with accepted academic practice. No use, distribution or reproduction is permitted which does not comply with these terms.



Current Standards and Recent Advances in Biomarkers of Major Endocrine Tumors

Yanhong Luo¹, Hua Zhu², Tao Tan² and Jianfeng He^{1*}

¹ Children's Hospital of Chongqing Medical University, Chongqing, China, ² Department of Surgery, Davis Heart and Lung Research Institute, The Ohio State University Wexner Medical Center, Columbus, OH, United States

OPEN ACCESS

Edited by:

Dong-Hua Yang,
St. John's University, United States

Reviewed by:

Yun Chen,
Albert Einstein College of Medicine,
United States
Yuqi Cui,
University of Missouri, United States
Yi Hong,
The University of Texas at Arlington,
United States

*Correspondence:

Jianfeng He
hjfdxyx@126.com

Specialty section:

This article was submitted to
Experimental Pharmacology
and Drug Discovery,
a section of the journal
Frontiers in Pharmacology

Received: 03 July 2018

Accepted: 03 August 2018

Published: 10 September 2018

Citation:

Luo Y, Zhu H, Tan T and He J (2018)
Current Standards and Recent
Advances in Biomarkers of Major
Endocrine Tumors.
Front. Pharmacol. 9:963.
doi: 10.3389/fphar.2018.00963

The complexity of endocrine tumor diagnosis stems from its variable symptoms and presentation that may mimic many other disease states, or display asymptomatic properties for a prolonged amount of time. Early and accurate disease identification is needed for better patient prognosis. The key to this may be in using validated biomarkers with enhanced sensitivity and specificity. Several biomarkers are consistently used across various endocrine tumor types, possibly indicating a deeper pathophysiological mechanism behind endocrine cancer genesis and development. For example, carbohydrate antigen (CA) is measured in both pancreatic adenocarcinoma as well as ovarian cancer for diagnosis, surveillance, and risk stratification. The discovery of measuring miRNAs that are highly expressed in malignant tumors is also a novel strategy across multiple endocrine tumor types, and is propelling the future advancement of biomarker development. This review introduces currently utilized biomarkers in some of the commonly known endocrine tumors, including thyroid, adrenal, pituitary, pancreatic, and gonadal carcinoma, as well as future research directions.

Keywords: biomarkers, thyroid carcinoma, neuroendocrine carcinoma, pituitary carcinoma, adrenal carcinoma

INTRODUCTION

Endocrinology comprises of a complex web of hormonal regulations. Understanding the intricacies of glands and hormones produced, as well as their downstream effects, is critical to the success of the field of endocrinology. It is difficult to categorize endocrinology strictly by organ systems, as its impact falls across multiple anatomic areas. On the other hand, the management of endocrinopathology is very simply summarized by initially assuming that most endocrine disorders can be treated by hormone replacement or suppression when accurately determined (Larry Jameson, 2015). However, variable symptoms and presentation that may mimic other disease states can make initial diagnosis difficult (Wolin et al., 2017). The key to correct disease identification may be in using biomarkers. Particularly for malignant tumors that require immediate medical attention, it is vital that clinically verified biomarkers be developed and utilized for timely diagnosis, and subsequently, to track treatment progress.

The current standard across most endocrine tumors includes an initial workup of measuring the level of offending hormone; yet this is generally low in specificity as abnormal hormone levels can also indicate other non-tumor disorders. Further biomarkers found in the serum and imaging diagnostics are required to confidently pinpoint the cancer diagnosis and monitor treatment success. However, many of these have not been shown to provide the specificity and sensitivity

required for accurate surveillance. With the advancement of biotechnologies, scientists may be turning increasingly to newer biomarkers such as micro RNAs (miRNAs). In this review, we discuss some of the most well-known endocrine tumors, including thyroid, adrenal, pituitary, pancreatic, and gonadal carcinoma, and their associated biomarkers, as well as future research directions.

THYROID CARCINOMA

Thyroid carcinoma is the malignant tumor of thyroid epithelia, which is also known as thyroid nodules. Thyroid carcinoma occurs infrequently when compared with the incidence of thyroid nodules. The lifetime diagnosis risk of thyroid carcinoma is 1.2% (Noone et al., 2018). The prevalence of thyroid nodules is currently about 5%, and the probability of developing thyroid nodules increases with older age (Noone et al., 2018). If tumors are present, identifying between aggressive and benign tumors can be a major challenge in thyroid pathology (Baloch et al., 2018). Thyroid carcinomas are categorized into differentiated (e.g., papillary, follicular, and Hürthle cell), medullary, and undifferentiated or anaplastic tumors (The National Comprehensive Cancer Network [NCCN], 2018e).

Diagnosis of Thyroid Carcinoma

Because both benign and malignant nodules can remain asymptomatic, diagnosis is often delayed and can lead to worse prognosis (The National Comprehensive Cancer Network [NCCN], 2018e). The protocol for evaluating thyroid carcinoma is well established. First and foremost, the thyroid-stimulating hormone (TSH) level is measured, and an ultrasound is performed to determine whether a fine-needle aspiration (FNA) is necessary (Czerwonka et al., 2014). Ultrasound features are often interpreted with high observer variability. As such, further tests may be required to confirm the diagnosis. Serum thyroglobulin (TG) levels can be taken, but are elevated in most thyroid diseases and may be relatively non-specific to tumors. Serum calcitonin levels can help with the early detection of medullary thyroid cancer (MTC) or tumors of C-cell origin. Focal (^{18}F) fluorodeoxyglucose positron emission tomography (^{18}FDG -PET) imaging is being increasingly utilized in malignant and non-malignant disease evaluation (Haugen et al., 2016). Soelberg et al. reported in a meta-analysis that approximately 35% of focal ^{18}FDG -PET positive thyroid nodules were cancerous (Soelberg et al., 2012). Contrastingly, diffuse ^{18}FDG -PET uptake is associated with benign disease. This test should be combined with sonographic evidence for further clinical confirmation. It is recommended that FNA cytology interpretation be standardized to the Bethesda System for Reporting Thyroid Cytopathology, which consists of six categories of malignancy risk (Crippa et al., 2010).

Molecular Testing of Thyroid Carcinoma

Recent advancement in molecular technology has made it possible to more conveniently test the molecular biomarkers in thyroid carcinoma. The most common molecular biomarkers

are involved in the analysis of gene mutation profile, epigenetic profile, microRNA profile, and cancer stem cell biomarkers. Molecular testing of FNA samples can further specify patient diagnosis, prognosis, therapeutic benefit, or aid in active observation (The National Comprehensive Cancer Network [NCCN], 2018e). Immunohistochemistry may be supplemental in confirming and differentiating thyroid tumors from other endocrine cancers, to further sub-classify tumor cell types or high-risk mutations. These biomarkers are critical in guiding individualized cancer treatment (Baloch et al., 2018). Most commonly studied genetic biomarkers include a seven-gene panel of mutations (*BRAF*, *RAS*, *RET/PTC*, and *PAX8/PPAR γ*) (Nikiforov et al., 2011), a gene expression classifier (mRNA expression of 167 genes) (Alexander et al., 2012), and galectin-3 immunohistochemistry (Bartolazzi et al., 2008). These tests have been shown to rule out malignancy in indeterminate cytology specimen or to guide surgical procedures. A variety of molecular marker test are also available in hospital-based laboratories for the ease of clinician.

Common Biomarkers in Thyroid Carcinoma

The biomarkers for thyroid carcinoma are numerous and diverse; therefore it is important to understand the nuances in biochemical and imaging test results to appropriately identify tumor types. For example, the human TG levels, though a rather insensitive form of measurement, can be significantly increased in patients with follicular-derived thyroid cancers as compared with those with benign conditions (Baloch et al., 2018). TG expression can give a clue to the thyroid follicular origin of the tumor, or can be decreased in the case of poorly differentiated thyroid carcinomas. Additional examination can reveal dense granular deposits localized to the perinuclear area or some cases of weak and focal expression in the case of oncocytic (Hürthle cell) tumors. Hürthle cell carcinoma can also look similar to medullary carcinoma on a frozen section (The National Comprehensive Cancer Network [NCCN], 2018e). Rare thyroid tumors can express both TG and calcitonin in the follicular cell- and C-cell-derived constituents, respectively. Other tests may be required to confirm the diagnosis (Baloch et al., 2018). On the imaging side, gallium-68 (^{68}Ga) radiolabelled somatostatin analog peptides in PET/CT have been well established for the diagnosis of neuroendocrine tumors. A study by Castroneves et al. showed that ^{68}Ga PET/CT may also be highly sensitive to identifying bone metastases in thyroid carcinoma (Castroneves et al., 2018).

Future Directions of Thyroid Carcinoma Biomarkers

Future research looks to optimize these molecular biomarkers for determining the diagnosis, prognosis, and treatment success. For example, mRNA (Lappinga et al., 2010) and miRNA (Agretti et al., 2012) markers have shown promise in diagnostic utility but have yet to be validated. Agretti et al. used data mining to identify miRNA with predictive enough expression to differentiate between benign and

TABLE 1 | Summary of biomarkers and diagnostic tests for endocrine tumors.

Endocrine tumor origin	Biomarkers	Diagnostic tests
Thyroid carcinoma	<ul style="list-style-type: none"> ● Thyroid-stimulating hormone (TSH) ● Thyroglobulin (TG) ● Calcitonin ● Genetic biomarkers <ul style="list-style-type: none"> ○ <i>BRAF</i> ○ <i>RAS</i> ○ <i>RET/PTC</i> ○ <i>PAX8/PPARγ</i> ○ mRNAs 	<ul style="list-style-type: none"> ● Fine-needle aspiration ● Imaging <ul style="list-style-type: none"> ○ (^{18}F) fluorodeoxyglucose positron emission tomography (^{18}FDG-PET) ○ Gallium-68 (^{68}Ga) radiolabelled somatostatin analog peptides PET/CT ● Immunohistochemistry <ul style="list-style-type: none"> ○ 7-gene mutation panel ○ Gene expression classifier ○ Galectin-3
Neuroendocrine carcinoma	<ul style="list-style-type: none"> ● Genetic biomarkers <ul style="list-style-type: none"> ○ <i>Menin</i> ○ <i>RET</i> ○ VHL ○ JAK3 ○ NRAS ○ RB1 ○ VHL1 ● Ki-67 ● Chromogranin A (CgA) ● 5-Hydroxyindoleacetic acid (5-HIAA) ● Mammalian target of rapamycin (mTOR) ● CDKN1B (p27) ● Circulating tumor cells (CTC) ● Hormonal markers <ul style="list-style-type: none"> ○ Insulin ○ Gastrin ○ Glucagon ○ Somatostatin ○ Growth hormone ○ Calcitonin ○ Substance P ○ Pancreastatin 	<ul style="list-style-type: none"> ● Imaging <ul style="list-style-type: none"> ○ CT and MRI ○ Somatostatin receptor scintigraphy (SRS) ○ ^{111}In-diethylenetriaminepentaacetic acid (^{111}In-DPTA)-octreotide scintigraphy ○ ^{18}F-fluorodopa and ^{68}Ga-labeled somatostatin analogs PET/CT ● Bloodwork to measure serum biomarkers
Pituitary carcinoma	<ul style="list-style-type: none"> ● Ki-67 ● p53 ● Cytokeratin ● Epithelial membrane antigen ● Glial fibrillary acidic protein ● CgA ● hTERT ● HER-2/neu ● COX-2 ● FGFR4 ● MMP ● Hormone markers <ul style="list-style-type: none"> ○ Adrenocorticotrophic hormone (ACTH) ○ Prolactin (PRL) ● Genetic mutational biomarkers <ul style="list-style-type: none"> ○ <i>Gsp</i> ○ <i>Ras</i> ○ <i>H-ras</i> ○ <i>Rb</i> ○ Chromosome 11 deletion ○ PTTG 	<ul style="list-style-type: none"> ● Imaging <ul style="list-style-type: none"> ○ ^{111}In-DPTA-octreotide SRS ● MIB-1 staining index ● Immunohistochemistry
Pancreatic adenocarcinoma	<ul style="list-style-type: none"> ● Carcinoembryonic antigen (CEA) ● Anti-oncofetal antigen ● Tissue polypeptide antigen ● Carbohydrate antigen (CA) 125 ● CA 19-9 ● TIMP1 ● LRG1 ● S100P 	

(Continued)

TABLE 1 | Continued

Endocrine tumor origin	Biomarkers	Diagnostic tests
Gonadal adenocarcinomas	<ul style="list-style-type: none"> Genetic mutational biomarkers <ul style="list-style-type: none"> <i>p16</i> <i>BRCA2</i> <i>KRAS</i> <i>TP53</i> <i>CDKN2A</i> <i>SMAD4</i> 	<ul style="list-style-type: none"> Imaging <ul style="list-style-type: none"> CT Endoscopic ultrasound (EUS) MRI FNA Immunoassays
	Testicular cancer <ul style="list-style-type: none"> Alpha-fetoprotein (AFP) Lactate dehydrogenase (LDH) Beta-human chorionic gonadotropin (beta-hCG) <i>XIST</i> gene expression miRNAs <ul style="list-style-type: none"> miR-371-3 miR-302/367 	Testicular cancer <ul style="list-style-type: none"> Bloodwork to measure serum markers PET MRI Ultrasound
	Ovarian cancer <ul style="list-style-type: none"> CA-125 Inhibin AFP Beta-hCG HE4 LDH CEA Cytokeratin 7 (CK7) PAX8 Estrogen receptor Genetic mutational markers <ul style="list-style-type: none"> <i>BRCA1</i> <i>BRCA2</i> miRNAs 	Ovarian cancer <ul style="list-style-type: none"> Abdominal, pelvic, or endovaginal ultrasound CT/MRI PAX8 immunostaining

malignant nodule. They found that miR-146b, miR-187, and miR-224 expressions were significantly increased in papillary thyroid carcinoma compared with in benign nodules (Agretti et al., 2012). Peripheral blood TSH receptor mRNA assay has been associated with high positive predictive value (90%) and negative predictive value (39%) in a single-center, prospective study (Milas et al., 2010). Longer-term studies are required to standardize and determine the validity of the diverse options for molecular testing.

NEUROENDOCRINE AND ADRENAL CARCINOMAS

Neuroendocrine carcinomas result from cells throughout the diffuse endocrine system (The National Comprehensive Cancer Network [NCCN], 2018a). Most common of these are well differentiated or carcinoid tumors, which are gastroenterohepatic and pulmonary in origin and exhibit a variety of symptoms (Gabriel et al., 2018). Patients may present with symptoms associated with hormonal hypersecretion (“functional” tumors) or those that are asymptomatic are considered to have “non-functional” disease (The National Comprehensive Cancer Network [NCCN], 2018a). Furthermore, due to the sporadic and gradual nature of tumor growth, as well as their small size, the lesions can be difficult to detect (Gabriel et al., 2018).

The most common inherited syndrome associated with neuroendocrine tumors is multiple endocrine neoplasia type (MEN) 1 (Oberg, 2013). Inherited genetic syndromes such as MEN types 1 and 2 are characterized by tumors of a number of origins depending on mutation type. For example, in MEN type 1, mutations in *menin* gene is associated with tumors of parathyroid, pituitary, and pancreatic glands, while MEN 2 is characterized by mutations in the *RET* proto-oncogene and leads to the development of medullary thyroid carcinoma, pheochromocytoma, and hyperparathyroidism (The National Comprehensive Cancer Network [NCCN], 2018a). Other genetic aberrations found upon mutational analysis include the VHL gene in pancreatic neuroendocrine tumors (NETs) and JAK3, NRAS, RB1, and VHL1 in pulmonary NETs (Oronsky et al., 2017).

Diagnosis of Neuroendocrine Carcinomas

Neuroendocrine carcinomas are histologically categorized by tumor differentiation (The National Comprehensive Cancer Network [NCCN], 2018a). Generally, tumor grade is positively correlated with mitotic count and Ki-67 proliferation index, while the classification method differs depending on tumor origin (Klimstra et al., 2010). Staging is according to the AJCC tumor, node, metastasis (TNM) system and determined similarly to other cancers of organs

in its physiologic vicinity (Edge et al., 2010). In other words, for example, carcinoids of the lung and bronchi are staged in the same manner as common lung carcinomas, and carcinoids of gastrointestinal origin are staged by other means.

Various imaging techniques are important in initial detection and evaluating the tumor grade of NETs. The current standard work-up includes CT and MRI; clinicians may additionally consider using somatostatin receptor scintigraphy (SRS) (The National Comprehensive Cancer Network [NCCN], 2018a). One of the standard imaging techniques utilizes ^{111}In -diethylenetriaminepentaacetic acid (^{111}In -DTPA)-octreotide. Newer, more sensitive PET radiotracers, such as ^{18}F -fluorodopa and ^{68}Ga -labeled somatostatin analogs are also utilized for more differentiated tumors (Gabriel et al., 2018).

Common Biomarkers of Neuroendocrine Carcinomas

One commonly used protein marker is chromogranin A (CgA), which is elevated and particularly useful in patients with non-functioning neuroendocrine tumors as well as in its ability to indicate poorer prognosis (Kapoor et al., 2014; Oronsky et al., 2017). Evaluating serotonin secretion using a 24-h urine collection of a serotonin metabolite, 5-Hydroxyindoleacetic acid (5-HIAA), is another biomarker assessment recommended for patients with metastatic lung or GI carcinoid tumors (Kapoor et al., 2014; Oronsky et al., 2017). Diet and drugs can affect 5-HIAA levels, however, and therefore proper patient counseling is warranted before this test (The National Comprehensive Cancer Network [NCCN], 2018a). Another study found that mammalian target of rapamycin (mTOR) overexpression correlated with decreased overall survival (OS) (Qian et al., 2013). Mutations in cyclin-dependent kinase inhibitor, CDKN1B (p27) or loss of CDKN1B expression have been observed in gastroenteropancreatic neuroendocrine tumors (Kim et al., 2014). Khan et al. (2013) hypothesized that circulating tumor cells (CTC) would suggest a more disseminated disease and found that the presence of CTC was associated with decreased progression-free survival and OS.

Future Directions of Neuroendocrine Carcinoma Biomarkers

Because of the heterogeneity of the disease, neuroendocrine neoplasms secrete a vast spectrum of protein or hormonal markers aside from CgA and 5-HIAA, such as insulin, gastrin, glucagon, somatostatin, growth hormone, calcitonin, substance P, pancreastatin, etc (Oronsky et al., 2017). This makes detection even more difficult for an already rare disease. Having a common biomarker may ease the process and facilitate earlier tumor diagnosis, as pursued, for example, by Gabriel and colleagues, who demonstrated that using ^{68}Ga -DOTATATE PET/CT for primary detection was superior than standard work-up (Gabriel et al., 2018). Yet, there is still a dearth of knowledge on the molecular

basis of neuroendocrine tumors, and therefore more studies are needed to validate these molecular assays for clinical application. To date, no single biomarker has been accepted for use in neuroendocrine tumors (Oberge et al., 2015).

PITUITARY ADENOCARCINOMAS

Pituitary tumors often present as sellar masses. Sellar masses can form as frequently as in about 10–15% of the adult population. In contrast, pituitary carcinomas (PCs) are one of the most rare but aggressive tumor types, representing only 0.1–0.2% of all pituitary tumors (Ragel and Couldwell, 2004).

Diagnosis of Pituitary Carcinoma

Pituitary carcinomas often present as invasive macroadenomas that metastasize systemically (Ragel and Couldwell, 2004). MRI is used to diagnose the extent of sellar masses (Ragel and Couldwell, 2004). In particular, imaging techniques that accurately measure the dimensions and invasions of the tumor site are recommended (Raverot et al., 2018). For example, SRS with ^{111}In -DTPA-octreotide can identify distant pituitary metastases (Ragel and Couldwell, 2004). Consistent tumor measurements are necessary to track tumor progression and guide treatment throughout the course of the disease (Raverot et al., 2018).

Common Biomarkers of Pituitary Carcinoma

Pituitary carcinomas harbor more commonly renowned neoplastic biomarkers such as Ki-67 and p53. Since the main characteristic of PCs is the mitoses of tumor cells, histopathological results often show an increase in MIB-1 staining index (for Ki-67) as well as a higher level of p53 protein (Ragel and Couldwell, 2004; Raverot et al., 2018). Immunohistochemical findings are often used as differential diagnosis from other diseases, such as Cushing's syndrome or other metastatic tumors (Hirohata et al., 2014). Majority of PCs are hormone-secreting tumors, including adrenocorticotrophic hormone (ACTH) secreting and prolactin (PRL) secreting tumors (Hirohata et al., 2014), and as such, antibodies for these hormones are used to aid in the diagnosis of pituitary tumor origin (Ragel and Couldwell, 2004). Other biomarkers that help identify tumor source are cytokeratin, epithelial membrane antigen, glial fibrillary acidic protein (GFAP), and CgA (Ragel and Couldwell, 2004).

Molecular Testing of Pituitary Carcinoma

Molecular and cytogenetic determination of PCs may play a role in better characterizing PCs. The *Gsp* gene is present in about 40% of growth hormone (GH)-producing tumors and the *Ras* oncogene is associated with anaplastic progression (Ragel and Couldwell, 2004). Higher level of p53 is indicative of an aggressive course of disease. A quantitative immunohistochemical study showed that p53 is expressed in 0

and 100% of non-invasive and metastatic disease, respectively (Ragel and Couldwell, 2004).

Future Directions of Pituitary Carcinoma Biomarkers

Early diagnosis of PC is challenging but extremely important due to the morbidity associated with the disease (Raverot et al., 2018). Despite advances in research, however, a single biomarker has yet to be found that accurately predicts tumor behavior (Raverot et al., 2018). Other observed molecular or cytogenetic markers that could be potential biomarkers includes the *H-ras* gene mutations, the presence or absence of D2 receptors, measured telomerase activity via hTERT expression, the expression of HER-2/neu, the detecting of cyclooxygenase-2 (COX-2) enzymes, and the involvement of the *Rb* gene (Ragel and Couldwell, 2004; Sav et al., 2012). For detecting high risk disease, FGFR4, MMP, PTTG, and deletions in chromosome 11 in addition to identifying levels of Ki-67 and p53 have been suggested as concerns for aggressive disease management (Mete et al., 2012). Finally, there is a dire research need for standardized criteria for evaluating biomarkers for PCs to validate them as having predictive value (Sav et al., 2012).

PANCREATIC ADENOCARCINOMAS

Pancreatic adenocarcinoma is the fourth most common cause of death in the United States (Siegel et al., 2017). Detection of pancreatic cancer is a challenge because early signs of pancreatic cancer are rarely seen (The National Comprehensive Cancer Network [NCCN], 2018c). Tumor presence is often predicted from astute observation of patient medical histories and presenting symptoms. Therefore, there is a strong consensus on the importance of developing biomarkers for the early diagnosis of pancreatic cancer to prevent further morbidity and mortality. Tumor-associated antigens that are related to pancreatic adenocarcinoma are numerous and include those such as carcinoembryonic antigen (CEA), pancreatic anti-oncofetal antigen, tissue polypeptide antigen, carbohydrate antigen (CA) 125, and CA 19-9 (The National Comprehensive Cancer Network [NCCN], 2018c).

Diagnosis of Pancreatic Adenocarcinoma

The primary means of diagnosis of pancreatic adenocarcinoma is through imaging. All patients with suspected disease should undergo initial CT evaluation, and continue imaging after every step of therapy (e.g., after neoadjuvant treatment), which provides constant assessment. The TNM staging criteria by the AJCC is utilized to determine whether the tumor is resectable (Edge et al., 2010). The initial recommendation is to screen with endoscopic ultrasounds (EUS) and/or MRI for high-risk individuals (i.e., those with cancer in the family or those that are carriers of *p16* or *BRCA2* mutations) (The National Comprehensive Cancer Network [NCCN], 2018c). A biopsy enhances the pathologic diagnosis of adenocarcinoma before the administration

of neoadjuvant therapy (Brugge et al., 2014). Fine-needle aspiration (FNA) guided by EUS is preferred (Brugge et al., 2014). Molecular analyses may supplement EUS by observing for some of the most common mutations in pancreatic cancer, including *KRAS*, *TP53*, *CDKN2A*, and *SMAD4* (Waddell et al., 2015).

Common Biomarkers of Pancreatic Adenocarcinoma

Carbohydrate antigen 19-9 is currently the most validated biomarker for early diagnosis and surveillance of pancreatic cancer. However, it is not tumor-specific, as CA 19-9 is often also expressed in other pancreatic diseases, other malignancies, as well as hepatobiliary disease (The National Comprehensive Cancer Network [NCCN], 2018c); nevertheless, it is still useful in differentiating from inflammatory conditions (The National Comprehensive Cancer Network [NCCN], 2018c). CA 19-9 has a sensitivity of 79–81% and a specificity of 80–90% in symptomatic patients (Huang and Liu, 2014). It is also beneficial to evaluate CA 19-9 as a prognostic biomarker, since a low level or a decreasing level were associated with better median survival in patients with resectable disease (Humphris et al., 2012; Bauer et al., 2013).

Furthermore, CA 19-9 may guide treatment in post-operative settings. In a study of 260 patients, those with CA 19-9 levels less than 90 U/mL benefited from adjuvant therapy by showing a longer disease-free survival (DFS), while those with higher CA 19-9 levels receiving adjuvant therapy showed no difference in DFS from untreated patients (Humphris et al., 2012). This prognostic benefit is also reflected in neoadjuvant or borderline resectable disease (Tzeng et al., 2014) and advanced disease (Bauer et al., 2013; Pelzer et al., 2013), as demonstrated by longer OS correlating with lower CA 19-9 levels. The NCCN guidelines recommend drawing serum CA 19-9 levels before and immediately following surgery, before administration of adjuvant therapy, and for surveillance (The National Comprehensive Cancer Network [NCCN], 2018c).

Molecular Testing of Pancreatic Adenocarcinoma

Novel biomarkers to screen for early pancreatic cancer are currently being investigated. Notably, there is much improvement in technology that identifies microRNAs in whole blood, profiles serum metabolism, and measures circulating cell-free DNA as possible biomarkers for screening (Schultz et al., 2014). Additionally, CA 19-9 (which is currently used as part of diagnostic testing) was also found to be elevated in pancreatic patients even before the cancer diagnosis, and therefore could be a potential biomarker for screening high-risk patients and for measuring response to chemotherapy (Morris-Stiff and Taylor, 2012). Another study, a meta-analysis, concluded that S100 calcium-binding protein P (S100P) shows high sensitivity (0.87; 95% CI, 0.83–0.90) and specificity (0.88; 95% CI, 0.82–0.93) for pancreatic cancer diagnosis (Hu et al., 2014).

Future Directions of Pancreatic Adenocarcinoma Biomarkers

While surgical removal of pancreatic cancer can result in better survival, only about 15 to 20% of patients still have localized disease at the time of diagnosis. Therefore, researchers are furiously validating biomarker candidates for earlier detection of disease. For example, Capello et al. (2017) demonstrated the validation of a panel of immunoassays as biomarker candidates, and found that TIMP1 and LRG1 in combination with CA 19-9 enhanced the detection of early-stage pancreatic cancer when compared with CA 19-9 alone. More evidence is needed for the optimal diagnosis and management of pancreatic lesions. Global experts are urging clinicians to share tissue samples to facilitate the research of potential diagnostic and prognostic biomarkers for pancreatic adenocarcinoma (The National Comprehensive Cancer Network [NCCN], 2018c).

GONADAL ADENOCARCINOMAS – TESTICULAR CANCER AND OVARIAN CANCER

Testicular Cancer, Its Diagnostic Biomarkers and Future Directions

Within all testicular cancer cases, 95% of them consist of germ cell tumors (GCTs) (The National Comprehensive Cancer Network [NCCN], 2018d). Biomarkers that aid in the diagnosis, prognosis, and to monitor treatment are well recognized in this disease state. Classic serum markers utilized for GCTs are alpha-fetoprotein (AFP), lactate dehydrogenase (LDH), and beta-human chorionic gonadotropin (beta-hCG) (Gilligan et al., 2010). Beta-hCG is often the most elevated serum biomarker in testicular cancer and its levels differ depending on the disease type (i.e., seminomatous and non-seminomatous) and metastatic risk, making it a useful diagnostic tool (Ferraro et al., 2018). Minor changes in beta-hCG should be interpreted cautiously, however, as it could be confounded with other conditions (Gilligan et al., 2010; Ferraro et al., 2018). Increased AFP levels are often associated with non-seminomatous disease and can be detected at any stage, but must also be analyzed with care; AFP levels that rise steadily can indicate metastasis, but clinicians may hold initial treatment in patients with only mildly increased and stable AFP levels (Gilligan et al., 2010). Another biomarker, LDH, is utilized in the risk-stratification of patients who are starting initial chemotherapy (Gilligan et al., 2010). LDH may be measured to check for relapse, but it is noteworthy that LDH is relatively non-specific with a high false-positive rate and should not be used alone to indicate treatment (Gilligan et al., 2010). These biomarkers guide clinicians in selecting further diagnostic tests (e.g., PET scan or MRI) and in choosing the appropriate course of treatment.

Testicular cancer is staged using the AJCC TNM system and based on the beta-hCG, LDH, and AFP levels (The National Comprehensive Cancer Network [NCCN], 2018d). Additionally,

an ultrasound can complement diagnosis by imaging testicular mass and its surrounding conditions. Treatment is mainly radical orchiectomy, and chemotherapy as required. After the procedure, serum biomarkers will be continuously monitored for their physiological kinetics to determine whether the levels are decreasing at target rates. A slower decline than expected can suggest metastatic disease (The National Comprehensive Cancer Network [NCCN], 2018d).

Despite the standardized approach to measuring beta-hCG, AFP, and LDH levels, these traditional serum biomarkers may not be elevated in a significant number of GCT patients (Looijenga et al., 2014). Therefore, other biomarker candidates have been suggested, such as analyzing the expression of *XIST* gene and detection of specific miRNAs such as from the miR-371-3 and miR-302/367 clusters (Looijenga et al., 2014; Mir et al., 2016). Recently, a number of newer protein markers have been identified to differentiate between histologic subtypes of testicular cancer, such as High Mobility Group A (HMGA), POZ-AT hook-zinc finger protein (PATZ), Aurora-B, Nek-2, c-kit, PLAP, NANOG, SOX2, and CDK10 (Mir et al., 2016). *In vitro* research shows varying levels of overexpression based on tumor differentiation (i.e., seminoma, embryonic carcinoma, or yolk cell tumors). Study of these biomarkers may hold promise for additional utility for diagnosis or active surveillance of testicular cancer (Mir et al., 2016).

Ovarian Cancer, Its Diagnostic Biomarkers and Future Directions

In contrast to testicular cancers, ovarian tumors consist of a more diverse collection of histopathologic entities (Kurman et al., 2014). Majority of ovarian cancer cases comprise of the epithelial type; others include germ cell tumors and sex-cord stromal cell tumors, as well as a number of rare pathological types (Prat, 2012). The difficulty in treating ovarian cancer mainly stems from the difference in therapy based on each tumor type (The National Comprehensive Cancer Network [NCCN], 2018b). As such, in the United States, it is the fifth most common cause of cancer death in women (The National Comprehensive Cancer Network [NCCN], 2018b).

Due to the physiological location of the ovaries, screening is extremely difficult at an earlier stage (The National Comprehensive Cancer Network [NCCN], 2018b). Therefore, it may be pertinent to find serum biomarkers that help detect less mature disease. While routine screening is not currently required in all women, clinicians may monitor high-risk patients by measuring cancer antigen 125 (CA-125) and performing endovaginal ultrasounds (Smith et al., 2015).

There are multivariate index assay tests previously used for ovarian cancer screening that may now be outdated (Ueland, 2017). Several professional health organizations are now stating that the OVA1 test (which uses five markers: transthyretin, apolipoprotein A1, transferrin, beta-2 microglobulin, and CA-125) should not be used to assess whether patients are candidates for surgery (Timmerman et al., 2016). Additionally, the OvaSure screening test (which uses six biomarkers: leptin, prolactin, osteopontin, insulin-like growth factor II, macrophage

inhibitory factor, and CA-125) is no longer reliable because some of the markers are not expressed timely enough to be useful for early stage detection of ovarian cancer (Mai et al., 2011).

What is recommended, on the other hand, may overlap between various histopathologic types. Initial work up of an undiagnosed pelvic mass combines laboratory studies with an abdominal or pelvic ultrasound and/or CT/MRI scan. Serum tumor markers such as CA-125, inhibin, AFP, and beta-hCG can be measured based on patient characteristics (The National Comprehensive Cancer Network [NCCN], 2018b). As an example, clinicians may consider measuring AFP levels in younger women if germ cell tumors are suspected. Furthermore, the FDA has approved HE4 and CA-125 as biomarkers to determine the risk of ovarian cancer in women with undiagnosed pelvic mass (Yoshida et al., 2016); however, measuring these biomarkers is not currently fully recommended by the NCCN and is regarded as optional by other professional organizations such as the Society of Gynecologic Oncologists (SGO) (Salani et al., 2011). If CA-125 levels were initially elevated, measures can be repeatedly taken for follow up post-treatment, but may be inconclusive in patients such as those that are asymptomatic with elevated levels of CA-125 (Lindemann et al., 2016). Others that may be useful in diagnostic tests may include the previously mentioned biomarkers, LDH and CEA (The National Comprehensive Cancer Network [NCCN], 2018b). The CA-125 to CEA ratio is occasionally taken before starting neoadjuvant chemotherapy to confirm the histology of the ovarian cancer along with biopsy results (The National Comprehensive Cancer Network [NCCN], 2018b). Family history plays a strong role in onset of ovarian cancer at an earlier age, particularly when associated with *BRCA1* and *BRCA2* genotypes (Nakonechny and Gilks, 2016); therefore, genetic analysis to identify *BRCA* mutations is important in risk-classification.

Less common histopathologies have other unique biomarkers for diagnosis and screening. In mucinous carcinoma, PAX8 immunostaining may be helpful to differentiate from adenocarcinomas that have metastasized to ovaries (Bruls et al., 2015). Endometrioid adenocarcinomas express higher levels of cytokeratin 7 (CK7), PAX8, CA-125, and estrogen receptors (McCluggage et al., 2015).

Determining an accurate sequential application of or crafting an individualized approach to diagnostic methods are some future strategies to be considered. Particularly in a tumor type with extremely diverse morphology, measuring only a serum biomarker may be insufficient and should be combined with ultrasound and CT scan (Ueland, 2017). For advancing the utility of ovarian cancer biomarkers, new types of biomarkers such as miRNAs hold promise and are also being studied extensively (Ueland, 2017). Circulating cell-free miRNAs are showing increasing potential in earlier detection in the general field of oncology (Schwarzenbach et al., 2014). A review by Nakamura et al. described the methodologies for obtaining miRNA samples and summarized studies of miRNAs with clinical relevance in ovarian cancer diagnosis, prognosis, and measuring treatment response (Nakamura et al., 2016). The ideal situation

is that a combination of serum nucleic markers and imaging techniques may provide for a simplified yet comprehensive screening panel in a single test.

FUTURE PERSPECTIVES

In reviewing the present biomarkers in various endocrine neoplasms, several recurring themes can be noted. Firstly, measuring hormone secretion is logical and is often the initial sign that a tumor should be suspected, but it is rarely the only way to diagnose tumors of endocrine origin. Rather, a combination of biochemical, imaging, and genetic analyses, as well as patient history and presented symptoms should aid in the tumor characterization. Some of the common serum biomarkers that are used across multiple endocrine tumors are CgA (Kapoor et al., 2014; Oronsky et al., 2017), CA (Bauer et al., 2013), beta-hCG (Gilligan et al., 2010; Looijenga et al., 2014), and AFP (Gilligan et al., 2010; Looijenga et al., 2014). Current standard biomarkers and methods used are summarized in **Table 1**. Perhaps these biomarkers will further elucidate the basis of endocrinopathy. Furthermore, in the exploration for novel biomarkers, researchers are increasingly turning to miRNAs across all tumor types (Looijenga et al., 2014; Mir et al., 2016; Nakamura et al., 2016; Ueland, 2017). In the age of advanced technology and globalization, it is also important to conduct research to standardize and validate these biomarkers for universal use across the diversity of the human race.

The complex nature of endocrine pathology requires detailed identification to differentiate an endocrine tumor from other conditions that may be suspected in the same physiologic region, or that may be metastases of other tumors (Wolin et al., 2017). As some of the endocrine malignancies are considered rare, often asymptomatic, and aggressive cancers, it is also imperative to develop biomarkers that enable earlier detection of disease. Similar to the management of other types of cancers, researchers are investigating the applicability of measuring circulating tumor cells in neuroendocrine tumors (Khan et al., 2013). New protein biomarkers have been identified for validation, such as p27 in gastroenteropancreatic neuroendocrine tumors (Kim et al., 2014), COX-2 enzyme in pituitary carcinoma (Ragel and Couldwell, 2004; Sav et al., 2012), TIMP1 and LRG1 in pancreatic adenocarcinoma (Capello et al., 2017), HMGA among others in testicular cancer (Mir et al., 2016), and various test panels recently approved by regulatory bodies for ovarian cancer (Yoshida et al., 2016).

Molecular and genetic testing combined is another strategy that may pave the way for potential uses of targeted therapies in endocrine neoplasms, which can help reduce unwanted adverse effects of systemic chemotherapy. The advent of immunotherapy is also becoming a clinical research area of interest in endocrinopathy such as thyroid carcinoma (Naoum et al., 2018). Finally, professional societies are urging clinicians and researchers to contribute to reporting programs or donate tumor samples. These collaborative efforts will facilitate the

acceleration of biomarker discovery and validation, in turn advancing the care of endocrine cancer patients.

CONCLUSION

The diagnosis and treatment of endocrine tumors are still challenging because of the complexity of their clinical presentations. Multiple biomarkers and modalities are required for diagnosis and management of endocrine tumors. Efforts must be warranted to develop newer biomarkers for better patient care.

REFERENCES

- Agretti, P., Ferrarini, E., Rago, T., Candelieri, A., De Marco, G., Dimida, A., et al. (2012). MicroRNA expression profile helps to distinguish benign nodules from papillary thyroid carcinomas starting from cells of fine-needle aspiration. *Eur. J. Endocrinol.* 167, 393–400. doi: 10.1530/eje-12-0400
- Alexander, E. K., Kennedy, G. C., Baloch, Z. W., Cibas, E. S., Chudova, D., Diggans, J., et al. (2012). Preoperative diagnosis of benign thyroid nodules with indeterminate cytology. *N. Engl. J. Med.* 367, 705–715. doi: 10.1056/NEJMoa1203208
- Baloch, Z., Mete, O., and Asa, S. L. (2018). Immunohistochemical biomarkers in thyroid pathology. *Endocr. Pathol.* doi: 10.1007/s12022-018-9532-9 [Epub ahead of print].
- Bartolazzi, A., Orlandi, F., Saggiorato, E., Volante, M., Arecco, F., Rossetto, R., et al. (2008). Galectin-3-expression analysis in the surgical selection of follicular thyroid nodules with indeterminate fine-needle aspiration cytology: a prospective multicentre study. *Lancet Oncol.* 9, 543–549. doi: 10.1016/s1470-2045(08)70132-3
- Bauer, T. M., El-Rayes, B. F., Li, X., Hammad, N., Philip, P. A., Shields, A. F., et al. (2013). Carbohydrate antigen 19-9 is a prognostic and predictive biomarker in patients with advanced pancreatic cancer who receive gemcitabine-containing chemotherapy: a pooled analysis of 6 prospective trials. *Cancer* 119, 285–292. doi: 10.1002/cncr.27734
- Brugge, W. R., De Witt, J., Klapman, J. B., Ashfaq, R., Shidham, V., Chhieng, D., et al. (2014). Techniques for cytologic sampling of pancreatic and bile duct lesions: the papanicolaou society of cytopathology guidelines. *Cytojournal* 11 (Suppl. 1):2. doi: 10.4103/1742-6413.133311
- Bruls, J., Simons, M., Overbeek, L. I., Bulten, J., Massuger, L. F., and Nagtegaal, I. D. (2015). A national population-based study provides insight in the origin of malignancies metastatic to the ovary. *Virchows Arch.* 467, 79–86. doi: 10.1007/s00428-015-1771-2
- Capello, M., Bantis, L. E., Scelo, G., Zhao, Y., Li, P., Dhillon, D. S., et al. (2017). Sequential validation of blood-based protein biomarker candidates for early-stage pancreatic cancer. *J. Natl. Cancer Inst.* 109:djw266. doi: 10.1093/jnci/djw266
- Castroneves, L. A., Coura Filho, G., de Freitas, R. M. C., Salles, R., Moyses, R. A., Lopez, R. V. M., et al. (2018). Comparison of 68Ga PET/CT to other imaging studies in medullary thyroid cancer: superiority in detecting bone metastases. *J. Clin. Endocrinol. Metab.* doi: 10.1210/jc.2018-00193 [Epub ahead of print].
- Crippa, S., Mazzucchelli, L., Cibas, E. S., and Ali, S. Z. (2010). The Bethesda system for reporting thyroid fine-needle aspiration specimens. *Am. J. Clin. Pathol.* 134, 343–344; author reply 345. doi: 10.1309/ajcpxm9wirq8jzbj
- Czerwonka, L., Freeman, J., McIver, B., Randolph, G. W., Shah, J. P., Shaha, A. R., et al. (2014). Summary of proceedings of the second world congress on thyroid cancer. *Head Neck* 36, 917–920. doi: 10.1002/hed.23631
- Edge, S. B., Byrd, D. R., and Compton, C. C. (2010). *AJCC Cancer Staging Manual*. New York, NY: Springer.
- Ferraro, S., Trevisiol, C., Gion, M., and Panteghini, M. (2018). Human chorionic gonadotropin assays for testicular tumors: closing the gap between clinical and laboratory practice. *Clin. Chem.* 64, 270–278. doi: 10.1373/clinchem.2017.275263
- Gabriel, S., Garrigue, P., Dahan, L., Castinetti, F., Sebarg, F., Baumstark, K., et al. (2018). Prospective evaluation of (68) Ga-DOTATATE PET/CT in

AUTHOR CONTRIBUTIONS

YL and JH conceived the general idea. YL, HZ, and TT wrote the first draft. JH revised the manuscript. All authors read and approved the final manuscript.

FUNDING

This study was supported by the 2006 TCM research project of Chongqing Health Bureau (No. 2006_B_37) to YL.

- limited disease neuroendocrine tumors and/or elevated serum neuroendocrine biomarkers. *Clin. Endocrinol.* doi: 10.1111/cen.13745 [Epub ahead of print].
- Gilligan, T. D., Seidenfeld, J., Basch, E. M., Einhorn, L. H., Fancher, T., Smith, D. C., et al. (2010). American society of clinical oncology clinical practice guideline on uses of serum tumor markers in adult males with germ cell tumors. *J. Clin. Oncol.* 28, 3388–3404. doi: 10.1200/jco.2009.26.4481
- Haugen, B. R., Alexander, E. K., Bible, K. C., Doherty, G. M., Mandel, S. J., Nikiforov, Y. E., et al. (2016). 2015 American thyroid association management guidelines for adult patients with thyroid nodules and differentiated thyroid cancer: the American thyroid association guidelines task force on thyroid nodules and differentiated thyroid cancer. *Thyroid* 26, 1–133. doi: 10.1089/thy.2015.0020
- Hirohata, T., Ishii, Y., and Matsuno, A. (2014). Treatment of pituitary carcinomas and atypical pituitary adenomas: a review. *Neurol. Med. Chir.* 54, 966–973. doi: 10.2176/nmc.ra.2014-0178
- Hu, H., Zhang, Q., Huang, C., Shen, Y., Chen, X., Shi, X., et al. (2014). Diagnostic value of S100P for pancreatic cancer: a meta-analysis. *Tumour Biol.* 35, 9479–9485. doi: 10.1007/s13277-014-2461-4
- Huang, Z., and Liu, F. (2014). Diagnostic value of serum carbohydrate antigen 19-9 in pancreatic cancer: a meta-analysis. *Tumour Biol.* 35, 7459–7465. doi: 10.1007/s13277-014-1995-9
- Humphris, J. L., Chang, D. K., Johns, A. L., Scarlett, C. J., Pajic, M., Jones, M. D., et al. (2012). The prognostic and predictive value of serum CA19.9 in pancreatic cancer. *Ann. Oncol.* 23, 1713–1722. doi: 10.1093/annonc/mdr561
- Kapoor, R., Bhattacharyya, T., Gupta, R., Mittal, B. R., and Kalra, N. (2014). A systematic review of management of neuroendocrine tumors: an experience from a tertiary care centre from India. *Clin. Cancer Invest. J.* 3, 363–372. doi: 10.4103/2278-0513.138052
- Khan, M. S., Kirkwood, A., Tsigani, T., Garcia-Hernandez, J., Hartley, J. A., Caplin, M. E., et al. (2013). Circulating tumor cells as prognostic markers in neuroendocrine tumors. *J. Clin. Oncol.* 31, 365–372. doi: 10.1200/jco.2012.44.2905
- Kim, H. S., Lee, H. S., Nam, K. H., Choi, J., and Kim, W. H. (2014). p27 loss is associated with poor prognosis in gastroenteropancreatic neuroendocrine tumors. *Cancer Res. Treat.* 46, 383–392. doi: 10.4143/crt.2013.102
- Klimstra, D. S., Modlin, I. R., Coppola, D., Lloyd, R. V., and Suster, S. (2010). The pathologic classification of neuroendocrine tumors: a review of nomenclature, grading, and staging systems. *Pancreas* 39, 707–712. doi: 10.1097/MPA.0b013e3181ec124e
- Kurman, R. J., Carcangiu, M. L., and Harrington, C. S. (2014). *WHO Classification of Tumours of Female Reproductive Organs*. Lyon: IARC Publications.
- Lappinga, P. J., Kip, N. S., Jin, L., Lloyd, R. V., Henry, M. R., Zhang, J., et al. (2010). HMGGA2 gene expression analysis performed on cytologic smears to distinguish benign from malignant thyroid nodules. *Cancer Cytopathol.* 118, 287–297. doi: 10.1002/cncy.20095
- Larry Jameson, J. (2015). “Approach to the patient with endocrine disorders,” in *Harrison's Principles of Internal Medicine*, 19th Edn, ed. J. Loscalzo (New York, NY: McGraw-Hill Education).
- Lindemann, K., Kristensen, G., Mirza, M. R., Davies, L., Hilpert, F., Romero, I., et al. (2016). Poor concordance between CA-125 and RECIST at the time of disease progression in patients with platinum-resistant ovarian cancer: analysis of the AURELIA trial. *Ann. Oncol.* 27, 1505–1510. doi: 10.1093/annonc/mdw238

- Looijenga, L. H., Stoop, H., and Biermann, K. (2014). Testicular cancer: biology and biomarkers. *Virchows Arch.* 464, 301–313. doi: 10.1007/s00428-013-1522-1
- Mai, P. L., Wentzensen, N., and Greene, M. H. (2011). Challenges related to developing serum-based biomarkers for early ovarian cancer detection. *Cancer Prev. Res.* 4, 303–306. doi: 10.1158/1940-6207.capr-11-0053
- McCluggage, W. G., Judge, M. J., Clarke, B. A., Davidson, B., Gilks, C. B., Hollema, H., et al. (2015). Data set for reporting of ovary, fallopian tube and primary peritoneal carcinoma: recommendations from the International Collaboration on Cancer Reporting (ICCR). *Mod. Pathol.* 28, 1101–1122. doi: 10.1038/modpathol.2015.77
- Mete, O., Ezzat, S., and Asa, S. L. (2012). Biomarkers of aggressive pituitary adenomas. *J. Mol. Endocrinol.* 49, R69–R78. doi: 10.1530/JME-12-0113
- Milas, M., Shin, J., Gupta, M., Novosel, T., Nasr, C., Brainard, J., et al. (2010). Circulating thyrotropin receptor mRNA as a novel marker of thyroid cancer: clinical applications learned from 1758 samples. *Ann. Surg.* 252, 643–651. doi: 10.1097/SLA.0b013e3181f5ba51
- Mir, M. C., Pavan, N., and Gonzalgo, M. L. (2016). Current clinical applications of testicular cancer biomarkers. *Urol. Clin. North Am.* 43, 119–125. doi: 10.1016/j.ucl.2015.08.011
- Morris-Stiff, G., and Taylor, M. A. (2012). Ca19-9 and pancreatic cancer: is it really that good? *J. Gastrointest. Oncol.* 3, 88–89. doi: 10.3978/j.issn.2078-6891.2012.016
- Nakamura, K., Sawada, K., Yoshimura, A., Kinose, Y., Nakatsuka, E., and Kimura, T. (2016). Clinical relevance of circulating cell-free microRNAs in ovarian cancer. *Mol. Cancer* 15:48. doi: 10.1186/s12943-016-0536-0
- Nakonechny, Q. B., and Gilks, C. B. (2016). Ovarian cancer in hereditary cancer susceptibility syndromes. *Surg. Pathol. Clin.* 9, 189–199. doi: 10.1016/j.path.2016.01.003
- Naoum, G. E., Morkos, M., Kim, B., and Arafat, W. (2018). Novel targeted therapies and immunotherapy for advanced thyroid cancers. *Mol. Cancer* 17:51. doi: 10.1186/s12943-018-0786-0
- Nikiforov, Y. E., Otori, N. P., Hodak, S. P., Carty, S. E., LeBeau, S. O., Ferris, R. L., et al. (2011). Impact of mutational testing on the diagnosis and management of patients with cytologically indeterminate thyroid nodules: a prospective analysis of 1056 FNA samples. *J. Clin. Endocrinol. Metab.* 96, 3390–3397. doi: 10.1210/jc.2011-1469
- Noone, A. M., Howlader, N., Krapcho, M., Miller, D., Brest, A., Yu, M., et al. (2018). 'SEER Cancer Statistics Review, 1975–2015'. Available at: https://seer.cancer.gov/csr/1975_2015/
- Oberg, K. (2013). The genetics of neuroendocrine tumors. *Semin. Oncol.* 40, 37–44. doi: 10.1053/j.seminoncol.2012.11.005
- Oberg, K., Modlin, I. M., De Herder, W., Pavel, M., Klimstra, D., Frilling, A., et al. (2015). Consensus on biomarkers for neuroendocrine tumour disease. *Lancet Oncol.* 16, e435–e446. doi: 10.1016/s1470-2045(15)00186-2
- Oronsky, B., Ma, P. C., Morgensztern, D., and Carter, C. A. (2017). Nothing but NET: a review of neuroendocrine tumors and carcinomas. *Neoplasia* 19, 991–1002. doi: 10.1016/j.neo.2017.09.002
- Pelzer, U., Hilbig, A., Sinn, M., Stieler, J., Bahra, M., Dorken, B., et al. (2013). Value of carbohydrate antigen 19-9 in predicting response and therapy control in patients with metastatic pancreatic cancer undergoing first-line therapy. *Front. Oncol.* 3:155. doi: 10.3389/fonc.2013.00155
- Prat, J. (2012). New insights into ovarian cancer pathology. *Ann. Oncol.* 23(Suppl. 10), x111–x117. doi: 10.1093/annonc/mds300
- Qian, Z. R., Ter-Minassian, M., Chan, J. A., Imamura, Y., Hooshmand, S. M., Kuchiba, A., et al. (2013). Prognostic significance of MTOR pathway component expression in neuroendocrine tumors. *J. Clin. Oncol.* 31, 3418–3425. doi: 10.1200/jco.2012.46.6946
- Ragel, B. T., and Couldwell, W. T. (2004). Pituitary carcinoma: a review of the literature. *Neurosurg. Focus* 16:E7. doi: 10.3171/foc.2004.16.4.8
- Raverot, G., Burman, P., McCormack, A., Heaney, A., Petersenn, S., Popovic, V., et al. (2018). European society of endocrinology clinical practice guidelines for the management of aggressive pituitary tumours and carcinomas. *Eur. J. Endocrinol.* 178, G1–G24. doi: 10.1530/EJE-17-0796
- Salani, R., Backes, F. J., Fung, M. F., Holschneider, C. H., Parker, L. P., Bristow, R. E., et al. (2011). Posttreatment surveillance and diagnosis of recurrence in women with gynecologic malignancies: society of gynecologic oncologists recommendations. *Am. J. Obstet. Gynecol.* 204, 466–478. doi: 10.1016/j.ajog.2011.03.008
- Sav, A., Rotondo, F., Syro, L. V., Scheithauer, B. W., and Kovacs, K. (2012). Biomarkers of pituitary neoplasms. *Anticancer Res.* 32, 4639–4654.
- Schultz, N. A., Dehlendorff, C., Jensen, B. V., Bjerregaard, J. K., Nielsen, K. R., Bojesen, S. E., et al. (2014). MicroRNA biomarkers in whole blood for detection of pancreatic cancer. *JAMA* 311, 392–404. doi: 10.1001/jama.2013.284664
- Schwarzenbach, H., Nishida, N., Calin, G. A., and Pantel, K. (2014). Clinical relevance of circulating cell-free microRNAs in cancer. *Nat. Rev. Clin. Oncol.* 11, 145–156. doi: 10.1038/nrclinonc.2014.5
- Siegel, R. L., Miller, K. D., and Jemal, A. (2017). Cancer Statistics, 2017. *CA Cancer J. Clin.* 67, 7–30. doi: 10.3322/caac.21387
- Smith, R. A., Manassaram-Baptiste, D., Brooks, D., Doroshenko, M., Fedewa, S., Saslow, D., et al. (2015). Cancer screening in the United States, 2015: a review of current American cancer society guidelines and current issues in cancer screening. *CA Cancer J. Clin.* 65, 30–54. doi: 10.3322/caac.21261
- Soelberg, K. K., Bonnema, S. J., Brix, T. H., and Hegedus, L. (2012). Risk of malignancy in thyroid incidentalomas detected by 18F-fluorodeoxyglucose positron emission tomography: a systematic review. *Thyroid* 22, 918–925. doi: 10.1089/thy.2012.0005
- The National Comprehensive Cancer Network [NCCN] (2018a). *NCCN Clinical Practice Guidelines in Oncology. (NCCN Guidelines®) for Neuroendocrine and Adrenal Tumors Version 2.2018*.
- The National Comprehensive Cancer Network [NCCN] (2018b). *NCCN Clinical Practice Guidelines in Oncology. (NCCN Guidelines®) for Ovarian Cancer Version 2.2018*.
- The National Comprehensive Cancer Network [NCCN] (2018c). *NCCN Clinical Practice Guidelines in Oncology. (NCCN Guidelines®) for Pancreatic Adenocarcinoma Version 1.2018*.
- The National Comprehensive Cancer Network [NCCN] (2018d). *NCCN Clinical Practice Guidelines in Oncology. (NCCN Guidelines®) for Testicular Cancer Version 2.2018*.
- The National Comprehensive Cancer Network [NCCN] (2018e). *NCCN Clinical Practice Guidelines in Oncology. (NCCN Guidelines®) for Thyroid Carcinoma Version 1.2018*.
- Timmerman, D., Van Calster, B., Testa, A., Savelli, L., Fischerova, D., Froyman, W., et al. (2016). Predicting the risk of malignancy in adnexal masses based on the simple rules from the international ovarian tumor analysis group. *Am. J. Obstet. Gynecol.* 214, 424–437. doi: 10.1016/j.ajog.2016.01.007
- Tzeng, C. W., Balachandran, A., Ahmad, M., Lee, J. E., Krishnan, S., Wang, H., et al. (2014). Serum carbohydrate antigen 19-9 represents a marker of response to neoadjuvant therapy in patients with borderline resectable pancreatic cancer. *HPB* 16, 430–438. doi: 10.1111/hpb.12154
- Ueland, F. R. (2017). A perspective on ovarian cancer biomarkers: past, present and Yet-To-Come. *Diagnostics* 7:E14. doi: 10.3390/diagnostics7010014
- Waddell, N., Pajic, M., Patch, A. M., Chang, D. K., Kassahn, K. S., Bailey, P., et al. (2015). Whole genomes redefine the mutational landscape of pancreatic cancer. *Nature* 518, 495–501. doi: 10.1038/nature14169
- Wolin, E. M., Leyden, J., Goldstein, G., Kolarova, T., Hollander, R., and Warner, R. R. P. (2017). Patient-reported experience of diagnosis, management, and burden of neuroendocrine tumors: results from a large patient survey in the United States. *Pancreas* 46, 639–647. doi: 10.1097/MPA.0000000000000818
- Yoshida, A., Derchain, S. F., Pitta, D. R., Andrade, L. A., and Sarian, L. O. (2016). Comparing the Copenhagen Index (CPH-I) and Risk of Ovarian Malignancy Algorithm (ROMA): two equivalent ways to differentiate malignant from benign ovarian tumors before surgery? *Gynecol. Oncol.* 140, 481–485. doi: 10.1016/j.ygyno.2016.01.023

Conflict of Interest Statement: The authors declare that the research was conducted in the absence of any commercial or financial relationships that could be construed as a potential conflict of interest.

Copyright © 2018 Luo, Zhu, Tan and He. This is an open-access article distributed under the terms of the Creative Commons Attribution License (CC BY). The use, distribution or reproduction in other forums is permitted, provided the original author(s) and the copyright owner(s) are credited and that the original publication in this journal is cited, in accordance with accepted academic practice. No use, distribution or reproduction is permitted which does not comply with these terms.



Inhibition of WEE1 Suppresses the Tumor Growth in Laryngeal Squamous Cell Carcinoma

Meng-Ling Yuan^{1†}, Pei Li^{2†}, Zi-Hao Xing¹, Jin-Ming Di³, Hui Liu⁴, An-Kui Yang⁵, Xi-Jun Lin², Qi-Wei Jiang¹, Yang Yang¹, Jia-Rong Huang¹, Kun Wang¹, Meng-Ning Wei¹, Yao Li¹, Jin Ye^{2*} and Zhi Shi^{1*}

¹ Department of Cell Biology – Institute of Biomedicine, National Engineering Research Center of Genetic Medicine, Provincial Key Laboratory of Bioengineering Medicine, College of Life Science and Technology, Jinan University, Guangzhou, China, ² Department of Otolaryngology-Head and Neck Surgery, The Third Affiliated Hospital, Sun Yat-sen University, Guangzhou, China, ³ Department of Urology, The Third Affiliated Hospital, Sun Yat-sen University, Guangzhou, China, ⁴ Division of Pulmonary and Critical Care, Department of Internal Medicine, The Third Affiliated Hospital, Sun Yat-sen University, Guangzhou, China, ⁵ Department of Head and Neck, Sun Yat-sen University Cancer Center, State Key Laboratory of Oncology in South China, Collaborative Innovation Center for Cancer Medicine, Guangzhou, China

OPEN ACCESS

Edited by:

Salvatore Salomone,
Università degli Studi di Catania, Italy

Reviewed by:

Claude Prigent,
Centre National de la Recherche
scientifique (CNRS), France
Andrew Burgess,
Anzac Research Institute, Australia

*Correspondence:

Jin Ye
yejin_sums@aliyun.com
Zhi Shi
tshizhi@jnu.edu.cn

[†]These authors have contributed
equally to this work

Specialty section:

This article was submitted to
Experimental Pharmacology
and Drug Discovery,
a section of the journal
Frontiers in Pharmacology

Received: 12 June 2018

Accepted: 27 August 2018

Published: 28 September 2018

Citation:

Yuan M-L, Li P, Xing Z-H, Di J-M,
Liu H, Yang A-K, Lin X-J, Jiang Q-W,
Yang Y, Huang J-R, Wang K,
Wei M-N, Li Y, Ye J and Shi Z (2018)
Inhibition of WEE1 Suppresses
the Tumor Growth in Laryngeal
Squamous Cell Carcinoma.
Front. Pharmacol. 9:1041.
doi: 10.3389/fphar.2018.01041

WEE1 is a tyrosine kinase that regulates G2/M cell cycle checkpoint and frequently overexpressed in various tumors. However, the expression and clinical significance of WEE1 in human laryngeal squamous cell carcinoma (LSCC) are still unknown. In this study, we found that WEE1 was highly expressed in LSCC tissues compared with adjacent normal tissues. Importantly, overexpression of WEE1 was correlated with T stages, lymph node metastasis, clinical stages and poor prognosis of LSCC patients. Furthermore, inhibition of WEE1 by MK-1775 induced cell growth inhibition, cell cycle arrest and apoptosis with the increased intracellular reactive oxygen species (ROS) levels in LSCC cells. Pretreatment with ROS scavenger *N*-acetyl-L-cysteine could reverse MK-1775-induced ROS accumulation and cell apoptosis in LSCC cells. MK-1775 also inhibited the growth of LSCC xenografts in nude mice. Altogether, these findings suggest that WEE1 is a potential therapeutic target in LSCC, and inhibition of WEE1 is the prospective strategy for LSCC therapy.

Keywords: laryngeal squamous cell carcinoma, WEE1, MK-1775, cell cycle, apoptosis, reactive oxygen species

INTRODUCTION

Laryngeal carcinoma is the second most common malignant tumor of the respiratory system in the male compared to its relative rare in the female (Siegel et al., 2018). The aggressive type of squamous cell carcinoma (LSCC), originating from the laryngeal epithelium, accounts for approximately 90% of laryngeal carcinoma cases (Li et al., 2017). In spite of therapeutic advances, the 5-year survival rate for LSCC patients remains generally unsatisfactory (~59.6–66.8%) (Hsueh et al., 2017). Thus, it is of great significance to comprehensively understand intrinsic molecular mechanisms underlying LSCC tumorigenesis and identify novel therapeutic targets for the diagnosis and prognostic assessment of LSCC.

WEE1 is a tyrosine kinase that phosphorylates CDC2 at Tyr15 residue and prevents progression through G2/M and S cell cycle checkpoint for DNA repair before mitotic entry (Matheson et al., 2016a). Prior work has demonstrated that ectopic high-expression of WEE1 has been identified in

several malignant tumors and associated with poor outcome, such as glioblastoma (Music et al., 2016), vulvar squamous cell carcinoma (Magnussen et al., 2013), ovarian carcinoma (Slipicevic et al., 2014), melanoma (Magnussen et al., 2012), and

colorectal carcinoma (Egeland et al., 2016; Ge et al., 2017). On the contrary, in non-small cell lung cancer and colon cancer, patients with absence of WEE1 expression had poor prognosis (Yoshida, 2004; Cormanich et al., 2009). Until now, the expression and

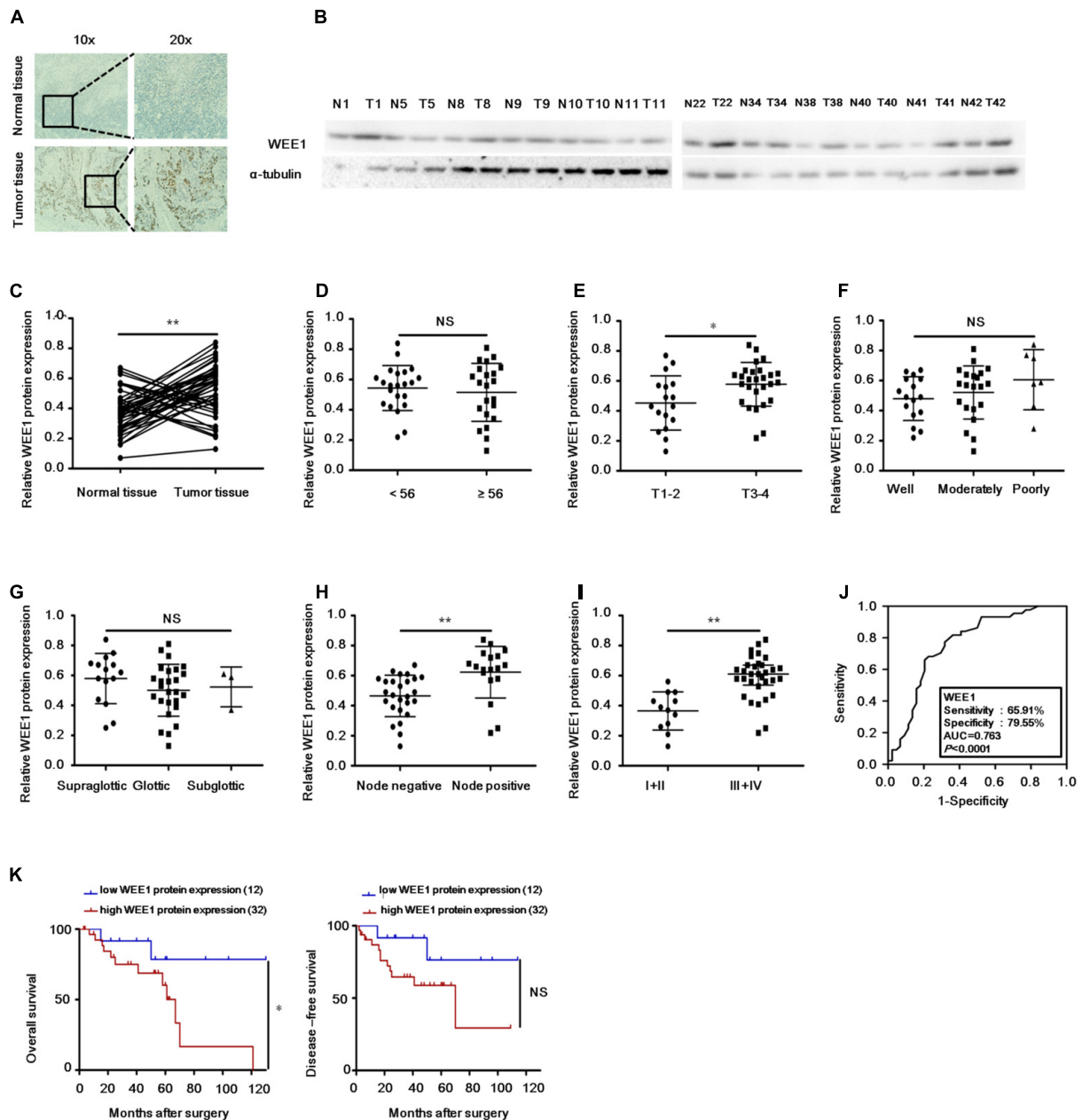


FIGURE 1 | Up-regulation of WEE1 protein in LSCC is correlated with T stages, lymph node metastasis, clinical stages, and poor prognosis.

(A) Immunohistochemistry analysis of WEE1 protein expression in the paired LSCC tissues and adjacent normal tissues. (B) Western blot analysis of WEE1 protein expression in the paired LSCC tissues and adjacent normal tissues. (C) Pearson's correlation scatter plot of the expressions and WEE1 protein in human LSCC tissues. The relative WEE1 protein expression in LSCC tissues and adjacent normal tissues were analyzed with Student's *t*-test. The relative WEE1 protein expression in two groups of LSCC tissues classified by age (D), T stage (E), lymph node metastasis (H), and clinical stage (I) were analyzed with Student's *t*-test. The relative WEE1 protein expression in three groups of LSCC tissues classified by differentiation (F) and primary location (G) were analyzed with one-way ANOVA. (J) ROC curve analysis of the discrimination between LSCC tissues and adjacent normal tissues by WEE1. (K) Kaplan-Meier analysis of overall survival and disease-free survival curves for LSCC patients with high or/and low expression of WEE1. Data are presented as mean \pm SD or median with the interquartile range.

P* < 0.05; *P* < 0.01; NS, no statistical significance.

clinical significance of WEE1 in LSCC are still unknown. Here, we have investigated the expression and clinical significance of WEE1 in LSCC, and the anti-tumor effects and mechanisms of WEE1 inhibition against LSCC.

MATERIALS AND METHODS

Patients and Specimens

A total 44 pairs of LSCC and corresponding adjacent normal tissues were obtained from patients who underwent partial or total laryngectomy without neoadjuvant radical or chemical therapy before and after surgery at the Department of Head and Neck, Cancer Center, Sun Yat-sen University (Guangzhou, China) from July 2008 to June 2015. The International Union against Cancer (UICC) 2002 norms for staging laryngeal carcinoma (clinical, endoscopic, and imaging) is strictly followed. Signed informed consents were obtained from all patients. The study was approved by the ethics committee of Sun Yat-sen University Cancer Center.

Cell Culture and Reagents

Normal human bronchial epithelium cells HBEC, LSCC cells KB-3-1 and TU212 were cultured in Dulbecco's modified Eagle's medium (DMEM) with 10% fetal bovine serum (FBS), penicillin (100 U/ml), and streptomycin (100 ng/ml) at 37°C with 5% CO₂ in a humidified incubator. MK-1775 was purchased from APExBio (Shanghai). Methylthiazolyldiphenyl-tetrazolium bromide (MTT), propidium iodide (PI) and other chemicals were

purchased from Sangon Biotech (Shanghai). *N*-acetyl-L-cysteine (NAC) and dihydroethidium (DHE) were purchased from Sigma-Aldrich. Anti-WEE1 (5285) and anti-pCDK T14/Y15 (28435) antibodies were from Santa Cruz Biotechnology. Anti-PARP (9542), anti-pHistone3 S10 (53348), and anti-C-Caspase3 (9964) were from Cell Signaling Technologies. Anti-γ-H2AX (AB55226) antibody was from Sangon Biotech. Anti-CDK1 (610037) antibody was from BD Biosciences. Anti-Ki-67 (2746-1) antibody was from Abcam. Anti-Vinculin (BM1611) antibody was from BOSTER Biological Technology.

MTT Assay

Cells were seeded into a 96-well plate at a density of 0.5×10^4 cells/well and treated with various concentrations of agents. After 3 days, MTT was added to each well at a final concentration of 0.5 mg/ml. After incubation for 4 h, the medium and MTT solution were removed from each well, and formazan crystals were dissolved in 100 μl of DMSO. Absorbance was measured at 570 nm by Multiscan Spectrum (Thermo Fisher). The data were analyzed by CompuSyn software with those results.

Western Blot Assay

Cells were harvested and washed twice with cold PBS, then resuspended and lysed in RIPA buffer (1% NP-40, 0.5% sodium deoxycholate, 0.1% SDS, 10 ng/ml PMSF, 0.03% aprotinin, 1 μM sodium orthovanadate) at 4°C for 30 min. Lysates were centrifuged for 10 min at $14,000 \times g$ and supernatants were stored at −80°C as whole cell extracts. Proteins were separated on 12% SDS-PAGE gels and transferred to polyvinylidene difluoride membranes. Membranes were blocked with 5% BSA and incubated with the indicated primary antibodies. Corresponding horseradish peroxidase-conjugated secondary antibodies were used against each primary antibody. Vinculin was used as a loading control. Signals were detected with the ChemiDoc XRS chemiluminescent gel imaging system (Analytik Jena).

Cell Cycle Assay

Cells were harvested and washed twice with phosphate-buffered saline (PBS), then permeabilized with 70% cold ethanol for 2 h at 4°C. After washing twice in PBS, cells were resuspended with 0.5 ml PBS containing PI (50 μg/ml), 0.1% Triton X-100, 0.1% sodium citrate, and DNase-free RNase (100 μg/ml), and assessed by flow cytometry (FCM) (Beckman Coulter) after incubation at room temperature in the dark for 15 min. Fluorescence was measured at an excitation wavelength of 480 nm through a FL-2filter. Data were analyzed using ModFit LT 4.1 software.

Cell Apoptosis Assay

Cells were harvested and washed twice with PBS, stained with Annexin V-FITC and PI in the binding buffer, and detected by FCM (Beckman Coulter) after 15 min incubation at room temperature in the dark. Fluorescence was measured at an excitation wave length of 480 nm through FL-1 (530 nm) and FL-2 filters (585 nm). The early apoptotic cells (Annexin V+/PI−) and late apoptotic cells (Annexin V+/PI+) were quantified.

TABLE 1 | Relationship between WEE1 protein expression level and clinicopathologic parameters.

Characteristics (n)	WEE1 protein level ^a	<i>p</i> ^b
Age		0.5880
<56 (22)	0.5436 ± 0.1482	
≥56 (22)	0.5155 ± 0.1915	
T classification		0.0103
T1-2 (17)	0.4529 ± 0.1807	
T3-4 (27)	0.5778 ± 0.1461	
Differentiation		0.5053
Well (16)	0.5479 ± 0.1970	
Moderately (21)	0.5082 ± 0.1179	
Poorly (7)	0.4728 ± 0.0858	
Primary location		0.3766
Supraglottis (15)	0.5793 ± 0.1680	
Glottis (26)	0.5015 ± 0.1734	
Subglottis (3)	0.5233 ± 0.1332	
Lymph node metastasis		0.0008
Negative (26)	0.4650 ± 0.1378	
Positive (18)	0.6228 ± 0.1716	
Clinical stage		<0.0001
I+II (12)	0.3650 ± 0.1267	
III+IV (32)	0.5913 ± 0.1411	

^aScores determined by Western blot in mean ± SD. ^bStudent's *t*-test (for two groups) or one-way ANOVA (for >2 groups).

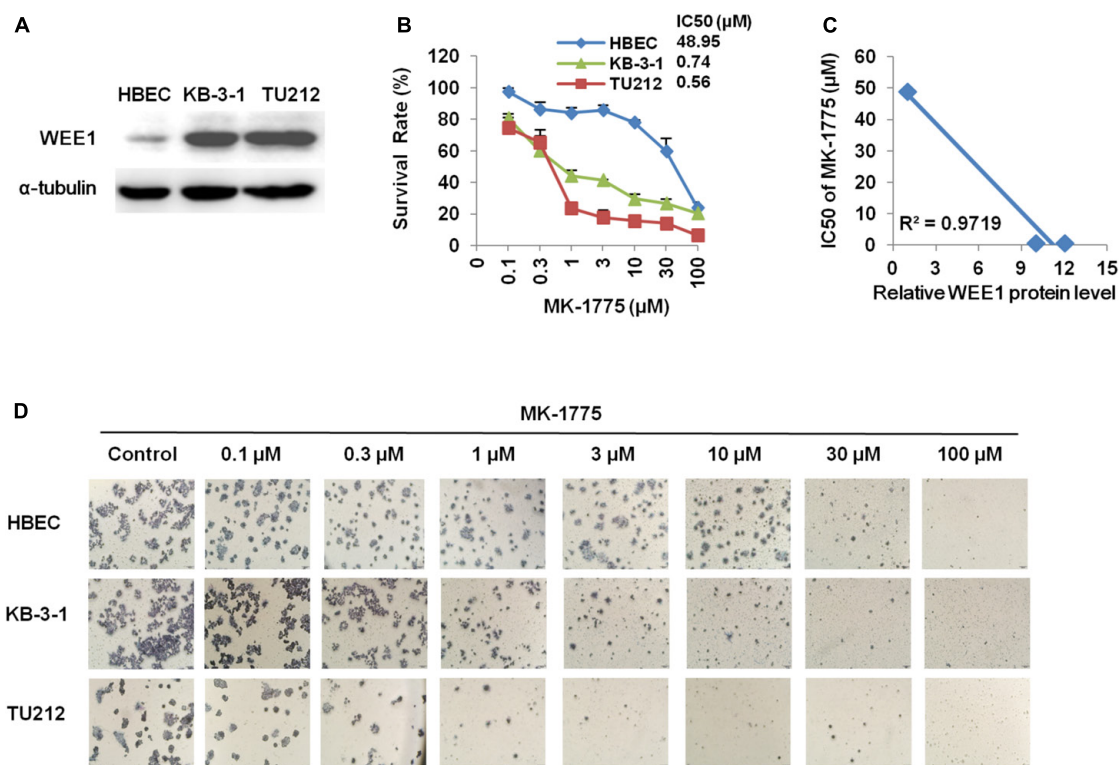


FIGURE 2 | The WEE1 inhibitor MK-1775 suppressed the growth of LSCC cells *in vitro*. **(A)** Western blot analysis of WEE1 protein expression in KB-3-1, TU212, and HBEC cells. Cells were treated with the indicated concentration of MK-1775 for 72 h. Cell survival was measured by MTT assay. The representative growth curves of KB-3-1, TU212, and HBEC cells treated with MK-1775 **(B)**, correlation analysis of MK-1775 IC₅₀ values and relative WEE1 protein levels **(C)**, and images of cells stained with MTT for 4-h **(D)** are shown.

Reactive Oxygen Species Assay

Cells were incubated with 10 μM of DHE for 30 min at 37°C, and observed under fluorescence microscope (Olympus, Japan) immediately after washing twice with PBS. Five fields were taken randomly for each well. After photographed under fluorescent microscope, cells were rapidly digested, harvested and then washed twice with cold PBS, and detected by FCM (Beckman Coulter). The DHE Fluorescence intensity was measured and quantified at an excitation wave length of 518 nm through PE filters.

Immunohistochemistry Assay

Formalin-fixed, paraffin embedded human LSCC tissues and KB-3-1 subcutaneous tumors in mice were stained with antibodies, respectively, using a microwave-enhanced avidin-biotin staining method. To quantify the protein expression, the following formula was used: immunohistochemical score = percentage of positive cells \times intensity score. The intensity was scored as follows: 0, negative (no staining); 1, weak (light yellow); 2, moderate (yellow brown); and 3, intense (brown).

Nude Mice Xenograft Assay

BALB/c nude mice were obtained from the Guangdong Medical Laboratory Animal Center and maintained with sterilized food

and water. Five female nude mice with 5 weeks old and 16–18 g weight were used for each group. Every mouse was injected subcutaneously of the KB-3-1 cells (3×10^6 in 100 μl of medium) under the right and left shoulders. When the subcutaneous tumors were approximately 0.3 cm \times 0.3 cm (two perpendicular diameters) in size, the mice were randomized into two groups and taken orally with vehicle alone (0.5% methylcellulose) or MK-1775 (50 mg/kg) twice daily. The body weights of mice and the two perpendicular diameters (A and B) of tumors were recorded every day. The tumor volume (V) was calculated as:

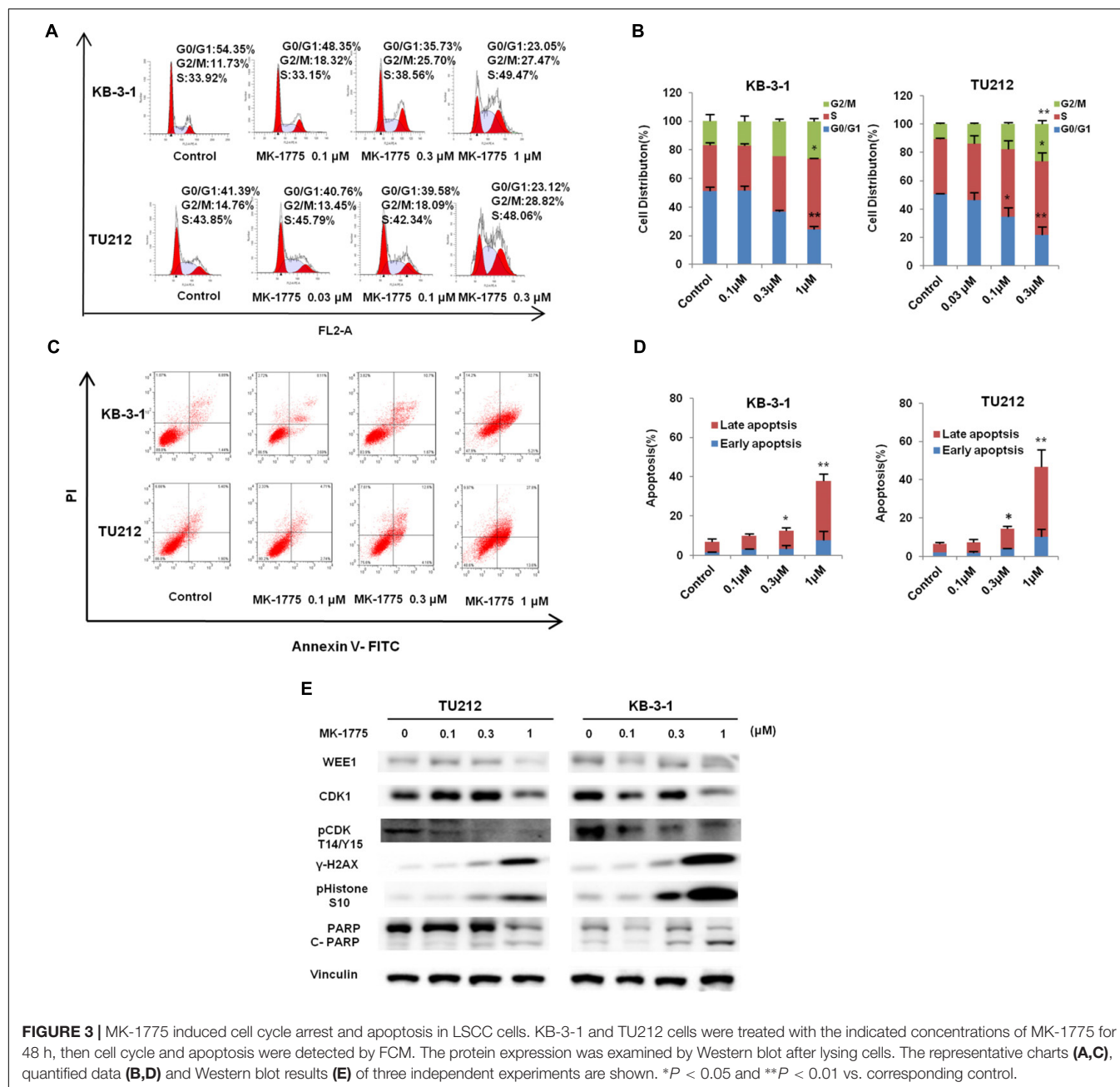
$$V = \pi/6(1/2(A + B))^3$$

The mice were anesthetized after experiment, and tumor tissue was excised from the mice and weighted. The rate of inhibition (IR) was calculated according to the formula:

$$\text{IR} = 1 - \frac{\text{Mean tumor weight of experimental group}}{\text{Mean tumor weight of control group}} \times 100\%.$$

Statistical Analysis

All statistical analyses were performed using the SPSS 20.0 statistical software package. Comparisons between two groups were performed using Student's *t*-test or Mann–Whitney *U*-test,



and comparisons among three groups were performed using one-way ANOVA or Kruskal–Wallis test. Fisher's exact test or Pearson's correlation were used to analyze the relationship between the expression levels of WEE1 protein. Kaplan–Meier method and the log-rank test were used to compare the survival of patients. ROC curve analyses were used to evaluate the prognostic ability. The difference in tumor volume between the two groups of mice was determined by repeated-measures analysis of variance. Data were presented as mean \pm SD or median with the interquartile range. $P < 0.05$ was considered statistically significant.

RESULTS

Up-Regulation of WEE1 Protein in LSCC Is Correlated With T Stages, Lymph Node Metastasis, Clinical Stages, and Poor Prognosis

To investigate the expression and clinical significance of WEE1 in LSCC, the expression of WEE1 protein was detected in the total 44 pair LSCC and adjacent normal tissues. Immunohistochemical staining and Western blot results revealed that the expression of

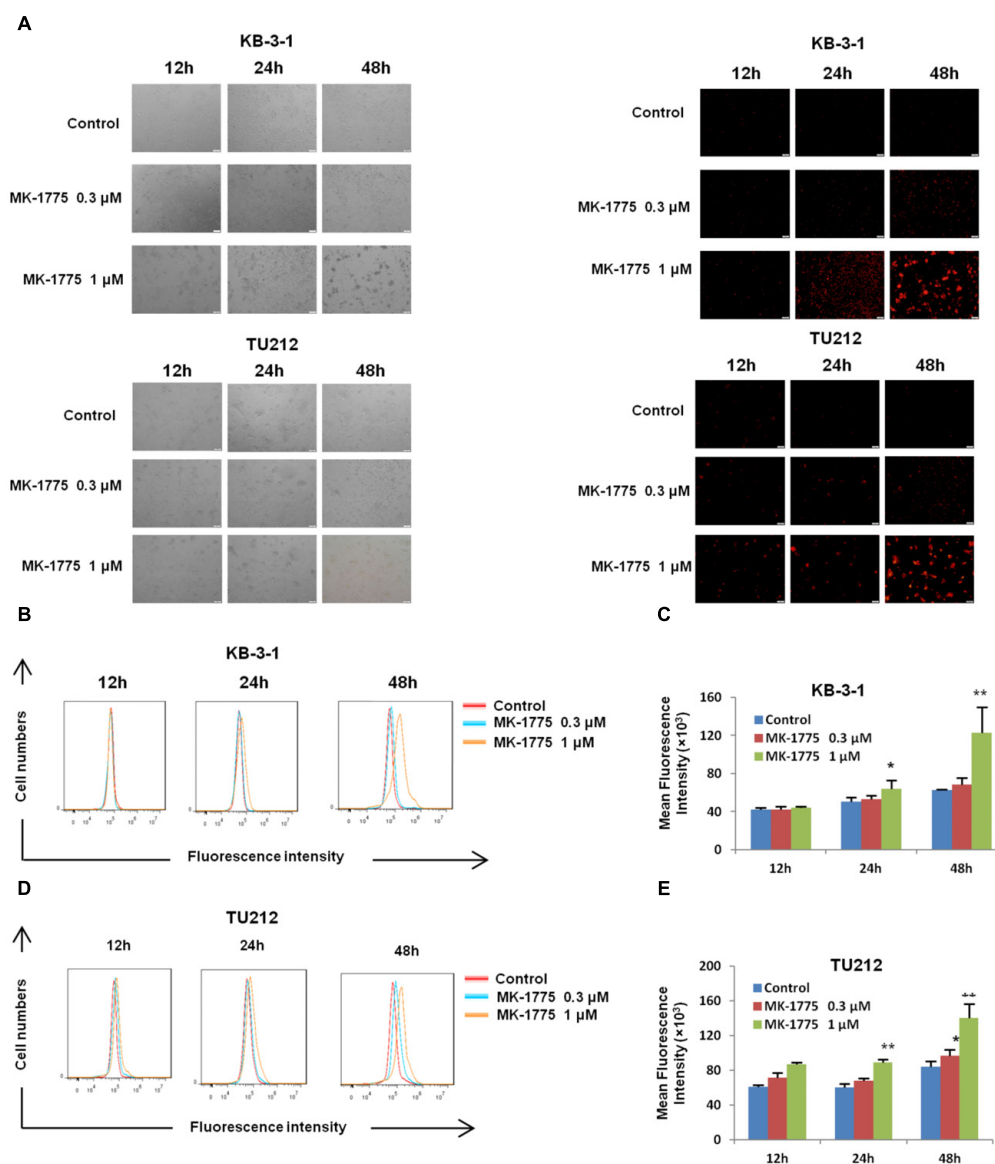


FIGURE 4 | MK-1775 enhanced the intracellular ROS levels in LSCC cells. KB-3-1 and TU212 cells were treated with MK-1775 at the indicated times and concentrations then stained with DHE, photographed and quantified respectively under fluorescent microscope and FCM. The representative micrographs (A), red fluorescent intensity charts by FCM (B,D) and quantified results of red fluorescence (C,E) of KB-3-1 and TU212 cells in three independent experiments were shown. * $P < 0.05$ and ** $P < 0.01$ vs. corresponding control.

WEE1 protein was higher in LSCC tissues than adjacent normal tissues (Figures 1A–C). Furthermore, statistic analysis indicated that the expression of WEE1 protein was associated with T stage, lymph node metastasis and stage, but not with age, tumor grades and tumor primary locations (Table 1 and Figures 1D–G). The expression of WEE1 protein in T1-2, negative lymph node metastasis and stage I+II groups were respectively lower than that in T3-4, positive lymph node metastasis and stage III+IV groups (Figures 1E,H,I). The levels of WEE1 protein could be a significant parameter to distinguish LSCC and adjacent non-tumorous tissues with an AUC of 0.763 (sensitivity = 65.91%, specificity = 79.55%; $P < 0.0001$) (Figure 1J). Moreover,

Kaplan–Meier analysis on the survival time of patients revealed that high WEE1 protein expression was correlated with poor overall survival, but not with disease-free survival (Figure 1K). Consequently, our results indicate that WEE1 may be a potential therapeutic target in LSCC.

The WEE1 Inhibitor MK-1775 Suppressed the Growth of LSCC Cells *in vitro*

To further explore whether WEE1 is a therapeutic target in LSCC, we examined the protein expression of WEE1 and cytotoxicity of a WEE1 inhibitor MK-1775 in LSCC cells. Two human LSCC cell lines KB-3-1 and TU212 expressed higher level of WEE1

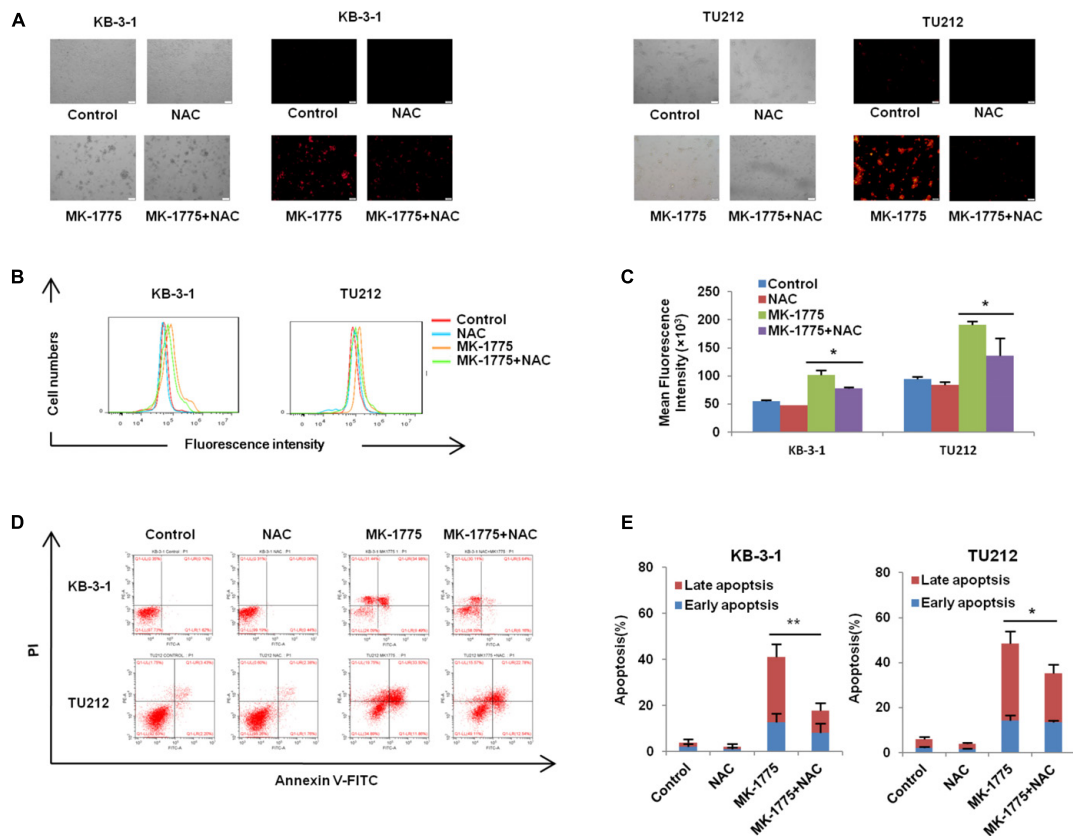


FIGURE 5 | NAC impeded MK-1775-induced ROS production and cell apoptosis. KB-3-1 and TU212 cells were treated with 1 μ M MK-1775 for 48 h in the presence or absence of 5 mM NAC pretreatment for 1 h, then stained with DHE, photographed and quantified respectively under fluorescent microscope and FCM. The apoptosis was detected by FCM with Annexin V/PI staining. The representative micrographs (A), red fluorescent intensity charts by FCM (B) and quantified results of red fluorescence (C), the apoptosis charts (D) and quantified results (E) of three independent experiments were shown. * $P < 0.05$ and ** $P < 0.01$ vs. corresponding control.

protein than one normal bronchial epithelium cell line HBEC (Figure 2A). Then these cells were treated with the increasing concentrations of MK-1775 for 72 h. As shown in Figures 2B,D, MK-1775 inhibited the growth of LSCC cells in a dose-dependent manner with the IC_{50} values of 0.74 μ M and 0.56 μ M in KB-3-1 and TU212 cells respectively. However, the IC_{50} value of MK-1775 in HBEC cell is 48.95 μ M, suggesting MK-1775 is significantly more cytotoxic to LSCC cells than normal cells. Moreover, the IC_{50} values of MK-1775 in these three cells were negatively correlated with their WEE1 protein levels (Figure 2C).

MK-1775 Induced Cell Cycle Arrest and Apoptosis in LSCC Cells

To determine whether the growth inhibition was due to cell cycle arrest, cell cycle distribution was examined after MK-1775 treatment. KB-3-1 and TU212 cells were treated with the incremental concentrations of MK-1775 for 48 h, stained with PI and examined by FCM. As shown in Figures 3A,B, MK-1775 induced the accumulation in S and G2/M phase and reduction in G0/G1 phase in these two cell lines. Next, the related proteins of cell cycle were detected by Western blot. Treatment with MK-1775 at 1 μ M for 48 h downregulated the protein expressions of

WEE1, CDK1, and pCDK T14/Y15, but upregulated the protein expression of γ -H2AX and pHistone3 S10 (Figure 3E).

To further determine whether MK-1775 could induce cell apoptosis in LSCC cells, TU212 and KB-3-1 cells were treated with 0.1, 0.3, 1 μ M of MK-1775 for 48 h, stained with Annexin V/PI and examined by FCM. As shown in Figures 3C,D, MK-1775 dose-dependently induced early apoptosis (Annexin V+/PI-) and late apoptosis (Annexin V+/PI+) in both cells. Furthermore, the protein levels of apoptosis marker cleaved-PARP was increased in a dose-depend manner after MK-1775 treatment in both cells (Figure 3E).

MK-1775 Enhanced the Intracellular ROS Levels in LSCC Cells

There was increasing evidence that extravagant production of ROS was relevant to carcinogenesis, malignant behavior, and mitochondria-mediated apoptosis (Chung, 2016; Miyata et al., 2017; Prasad et al., 2017), and cancer cells generally have higher ROS levels than their normal counterparts (Chung, 2016; De Sa Junior et al., 2017). Thus, we speculated that MK-1775 caused apoptosis in LSCC cells in relation to excessive ROS generation. Firstly, the cellular ROS was tagged by DHE fluorescence staining

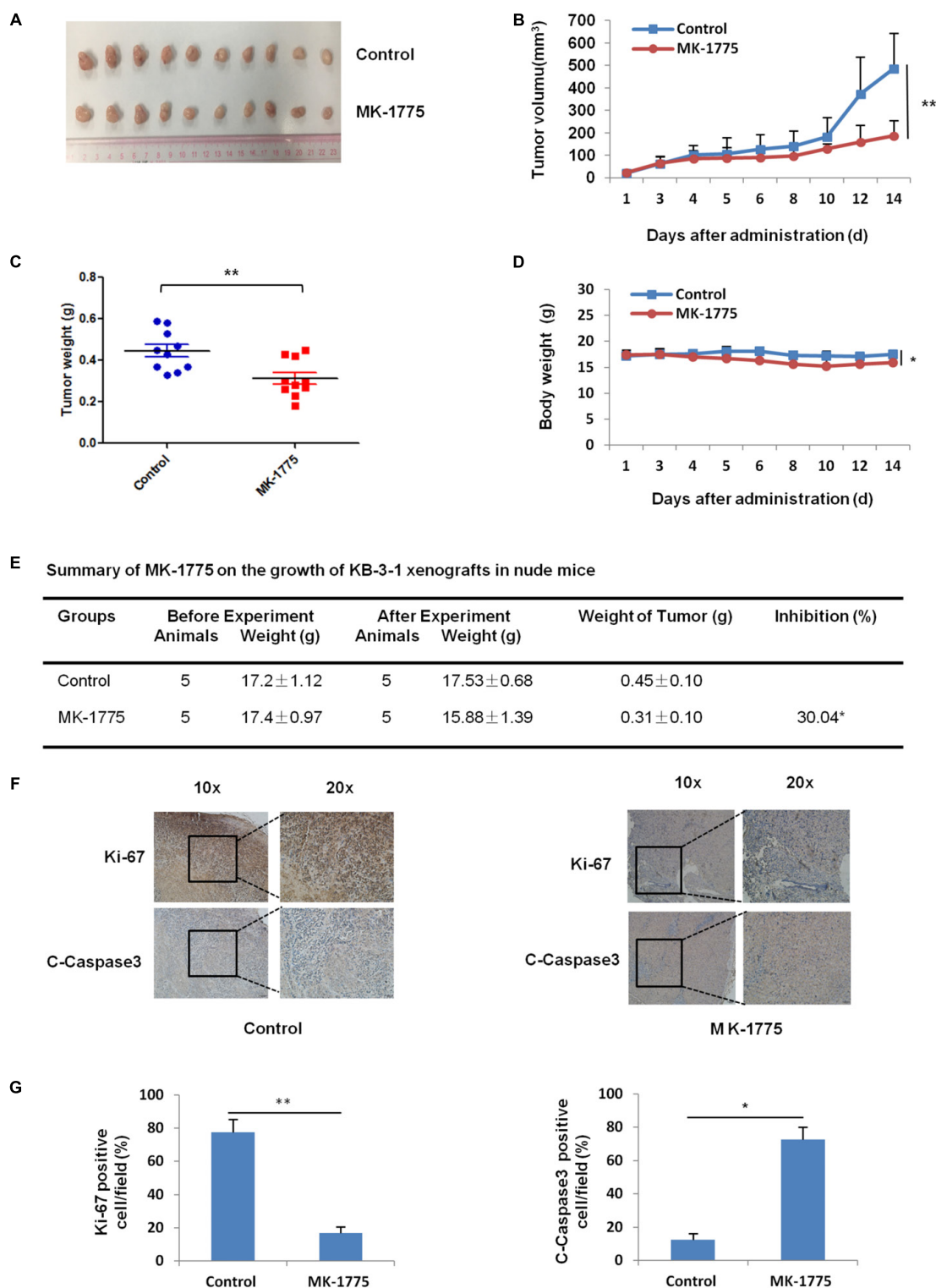


FIGURE 6 | MK-1775 inhibited the growth of KB-3-1 xenografts in nude mice. Each mouse was injected subcutaneously with KB-3-1 cells (3×10^6 in 100 μ l of medium) under the right and left shoulders. When the subcutaneous tumors were approximately 0.3 cm \times 0.3 cm² (two perpendicular diameters) in size, mice were randomized into two groups, and were taken orally with vehicle alone (0.5% methylcellulose) or MK-1775 (50 mg/kg) twice daily. The body weights of mice and tumor volume were recorded. The mice were anesthetized after experiment, and tumor tissue was excised from the mice and weighted. The original tumors (**A**), tumor volume (**B**), tumor weight (**C**), body weight (**D**), summary data (**E**), immunohistochemical staining of Ki-67 and C-caspase3 in subcutaneous tumors (**F**) and quantified of Ki-67 and C-caspase3 positive cells (**G**) were also shown. The values presented are the means \pm SD for each group. * $P < 0.05$ and ** $P < 0.01$ vs. corresponding control.

in MK-1775-treated cells. As illustrated in **Figures 4A–E**, MK-1775 enhanced the detectable red fluorescent signals of DHE in both KB-3-1 and TU212 cells in the concentration- and time-dependent manners, indicating the intracellular ROS levels were increased after MK-1775 treatment.

NAC Impeded MK-1775-Induced ROS Production and Cell Apoptosis

To investigate whether ROS generation was involved in the MK-1775-induced cell apoptosis, a specific ROS scavenger (NAC) was co-treated with MK-1775 in both KB-3-1 and TU212 cells. MK-1775-induced DHE fluorescent signals were attenuated by NAC in both cells (**Figures 5A–C**). Moreover, a reduction of cell apoptosis after co-treatment with MK-1775 and NAC was observed compared with MK-1775 treatment alone in both cells (**Figures 5D,E**). Collectively, these results suggest that NAC impedes MK-1775-induced ROS production and cell apoptosis.

MK-1775 Inhibited the Growth of KB-3-1 Xenografts in Nude Mice

To confirm the antitumor effects of MK-1775 *in vivo*, KB-3-1 subcutaneous xenografts were generated in the nude mice. As shown in **Figures 6A–E**, treatment with MK-1775 inhibited the growth of KB-3-1 xenografts with the inhibition ratio of 30.04% by reducing the tumor volumes and weights. Furthermore, mice body weight in MK-1775 group was lower than that of control group, suggesting that MK-1775 at the indicated dose did cause toxicity in mice (**Figure 6D**). Additionally, the results of immunohistochemical staining showed that the percentage of proliferation marker Ki-67 positive cells was decreased, while apoptosis marker cleaved-caspase 3 positive cells was increased in KB-3-1 xenografts after MK-1775 treatment (**Figures 6F,G**).

DISCUSSION

In this study, we reported that WEE1 was significantly expressed in LSCC tissues than adjacent normal tissues, and the expression level of WEE1 was associated with T stage, lymph node metastasis and poor survival of patients with LSCC. These data are similar with previous studies which have shown that WEE1 has served a crucial role in tumorigenesis and related with poor prognosis in several cancers that harbor WEE1 amplifications (Magnussen et al., 2012, 2013; Slipicevic et al., 2014; Music et al., 2016). Therefore, targeting WEE1 has emerged as a promising therapy for human cancers (Matheson et al., 2016a; Geenen and Schellens, 2017). MK-1775, a first-in-class small-molecule inhibitor of WEE1 with undergoing clinical evaluation, abated phosphorylation of CDK1 at Tyr15 and caused mitotic catastrophe in cancer cells (Kreahling et al., 2013). Early preclinical studies suggested MK-1775 was capable of abrogating the G2/M checkpoint allowing for premature entry into mitosis to exert a toxic effect specifically in p53 deficient tumor cells (Guertin et al., 2013; Hirai et al., 2014). Our results showed that inhibition of WEE1 with MK-1775 caused decreased viability, cell cycle arrest, and cell apoptosis, suggesting WEE1 was essential for cell proliferation and tumorigenicity in LSCC cells. MK-1775 has been reported that sensitizes cancers of head and

neck (Osman et al., 2015), brain (Matheson et al., 2016b), and non-small cell lung cancer (Richer et al., 2017) to the DNA-damage drug cisplatin as well as pancreatic cancer cells (Kausar et al., 2015) to gemcitabine. Additionally, MK-1775 has promising synergistic antitumor effect when combined with CHK1 inhibitors LY2603618 and Sirt1 inhibitor Ex527 in various malignancies (Chen et al., 2017; Hauge et al., 2017), suggesting a novel strategy for MK-1775-mediated cancer treatment.

Biological roles of ROS were intricate and contradictory in cancers (Halliwell, 2013). Under a low or moderate increase, ROS is vital for regulating various cell physiological processes and maintaining cellular homeostasis, which functions as signaling molecules favoring tumorigenesis (Miyata et al., 2017). On the contrary, exorbitant production of ROS acts to cause DNA damage and oxidative stress to engender genotoxic or even proapoptotic and autophagic effect on cancer cells (Trachootham et al., 2009; Schieber and Chandel, 2014; Kruk and Aboul-Enein, 2017). Accordingly, this oxidative stress causing the cumulative effects may induce cancer cells susceptible to chemotherapeutic agents treatment that perform by amplifying ROS generation (Schumacker, 2006). ROS goes up when cells prematurely enter mitosis, and that the increased ROS drives cell death (Marchetti et al., 2006). To confirm that this was occurring we detected the intracellular level of ROS in MK-1775-treated LSCC cells, we found ROS significantly increased following Wee1 inhibition, and we could limit death by reducing ROS with NAC.

CONCLUSION

Our findings suggest that WEE1 is a potential therapeutic target in LSCC, and inhibition of WEE1 is the prospective strategy for LSCC therapy.

AUTHOR CONTRIBUTIONS

M-LY, PL, JY and ZS designed the experiments, performed the experiments, analyzed the data, and wrote the paper. Z-HX, J-MD, HL, A-KY, X-JL, Q-WJ, YY, J-RH, KW, M-NW, and YL performed the experiments. All authors read and approved the final manuscript.

FUNDING

This work was supported by funds from the National Key Research and Development Program of China No. 2017YFA0505104 (ZS), the National Natural Science Foundation of China Nos. 81772540 (ZS) and 81772752 (J-MD), the Guangdong Natural Science Funds for Distinguished Young Scholar No. 2014A030306001 (ZS), the Guangdong Special Support Program for Young Talent No. 2015TQ01R350 (ZS), the Science and Technology Program of Guangdong Nos. 2016A050502027 (ZS) and 2017A020215122 (J-MD), and the Science and Technology Program of Guangzhou Nos. 201704030058 (ZS) and 201709010038 (J-MD).

REFERENCES

- Chen, G., Zhang, B., Xu, H., Sun, Y., Shi, Y., Luo, Y., et al. (2017). Suppression of Sirt1 sensitizes lung cancer cells to WEE1 inhibitor MK-1775-induced DNA damage and apoptosis. *Oncogene* 36, 6863–6872. doi: 10.1038/onc.2017.297
- Chung, W. H. (2016). Mechanisms of a novel anticancer therapeutic strategy involving atmospheric pressure plasma-mediated apoptosis and DNA strand break formation. *Arch. Pharm. Res.* 39, 1–9. doi: 10.1007/s12272-015-0644-1
- Cormanich, R. A., Goodarzi, M., and Freitas, M. P. (2009). Improvement of multivariate image analysis applied to quantitative structure-activity relationship (QSAR) analysis by using wavelet-principal component analysis ranking variable selection and least-squares support vector machine regression: QSAR study of checkpoint kinase WEE1 inhibitors. *Chem. Biol. Drug Des.* 73, 244–252. doi: 10.1111/j.1747-0285.2008.00764.x
- De Sa Junior, P. L., Camara, D. A. D., Porcacchia, A. S., Fonseca, P. M. M., Jorge, S. D., Araldi, R. P., et al. (2017). The roles of ROS in cancer heterogeneity and therapy. *Oxid. Med. Cell Longev.* 2017:2467940.
- Egeland, E. V., Flatmark, K., Nesland, J. M., Florenes, V. A., Maelandsmo, G. M., and Boye, K. (2016). Expression and clinical significance of Wee1 in colorectal cancer. *Tumour Biol.* 37, 12133–12140.
- Ge, X. C., Wu, F., Li, W. T., Zhu, X. J., Liu, J. W., and Wang, B. L. (2017). Upregulation of WEE1 is a potential prognostic biomarker for patients with colorectal cancer. *Oncol. Lett.* 13, 4341–4348. doi: 10.3892/ol.2017.5984
- Geenen, J. J., and Schellens, J. H. M. (2017). Molecular pathways: targeting the protein kinase wee1 in cancer. *Clin. Cancer Res.* 23, 4540–4544. doi: 10.1158/1078-0432.CCR-17-0520
- Guertin, A. D., Li, J., Liu, Y., Hurd, M. S., Schuller, A. G., Long, B., et al. (2013). Preclinical evaluation of the WEE1 inhibitor MK-1775 as single-agent anticancer therapy. *Mol. Cancer Ther.* 12, 1442–1452. doi: 10.1158/1535-7163.MCT-13-0025
- Halliwell, B. (2013). The antioxidant paradox: less paradoxical now? *Br. J. Clin. Pharmacol.* 75, 637–644. doi: 10.1111/j.1365-2125.2012.04272.x
- Hauge, S., Naucke, C., Hasvold, G., Joel, M., Rodland, G. E., Juzenas, P., et al. (2017). Combined inhibition of Wee1 and Chk1 gives synergistic DNA damage in S-phase due to distinct regulation of CDK activity and CDC45 loading. *Oncotarget* 8, 10966–10979. doi: 10.18632/oncotarget.14089
- Hirai, H., Arai, T., Okada, M., Nishibata, T., Kobayashi, M., Sakai, N., et al. (2014). MK-1775, a small molecule Wee1 inhibitor, enhances anti-tumor efficacy of various DNA-damaging agents, including 5-fluorouracil. *Cancer Biol. Ther.* 9, 514–522.
- Hsueh, C., Tao, L., Zhang, M., Cao, W., Gong, H., Zhou, J., et al. (2017). The prognostic value of preoperative neutrophils, platelets, lymphocytes, monocytes and calculated ratios in patients with laryngeal squamous cell cancer. *Oncotarget* 8, 60514–60527. doi: 10.18632/oncotarget.16234
- Kausar, T., Schreiber, J. S., Karnak, D., Parsels, L. A., Parsels, J. D., Davis, M. A., et al. (2015). Sensitization of pancreatic cancers to gemcitabine chemoradiation by WEE1 Kinase inhibition depends on homologous recombination repair. *Neoplasia* 17, 757–766. doi: 10.1016/j.neo.2015.09.006
- Kreahling, J. M., Foroutan, P., Reed, D., Martinez, G., Razaboudski, T., Bui, M. M., et al. (2013). Wee1 inhibition by MK-1775 leads to tumor inhibition and enhances efficacy of gemcitabine in human sarcomas. *PLoS One* 8:e57523. doi: 10.1371/journal.pone.0057523
- Kruk, J., and Aboul-Enein, H. Y. (2017). Reactive oxygen and nitrogen species in carcinogenesis: implications of oxidative stress on the progression and development of several cancer types. *Mini Rev. Med. Chem.* 17, 904–919. doi: 10.2174/1389557517666170228115324
- Li, P., Yang, Y., Liu, H., Yang, A. K., Di, J. M., Tan, G. M., et al. (2017). MiR-194 functions as a tumor suppressor in laryngeal squamous cell carcinoma by targeting Wee1. *J. Hematol. Oncol.* 10:32. doi: 10.1186/s13045-017-0402-6
- Magnussen, G. I., Holm, R., Emilsen, E., Rosnes, A. K., Slipicevic, A., and Florenes, V. A. (2012). High expression of Wee1 is associated with poor disease-free survival in malignant melanoma: potential for targeted therapy. *PLoS One* 7:e38254. doi: 10.1371/journal.pone.0038254
- Magnussen, G. I., Hellesylt, E., Nesland, J. M., Trope, C. G., Florenes, V. A., and Holm, R. (2013). High expression of wee1 is associated with malignancy in vulvar squamous cell carcinoma patients.pdf. *BMC Cancer* 13:288. doi: 10.1186/1471-2407-13-288
- Marchetti, M. A., Weinberger, M., Murakami, Y., Burhans, W. C., and Huberman, J. A. (2006). Production of reactive oxygen species in response to replication stress and inappropriate mitosis in fission yeast. *J. Cell Sci.* 119, 124–131.
- Matheson, C. J., Backos, D. S., and Reigan, P. (2016a). Targeting WEE1 Kinase in cancer. *Trends Pharmacol. Sci.* 37, 872–881.
- Matheson, C. J., Venkataraman, S., Amani, V., Harris, P. S., Backos, D. S., Donson, A. M., et al. (2016b). A WEE1 inhibitor analog of AZD1775 maintains synergy with cisplatin and demonstrates reduced single-agent cytotoxicity in medulloblastoma cells. *ACS Chem. Biol.* 11, 2066–2067.
- Miyata, Y., Matsuo, T., Sagara, Y., Ohba, K., Ohya, K., and Sakai, H. (2017). A mini-review of reactive oxygen species in urological cancer: correlation with nadph oxidases, angiogenesis, and apoptosis. *Int. J. Mol. Sci.* 18: E2214.
- Music, D., Dahlrot, R. H., Hermansen, S. K., Hjelmberg, J., De Stricker, K., Hansen, S., et al. (2016). Expression and prognostic value of the WEE1 kinase in gliomas. *J. Neurooncol.* 127, 381–389. doi: 10.1007/s11060-015-2050-4
- Osman, A. A., Monroe, M. M., Ortega Alves, M. V., Patel, A. A., Katsonis, P., Fitzgerald, A. L., et al. (2015). Wee-1 kinase inhibition overcomes cisplatin resistance associated with high-risk TP53 mutations in head and neck cancer through mitotic arrest followed by senescence. *Mol. Cancer Ther.* 14, 608–619. doi: 10.1158/1535-7163.MCT-14-0735-T
- Prasad, S., Gupta, S. C., and Tyagi, A. K. (2017). Reactive oxygen species (ROS) and cancer: role of antioxidative nutraceuticals. *Cancer Lett.* 387, 95–105. doi: 10.1016/j.canlet.2016.03.042
- Richer, A. L., Cala, J. M., O'Brien, K., Carson, V. M., Inge, L. J., and Whitsett, T. G. (2017). WEE1 kinase inhibitor AZD1775 has preclinical efficacy in LKB1-deficient non-small cell lung cancer. *Cancer Res.* 77, 4663–4672. doi: 10.1158/0008-5472.CAN-16-3565
- Schieber, M., and Chandel, N. S. (2014). ROS function in redox signaling and oxidative stress. *Curr. Biol.* 24, R453–R462. doi: 10.1016/j.cub.2014.03.034
- Schumacker, P. T. (2006). Reactive oxygen species in cancer cells: live by the sword, die by the sword. *Cancer Cell* 10, 175–176.
- Siegel, R. L., Miller, K. D., and Jemal, A. (2018). Cancer statistics, 2018. *CA Cancer J. Clin.* 68, 7–30. doi: 10.3322/caac.21442
- Slipicevic, A., Holth, A., Hellesylt, E., Trope, C. G., Davidson, B., and Florenes, V. A. (2014). Wee1 is a novel independent prognostic marker of poor survival in post-chemotherapy ovarian carcinoma effusions. *Gynecol. Oncol.* 135, 118–124. doi: 10.1016/j.ygyno.2014.07.102
- Trachootham, D., Alexandre, J., and Huang, P. (2009). Targeting cancer cells by ROS-mediated mechanisms: a radical therapeutic approach? *Nat. Rev. Drug Discov.* 8, 579–591. doi: 10.1038/nrd2803
- Yoshida, T. (2004). The clinical significance of Cyclin B1 and Wee1 expression in non-small-cell lung cancer. *Ann. Oncol.* 15, 252–256.

Conflict of Interest Statement: The authors declare that the research was conducted in the absence of any commercial or financial relationships that could be construed as a potential conflict of interest.

Copyright © 2018 Yuan, Li, Xing, Di, Liu, Yang, Lin, Jiang, Yang, Huang, Wang, Wei, Li, Ye and Shi. This is an open-access article distributed under the terms of the Creative Commons Attribution License (CC BY). The use, distribution or reproduction in other forums is permitted, provided the original author(s) and the copyright owner(s) are credited and that the original publication in this journal is cited, in accordance with accepted academic practice. No use, distribution or reproduction is permitted which does not comply with these terms.



Olmudinib (BI1482694/HM61713), a Novel Epidermal Growth Factor Receptor Tyrosine Kinase Inhibitor, Reverses ABCG2-Mediated Multidrug Resistance in Cancer Cells

OPEN ACCESS

Edited by:

Pascale Cohen,
Claude Bernard University Lyon 1,
France

Reviewed by:

Hua Zhu,
The Ohio State University,
United States
Sara Galimberti,
Università degli Studi di Pisa, Italy

*Correspondence:

Zhe-Sheng Chen
chenz@stjohns.edu

[†] These authors have contributed
equally to this work

Specialty section:

This article was submitted to
Experimental Pharmacology
and Drug Discovery,
a section of the journal
Frontiers in Pharmacology

Received: 03 June 2018

Accepted: 07 September 2018

Published: 09 October 2018

Citation:

Zhang W, Fan Y-F, Cai C-Y,
Wang J-Q, Teng Q-X, Lei Z-N,
Zeng L, Gupta P and Chen Z-S (2018)
Olmudinib (BI1482694/HM61713),
a Novel Epidermal Growth Factor
Receptor Tyrosine Kinase Inhibitor,
Reverses ABCG2-Mediated Multidrug
Resistance in Cancer Cells.
Front. Pharmacol. 9:1097.
doi: 10.3389/fphar.2018.01097

**Wei Zhang^{1,2†}, Ying-Fang Fan^{2,3†}, Chao-Yun Cai², Jing-Quan Wang², Qiu-Xu Teng²,
Zi-Ning Lei², Leli Zeng^{2,4}, Pranav Gupta² and Zhe-Sheng Chen^{2*}**

¹ Institute of Plastic Surgery, Weifang Medical University, Weifang, China, ² Department of Pharmaceutical Sciences, College of Pharmacy and Health Sciences, St. John's University, Queens, NY, United States, ³ Department of Hepatobiliary Surgery, Zhujiang Hospital, Southern Medical University, Guangzhou, China, ⁴ MOE Key Laboratory of Bioinorganic and Synthetic Chemistry, School of Chemistry, Sun Yat-sen University, Guangzhou, China

The main characteristic of tumor cell resistance is multidrug resistance (MDR). MDR is the principle cause of the decline in clinical efficacy of chemotherapeutic drugs. There are several mechanisms that could cause MDR. Among these, one of the most important mechanisms underlying MDR is the overexpression of adenosine triphosphate (ATP)-binding cassette (ABC) super-family of transporters, which effectively pump out cytotoxic agents and targeted anticancer drugs across the cell membrane. In recent years, studies found that ABC transporters and tyrosine kinase inhibitors (TKIs) interact with each other. TKIs may behave as substrates or inhibitors depending on the expression of specific pumps, drug concentration, their affinity for the transporters and types of co-administered agents. Therefore, we performed *in vitro* experiments to observe whether olmutinib could reverse MDR in cancer cells overexpressing ABCB1, ABCG2, or ABCC1 transporters. The results showed that olmutinib at 3 μ M significantly reversed drug resistance mediated by ABCG2, but not by ABCB1 and ABCC1, by antagonizing the drug efflux function in ABCG2-overexpressing cells. In addition, olmutinib at reversal concentration affected neither the protein expression level nor the localization of ABCG2. The results observed from the accumulation/efflux study of olmutinib showed that olmutinib reversed ABCG2-mediated MDR with an increasing intracellular drug accumulation due to inhibited drug efflux. We also had consistent results with the ATPase assay that olmutinib stimulated ATPase activity of ABCG2 up to 3.5-fold. Additionally, the molecular interaction between olmutinib and ABCG2 was identified by docking simulation. Olmutinib not only interacts directly with ABCG2 but

also works as a competitive inhibitor of the transport protein. In conclusion, olmutinib could reverse ABCG2-mediated MDR. The reversal effect of olmutinib on ABCG2-mediated MDR cells is not due to ABCG2 expression or intracellular localization, but rather related to its interaction with ABCG2 protein resulting in drug efflux inhibition and ATPase stimulation.

Keywords: multidrug resistance (MDR), ATP-binding cassette (ABC) transporter, tyrosine kinase inhibitor (TKI), olmutinib, breast cancer resistance protein (BCRP/ABCG2)

INTRODUCTION

The main characteristic of tumor cell resistance is MDR, in which cancer cells exhibit a cross-resistant phenotype against multiple unrelated drugs that are structurally and/or functionally different and may also have varying molecular targets (Saraswathy and Gong, 2013). MDR is the main cause of the decline in clinical efficacy of chemotherapeutic drugs. There are several mechanisms that could cause MDR, such as reduced uptake of drugs, overexpression of energy-dependent efflux proteins, increased efflux of drugs by drug transporters, inhibition of apoptosis, activation of DNA repair mechanisms, cell cycle arrest and modification of cell cycle checkpoints (Gillet and Gottesman, 2010; Hu et al., 2016; Kartal-Yandim et al., 2016; Pan et al., 2016). Among these, one of the most important mechanisms underlying MDR is the overexpression of the adenosine triphosphate (ATP)-binding cassette (ABC) super-family of transporters, which effectively pump out cytotoxic agents and targeted anticancer drugs across the cell membrane (Zhang et al., 2017; Fan et al., 2018). ABC transporters that cause drug resistance are currently divided into three main categories: ABCB, ABCC, and ABCG. Among them, ABCB1 (P-glycoprotein, P-gp), ABCC1 (MDR protein 1, MRP1), and ABCG2 (breast cancer resistance protein, BCRP) are the most common ones (Strouse et al., 2013; Miklos et al., 2015).

P-gp was the first ABC transporter that was isolated from colchicine-resistant Chinese hamster ovary cells by Juliano and Ling (1976). P-gp pumps substrates out of tumor cells through an ATP-dependent mechanism (Juliano and Ling, 1976; Kartner et al., 1983; Krishna and Mayer, 2000). MRP1 was first reported in 1992 as the mediator of acquired drug resistance in a small cell lung cancer cell line selected by repeated exposure to doxorubicin (Cole et al., 1992; Fletcher et al., 2016). Although associated with drug resistance properties, it also has been identified as an organic anion transporter in its normal physiological role (Borst et al., 1997). BCRP, encoded by ABCG2, was the third member of the ABC transporter family that was identified (Doyle et al., 1998; Miyake et al., 1999; Robey et al., 2018). A number of chemotherapeutic agents, such as MX, 9-aminocamptothecin, topotecan, irinotecan and SN-38 have been shown to be transported by BCRP (Robey et al., 2007). ABC transporters mainly contribute to MDR by altering drug absorption, distribution, excretion and metabolism (Kathawala

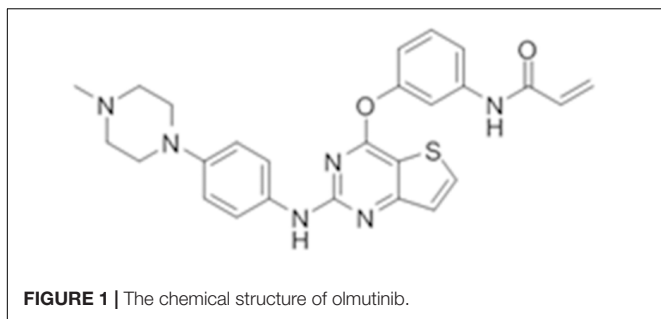
et al., 2017). Numerous studies have found that ABC transporters are over expressed in many tumor tissues. For this reason, reversal of MDR caused by ABC transporters is one of the main strategies for tumor treatment. Researchers have been working to find new ways to inhibit ABC transporters and re-sensitize cancer cells to chemotherapeutic drugs (Kathawala et al., 2017).

Tyrosine kinases (TKs) are widely expressed in cells, and they play important roles in various cellular processes. The expression of TKs is related to the proliferation, differentiation, migration, apoptosis, angiogenesis, and metastasis of cancer cells in key signaling events/pathways (van der Geer et al., 1994; Pytel et al., 2009; Shukla et al., 2012). The phosphatidyl inositol-3-kinase (PI3K)/AKT, protein kinase C (PKC) family, and mitogen-activated protein kinase (MAPK)/Ras signaling cascades are activated by TKs and play important roles in cell proliferation and homeostasis (Faivre et al., 2006). TKs can catalyze the transfer of a phosphate group from ATP to target proteins. Therefore, TKIs have become one of the effective targets in cancer treatments (Dohse et al., 2010; Russo et al., 2017). TKIs have achieved significant clinical efficacy as anti-tumor agents. Among them, small-molecule TK inhibitors are the most promising new drugs and have shown good prospects in both clinical and experimental treatments (Chen et al., 2017; Hocker et al., 2017; Chikhale et al., 2018; Parikh and Ghate, 2018).

In recent years, studies have found that ABC transporters and several TKIs interact with each other (e.g., imatinib, sunitinib, nilotinib, and gefitinib). On the one hand, ABC transporters can cause a decrease in the function of TKIs, leading to the occurrence of MDR (Beretta et al., 2017). Parts of TKIs can be the substrates of ABC transporters. The ABC transporters pump them out of the cell and cause drug resistance (Herbrink et al., 2015). On the other hand, more and more studies have shown that some TKIs can reverse ABC transporter-mediated MDR (Ma et al., 2014). The reversal mechanisms include inhibiting the protein expression of ABC transporters, inhibiting the protein pumping function and other signaling pathways (Zhang et al., 2016a,b; Beretta et al., 2017; Kathawala et al., 2017).

Olmudinib (HM61713/BI1482694) is a novel third-generation that is orally active and selectively inhibits EGFR mutations (Figure 1), including both activating mutations and T790M, but not EGFR wild-type (Kim, 2016). It was approved in South Korea on May 13, 2016 for the treatment of patients with locally advanced or metastatic EGFR T790M mutation-positive NSCLC previously treated with an EGFR TKI (Singh and Jadhav, 2018). At present, olmutinib is waiting for the phase III clinical efficacy observation.

Abbreviations: ABC, ATP-binding cassette; EGFR, epidermal growth factor receptor; IFD, induced-fit docking; MDR, multidrug resistance; MTT, 3-(4, 5-dimethylthiazol-yl)-2, 5- diphenyltetrazolium bromide; MX, mitoxantrone; TK, tyrosine kinase; TKI, tyrosine kinase inhibitor; TMD, transmembrane domain.



Tyrosine kinase inhibitors may behave as substrates or inhibitors of ABC transporters depending on the expression of specific pumps, drug concentration, affinity for transporters and types of co-administered agents (Beretta et al., 2017). Therefore, we performed *in vitro* experiments to evaluate if olmutinib could reverse MDR in cancer cells overexpressing ABCB1, ABCG2, or ABCC1 transporters.

MATERIALS AND METHODS

Chemicals and Reagents

Dulbecco's modified Eagle's medium (DMEM), fetal bovine serum (FBS), bovine calf serum (BS), penicillin/streptomycin and trypsin 0.25% were purchased from Hyclone (GE Healthcare Life Sciences, Pittsburgh, PA, United States). 10X solution of phosphate buffered saline (PBS), SN-38, and Alexa Fluor 488 conjugated rabbit anti-mouse IgG secondary antibody were purchased from Thermo Fisher Scientific Inc. (Rockford, IL, United States). The monoclonal antibodies for ABCG2 (BXP-34), paclitaxel, vincristine, vinblastine, cisplatin, MX, verapamil, 3-(4, 5-dimethylthiazol-yl)-2, 5-diphenyltetrazolium bromide (MTT), dimethyl sulfoxide (DMSO), propidium iodide (PI), and Triton X-100, were obtained from Sigma Chemical Co. (St. Louis, MO, United States). Ko-143 and MK-571 were products from Enzo Life Sciences (Farmingdale, NY, United States). Monoclonal antibodies sc-47778 (against β -actin) and secondary HRP-labeled rabbit anti-mouse IgG were purchased from Santa Cruz Biotechnology, Inc. (Dallas, TX, United States). [3 H]-MX (2.5 Ci/mmol) was purchased from Moravsek Biochemicals (Brea, CA, United States). Liquid scintillation cocktail was a product from MP Biomedicals, Inc. (Santa Ana, CA, United States). All other chemicals were purchased from Sigma Chemical Co. (St. Louis, MO, United States).

Cell Lines and Cell Culture

The non-small cell lung cancer cell line NCI-H460 and its drug-resistant ABCG2-overexpressing NCI-H460/MX20 cells, which was maintained in medium with an addition of 20 nM MX, were kindly provided by Drs. Susan Bates and Robert Robey (NIH, Bethesda, MD, United States). The human epidermal carcinoma cell line KB-3-1 and its drug-resistant ABCB1-overexpressing KB-C2 cells, which were cloned from KB-3-1 and maintained in medium with 2 mg/ml of colchicine, and its drug-resistant ABCC1-overexpressing cell line KB-CV60,

maintained in medium with 1 μ g/mL of cepharanthine and 60 ng/mL of vincristine, were also used in this study (Aoki et al., 2001). HEK293/pcDNA3.1, HEK293/ABCB1, HEK293/ABCG2, and HEK293/ABCC1 cell lines were established by transfecting HEK293 cells with either the empty pcDNA3.1 vector or the vector containing full length ABCB1 (HEK293/ABCB1), ABCG2 (HEK293/ABCG2), and ABCC1 (HEK293/ABCC1) DNA, respectively, and were cultured in medium containing 2 mg/mL of G418 (Enzo Life Sciences, Farmingdale, NY, United States) (Zhang et al., 2015). All cell lines were cultured in DMEM medium with 10% FBS and 1% penicillin/streptomycin at 37°C with 5% CO₂. All drug-resistant cell lines were grown in a drug-free culture medium for more than 2 weeks prior to use.

Cell Cytotoxicity by MTT Assay

The cytotoxicity of anticancer drugs with or without modulator agents was determined by modified MTT colorimetric assay (Fan et al., 2018). Briefly, 5000 cells were seeded evenly into each well in coated 96-well microplates overnight. Olmutinib and parallel control modulators were added 2 h prior to the addition of chemotherapeutic drugs in a designated concentration gradient. After 68 h of incubation, 20 μ L of MTT solution (4 mg/mL) was added into each well with further incubation of 4 h. The medium was aspirated and 100 μ L of DMSO was added to dissolve the formazan crystals in each well. The absorbance was determined at 570 nm by the accuScan GO UV/Vis Microplate Spectrophotometer (Fisher Scientific, Fair Lawn, NJ, United States). Verapamil, KO-143 and MK-571 was used as a inhibitors for ABCB1-overexpressing, ABCG2-overexpressing, and ABCC1-overexpressing cell lines, respectively.

Western Blotting Analysis

After treatment with 0, 3, and 6 μ M olmutinib for 72 h, and after treatment with 3 μ M olmutinib for 24, 48, and 72 h in NCI-H460/MX20 cells, the cells were incubated with a lysis buffer (2.5% 1M Tris, 0.15% EDTA, 1% sodium deoxycholate, 0.1% SDS, 0.88% NaCl, 1% Triton-X and protease inhibitor cocktail) on ice for 20 min, followed by centrifugation at 12,000 g at 4°C for 20 min. The supernatant was collected, and the protein concentration was determined by a bicinchoninic acid (BCA)-based protein assay (Thermo Scientific, Rockford, IL, United States). 25 μ g of protein in 30 μ L loading sample was separated by SDS-polyacrylamide gel electrophoresis and transferred to a polyvinylidene difluoride (PVDF) membrane. After blocked by 5% dry milk for 2 h, the membrane was incubated with primary antibody BXP-34 (1:1000, detects BCRP) overnight at 4°C. The signal was detected using enhanced chemiluminescence followed by incubation with secondary HRP-labeled antibody (1:1000). The protein expression was quantified by ImageJ software (NIH, Bethesda, MD, United States).

Immunofluorescence Assay

NCI-H460 and NCI-H460/MX20 cells were seeded as 1×10^5 per well in 24-well plates and cultured at 37°C for 24 h,

followed by incubation with 3 μM olmutinib for 0, 24, 48, and 72 h, or followed by incubation with 0, 1, 3, or 6 μM olmutinib. The cells were then washed with cold PBS solution twice and fixed in 4% formaldehyde for 15 min. Subsequently, after incubation with 0.5% Triton X-100 for 15 min, cells were incubated with BSA (2 mg/ml) for 1 h followed by monoclonal antibodies for ABCG2 (BXP-34, 1:1000) overnight at 4°C. Cells were further incubated with Alexa Fluor 488 conjugated IgG secondary antibody for 1 h in dark. PI solution was used to counterstain the nuclei. Immunofluorescence images were collected using a Nikon TE-2000S fluorescence microscope (Nikon Instruments Inc., Melville, NY, United States).

ABCG2 ATPase Assay

The ABCG2 ATPase activity based on vanadate-sensitive membrane vesicles of High Five insect cells was measured as previously described (Zhang et al., 2017). Briefly, the membrane vesicles (10 μg of protein) were incubated in ATPase assay buffer with or without 0.3 mM vanadate at 37°C for 5 min. After that, the assay buffer was incubated with 0–40 μM varying concentrations of olmutinib at 37°C for 3 min. The ATPase reaction was induced by adding 5 mM MgATP with a total volume of 0.1 ml. After 20 min incubation at 37°C, the reaction was stopped by adding 100 μl 5% SDS solution to the reaction mix. The ATPase activity due to ABCG2 is calculated from the amount of inorganic phosphate (IP) released detected at 880 nm using a spectrophotometer.

Accumulation and Efflux Assay

We used the drug accumulation and efflux assays as previously described (Fan et al., 2018). For the accumulation assay, NCI-H460 and NCI-H460/MX20 cells were seeded into 24-well plate (100,000 cells/well) and incubated at 37°C for 12 h. Then the cells were incubated with or without inhibitors for 2 h. The medium was discarded, followed by the addition of medium containing 0.01 μM [^3H]-MX, and then the inhibitors were added into the wells. After 2 h incubation, the medium was discarded and the cells were washed with ice-cold PBS three times, lysed, and then transferred to the scintillation fluid. For the efflux assay, we performed similar procedures as the accumulation assay. After discarding the medium containing [^3H]-MX, the cells were washed with ice-cold PBS and incubated with medium in the absence or presence of inhibitors. The cells were washed three times, lysed, and then transferred to the scintillation fluid at different time points of 0, 30, 60, and 120 min, respectively. The radioactivity was measured using the Packard TRI-CARB1 190A liquid scintillation analyzer.

Molecular Modeling

Molecular modeling was performed in Maestro v11.1 (Schrödinger, LLC) software as described previously (Zhang et al., 2017). Human ABCG2 (PDB ID: 5NJ3) (Taylor et al., 2017) protein preparation was performed and the grid was generated by selecting residues (Phe432, Phe 439, Leu539, Ile543, Val546,

and Met549) at a substrate-binding pocket in TMD of ABCG2. The best-scored ligand was obtained through Glide XP docking then the receptor grid for IFD was generated. The IFD protocol with default parameters was performed. The conformation of ligand with the highest docking score (kcal/mol) was used for docking analysis.

Statistical Analysis

All experiments were repeated at least three times and the result values are presented as mean \pm SD. Statistical differences between two groups were determined by the two-tailed Student's *t*-test and *p* values equal or below 0.05 were considered significant.

RESULTS

Effects of Olmutinib on Cells Overexpressing ABCB1, ABCG2, and ABCC1 Transporters

To determine the effects of olmutinib on ABC transporters, the sensitivity of ABCB1-, ABCG2-, and ABCC1-overexpressing cells to olmutinib were determined. The cytotoxicity assay indicated that the IC₅₀ values of olmutinib for ABCB1-, ABCG2-, and ABCC1-overexpressing cancer cells (KB-C2, NCI-H460/MX20 and KB-CV60) were 11.42, 12.19, and 17.14 μM . The IC₅₀ values of olmutinib for their parental cells (KB-3-1, NCI-H460, and KB-3-1) were 18.85, 15.58, and 12.62 μM , respectively, (Figure 2). As the concentration of 3 μM olmutinib did not produce significant cytotoxicity, this concentration was used for reversal experiments.

Effects of Olmutinib on Reversing Drug-Resistance of ABCG2-Overexpressing Cells

To further determine whether olmutinib in the above cell lines reverses the multi-drug resistance (MDR) mediated by ABC transporters, the drug-induced resistant human cancer cell line (KB-C2, NCI-H460/MX20, and KB-CV60) and the transfected resistant cell line (HEK293/ABCB1, HEK293/G2, and HEK293/MRP1) and their corresponding parental cell lines (KB-3-1, NCI-H460, and HEK293/pcDNA3.1) were used to perform the cytotoxicity assay. As shown in Tables 1–3, the IC₅₀ values of KB-C2 and KB-CV60 cell lines were much higher than those of the corresponding parental cell lines. On the other hand, the result in the NCI-H460/MX20 cell line was the opposite. As compared with the NCI-H460 and HEK293/pcDNA3.1 cell lines, olmutinib significantly decreased the IC₅₀ values of MX and SN-38 in the NCI-H460/MX20 and HEK293/ABCG2 cell lines, but it did not affect the values of paclitaxel and vincristine in the KB-C2 and HEK293/ABCB1 cell lines, compared to parental KB-3-1 and HEK293/pcDNA3.1 cell lines. It also did not affect the IC₅₀ values of vinblastine and vincristine in KB-CV60 and HEK293/MRP1 cell lines, compared to parental KB-3-1 and HEK293/pcDNA3.1 cell lines. Cisplatin is not a

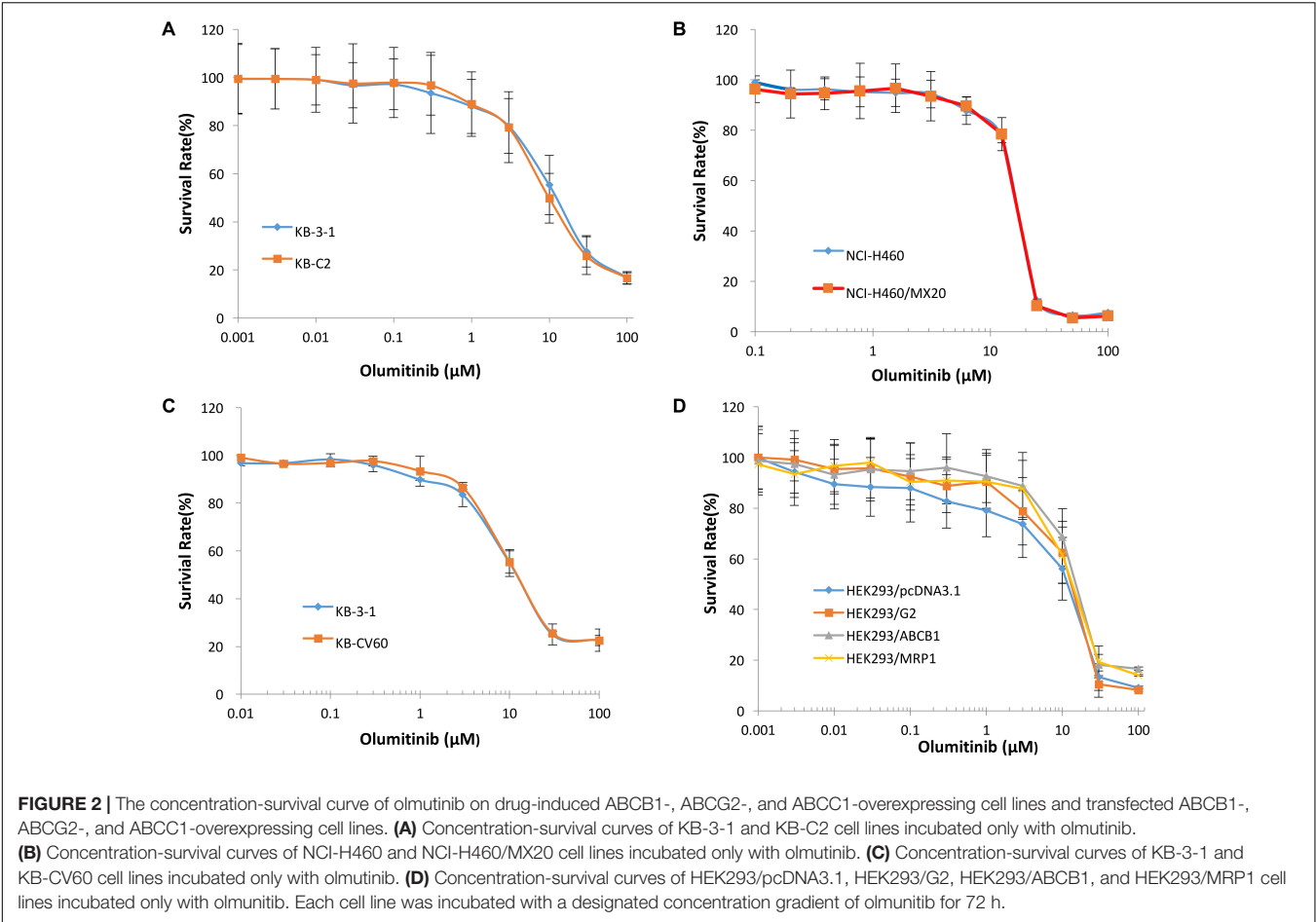


TABLE 1 | The effect of olmutinib on drug resistance to paclitaxel, vincristine, and cisplatin in ABCB1-overexpressing cell lines (KB-3-1 and KB-C2, HEK293/pcDNA3.1, and HEK293/ABCB1).

Treatment	IC ₅₀ ± SD ^a (RF ^b)			
	KB-3-1 (μM)	KB-C2 (μM)	HEK293/pcDNA3.1 (μM)	HEK293/ABCB1 (μM)
Paclitaxel	0.034 ± 0.007(1.00)	2.389 ± 0.541(70.26)	0.173 ± 0.072(1.00)	4.464 ± 0.466(25.80)
+ Olmutinib (1 μM)	0.038 ± 0.009(1.12)	2.237 ± 0.487(65.79)	0.158 ± 0.025(0.91)	3.653 ± 1.096(21.12)
+ Olmutinib (3 μM)	0.036 ± 0.007(1.06)	2.174 ± 0.641(63.94)	0.134 ± 0.074(0.77)	3.462 ± 0.981(20.01)
+ Verapamil (3 μM)	0.054 ± 0.016(1.59)	0.495 ± 0.144(14.56)**	0.153 ± 0.146(0.88)	0.263 ± 0.034(1.52)**
Vincristine	0.028 ± 0.006(1.00)	1.299 ± 0.361(46.39)	0.086 ± 0.221(1.00)	0.763 ± 0.647(8.87)
+ Olmutinib (1 μM)	0.024 ± 0.006(0.86)	1.217 ± 0.389(43.46)	0.071 ± 0.016(0.83)	0.733 ± 0.068(8.52)
+ Olmutinib (3 μM)	0.021 ± 0.007(0.75)	1.132 ± 0.238(40.43)	0.063 ± 0.017(0.73)	0.651 ± 0.692(7.57)
+ Verapamil (3 μM)	0.032 ± 0.015(1.14)	0.056 ± 0.011(2.00)**	0.077 ± 0.013(0.90)	0.126 ± 0.051(1.47)
Cisplatin	1.194 ± 0.876(1.00)	1.863 ± 0.428(1.56)	1.523 ± 0.285(1.00)	1.945 ± 0.876(1.28)
+ Olmutinib (3 μM)	1.123 ± 0.473(0.94)	1.346 ± 0.283(1.13)	1.433 ± 0.465(0.94)	1.683 ± 0.464(1.11)
+ Verapamil (3 μM)	1.744 ± 0.452(1.46)	1.643 ± 0.233(1.38)	1.245 ± 0.337(0.82)	1.534 ± 0.344(1.01)

^aIC₅₀ values represent the mean ± SD of three independent experiments which were performed in triplicate. ^bResistance Fold (RF) was calculated by dividing the IC₅₀ values of substrates in the presence or absence of an inhibitor by the IC₅₀ values of parental cells without an inhibitor. **P < 0.01 versus no inhibitor group.

substrate for ABCB1 and ABCG2. It has no reversal effect on ABCB1-mediated and ABCG2-mediated MDR. So there was no significant change in the IC₅₀ values of cisplatin in the human cancer cell lines (KB-C2, NCI-H460/MX20, and KB-CV60) or transfected cell lines (HEK293/ABCB1, HEK293/G2, and HEK293/MRP1) compared with the corresponding parental cells (Tables 1–3). These results indicate that olmutinib could selectively reverse MDR mediated by ABCG2-overexpression but could not reverse ABCB1- and ABCC1-overexpressing mediated MDR.

TABLE 2 | The effect of olmutinib on drug resistance to MX, SN38, and cisplatin in ABCG2-overexpressing cell lines (NCI-H460 and NCI-H460/MX20, and HEK293/pcDNA3.1 and HEK293/ABCG2).

Treatment	IC ₅₀ ± SD ^a (RF ^b)			
	NCI-H460 (nM)	NCI-H460/MX20 (μM)	HEK293/pcDNA3.1 (nM)	HEK293/ABCG2 (μM)
MX	22.987 ± 4.145(1.00)	2.327 ± 0.642(101.23)	72.245 ± 10.834(1.00)	1.974 ± 0.846(27.32)
+ Olmutinib (1 μM)	18.642 ± 4.101(0.81)	0.039 ± 0.009(1.70)**	70.563 ± 20.169(0.98)	0.261 ± 0.052(3.61)*
+ Olmutinib (3 μM)	17.067 ± 2.241(0.74)	0.027 ± 0.017(1.17)**	68.125 ± 14.824(0.94)	0.146 ± 0.038(2.02)*
+ Ko 143 (3 μM)	16.947 ± 2.643(0.74)	0.022 ± 0.012(0.96)**	62.234 ± 11.216(0.86)	0.183 ± 0.022(2.53)*
SN-38	13.454 ± 1.156(1.00)	2.197 ± 0.342(163.30)	56.462 ± 9.243(1.00)	2.389 ± 0.279(42.31)
+ Olmutinib (1 μM)	12.592 ± 2.392(0.94)	0.033 ± 0.012(2.45)**	56.427 ± 10.421(1.00)	0.288 ± 0.038(5.10)**
+ Olmutinib (3 μM)	12.346 ± 3.243(0.92)	0.019 ± 0.034(1.41)**	54.364 ± 5.826(0.96)	0.176 ± 0.029(3.12)**
+ Ko 143 (3 μM)	12.456 ± 4.024(0.93)	0.021 ± 0.032(1.56)**	57.522 ± 8.024(1.02)	0.164 ± 0.027(2.90)**
IC ₅₀ ± SD ^a (μM) (RF ^b)				
Cisplatin	1.426 ± 0.543(1.00)	1.745 ± 0.224(1.22)	1.628 ± 0.252(1.00)	1.463 ± 0.663(0.90)
+ Olmutinib (3 μM)	1.313 ± 0.512(0.92)	1.654 ± 0.443(1.16)	1.214 ± 0.478(0.75)	1.126 ± 0.275(0.69)
+ Ko 143 (3 μM)	1.226 ± 0.861(0.86)	1.494 ± 0.268(1.05)	1.354 ± 0.368(0.83)	1.425 ± 0.264(0.88)

^aIC₅₀ values represent the mean ± SD of three independent experiments which were performed in triplicate. ^bResistance Fold (RF) was calculated by dividing the IC₅₀ values of substrates in the presence or absence of an inhibitor by the IC₅₀ values of parental cells without an inhibitor. *P < 0.05, **P < 0.01 versus no inhibitor group.

TABLE 3 | The effect of olmutinib on drug resistance to vincristine, vinblastine, and cisplatin in ABCC1-overexpressing cell lines (KB-3-1 and KB-CV60, HEK293/pcDNA3.1, and HEK293/ABCC1).

Treatment	IC ₅₀ ± SD ^a (RF ^b)			
	KB-3-1 (nM)	KB-CV60 (nM)	HEK293/pcDNA3.1 (nM)	HEK293/ABCC1 (nM)
Vincristine	18.424 ± 1.783(1.00)	253.243 ± 11.45(13.75)	13.254 ± 1.884(1.00)	258.344 ± 16.76(19.49)
+ Olmutinib (1 μM)	17.019 ± 2.354(0.92)	230.565 ± 14.081(12.51)	13.136 ± 2.372(0.99)	221.357 ± 20.731(16.70)
+ Olmutinib (3 μM)	16.564 ± 2.165(0.90)	224.363 ± 13.47(12.18)	12.136 ± 2.565(0.92)	213.564 ± 18.672(16.11)
+ MK 571 (25 μM)	17.434 ± 1.624(0.95)	22.467 ± 9.744(1.22)**	11.457 ± 1.343(0.86)	45.348 ± 7.238(3.42)**
Vinblastine	56.514 ± 9.584(1.00)	275.345 ± 13.545(4.87)	8.864 ± 0.843(1.00)	58.462 ± 6.453(6.60)
+ Olmutinib (1 μM)	56.235 ± 7.956(1.00)	234.864 ± 18.452(4.16)	8.233 ± 0.571(0.93)	46.892 ± 7.563(5.29)
+ Olmutinib (3 μM)	56.184 ± 4.763(0.99)	213.585 ± 10.842(3.80)	8.164 ± 0.263(0.92)	45.364 ± 6.837(5.12)
+ MK 571 (25 μM)	45.527 ± 6.254(0.81)	75.613 ± 8.124(1.34)**	7.852 ± 0.144(0.89)	9.823 ± 0.453(1.11)**
IC ₅₀ ± SD ^a (μM) (RF ^b)				
Cisplatin	1.683 ± 0.562(1.00)	1.896 ± 0.323(1.13)	1.644 ± 0.253(1.00)	1.864 ± 0.362(1.13)
+ Olmutinib (3 μM)	1.724 ± 0.233(1.02)	1.657 ± 0.546(0.98)	1.775 ± 0.265(1.08)	1.626 ± 0.164(0.99)
+ MK 571 (25 μM)	1.326 ± 0.364(0.79)	1.469 ± 0.328(0.87)	1.527 ± 0.263(0.93)	1.454 ± 0.246(0.88)

^aIC₅₀ values represent the mean ± SD of three independent experiments which were performed in triplicate. ^bResistance Fold (RF) was calculated by dividing the IC₅₀ values of substrates in the presence or absence of an inhibitor by the IC₅₀ values of parental cells without an inhibitor. **P < 0.01 versus no inhibitor group.

Effect of Olmutinib on the Protein Expression of ABCG2 Transporters

Western blot analysis was performed to confirm whether olmutinib could affect the protein expression of ABCG2 transporters in cell lysates. As shown in **Figures 3A,C**, different concentrations (1, 3, and 6 μM) of olmutinib treatment did not significantly alter the expression of the ABCG2 protein (72 kDa) in ABCG2-overexpressing NCI-H460/MX20 cell line compared to control. **Figures 3B,D** indicated that the protein expression level of ABCG2 was quite low in the parental NCI-H460 cell line, and the treatment of olmutinib (3 μM) for 0, 24, 48, and 72 h did not significantly alter expression of the ABCG2 protein (72 kDa) in the ABCG2-overexpressing NCI-H460/MX20 cell line.

Effect of Olmutinib on the Expression and Intracellular Localization of ABCG2

To further confirm whether olmutinib altered the expression and cellular localization of the ABCG2 protein, immunofluorescence staining was performed after cells were processed with different time of incubation or with different concentrations of olmutinib. As shown in **Figure 4**, the ABCG2 transporters are located on the membrane of NCI-H460/MX20 cells. **Figure 4A** showed that incubation of cells with 3 μM of olmutinib did not significantly alter the subcellular distribution of ABCG2 in NCI-H460/MX20 cells when compared at 0, 24, 48, and 72 h. Similarly, **Figure 4B** showed that incubation of cells after 72 h with 0, 1, 3, and 6 μM of olmutinib did not significantly

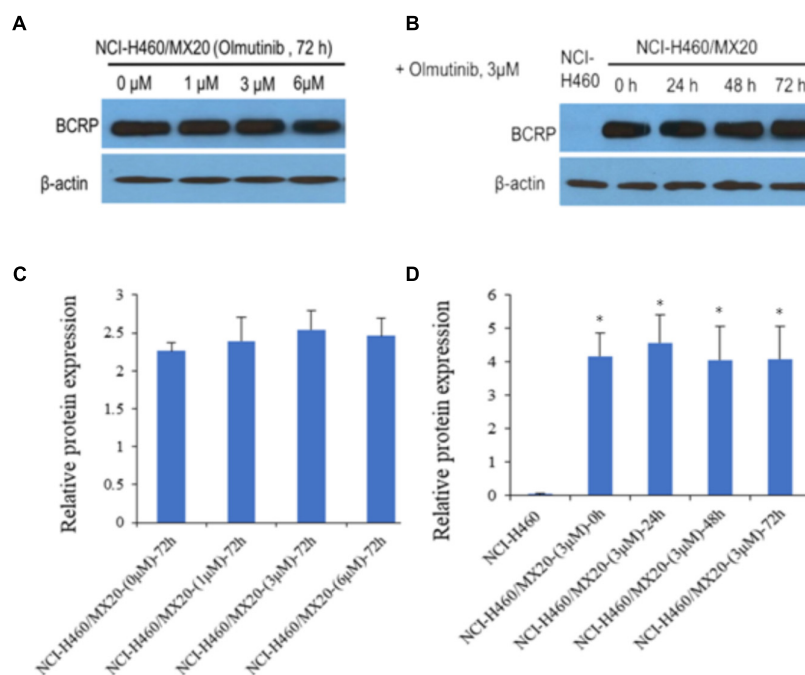


FIGURE 3 | Western blotting to detect ABCG2 expression in ABCG2-over-expressing cell lines. **(A)** The effect of olmutinib at 1, 3, and 6 μ M on the expression levels of ABCG2 in NCI-H460 and NCI-H460/MX20 cells at 72 h. **(B)** The effect of olmutinib at 3 μ M on the expression levels of ABCG2 in NCI-H460 and NCI-H460/MX20 cells at 0, 24, 48, and 72 h. **(C)** The effect of olmutinib at 0, 1, 3, and 6 μ M on the expression levels of ABCG2 in NCI-H460 and NCI-H460/MX20 cells at 72 h. **(D)** The effect of olmutinib at 3 μ M on the expression levels of ABCG2 in NCI-H460 and NCI-H460/MX20 cells at 0, 24, 48, and 72 h. Equal amounts of total cell lysate were used for each sample. * $P < 0.05$ versus the control group (**B,D** versus NCI-H460).

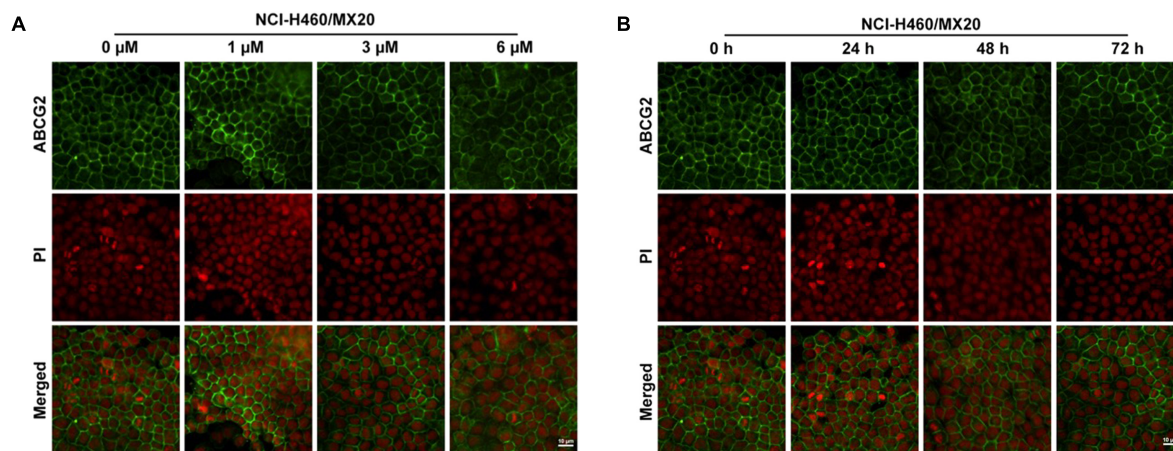


FIGURE 4 | Effect of olmutinib on the expression and cell localization of ABCG2. **(A)** Micrographs are representatives of immunostaining of NCI-H460/MX20 cells incubated with 3 μ M olmutinib after 0, 24, 48, and 72 h. **(B)** The effect of olmutinib at 0, 1, 3, and 6 μ M on NCI-H460/MX20 cells after being processed for 72 h.

alter the subcellular distribution of ABCG2 in NCI-H460/MX20 cells.

Effect of Olmutinib on [3 H]-MX Accumulation and Efflux

The accumulation and efflux effects of the olmutinib were investigated by comparing the quantity of [3 H]-MX in NCI-H460 and ABCG2-mediated NCI-H460/MX20 cells. As shown

in **Figure 5A**, intracellular [3 H]-MX level in NCI-H460/MX20 cells was approximately 2.5-fold lower than that in NCI-H460 cells after 2 h incubation without an inhibitor. Compared with the control group, the accumulation of [3 H]-MX in NCI-H460/MX20 cells was significantly increased in the olmutinib (3 μ M) group. The accumulation effect of olmutinib (3 μ M) is comparable to that of Ko 143 (3 μ M), which is a positive inhibitor of ABCG2. **Figure 5B** indicated that the intracellular

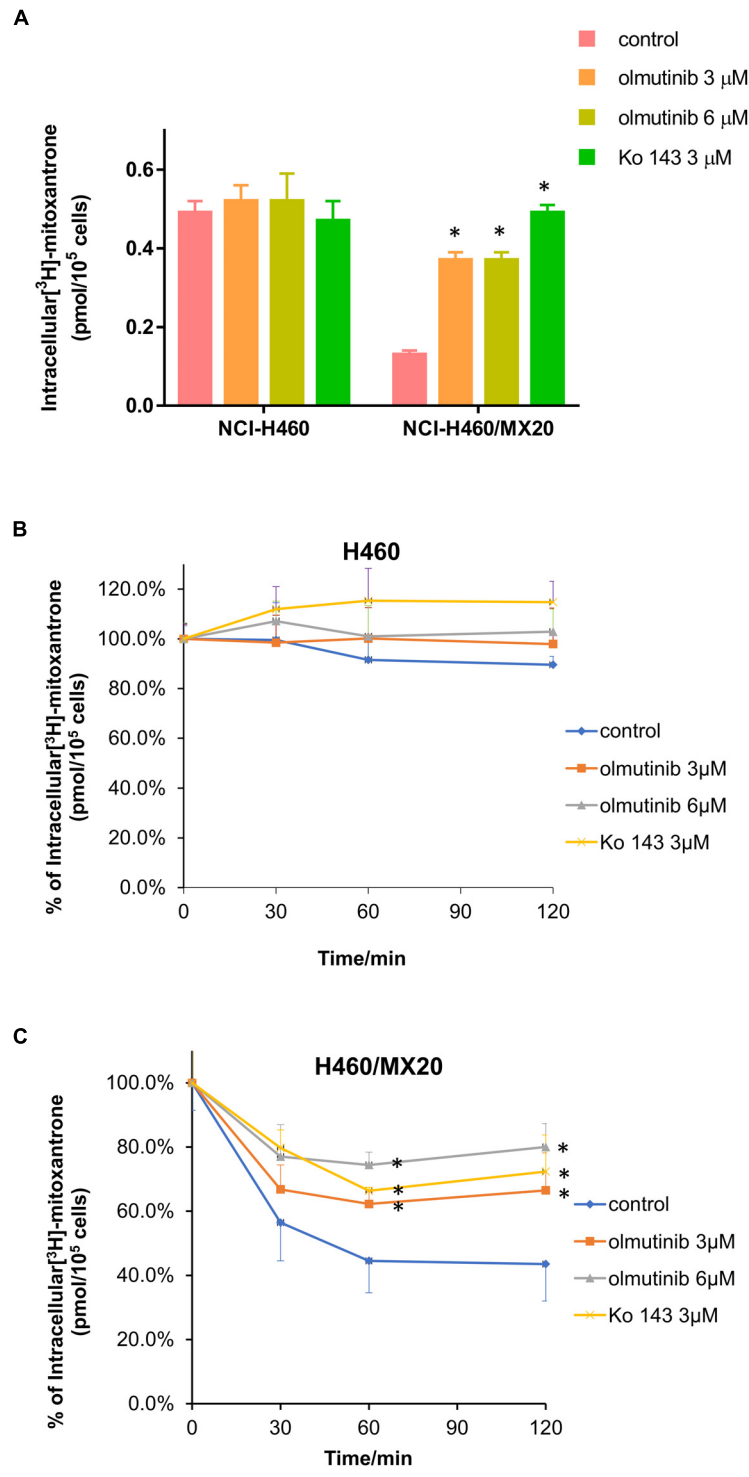


FIGURE 5 | Effects of olmutinib on intracellular accumulation and efflux of [³H]-MX in NCI-H460 and NCI-H460/MX20 cells. **(A)** The effects of olmutinib on the accumulation of [³H]-MX in NCI-H460 and NCI-H460/MX20 cells. **(B)** The effects of olmutinib on the efflux function of NCI-H460 cells. **(C)** The effects of olmutinib on the efflux function of NCI-H460/MX20 cells. Error bars represent the SD value. Ko 143 (3 μM) is used as positive control for ABCG2-overexpressing cells. **P* < 0.05 versus control group, two-way ANOVA.

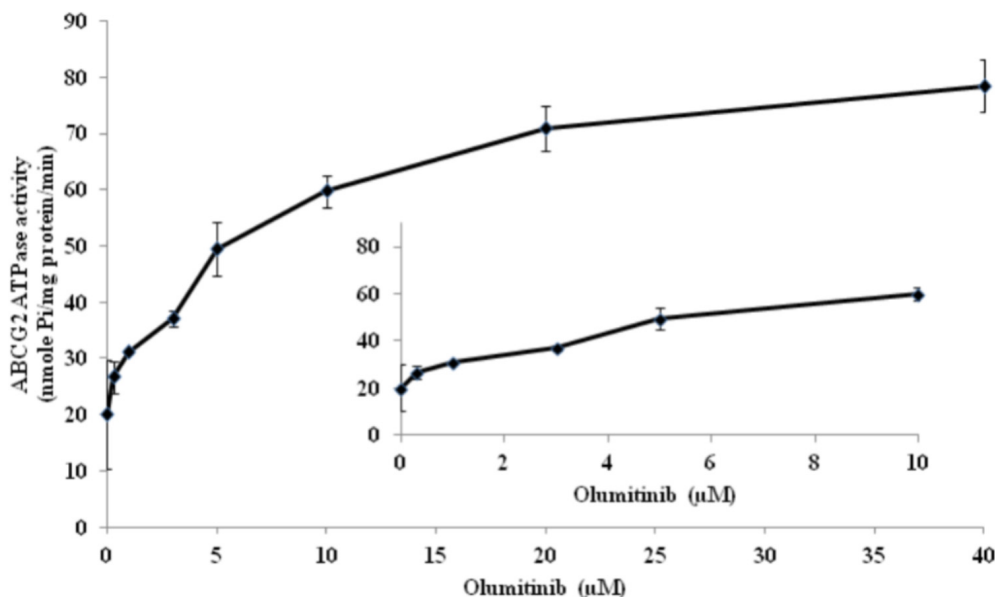


FIGURE 6 | ABCG2 transporter specific ATPase activity was stimulated by olmutinib. The effect of olmutinib on the subcellular localization of BCRP in NCI-H460/MX20 cells. The graph shows that ATPase activity was plotted with SD as a function of concentration of olmutinib. The inset shows stimulation of ATP hydrolysis at lower (0–10 μ M) concentration of olmutinib.

[3 H]-MX level in NCI-H460 cells did not significantly change after 120 min, and treatment with inhibitors did not alter the efflux function in NCI-H460 cells. However, the intracellular [3 H]-MX level in NCI-H460/MX20 cells decreased dramatically by about 60% without the treatment of inhibitors (Figure 5C). With the treatment of olmutinib (3 μ M), the efflux function of NCI-H460/MX20 cells could be effectively inhibited; this inhibition of efflux function would increase with olmutinib at 6 μ M.

Effect of Olmutinib on ATPase Activity of ABCG2 Transporters

ABCG2-mediated ATP hydrolysis, in the presence of olmutinib at various concentrations from 0 to 40 μ M, was measured to assess the effect of olmutinib on the ATPase activity of ABCG2. Olmutinib stimulated the ATPase activity of ABCG2 in a concentration-dependent manner, with a maximal stimulation of 3.5-fold of the basal activity as shown in Figure 6. The concentration of olmutinib required to obtain 50% stimulation is 2.2 μ M. This result indicated that olmutinib interacts at the drug-substrate binding site and affects the ATPase activity of ABCG2.

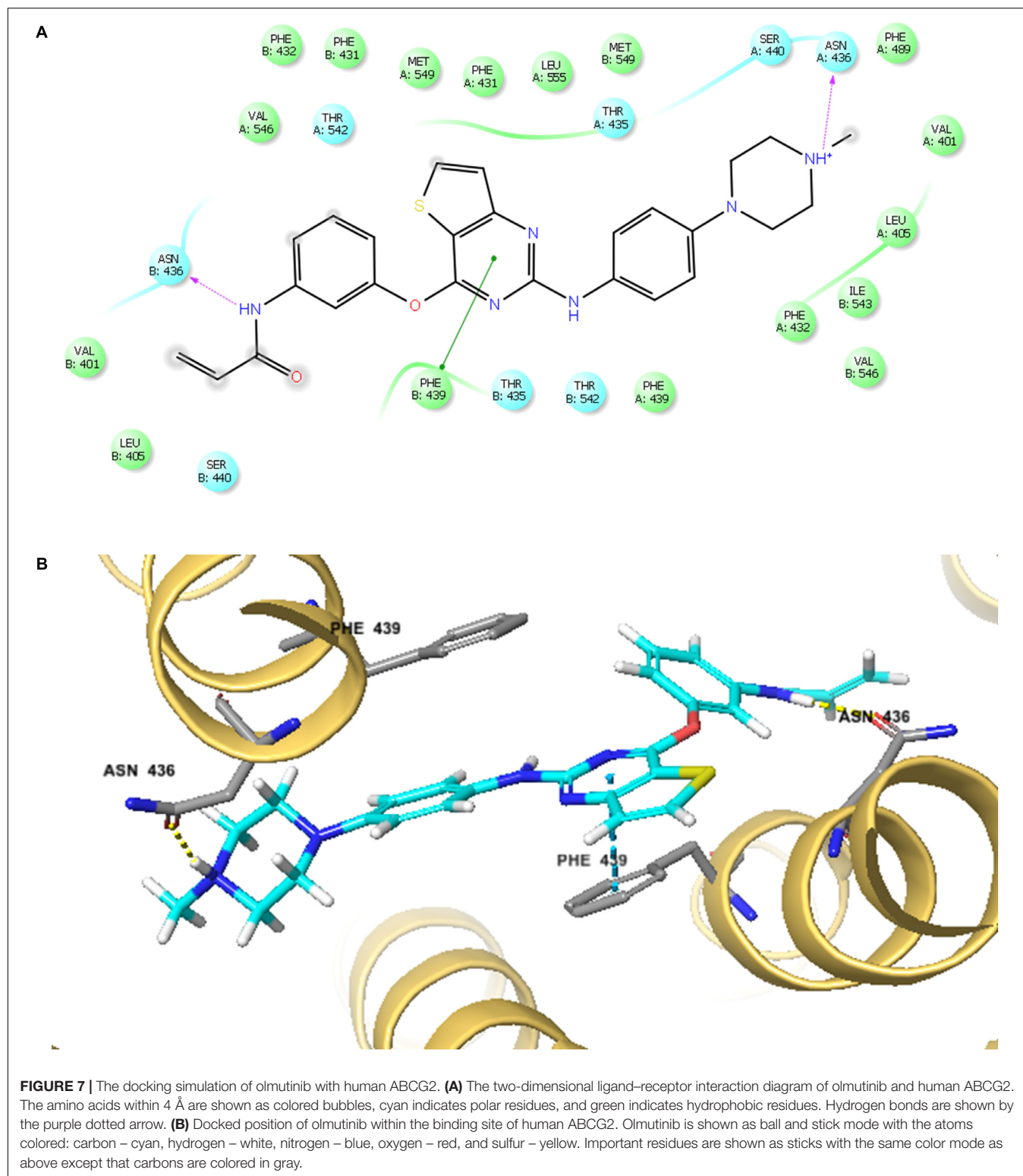
Docking Analysis of the Binding of Olmutinib With Human Wild-Type ABCG2 Model

The best-scored docked (−10.902 kcal/mol) position of olmutinib within the binding pocket of human ABCG2 (5NJ3) is shown in Figure 7. Figure 7A showed that there were two hydrogen bonds and one π – π interaction between

olmutinib and human ABCG2. Interestingly, the nitrogen in piperazine group of olmutinib was ionized and formed a hydrogen bond with Asn436 in the A chain. It was reported that acidic microenvironment is a major feature of tumor (Kato et al., 2013). Acidic extracellular pH could facilitate the ionization of olmutinib and generate the hydrogen bonding with ABCG2. The nitrogen in the enamide group of olmutinib could have another hydrogen bonding with Asn436 in the B chain of ABCG2. Besides the interactions mentioned above, olmutinib could be stabilized in the hydrophobic pocket of ABCG2 by the hydrophobic interactions with residues such as Met431, Phe432, Ile543, Phe549, and Leu555.

DISCUSSION

According to previous studies, small molecule cell signaling inhibitors, such as TK inhibitors, are of crucial importance in chemotherapeutic drug resistance (Wu et al., 2014). ABC transporters are known as mediators of MDR, which is significantly reversed by many clinically used TKIs. Cancer cells acquire MDR via various types of ABC transporters; for example NSCLC cells obtain MDR due to overexpression of ABCG2. ABC transporter-mediated MDR has been found partially or completely reversed by other TKIs such as fumitremorgin C (FTC) (Kim, 2016). As a third-generation EGFR TKI, olmutinib has been approved for the treatment of locally advanced or metastatic EGFR T790M mutation-positive NSCLC (Ni et al., 2010). Therefore, in this study, we aimed to further explore whether olmutinib has potential reversal effects in different



types of ABC transporter-mediated MDR. The results indicated that olmutinib greatly reversed ABCG2-mediated MDR, while ABCB1- and ABCC1-mediated MDR were not significantly influenced.

According to our MTT assay, MX-selected NCI-H460/MX20 cells also acquired resistance to SN-38 and were sensitized to both MX and SN-38 by incubation with olmutinib. IC₅₀ of cisplatin, which is not a substrate of ABCG2, did not vary

significantly with or without pre-incubation with olmutinib. To further explore the specificity of its reversal effects, we also determined the effects of olmutinib on ABCB1-overexpressing cells. Both ABCB1-transfected HEK293 cell and colchicine-selected ABCB1-overexpressing KB-C2 cells had shown drug resistance toward paclitaxel and vincristine. After olmutinib incubation, the results showed that ABCB1-overexpressing cells were not significantly sensitized. Similarly, olmutinib did not show statistically significant reversal effects in ABCC1-overexpressing KB-CV60 and HEK293/ABCC1 cells.

Moreover, to explore the possible mechanism of olmutinib, its effect on ABCG2 expression was tested. Based on the result, ABCG2 expression was not significantly altered with different incubation time or olmutinib concentration. Additionally, intracellular localization of ABCG2 did not vary after 72 h of treatment, as demonstrated by the immunofluorescence results. Based on these findings, we can conclude that the reversal of drug resistance by olmutinib is not related to down-regulated ABCG2 protein expression or altered intracellular location. Instead, the reversal function of olmutinib may be generated by interacting with the ABCG2 protein.

To further determine the interaction between olmutinib and ABCG2, we investigated the accumulation/efflux effect of olmutinib. The results indicated a significant increase in [^3H]-MX accumulation in NCI-H460MX20 cells when incubated with 3 μM olmutinib. The accumulation effect of olmutinib was comparable to that of a positive ABCG2 inhibitor Ko 143. In addition, according to the efflux time-course, MDR cells showed an inhibited MX efflux when treated with olmutinib compared with control group. In conclusion, olmutinib reversed ABCG2-mediated MDR due to inhibited drug efflux, leading to an increased intracellular drug accumulation. A large proportion of TKIs that are involved in ABC transporter-mediated MDR reversal stimulate ATP hydrolysis (Anreddy et al., 2014); we saw consistent results in the ATPase assay that olmutinib stimulated ATPase activity of ABCG2 up to 3.5-fold. Additionally, the molecular interaction between olmutinib and ABCG2 was identified by a docking simulation. The best-score (-10.902 kcal/mol) docking position of olmutinib within human ABCG2 implied direct interaction with $\pi - \pi$ bonds and hydrogen bonds, which stabilized olmutinib in the hydrophobic pocket of ABCG2. The results showed that olmutinib not only interacts directly with ABCG2 but also works as a competitive inhibitor of the transport protein. In conclusion, the reversal effect of olmutinib on ABCG2 in MDR cells is not due to ABCG2 expression or intracellular localization, but is related to its interaction with the ABCG2 protein including drug efflux inhibition and ATPase stimulation.

REFERENCES

Anreddy, N., Gupta, P., Kathawala, R. J., Patel, A., Wurlpel, J. N., and Chen, Z. S. (2014). Tyrosine kinase inhibitors as reversal agents for ABC transporter mediated drug resistance. *Molecules* 19, 13848–13877. doi: 10.3390/molecules190913848

The mechanism involved in resistance of olmutinib is very complex. In recent years, some studies have shown that the nucleotide polymorphism of ABCG2 gene may play a role in the expression level and function of ABCG2 (Tanaka et al., 2011; Chen et al., 2015; Tang et al., 2018). In addition, the nucleotide polymorphism of ABCG2 gene is also associated with drug resistance. Therefore, the effect of ABCG2 single nucleotide polymorphism on ABCG2 function, pharmacokinetics and the mechanism of ABCG2 effect on tumor will be the focus of our future research.

CONCLUSION

Overall, in this study we reported that a newly approved TKI olmutinib reversed ABCG2-mediated MDR by inhibiting chemotherapeutic drug efflux and increasing intracellular drug accumulation. Collectively, our study suggested that ABCG2-mediated drug resistance to conventional chemotherapeutic drugs could be reversed by a combination regimen of olmutinib with other chemotherapeutic drugs.

AUTHOR CONTRIBUTIONS

Z-SC conceived and designed the experiments. WZ, Y-FF, C-YC, J-QW, Q-XT, Z-NL, LZ, and PG performed the experiments and wrote the manuscript. Z-SC finalized the manuscript. All authors read and approved the manuscript.

FUNDING

This work was supported by funds from NIH (No. 1R15CA143701) to Z-SC, project of scientific research and development of universities in Shandong Province (J18KB112) and Natural Science Foundation of Shandong Province (ZR2013HQ025) to WZ, and the National Key Research Program of China (2016YPC1201802) to Y-FF.

ACKNOWLEDGMENTS

We would like to thank Tanaji T. Talele (St. John's University, New York, NY, United States) for providing the computing resources for the docking analysis; Drs. Susan E. Bates and Robert W. Robey (NCI, NIH, Bethesda, MD, United States) for providing the cell lines; Xiao-yu Zhang for her help in the MTT experiment.

Aoki, S., Chen, Z. S., Higasiyama, K., Setiawan, A., Akiyama, S., and Kobayashi, M. (2001). Reversing effect of agosterol A, a spongy sterol acetate, on multidrug resistance in human carcinoma cells. *Jpn. J. Cancer. Res.* 92, 886–895. doi: 10.1111/j.1349-7006.2001.tb01177.x

Beretta, G. L., Cassinelli, G., Pennati, M., Zuco, V., and Gatti, L. (2017). Overcoming ABC transporter-mediated multidrug resistance: the dual role of

- tyrosine kinase inhibitors as multitargeting agents. *Eur. J. Med. Chem.* 142, 271–289. doi: 10.1016/j.ejmech.2017.07.062
- Borst, P., Kool, M., and Evers, R. (1997). Do cMOAT (MRP2), other MRP homologues, and LRP play a role in MDR? *Semin. Cancer Biol.* 8, 205–213. doi: 10.1006/scbi.1997.0071
- Chen, X., Chen, D., Yang, S., Ma, R., Pan, Y., Li, X., et al. (2015). Impact of ABCG2 polymorphisms on the clinical outcome of TKIs therapy in Chinese advanced non-small-cell lung cancer patients. *Cancer Cell Int.* 15, 43. doi: 10.1186/s12935-015-0191-3
- Chen, Y., Zhang, H., and Zhang, Y. (2017). Targeting receptor tyrosine kinase EphB4 in cancer therapy. *Semin. Cancer Biol.* doi: 10.1016/j.semcancer.2017.10.002 [Epub ahead of print].
- Chikhale, R., Thorat, S., Choudhary, R. K., Gadewal, N., and Khedekar, P. (2018). Design, synthesis and anticancer studies of novel aminobenzazoly pyrimidines as tyrosine kinase inhibitors. *Bioorg. Chem.* 77, 84–100. doi: 10.1016/j.bioorg.2018.01.008
- Cole, S. P., Bhardwaj, G., Gerlach, J. H., Mackie, J. E., Grant, C. E., Almquist, K. C., et al. (1992). Overexpression of a transporter gene in a multidrug-resistant human lung cancer cell line. *Science* 258, 1650–1654. doi: 10.1126/science.1360704
- Dohse, M., Scharenberg, C., Shukla, S., Robey, R. W., Volkmann, T., Deeken, J. F., et al. (2010). Comparison of ATP-binding cassette transporter interactions with the tyrosine kinase inhibitors imatinib, nilotinib, and dasatinib. *Drug Metab. Dispos.* 38, 1371–1380. doi: 10.1124/dmd.109.031302
- Doyle, L. A., Yang, W., Abruzzo, L. V., Krogmann, T., Gao, Y., Rishi, A. K., et al. (1998). A multidrug resistance transporter from human MCF-7 breast cancer cells. *Proc. Natl. Acad. Sci. U.S.A.* 95, 15665–15670. doi: 10.1073/pnas.95.26.15665
- Faivre, S., Djelloul, S., and Raymond, E. (2006). New paradigms in anticancer therapy: targeting multiple signaling pathways with kinase inhibitors. *Semin. Oncol.* 33, 407–420. doi: 10.1053/j.seminoncol.2006.04.005
- Fan, Y. F., Zhang, W., Zeng, L., Lei, Z. N., Cai, C. Y., Gupta, P., et al. (2018). Dacomitinib antagonizes multidrug resistance (MDR) in cancer cells by inhibiting the efflux activity of ABCB1 and ABCG2 transporters. *Cancer Lett.* 421, 186–198. doi: 10.1016/j.canlet.2018.01.021
- Fletcher, J. I., Williams, R. T., Henderson, M. J., Norris, M. D., and Haber, M. (2016). ABC transporters as mediators of drug resistance and contributors to cancer cell biology. *Drug Resist. Updat.* 26, 1–9. doi: 10.1016/j.drug.2016.03.001
- Gillet, J. P., and Gottesman, M. M. (2010). Mechanisms of multidrug resistance in cancer. *Methods Mol. Biol.* 596, 47–76. doi: 10.1007/978-1-60761-416-6_4
- Herbrink, M., Nuijen, B., Schellens, J. H., and Beijnen, J. H. (2015). Variability in bioavailability of small molecular tyrosine kinase inhibitors. *Cancer Treat. Rev.* 41, 412–422. doi: 10.1016/j.ctrv.2015.03.005
- Hocker, S. E., Higginbotham, M. L., Schermerhorn, T., and Henningson, J. (2017). Receptor tyrosine kinase expression and phosphorylation in canine nasal carcinoma. *Res. Vet. Sci.* 115, 484–489. doi: 10.1016/j.rvsc.2017.07.030
- Hu, T., Li, Z., Gao, C. Y., and Cho, C. H. (2016). Mechanisms of drug resistance in colon cancer and its therapeutic strategies. *World J. Gastroenterol.* 22, 6876–6889. doi: 10.3748/wjg.v22.i30.6876
- Juliano, R. L., and Ling, V. (1976). A surface glycoprotein modulating drug permeability in Chinese hamster ovary cell mutants. *Biochim. Biophys. Acta* 455, 152–162. doi: 10.1016/0005-2736(76)90160-7
- Kartal-Yandim, M., Adan-Gokbulut, A., and Baran, Y. (2016). Molecular mechanisms of drug resistance and its reversal in cancer. *Crit. Rev. Biotechnol.* 36, 716–726. doi: 10.3109/07388551.2015.1015957
- Kartner, N., Riordan, J. R., and Ling, V. (1983). Cell surface P-glycoprotein associated with multidrug resistance in mammalian cell lines. *Science* 221, 1285–1288. doi: 10.1126/science.6137059
- Kathawala, R. J., Li, T., Yang, D., Guo, H. Q., Yang, D. H., Chen, X., et al. (2017). 2-trifluoromethyl-2-hydroxypropionamide derivatives as novel reversal agents of ABCG2 (BCRP)-mediated multidrug resistance: synthesis and biological evaluations. *J. Cell. Biochem.* 118, 2420–2429. doi: 10.1002/jcb.25908
- Kato, Y., Ozawa, S., Miyamoto, C., Maehata, Y., Suzuki, A., Maeda, T., et al. (2013). Acidic extracellular microenvironment and cancer. *Cancer Cell Int.* 13:89. doi: 10.1186/1475-2867-13-89
- Kim, E. S. (2016). Olmutinib: first global approval. *Drugs* 76, 1153–1157. doi: 10.1007/s40265-016-0606-z
- Krishna, R., and Mayer, L. D. (2000). Multidrug resistance (MDR) in cancer. Mechanisms, reversal using modulators of MDR and the role of MDR modulators in influencing the pharmacokinetics of anticancer drugs. *Eur. J. Pharm. Sci.* 11, 265–283. doi: 10.1016/S0928-0987(00)00114-7
- Ma, S. L., Hu, Y. P., Wang, F., Huang, Z. C., Chen, Y. F., Wang, X. K., et al. (2014). Lapatinib antagonizes multidrug resistance-associated protein 1-mediated multidrug resistance by inhibiting its transport function. *Mol. Med.* 20, 390–399. doi: 10.2119/molmed.2014.00059
- Miklos, W., Pelivan, K., Kowol, C. R., Pirker, C., Dornetshuber-Fleiss, R., Spitzwieser, M., et al. (2015). Triapine-mediated ABCB1 induction via PKC induces widespread therapy unresponsiveness but is not underlying acquired triapine resistance. *Cancer Lett.* 361, 112–120. doi: 10.1016/j.canlet.2015.02.049
- Miyake, K., Mickley, L., Litman, T., Zhan, Z., Robey, R., Cristensen, B., et al. (1999). Molecular cloning of cDNAs which are highly overexpressed in mitoxantrone-resistant cells: demonstration of homology to ABC transport genes. *Cancer Res.* 59, 8–13.
- Ni, Z., Bikadi, Z., Rosenberg, M. F., and Mao, Q. (2010). Structure and function of the human breast cancer resistance protein (BCRP/ABCG2). *Curr. Drug Metab.* 11, 603–617. doi: 10.2174/138920010792927325
- Pan, S. T., Li, Z. L., He, Z. X., Qiu, J. X., and Zhou, S. F. (2016). Molecular mechanisms for tumour resistance to chemotherapy. *Clin. Exp. Pharmacol. Physiol.* 43, 723–737. doi: 10.1111/1440-1681.12581
- Parikh, P. K., and Ghate, M. D. (2018). Recent advances in the discovery of small molecule c-Met kinase inhibitors. *Eur. J. Med. Chem.* 143, 1103–1138. doi: 10.1016/j.ejmech.2017.08.044
- Pytel, D., Sliwinski, T., Poplawski, T., Ferriola, D., and Majsterek, I. (2009). Tyrosine kinase blockers: new hope for successful cancer therapy. *Anticancer Agents Med. Chem.* 9, 66–76. doi: 10.2174/187152009787047752
- Robey, R. W., Pluchino, K. M., Hall, M. D., Fojo, A. T., Bates, S. E., and Gottesman, M. M. (2018). Revisiting the role of ABC transporters in multidrug-resistant cancer. *Nat. Rev. Cancer* 18, 452–464. doi: 10.1038/s41568-018-0005-8
- Robey, R. W., Polgar, O., Deeken, J., To, K. W., and Bates, S. E. (2007). ABCG2: determining its relevance in clinical drug resistance. *Cancer Metastasis Rev.* 26, 39–57. doi: 10.1007/s10555-007-9042-6
- Russo, A., Franchina, T., Ricciardi, G. R. R., Smirardo, V., Picciotto, M., Zanghi, M., et al. (2017). Third generation EGFR TKIs in EGFR-mutated NSCLC: where are we now and where are we going. *Crit. Rev. Oncol. Hematol.* 117, 38–47. doi: 10.1016/j.critrevonc.2017.07.003
- Saraswathy, M., and Gong, S. (2013). Different strategies to overcome multidrug resistance in cancer. *Biotechnol. Adv.* 31, 1397–1407. doi: 10.1016/j.biotechadv.2013.06.004
- Shukla, S., Chen, Z. S., and Ambudkar, S. V. (2012). Tyrosine kinase inhibitors as modulators of ABC transporter-mediated drug resistance. *Drug Resist. Updat.* 15, 70–80. doi: 10.1016/j.drug.2012.01.005
- Singh, M., and Jadhav, H. R. (2018). Targeting non-small cell lung cancer with small-molecule EGFR tyrosine kinase inhibitors. *Drug Discov. Today* 23, 745–753. doi: 10.1016/j.drudis.2017.10.004
- Strouse, J. J., Ivnitiski-Steele, I., Waller, A., Young, S. M., Perez, D., Evangelisti, A. M., et al. (2013). Fluorescent substrates for flow cytometric evaluation of efflux inhibition in ABCB1, ABCC1, and ABCG2 transporters. *Anal. Biochem.* 437, 77–87. doi: 10.1016/j.ab.2013.02.018
- Tanaka, M., Okazaki, T., Suzuki, H., Abbruzzese, J. L., and Li, D. (2011). Association of multi-drug resistance gene polymorphisms with pancreatic cancer outcome. *Cancer* 117, 744–751. doi: 10.1002/cncr.25510
- Tang, L., Zhang, C., He, H., Pan, Z., Fan, D., He, Y., et al. (2018). Associations between ABCG2 gene polymorphisms and gefitinib toxicity in non-small cell lung cancer: a meta-analysis. *Onco Targets Ther.* 11, 665–675. doi: 10.2147/OTT.S154244
- Taylor, N. M. I., Manolaridis, I., Jackson, S. M., Kowal, J., Stahlberg, H., and Locher, K. P. (2017). Structure of the human multidrug transporter ABCG2. *Nature* 546, 504–509. doi: 10.1038/nature22345
- van der Geer, P., Hunter, T., and Lindberg, R. A. (1994). Receptor protein-tyrosine kinases and their signal transduction pathways. *Annu. Rev. Cell Biol.* 10, 251–337. doi: 10.1146/annurev.cb.10.10194.001343

- Wu, Q., Yang, Z., Nie, Y., Shi, Y., and Fan, D. (2014). Multi-drug resistance in cancer chemotherapeutics: mechanisms and lab approaches. *Cancer Lett.* 347, 159–166. doi: 10.1016/j.canlet.2014.03.013
- Zhang, X. Y., Zhang, Y. K., Wang, Y. J., Gupta, P., Zeng, L., Xu, M., et al. (2016a). Osimertinib (AZD9291), a mutant-selective EGFR inhibitor, reverses ABCB1-mediated drug resistance in cancer cells. *Molecules* 21:E1236. doi: 10.3390/molecules21091236
- Zhang, Y. K., Zhang, G. N., Wang, Y. J., Patel, B. A., Talele, T. T., Yang, D. H., et al. (2016b). Bafetinib (INNO-406) reverses multidrug resistance by inhibiting the efflux function of ABCB1 and ABCG2 transporters. *Sci. Rep.* 6:25694. doi: 10.1038/srep25694
- Zhang, Y. K., Zhang, H., Zhang, G. N., Wang, Y. J., Kathawala, R. J., Si, R., et al. (2015). Semi-synthetic ocotillol analogues as selective ABCB1-mediated drug resistance reversal agents. *Oncotarget* 6, 24277–24290. doi: 10.18632/oncotarget.4493
- Zhang, Y. K., Zhang, X. Y., Zhang, G. N., Wang, Y. J., Xu, H., Zhang, D., et al. (2017). Selective reversal of BCRP-mediated MDR by VEGFR-2 inhibitor ZM323881. *Biochem. Pharmacol.* 132, 29–37. doi: 10.1016/j.bcp.2017.02.019
- Conflict of Interest Statement:** The authors declare that the research was conducted in the absence of any commercial or financial relationships that could be construed as a potential conflict of interest.
- Copyright © 2018 Zhang, Fan, Cai, Wang, Teng, Lei, Zeng, Gupta and Chen. This is an open-access article distributed under the terms of the Creative Commons Attribution License (CC BY). The use, distribution or reproduction in other forums is permitted, provided the original author(s) and the copyright owner(s) are credited and that the original publication in this journal is cited, in accordance with accepted academic practice. No use, distribution or reproduction is permitted which does not comply with these terms.



VS-4718 Antagonizes Multidrug Resistance in ABCB1- and ABCG2-Overexpressing Cancer Cells by Inhibiting the Efflux Function of ABC Transporters

Ning Ji^{1,2}, Yuqi Yang², Chao-Yun Cai², Zi-Ning Lei², Jing-Quan Wang², Pranav Gupta², Qiu-Xu Teng², Zhe-Sheng Chen², Dexin Kong^{1*} and Dong-Hua Yang^{2*}

¹ Tianjin Key Laboratory on Technologies Enabling Development of Clinical Therapeutics and Diagnostics, School of Pharmacy, Tianjin Medical University, Tianjin, China, ² Department of Pharmaceutical Sciences, College of Pharmacy and Health Sciences, St. John's University, Queens, NY, United States

OPEN ACCESS

Edited by:

Tea Lanisnik Rizner,
University of Ljubljana, Slovenia

Reviewed by:

Antonello Di Paolo,
Università degli Studi di Pisa, Italy
Marialessandra Contino,
Università degli Studi di Bari, Italy

*Correspondence:

Dexin Kong
kongdexin@tmu.edu.cn
Dong-Hua Yang
yangd1@stjohns.edu

Specialty section:

This article was submitted to
Experimental Pharmacology and Drug
Discovery,
a section of the journal
Frontiers in Pharmacology

Received: 22 August 2018

Accepted: 11 October 2018

Published: 30 October 2018

Citation:

Ji N, Yang Y, Cai C-Y, Lei Z-N,
Wang J-Q, Gupta P, Teng Q-X,
Chen Z-S, Kong D and Yang D-H
(2018) VS-4718 Antagonizes
Multidrug Resistance in ABCB1- and
ABCG2-Overexpressing Cancer Cells
by Inhibiting the Efflux Function of
ABC Transporters.
Front. Pharmacol. 9:1236.
doi: 10.3389/fphar.2018.01236

Overexpression of ATP-binding cassette (ABC) transporters is one of the most important mechanisms responsible for multi-drug resistance (MDR). VS-4718, a tyrosine kinase inhibitor targeting focal adhesion kinase (FAK) with a potential anticancer effect, is currently evaluated in clinical trials. In this study, we investigated whether VS-4718 could reverse MDR mediated by ABC transporters, including ABCB1, ABCG2, and ABCC1. The results showed that VS-4718 significantly reversed ABCB1- and ABCG2-mediated MDR, but not MDR mediated by ABCC1. Treatment of VS-4718 did not alter the protein level and subcellular localization of ABCB1 or ABCG2. Mechanism studies indicated that the reversal effects of VS-4718 were related to attenuation of the efflux activity of ABCB1 and ABCG2 transporters. ATPase analysis indicated that VS-4718 stimulated the ATPase activity of ABCB1 and ABCG2. Docking study showed that VS-4718 interacted with the substrate-binding sites of both ABCB1 and ABCG2, suggesting that VS-4718 may affect the activity of ABCB1 and ABCG2 competitively. This study provided a novel insight for MDR cancer treatment. It indicated that combination of VS-4718 with antineoplastic drugs could attenuate MDR mediated by ABCB1 or ABCG2 in ABCB1- or ABCG2-overexpressing cancer cells.

Keywords: VS-4718, multidrug resistance (MDR), ATP-binding cassette (ABC) transporter, P-glycoprotein (P-gp/ABCB1), breast cancer resistance protein (BCRP/ABCG2)

INTRODUCTION

Multidrug resistance (MDR) remains a major challenge that contributes to the failure of cancer chemotherapy (Szakács et al., 2006; Kartal-Yandim et al., 2016). MDR in cancer leads to synchronous resistance of cancer cells to structurally unrelated anticancer drugs. Several mechanisms contribute to cancer MDR, including reduced apoptosis, advanced DNA damage repair mechanisms, or altered drug metabolism. However, ATP binding cassette (ABC) transporters play a critical role in inducing MDR in cancer cells (Gottesman et al., 2002; Eckford and Sharom, 2009).

The ABC transporters contain diverse groups of active membrane transporters with important physiological and pharmacological roles (Dassa and Bouige, 2001). Divided into 7 subfamilies from ABCA to ABCG, the human ABC protein family has 49 ABC proteins and 48 of them have functions (Stavrovskaya and Stromskaya, 2008; Eckford and Sharom, 2009). Collectively, they are widely expressed in the placenta, blood brain barrier (BBB), intestines, liver, and kidneys to restrict the bioavailability of administered drugs (Linton, 2007; Linton and Higgins, 2007), transporting and regulating levels of physiological substrates such as lipids, porphyrins, and sterols (Wu and Ambudkar, 2014). The ABC transporters also play an important role in MDR, especially the ABC transporter subfamily B member 1 (ABCB1/P-glycoprotein, P-gp) and-subfamily G member 2 (ABCG2/breast cancer resistance protein, BCRP). The ABC transporters significantly decrease the intracellular concentration of certain anticancer drugs by pumping substrate drugs out of cancer cells, which becomes a major impediment to chemotherapy. It is well documented that the expression of ABC transporters are associated with the level of response of chemotherapy and the progression of malignancy (Liu et al., 2013, 2014; Ali and Elsalakawy, 2014; Xie et al., 2014; Yang et al., 2015). Thus, inhibiting the efflux function of ABC transporters is of great importance to enhance the efficacy of chemotherapy (Shukla et al., 2008).

Previously, we found that some tyrosine kinase inhibitors (TKIs) could attenuate ABC transporter-mediated MDR. For example, dacomitinib, an epidermal growth factor receptor (EGFR) inhibitor, directly inhibits the efflux activity of ABCB1 and ABCG2, thereby decreasing the efflux of certain anticancer drugs and subsequently increases their intracellular accumulation, finally reversing the MDR (Zhang et al., 2018).

VS-4718 (PND-1186) is a selective focal adhesion kinase (FAK) inhibitor with potential anti-cancer activity in breast cancer and ovarian cancer (Tanjoni et al., 2010; Tancioni et al., 2014). It is currently evaluated in clinical trials (NCT02215629, NCT01849744, and NCT02651727). Recent studies have shown that VS-4718 could drive depletion of regulatory T cells (Tregs) and promotes CD8⁺ T cell-mediated anti-tumor response (Serrels et al., 2015). However, there is hardly any research indicating the sensitizing effects of VS-4718 in ABC transporter-overexpressing cancer cells. Here we report for the first time that VS-4718 shows a significant effect on reversing ABCB1- and ABCG2-mediated MDR at non-toxic concentrations.

MATERIALS AND METHODS

Chemicals

VS-4718 (PND-1186) was a gift from Chemie Tek (Indianapolis, IN). Bovine serum albumin (BSA), fetal bovine serum (FBS), Dulbecco's modified Eagle's Medium (DMEM), penicillin/streptomycin and 0.25% trypsin were purchased from Corning Incorporated (Corning, NY). The monoclonal antibodies for ABCG2 (catalog number MAB4146, Lot number 3026758, clone BXP-21) were purchased from Millipore (Billerica, MA). Paclitaxel, doxorubicin, cisplatin, vincristine, mitoxantrone, verapamil, the monoclonal antibodies for

ABCB1 (catalog number P7965, Lot number 067M4761V, clone F4), dimethylsulfoxide (DMSO), 3-(4,5-dimethylthiazolyl)-2,5-diphenyltetrazolium bromide (MTT), Triton X-100, 4',6-diamidino-2-phenylindole (DAPI), and paraformaldehyde, were purchased from Sigma-Aldrich (St. Louis, MO). The monoclonal antibody for GAPDH (catalog number MA5-15738, Lot number SA247966, clone GA1R), Alexa Fluor 488 conjugated goat anti-mouse IgG secondary antibody, SN-38 and MK571, were purchased from Thermo Fisher Scientific Inc (Rockford, IL). HRP-conjugated rabbit anti-mouse IgG secondary antibody (catalog number 7076S, Lot number 32) were purchased from Cell Signaling Technology Inc (Danvers, MA). Ko143 was a product from Enzo Life Sciences (Farmingdale, NY). [³H]-paclitaxel (15 Ci/mmol) and [³H]-mitoxantrone (2.5 Ci/mmol) were purchased from Moravsek Biochemicals, Inc., (Brea, CA). All other chemicals were purchased from Sigma Chemical Co (St. Louis, MO).

Cell Lines and Cell Culture

The ABCB1-overexpressing resistant KB-C2 cells were established by step-wise increased concentration of colchicine to parental human epidermoid carcinoma KB-3-1 cells and were cultured in medium with 2 µg/mL colchicine (Akiyama et al., 1985). The ABCG2-overexpressing KB-CV60 cells were cloned from KB-3-1 cells and were maintained in medium with 1 µg/mL cepharanthine and 60 ng/mL vincristine (Taguchi et al., 1997). Both KB-C2 and KB-CV60 and their parental KB-3-1 cells were kindly provided by Dr. Shin-ichi Akiyama (Kagoshima University, Kagoshima, Japan). The human colon cancer SW620 cells and the doxorubicin-selected ABCB1-overexpressing resistant subline SW620/Ad300 were used for ABCB1 reversal study and the SW620/Ad300 cells were cultured in medium with 300 ng/mL doxorubicin (Bates et al., 1993). The human non-small cell lung cancer (NSCLC) NCI-H460 cells and the mitoxantrone-selected subline ABCG2-overexpressing NCI-H460/MX20 cells were used for ABCG2 reversal study and the NCI-H460/MX20 cells were maintained in medium with 20 ng/mL mitoxantrone (Robey et al., 2001). The human colon carcinoma cell line S1 and its mitoxantrone-selected derivative ABCG2 overexpressing S1-M1-80 cells were used for ABCG2 reversal study and the S1-M1-80 cells were maintained in the medium with 80 µM mitoxantrone (Miyake et al., 1999). HEK293/pcDNA3.1 and HEK293/ABCB1 were established by transfecting the human embryonic kidney HEK293 cells with empty and ABCB1 expressing vector respectively (Fung et al., 2014). HEK293/pcDNA3.1 and HEK293/ABCG2 were transfected with either an empty vector pcDNA3.1 or a pcDNA3.1 vector containing a full length ABCG2. Transfected cells were selected with complete culture medium containing G418 (2 mg/ml). SW620 and SW620/Ad300, NCI-H460 and NCI-H460/MX20, S1 and S1-M1-80, HEK293/ABCG2 were kindly provided by Drs. Susan Bates and Robert Robey (NCI, NIH, Bethesda, MD). HEK293/ABCB1 were kindly provided by Dr. Suresh V. Ambudkar (NCI, NIH, Bethesda, MD). Each aforementioned cell line was cultured in DMEM medium containing 10% fetal bovine serum and 1% penicillin/streptomycin at 37°C in a humidified atmosphere

containing 5% CO₂. All cells were grown as an adherent monolayer and drug-resistant cells were grown in drug-free culture media for more than 2 weeks before assay. All cells were tested by DAPI staining and found free of mycoplasma contamination before being used for experiments.

Cell Viability and Reversal Experiments

Cell viability and reversal fold were determined using MTT assay as previously described (Zhang X. Y. et al., 2016). Briefly, for the reversal study, each type of cells were harvested and resuspended, and seeded evenly onto a 96-well plate at a final concentration of 5×10^3 cells per well in 160 μ l medium. After incubating for 24 h, VS-4718 (1 and 3 μ M) was added 2 h prior to incubation with anticancer drugs. After 72 h of incubation, MTT solution (4 mg/ml) was added to each well and the cells were further incubated for 4 h. Then, the supernatant was discarded and 100 μ L of DMSO was used to dissolve the formazan crystals. An accuScanTM GO UV/Vis Microplate Spectrophotometer (Fisher Sci., Fair Lawn, NJ) was used to determine the absorbance at 570 nm. The concentration for 50% inhibition of cell viability (IC₅₀) of the anticancer drug was calculated as previously described (Zhang et al., 2015). Verapamil (3 μ M), Ko 143 (3 μ M), and MK 571 (25 μ M) were used to reverse ABCB1-, ABCG2- and ABCC1-mediated MDR, respectively, as positive controls. Cisplatin, known as a non-substrate of ABCB1, ABCG2, or ABCC1, was used as a negative control of anticancer drug.

Western Blotting Analysis

Western blotting analysis was carried out as previously described (Zhang X. Y. et al., 2016). Briefly, cells were incubated with or without VS-4718 for varying amounts of time (0, 24, 48, 72 h) before being lysed. Protein concentrations were determined with BCA Protein Assay Kit (Pierce, Rockford, IL). Equal amounts (20 μ g) of proteins were subjected to 10% sodium dodecyl sulfate polyacrylamide gel electrophoresis (SDS-PAGE) and transferred to PVDF membranes (Millipore, Billerica, MA). The presence of ABCB1 and ABCG2 was determined using monoclonal antibody F4 (dilution 1:500) and BXP-21 (dilution 1:1,000), respectively. GAPDH was used as a loading control. The resulting protein bands were analyzed using Image J software.

Immunofluorescence Assay

The immunofluorescence assay was performed as previously described (Zhang X. Y. et al., 2016). After being cultured overnight in 24-well plates, the cells (2×10^4) were treated with VS-4718 for 0, 24, 48, and 72 h. Then cells were fixed in 4% paraformaldehyde for 10 min and permeabilized by 0.1% Triton X-100 for 10 min before blocking with 6% BSA for 1 h. Cells were incubated with monoclonal antibodies ABCB1 (F4, dilution 1:100) and ABCG2 (BXP-21, dilution 1:150) at 4 °C overnight. Alexa Fluor 488 conjugated secondary antibody (1:1,000) was used after washing with iced PBS. DAPI was used to counterstain the nuclei. Immunofluorescence images were collected using an EVOS FL Auto fluorescence microscope (Life Technologies Corporation, Gaithersburg, MD).

ATPase Assay

The ABCB1- and ABCG2-associated ATPase activities were measured using PREDEASY ATPase Kits (TEBU-BIO nv, Boechout, Belgium) with modified protocols. In short, cell membranes that overexpressed ABCB1 or ABCG2 were thawed and diluted before used. Sodium orthovanadate (Na₃VO₄) was used as an ATPase inhibitor. Various concentrations of VS-4718 were incubated with membranes for 5 min. The ATPase reactions were initiated by adding 5 mM Mg²⁺ ATP. Luminescence signals of P_i were initiated and measured after incubation at 37°C for 40 min with brief mixing. The changes of relative light units were determined by comparing Na₃VO₄-treated samples with VS-4718 treated groups.

[³H]-Paclitaxel and [³H]-mitoxantrone Accumulation Assay

For the [³H]-paclitaxel accumulation assay, KB-3-1 and its drug resistant subline KB-C2 were used. Briefly, 5×10^5 cells were cultured in 24-well plates overnight before the assay, and VS-4718 was added 2 h prior to the addition of [³H]-paclitaxel. After incubating with [³H]-paclitaxel with or without VS-4718 for 2 h at 37°C, cells were washed twice with iced PBS, and lysed with 0.25% trypsin before being placed in 5 mL scintillation fluid. Radioactivity of cells was measured in the Packard TRI-CARB 1900CA liquid scintillation analyzer (Packard Instrument, Downers Grove, IL). NCI-H460, NCI-H46/MX20, were used for [³H]-mitoxantrone accumulation assay as previously described (Sun et al., 2012).

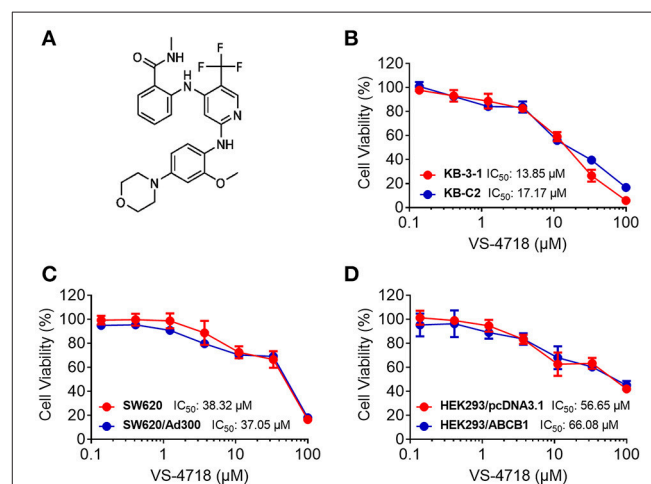


FIGURE 1 | Chemical structure of VS-4718 and concentration-dependent viability curves for parental and ABCB1-overexpressing cells incubated with VS-4718. **(A)** Chemical structure of VS-4718. **(B)** Concentration-viability curves for KB-3-1 and KB-C2 cells incubated with VS-4718 for 72 h. **(C)** Concentration-viability curves for SW620 and SW620/Ad300 cells incubated with VS-4718 for 72 h. **(D)** Concentration-viability curves for HEK293/pcDNA3.1 and HEK293/ABCB1 cells incubated with VS-4718 for 72 h. The cell viability was determined by MTT assay. Data are expressed as mean \pm SD, and representative of three independent experiments in triplicate are shown.

³H]-Paclitaxel and ³H]-mitoxantrone Efflux Assay

For the efflux assay, cells were incubated with VS-4718 for 2 h followed by incubation with [³H]-paclitaxel or [³H]-mitoxantrone with or without VS-4718 for 2 h at 37°C. The cells were washed with iced PBS twice and then lysed at various time points (0, 30, 60, and 120 min) with trypsin. Subsequently, cells were placed in 5 mL of scintillation fluid, and radioactivity was measured in the Packard TRI-CARB 1900CA liquid scintillation analyzer (Packard Instrument, Downers Grove, IL). KB-3-1 and KB-C2 were used for [³H]-paclitaxel efflux assay. NCI-H460, NCI-H46/MX20 were used for [³H]-mitoxantrone efflux assay (Sun et al., 2012).

Molecular Modeling of Human ABCB1 Homology Model and Wild-Type Human ABCG2 Model

All docking experiments were performed with software Schrödinger 2018-1 (Schrödinger, LLC, New York, NY, 2018) as described previously (Zhang Y. K. et al., 2016; Fan et al., 2018). Ligand preparation and protein preparation were essentially performed. Human ABCB1 homology model was established based on refined mouse ABCB1 (PDB ID: 4M1M), and the docking grid at drug-binding pocket was generated (Li et al., 2014). The grid of ABCG2 was generated by selecting residues at a substrate-binding pocket of ABCG2 (PDB ID: 5NJ3, selected

residues: Phe432, Phe-439, Leu539, Ile543, Val546, and Met549) (Taylor et al., 2017). Glide XP docking was performed and the receptor grid for induced-fit docking (IFD) was generated by selecting the best scoring ligand. The Induced-fit docking was performed with the default protocol.

Statistical Analysis

All data are expressed as the mean \pm SD and analyzed using one-way ANOVA. All experiments were repeated at least three times. Differences were considered significant when $P < 0.05$.

RESULTS

The Effect of VS-4718 on the Efficacy of Anticancer Drugs in Cells Overexpressing ABCB1 and ABCG2 Transporters

We first determined the toxicity of VS-4718 in the cells we would use to choose concentrations of VS-4718 that would not significantly alter cell survival rate. Concentrations of VS-4718 below IC₂₀ upon 72 h-incubation with cells were selected. Based on the results (Figures 1, 2), we conducted the following assays with VS-4718 at concentrations of 1 and 3 μ M.

VS-4718 significantly reduced the IC₅₀ values of KB-C2 and SW620/Ad300 cells to doxorubicin and paclitaxel compared to their control cells in a dose-dependent manner (Table 1). After treatment with VS-4718, the IC₅₀ values of mitoxantrone, topotecan, and SN-38 to NCI-H460/MX20 and S1-M1-80 cells

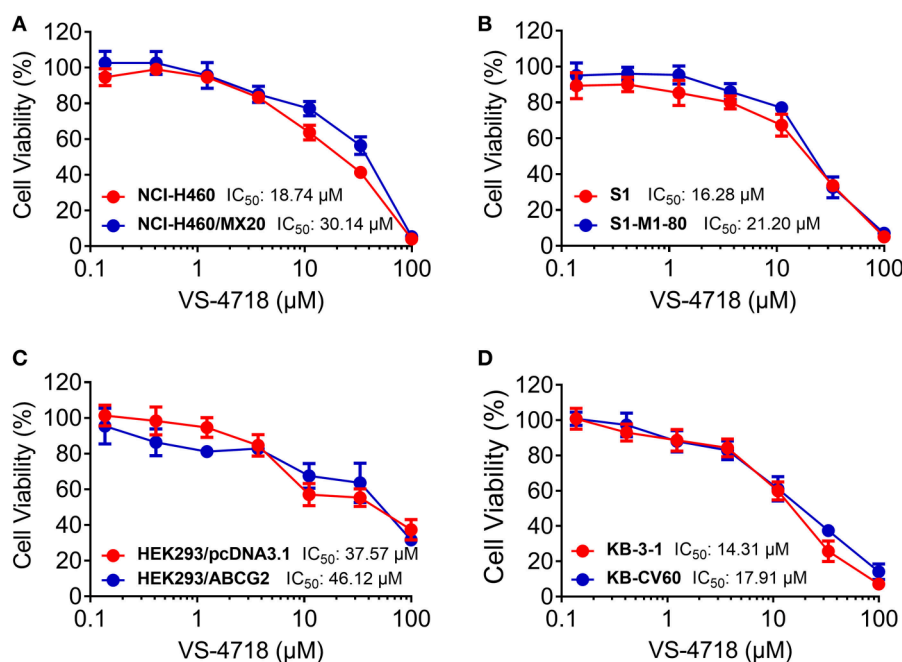


FIGURE 2 | Concentration-viability curves for parental and ABCG2- and ABCB1-overexpressing cells incubated with VS-4718. **(A)** Concentration-viability curves for NCI-H460 and NCI-H460/MX20 cells incubated with VS-4718 for 72 h. **(B)** Concentration-viability curves for S1 and S1-M1-80 cells incubated with VS-4718 for 72 h. **(C)** Concentration-viability curves for HEK293/pcDNA3.1 and HEK293/ABCG2 cells incubated with VS-4718 for 72 h. **(D)** Concentration-viability curves for KB-3-1 and KB-CV60 cells incubated with VS-4718 for 72 h. The cell viability was determined by MTT assay. Data are expressed as mean \pm SD, representative of three independent experiments in triplicate.

TABLE 1 | VS-4718 sensitized ABCB1-substrate-selected resistant cells to ABCB1 substrates.

Treatment	IC ₅₀ ± SD ^a (RF ^b)			
	KB-3-1 (μM)	KB-C2 (μM)	SW620 (μM)	SW620/Ad300 (μM)
Doxorubicin	0.035 ± 0.002 (1.00)	2.560 ± 0.250 (72.62)	0.061 ± 0.007 (1.00)	5.494 ± 0.600 (90.19)
+VS-4718 (1 μM)	0.030 ± 0.005 (0.85)	0.346 ± 0.128 (9.82)*	0.058 ± 0.012 (0.96)	1.120 ± 0.424 (18.39)*
+VS-4718 (3 μM)	0.026 ± 0.005 (0.74)	0.092 ± 0.007 (2.61)*	0.066 ± 0.004 (1.08)	0.382 ± 0.041 (6.27)*
+Verapamil (3 μM)	0.029 ± 0.007 (0.83)	0.051 ± 0.013 (1.44)*	0.069 ± 0.012 (1.12)	0.356 ± 0.030 (5.84)*
Paclitaxel	0.005 ± 0.001 (1.00)	2.348 ± 0.233 (521.83)	0.028 ± 0.003 (1.00)	2.411 ± 0.687 (86.10)
+VS-4718 (1 μM)	0.004 ± 0.001 (0.97)	0.491 ± 0.031 (109.10)*	0.029 ± 0.005 (1.03)	0.358 ± 0.138 (12.79)*
+VS-4718 (3 μM)	0.003 ± 0.001 (0.67)	0.053 ± 0.018 (11.79)*	0.024 ± 0.002 (0.86)	0.146 ± 0.097 (5.23)*
+Verapamil (3 μM)	0.004 ± 0.001 (0.89)	0.061 ± 0.011 (13.60)*	0.023 ± 0.002 (0.83)	0.100 ± 0.042 (3.57)*
Cisplatin	1.135 ± 0.038 (1.00)	1.921 ± 0.139 (1.69)	1.195 ± 0.094 (1.00)	1.228 ± 0.674 (1.00)
+VS-4718 (1 μM)	1.476 ± 0.007 (1.30)	1.862 ± 0.210 (1.64)	1.272 ± 0.347 (1.06)	1.221 ± 0.119 (0.99)
+VS-4718 (3 μM)	1.462 ± 0.022 (1.29)	2.544 ± 0.145 (2.24)	1.365 ± 0.763 (1.14)	1.490 ± 0.073 (1.21)
+Verapamil (3 μM)	1.113 ± 0.045 (0.98)	2.221 ± 0.162 (1.96)	1.374 ± 0.655 (1.15)	1.474 ± 0.169 (1.20)

^aIC₅₀ values were determined by MTT assay as described in "Materials and Methods," and were obtained from three independent experiments in triplicate.

^bResistance fold (RF) was calculated from dividing the IC₅₀ values of resistant cells (KB-C2 and SW620/Ad300) by the IC₅₀ of parental cells (KB-3-1 and SW620) in the presence or absence of VS-4718 or positive control inhibitor. *indicates $p < 0.05$ vs. group treated with antineoplastic drug only.

were much lower than those in their control resistant cells (Table 3). Similarly, VS-4718 significantly increased the efficacy of doxorubicin and paclitaxel in the HEK293/ABCB1 cells compared with that in the control resistant cells (Table 2). Furthermore, after treatment with VS-4718, the ABCG2-transfected cells were much more sensitive to mitoxantrone, topotecan, and SN-38 compared with the control group (Table 4). VS-4718 did not alter the sensitivity of KB-CV60 to vincristine (Tables 5). In addition, VS-4718 did not significantly alter the cytotoxic effect of cisplatin, a drug that is neither a substrate of ABCB1 nor ABCG2 (Tables 1–5). These results suggested that VS-4718 could reverse ABCB1- and ABCG2-mediated MDR, but not MDR mediated by ABCG1.

The Effect of VS-4718 on the Protein Expression and Subcellular Localization of ABCB1 and ABCG2 Transporters

Since VS-4718 antagonized ABCB1- and ABCG2-mediated MDR, the mechanisms may result from down-regulation of the protein level and/or change of the subcellular localization of the ABC transporters. Thus, we performed Western blotting and immunofluorescence assay to determine whether VS-4718 could alter the expression level and/or the subcellular localization of ABCB1 and ABCG2 transporters. As shown in Figures 3A,B, after incubating for 24, 48, and 72 h, VS-4718 did not significantly alter the expression of ABCB1 protein (170 kDa) in ABCB1-overexpressing KB-C2 and SW620/Ad300 cells. Similarly, the expression of ABCG2 protein (72 kDa) in ABCG2-overexpressing cells NCI-H460/MX20 and S1-M1-80 was not altered significantly after treatment with VS-4718 for up to 72 h (Figures 3C,D). As shown in Figures 3E,F, ABCB1 and ABCG2 transporters were located on the membrane of KB-C2 and NCI-H460/MX20 cells separately after being treated with VS-4718 for 24 to 72 h, indicating that VS-4718 did not alter subcellular localization of the ABCB1 and ABCG2 transporters. In this study,

TABLE 2 | VS-4718 sensitized ABCB1-gene-transfected cells to ABCB1 substrates.

Treatment	IC ₅₀ ± SD ^a (RF ^b)	
	HEK293/pcDNA3.1 (μM)	HEK293/ABCB1 (μM)
Doxorubicin	0.065 ± 0.008 (1.00)	1.375 ± 0.079 (21.15)
+VS-4718 (1 μM)	0.066 ± 0.009 (1.01)	0.491 ± 0.049 (7.55)*
+VS-4718 (3 μM)	0.055 ± 0.013 (0.84)	0.220 ± 0.034 (3.39)*
+Verapamil (3 μM)	0.064 ± 0.007 (0.99)	0.121 ± 0.017 (1.85)*
Paclitaxel	0.043 ± 0.001 (1.00)	1.054 ± 0.200 (24.80)
+VS-4718 (1 μM)	0.047 ± 0.004 (1.11)	0.498 ± 0.062 (11.73)*
+VS-4718 (3 μM)	0.037 ± 0.005 (0.86)	0.313 ± 0.053 (7.37)*
+Verapamil (3 μM)	0.032 ± 0.009 (0.74)	0.297 ± 0.055 (6.99)*
Cisplatin	1.071 ± 0.144 (1.00)	1.259 ± 0.425 (1.18)
+VS-4718 (1 μM)	1.186 ± 0.443 (1.11)	1.260 ± 0.563 (1.18)
+VS-4718 (3 μM)	1.105 ± 0.371 (1.03)	1.272 ± 0.217 (1.19)
+Verapamil (3 μM)	0.971 ± 0.206 (0.91)	1.293 ± 0.368 (1.21)

^aIC₅₀ values were determined by MTT assay as described in "Materials and Methods," and were obtained from three independent experiments in triplicate.

^bResistance fold (RF) was calculated from dividing the IC₅₀ values of resistance cells (HEK293/ABCB1) by the IC₅₀ of parental cells (HEK293/pcDNA3.1) in the presence or absence of VS-4718 or positive control inhibitor. *indicates $p < 0.05$ vs. group treated with antineoplastic drug only.

KB-3-1 and SW620, and NCI-H460 and S1 that did not express ABCB1 and ABCG2 transporters were used as negative controls (Figure 3).

The Effect of VS-4718 on the Intracellular Accumulation of Antineoplastic Drugs in Cancer Cells Overexpressing ABCB1 and ABCG2 Transporters

The above results indicated that VS-4718 significantly weakened ABCB1- and ABCG2-mediated MDR. However, VS-4718 did

TABLE 3 | VS-4718 sensitized ABCG2-substrate-selected resistant cells to ABCG2 substrates.

Treatment	IC ₅₀ ± SD ^a (RF ^b)			
	NCI-H460 (μM)	NCI-H460/MX20 (μM)	S1 (μM)	S1-M1-80 (μM)
Mitoxantrone	0.036 ± 0.008 (1.00)	4.361 ± 0.609 (120.30)	0.032 ± 0.002 (1.00)	4.559 ± 1.607 (143.23)
+VS-4718 (1 μM)	0.037 ± 0.013 (1.01)	1.247 ± 0.456 (34.40)*	0.029 ± 0.006 (0.91)	2.098 ± 0.916 (65.90)*
+VS-4718 (3 μM)	0.030 ± 0.015 (0.82)	0.496 ± 0.193 (13.68)*	0.027 ± 0.004 (0.85)	0.577 ± 0.182 (18.12)*
+Ko 143 (3 μM)	0.022 ± 0.006 (0.62)	0.302 ± 0.018 (8.32)*	0.026 ± 0.005 (0.81)	0.034 ± 0.015 (1.08)*
SN-38	0.038 ± 0.012 (1.00)	3.169 ± 0.493 (83.51)	0.043 ± 0.003 (1.00)	3.628 ± 1.819 (85.36)
+VS-4718 (1 μM)	0.031 ± 0.013 (0.82)	0.436 ± 0.287 (11.49)*	0.041 ± 0.009 (0.95)	0.365 ± 0.026 (8.59)*
+VS-4718 (3 μM)	0.030 ± 0.012 (0.78)	0.071 ± 0.015 (1.88)*	0.053 ± 0.006 (1.25)	0.097 ± 0.042 (2.27)*
+Ko 143 (3 μM)	0.031 ± 0.021 (0.81)	0.039 ± 0.003 (1.02)*	0.052 ± 0.013 (1.21)	0.045 ± 0.035 (1.05)*
Topotecan	0.067 ± 0.009 (1.00)	4.471 ± 0.644 (66.85)	0.064 ± 0.007 (1.00)	4.940 ± 0.701 (77.79)
+VS-4718 (1 μM)	0.058 ± 0.034 (0.87)	1.170 ± 0.398 (17.50)*	0.061 ± 0.001 (0.95)	1.801 ± 0.791 (28.36)*
+VS-4718 (3 μM)	0.053 ± 0.026 (0.79)	0.503 ± 0.053 (7.53)*	0.057 ± 0.002 (0.90)	0.434 ± 0.120 (6.84)*
+Ko 143 (3 μM)	0.034 ± 0.013 (0.71)	0.264 ± 0.034 (3.94)*	0.051 ± 0.029 (0.80)	0.306 ± 0.037 (4.81)*
Cisplatin	1.658 ± 0.261 (1.00)	1.696 ± 0.300 (1.02)	1.447 ± 0.064 (1.00)	1.508 ± 0.159 (1.04)
+VS-4718 (1 μM)	2.024 ± 0.421 (1.22)	1.672 ± 0.271 (1.01)	1.347 ± 0.196 (0.93)	1.873 ± 0.202 (1.29)
+VS-4718 (3 μM)	1.550 ± 1.055 (0.93)	1.699 ± 0.245 (1.02)	1.290 ± 0.051 (0.89)	1.840 ± 0.744 (1.27)
+Ko 143 (3 μM)	1.812 ± 0.801 (1.09)	1.721 ± 0.245 (1.04)	1.417 ± 0.188 (0.98)	1.506 ± 0.441 (1.04)

^aIC₅₀ values were determined by MTT assay as described in "Materials and Methods," and were obtained from three independent experiments in triplicate.

^bResistance fold (RF) was calculated from dividing the IC₅₀ values of resistant cells (NCI-H460/MX20 and S1-M1-80) by the IC₅₀ of parental cells (NCI-H460 and S1) in the presence or absence of VS-4718 or positive control inhibitor. *indicates $p < 0.05$ vs. group treated with antineoplastic drug only.

not significantly alter ABCB1 and ABCG2 protein expression or subcellular localization. To gain insight into the mechanisms of VS-4718 in reversing MDR, an accumulation assay was performed. The intracellular levels of [³H]-paclitaxel and [³H]-mitoxantrone were measured respectively in cells that overexpress ABCB1 and ABCG2 transporters in the presence or absence of VS-4718. As shown in **Figure 4A**, VS-4718 significantly increased the intracellular level of [³H]-paclitaxel in KB-C2 cells, that overexpress ABCB1 transporters, but not in its parental cell line KB-3-1 cells. Similarly, the intracellular level of [³H]-mitoxantrone in ABCG2-overexpressing NCI-H460/MX20 cells significantly increased after treatment with VS-4718, compared to its parental NCI-H460 cells (**Figure 4B**). These results suggested that VS-4718 may increase the intracellular accumulation of antineoplastic drugs by inhibiting the function of ABCB1 and ABCG2 transporters.

The Effect of VS-4718 on the Efflux Activity in Cancer Cells Overexpressing ABCB1 and ABCG2 Transporters

In order to further understand the mechanism of VS-4718 in antagonizing ABCB1- and ABCG2-mediated MDR, we performed the efflux assay to determine the effect of VS-4718 on the efflux function of ABCB1 and ABCG2 transporters. As shown in **Figures 5B,D**, VS-4718 significantly reduced the efflux of [³H]-paclitaxel in ABCB1-overexpressing KB-C2 cells, and [³H]-mitoxantrone efflux in ABCG2-overexpressing NCI-H460/MX20 cells. Nevertheless, VS-4718 did not significantly alter the efflux of [³H]-paclitaxel or [³H]-mitoxantrone in their parental KB-3-1 or NCI-H460 cells (**Figures 5A,C**). These results suggested that

VS-4718 could increase the accumulation of anticancer drugs by impeding the efflux function mediated by ABCB1 and ABCG2.

VS-4718 Stimulated the ATPase Activity of ABCB1 and ABCG2

As the above results showed that VS-4718 significantly antagonized ABCB1- and ABCG2-mediated MDR by inhibiting the efflux function of ABCB1 and ABCG2 transporters, it is likely that VS-4718 could affect the ATPase activity of ABCB1 and ABCG2 transporters. Hence, we measured ABCB1- or ABCG2-mediated ATP hydrolysis in the presence or absence of VS-4718 at various concentration from 0 to 40 μM to verify this hypothesis. As shown in **Figure 6A**, VS-4718 stimulated the ATPase activity of ABCB1 transporters in a dose-dependent manner with a maximal stimulation of 4.89-fold of the basal activity, and the concentration of VS-4718 required to obtain 50% of maximal stimulation is 1.72 μM. Similarly, VS-4718 stimulated the ATPase activity of ABCG2 transporters (**Figure 6B**), the concentration of VS-4718 required to obtain 50% of maximal stimulation is 9.60 μM, with 3.01-fold of maximum stimulation. These results suggested that VS-4718 may interact with the drug-substrate-binding site and affect the ATPase activity of ABCB1 and ABCG2 thereby restraining their efflux functions.

Docking Analysis of the Binding of VS-4718 With Human ABCB1 Homology Model and ABCG2 Model

The best-scored docked position of VS-4718 within the binding pocket of human homology modeled ABCB1 and ABCG2 (5NJ3)

TABLE 4 | VS-4718 sensitized ABCG2-gene-transfected cells to ABCG2 substrates.

Treatment	IC ₅₀ ± SD ^a (RF ^b)	
	HEK293/pcDNA3.1 (μM)	HEK293/ABCG2 (μM)
Mitoxantrone	0.040 ± 0.004 (1.00)	0.556 ± 0.083 (13.90)
+VS-4718 (1 μM)	0.048 ± 0.009 (1.19)	0.306 ± 0.054 (7.66)*
+VS-4718 (3 μM)	0.033 ± 0.009 (0.81)	0.052 ± 0.004 (1.31)*
+Ko 143 (3 μM)	0.040 ± 0.005 (0.99)	0.036 ± 0.010 (0.89)*
SN-38	0.022 ± 0.002 (1.00)	0.307 ± 0.078 (13.95)
+VS-4718 (1 μM)	0.022 ± 0.002 (1.00)	0.109 ± 0.008 (4.95)*
+VS-4718 (3 μM)	0.019 ± 0.009 (0.85)	0.034 ± 0.001 (1.53)*
+Ko 143 (3 μM)	0.024 ± 0.008 (1.09)	0.024 ± 0.009 (1.09)*
Topotecan	0.042 ± 0.000 (1.00)	0.611 ± 0.161 (14.54)
+VS-4718 (1 μM)	0.042 ± 0.001 (0.99)	0.097 ± 0.039 (2.30)*
+VS-4718 (3 μM)	0.033 ± 0.005 (0.77)	0.033 ± 0.001 (0.80)*
+Ko 143 (3 μM)	0.041 ± 0.001 (0.96)	0.039 ± 0.006 (0.93)*
Cisplatin	1.088 ± 0.446 (1.00)	1.281 ± 0.206 (1.18)
+VS-4718 (1 μM)	1.009 ± 0.058 (0.93)	1.123 ± 0.057 (1.03)
+VS-4718 (3 μM)	0.840 ± 0.278 (0.77)	1.410 ± 0.230 (1.30)
+Ko 143 (3 μM)	1.014 ± 0.317 (0.93)	1.228 ± 0.526 (1.13)

^aIC₅₀ values were determined by MTT assay as described in "Materials and Methods," and were obtained from three independent experiments in triplicate.

^bResistance fold (RF) was calculated from dividing the IC₅₀ values of resistant cells (HEK293/ABCG2) by the IC₅₀ of parental cells (HEK293/pcDNA3.1) in the presence or absence of VS-4718 or positive control inhibitor. *indicates $p < 0.05$ vs. group treated with antineoplastic drug only.

are shown in **Figure 7**. The docking score of the binding of VS-4718 and ABCB1 is -10.782 kcal/mol and that of the binding of VS-4718 and human ABCG2 is -10.767 kcal/mol. There are two π - π interactions between VS-4718 and human homology ABCB1 (**Figure 7A**). The pyridine ring of VS-4718 has π - π interaction with both Phe732 and Phe983 of ABCB1. The oxygen in the amide group and the morpholinyl have hydrogen bonding with Tyr307 and Tyr118 in chain A, respectively. Moreover, VS-4718 could be stabilized in the pocket of ABCB1 by hydrophobic interaction with residues such as Phe72, Phe303, Tyr310, Phe336, Phe953, Phe978, Met986, and Ala987 (**Figure 7C**). As shown in **Figure 7B**, the binding of VS-4718 and ABCG2 include hydrogen bonding interaction and π - π interaction. The phenyl ring in the benzamide group of VS-4718 has π - π interaction with Phe439 in the A chain. The amino group in VS-4718 as hydrogen bond ($\text{NH}_2 \cdots \text{NH}_2$ -Asn436) has hydrogen bonding interaction with residue Asn436 in the A chain. Besides, VS-4718 could also have hydrophilic interaction with the residues (Thr435, Asn436, Ser440, Ser443, Thr542) in the drug-binding pocket of ABCG2 (**Figure 7D**).

DISCUSSION

It is well documented that the ABC transporters expressed on cancer cell membrane are responsible for MDR, which finally leads to the failure of chemotherapy (Dassa and Bouige, 2001; Szakács et al., 2006; Shukla et al., 2008; Stavrovskaya and Stromskaya, 2008; Eckford and Sharom, 2009; Kartal-Yandim

TABLE 5 | VS-4718 did not affect ABCC1-mediated MDR.

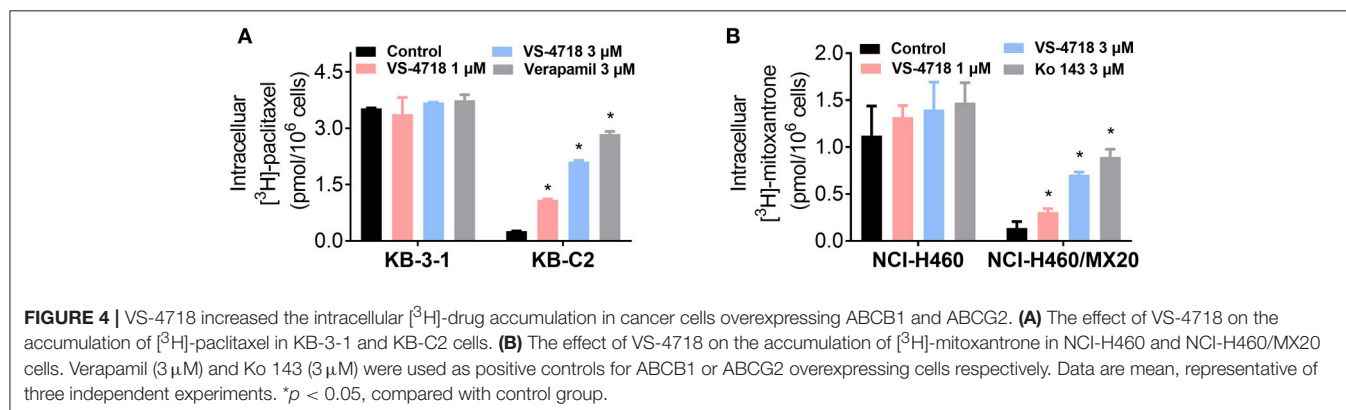
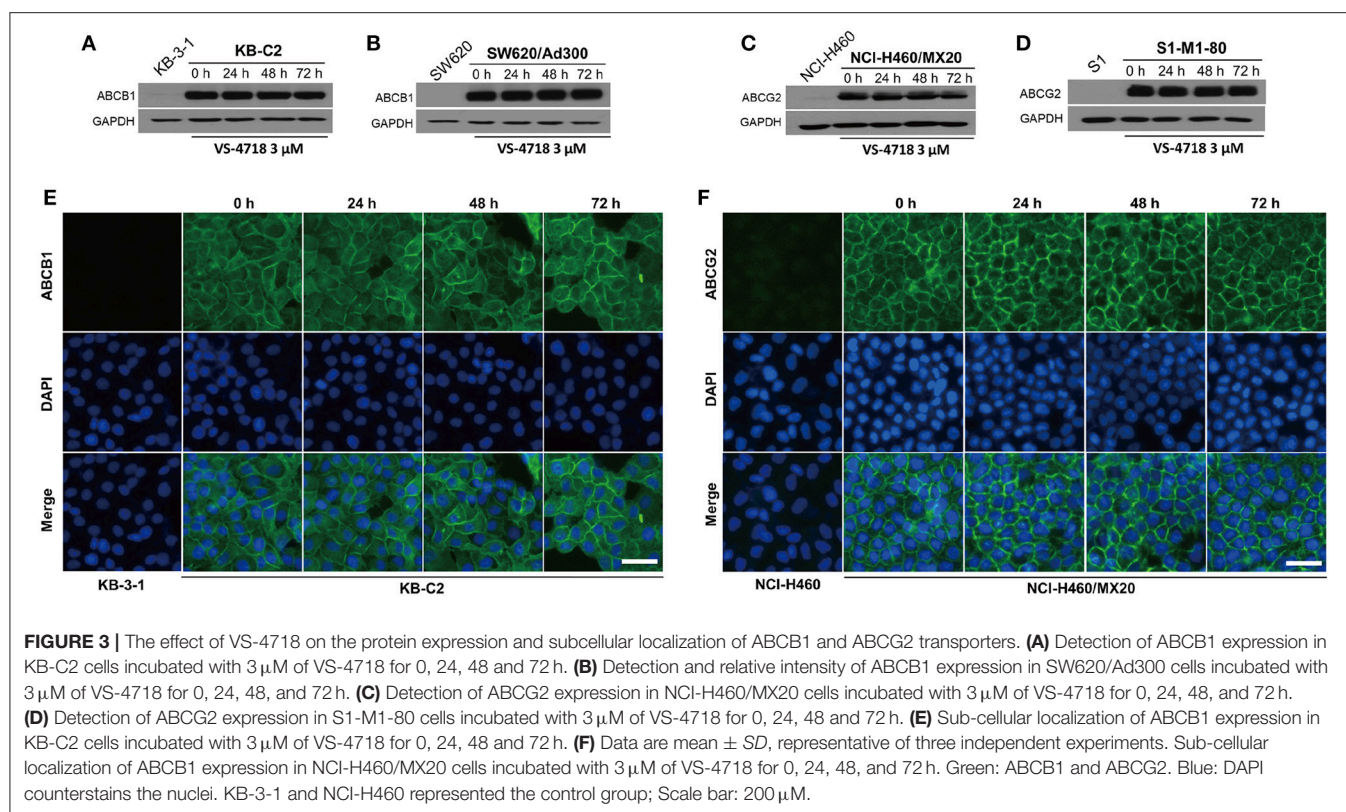
Treatment	IC ₅₀ ± SD ^a (RF ^b)	
	KB-3-1 (μM)	KB-CV60 (μM)
Vincristine	0.012 ± 0.001 (1.00)	0.207 ± 0.011 (17.96)
+VS-4718 (1 μM)	0.013 ± 0.005 (1.09)	0.203 ± 0.005 (17.68)
+VS-4718 (3 μM)	0.013 ± 0.003 (1.09)	0.220 ± 0.035 (19.12)
+MK 571 (25 μM)	0.016 ± 0.007 (1.35)	0.092 ± 0.020 (7.98)*
Cisplatin	1.023 ± 0.275 (1.00)	1.261 ± 0.218 (1.23)
+VS-4718 (1 μM)	1.015 ± 0.236 (0.99)	1.381 ± 0.591 (1.35)
+VS-4718 (3 μM)	0.988 ± 0.356 (0.97)	1.344 ± 0.375 (1.31)
+MK 571 (25 μM)	1.036 ± 0.125 (1.01)	1.254 ± 0.417 (1.23)

^aIC₅₀ values were determined by MTT assay as described in "Materials and Methods," and were obtained from three independent experiments in triplicate.

^bResistance fold (RF) was calculated from dividing the IC₅₀ values of resistant cells (KB-CV60) by the IC₅₀ of parental cells (KB-3-1) in the presence or absence of VS-4718 or positive control inhibitor. *indicates $p < 0.05$ vs. group treated with antineoplastic drug only.

et al., 2016). In decades, studies have shown that a series of small-molecule inhibitors have the capacity to reverse ABC transporter-mediated MDR, including EGFR inhibitor gefitinib, erlotinib, AG1478, PD153035, and dacomitinib, an EGFR and HER-2 inhibitor lapatinib, a pan-HER inhibitor canertinib, a BCR-ABL inhibitor imatinib, a Bruton tyrosine kinase (BTK) inhibitor ibrutinib, and certain multi-kinase inhibitors such as sunitinib (Erllichman et al., 2001; Ozvegy-Laczka et al., 2005; Dai et al., 2008; Shukla et al., 2009; Tiwari et al., 2009; Fan et al., 2018; Zhang et al., 2018). Reversing MDR by a combination of a chemotherapeutic drug with a reversal agent against the function of ABC transporters is a potential pharmacological approach to cancer treatments.

In this study, we found that VS-4718, at non-toxic concentrations, significantly sensitized ABCB1- and ABCG2-overexpressing cancer cells to their substrates in a dose-dependent manner. However, the re-sensitizing effects were not shown in ABCC1-overexpressing cells. First of all, an MTT assay was performed to obtain non-toxic concentrations of VS-4718 in the cells that we would use to avoid possible bias of VS-4718-induced cytotoxicity in evaluating its reversal effects. Based on the MTT results, 1 and 3 μM of VS-4718 were adopted for reversal studies. Our results indicated that VS-4718 significantly increased the efficacy of doxorubicin and paclitaxel on the ABCB1-overexpressing KB-C2 and SW620/Ad300 cells compared to their control resistant cells in a dose-dependent manner. Similarly, VS-4718 significantly reduced the IC₅₀ values of substrate drugs in HEK293/ABCB1 cells dose dependently. In addition, VS-4718 sensitized ABCG2-overexpressing cells, NCI-H460/MX20 and S1-MI-80, and the ABCG2-transfected HEK293 cells to mitoxantrone, topotecan, and SN-38 in a dose-dependent manner. However, VS-4718, up to 3 μM, did not significantly sensitize the parental cells such as KB-3-1, SW620, NCI-H460, S1, and HEK293/pcDNA3.1 cells. Moreover, there was no significant alteration of insensitivity of cancer cells to cisplatin, which was neither an ABCB1 nor ABCG2 substrate. Furthermore, at 1 and 3 μM, VS-4718 did not significantly alter the IC₅₀ value of



ABCC1-overexpressing KB-CV60 cells. These findings suggested that the reversal effect of VS-4718 is specific to ABCB1- and ABCG2-mediated MDR.

The reversal of ABC transporter-mediated MDR may due to the down-regulation of ABC protein expression or change of subcellular localization. We performed Western blotting and immunofluorescence assay to investigate the potential mechanisms. We found that there was no significant decrease in the protein level of ABCB1 or ABCG2 transporters after treatment with VS-4718 (3 μ M) up to 72 h. Likewise, VS-4718 at 3 μ M did not significantly change the ABCB1 and ABCG2 transporters subcellular localization after incubating for up to 72 h, suggesting that the reversal effects of VS-4718 on MDR were not related to alteration of the protein level or

subcellular localization of ABC transporters. However, further studies should determine the indirect effect of VS-4718 on the expression of ABCB1 and ABCG2 at a higher concentration and a longer incubation time. Moreover, we could not exclude the possibility that part of the reversal effect of VS-4718 could involve its effect on some proteins and/or cross-talk with other proteins, which may affect the function of ABCB1 and ABCG2. This needs to be studied further to exclude this possibility. Furthermore, we could not fully exclude the possible effect of VS-4718 on ABCC1 transporter, though this kind of effect may not result in reversing ABCC1-mediated MDR, further study should be performed in the future to determine the effect of VS-4718 on protein level and/or subcellular localization of ABCC1 transporter.

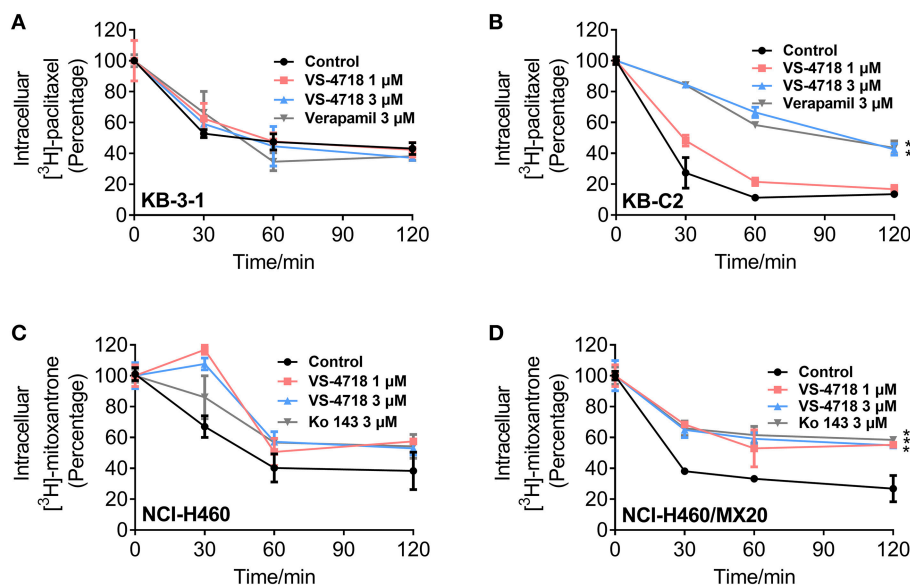


FIGURE 5 | VS-4718 inhibited the efflux function of ABCB1 and ABCG2 transporters. (A,B) The effects of VS-4718 on efflux of [³H]-paclitaxel in KB-3-1 and KB-C2 cells. (C,D) The effects of VS-4718 on efflux of [³H]-mitoxantrone in NCI-H460 and NCI-H460/MX20 cells. Data are mean ± SD, representative of three independent experiments. **p* < 0.05, compared with control group.

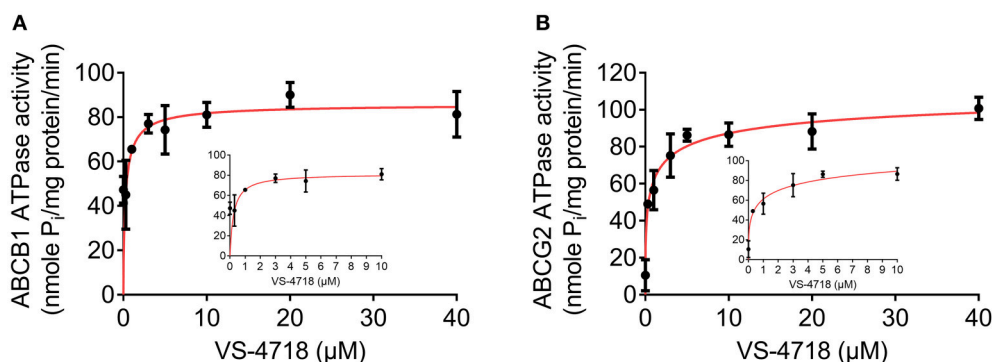


FIGURE 6 | VS-4718 stimulated the ATPase activity of ABCB1 and ABCG2. (A) Effect of VS-4718 on the ATPase activity of ABCB1. (B) Effect of VS-4718 on the ATPase activity of ABCG2. The inset graphs illustrate the effect of 0–10 μM VS-4718 on the ATPase activity of ABCB1 (A) or ABCG2 (B). Data are mean ± SD, representative of three independent experiments.

In accumulation and efflux assays, we found that VS-4718 significantly increased the intracellular [³H]-paclitaxel concentration in ABCB1-overexpressing KB-C2 cells, and [³H]-mitoxantrone in ABCG2-overexpressing NCI-H460/MX20 cells, in a dose-dependent manner, while no significant [³H]-drug alteration was found in their corresponding parental cells. Furthermore, VS-4718 significantly prevented [³H]-drugs being pumped out of ABCB1- and ABCG2-overexpressing cells in a dose-dependent manner, while no significant change of efflux was observed in their corresponding parental cells. The results of the accumulation and efflux experiments were congruent with the reversal effects of VS-4718 shown in anti-cancer efficacy testing when co-administered with substrate-drugs, suggesting that VS-4718 may increase the accumulation of substrate-drugs

in ABCB1- and ABCG2-overexpressing cancer cells by inhibiting the ABCB1- and ABCG2-mediated efflux activity, which led to the decline of IC₅₀ of substrate-drugs and finally attenuated the ABC transporter-mediated MDR. The results are also consistent with studies of our other small-molecule reversal reagents (Zhang et al., 2017, 2018; Gupta et al., 2018).

It is known that the function of ABC transporters relies on the energy from the hydrolysis of ATP by the enzyme ATPase, which can be modulated by the presence of substrates or inhibitors (Gottesman and Ambudkar, 2001; Wilkens, 2015). Our results indicated that VS-4718 stimulated the ATPase activity of both ABCB1 and ABCG2, with a 4.89-fold in ABCB1 and a 3.01-fold in ABCG2. The results suggested that VS-4718 probably acts as a substrate of ABCB1 and ABCG2, which may competitively

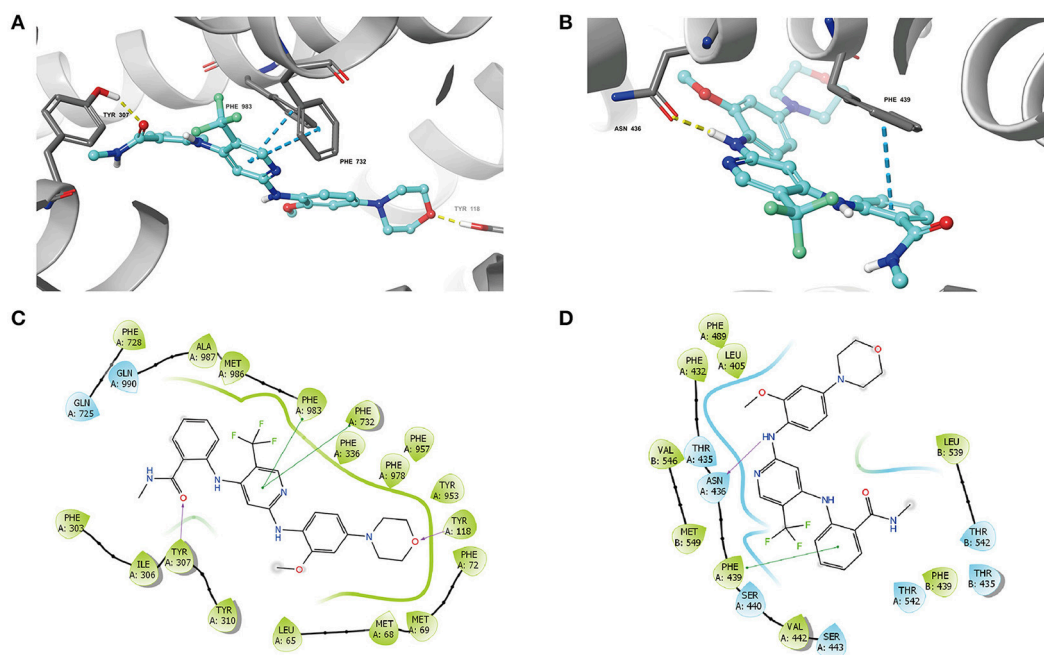


FIGURE 7 | The molecular modeling study of VS-4718 with human homology ABCB1 and human ABCG2. **(A)** Docked position of VS-4718 within the drug-binding site of human ABCB1 homology model. **(B)** Docked position of VS-4718 within the binding site of ABCG2. VS-4718 is shown as ball and stick mode with the atoms colored: carbon-cyan, hydrogen-white, nitrogen-blue, oxygen-red, fluorine-green, hydrogen-white. Important residues are shown as sticks with gray color. π - π stacking interactions are indicated with cyan dotted short line. Hydrogen bonds are shown by the yellow dotted line. **(C)** The two-dimensional ligand-receptor interaction diagram of VS-4718 and human ABCB1. **(D)** The two-dimensional ligand-receptor interaction diagram of VS-4718 and human ABCG2. The amino acids within 3 Å are shown as colored bubbles, cyan indicates polar residues, and green indicates hydrophobic residues. The purple arrow indicates hydrogen bond and green short line shows π - π stacking interaction.

occupy the drug binding site of both ABCB1 and ABCG2 transporters.

Although VS-4718 presents similar up-regulated ATPase activity of ABCB1 and ABCG2, the accurate binding site still remain unclear, so molecular docking simulations of VS-4718 with substrate-binding sites of ABCB1 and ABCG2 was performed. Modeling study suggested that VS-4718 could interact with the TMD of both ABCB1 and ABCG2 with docking scores of -10.782 kcal/mol and -10.767 kcal/mol, respectively, and hydrogen bonding interactions and π - π interactions were predicted between VS-4718 and lining residues of drug-binding cavities from ABCB1 and ABCG2. In conclusion, this suggested, along with our other results, that VS-4718 acts as a potential competitive substrate that increases the ATPase activity and displaces chemotherapy drugs from ABCB1 and ABCG2 transporters, thereby inhibiting the efflux function of ABCB1 and ABCG2, and increasing the intracellular accumulation of certain substrate drugs into the MDR cells, and finally reversing MDR.

In recent years, research has shown that a series of small-molecule targeted drugs have the capacity to reverse ABC transporter-mediated MDR. However, strategies to develop ABC transporters as a therapeutic target to overcome drug resistance have, to date, failed in the clinic, due to the unpredictable fate of the co-administrated reversal reagents with anticancer drugs. Nonetheless, it has been reported that clinical resistance to chemotherapy in a series of cancers is strongly associated with

the overexpression of the ABC transporters, and overexpression of ABCB1 and ABCG2 in cancers may come with poor prognosis and high risk of death (Marsh et al., 2007; Campa et al., 2012; Hlavata et al., 2012; Litviakov et al., 2013; Bartholomae et al., 2016). Our study provides a clue that the combination of VS-4718 with ABCB1 or ABCG2 substrate-drugs, like doxorubicin or topotecan, as well as SN-38, could be a novel treatment strategy to antagonize resistance in cancer patients. Furthermore, in this study, though VS-4718 (1 and 3 μ M) showed relative non-toxic and significant reversal effect in the cells we used, we could not conclude that VS-4718 would work in a *in vivo* model at a non-toxic dose. Therefore, *in vivo* study should be performed in the future to support the current findings.

In conclusion, this study indicates that VS-4718 could reverse ABCB1- and ABCG2-mediated MDR by competitively inhibiting the anticancer drugs being pumped out by ABC transporters. The combination of VS-4718 with substrate drugs of ABCB1 and ABCG2 transporters might be used for cancer clinical treatment to elude MDR if it could be validated in *in vivo* models.

AUTHOR CONTRIBUTIONS

DK and D-HY conceived the general idea. NJ, YY, C-YC, Z-NL, J-QW, PG, and Q-XT performed experiments. NJ, Z-SC, DK, and D-HY analyzed the results. NJ, YY, C-YC, Z-NL,

J-QW, and PG wrote the first draft. DK and D-HY revised the manuscript.

FUNDING

This work was supported by St. John's University Research Seed Grant (No. 579-1110-7002), National Natural Science Foundation of China (81673464), Grant for Major Project of Tianjin for New Drug Development (17ZXXYSY00050), and the Postgraduate Innovation Fund of 13th Five-Year comprehensive investment, Tianjin Medical University (YJSCX201712).

REFERENCES

- Akiyama, S., Fojo, A., Hanover, J. A., Pastan, I., and Gottesman, M. M. (1985). Isolation and genetic characterization of human KB cell lines resistant to multiple drugs. *Somat. Cell Mol. Genet.* 11, 117–126.
- Ali, M. A., and Elsalakawy, W. A. (2014). ABCB1 haplotypes but not individual SNPs predict for optimal response/failure in Egyptian patients with chronic-phase chronic myeloid leukemia receiving imatinib mesylate. *Med. Oncol.* 31:279. doi: 10.1007/s12032-014-0279-y
- Bartholomae, S., Gruhn, B., Debatin, K. M., Zimmermann, M., Creutzig, U., Reinhardt, D., et al. (2016). Coexpression of multiple ABC-transporters is strongly associated with treatment response in childhood acute myeloid leukemia. *Pediatr. Blood Cancer* 63, 242–247. doi: 10.1002/pbc.25785
- Bates, S. E., Lee, J. S., Dickstein, B., Spolyar, M., and Fojo, A. T. (1993). Differential modulation of P-glycoprotein transport by protein kinase inhibition. *Biochemistry* 32, 9156–9164.
- Campa, D., Müller, P., Edler, L., Knoefel, L., Barale, R., Heussel, C. P., et al. (2012). A comprehensive study of polymorphisms in ABCB1, ABCG2 and ABCG2 and lung cancer chemotherapy response and prognosis. *Int. J. Cancer* 131, 2920–2928. doi: 10.1002/ijc.27567
- Dai, C. L., Tiwari, A. K., Wu, C. P., Su, X. D., Wang, S. R., Liu, D. G., et al. (2008). Lapatinib (Tykerb, GW572016) reverses multidrug resistance in cancer cells by inhibiting the activity of ATP-binding cassette subfamily B member 1 and G member 2. *Cancer Res.* 68, 7905–7914. doi: 10.1158/0008-5472.CAN-08-0499
- Dassa, E., and Bouige, P. (2001). The ABC of ABCs: a phylogenetic and functional classification of ABC systems in living organisms. *Res. Microbiol.* 152, 211–229. doi: 10.1016/S0923-2508(01)01194-9
- Eckford, P. D., and Sharom, F. J. (2009). ABC efflux pump-based resistance to chemotherapy drugs. *Chem. Rev.* 109, 2989–3011. doi: 10.1021/cr9000226
- Erlhman, C., Boerner, S. A., Hallgren, C. G., Spieker, R., Wang, X. Y., James, C. D., et al. (2001). The HER tyrosine kinase inhibitor CI1033 enhances cytotoxicity of 7-ethyl-10-hydroxycamptothecin and topotecan by inhibiting breast cancer resistance protein-mediated drug efflux. *Cancer Res.* 61, 739–748. Available online at: <http://cancerres.aacrjournals.org/content/61/2/739.full-text.pdf>
- Fan, Y. F., Zhang, W., Zeng, L., Lei, Z. N., Cai, C. Y., Gupta, P., et al. (2018). Dacomitinib antagonizes multidrug resistance (MDR) in cancer cells by inhibiting the efflux activity of ABCB1 and ABCG2 transporters. *Cancer Lett.* 421, 186–198. doi: 10.1016/j.canlet.2018.01.021
- Fung, K. L., Pan, J., Ohnuma, S., Lund, P. E., Pixley, J. N., Kimchi-Sarfaty, C., et al. (2014). MDR1 synonymous polymorphisms alter transporter specificity and protein stability in a stable epithelial monolayer. *Cancer Res.* 74, 598–608. doi: 10.1158/0008-5472.CAN-13-2064
- Gottesman, M. M., and Ambudkar, S. V. (2001). Overview: ABC transporters and human disease. *J. Bioenerg. Biomembr.* 33, 453–458.
- Gottesman, M. M., Fojo, T., and Bates, S. E. (2002). Multidrug resistance in cancer: role of ATP-dependent transporters. *Nat. Rev. Cancer* 2, 48–58. doi: 10.1038/nrc706
- Gupta, P., Zhang, Y. K., Zhang, X. Y., Wang, Y. J., Lu, K. W., Hall, T., et al. (2018). Voruciclib, a potent CDK4/6 inhibitor, antagonizes ABCB1 and ABCG2-mediated multi-drug resistance in cancer cells. *Cell. Physiol. Biochem.* 45, 1515–1528. doi: 10.1159/000487578

ACKNOWLEDGMENTS

We would like to thank Chemie Tek (Indianapolis, IN) for providing us with the VS-4718 compound. We would like to thank Dr. Stephen Aller (The University of Alabama at Birmingham, Birmingham) for kindly providing the human ABCB1 homology model. We thank Tanaji T. Talele (St. John's University, New York, NY) for providing the computing resources for the docking analysis. We thank Drs. Susan E. Bates and Robert W. Robey (NCI, NIH, Bethesda, MD) for providing the cell lines. The first author thanks China Scholarship Council for reimbursing daily expenditures in America.

- Hlavata, I., Mohelnikova-Duchonova, B., Vaclavikova, R., Liska, V., Pitule, P., Novak, P., et al. (2012). The role of ABC transporters in progression and clinical outcome of colorectal cancer. *Mutagenesis* 27, 187–196. doi: 10.1093/mutage/ger075
- Kartal-Yandim, M., Adan-Gokbulut, A., and Baran, Y. (2016). Molecular mechanisms of drug resistance and its reversal in cancer. *Crit. Rev. Biotechnol.* 36, 716–726. doi: 10.3109/07388551.2015.1015957
- Li, J., Jaimes, K. F., and Aller, S. G. (2014). Refined structures of mouse P-glycoprotein. *Protein Sci.* 23, 34–46. doi: 10.1002/pro.2387
- Linton, K. J. (2007). Structure and function of ABC transporters. *Physiology* 22, 122–130. doi: 10.1152/physiol.00046.2006
- Linton, K. J., and Higgins, C. F. (2007). Structure and function of ABC transporters: the ATP switch provides flexible control. *Pflugers Arch.* 453, 555–567. doi: 10.1007/s00424-006-0126-x
- Litviakov, N. V., Cherdynseva, N. V., Tsyganov, M. M., Denisov, E. V., Garbukov, E. Y., Merzliakova, M. K., et al. (2013). Changing the expression vector of multidrug resistance genes is related to neoadjuvant chemotherapy response. *Cancer Chemother. Pharmacol.* 71, 153–163. doi: 10.1007/s00280-012-1992-x
- Liu, L., Zuo, L. F., and Guo, J. W. (2014). ABCG2 gene amplification and expression in esophageal cancer cells with acquired adriamycin resistance. *Mol. Med. Rep.* 9, 1299–1304. doi: 10.3892/mmr.2014.1949
- Liu, Y. S., Hsu, H. C., Tseng, K. C., Chen, H. C., and Chen, S. J. (2013). Lgr5 promotes cancer stemness and confers chemoresistance through ABCB1 in colorectal cancer. *Biomed. Pharmacother.* 67, 791–799. doi: 10.1016/j.biopha.2013.08.001
- Marsh, S., Somlo, G., Li, X., Frankel, P., King, C. R., Shannon, W. D., et al. (2007). Pharmacogenetic analysis of paclitaxel transport and metabolism genes in breast cancer. *Pharmacogenomics J.* 7, 362–365. doi: 10.1038/sj.tpj.6500434
- Miyake, K., Mickle, L., Litman, T., Zhan, Z., Robey, R., Cristensen, B., et al. (1999). Molecular cloning of cDNAs which are highly overexpressed in mitoxantrone-resistant cells: demonstration of homology to ABC transport genes. *Cancer Res.* 59, 8–13.
- Ozvegy-Laczka, C., Cserepes, J., Elkind, N. B., and Sarkadi, B. (2005). Tyrosine kinase inhibitor resistance in cancer: role of ABC multidrug transporters. *Drug Resist. Updat.* 8, 15–26. doi: 10.1016/j.drug.2005.02.002
- Robey, R. W., Honjo, Y., van de Laar, A., Miyake, K., Regis, J. T., Litman, T., et al. (2001). A functional assay for detection of the mitoxantrone resistance protein, MXR (ABCG2). *Biochim. Biophys. Acta* 1512, 171–182. doi: 10.1016/S0005-2736(01)00308-X
- Serrels, A., Lund, T., Serrels, B., Byron, A., McPherson, R. C., von Kriegsheim, A., et al. (2015). Nuclear FAK controls chemokine transcription, Tregs, and evasion of anti-tumor immunity. *Cell* 163, 160–173. doi: 10.1016/j.cell.2015.09.001
- Shukla, S., Robey, R. W., Bates, S. E., and Ambudkar, S. V. (2009). Sunitinib (Sutent, SU11248), a small-molecule receptor tyrosine kinase inhibitor, blocks function of the ATP-binding cassette (ABC) transporters P-glycoprotein (ABCB1) and ABCG2. *Drug Metab. Dispos.* 37, 359–365. doi: 10.1124/dmd.108.024612
- Shukla, S., Wu, C. P., and Ambudkar, S. V. (2008). Development of inhibitors of ATP-binding cassette drug transporters: present status and challenges. *Expert Opin. Drug Metab. Toxicol.* 4, 205–223. doi: 10.1517/17425255.4.2.205

- Stavrovskaya, A. A., and Stromskaya, T. P. (2008). Transport proteins of the ABC family and multidrug resistance of tumor cells. *Biochem. Mosc.* 73, 592–604. doi: 10.1134/S0006297908050118
- Sun, Y. L., Kathawala, R. J., Singh, S., Zheng, K., Talele, T. T., Jiang, W. Q., et al. (2012). Zafirlukast antagonizes ATP-binding cassette subfamily G member 2-mediated multidrug resistance. *Anticancer. Drugs* 23, 865–873. doi: 10.1097/CAD.0b013e328354a196
- Szakács, G., Paterson, J. K., Ludwig, J. A., Booth-Genthe, C., and Gottesman, M. M. (2006). Targeting multidrug resistance in cancer. *Nat. Rev. Drug Discov.* 5, 219–234. doi: 10.1038/nrd1984
- Taguchi, Y., Yoshida, A., Takada, Y., Komano, T., and Ueda, K. (1997). Anti-cancer drugs and glutathione stimulate vanadate-induced trapping of nucleotide in multidrug resistance-associated protein (MRP). *FEBS Lett.* 401, 11–14.
- Tancioni, I., Uryu, S., Sulzmaier, F. J., Shah, N. R., Lawson, C., Miller, N. L., et al. (2014). FAK Inhibition disrupts a beta5 integrin signaling axis controlling anchorage-independent ovarian carcinoma growth. *Mol. Cancer Ther.* 13, 2050–2061. doi: 10.1158/1535-7163.MCT-13-1063
- Tanjoni, I., Walsh, C., Uryu, S., Tomar, A., Nam, J. O., Mielgo, A., et al. (2010). PND-1186 FAK inhibitor selectively promotes tumor cell apoptosis in three-dimensional environments. *Cancer Biol. Ther.* 9, 764–777.
- Taylor, N. M. I., Manolaridis, I., Jackson, S. M., Kowal, J., Stahlberg, H., and Locher, K. P. (2017). Structure of the human multidrug transporter ABCG2. *Nature* 546, 504–509. doi: 10.1038/nature22345
- Tiwari, A. K., Sodani, K., Wang, S. R., Kuang, Y. H., Ashby, C. R. Jr., Chen, X., et al. (2009). Nilotinib (AMN107, Tasigna) reverses multidrug resistance by inhibiting the activity of the ABCB1/Pgp and ABCG2/BCRP/MXR transporters. *Biochem. Pharmacol.* 78, 153–161. doi: 10.1016/j.bcp.2009.04.002
- Wilkens, S. (2015). Structure and mechanism of ABC transporters. *F1000Prime Rep.* 7:14. doi: 10.12703/P7-14
- Wu, C. P., and Ambudkar S. V. (2014). The pharmacological impact of ATP-binding cassette drug transporters on vemurafenib-based therapy. *Acta Pharm. Sin. B* 4, 105–111. doi: 10.1016/j.apsb.2013.12.001
- Xie, Z. Y., Lv, K., Xiong, Y., and Guo, W. H. (2014). ABCG2-mediated multidrug resistance and tumor-initiating capacity of side population cells from colon cancer. *Oncol Res Treat.* 37, 666–668, 670–662. doi: 10.1159/000368842
- Yang, B., Ma, Y. F., and Liu, Y. (2015). Elevated expression of Nrf-2 and ABCG2 involved in multi-drug resistance of lung cancer SP cells. *Drug Res.* 65, 526–531. doi: 10.1055/s-0034-1390458
- Zhang, G. N., Zhang, Y. K., Wang, Y. J., Gupta, P., Ashby, C. R. Jr., Alqahtani, S., et al. (2018). Epidermal growth factor receptor (EGFR) inhibitor PD153035 reverses ABCG2-mediated multidrug resistance in non-small cell lung cancer: *in vitro* and *in vivo*. *Cancer Lett.* 424, 19–29. doi: 10.1016/j.canlet.2018.02.040
- Zhang, H., Patel, A., Wang, Y. J., Zhang, Y. K., Kathawala, R. J., Qiu, L. H., et al. (2017). The BTK inhibitor ibrutinib (PCI-32765) overcomes paclitaxel resistance in ABCB1- and ABCC10-overexpressing cells and tumors. *Mol. Cancer Ther.* 16, 1021–1030. doi: 10.1158/1535-7163.MCT-16-0511
- Zhang, X. Y., Zhang, Y. K., Wang, Y. J., Gupta, P., Zeng, L., Xu, M., et al. (2016). Osimertinib (AZD9291), a Mutant-selective EGFR inhibitor, reverses ABCB1-mediated drug resistance in cancer cells. *Molecules* 21:E1236. doi: 10.3390/molecules21091236
- Zhang, Y. K., Zhang, G. N., Wang, Y. J., Patel, B. A., Talele, T. T., Yang, D. H., et al. (2016). Bafetinib (INNO-406) reverses multidrug resistance by inhibiting the efflux function of ABCB1 and ABCG2 transporters. *Sci. Rep.* 6:25694. doi: 10.1038/srep25694
- Zhang, Y. K., Zhang, H., Zhang, G. N., Wang, Y. J., Kathawala, R. J., Si, R., et al. (2015). Semi-synthetic ocotillol analogues as selective ABCB1-mediated drug resistance reversal agents. *Oncotarget* 6, 24277–24290. doi: 10.18632/oncotarget.4493

Conflict of Interest Statement: The authors declare that the research was conducted in the absence of any commercial or financial relationships that could be construed as a potential conflict of interest.

Copyright © 2018 Ji, Yang, Cai, Lei, Wang, Gupta, Teng, Chen, Kong and Yang. This is an open-access article distributed under the terms of the Creative Commons Attribution License (CC BY). The use, distribution or reproduction in other forums is permitted, provided the original author(s) and the copyright owner(s) are credited and that the original publication in this journal is cited, in accordance with accepted academic practice. No use, distribution or reproduction is permitted which does not comply with these terms.



Peptides/Proteins Encoded by Non-coding RNA: A Novel Resource Bank for Drug Targets and Biomarkers

Song Zhu^{1,2†}, Jizhong Wang^{1,2†}, Yutian He^{1,2†}, Nan Meng^{1,2†} and Guang-Rong Yan^{1,2*}

¹ Biomedicine Research Center, The Third Affiliated Hospital of Guangzhou Medical University, Guangzhou, China, ² Key Laboratory of Protein Modification and Degradation, Guangzhou Medical University, Guangzhou, China

OPEN ACCESS

Edited by:

Zhi Shi,
Jinan University, China

Reviewed by:

Shengtao Zhou,
West China Second University
Hospital of Sichuan University, China
Weiyi Fang,
Southern Medical University, China

*Correspondence:

Guang-Rong Yan
jxygr007@yahoo.com;
jxygr007@126.com

[†] These authors have contributed
equally to this work

Specialty section:

This article was submitted to
Experimental Pharmacology
and Drug Discovery,
a section of the journal
Frontiers in Pharmacology

Received: 19 September 2018

Accepted: 22 October 2018

Published: 13 November 2018

Citation:

Zhu S, Wang J, He Y, Meng N and
Yan G-R (2018) Peptides/Proteins
Encoded by Non-coding RNA:
A Novel Resource Bank for Drug
Targets and Biomarkers.
Front. Pharmacol. 9:1295.
doi: 10.3389/fphar.2018.01295

Non-coding RNAs (ncRNAs) are defined as RNA molecules that do not encode proteins, but recent evidence has proven that peptides/proteins encoded by ncRNAs do indeed exist and usually contain less than 100 amino acids. These peptides/proteins play an important role in regulating tumor energy metabolism, epithelial to mesenchymal transition of cancer cells, the stability of the c-Myc oncoprotein, and the ubiquitination and degradation of proliferating cell nuclear antigen (PCNA). These peptides/proteins represent promising drug targets for fighting against tumor growth or biomarkers for predicting the prognosis of cancer patients. In this review, we summarize the characteristics of peptides/proteins that have recently been identified as putative ncRNA translation products and their outlook for small molecule peptide drugs, drug targets, and biomarkers.

Keywords: long non-coding RNA (lncRNA), circular RNA (circRNA), primary miRNA (pri-miRNA), small ORF, small peptide, drug target, biomarker

INTRODUCTION

Non-coding RNAs (ncRNAs) comprise a class of RNA nucleic acid molecules that are transcribed from DNA but do not encode proteins (Guttman et al., 2013). However, ncRNAs are involved in many diseases (Cho, 2011; Esteller, 2011; Hu et al., 2015; Zhou et al., 2016; Nan et al., 2017; Luo et al., 2018) and utilize a variety of mechanisms to participate in gene regulation, including DNA methylation, chromatin modifications, transcriptional regulation, mRNA splicing, translation control, RNA stability, and so on (Muro et al., 2011; Pelechano and Steinmetz, 2013; Xing et al., 2014; Huang and Shan, 2015).

For a long time, there has been widespread recognition that ncRNA are unable to encode proteins (Guttman et al., 2013). However, with the development of deep ribosome profiling sequencing (Ribo-Seq) technology, mass spectrometry and algorithms including fragment length organization similarity score (FLOSS; Ingolia et al., 2014), ORF-RATER (Fields et al., 2015), and Ribo taper (Calviello et al., 2016), a subset of ncRNA have been identified to be able to encode peptides (<100 amino acids) or proteins, such as HOXB-AS3 (Huang et al., 2017), SPAR (Matsumoto et al., 2017), FBXW7-185aa (Yang et al., 2018), SHPRH-146aa (Zhang et al., 2018), miPEP-200a, and miPEP-200b (Fang et al., 2017; **Figure 1**). HOXB-AS3 and SPAR are encoded by long non-coding RNA (lncRNA). HOXB-AS3 plays an important role in regulating tumor energy metabolism, and SPAR interacts with the lysosomal v-ATPase to negatively regulate mTORC1 activation. FBXW7-185aa and SHPRH-146aa are encoded by circular RNA (circRNA), regulating the stability of the c-Myc oncoprotein and mediating ubiquitination and degradation

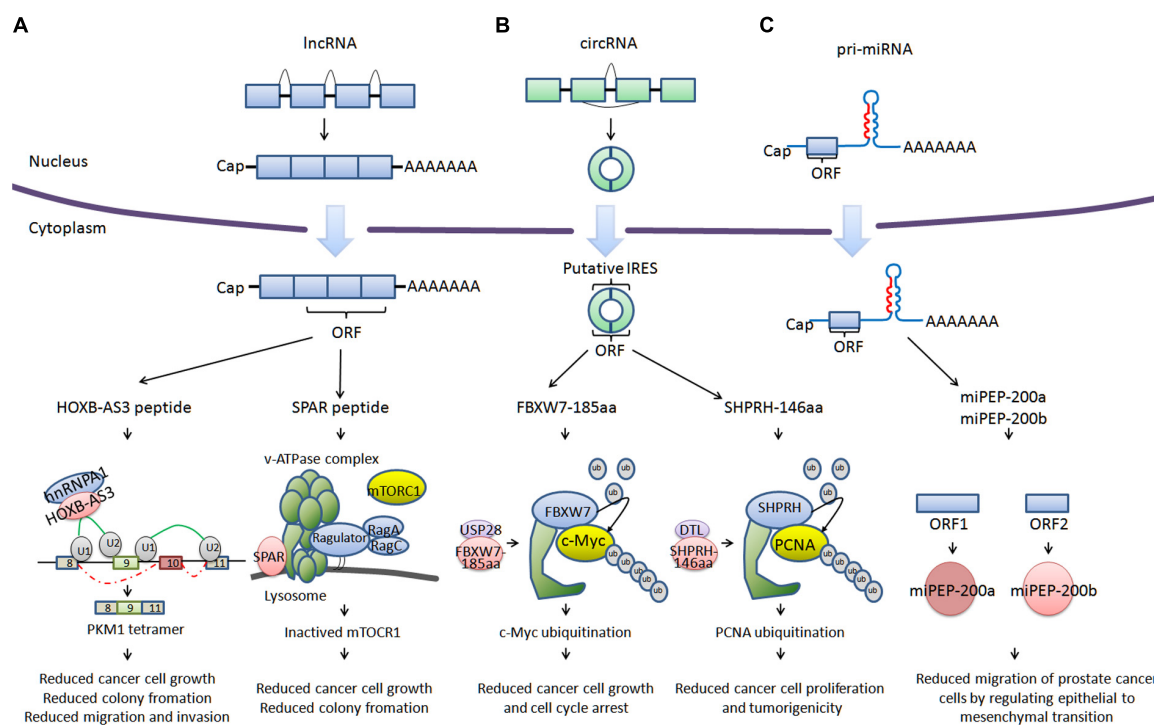


FIGURE 1 | Cancer-related peptides/proteins encoded by ncRNAs. **(A)** Cancer-related peptides encoded by lncRNA. HOXB-AS3 is encoded by the lncRNA *HOXB-AS3*. HOXB-AS3 regulates tumor energy metabolism by antagonizing hnRNP A1, mediating PKM splicing. SPAR is encoded by *LINC00961*. SPAR interacts with the lysosomal v-ATPase to negatively regulate mTORC1 activation. **(B)** Cancer-related proteins encoded by circRNA. FBXW7-185aa is encoded by circ-*FBXW7*. FBXW7-185aa regulates the stability of the c-Myc oncoprotein. SHPRH-146aa is encoded by circ-*SHPRH*. SHPRH-146aa mediates the ubiquitination and degradation of PCNA. **(C)** Cancer-related proteins encoded by pri-miRNA. miPEP-200a and miPEP-200b are encoded by pri-miRNA (miR-200a and miR-200b). miPEP-200a and miPEP-200b affect the epithelial to mesenchymal transition of prostate cancer cells.

of proliferating cell nuclear antigen (PCNA). miPEP-200a and miPEP-200b are encoded by primary miRNA (pri-miRNA). miPEP-200a and miPEP-200b affect epithelial to mesenchymal transition of cancer cells. We describe a bank of biologically functional peptides/proteins encoded by lncRNA, circRNA, and pri-miRNA. The biological activity of ncRNA encoded peptides/proteins may provide possibilities for developing new therapies for current refractory and other diseases.

Peptides/proteins encoded by ncRNAs represent promising drug targets for fighting against tumor growth or biomarkers for predicting the prognosis of cancer patients. In this review, we summarize the characteristics of peptides/proteins encoded by ncRNA and their outlook for small molecule peptide drugs, drug targets, and biomarkers.

PEPTIDES/SMALL PROTEINS ENCODED BY NCRNA AS PROMISING CANDIDATES IN ANTITUMOR DRUGS

Advantages and Development Status of Anti-tumor Peptide/Small Protein Drugs

It is generally known that some peptide/protein drugs (such as antibacterial peptides) have been widely used in the field of

animal medicine and have achieved good results (Broegden et al., 2003). In addition, the use of peptides/small protein drugs has a long successful history in the treatment of human disease, for instance, insulin for the treatment of diabetes (Kaur et al., 2018). Some anti-tumor peptides/small proteins such as mifamurtide (Brosa et al., 2014), interferon- γ (INF- γ ; Berek, 2000), and interleukin-2 (IL-2; Liang et al., 2012), have been used in clinics and achieved a certain curative efficacy. Although chemotherapy is the major treatment method for cancer, it has fierce side effects, including the insufficient uptake of drugs in tumor cells, non-specific cytotoxicity of chemotherapeutic drugs and the rapid emergence of drug resistance, which largely limit clinical application (Gandhi et al., 2014; He et al., 2016). Compared with traditional chemotherapy agents, peptide and protein drugs possess unique advantages, including high specificity and activity, low immunogenicity and less cytotoxicity to normal tissues (Leader et al., 2008). Therefore, peptide and protein therapeutics have emerged as crucial approaches in recent clinical cancer treatment. The anti-cancer mechanisms of peptides and proteins are mainly divided into two types: one is usually related to direct induction of apoptosis in tumor cells via specific pathways, and the other is related to direct inhibition of tumor cell growth through targeting tumor angiogenesis or stimulating an immune response (Vaishya et al., 2015; Redington et al., 2017). Some protein drugs, such as tumor necrosis factor alpha

(TNF- α), INF- γ , and IL-2, have been widely used in clinical cancer treatment (Berek, 2000; Calzascia et al., 2007; Liang et al., 2012). Nevertheless, despite TNF- α , INF- γ , and IL-2 possessing anti-tumor potency, the systemic clinical applications of high doses of these drugs are severely limited due to their systemic toxicities, for instance, inflammatory response, and underlying cardiotoxicity (Ashkenazi et al., 1999; Berek, 2000; Liang et al., 2012). Therefore, it is necessary and urgent to continue looking for higher efficiency and lower toxicity anti-tumor drugs.

Application Prospect of Peptides/Small Proteins Encoded by lncRNAs in the Treatment of Tumors

Only 2% of the human genome is able to code for proteins or peptides, and the rest is actively transcribed into ncRNAs (Fang et al., 2017). Surprisingly, a limited number of “ncRNAs” have recently shown the ability to encode proteins or peptides. *HOXB-AS3* was annotated as lncRNA in the NCBI and lncRNA databases. Our research team has recently discovered that the lncRNA *HOXB-AS3* could actually encode a conserved 53-aa peptide, called *HOXB-AS3* peptide (Huang et al., 2017). *In vitro* studies showed that *HOXB-AS3*, rather than its lncRNA, inhibited proliferation, migration, invasion, and colony formation of colon cancer cells (CRC) via antagonizing hnRNP A1 protein (Huang et al., 2017). More importantly, the *HOXB-AS3* peptide clearly impaired the *in vivo* growth of CRC xenografts and decreased the number and size of lung metastatic nodules (Huang et al., 2017). Therefore, *HOXB-AS3* has great potential for the treatment of colon cancer via antagonizing hnRNP A1. Moreover, a conserved lncRNA *LINC00961*, encodes a novel peptide, called “small regulatory peptide of amino acid response” (SPAR). SPAR locates at the late endosome/lysosome and interacts with the lysosomal v-ATPase to negatively regulate mTORC1 activation (Matsumoto et al., 2017).

Application Prospect of Peptides/Small Proteins Encoded by circRNAs in the Treatment of Tumors

Very few circRNAs have been shown to encode small proteins with antitumor activity based on small-ORFs. Zhang et al. (2018) reported that a novel antitumor protein, SHPRH-146aa, was encoded by the circular RNA *SHPRH* and was driven by internal ribosome entry site (IRES) elements. SHPRH-146aa was able to protect full-length SHPRH from degradation by the ubiquitin-proteasome. Stabilized SHPRH inhibited glioblastoma cell proliferation and tumorigenicity via sequentially ubiquitinating PCNA as an E3 ligase (Zhang et al., 2018). In addition, Yang et al. (2018) also found that a novel 21-kDa protein, named FBXW7-185aa, was encoded by the circular RNA *FBXW7*. The FBXW7-185aa protein can reduce the half-life of the c-Myc oncoprotein, which is known to regulate the transcription of numerous genes and pathways, via antagonizing ubiquitin carboxyl-terminal hydrolase 28 (USP28) induced c-Myc stabilization in glioma cells (Yang et al., 2018). Therefore, the FBXW7-185aa protein can inhibit the proliferation and cell cycle acceleration of malignant

glioma cells by downregulating the protein expression of c-Myc (Yang et al., 2018).

Application Prospect of Peptides/Small Proteins Encoded by pri-miRNAs in the Treatment of Tumors

Impressively, Fang et al. (2017) found that two proteins (miPEP-200a and miPEP-200b) were encoded by miR-200a and miR-200b, respectively. The experiment results indicated that miPEP-200a and miPEP-200b suppressed the migration of prostate cancer cells through regulating the epithelial to mesenchymal transition of tumor cells.

Application of Peptide/Small Protein Drugs Encoded by ncRNA

The ideal drug not only has specificity and pharmacological activity, but can also reach the target site to play a role. Whether these cancer-suppressive peptides/small proteins (SPAR, *HOXB-AS3*, FBXW7-185aa, SHPRH-146aa, miPEP-200a, and miPEP-200b) encoded by ncRNAs, are secreted into human serum remains unknown. Whether they can enter tumor cells through transporters on the cell membrane and play an inhibitory role remains unknown. Due to the potential developmental value and clinical applications, these problems will become a hot topic of research. In the past few decades, nanoscale carriers have become one of the key strategies for enhancing cancer treatment, which is attributed to the markedly enhanced tumor accumulation of drugs, prolonged blood circulation of the drug-loaded nanoparticles, and improved intracellular delivery efficiency (Elsababy and Wooley, 2012; He et al., 2016). Therefore, if these peptides/small proteins have a very short half-life *in vivo* and are difficult to pass the biofilm barrier, they could be wrapped in nanomaterials to avoid being quickly metabolized and be delivered to tumor cells through nanoparticles to play an anti-cancer role. Moreover, these peptides/small proteins could interact with chemical drugs to treat tumors through nanoscale codelivery systems. Recombinant human adenovirus-p53 injection has become a new method for the clinical treatment of cancer. After the coding sequence of these peptides/small proteins is recombined with adenovirus, it could be injected into patients to treat tumors.

PEPTIDES/SMALL PROTEINS ENCODED BY NCRNA AS PROMISING CANCER DRUG TARGETS

Targeted Therapy

Targeted therapy refers to a type of treatment that uses drugs or other substances to attack specific targeted molecules (e.g., certain enzymes, proteins, DNA, RNA or other molecules), thereby maximizing efficacy and minimizing toxicity (Sawyers, 2008). This is also called “molecularly targeted therapy” and “precision medicine.” The purpose of targeted therapy in cancer is to restrict the growth and survival of cancer cells without injury to normal cells. In view of tumor heterogeneity, several types

of targeted therapies, including monoclonal antibodies (e.g., Rituximab and Infliximab) (Maifrede et al., 2018), angiogenesis inhibitors (e.g., Pemetrexed and FGFR inhibitors) (Rojas et al., 2016), hormone therapies (e.g., Palbociclib) (Lynce et al., 2018), immune therapies (e.g., Durvalumab) (Raja et al., 2018), and rapamycin target inhibitor (e.g., Everolimus) (Kornblum et al., 2018), have been approved for cancer treatment. Additionally, tumor suppressor have also been studied as targets for targeted therapies in cancer. An example is the most important tumor suppressor protein, p53, which is associated with carcinogenesis by missense mutation (Brosh and Rotter, 2009). It was reported that 96.7% of high-grade serous ovarian carcinoma (HGSOC) cases contain pathogenic TP53 mutations (Ahmed et al., 2010). More recently, Soragni et al. (2016) designed a peptide inhibitor of p53 amyloid aggregation, ReACp53, which penetrated cells and restored the p53 function of tumor suppression in HGSOCs.

Application of ncRNA Encoded Peptides/Proteins as Promising Therapy Targets

ncRNA encoded peptides/proteins (HOXB-AS3, FBXW7-185aa, SHPRH-146aa, miPEP-200a, and miPEP-200b) have been proved to suppress tumorigenesis, which has enriched the research of ncRNAs in cancer development. Whether or not these tumor suppressor ncRNAs present mutations, like TP53 does, in tumors is still unknown. Strategies for rescuing or strengthening the function of tumor suppressor peptides/proteins, including vaccination with synthesized peptides or viral vector vaccines that encode relevant peptides sequences for cancer therapies, are now in development (Efremova et al., 2017; Radvanyi, 2018). Meanwhile, in the human genome, increasing evidence suggests that numerous ncRNAs are functional and play pivotal roles in many aspects of biology (Esteller, 2011). Maybe there are some hidden oncopeptides/oncoproteins encoded by ncRNAs that need to be identified; these hidden oncopeptides/oncoproteins may be exploited as novel targets for targeted therapies in cancer.

PEPTIDES/PROTEINS ENCODED BY NCRNA AS PROMISING CANCER BIOMARKERS

Biomarkers in Clinical Detection

With the advancement of treatment modalities, the survival rate and quality of life for early-stage cancer patients have been improved. However, due to the lack of specific symptoms and signs of early-stage cancer, and limited by cancer heterogeneity, only a portion of cancer patients are diagnosed early. Most cancer patients experience tumor recurrence and metastasis at regional or distant sites, which seriously shortens their survival time and greatly diminished quality of life. It is obvious that cancer bring devastating effects on patients and their families, which is a tremendous burden on society. Bray estimated there would be 22.2 million new cancer cases in 184 countries by 2030 (Bray et al., 2012). Cancer has been a severe challenge to society, and the early detection of cancer is highly important for clinical work.

It has been widely recognized that cancer is a very heterogeneous disease, and implementing precision medicine for patients is widely accepted. The molecular subtype of cancer provides us a new perspective: for different molecular subtypes, we can develop different, appropriate therapies and monitor the disease progression in the most suitable way. For instance, patients with triple-negative breast cancer (TNBC) have an increased risk of death compared with women with other types of breast cancer (Mayer et al., 2014). Gene expression analyses recently showed that TNBC has six distinct subtypes, each displaying a unique biology and showing distinct responses to standard treatment (Lehmann et al., 2011; Masuda et al., 2013). It is urgent to develop more biology-specific cancer biomarkers so that patients can receive the most appropriate therapy. Developing more suitable biomarkers for different molecular typing of tumors will be an inevitable biological challenge for cancer treatment. Therefore, biology-specific cancer biomarkers urgently need to be discovered and developed.

Peptides/Proteins Encoded by ncRNA as Promising Cancer Biomarkers HOXB-AS3 Encoded by lncRNA Is a Potential Prognostic Biomarker

Our research team reported that the HOXB-AS3, encoded by the lncRNA *HOXB-AS3*, has been proven to play an important role in the development of cancer metabolism reprogramming. In mice, the *in vivo* growth of CRC xenografts with *HOXB-AS3* ORF and 5' UTR-ORF stably transfected cells was clearly impaired, including inhibition of tumor growth and lung metastasis. The HOXB-AS3 levels were decreased in primary CRC tissues compared with their paired non-tumoral tissues. Comparing the correlations between the level of HOXB-AS3 and clinic pathological features in 90 CRC cases, we found that patients with the clinical stage between IIB to IV have significantly lower levels of HOXB-AS3. The mean overall survival time for CRC patients with high levels of HOXB-AS3 was 1.6 times that of CRC patients with low levels of HOXB-AS3. Kaplan-Meier survival analyses revealed that patients with lower HOXB-AS3 levels were at increased risk of CRC-related death. Therefore, the low level of the HOXB-AS3 was correlated with a poor prognosis in CRC patients (Huang et al., 2017).

The Potential of Peptides/Proteins Encoded by circRNAs as Cancer Biomarkers

Nu Zhang's research team reported that circ-*FBXW7* can encode a 21-kDa protein, called FBXW7-185aa, which is assumed as a prognostic marker for glioblastoma. The mice injected with glioblastoma multiforme cells that stably overexpressed circ-*FBXW7* had longer survival times and exhibited a much lower tumorigenicity than mice injected with the corresponding control cells. In 38 pairs of glioblastoma samples compared with their paired tumor-adjacent tissues, the expression of FBXW7-185aa was obviously decreased. The protein expression was investigated to demonstrate that glioblastoma patients with higher FBXW7-185aa expression had an increased total survival time (Yang et al., 2018).

Another study focused on SHPRH-146aa, which is encoded by circ-SHPRH, and showed that the SHPRH-146aa expression was significantly downregulated in 60 glioblastoma samples compared with their adjacent normal tissues. The subcutaneous injection with SHPRH-146aa stably overexpressing cells resulted in substantially lower tumorigenicity compared with the injection of the corresponding control cells in mice. Cancer patients with higher SHPRH-146aa expression had a longer survival time than those with lower SHPRH-146aa expression in glioblastoma patient samples. The result suggested SHPRH-146aa is a prognostic marker for glioblastoma in clinics (Zhang et al., 2018).

The Potential of Peptides/Proteins Encoded by pri-miRNAs as Cancer Biomarkers

The primary microRNA, miR-200a and miR-200b, that encode proteins (miPEP-200a and miPEP-200b) can inhibit the migration of prostate cancer cells, and it was observed that low-level expression of miPEP-200a and miPEP-200b were associated with poor survival outcome in cancer patients. This evidence indicated that miPEP-200a and miPEP-200b have the potential to be used as diagnostic and prognostic markers (Fang et al., 2017).

The Expectation of Peptides/Proteins Encoded by ncRNA Used as the Cancer Biomarkers

Accumulating evidence has shown that peptides/proteins encoded by ncRNA represent a promising source for prognostic biomarkers. Although the differential expression and prognostic correlation of the five peptides/proteins HOXB-AS3, SHPRH-146aa, FBXW7-185aa, miPEP-200a and miPEP-200b in cancer have been confirmed by the IHC analysis of paraffin sections of tumor tissues and western blot analysis of protein samples, we do not see a clear report that the peptides/proteins encoded by ncRNA are detected in body fluid (including blood, serum, urine, chest fluid, etc.). If these biology-specific peptides/proteins can be found in body fluid, the widespread progress of using them as cancer biomarkers in clinical applications will be greatly promoted. The tremendous research space of peptides/proteins encoded by ncRNAs used as cancer biomarkers will encourage researchers to continuously devote great effort in this field so that

they can meet the requirements of being reliable, cost-effective, and capable of precise detection and monitoring.

CONCLUSION

ncRNA-encoded peptides/proteins open up a new field. The peptides/proteins mentioned in this review affect multiple steps in the development of tumorigenesis. These peptides/proteins regulate tumor energy metabolism, the stability of oncoproteins and the epithelial to mesenchymal transition of cancer cells. They are the new stars of the future drug targets for fighting against tumor growth or may be used as biomarkers for predicting the prognosis of cancer patients.

However, the ncRNA-encoded peptides/proteins that have been discovered so far are only the beginning, and those that are undiscovered will provide a wealth of opportunities for small molecule peptide drugs, drug targets, and biomarkers. Currently, whether these ncRNA-encoded peptides/proteins can be used in clinical practice requires a large sample of clinical studies. Follow-up treatment effects of ncRNA-encoded peptides/proteins and detecting these as biomarkers in more samples will be needed.

AUTHOR CONTRIBUTIONS

G-RY conceived the general idea. SZ, JW, YH, and NM wrote the first draft. G-RY revised the manuscript. All authors read and approved the final manuscript.

FUNDING

This work was supported by the National Natural Science Foundation of China (81772998 and 81672393), the R&D Plan of Guangzhou (201704020115), the Yangcheng Scholars Program from the Ministry of Education of Guangzhou (1201561583), Innovative Research Team of Ministry of Education of Guangzhou (1201610015), the R&D Plan of Guangdong (2017A020215096), and the National Funds of Developing Local Colleges and Universities (B16056001).

REFERENCES

- Ahmed, A. A., Etemadmoghadam, D., Temple, J., Lynch, A. G., Riad, M., Sharma, R., et al. (2010). Driver mutations in TP53 are ubiquitous in high grade serous carcinoma of the ovary. *J. Pathol.* 221, 49–56. doi: 10.1002/path.2696
- Ashkenazi, A., Pai, R. C., Fong, S., Leung, S., Lawrence, D. A., Marsters, A., et al. (1999). Safety and antitumor activity of recombinant soluble Apo2 ligand. *J. Clin. Invest.* 104, 155–162. doi: 10.1172/JCI6926
- Berek, J. S. (2000). Interferon plus chemotherapy for primary treatment of ovarian cancer. *Lancet* 356, 6–7. doi: 10.1016/S0140-6736(00)02422-3
- Bray, F., Jemal, A., Grey, N., Ferlay, J., and Forman, D. (2012). Global cancer transitions according to the human development index (2008–2030): a population-based study. *Lancet Oncol.* 13, 790–801. doi: 10.1016/S1470-2045(12)70211-5
- Brogden, K. A., Ackermann, M., McCray, P. J., and Tack, B. F. (2003). Antimicrobial peptides in animals and their role in host defences. *Int. J. Antimicrob. Agents* 22, 465–478. doi: 10.1016/S0924-8579(03)00180-8
- Brosa, M., Garcia, D. M., Mora, J., Villacampa, A., Pozo, T., Adán, C., et al. (2014). Economic considerations on the use of mifamurtide in the treatment of osteosarcoma in Spain. *Value Health* 17, A526–A527. doi: 10.1016/j.jval.2014.08.1662
- Brosh, R., and Rotter, V. (2009). When mutants gain new powers: news from the mutant p53 field. *Nat. Rev. Cancer* 9, 701–713. doi: 10.1038/nrc2693
- Calviello, L., Mukherjee, N., Wyler, E., Zaubner, H., Hirsekorn, A., Selbach, M., et al. (2016). Detecting actively translated open reading frames in ribosome profiling data. *Nat. Methods* 13, 165–170. doi: 10.1038/nmeth.3688
- Calzascia, T., Pellegrini, M., Hall, H., Sabbagh, L., Ono, N., Elford, A. R., et al. (2007). TNF- α is critical for antitumor but not antiviral T cell immunity in mice. *J. Clin. Invest.* 117, 3833–3845. doi: 10.1172/JCI32567
- Cho, W. C. (2011). Grand challenges and opportunities in deciphering the role of non-coding RNAs in human diseases. *Front. Genet.* 2:1. doi: 10.3389/fgene.2011.00001
- Efremova, M., Finotello, F., Rieder, D., and Trajanoski, Z. (2017). Neoantigens generated by individual mutations and their role in cancer immunity

- and immunotherapy. *Front. Immunol.* 8:1679. doi: 10.3389/fimmu.2017.01679
- Elsababy, M., and Wooley, K. L. (2012). Design of polymeric nanoparticles for biomedical delivery applications. *Chem. Soc. Rev.* 41, 2545–2561. doi: 10.1039/c2cs15327k
- Esteller, M. (2011). Non-coding RNAs in human disease. *Nat. Rev. Genet.* 12, 861–874. doi: 10.1038/nrg3074
- Fang, J., Morsalin, S., Rao, V. N., and Reddy, E. S. P. (2017). Decoding of non-coding DNA and non-coding RNA: pri-micro RNA-encoded novel peptides regulate migration of cancer cells. *J. Pharm. Sci. Pharm.* 3, 23–27. doi: 10.1166/jpsp.2017.1070
- Fields, A. P., Rodriguez, E. H., Jovanovic, M., Stern-Ginossar, N., Haas, B. J., Mertins, P., et al. (2015). A regression-based analysis of ribosome-profiling data reveals a conserved complexity to mammalian translation. *Mol. Cell* 60, 816–827. doi: 10.1016/j.molcel.2015.11.013
- Gandhi, N. S., Tekade, R. K., and Chougule, M. B. (2014). Nanocarrier mediated delivery of siRNA/miRNA in combination with chemotherapeutic agents for cancer therapy: current progress and advances. *J. Control. Release* 194, 238–256. doi: 10.1016/j.jconrel.2014.09.001
- Guttman, M., Russell, P., Ingolia, N. T., Weissman, J. S., and Lander, E. S. (2013). Ribosome profiling provides evidence that large noncoding RNAs do not encode proteins. *Cell* 154, 240–251. doi: 10.1016/j.cell.2013.06.009
- He, C., Tang, Z., Tian, H., and Chen, X. (2016). Co-delivery of chemotherapeutics and proteins for synergistic therapy. *Adv. Drug Deliv. Rev.* 98, 64–76. doi: 10.1016/j.addr.2015.10.021
- Hu, G., Yang, T., Zheng, J., Dai, J., Nan, A., Lai, Y., et al. (2015). Functional role and mechanism of lncRNA LOC728228 in malignant 16HBE cells transformed by anti-benzopyrene-trans-7,8-dihydrodiol-9,10-epoxide. *Mol. Carcinog.* 54(Suppl. 1), E192–E204. doi: 10.1002/mc.22314
- Huang, C., and Shan, G. (2015). What happens at or after transcription: insights into circRNA biogenesis and function. *Transcription* 6, 61–64. doi: 10.1080/21541264.2015.1071301
- Huang, J. Z., Chen, M., Chen, D., Gao, X. C., Zhu, S., Huang, H., et al. (2017). A peptide encoded by a putative lncRNA HOXB-AS3 suppresses colon cancer growth. *Mol. Cell* 68, 171–184. doi: 10.1016/j.molcel.2017.09.015
- Ingolia, N. T., Brar, G. A., Sterniginossar, N., Harris, M. S., Talhouarne, G. J. S., Jackson, S. E., et al. (2014). Ribosome profiling reveals pervasive translation outside of annotated protein-coding genes. *Cell Rep.* 8, 1365–1379. doi: 10.1016/j.celrep.2014.07.045
- Kaur, R., Kaur, M., and Singh, J. (2018). Endothelial dysfunction and platelet hyperactivity in type 2 diabetes mellitus: molecular insights and therapeutic strategies. *Cardiovasc. Diabetol.* 17:121. doi: 10.1186/s12933-018-0763-3
- Kornblum, N., Zhao, F., Manola, J., Klein, P., Ramaswamy, B., Brufsky, A., et al. (2018). Randomized phase II trial of fulvestrant plus everolimus or placebo in postmenopausal women with hormone receptor-positive, human epidermal growth factor receptor 2-negative metastatic breast cancer resistant to aromatase inhibitor therapy: results of PrE0102. *J. Clin. Oncol.* 36, 1556–1563. doi: 10.1200/JCO.2017.76.9331
- Leader, B., Baca, Q. J., and Golan, D. E. (2008). Protein therapeutics: a summary and pharmacological classification. *Nat. Rev. Drug Discov.* 7, 21–39. doi: 10.1038/nrd2399
- Lehmann, B. D., Bauer, J. A., Chen, X., Sanders, M. E., Chakravarthy, A. B., Shyr, Y., et al. (2011). Identification of human triple-negative breast cancer subtypes and preclinical models for selection of targeted therapies. *J. Clin. Invest.* 121, 2750–2767. doi: 10.1172/JCI45014
- Liang, X., De Vera, M. E., Buchser, W. J., Romo, D. V. C. A., Loughran, P., Beer Stolz, D., et al. (2012). Inhibiting systemic autophagy during interleukin 2 immunotherapy promotes long-term tumor regression. *Cancer Res.* 72, 2791–2801. doi: 10.1158/0008-5472.CAN-12-0320
- Luo, Y., Liang, M., Yao, W., Liu, J., Niu, Q., Chen, J., et al. (2018). Functional role of lncRNA LOC101927497 in N-methyl-N'-nitro-N-nitrosoguanidine-induced malignantly transformed human gastric epithelial cells. *Life Sci.* 193, 93–103. doi: 10.1016/j.lfs.2017.12.007
- Lynce, F., Shajahan-Haq, A. N., and Swain, S. M. (2018). CDK4/6 inhibitors in breast cancer therapy: current practice and future opportunities. *Pharmacol. Ther.* 191, 65–73. doi: 10.1016/j.pharmthera.2018.06.008
- Maifrede, S., Nieborowskaskorska, M., Sullivan, K., Dasgupta, Y., and Podszyslawowbartnicka, P. (2018). Tyrosine kinase inhibitor-induced defects in DNA repair sensitize FLT3(ITD)-positive leukemia cells to PARP1 inhibitors. *Blood* 132, 67–77. doi: 10.1182/blood-2018-02-834895
- Masuda, H., Baggerly, K. A., Wang, Y., Zhang, Y., Gonzalez-Angulo, A. M., Meric-Bernstam, F., et al. (2013). Differential response to neoadjuvant chemotherapy among 7 triple-negative breast cancer molecular subtypes. *Clin. Cancer Res.* 19, 5533–5540. doi: 10.1158/1078-0432.CCR-13-0799
- Matsumoto, A., Pasut, A., Matsumoto, M., Yamashita, R., Fung, J., Monteleone, E., et al. (2017). mTORC1 and muscle regeneration are regulated by the LINC00961-encoded SPAR polypeptide. *Nature* 541, 228–232. doi: 10.1038/nature21034
- Mayer, I. A., Abramson, V. G., Lehmann, B. D., and Pietenpol, J. A. (2014). New strategies for triple-negative breast cancer—deciphering the heterogeneity. *Clin. Cancer Res.* 20, 782–790. doi: 10.1158/1078-0432.CCR-13-0583
- Muro, E. M., Mah, N., and Andradenavarro, M. A. (2011). Functional evidence of post-transcriptional regulation by pseudogenes. *Biochimie* 93, 1916–1921. doi: 10.1016/j.biochi.2011.07.024
- Nan, A., Chen, L., Zhang, N., Liu, Z., Yang, T., Wang, Z., et al. (2017). A novel regulatory network among lncRpa, CircRar1, MiR-671 and apoptotic genes promotes lead-induced neuronal cell apoptosis. *Arch. Toxicol.* 91, 1671–1684. doi: 10.1007/s00204-016-1837-1
- Pelechano, V., and Steinmetz, L. M. (2013). Gene regulation by antisense transcription. *Nat. Rev. Genet.* 14:880. doi: 10.1038/nrg3594
- Radvanyi, L. G. (2018). Targeting the cancer mutanome of breast cancer. *Nat. Med.* 24, 703–704. doi: 10.1038/s41591-018-0065-z
- Raja, R., Kuziora, M., Brohawn, P., Higgs, B. W., Gupta, A., Dennis, P. A., et al. (2018). Early reduction in ctDNA predicts survival in lung and bladder cancer patients treated with durvalumab. *Clin. Cancer Res.* doi: 10.1158/1078-0432.CCR-18-0386 [Epub ahead of print].
- Redington, J. M., Breydo, L., and Uversky, V. N. (2017). When good goes awry: the aggregation of protein therapeutics. *Protein Pept. Lett.* 24, 340–347. doi: 10.2174/0929866524666170209153421
- Rojas, L., Cardona, A. F., Arrieta, O., Wills, B., and Corrales-Rodriguez, L. (2016). PD2.04 (also presented as P1.42): PEM/CBP/BEV followed by maintenance PEM/BEV in hispanic patients with NSCLC: outcomes according to TS, ERCC1 and VEGF. *J. Thorac. Oncol.* 11, S177–S178. doi: 10.1016/j.jtho.2016.08.018
- Sawyers, C. L. (2008). The cancer biomarker problem. *Nature* 452, 548–552. doi: 10.1038/nature06913
- Soragni, A., Janzen, D. M., Johnson, L. M., Lindgren, A. G., Thaikunh, N. A., Tiourin, E., et al. (2016). A designed inhibitor of p53 aggregation rescues p53 tumor suppression in ovarian carcinomas. *Cancer Cell* 29, 90–103. doi: 10.1016/j.jccell.2015.12.002
- Vaishya, R., Khurana, V., Patel, S., and Mitra, A. K. (2015). Long-term delivery of protein therapeutics. *Expert Opin. Drug Del.* 12, 415–440. doi: 10.1517/17425247.2015.961420
- Xing, Z., Lin, A., Li, C., Liang, K., Wang, S., Liu, Y., et al. (2014). lncRNA directs cooperative epigenetic regulation downstream of chemokine signals. *Cell* 159, 1110–1125. doi: 10.1016/j.cell.2014.10.013
- Yang, Y., Gao, X., Zhang, M., Yan, S., Sun, C., Xiao, F., et al. (2018). Novel role of FBXW7 circular RNA in repressing glioma tumorigenesis. *J. Natl. Cancer Ins.* 110, 304–315. doi: 10.1093/jnci/djx166
- Zhang, M., Huang, N., Yang, X., Luo, J., Yan, S., Xiao, F., et al. (2018). A novel protein encoded by the circular form of the SHPRH gene suppresses glioma tumorigenesis. *Oncogene* 37, 1805–1814. doi: 10.1038/s41388-017-0019-9
- Zhou, Y., Xu, X., Lv, H., Wen, Q., Li, J., Tan, L., et al. (2016). The long noncoding RNA MALAT-1 is highly expressed in ovarian cancer and induces cell growth and migration. *PLoS One* 11:e0155250. doi: 10.1371/journal.pone.0155250

Conflict of Interest Statement: The authors declare that the research was conducted in the absence of any commercial or financial relationships that could be construed as a potential conflict of interest.

Copyright © 2018 Zhu, Wang, He, Meng and Yan. This is an open-access article distributed under the terms of the Creative Commons Attribution License (CC BY). The use, distribution or reproduction in other forums is permitted, provided the original author(s) and the copyright owner(s) are credited and that the original publication in this journal is cited, in accordance with accepted academic practice. No use, distribution or reproduction is permitted which does not comply with these terms.



ORY-1001 Suppresses Cell Growth and Induces Apoptosis in Lung Cancer Through Triggering HK2 Mediated Warburg Effect

Zhaoliang Lu¹, Yanke Guo¹, Xiaoya Zhang¹, Jing Li², Leilei Li¹, Shuai Zhang^{3,4*} and Changliang Shan^{1,2*}

¹ The First Affiliated Hospital, Biomedical Translational Research Institute, Jinan University, Guangzhou, China, ² State Key Laboratory of Medicinal Chemical Biology, College of Pharmacy and Tianjin Key Laboratory of Molecular Drug Research, Nankai University, Tianjin, China, ³ School of Integrative Medicine, Tianjin University of Traditional Chinese Medicine, Tianjin, China, ⁴ Department of Medical Biochemistry and Molecular Biology, School of Medicine, Jinan University, Guangzhou, China

OPEN ACCESS

Edited by:

Dong-Hua Yang,
St. John's University, United States

Reviewed by:

Guo Chen,
Emory University, United States
Lingtao Jin,
University of Florida, United States
Dan Li,
National Cancer Centre Singapore,
Singapore

*Correspondence:

Changliang Shan
changliangshan@jnu.edu.cn
Shuai Zhang
shuaizhang@tjutcm.edu.cn

Specialty section:

This article was submitted to
Experimental Pharmacology and Drug
Discovery,
a section of the journal
Frontiers in Pharmacology

Received: 27 September 2018

Accepted: 16 November 2018

Published: 04 December 2018

Citation:

Lu Z, Guo Y, Zhang X, Li J, Li L,
Zhang S and Shan C (2018)
ORY-1001 Suppresses Cell Growth
and Induces Apoptosis in Lung
Cancer Through Triggering HK2
Mediated Warburg Effect.
Front. Pharmacol. 9:1411.
doi: 10.3389/fphar.2018.01411

ORY-1001, an inhibitor of covalent lysine (K)-specific demethylase 1A (KDM1A), has been used as a therapy for the treatment of acute leukemia. However, the underlying mechanisms of anticancer are still not fully elucidated. Here, we report that KDM1A is highly expressed in lung cancers, where it appears to drive aggressive growth. Furthermore, lung cancer patients with higher KDM1A levels have worse survival outcomes than patients with lower KDM1A levels. Interestingly, ORY-1001 significantly inhibited the cell proliferation, colony formation, cell cycle, and induced apoptosis, by regulating the Warburg effect through controlling Hexokinases 2 (HK2) expression. In summary, these results indicate that ORY-1001 could inhibit the growth of lung cancer cells via regulating the Warburg effect by controlling HK2.

Keywords: lysine (K)-specific demethylase 1A, Warburg effect, Hexokinases 2, cell proliferation, lung cancer

INTRODUCTION

Energy metabolism reprogramming is a hallmark of cancer. Cancer cells increase glucose uptake, which then leads to an increase in the aerobic glycolysis rate and enhances lactate and energy production, known as the Warburg effect (Cairns et al., 2011; Fan et al., 2014). Mounting evidence supports that deregulated energy metabolism reprogramming is closely related to drug resistance in cancer therapy (Liu et al., 2008; Wang et al., 2010; Zhou et al., 2010; Zhao et al., 2011, 2013; Zheng et al., 2017). The enzymes involved in energy metabolism reprogramming can be regulated at the gene expression and post-translation modification level, in response to extracellular and intracellular signaling, to cope with the adaptive metabolic remodeling, in response to severe environmental conditions. Blocking the epigenetic regulation of metabolic enzymes is not only an intellectual pursuit, but also provides a way to help diagnose and treat cancers.

Lysine (K)-specific demethylase 1A (KDM1A), also known as Lysine-specific demethylase-1 (LSD1), is the first reported histone demethylase, that can remove histone H3 Lys 4 and Lys 9's mono- and di-methylation modification (Sehrawat et al., 2018). KDM1A has been characterized as a potential oncogene and a therapeutic target in various cancers (Hayami et al., 2011; Schildhaus et al., 2011; Yu et al., 2013). Several studies showed that various cancers with higher KDM1A expression correction, have high cell proliferation rates (Lv et al., 2012; Zhao et al., 2012; Jie et al., 2013; Yu et al., 2013). In acute myeloid leukemia (AML), KDM1A overexpression blocks

differentiation and results in a poor prognosis (Fang et al., 2017; Fiskus et al., 2017). Sakamoto et al. (2015) recently found that KDM1A suppresses murine adipocytes mitochondrial respiration and maintains energy storage under obese conditions (Sakamoto et al., 2015). Targeting KDM1A by small molecule inhibitors, blocks cell proliferation in leukemia (Magliulo et al., 2018). It is therefore interesting to test whether targeting KDM1A, would block metabolic reprogramming in cancer cells driven by KDM1A. To better understand tumorigenesis, we must understand the metabolic reprogramming of cancerous cells. For this reason, the cancer metabolic reprogramming driven by KDM1A, has attracted much attention. Nevertheless, the precise contribution of KDM1A to cancer metabolism remains unclear.

Maes et al. have developed ORY-1001, a potent and selective inhibitor of KDM1A, for the inhibition of acute leukemia cell growth (Maes et al., 2018). But, the anti-cancer activity of ORY-1001 in lung cancer is unknown. In this study, we reported that KDM1A is highly expressed in lung cancer tissues and lung cancer cells and regulated cell proliferation. Furthermore, we found that ORY-1001 inhibited lung cancer cell proliferation, cell cycle and induced apoptosis by triggering the Warburg effect, by regulating HK2 expression. These results suggest the hypothesis that cancer cells are transmitted more on the glycolytic pathway than normal cells and targeting KDM1A may represent a promising approach for selectively causing cell proliferation in cancer cells.

MATERIALS AND METHODS

Cell Lines

H1299, H157, H1944, H226, and H460 cells were cultured in a RPMI 1,640 medium with 10% FBS at 37°C and 5% CO₂. The human lung adenocarcinoma epithelial cells A549, were gifted by Dr. Zhi Shi (Jinan University, Guangdong, China). The A549 cells were cultured in a Dulbecco Modified Eagle Medium (DMEM) with 10% FBS. Normal proliferating Human Bronchial Epithelial Cell Line (BEAS-2B) was gifted by Dr. Chenglai Xia (Guangzhou Medical University, Guangdong, China) and were cultured in a RPMI 1,640 medium with 10% FBS at 37°C and 5% CO₂.

Cell Proliferation Assay

For cell proliferation assay, 5×10^4 cells were seeded into 6-well plates and cultured at 37°C and 5% CO₂ for 12 h. The cells were then treated with ORY1001, with an increased concentration (80 and 160 μ M) or vehicle alone for 1, 2, 3, and 4 days, and the cell number was counted.

Colony Formation Assay

Eight hundred cells (H1299 and A549) were plated into 6-well plates and were cultured in a RPMI 1,640 or DMEM medium at 37°C and 5% CO₂, in a humidified incubator. The cells were then replenished with a fresh RPMI 1,640 or DMEM medium containing ORY1001 (80 and 160 μ M) after 10 days and incubated for another 5 days. The treated cells were washed with pre-warmed PBS three times, fixed with methanol for 20 min, and stained with crystal violet for

15 min. The residual crystal violet was then removed using double distilled H₂O, and the plates were then air-dried. The colony numbers were counted using Image plus software. Each experiment was assayed in triplicate with three independent experiments.

Apoptosis Assay

Cell apoptosis was determined by flow cytometry. Firstly, the cells were harvested and washed with PBS. Subsequently, an Annexin V fluorescein (FITC)/propidium iodide (PI) double staining solution was used on the cell sample, to detect apoptosis following the manufacturer's protocol. The samples were analyzed using the BD FACScalibur flow cytometer (BD Biosciences), and subsequent analyses were performed with FlowJo software. All assays were performed in triplicate.

Cell Cycle Assay

H1299 and A549 cells were seeded into 6-well plates and treated with 80 and 160 μ M ORY1001 for 48 h. The cells were then harvested, washed with PBS, centrifuged and fixed in cold 70% ethanol at 4°C for 12 h. The samples were washed with PBS after fixation to remove the ethanol. Subsequently, PBS containing 10 mg/mL propidium iodide (PI; Sigma-Aldrich) and RNase A (100 mg/mL, Solarbio) was added to the cell sample, at room temperature for 10 min under darkness. Finally, the samples were analyzed using the BD FACScalibur flow cytometer (BD Biosciences).

Western Blotting

Cells were lysed with lysis buffer [1.5 M NaCl, 1 M HEPES(pH = 7.0), 1%NP40, 0.1 M Na₄P₂O₇, 0.1 M NaF, 0.1 M Na₃VO₄, protease inhibitor] on ice for 30 min and then centrifuged at 12,000 rpm for 15 min at 4°C. Protein samples were loaded into 12% SDS-PAGE, then separated by running different Voltages, and transferred onto PVDF membranes (Millipore). The membranes were blocked with 5% non-fat milk for 2 h and then incubated overnight at 4°C, or at room temperature for 2 h with the primary antibody and for 1 h at room temperature with the secondary antibody. Signals were detected using a Luminol substrate solution.

Small Interference RNA Transfection

H1299 and A549 cells (2×10^5) were seeded into 6-well plates and cultured in a humidified incubator at 37°C and 5% CO₂ for 12 h. Cells were transfected with a siRNA control and three independent siRNA targeting KDM1A by TransIT LT1 (Mirus corporation-). Transfected cells were cultured for 48 h before being used for further experiments. The KDM1A siRNA target sequences were as follows: KDM1A siRNA-1: GCTCGA CAGTTACAAAGTT; KDM1A siRNA-2: GTTGGATAATCC AAAGATT; KDM1A siRNA-3: GAAGCTACATCTTACCTTA, and all siRNA sequences were purchased from the Ribobio corporation of Guangzhou.

Cell Metabolism Determination

The extracellular acidification rate (ECAR), was determined by the Seahorse XF96 Extracellular Flux Analyzer (Agilent

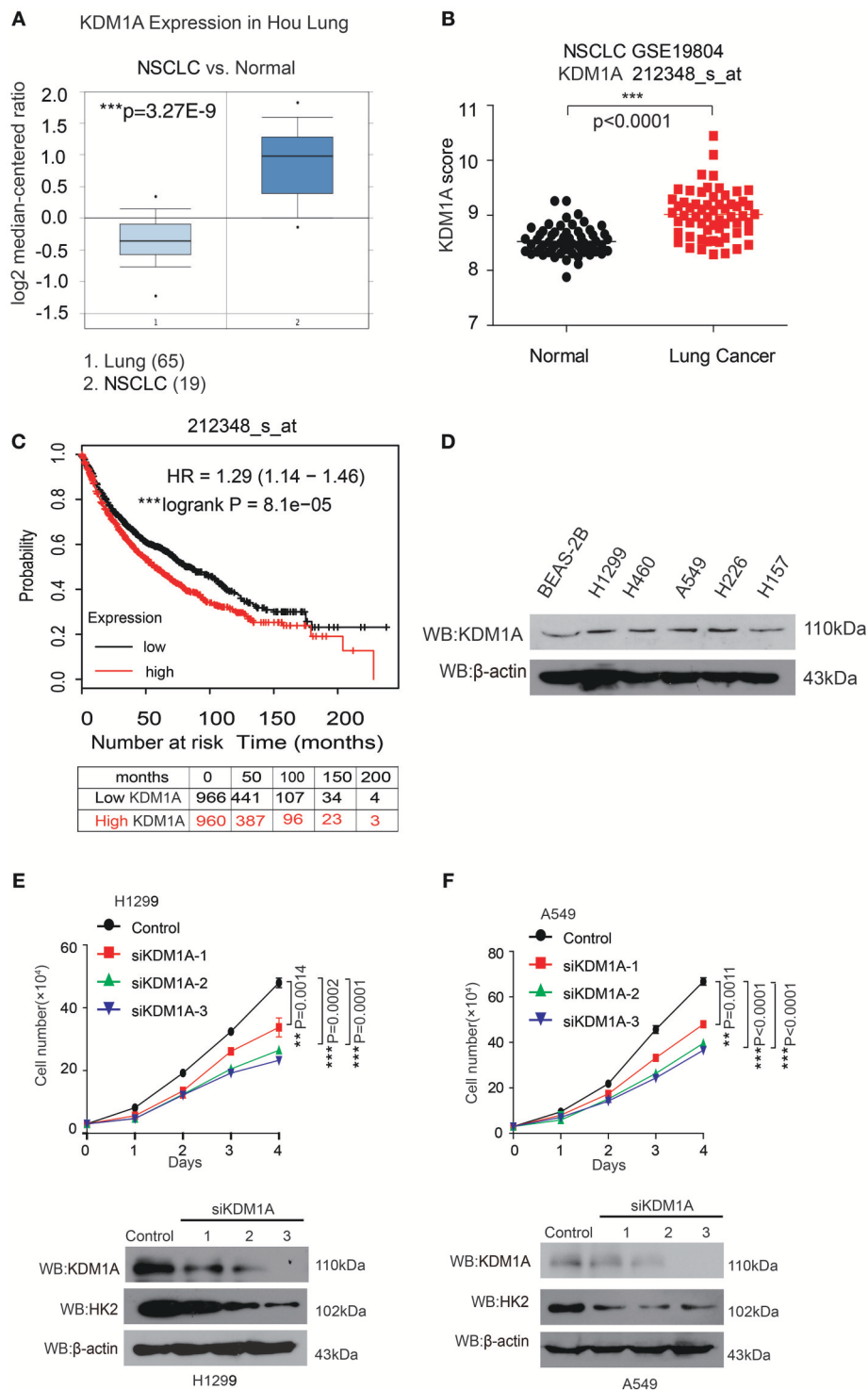


FIGURE 1 | KDM1A expression is evaluated in lung cancer and is important for cancer cell proliferation and tumor growth. **(A)** Oncomine data for the expression of KDM1A in lung and non-small cell lung cancer (NSCLC). **(B)** Expression of KDM1A in lung cancer tissues and matched non-cancerous, calculated from GEO profiles (GSE19804, $n = 60$). **(C)** Kaplan–Meier curves of overall survival in lung cancer patients with high and low expression of KDM1A, calculated from (<http://kmplot.com/analysis>). **(D)** KDM1A protein levels were analyzed in the majority of a spectrum of diverse human lung cancer cells, including H1944, H460, H1299, H157, H226, A549 cells, and normal proliferating Human Bronchial Epithelial Cell Line (BEAS-2B). **(E,F)** Cell proliferation rates determined by cell counting in human lung cancer H1299 and A549 cells with knockdown of KDM1A. The error bars represent mean values \pm SD from three replicates of each sample (*: $0.01 < p < 0.05$; **: $0.001 < p < 0.01$; *** $p < 0.001$).

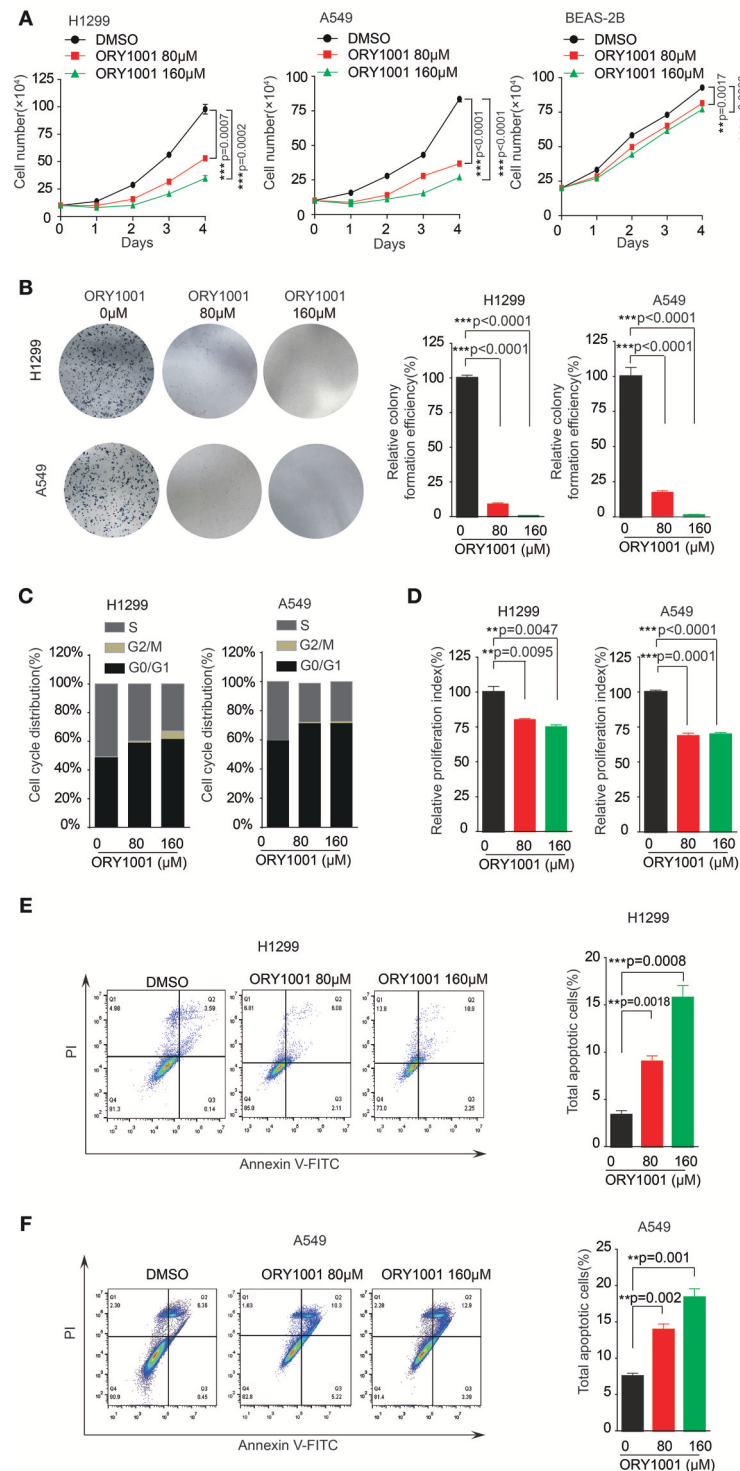


FIGURE 2 | Targeting KDM1A inhibits lung cancer cell proliferation and cell cycle. **(A)** Cell proliferation was determined in H1299, A549, and BEAS-2B cells in the presence of increasing concentrations of ORY-1001. **(B)** Colony formation was determined in H1299 and A549 cells in the presence of increasing concentrations of ORY-1001. **(C,D)** H1299 and A549 cells were treated with increasing concentrations of ORY-1001 for 48 h and stained with propidium iodide (PI) for flow cytometer analysis. **(C)** Bar charts of the cell cycle phases from three independent experiments were shown. **(D)** Cell proliferation index (PI) was calculated based on the indicated equation and is shown. **(E)** H1299 cells were treated with ORY-1001 at the indicating concentrations for 48 h, and then labeled with annexin V-FITC and PI for flow cytometer analysis. A set of representative dot plots of H1299 flow cytometer analysis were shown, and the bar charts show total apoptotic cells from three independent experiments. **(F)** A549 cells were treated with ORY-1001 at the indicating concentrations for 48 h, and then labeled with annexin V-FITC and PI for flow cytometer analysis. A set of representative dot plots of A549 flow cytometer analysis were shown, and the bar charts show total apoptotic cells from three independent experiments. The error bars represent mean values \pm SD from three replicates of each sample (*: $0.01 < p < 0.05$; **: $0.001 < p < 0.01$; *** $p < 0.001$).

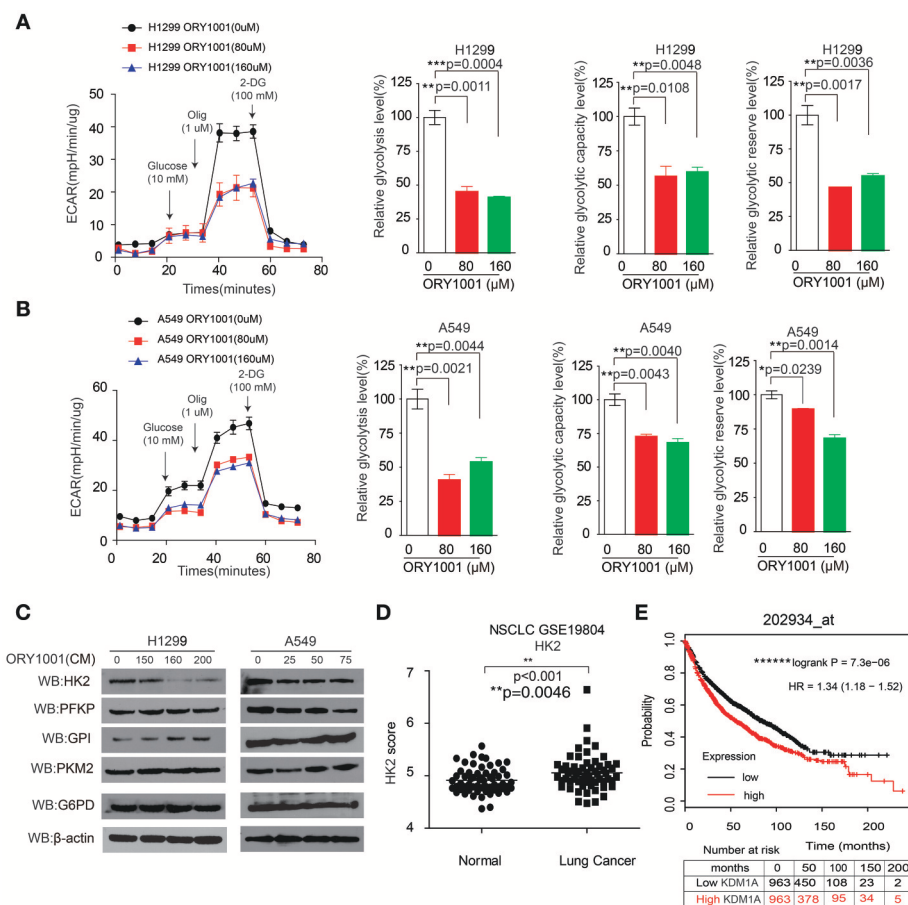


FIGURE 3 | KDM1A inhibition by ORY-1001 affects the Warburg effect in lung cancer cells. **(A,B)** ECAR rate (a proxy for the rate of glycolysis) was used to assess the glycolysis using a Seahorse 96XF extracellular flux analyzer following sequential addition of glucose (10 mM), oligomycin (1.0 μM), and 2-DG (100 mM) as arrows indicated in H1299 and A549 cells in the presence of increasing concentrations of ORY-1001. **(C)** Western blotting assay for the expression of glycolytic enzymes in H1299 and A549 cells in the presence of ORY-1001. **(D)** Expression of HK2 in lung cancer tissues and matched non-cancerous, calculated from GEO profiles (GSE19804, $n = 60$). **(E)** Kaplan–Meier curves of overall survival in lung cancer patients with high and low expression of HK2, calculated from (<http://kmplot.com/analysis/>). The error bars represent mean values \pm SD from three replicates of each sample (*: $0.01 < p < 0.05$; **: $0.001 < p < 0.01$; ns, not significant).

Technologies, Santa Clara, CA, USA) according to the manufacturer's protocol. Briefly, H1299 and A549 cells were seeded into 6-well plates and cultured in a humidified incubator at 37°C and 5% CO₂ for 12 h. Cells treated with ORY1001 (80 and 160 μM) or vehicle alone for 24 h, were then seeded into 96-well cell plates. At the same time, the calibration plate was incubated at 37°C, in a non-CO₂ incubator for 12 h. To determine the cellular aerobic glycolysis profile, ECAR was estimated after sequential injections of glucose (10 mM), oligomycin (1 μM), and 2-DG (100 mM). Protein concentration was quantified using the BCA kit to normalize the data and plotted as the mean \pm SD.

Bioinformatics Analysis

The public Gene Expression Omnibus datasets (GSE19804) and the human protein atlas (<https://www.proteinatlas.org>) dataset were used for bioinformatics analysis. Kaplan–Meier Plotter (<http://kmplot.com/analysis/>) was used for overall survival.

Statistical Analysis

Statistical analyses were performed using the Student's *t*-test. All data were obtained from three independent experiments performed in triplicate and were presented as the mean \pm SD. Statistical analyses of the KM curve were performed using the Log-Rank test. We considered a $P < 0.05$, to indicate a statistically significant difference.

RESULTS

KDM1A Expression Is Elevated in Lung Cancer and Regulates Cell Proliferation

In an effort to explore the role of KDM1A in lung cancer, we analyzed the correlation between KDM1A expression levels and the outcomes of lung cancer patients. We first examined the expression of KDM1A in lung cancer tissues using Oncomine data. **Figure 1A** shows that KDM1A was increased in non-small cell lung cancer (NSCLC) tissue (19) compared with lung tissue

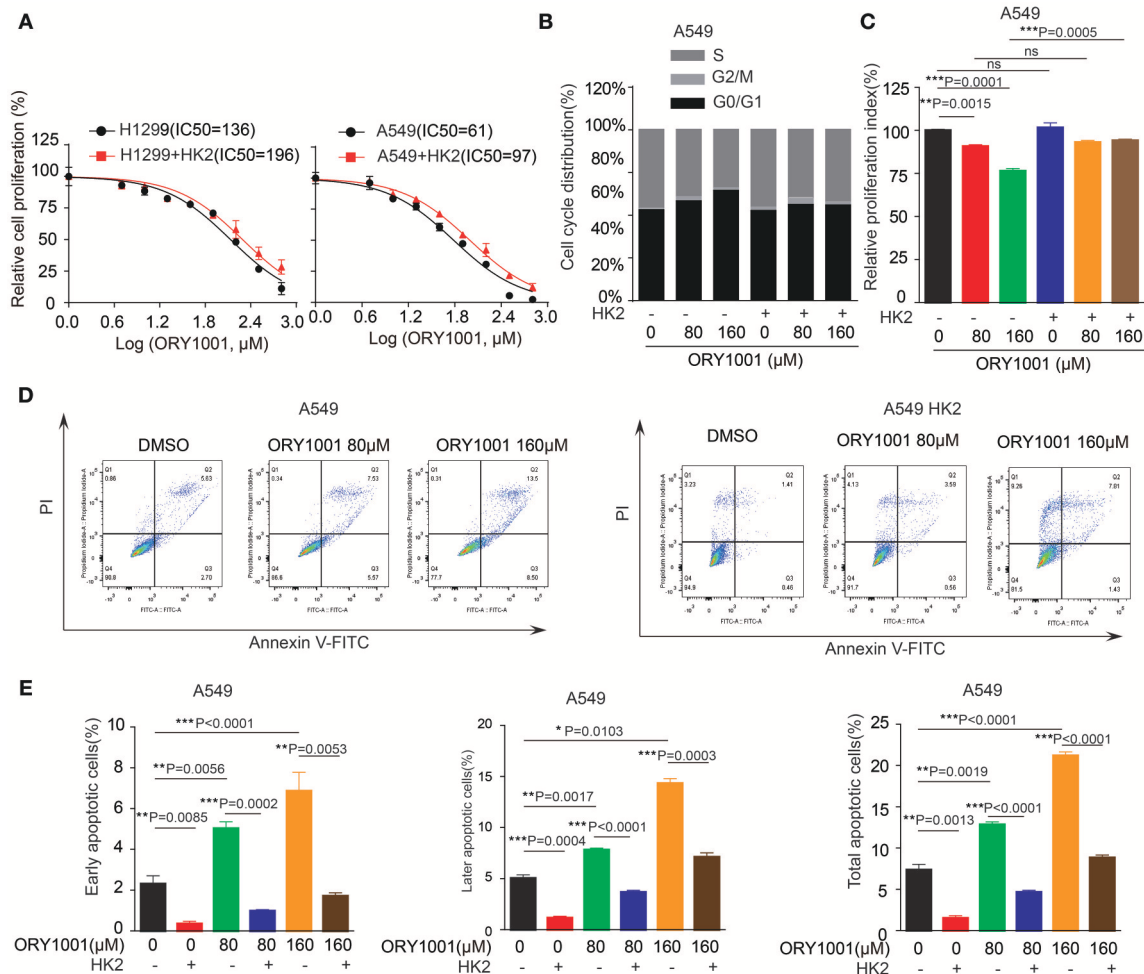


FIGURE 4 | Overexpress HK2 would rescue the effect of ORY-1001 on cells proliferation, cell cycle and apoptosis. **(A)** Cell proliferation was determined in H1299 and A549 cells in the presence of increasing concentrations of ORY-1001 when overexpress HK2. **(B,C)** HK2 overexpress A549 cells were treated with increasing concentrations of ORY-1001 for 48 h and stained with propidium iodide (PI) for flow cytometer analysis. **(B)** Bar charts of the cell cycle phases from three independent experiments were shown. **(C)** Cell proliferation index (PI) was calculated based on the indicated equation and is shown. **(D,E)** HK2 overexpress A549 cells were treated with ORY-1001 at the indicating concentrations for 48 h, and then labeled with annexin V-FITC and PI for flow cytometer analysis. **(D)** A set of representative dot plots of A549 flow cytometer analysis was shown, **(E)** The apoptosis bar charts from three independent experiments were shown. The error bars represent mean values \pm SD from three replicates of each sample (*: $0.01 < p < 0.05$; **: $0.001 < p < 0.01$; ***: $p < 0.001$).

(65) (Hou et al., 2010). We also used Gene Expression Omnibus (GEO) profiles (GSE19804) to analyze KDM1A expression and confirmed that the expression of KDM1A was higher in cancer tissues than in non-tumors (Figure 1B). To further substantiate the importance of KDM1A expression in lung cancer progression, we also used the Kaplan-Meier survival analysis in lung cancer patients, based on the publicly available Kaplan-Meier Plotter (<http://kmplot.com/analysis/> (KDM1A: accession number 212348_s_at). Higher levels of KDM1A (red) are significantly correlated with reduced overall survival compared to low KDM1A levels (black) (Figure 1C). To validate our findings using the publish data, we also checked the expression of KDM1A in the various human lung cancer cells, including H1944, H460, H1299, H157, and H226 cells, compared to the normal proliferating Human Bronchial Epithelial Cell

Line (BEAS-2B), but there were not significant differences (Figure 1D).

To determine the role of KDM1A in lung cancer cell proliferation, we found that knockdown of KDM1A by siRNA transient transfection, resulted in decreased cell proliferation in the human lung cancer H1299 and A549 cells (Figures 1E,F). Together these data demonstrated that KDM1A was highly expressed in lung cancer and correlated with overall survival, and that KDM1A plays an important role in cancer cell proliferation, suggesting that KDM1A is a promising anti-cancer target.

Targeting KDM1A Inhibit Lung Cancer Cell Proliferation and Cell Cycle

ORY-1001 was identified as a potent and selective covalent inhibitor of KDM1A for the inhibition cell proliferation of

acute leukemia. In this study, we explored the role of ORY-1001 in lung cancer. Firstly, ORY-1001 treatment resulted in a decreased cell proliferation of lung cancer cells including H1299 and A549 cells, in a time and dose-dependent manner, but did not significantly affect normal BEAS-2B cell proliferation (Figure 2A). Secondly, the colony formation assays revealed that the inhibition of KDM1A by ORY-1001 reduced the colony formation of H1299 and A549 cells (Figure 2B). Thirdly, ORY-1001 treatment resulted in the decreased cell cycle of H1299 and A549 cells (Figures 2C,D). Together these data demonstrated that ORY-1001 treatment suppressed lung cancer cell proliferation, colony formation and the cell cycle. To evaluate the anti-survival effect of KDM1A inhibition by ORY-1001, H1299, and A549 cells were treated with ORY-1001 at different concentrations, and apoptosis of the cells were analyzed by flow cytometry. The results revealed that ORY-1001 induced robust apoptosis in H1299 and A549 cells in a dose-dependent manner (Figures 2E,F). Together these results demonstrated that ORY-1001 inhibited lung cancer cell growth and induced apoptosis.

KDM1A Inhibition by ORY-1001 Affects the Warburg Effect in Lung Cancer Cells

Next, we attempted to verify whether the effect of KDM1A inhibition by ORY-1001 on the Warburg effect, involved lung cancer cell proliferation and apoptosis. KDM1A inhibition by ORY-1001 decreased glycolysis in H1299 and A549 cells (Figures 3A,B). We further assessed the various parameters of the glycolysis function by analyzing ECAR data at each time point. Our results showed that glycolysis, glycolytic capacity and the glycolytic reserve were markedly decreased in H1299 and A549 cells treated with ORY-1001 (Figures 3A,B). In addition, the protein levels of HK2, were decreased in the ORY-1001 treated cells (Figure 3C). These results suggest that ORY-1001 decreased glycolysis in lung cancer cells by decreasing HK2 expression.

In an effort to determine the role of HK2 in lung cancer mediated by KDM1A, we analyzed the correlation between HK2 expression levels and the outcomes of lung cancer patients. We also analyzed HK2 expression utilizing Gene Expression Omnibus (GEO) profiles (GSE19804) (Figure 3D). To further substantiate the importance of HK2 expression in lung cancer progression, we also used the Kaplan-Meier survival analysis in lung cancer patients based on the publicly available Kaplan-Meier Plotter (<http://kmplot.com/analysis/>) (HK2: accession number 202934_at). Patients with higher HK2 levels (red) were significantly correlated with reduced overall survival compared to patients with lower HK2 levels (black) (Figure 3E). Together, these data suggest that ORY-1001 affects the Warburg effect in lung cancer cells by targeting KDM1A, leading to the regulation of HK2 expression.

ORY-1001 Affects Lung Cancer Cell Proliferation and Apoptosis Through Regulating HK2 Expression

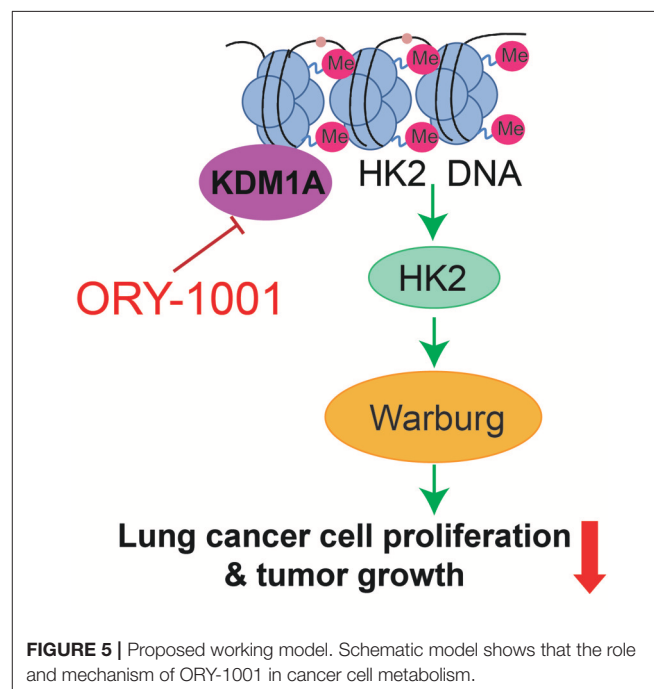
We wanted to explore the mechanism of how ORY-1001 inhibits lung cancer cell proliferation and induces apoptosis. Firstly,

ORY-1001 treatment resulted in decreased cell proliferation of lung cancer cells, including H1299 and A549 cells, in a time and dose-dependent manner, but this effect was rescued in H1299 and A549 cells, when HK2 was over expressed (Figure 4A). At the same time, the decreased cell cycle of lung cancer cells was also rescued by the overexpression of HK2 (Figures 4B,C). Thirdly, ORY-1001 induced robust apoptosis in H1299 and A549 cells, in a dose-dependent manner and was also rescued by the overexpression of HK2 (Figures 4D,E). Together, these results suggest that ORY-1001 affects lung cancer cell proliferation and apoptosis through regulating HK2 expression.

DISCUSSION

The Warburg effect describes cancer cells with high rates of aerobic glycolysis and increased glucose uptake, which are hallmarks of cancer (Cairns et al., 2011; Zheng et al., 2017; Zhong et al., 2018). The increased aerobic glycolysis rate gives cancer cells a growth advantage, which provides energy and intermediates the rapid growth of a cancer cell. In this study, we established the KDM1A-HK2 axis as a critical regulatory pathway in regulating the Warburg effect. KDM1A directly promotes the expression of key glycolytic genes that facilitate the Warburg effect, which involves the regulation of cell proliferation, cell cycle and apoptosis. Our data indicated that KDM1A is a key factor in the regulation of the Warburg effect and also indicated the causal role of KDM1A in glycolysis regulation mediated by HK2 expression (Figure 5).

Cancer metabolism has been extensively studied, and recent studies have suggested that targeting the enzymes in the



metabolic pathways for cancer therapy, seems appealing at first glance. Regulation of cell metabolism to support all fundamental cellular activities is essential for the maintenance of cellular redox homeostasis, reactive oxygen species, growth, proliferation and migration. In the current study, we demonstrated that KDM1A is commonly upregulated in lung cancer and is important for cell proliferation. Using different lung cancer cell lines, we showed that targeting KDM1A by ORY-1001 can facilitate cell proliferation, cell cycle and apoptosis. For the first time we revealed the role that targeting KDM1A plays in controlling cell proliferation, the cell cycle and the role it place in inducing apoptosis, through the promotion of the Warburg effect by regulating the expression of the key enzyme HK2, which is necessary for cell proliferation and rapidly growing tumors. However, we did not exclude the possibility that KDM1A directly demethylates the enzymes in the glycolysis pathway, regulating the Warburg effect by controlling their enzyme activity.

From a translational point of view, therapeutic targeting of KDM1A might be an effective therapeutic option for the advanced growth of lung cancer, as it is sufficient to block the glycolysis signaling pathway. Taken together, our data clearly indicated that targeting the KDM1A would rewire the Warburg effect and inhibit cancer

cell proliferation, by regulating the key enzyme HK2 expression.

AUTHOR CONTRIBUTIONS

ZL and XZ performed and analyzed all the experiments. JL and LL drafted the work for important intellectual content. YG edited the language and figures. SZ and CS wrote the manuscript and designed the study.

FUNDING

We are grateful to grants from the Startup Fund for Distinguished Scholars from Jinan University, National Nature Science Foundation of China (81672781 and 81702746), China Postdoctoral Science Foundation (2017M612839), and the Fundamental Research Funds for the Central Universities (21616323, 21617433). This work was also supported by The Program from the Science and Technology Department of Guangdong Province of China (Grant 2017A030313890) and the Science and Technology Program of Guangzhou (Grant 201807010003). This work was also supported by the Program of Introducing Talents of Discipline to Universities (111 Project, No. B16021).

REFERENCES

- Cairns, R. A., Harris, I. S., and Mak, T. W. (2011). Regulation of cancer cell metabolism. *Nat. Rev. Cancer* 11, 85–95. doi: 10.1038/nrc2981
- Fan, J., Shan, C., Kang, H. B., Elf, S., Xie, J., Tucker, M., et al. (2014). Tyr phosphorylation of PDP1 toggles recruitment between ACAT1 and SIRT3 to regulate the pyruvate dehydrogenase complex. *Mol. Cell* 53, 534–548. doi: 10.1016/j.molcel.2013.12.026
- Fang, J., Ying, H., Mao, T., Fang, Y., Lu, Y., Wang, H., et al. (2017). Upregulation of CD11b and CD86 through LSD1 inhibition promotes myeloid differentiation and suppresses cell proliferation in human monocytic leukemia cells. *Oncotarget* 8, 85085–85101. doi: 10.18632/oncotarget.18564
- Fiskus, W., Sharma, S., Shah, B., Portier, B. P., Devaraj, S. G. T., Liu, K., et al. (2017). Highly effective combination of LSD1 (KDM1A) antagonist and pan-histone deacetylase inhibitor against human AML cells. *Leukemia* 31:1658. doi: 10.1038/leu.2017.77
- Hayami, S., Kelly, J. D., Cho, H. S., Yoshimatsu, M., Unoki, M., Tsunoda, T., et al. (2011). Overexpression of LSD1 contributes to human carcinogenesis through chromatin regulation in various cancers. *Int. J. Cancer* 128, 574–586. doi: 10.1002/ijc.25349
- Hou, J., Aerts, J., Den Hamer, B., Van Ijcken, W., Den Bakker, M., Riegman, P., et al. (2010). Gene expression-based classification of non-small cell lung carcinomas and survival prediction. *PLoS ONE* 5:e10312. doi: 10.1371/journal.pone.0010312
- Jie, D., Zhongmin, Z., Guoqing, L., Sheng, L., Yi, Z., Jing, W., et al. (2013). Positive expression of LSD1 and negative expression of E-cadherin correlate with metastasis and poor prognosis of colon cancer. *Dig. Dis. Sci.* 58, 1581–1589. doi: 10.1007/s10620-012-2552-2
- Liu, H., Liu, Y., and Zhang, J. T. (2008). A new mechanism of drug resistance in breast cancer cells: fatty acid synthase overexpression-mediated palmitate overproduction. *Mol. Cancer Ther.* 7, 263–270. doi: 10.1158/1535-7163.MCT-07-0445
- Lv, T., Yuan, D., Miao, X., Lv, Y., Zhan, P., Shen, X., et al. (2012). Over-expression of LSD1 promotes proliferation, migration and invasion in non-small cell lung cancer. *PLoS ONE* 7:e35065. doi: 10.1371/journal.pone.0035065
- Maes, T., Mascaró, C., Tirapu, I., Estiarte, A., Ciceri, F., Lunardi, S., et al. (2018). ORY-1001, a potent and selective covalent KDM1A inhibitor, for the treatment of acute leukemia. *Cancer Cell* 33, 495–511 e412. doi: 10.1016/j.ccell.2018.02.002
- Magliulo, D., Bernardi, R., and Messina, S. (2018). Lysine-specific demethylase 1A as a promising target in acute myeloid leukemia. *Front. Oncol.* 8:255. doi: 10.3389/fonc.2018.00255
- Sakamoto, A., Hino, S., Nagaoka, K., Anan, K., Takase, R., Matsumori, H., et al. (2015). Lysine demethylase LSD1 coordinates glycolytic and mitochondrial metabolism in hepatocellular carcinoma cells. *Cancer Res.* 75, 1445–1456. doi: 10.1158/0008-5472.CAN-14-1560
- Schildhaus, H. U., Riegel, R., Hartmann, W., Steiner, S., Wardelmann, E., Merkelbach-Bruse, S., et al. (2011). Lysine-specific demethylase 1 is highly expressed in solitary fibrous tumors, synovial sarcomas, rhabdomyosarcomas, desmoplastic small round cell tumors, and malignant peripheral nerve sheath tumors. *Hum. Pathol.* 42, 1667–1675. doi: 10.1016/j.humpath.2010.12.025
- Sehrawat, A., Gao, L., Wang, Y., Bankhead, A. III, Mcweeney, S. K., King, C. J., et al. (2018). LSD1 activates a lethal prostate cancer gene network independently of its demethylase function. *Proc. Natl. Acad. Sci. U. S. A.* 115, E4179–E4188. doi: 10.1073/pnas.1719168115
- Wang, J. B., Erickson, J. W., Fuji, R., Ramachandran, S., Gao, P., Dinavahi, R., et al. (2010). Targeting mitochondrial glutaminase activity inhibits oncogenic transformation. *Cancer Cell* 18, 207–219. doi: 10.1016/j.ccr.2010.08.009
- Yu, Y., Wang, B., Zhang, K., Lei, Z., Guo, Y., Xiao, H., et al. (2013). High expression of lysine-specific demethylase 1 correlates with poor prognosis of patients with esophageal squamous cell carcinoma. *Biochem. Biophys. Res. Commun.* 437, 192–198. doi: 10.1016/j.bbrc.2013.05.123
- Zhao, Y., Butler, E. B., and Tan, M. (2013). Targeting cellular metabolism to improve cancer therapeutics. *Cell Death Dis.* 4:e532. doi: 10.1038/cddis.2013.60
- Zhao, Y., Liu, H., Liu, Z., Ding, Y., Ledoux, S. P., Wilson, G. L., et al. (2011). Overcoming trastuzumab resistance in breast cancer by targeting dysregulated glucose metabolism. *Cancer Res.* 71, 4585–4597. doi: 10.1158/0008-5472.CAN-11-0127

- Zhao, Z. K., Yu, H. F., Wang, D. R., Dong, P., Chen, L., Wu, W. G., et al. (2012). Overexpression of lysine specific demethylase 1 predicts worse prognosis in primary hepatocellular carcinoma patients. *World J. Gastroenterol.* 18, 6651–6656. doi: 10.3748/wjg.v18.i4.5.6651
- Zheng, W., Feng, Q., Liu, J., Guo, Y., Gao, L., Li, R., et al. (2017). Inhibition of 6-phosphogluconate dehydrogenase reverses cisplatin resistance in ovarian and lung cancer. *Front. Pharmacol.* 8:421. doi: 10.3389/fphar.2017.00421
- Zhong, X. Y., Yuan, X. M., Xu, Y. Y., Yin, M., Yan, W. W., Zou, S. W., et al. (2018). CARM1 methylates GAPDH to regulate glucose metabolism and is suppressed in liver cancer. *Cell Rep.* 24, 3207–3223. doi: 10.1016/j.celrep.2018.08.066
- Zhou, M., Zhao, Y., Ding, Y., Liu, H., Liu, Z., Fodstad, O., et al. (2010). Warburg effect in chemosensitivity: targeting lactate dehydrogenase-a re-sensitizes

taxol-resistant cancer cells to taxol. *Mol. Cancer* 9:33. doi: 10.1186/1476-4598-9-33

Conflict of Interest Statement: The authors declare that the research was conducted in the absence of any commercial or financial relationships that could be construed as a potential conflict of interest.

Copyright © 2018 Lu, Guo, Zhang, Li, Li, Zhang and Shan. This is an open-access article distributed under the terms of the Creative Commons Attribution License (CC BY). The use, distribution or reproduction in other forums is permitted, provided the original author(s) and the copyright owner(s) are credited and that the original publication in this journal is cited, in accordance with accepted academic practice. No use, distribution or reproduction is permitted which does not comply with these terms.



CDH1 Gene and Hereditary Diffuse Gastric Cancer Syndrome: Molecular and Histological Alterations and Implications for Diagnosis And Treatment

Wenyi Luo¹, Faysal Fedda¹, Patrick Lynch² and Dongfeng Tan^{1*}

¹ Department of Pathology, The University of Texas MD Anderson Cancer Center, Houston, TX, United States, ² Department of Gastroenterology, Hepatology and Nutrition, The University of Texas MD Anderson Cancer Center, Houston, TX, United States

OPEN ACCESS

Edited by:

Dong-Hua Yang,
St. John's University, United States

Reviewed by:

Valli De Re,
Centro di Riferimento Oncologico di
Aviano (CRO), Italy
Yuji Naito,
Kyoto Prefectural University of
Medicine, Japan

*Correspondence:

Dongfeng Tan
dtan@mdanderson.org

Specialty section:

This article was submitted to
Experimental Pharmacology and Drug
Discovery,
a section of the journal
Frontiers in Pharmacology

Received: 14 October 2018

Accepted: 19 November 2018

Published: 05 December 2018

Citation:

Luo W, Fedda F, Lynch P and Tan D
(2018) CDH1 Gene and Hereditary
Diffuse Gastric Cancer Syndrome:
Molecular and Histological Alterations
and Implications for Diagnosis And
Treatment. *Front. Pharmacol.* 9:1421.
doi: 10.3389/fphar.2018.01421

Gastric cancer, a group of common malignancies, results in the most cancer mortality worldwide after only lung and colorectal cancer. Although familial gastric cancers have long been recognized, it was not until recently that they were discovered to be associated with mutations of specific genes. Mutations of *CDH1*, the gene encoding E-cadherin, are the most common germline mutations detected in gastric cancer and underlie hereditary diffuse gastric cancer (HDGC) syndrome. All reported HDGCs are the pure diffuse type by Lauren classification and are associated with dismal prognosis once the tumor invades the submucosa. Because *CDH1* germline mutations are inherited in an autosomal-dominant fashion and have high penetrance, the International Gastric Cancer Linkage Consortium (IGCLC) developed criteria to facilitate the screening of *CDH1* mutation carriers; these criteria have been proven to have excellent sensitivity and specificity. Recent histologic studies suggest that HDGC progresses through several stages. Even when the tumor becomes “invasive” in lamina propria, it may stay indolent for a long time. However, the molecular mechanisms that induce the transitions between stages and determine the length of the indolent phase remain to be determined. Although the standard management for *CDH1* mutation carriers is prophylactic total gastrectomy, many questions must be answered before the surgery can be done. These include the optimal surveillance strategy, the best strategy to choose surgical candidates, and the ideal time to perform surgery. In addition to increasing the risk of gastric cancer, *CDH1* germline mutations also increase the risk of invasive lobular carcinoma of the breast, and possibly colorectal adenocarcinoma, and are associated with blepharocheilodontic syndrome (a congenital development disorder). However, the optimal management of these conditions is less established owing to insufficient data regarding the risk of cancer development. This review focuses on molecular and histological findings in HDGC, as opposed to sporadic diffuse gastric cancer, and their implications for the management of *CDH1* mutation carriers and the diagnosis and treatment of HDGC. Other conditions associated with *CDH1* germline mutations and future research directions are also discussed.

Keywords: CDH1 cadherin-1 gene, lobular breast cancer, management, familial gastric cancer (FGC), signet ring cell carcinoma

OVERVIEW OF HEREDITARY DIFFUSE GASTRIC CANCER

Gastric cancer is the fifth most common malignancy in the world and the third leading cause of cancer death in both sexes worldwide after lung cancer and colorectal cancer (Ferlay et al., 2013). Although the overall incidence and mortality of non-cardia gastric cancer has declined over the past four decades, the rates are increasing among persons younger than 50 years (Wang et al., 2018); these increases are associated with the rapidly increased recognition of diffuse gastric cancer from 1978 to 2000, after this recognition decreased slightly from 2001 to 2005 (Wu et al., 2009). Gastric cancer in the young is associated with a high incidence of poorly-differentiated and signet ring cell morphology and demonstrates advanced stage at presentation and poor survival even with surgical intervention (Rona et al., 2017).

Familial clustering of gastric cancer has long been noticed (Maimon and Zininger, 1953). Approximately 8–30% of gastric cancer patients have a positive family history (van der Post et al., 2015a). However, not all these cancers are hereditary. Countries with a high incidence of sporadic gastric cancer, such as Japan and Korea, have a lower frequency of germline mutations in familial gastric cancers than low-incidence countries do (Lee et al., 2014). The cause of familial clustering in high-incidence countries is more likely environmental than hereditary.

Approximately 1–3% of gastric cancers are truly hereditary (Fitzgerald et al., 2010). The underlying genetic alteration in 60% of cases remains unknown (Gaston et al., 2014). Gastric cancer predisposition has been linked to familial cancer syndromes, including Lynch syndrome (Capelle et al., 2010), Peutz-Jeghers syndrome (van Lier et al., 2010), Li-Fraumeni syndrome (Masciari et al., 2011), familial adenomatous polyposis syndrome (Fornasari et al., 2018) and recently described gastric adenocarcinoma and proximal polyposis syndrome of the stomach (Worthley et al., 2012). Similar to sporadic gastric cancer, gastric cancer in these syndromic patients can be either intestinal or diffuse type. Diffuse type gastric cancer does not appear to be overrepresented in these syndromes (Fewings et al., 2018). A higher frequency of deleterious germline *ATM* mutations has been detected in gastric cancer patients; however, the histologic types have not been studied (Huang et al., 2015). Gastric cancer containing a significant diffuse component can occur in patients bearing certain germline mutations. For example, *MAP3K6* germline mutations have also been associated with familial gastric cancer, and the gastric cancers associated with *MAP3K6* predominantly have a signet ring cell morphology, although a minor glandular component has been described (Gaston et al., 2014). Some syndromic patients develop pure diffuse type gastric cancer, referred to as hereditary diffuse gastric carcinoma (HDGC). In addition to *CDH1*, the gene encoding E-cadherin, germline pathogenic variants in *PALB2* and other cancer-predisposing genes have been identified by whole-exome sequencing of HDGC families (Fewings et al., 2018). The clinical implications of these genes remain to be elucidated.

HDGC accounts for 1–3% of gastric cancers (Guilford et al., 1998). Although *CDH1* somatic mutations are present in up to 50% of sporadic diffuse gastric carcinoma (SDGC) (Becker et al., 1994) and epigenetic inactivation of *CDH1* had been detected in several tumor types (Yoshiura et al., 1995), it was not until 1998 that Guilford (Guilford et al., 1998) reported the presence of a *CDH1* mutation in a large kindred from New Zealand with early-onset diffuse gastric cancer. This seminal study, for the first time, established the pathogenic role of *CDH1* mutations in HDGC. *CDH1* germline mutations are detected in approximately 25% of HDGC patients and are inherited in an autosomal-dominant fashion (Caldas et al., 1999). The estimated cumulative incidence of gastric cancer by age 80 years is 70% in male carriers and 56% in female carriers. In addition to having an increased risk of gastric cancer, *CDH1* mutation carriers also have an increased risk of lobular breast carcinoma. The estimated cumulative incidence of lobular breast cancer in female carriers is as high as 60% (Fitzgerald et al., 2010; Guilford et al., 2010; Hansford et al., 2015). HDGC patients with germline *CDH1* mutations have lower 1 and 5 years survival rates (36 and 4%, respectively) than HDGC patients without germline *CDH1* mutations do (48 and 13%, respectively) (van der Post et al., 2015a), emphasizing the importance of screening for *CDH1* germline mutations (Benusiglio et al., 2015).

The International Gastric Cancer Linkage Consortium (IGCLC) defined the clinical criteria to select patients eligible for *CDH1* germline mutations: (1) two or more documented cases of gastric cancer in first- or second-degree relatives regardless of age, with at least one confirmed diffuse gastric cancer; (2) diffuse gastric cancer before age 40 years without a family history; or (3) families with diagnoses of both diffuse gastric cancer and lobular breast carcinoma, at least one before age 50 years (van der Post et al., 2015b). These criteria have a sensitivity of 0.79–0.89, specificity of 0.70, positive predictive value of 0.14–0.19, and negative predictive value of 0.97 (Benusiglio et al., 2015; van der Post et al., 2015a). One study showed that HDGC patients without a known *CDH1* mutation diagnosed by multigene cancer panel before surgery were more likely to have metastatic disease and die of their disease than were patients with known *CDH1* mutation status (Moslim et al., 2018), suggesting that genetic counseling and detection of *CDH1* mutations in asymptomatic carriers improves HDGC patient survival.

This review will discuss current molecular and histological findings in HDGC, as opposed to SDGC, and their implications for the management of *CDH1* mutation carriers and the diagnosis and treatment of HDGC. Other conditions associated with *CDH1* germline mutations and future research directions will also be discussed briefly.

MOLECULAR PATHOGENESIS, CELLULAR ORIGIN, AND INITIATION

The gene *CDH1*, the coding gene for E-cadherin, is located on chromosome 16q22.1 and consists of 16 exons (Berx et al., 1995). More than 100 *CDH1* pathogenic germline variants have been described in HDGC families (Hansford et al., 2015), and

they are scattered across the entire gene, including introns and each of 16 exons (Corso et al., 2012; Melo et al., 2017; Li et al., 2018). A minority (27%) of the reported pathogenic mutations have been reported in multiple families, likely owing to a common ancestor or mutation in hot spots (Hansford et al., 2015; Li et al., 2018). Cases of sporadic gastric cancer with pathologic germline mutations have also been reported (Garziera et al., 2013). Overall, the most common mutations are small insertions and deletions (35%). Other mutations include nonsense mutations (16%), splice site mutations (16%), and large exon deletions and missense mutations (28%) (Guilford et al., 2010). Phenotype is not correlated with the location or type of germline *CDH1* mutation (Guilford et al., 2010). In particular, genotype is not correlated with the presence of lobular breast cancer in HDGC families (Schrader et al., 2008).

E-cadherin is a member of the cadherin family, which consists of a group of glycoproteins that mediate cell-cell adhesion in a calcium-dependent manner (Takeichi, 1991). Mature E-cadherin has an ectodomain consisting of five tandem repeats, a transmembrane domain, a single transmembrane domain, and a cytoplasmic domain (Takeichi, 1995). The extracellular domain is critical for cell-cell adhesion, correct folding, and dimerization (Shapiro et al., 1995; Nagar et al., 1996). The cytoplasmic domain of E-cadherin interacts with β -, p120-, and α -catenins anchored to the actin cytoskeleton (Blaschuk et al., 1990). The interaction with actin is required for membrane deformation processes such as endocytosis, exocytosis, autophagy and receptor/channel recycling, and is involved in cell membrane maintenance, tension, ion channel activity among others (Gumbiner, 1996; Godwin et al., 2018). E-cadherin deficiency undermines the efficiency of these different processes and potentially cell survivability (Godwin et al., 2018). E-cadherin plays an important role in blastomere adhesion during development, which polarizes the cells and allows differentiation to occur (Fleming et al., 1992). In normal adult tissue, E-cadherin is involved in the maintenance and homeostasis of the epithelium (Gumbiner, 1996). In addition to its structural role, E-cadherin can also transduce signals from the extracellular domain through the cytoplasmic tail into the nucleus to alter gene expression (Bershadsky, 2004). The reduction or complete absence of E-cadherin, which has been detected in many cancer types, is associated with loss of epithelial morphology and increased invasiveness through epithelial-mesenchymal transition (Berx et al., 1998; Machado et al., 1999) and is correlated with high grade, advanced stage, and poor prognosis (Guilford, 1999).

Reduced or absent E-cadherin expression is seen in both the *in situ* and invasive components of HDGC, suggesting that inactivation of E-cadherin is an early event (Carneiro et al., 2004). E-cadherin loss generally correlates with the identification of an alteration of the second *CDH1* allele (i.e., a second hit) (Barber et al., 2008a). The most frequent second hit inactivation mechanism is *CDH1* promoter hypermethylation, which occurs in approximately 50% of primary tumors, whereas a second mutation or loss of heterozygosity is less frequently identified (Grady et al., 2000; Oliveira et al., 2009). The methylation is allele-specific and is uncommon in HDGC patients without *CDH1*

germline mutations (Barber et al., 2008a). In patients with *CDH1* germline mutations, methylation occurs only when the wild-type allele is methylated (Grady et al., 2000). The trigger of the second hit remains unclear. The normal expression of E-cadherin in tissue between tumor foci and the variable expression levels of E-cadherin between HDGC tumor foci suggest that these tumor foci are multiclonal and develop independently (Charlton et al., 2004). Therefore, certain environmental factors affecting the entire gastric mucosa may be present as a trigger. However, the well-characterized risk factor for sporadic gastric cancer, *Helicobacter pylori*, together with other lesions commonly seen in the background of sporadic gastric cancer, are rarely detected in the total gastrectomy specimens from asymptomatic HDGC patients (Carneiro et al., 2004; Humar and Guilford, 2009; Rocha et al., 2018).

Different from other tumor repressors, complete loss of *CDH1* expression is not sufficient for the development of invasive carcinoma, as has been demonstrated in transgenic animal models. Conditional knockout of *CDH1* in mouse stomach induces signet ring-like cells in stroma (analogous to intramucosal signet ring cell carcinoma) but not the development of carcinoma invading into submucosa (Mimata et al., 2011). Other modifying genes, such as *Smad4* and *p53*, are required for aggressive diffuse gastric cancer or metastasis to occur in mice (Pereira et al., 2006; Park et al., 2014, 2018). Similar findings were also reported in lobular mammary carcinoma (Derksen et al., 2006). These findings recapitulated those in humans, in which lesions of various morphologies are seen, with some confined within basement membrane (meeting the conventional definition of carcinoma *in situ*), some existing in the lamina propria, and others invading into submucosa. Intramucosal carcinoma can remain indolent for a long time before submucosal invasion and lymph node metastasis ensue (van der Post et al., 2016). Therefore, the progression of HDGC is most likely a multi-stage process, with the initial loss of E-cadherin enabling tumor cells to detach from basement membrane and the subsequent loss of other modifying genes rendering the cells truly invasive. In humans, different or additional molecular mechanisms might be involved. C-Src kinase, a well-characterized inducer of epithelium mesenchymal transition, was found to be differentially expressed and activated in signet ring cells at different stages: C-Src was strongly expressed in poorly-differentiated and dedifferentiated cells in the mucosal layer and in the cells invading the muscularis mucosae but was not expressed in intramucosal signet ring cells. Consistent with this, downstream targets of c-Src, such as fibronectin, Fak, and Stat3, were differentially activated (Humar et al., 2007).

The upregulation of c-Src in HDGC has been linked to the loss of inhibition of epidermal growth factor receptor (EGFR), the upstream tyrosine receptor kinase of c-Src. E-cadherin has an inhibitory effect on EGFR, and the effect relies on the integrity of the extracellular domains of E-cadherin (Qian et al., 2004). Cell lines derived from HDGC patients with impaired extracellular domains of E-cadherin were less able to suppress EGFR signaling than cell lines with wild type E-cadherin were (Mateus et al., 2007). Loss of EGFR inhibition increases the activation of EGFR

and its downstream components, such as phosphoinositide 3-kinase and c-Src. This theory is supported by the finding that some HDGC-derived cell lines demonstrate sensitivity to EGFR inhibition (Li et al., 2018).

Interestingly, studies also support a functional interaction between HER2 and the E-cadherin through interactions with β -, p120-, and α -catenins which leads to a decrease of the E-cadherin-mediated cell adhesion and facilitates tumor cell invasion and migration. Association between specific CDH1 polymorphisms with a subset of HER2-positive gastric cancer and possibly favorable prognosis has been described (Caggiari et al., 2017).

There are multiple theories regarding the cell of origin of signet ring cell carcinoma in HDGC patients. Gastric stem cells are candidates because they reside in the upper neck region (Karam et al., 2003), where HDGC seems to originate (Humar et al., 2007). An epithelial origin has also been suggested, and direct conversion from gastric epithelium to mucous containing signet ring cells is believed to be the first step of carcinogenesis (Charlton et al., 2004). A neuroendocrine cell of origin has also been proposed because normal neuroendocrine cells of the upper gastrointestinal tract lack E-cadherin expression (Waldum et al., 2014). This proposal explains the discrepancy between the lack of atypia and malignant biological behavior. Studies in a *CDH1* knock-out animal model showed that parietal cells can “float” in the lamina propria, mimicking signet ring cell carcinoma, suggesting that parietal cells are possible cell of origin for signet ring cell carcinoma (Mimata et al., 2011).

HISTOPATHOLOGY AND PROGRESSION MODEL

No gross lesion can be detected in the early stages of disease (Rogers et al., 2008). Advanced HDGC demonstrates linitis plastica (Guilford et al., 2010). Owing to the lack of a gross lesion, histologic examination of the entire grossly normal gastric mucosa of the prophylactic gastrectomy specimen is still the standard practice for asymptomatic *CDH1* mutation carriers (Corso et al., 2014). Careful examination can identify signet ring cell carcinoma (mostly multifocal and intramucosal) as well as signet ring carcinoma *in situ* in over 90% of these specimens (Corso et al., 2014).

Between 0 and 200 cancer foci have been detected in prophylactic gastrectomy specimens. The sizes of the foci vary from 0 to 14 mm. No correlations between the number or location of foci identified and the age or sex of the patients or their specific germline mutations have been identified (Barber et al., 2008b). The topological mapping of tumor foci in gastrectomy specimens to assess the feasibility of targeted biopsies has yielded mixed results. Two studies showed that most cancer foci were concentrated in the proximal stomach (Rogers et al., 2008; Black et al., 2014). Similarly, in another study of seven patients, the majority of foci were identified in the fundus (44.7% of all foci) and body (40.2%), and all patients had lesions in these two areas (Barber et al., 2008b). Another study based on 6 fully mapped cases revealed predominant localization of tumor foci in

the distal stomach body-antral transitional zone (Charlton et al., 2004). No topographic association was found in a different study (Huntsman et al., 2001).

Because of the considerable time commitment, researchers have sought methods to facilitate the detection of foci of signet ring cell carcinoma. Periodic acid-Schiff (PAS) staining is superior to hematoxylin and eosin (HE) staining for screening prophylactic gastrectomy specimens from *CDH1* mutation carriers (Lee et al., 2010). In contrast to HE staining, PAS staining increases the contrast between signet ring cells (which show magenta cytoplasm in PAS staining) and lamina propria (PAS-negative) and therefore significantly reduces the screening time and number of missed foci.

All reported gastric cancers identified in HDGC families are the pure diffuse type by Lauren classification. No pathogenic germline mutations have been found in families with the intestinal, medullary, or mixed types (van der Post et al., 2015a). Although signet ring cell morphology is common, especially if the tumor is intramucosal, poorly-differentiated carcinomas without signet ring cell features are also seen (Guilford et al., 2007; Humar et al., 2007). Various histological morphologies have been observed in lesions containing signet ring cells, including signet ring cell carcinoma *in situ*, in which the signet ring cells are confined within the epithelium by basement membrane; pagetoid spread, in which the signet ring cells spread below the preserved epithelium of glands/foveolae without breaking the basement membrane (essentially another form of signet ring cell carcinoma *in situ*); and invasive carcinoma (Huntsman et al., 2001; Carneiro et al., 2004).

Because it frequently occurs distant from the intramucosal carcinoma, signet ring cell carcinoma is probably a distinctive lesion instead of colonization of the epithelium by invasive carcinoma (Carneiro et al., 2004). Many intramucosal signet ring cell carcinoma foci in preventive gastrectomy specimens do not have an adjacent *in situ* component. The discrepancy between the numerous invasive carcinoma foci and the low number of *in situ* carcinoma lesions suggests that signet ring cell carcinoma *in situ* is not an obligated precursor of invasive carcinoma in HDGC (Milne et al., 2007). The process of basement membrane breakthrough, which is still hypothetical, may be induced by the expression of type IV collagenases, which have been found to be upregulated when E-cadherin is downregulated through the inactivation of the other copy of *CDH1* gene (Margulis et al., 2005). Although the secretion of these enzymes is limited, it is sufficient for cells to penetrate the basement membrane in the absence of adhesion and polarity (Humar and Guilford, 2009).

Several morphologies are seen in tumor cells outside the basement membrane. Two morphological populations of signet ring cells are present in the intramucosal carcinoma. “Well-differentiated large cells” are signet ring cells with abundant mucin and eccentrically located flattened nuclei with mild atypia. They are positive for mucicarmine and pCEA and mostly located beneath the surface epithelium. “Small cells” are signet ring cells with less mucin and have hyperchromatic and atypical nuclei. They are located in the neck region and are rarely positive for mucicarmine or pCEA (Lee et al.,

2018). The small cells have the highest proliferative index, which is similar to that of normal gastric cells in the upper neck region. Immunofluorescence studies have also demonstrated that the base of the intramucosal carcinoma in HDGC has a proliferative index and a differentiation marker expression profile similar to those of the upper neck region of normal gastric units which is therefore the likely origin of the disease (Humar et al., 2007). The locations of large and small cells and their differences in proliferation suggest an initial upper migration stage when maturation occurs.

The small cells can be further classified as well-differentiated or poorly-differentiated, with the latter showing nuclear and cytoplasmic reactivity to p16 immunohistochemical staining and displaying more aggressive behavior. Most of the foci studied have demonstrated combined morphology (Lee et al., 2018). Despite the seemingly different differentiation, both large and small cells express the epithelial markers cytokeratin 8 and 18 but not markers of epithelial-mesenchymal transition such as vimentin, high Ki67 (Barber et al., 2008b), and c-Src (Humar et al., 2007). Conversely, epithelial-mesenchymal transition, the hallmark feature once the tumor invades the submucosa, is associated with poor differentiation and increased proliferation. This is achieved by increased activation of c-Src kinase and its downstream targets fibronectin, Fak, and Stat3 (Humar et al., 2007). The long and asymptomatic presence of intramucosal carcinoma in *CDH1* mutation carriers and the low proliferative index suggest that intramucosal carcinoma has an indolent nature. However, the trigger of the progression from well-differentiated cells to poorly-differentiated cells and further to submucosal invasion is still unknown. The small cells, particularly the poorly-differentiated small cells, are morphologically similar to metastatic lobular carcinoma of the breast. When breast carcinoma is a diagnostic possibility, immunohistochemical staining for estrogen receptor, progesterone receptor, GATA3 and gross cystic disease fluid protein-15, among others, may be used to aid in the differential diagnosis. The mentioned immunohistochemical stains are most commonly positive in metastatic lobular carcinoma of the breast (Kim et al., 2018), however a panel approach is preferred.

Several patterns of E-cadherin have been detected immunohistochemically, including complete loss of staining, attenuated staining, and aberrant staining. However, screening by E-cadherin immunohistochemical staining is not feasible, because 60% of gastric cancers without E-cadherin expression and 70% of gastric cancers with aberrant expression are negative for *CDH1* alterations (Corso et al., 2013).

Although morphologically similar, HDGC and SDGC are different histologically and immunohistochemically. Signet ring cell carcinoma *in situ*, including pagetoid spread of signet ring cells, appears specific to HDGC with *CDH1* mutations, as it has not been reported in SDGC (Carneiro et al., 2004; Fitzgerald et al., 2010) or HDGC without germline *CDH1* mutations (van der Post et al., 2015b). The presence of signet ring carcinoma *in situ* cells should trigger genetic testing for possible HDGC. The tumor cells in HDGC patients are negative for CDX2,

whereas most SDGC cases (with one exception), have shown positive CDX2 expression (Lee et al., 2018), implying that HDGC and SDGC have different pathogeneses. Accordingly, the absence of CDX2 in signet ring cell carcinomas in patients without a family history may prompt genetic screening for HDGC.

Background alterations in the gastric mucosa of HDGC include infrequent *Helicobacter pylori* and intestinal metaplasia. Other changes include mild chronic gastritis, foveolar hyperplasia, tufting, vacuolization of superficial epithelium, and fundic and hyperplastic polyps (Carneiro et al., 2004; Rocha et al., 2018). Mimickers of signet ring cell carcinoma, including clear changes, globoid changes, xanthomatous cells, and pseudo-signet ring cells associated with lymphoid aggregates, are also seen (Rocha et al., 2018).

OTHER DISEASE ASSOCIATION

Female kindreds of an HDGC family have increased risk of invasive lobular carcinoma, with a lifetime risk of 50–60% (Fitzgerald et al., 2010; Guilford et al., 2010; Hansford et al., 2015). Invasive lobular carcinoma may be the first manifestation of HDGC (Benusiglio et al., 2013). Invasive lobular carcinoma was also recently discovered in *CDH1* germline mutation carriers who never developed HDGC (Corso et al., 2016). The hallmark molecular alterations of all lobular neoplasia (atypical lobular hyperplasia, lobular carcinoma *in situ*, and invasive lobular carcinoma) are loss of cellular adhesion and loss or decreased expression of E-cadherin (Zou et al., 2009). Although atypical lobular hyperplasia and lobular carcinoma *in situ* are considered markers of increased risk of sporadic invasive lobular carcinoma, their roles and characteristics in invasive lobular carcinoma in *CDH1* germline mutation carriers have rarely been studied. One recent study showed that up to 8% of patients with bilateral LCIS have germline mutations in *CDH1* (Petridis et al., 2014). Earlier studies showed a lower prevalence of *CDH1* germline mutations in patients with no history of gastric carcinoma (Rahman et al., 2000; Masciari et al., 2007).

HDGC syndrome is also possibly associated with colorectal carcinoma because colorectal carcinoma has been observed in HDGC families, and loss of E-cadherin has been detected in both the tumor and adjacent normal colonic tissue. In one study, a *CDH1* missense germline mutation co-segregated with colorectal carcinoma; however, the same mutation was also present in the normal population. Interestingly, the colorectal adenocarcinoma associated with HDGC syndrome is not necessarily signet ring cell carcinoma; instead, it can be intestinal adenocarcinoma (Salahshor et al., 2001). One case of an appendiceal signet ring cell carcinoma occurring with a gastric intramucosal signet ring cell carcinoma has been reported (Hamilton et al., 2013).

CDH1 mutations have also been identified in patients with blepharocheilodontic syndrome, a congenital development disorder causing dysmorphic features, which can be accompanied by imperforate anus, hypothyroidism, and neural tube defect. However, the mutations identified in blepharocheilodontic syndrome all occur in extracellular

calcium binding repeats and are functionally distinct from those identified in HDGC (Kievit et al., 2018).

CLINICAL MANAGEMENT

Guidelines recommend genetic screening offered from the age of consent (16–18 years) (van der Post et al., 2015b). Factors such as the emotional and physical health of the individual and the earliest age of gastric cancer in the family should be considered (Guilford et al., 2010). With newer technologies, screening of HDGC carriers is becoming more efficient. A next-generation sequencing panel covering all 16 exons has been developed and validated (El-Husny et al., 2016). Liquid biopsies based on cell-free circulating DNA have been used to detect *CDH1* promoter methylation in the plasma/serum of gastric cancer patients (Tsujiura et al., 2014).

CDH1 mutation types are important in determining the management of patients at risk. Truncating germline mutations are deleterious, and a total prophylactic gastrectomy should be offered. However, the management of carriers of missense mutations is not straightforward, and the burden is to prove or disprove pathogenic relevance. In contrast to SDGCs, which have mutations clustered in exons 7 and 9, HDGC has no hotspot for germline mutations. Only 17% of germline mutations are shared by more than one family or isolated individual (Suriano et al., 2006). Therefore, the pathogenic relevance of most missense mutations has to be individually validated. This can be achieved using computational methods including frequency in normal controls, co-segregation, recurrence, and *in silico* tools such as structural modeling and SIFT software in combination with databases containing *CDH1* sequencing data, such as The Exome Variant Server of the University of Washington and the variant database <http://www.LOVD.nl/CDH1> (Suriano et al., 2006; van der Post et al., 2015a). For difficult cases, functional assessment, such as *in vitro* evaluation of an E-cadherin-induced cell adhesion and invasion assay, may be ultimately needed to ascertain the role of *CDH1* missense mutations (Suriano et al., 2006; Barber et al., 2008b; Corso et al., 2011). A functional cell model (Suriano et al., 2003) and several animal models (Pereira et al., 2006; Caldeira et al., 2009) have been established for this purpose.

The recommended management for HDGC patients is prophylactic total gastrectomy (van der Post et al., 2015b). Prophylactic gastrectomy carries a 3–6% mortality rate and a 100% morbidity rate owing to eating habit changes, dumping syndrome, diarrhea, and weight loss (Lewis et al., 2001). Although guidelines recommend prophylactic gastrectomy for germline *CDH1* mutation carriers in their 20 or 30 s, the optimal time for gastrectomy is debatable and should be individualized. Carriers can develop advanced gastric carcinoma as early as age 14 years or may never develop cancer owing to incomplete penetrance, which occurs in 20–30% of *CDH1* germline mutation carriers. The onset age among families varies widely; this variation may be caused by different types of mutations, with missense mutations having less penetrance. Even within the same family, cancer develops at different ages, probably owing

to when and how the second allele is inactivated. It has been recommended that prophylactic gastrectomy may be considered at an age younger than that of the youngest affected person in the family but should not be considered for family members in whom a causative mutation has not been identified or who have less penetrant forms of susceptibility to gastric cancer (Huntsman et al., 2001).

Endoscopic surveillance is needed if gastrectomy is contraindicated owing to comorbidity, if the patient is younger than the age recommended for surgery, or if the patient refuses surgery. The probability of detecting intramucosal carcinoma depends on the total number of lesions for a given total area of abnormal mucosa. The probability is higher for a large number of small lesions. The probability of detecting intramucosal carcinomas by five blind random biopsies has been estimated to be lower than 5% in cases with small numbers of lesions (Carneiro et al., 2004). In one theoretical estimation, 1,768 biopsies are needed to assure a 90% rate of detecting at least 1 cancer focus (Fujita et al., 2012). Current guidelines recommended that individuals be offered annual high-definition white light endoscopy (van der Post et al., 2015b). Chromoendoscopy with Congo red/methylene blue, which had been used successfully to detect lesions harboring tumor foci, has been discontinued owing to concerns about Congo red toxicity (Shaw et al., 2005). In addition to sampling endoscopically visible lesions, random sampling covering the pre-pyloric area, antrum, transitional zone, body, fundus, and cardia is also recommended (van der Post et al., 2015b). A minimum of 30 biopsies is recommended, as described in the Cambridge protocol (Fitzgerald et al., 2010). It is possible to increase the yield of signet ring cell carcinoma by adhering strictly to the Cambridge protocol. Using careful white-light examination with targeted biopsies and 24 random biopsies (4 each of the prepylorus, antrum, T zone, body, fundus, and cardia) combined with detailed histopathology, Lim et al (van der Post et al., 2015a) found signet ring cell carcinomas in 14 of 22 patients with, and 2 of 7 patients without, *CDH1* mutations fulfilling the 2010 HDGC criteria.

Surgical intervention for HDGC is no different from that for sporadic gastric cancer. Current guidelines recommend a total gastrectomy with Roux-en-Y reconstruction (van der Post et al., 2015a). A D1 lymph node dissection can be considered because most tumors in HDGC patients are at least T1a, and the presence of T1b lesions cannot be ruled out preoperatively (van der Post et al., 2015a). The management of gastric heterotopia has been controversial. Theoretically, signet ring cell carcinoma can arise from any gastric mucosa, including ectopic gastric mucosa and this forms the basis of the recommendation that all gastric mucosa should be removed during surgery (van der Post et al., 2015b). In some institutions, including MD Anderson Cancer Center, absence of gastric mucosa (including ectopic gastric mucosa) at the margins is required and can be confirmed by frozen section (van der Post et al., 2015a).

Because of the high lifetime risk of invasive lobular carcinoma, women with *CDH1* mutations should undergo annual radiologic surveillance, with bilateral breast magnetic resonance imaging

being the preferred modality, along with annual clinical breast examination (van der Post et al., 2015b). The suggested age at which breast surveillance should start varies from 25 to 35 years, whereas the role of chemoprevention remains unclear (Cisco and Norton, 2008; van der Post et al., 2015b; Corso et al., 2016; Wright et al., 2018). On the other hand, prophylactic bilateral mastectomy is not routinely recommended, and breast surveillance is preferred (Corso et al., 2014). Contralateral

mastectomy for *CDH1* mutation carriers diagnosed with invasive lobular carcinoma may be considered on an individual basis (Wright et al., 2018).

AUTHOR CONTRIBUTIONS

DT conceived, designed, and reviewed the paper; WL and FF wrote the paper; PL reviewed clinical management.

REFERENCES

- Barber, M., Murrell, A., Ito, Y., Maia, A. T., Hyland, S., Oliveira, C., et al. (2008a). Mechanisms and sequelae of E-cadherin silencing in hereditary diffuse gastric cancer. *J. Pathol.* 216, 295–306. doi: 10.1002/path.2426
- Barber, M. E., Save, V., Carneiro, F., Derryhouse, S., Lao-Sirieix, P., Hardwick, R. H., et al. (2008b). Histopathological and molecular analysis of gastrectomy specimens from hereditary diffuse gastric cancer patients has implications for endoscopic surveillance of individuals at risk. *J. Pathol.* 216, 286–294. doi: 10.1002/path.2415
- Becker, K. F., Atkinson, M. J., Reich, U., Becker, I., Nekarda, H., Siewert, J. R., et al. (1994). E-cadherin gene mutations provide clues to diffuse type gastric carcinomas. *Cancer Res.* 54, 3845–3852.
- Benusiglio, P. R., Colas, C., Rouleau, E., Uhrhammer, N., Romero, P., Remenieras, A., et al. (2015). Hereditary diffuse gastric cancer syndrome: improved performances of the 2015 testing criteria for the identification of probands with a *CDH1* germline mutation. *J. Med. Genet.* 52, 563–565. doi: 10.1136/jmedgenet-2015-103153
- Benusiglio, P. R., Malka, D., Rouleau, E., De Pauw, A., Buecher, B., Noguès, C., et al. (2013). *CDH1* germline mutations and the hereditary diffuse gastric and lobular breast cancer syndrome: a multicentre study. *J. Med. Genet.* 50, 486–489. doi: 10.1136/jmedgenet-2012-101472
- Bershadsky, A. (2004). Magic touch: how does cell-cell adhesion trigger actin assembly? *Trends Cell Biol.* 14, 589–593. doi: 10.1016/j.tcb.2004.09.009
- Berx, G., Becker, K. F., Höfler, H., and van Roy, F. (1998). Mutations of the human E-cadherin (*CDH1*) gene. *Hum. Mutat.* 12, 226–237. doi: 10.1002/(SICI)1098-1004(1998)12:4<226::AID-HUMU2>3.0.CO;2-D
- Berx, G., Staes, K., van Hengel, J., Molemans, F., Bussemakers, M. J., van Bokhoven, A., et al. (1995). Cloning and characterization of the human invasion suppressor gene E-cadherin (*CDH1*). *Genomics.* 26, 281–289. doi: 10.1016/0888-7543(95)80212-5
- Black, M. D., Kaneshiro, R., Lai, J. I., and Shimizu, D. M. (2014). Hereditary diffuse gastric cancer associated with E-cadherin germline mutation: a case report. *Hawaii. J. Med. Public Health.* 73, 204–207.
- Blaschuk, O. W., Sullivan, R., David, S., and Pouliot, Y. (1990). Identification of a cadherin cell adhesion recognition sequence. *Dev. Biol.* 139, 227–229. doi: 10.1016/0012-1606(90)90290-Y
- Caggiari, L., Miolo, G., Buonadonna, A., Basile, D., Santeufemia, D. A., Cossu, A., et al. (2017). Characterizing metastatic HER2-positive gastric cancer at the *CDH1* haplotype. *Int. J. Mol. Sci.* 19:47. doi: 10.3390/ijms19010047
- Caldas, C., Carneiro, F., Lynch, H. T., Yokota, J., Wiesner, G. L., Powell, S. M., et al. (1999). Familial gastric cancer: overview and guidelines for management. *J. Med. Genet.* 36, 873–880.
- Caldeira, J., Pereira, P. S., Suriano, G., and Casares, F. (2009). Using fruitflies to help understand the molecular mechanisms of human hereditary diffuse gastric cancer. *Int. J. Dev. Biol.* 53, 1557–1561. doi: 10.1387/ijdb.072277jc
- Capelle, L. G., Van Grieken, N. C., Lingsma, H. F., Steyerberg, E. W., Klokman, W. J., Bruno, M. J., et al. (2010). Risk and epidemiological time trends of gastric cancer in Lynch syndrome carriers in the Netherlands. *Gastroenterology.* 138, 487–492. doi: 10.1053/j.gastro.2009.10.051
- Carneiro, F., Huntsman, D. G., Smyrk, T. C., Owen, D. A., Seruca, R., Pharoah, P., et al. (2004). Model of the early development of diffuse gastric cancer in E-cadherin mutation carriers and its implications for patient screening. *J. Pathol.* 203, 681–687. doi: 10.1002/path.1564
- Charlton, A., Blair, V., Shaw, D., Parry, S., Guilford, P., and Martin, I. G. (2004). Hereditary diffuse gastric cancer: predominance of multiple foci of signet ring cell carcinoma in distal stomach and transitional zone. *Gut* 53, 814–820. doi: 10.1136/gut.2002.010447
- Cisco, R. M., and Norton, J. A. (2008). Hereditary diffuse gastric cancer: surgery, surveillance and unanswered questions. *Future Oncol.* 4, 553–559. doi: 10.2217/14796694.4.4.553
- Corso, G., Carvalho, J., Marrelli, D., Vindigni, C., Carvalho, B., Seruca, R., et al. (2013). Somatic mutations and deletions of the E-cadherin gene predict poor survival of patients with gastric cancer. *J. Clin. Oncol.* 31, 868–875. doi: 10.1200/JCO.2012.44.4612
- Corso, G., Figueiredo, J., Biffi, R., Trentin, C., Bonanni, B., Feroce, I., et al. (2014). E-cadherin germline mutation carriers: clinical management and genetic implications. *Cancer Metastasis Rev.* 33, 1081–1094. doi: 10.1007/s10555-014-9528-y
- Corso, G., Intra, M., Trentin, C., Veronesi, P., and Galimberti, V. (2016). *CDH1* germline mutations and hereditary lobular breast cancer. *Fam. Cancer* 15, 215–219. doi: 10.1007/s10689-016-9869-5
- Corso, G., Marrelli, D., Pascale, V., Vindigni, C., and Roviello, F. (2012). Frequency of *CDH1* germline mutations in gastric carcinoma coming from high- and low-risk areas: metanalysis and systematic review of the literature. *BMC Cancer.* 12:8. doi: 10.1186/1471-2407-12-8
- Corso, G., Pedrazzani, C., Pinheiro, H., Fernandes, E., Marrelli, D., Rinnovati, A., et al. (2011). E-cadherin genetic screening and clinico-pathologic characteristics of early onset gastric cancer. *Eur. J. Cancer* 47, 631–639. doi: 10.1016/j.ejca.2010.10.011
- Derksen, P. W., Liu, X., Saridin, F., van der Gulden, H., Zevenhoven, J., Evers, B., et al. (2006). Somatic inactivation of E-cadherin and p53 in mice leads to metastatic lobular mammary carcinoma through induction of anoikis resistance and angiogenesis. *Cancer Cell* 10, 437–449. doi: 10.1016/j.ccr.2006.09.013
- El-Husny, A., Raiol-Moraes, M., Amador, M., Ribeiro-Dos-Santos, A. M., Montagnini, A., Barbosa, S., et al. (2016). *CDH1* mutations in gastric cancer patients from northern Brazil identified by Next- Generation Sequencing (NGS). *Genet. Mol. Biol.* 39, 189–198. doi: 10.1590/1678-4685-gmb-2014-0342
- Ferlay, J., Soerjomataram, I., Ervik, M., Dikshit, R., Eser, S., Mathers, C., et al. (2013). *Cancer Incidence and Mortality Worldwide: IARC CancerBase No. 11*. Lyon: International Agency for Research on Cancer, GLOBOCAN 2012. v1.v0.
- Fewings, E., Larionov, A., Redman, J., Goldgraben, M. A., Scarth, J., Richardson, S., et al. (2018). Germline pathogenic variants in *PALB2* and other cancer-predisposing genes in families with hereditary diffuse gastric cancer without *CDH1* mutation: a whole-exome sequencing study. *Lancet Gastroenterol. Hepatol.* 3, 489–498. doi: 10.1016/S2468-1253(18)30079-7
- Fitzgerald, R. C., Hardwick, R., Huntsman, D., Carneiro, F., Guilford, P., Blair, V., et al. (2010). Hereditary diffuse gastric cancer: updated consensus guidelines for clinical management and directions for future research. *J. Med. Genet.* 47, 436–444. doi: 10.1136/jmg.2009.074237
- Fleming, T. P., Javed, Q., and Hay, M. (1992). Epithelial differentiation and intercellular junction formation in the mouse early embryo. *Dev. Suppl.* 1992, 105–12.
- Fornasarig, M., Magris, R., De Re, V., Bidoli, E., Canzonieri, V., Maiero, S., et al. (2018). Molecular and pathological features of gastric cancer in lynch syndrome and familial adenomatous polyposis. *Int. J. Mol. Sci.* 19:E1682. doi: 10.3390/ijms19061682

- Fujita, H., Lennerz, J. K., Chung, D. C., Patel, D., Deshpande, V., Yoon, S. S., et al. (2012). Endoscopic surveillance of patients with hereditary diffuse gastric cancer: biopsy recommendations after topographic distribution of cancer foci in a series of 10 CDH1-mutated gastrectomies. *Am. J. Surg. Pathol.* 36, 1709–1717. doi: 10.1097/PAS.0b013e31826ca204
- Garziera, M., Canzonieri, V., Cannizzaro, R., Geremia, S., Caggiari, L., De Zorzi, M., et al. (2013). Identification and characterization of CDH1 germline variants in sporadic gastric cancer patients and in individuals at risk of gastric cancer. *PLoS ONE* 8:e77035. doi: 10.1371/journal.pone.0077035
- Gaston, D., Hansford, S., Oliveira, C., Nightingale, M., Pinheiro, H., Macgillivray, C., et al. (2014). Germline mutations in MAP3K6 are associated with familial gastric cancer. *PLoS Genet.* 10:e1004669. doi: 10.1371/journal.pgen.1004669
- Godwin, T. D., Kelly, S. T., Brew, T. P., Bougen-Zhukov, N. M., Single, A. B., Chen, A., et al. (2018). E-cadherin-deficient cells have synthetic lethal vulnerabilities in plasma membrane organisation, dynamics and function. *Gastric Cancer*. doi: 10.1007/s10120-018-0859-1. [Epub ahead of print].
- Grady, W. M., Willis, J., Guilford, P. J., Dunbier, A. K., Toro, T. T., Lynch, H., et al. (2000). Methylation of the CDH1 promoter as the second genetic hit in hereditary diffuse gastric cancer. *Nat. Genet.* 26, 16–17. doi: 10.1038/79120
- Guilford, P. (1999). E-cadherin downregulation in cancer: fuel on the fire? *Mol. Med. Today* 5, 172–177. doi: 10.1016/S1357-4310(99)01461-6
- Guilford, P., Blair, V., More, H., and Humar, B. (2007). A short guide to hereditary diffuse gastric cancer. *Hered. Cancer Clin. Pract.* 5, 183–194. doi: 10.1186/1897-4287-5-4-183
- Guilford, P., Hopkins, J., Harraway, J., McLeod, M., McLeod, N., Harawira, P., et al. (1998). E-cadherin germline mutations in familial gastric cancer. *Nature* 392, 402–405. doi: 10.1038/32918
- Guilford, P., Humar, B., and Blair, V. (2010). Hereditary diffuse gastric cancer: translation of CDH1 germline mutations into clinical practice. *Gastric Cancer* 13, 1–10. doi: 10.1007/s10120-009-0531-x
- Gumbiner, B. M. (1996). Cell adhesion: the molecular basis of tissue architecture and morphogenesis. *Cell* 84, 345–57. doi: 10.1016/S0092-8674(00)81279-9
- Hamilton, L. E., Jones, K., Church, N., and Medlicott, S. (2013). Synchronous appendiceal and intramucosal gastric signet ring cell carcinomas in an individual with CDH1-associated hereditary diffuse gastric carcinoma: a case report of a novel association and review of the literature. *BMC Gastroenterol.* 13:114. doi: 10.1186/1471-230X-13-114
- Hansford, S., Kaurah, P., Li-Chang, H., Woo, M., Senz, J., Pinheiro, H., et al. (2015). Hereditary diffuse gastric cancer syndrome: CDH1 mutations and beyond. *JAMA Oncol.* 1, 23–32. doi: 10.1001/jamaoncol.2014.168
- Huang, D. S., Tao, H. Q., He, X. J., Long, M., Yu, S., Xia, Y. J., et al. (2015). Prevalence of deleterious ATM germline mutations in gastric cancer patients. *Oncotarget* 6, 40953–40958. doi: 10.18632/oncotarget.5944
- Humar, B., Fukuzawa, R., Blair, V., Dunbier, A., More, H., Charlton, A., et al. (2007). Destabilized adhesion in the gastric proliferative zone and c-Src kinase activation mark the development of early diffuse gastric cancer. *Cancer Res.* 67, 2480–2489. doi: 10.1158/0008-5472.CAN-06-3021
- Humar, B., and Guilford, P. (2009). Hereditary diffuse gastric cancer: a manifestation of lost cell polarity. *Cancer Sci.* 100, 1151–7. doi: 10.1111/j.1349-7006.2009.01163.x
- Huntsman, D. G., Carneiro, F., Lewis, F. R., MacLeod, P. M., Hayashi, A., Monaghan, K. G., et al. (2001). Early gastric cancer in young, asymptomatic carriers of germ-line E-cadherin mutations. *N. Engl. J. Med.* 344, 1904–1909. doi: 10.1056/NEJM200106213442504
- Karam, S. M., Straiton, T., Hassan, W. M., and Leblond, C. P. (2003). Defining epithelial cell progenitors in the human oxyntic mucosa. *Stem Cells* 21, 322–336. doi: 10.1634/stemcells.21-3-322
- Kievit, A., Tessadori, F., Douben, H., Jordens, I., Maurice, M., Hoogeboom, J., et al. (2018). Variants in members of the cadherin-catenin complex, CDH1 and CTNND1, cause blepharochelodontic syndrome. *Eur. J. Hum. Genet.* 26, 210–219. doi: 10.1038/s41431-017-0010-5
- Kim, D. H., Son, S. M., and Choi, Y. J. (2018). Gastric metastasis from invasive lobular breast cancer, mimicking primary gastric cancer: a case report. *Medicine* 97:e0258. doi: 10.1097/MD.00000000000010258
- Lee, A. F., Rees, H., Owen, D. A., and Huntsman, D. G. (2010). Periodic acid-schiff is superior to hematoxylin and eosin for screening prophylactic gastrectomies from CDH1 mutation carriers. *Am. J. Surg. Pathol.* 34, 1007–1013. doi: 10.1097/PAS.0b013e3181e28985
- Lee, H. E., Smyrk, T. C., and Zhang, L. (2018). Histologic and immunohistochemical differences between hereditary and sporadic diffuse gastric carcinoma. *Hum. Pathol.* 74, 64–72. doi: 10.1016/j.humpath.2017.12.023
- Lee, Y. S., Cho, Y. S., Lee, G. K., Lee, S., Kim, Y. W., Jho, S., et al. (2014). Genomic profile analysis of diffuse-type gastric cancers. *Genome Biol.* 15:R55. doi: 10.1186/gb-2014-15-4-r55
- Lewis, F. R., Mellinger, J. D., Hayashi, A., Lorelli, D., Monaghan, K. G., Carneiro, F., et al. (2001). Prophylactic total gastrectomy for familial gastric cancer. *Surgery* 130, 612–617; discussion 617–9. doi: 10.1067/msy.2001.117099
- Li, D., Lo, W., and Rudloff, U. (2018). Merging perspectives: genotype-directed molecular therapy for hereditary diffuse gastric cancer (HDGC) and E-cadherin-EGFR crosstalk. *Clin. Transl. Med.* 7:7. doi: 10.1186/s40169-018-0184-7
- Machado, J. C., Soares, P., Carneiro, F., Rocha, A., Beck, S., Blin, N., et al. (1999). E-cadherin gene mutations provide a genetic basis for the phenotypic divergence of mixed gastric carcinomas. *Lab. Invest.* 79, 459–465. doi: 10.1097/00008469-199908000-00035
- Maimon, S. N., and Zininger, M. M. (1953). Familial gastric cancer. *Gastroenterology* 25, 139–152; discussion, 153–5.
- Margulis, A., Zhang, W., Alt-Holland, A., Crawford, H. C., Fusenig, N. E., and Garlick, J. A. (2005). E-cadherin suppression accelerates squamous cell carcinoma progression in three-dimensional, human tissue constructs. *Cancer Res.* 65, 1783–1791. doi: 10.1158/0008-5472.CAN-04-3399
- Masciari, S., Dewanwala, A., Stoffel, E. M., Lauwers, G. Y., Zheng, H., Achatz, M. I., et al. (2011). Gastric cancer in individuals with Li-Fraumeni syndrome. *Genet. Med.* 13, 651–657. doi: 10.1097/GIM.0b013e31821628b6
- Masciari, S., Larsson, N., Senz, J., Boyd, N., Kaurah, P., Kandel, M. J., et al. (2007). Germline E-cadherin mutations in familial lobular breast cancer. *J. Med. Genet.* 44, 726–731. doi: 10.1136/jmg.2007.051268
- Mateus, A. R., Seruca, R., Machado, J. C., Keller, G., Oliveira, M. J., Suriano, G., et al. (2007). EGFR regulates RhoA-GTP dependent cell motility in E-cadherin mutant cells. *Hum. Mol. Genet.* 16, 1639–1647. doi: 10.1093/hmg/ddm113
- Melo, S., Figueiredo, J., Fernandes, M. S., Gonçalves, M., Morais-de-Sá, E., Sanches, J. M., et al. (2017). Predicting the functional impact of CDH1 missense mutations in hereditary diffuse gastric cancer. *Int. J. Mol. Sci.* 18: E2687. doi: 10.3390/ijms18122687
- Milne, A. N., Sitarz, R., Carvalho, R., Carneiro, F., and Offerhaus, G. J. (2007). Early onset gastric cancer: on the road to unraveling gastric carcinogenesis. *Curr. Mol. Med.* 7, 15–28. doi: 10.2174/156652407779940503
- Mimata, A., Fukumachi, H., Eishi, Y., and Yuasa, Y. (2011). Loss of E-cadherin in mouse gastric epithelial cells induces signet ring-like cells, a possible precursor lesion of diffuse gastric cancer. *Cancer Sci.* 102, 942–950. doi: 10.1111/j.1349-7006.2011.01890.x
- Moslim, M. A., Heald, B., Tu, C., Burke, C. A., and Walsh, R. M. (2018). Early genetic counseling and detection of CDH1 mutation in asymptomatic carriers improves survival in hereditary diffuse gastric cancer. *Surgery* 164, 754–759. doi: 10.1016/j.surg.2018.05.059
- Nagar, B., Overduin, M., Ikura, M., and Rini, J. M. (1996). Structural basis of calcium-induced E-cadherin rigidification and dimerization. *Nature* 380, 360–364. doi: 10.1038/380360a0
- Oliveira, C., Sousa, S., Pinheiro, H., Karam, R., Bordeira-Carriço, R., Senz, J., et al. (2009). Quantification of epigenetic and genetic 2nd hits in CDH1 during hereditary diffuse gastric cancer syndrome progression. *Gastroenterology* 136, 2137–2148. doi: 10.1053/j.gastro.2009.02.065
- Park, J. W., Jang, S. H., Park, D. M., Lim, N. J., Deng, C., Kim, D. Y., et al. (2014). Cooperativity of E-cadherin and Smad4 loss to promote diffuse-type gastric adenocarcinoma and metastasis. *Mol. Cancer Res.* 12, 1088–1099. doi: 10.1158/1541-7786.MCR-14-0192-T
- Park, J. W., Kim, M. S., Voon, D. C., Kim, S. J., Bae, J., Mun, D. G., et al. (2018). Multi-omics analysis identifies pathways and genes involved in diffuse-type gastric carcinogenesis induced by E-cadherin, p53, and Smad4 loss in mice. *Mol. Carcinog.* 57, 947–954. doi: 10.1002/mc.22803
- Pereira, P. S., Teixeira, A., Pinho, S., Ferreira, P., Fernandes, J., Oliveira, C., et al. (2006). E-cadherin missense mutations, associated with hereditary diffuse gastric cancer (HDGC) syndrome, display distinct invasive behaviors and genetic interactions with the Wnt and Notch pathways in *Drosophila* epithelia. *Hum. Mol. Genet.* 15, 1704–1712. doi: 10.1093/hmg/ddl093

- Petridis, C., Shinomiya, I., Kohut, K., Gorman, P., Caneppele, M., Shah, V., et al. (2014). Germline CDH1 mutations in bilateral lobular carcinoma in situ. *Br. J. Cancer* 110, 1053–1057. doi: 10.1038/bjc.2013.792
- Qian, X., Karpova, T., Sheppard, A. M., McNally, J., and Lowy, D. R. (2004). E-cadherin-mediated adhesion inhibits ligand-dependent activation of diverse receptor tyrosine kinases. *EMBO J.* 23, 1739–1748. doi: 10.1038/sj.emboj.7600136
- Rahman, N., Stone, J. G., Coleman, G., Gusterson, B., Seal, S., Marossy, A., et al. (2000). Lobular carcinoma in situ of the breast is not caused by constitutional mutations in the E-cadherin gene. *Br. J. Cancer* 82, 568–570. doi: 10.1054/bjoc.1999.0965
- Rocha, J. P., Gullo, I., Wen, X., Devezas, V., Baptista, M., Oliveira, C., et al. (2018). Pathological features of total gastrectomy specimens from asymptomatic hereditary diffuse gastric cancer patients and implications for clinical management. *Histopathology* 73, 878–886. doi: 10.1111/his.13715
- Rogers, W. M., Dobo, E., Norton, J. A., Van Dam, J., Jeffrey, R. B., Huntsman, D. G., et al. (2008). Risk-reducing total gastrectomy for germline mutations in E-cadherin (CDH1): pathologic findings with clinical implications. *Am. J. Surg. Pathol.* 32, 799–809. doi: 10.1097/PAS.0b013e31815e7f1a
- Rona, K. A., Schwameis, K., Zehetner, J., Samakar, K., Green, K., Samaan, J., et al. (2017). Gastric cancer in the young: An advanced disease with poor prognostic features. *J. Surg. Oncol.* 115, 371–375. doi: 10.1002/jso.24533
- Salahshor, S., Hou, H., Diep, C. B., Loukola, A., Zhang, H., Liu, T., et al. (2001). A germline E-cadherin mutation in a family with gastric and colon cancer. *Int. J. Mol. Med.* 8, 439–443. doi: 10.3892/ijmm.8.4.439
- Schrader, K. A., Masciari, S., Boyd, N., Wiyrick, S., Kaurah, P., Senz, J., et al. (2008). Hereditary diffuse gastric cancer: association with lobular breast cancer. *Fam. Cancer* 7, 73–82. doi: 10.1007/s10689-007-9172-6
- Shapiro, L., Fannon, A. M., Kwong, P. D., Thompson, A., Lehmann, M. S., Grubel, G., et al. (1995). Structural basis of cell-cell adhesion by cadherins. *Nature* 374, 327–337. doi: 10.1038/374327a0
- Shaw, D., Blair, V., Framp, A., Harawira, P., McLeod, M., Guilford, P., et al. (2005). Chromoendoscopic surveillance in hereditary diffuse gastric cancer: an alternative to prophylactic gastrectomy? *Gut* 54, 461–468. doi: 10.1136/gut.2004.049171
- Suriano, G., Oliveira, C., Ferreira, P., Machado, J. C., Bordin, M. C., De Wever, O., et al. (2003). Identification of CDH1 germline missense mutations associated with functional inactivation of the E-cadherin protein in young gastric cancer probands. *Hum. Mol. Genet.* 12, 575–582. doi: 10.1093/hmg/ddg048
- Suriano, G., Seixas, S., Rocha, J., and Seruca, R. (2006). A model to infer the pathogenic significance of CDH1 germline missense variants. *J. Mol. Med.* 84, 1023–1031. doi: 10.1007/s00109-006-0091-z
- Takeichi, M. (1991). Cadherin cell adhesion receptors as a morphogenetic regulator. *Science* 251, 1451–1455. doi: 10.1126/science.2006419
- Takeichi, M. (1995). Morphogenetic roles of classic cadherins. *Curr. Opin. Cell Biol.* 7, 619–27. doi: 10.1016/0955-0674(95)80102-2
- Tsujiura, M., Ichikawa, D., Konishi, H., Komatsu, S., Shiozaki, A., and Otsuji, E. (2014). Liquid biopsy of gastric cancer patients: circulating tumor cells and cell-free nucleic acids. *World J. Gastroenterol.* 20, 3265–3286. doi: 10.3748/wjg.v20.i12.3265
- van der Post, R. S., Gullo, I., Oliveira, C., Tang, L. H., Grabsch, H. I., O'Donovan, M., et al. (2016). Histopathological, molecular, and genetic profile of hereditary diffuse gastric cancer: current knowledge and challenges for the future. *Adv. Exp. Med. Biol.* 908, 371–391. doi: 10.1007/978-3-319-41388-4_18
- van der Post, R. S., Vogelaar, I. P., Carneiro, F., Guilford, P., Huntsman, D., Hoogerbrugge, N., et al. (2015b). Hereditary diffuse gastric cancer: updated clinical guidelines with an emphasis on germline CDH1 mutation carriers. *J. Med. Genet.* 52, 361–374. doi: 10.1136/jmedgenet-2015-103094
- van der Post, R. S., Vogelaar, I. P., Manders, P., van der Kolk, L. E., Cats, A., van Hest, L. P., et al. (2015a). Accuracy of hereditary diffuse gastric cancer testing criteria and outcomes in patients with a germline mutation in CDH1. *Gastroenterology* 149, 897–906.e19. doi: 10.1053/j.gastro.2015.06.003
- van Lier, M. G., Wagner, A., Mathus-Vliegen, E. M., Kuipers, E. J., Steyerberg, E. W., and van Leerdam, M. E. (2010). High cancer risk in Peutz-Jeghers syndrome: a systematic review and surveillance recommendations. *Am. J. Gastroenterol.* 105, 1258–1264; author reply 1265. doi: 10.1038/ajg.2009.725
- Waldum, H. L., Ringnes, E., Nordbø, H., Sørda, Ø., Nordrum, I. S., and Hauso, Ø. (2014). The normal neuroendocrine cells of the upper gastrointestinal tract lack E-cadherin. *Scand. J. Gastroenterol.* 49, 974–978. doi: 10.3109/00365521.2014.909275
- Wang, Z., Graham, D. Y., Khan, A., Balakrishnan, M., Abrams, H. R., El-Serag, H. B., et al. (2018). Incidence of gastric cancer in the USA during 1999 to 2013: a 50-state analysis. *Int. J. Epidemiol.* 47, 966–975. doi: 10.1093/ije/dyy055
- Worthley, D. L., Phillips, K. D., Wayte, N., Schrader, K. A., Healey, S., Kaurah, P., et al. (2012). Gastric adenocarcinoma and proximal polyposis of the stomach (GAPPS): a new autosomal dominant syndrome. *Gut* 61, 774–779. doi: 10.1136/gutjnl-2011-300348
- Wright, F. C., Look Hong, N. J., Quan, M. L., Beyfuss, K., Temple, S., Covelli, A., et al. (2018). Indications for contralateral prophylactic mastectomy: a consensus statement using modified delphi methodology. *Ann. Surg.* 267, 271–279. doi: 10.1097/SLA.0000000000002309
- Wu, H., Rusiecki, J. A., Zhu, K., Potter, J., and Devesa, S. S. (2009). Stomach carcinoma incidence patterns in the United States by histologic type and anatomic site. *Cancer Epidemiol. Biomarkers Prev.* 18, 1945–1952. doi: 10.1158/1055-9965.EPI-09-0250
- Yoshiura, K., Kanai, Y., Ochiai, A., Shimoyama, Y., Sugimura, T., and Hirohashi, S. (1995). Silencing of the E-cadherin invasion-suppressor gene by CpG methylation in human carcinomas. *Proc. Natl. Acad. Sci. U.S.A.* 92, 7416–7419. doi: 10.1073/pnas.92.16.7416
- Zou, D., Yoon, H. S., Perez, D., Weeks, R. J., Guilford, P., and Humar, B. (2009). Epigenetic silencing in non-neoplastic epithelia identifies E-cadherin (CDH1) as a target for chemoprevention of lobular neoplasia. *J. Pathol.* 218, 265–272. doi: 10.1002/path.2541

Conflict of Interest Statement: The authors declare that the research was conducted in the absence of any commercial or financial relationships that could be construed as a potential conflict of interest.

Copyright © 2018 Luo, Fedda, Lynch and Tan. This is an open-access article distributed under the terms of the Creative Commons Attribution License (CC BY). The use, distribution or reproduction in other forums is permitted, provided the original author(s) and the copyright owner(s) are credited and that the original publication in this journal is cited, in accordance with accepted academic practice. No use, distribution or reproduction is permitted which does not comply with these terms.



DT-13 Inhibits Proliferation and Metastasis of Human Prostate Cancer Cells Through Blocking PI3K/Akt Pathway

Zhengming Wang¹, Yingying Wang¹, Shan Zhu¹, Yao Liu¹, Xin Peng¹, Shaolu Zhang^{1,2}, Zhe Zhang¹, Yuling Qiu¹, Meihua Jin¹, Ran Wang^{1*}, Yuxu Zhong^{2*} and Dexin Kong^{1*}

¹ Tianjin Key Laboratory on Technologies Enabling Development of Clinical Therapeutics and Diagnostics, School of Pharmacy, Tianjin Medical University, Tianjin, China, ² State Key Laboratory of Toxicology and Medical Countermeasures, Beijing Institute of Pharmacology and Toxicology, Beijing, China

OPEN ACCESS

Edited by:

Zhi Shi,
Jinan University, China

Reviewed by:

Revati Wani,
Pfizer, United States
Gabriella D'Orazi,
Università degli Studi 'G. d'Annunzio'
Chieti – Pescara, Italy

*Correspondence:

Ran Wang
wangran@tmu.edu.cn
Yuxu Zhong
yuxuzhong2008@aliyun.com
Dexin Kong
kongdexin@tmu.edu.cn

Specialty section:

This article was submitted to
Experimental Pharmacology
and Drug Discovery,
a section of the journal
Frontiers in Pharmacology

Received: 29 August 2018

Accepted: 26 November 2018

Published: 07 December 2018

Citation:

Wang Z, Wang Y, Zhu S, Liu Y,
Peng X, Zhang S, Zhang Z, Qiu Y,
Jin M, Wang R, Zhong Y and Kong D
(2018) DT-13 Inhibits Proliferation
and Metastasis of Human Prostate
Cancer Cells Through Blocking
PI3K/Akt Pathway.
Front. Pharmacol. 9:1450.
doi: 10.3389/fphar.2018.01450

DT-13, a saponin monomer 13 from the dwarf lilyturf tuber, was reported to exhibit anti-inflammatory, hepatoprotective, cardioprotective as well as antitumor activities in a number of tumor cells. Prostate cancer is the second leading cause of cancer death in males, discovery of novel antitumor drug for therapy of prostate cancer is expected. Aiming to evaluate whether DT-13 could become a candidate to treat prostate cancer, we recently investigated the antitumor effect of DT-13 on human prostate cancer cells and the underlying mechanism. DT-13 was found to effectively inhibit proliferation and metastasis of prostate cancer PC3 and DU145 cell lines in a dose-dependent manner. Treatment by DT-13 resulted in a mitochondria-mediated apoptosis, which was accompanied by the chromatin condensation and nuclear shrinkage in the prostate cancer cells. Moreover, DT-13 caused remarkable upregulation of Bax, Bad, Cytochrome C, cleaved -caspase 3, -caspase 9 and -PARP, in contrast to the downregulation of Bcl-2. Nevertheless, no obvious change in intracellular ROS level was observed after DT-13 treatment. We further demonstrated that DT-13 could inhibit PC3 cell metastasis in which suppression of Integrin β 1 and MMP2/9 might be involved. Western blot analysis indicated DT-13 significantly decreased the phosphorylation of PDK1, Akt, mTOR as well as p70S6K, suggesting the pro-apoptotic and anti-metastatic effects of DT-13 on prostate cancer cells might be attributed to the blockade of PI3K/Akt pathway. Collectively, our findings suggest DT-13 is worthy of further investigation as a drug candidate for the treatment of prostate cancer.

Keywords: DT-13, prostate cancer, anti-proliferation, anti-metastasis, apoptosis, PI3K/Akt pathway

INTRODUCTION

Prostate cancer is the most commonly diagnosed cancer and the second leading lethal disease in males (Siegel et al., 2018). In worldwide, about 300,000 men die from prostate cancer each year (Center et al., 2012). Some types of prostate cancer grow slowly or even they would stay that way, other types are aggressive and move fast in the body. According to recent statistics, between the year of 2005 and 2011, patients with non-metastatic prostate cancer had a 98.9% five-year

survival rate, but that for patients with metastatic prostate cancer is only 28.2%, suggesting most patients eventually die from cancer metastasis (Siegel et al., 2018; Wade and Kyprianou, 2018). Chemotherapeutic drugs and surgeries are common options applied in treating prostate cancer, but chemotherapy produces a series of side-effects (Perez-Gracia et al., 2018). These situations urgently require innovative pharmacotherapies to implement the control of prostate cancer development and metastasis. Recently, a number of compounds from natural products were evaluated for their chemopreventive potential against various tumors, providing new opportunity for alternative treatment of prostate cancer (Lawania and Mishra, 2013).

The steroidal saponin DT-13, [25(R,S)-ruscogenin-1-O- β -D-glucopyranosyl-(1 \rightarrow 2)][β -D-xylopyranosyl-(1 \rightarrow 3)]- β -D-fucopyranoside, one of the major active compounds derived from Dwarf lilyturf tuber, has been widely studied and demonstrated to possess multiple pharmacological activities (Khan et al., 2018). This compound has shown anti-inflammatory, hepatoprotective, cardioprotective as well as immunomodulating effects with little toxicities (Khan et al., 2018). Besides, it is highlighted that DT-13 exhibited great potential in combating cancer against a variety of cancer cell lines such as lung, breast and gastric cancer, which might be attributed to its pro-apoptotic effect on cancer cells (Zhang et al., 2012; Ren-Ping et al., 2014; Li et al., 2016, 2017b; Wei et al., 2016; Yu et al., 2016; Du et al., 2018; Khan et al., 2018). It was also found that DT-13 could inhibit tissue factors and angiogenesis to suppress tumor metastasis (Zhang et al., 2012; Zhao R. et al., 2013).

Phosphatidylinositol-3 kinases (PI3Ks) are a family of phosphokinase that plays vital roles in multiple cellular processes, such as cell growth, differentiation, apoptosis, transcription and cell migration. PI3Ks transmit signals from various cytokines, growth factors and chemotherapeutic agents into intracellular messages by generating phospholipid PI(3,4,5)P₃, which in turn activate protein kinase B (Akt) and other downstream effectors (Kong and Yamori, 2009). It is well known the PI 3-kinase is often mutationally activated or over expressed in many cancers, which results in the development of cancer. Hence, many pharmaceutical researchers are actively developing inhibitors targeting PI3K and other key components in the pathway (Yap et al., 2015). At present, great efforts have been made to discover inhibitors of PI3K/Akt pathway for the treatment of cancer and a number of these inhibitors have been approved or are evaluated in clinical trials, such as Idelalisib, BEZ-235, ZSTK474, PI-103, XL-765, BYL-719, and PX-866 (Cohen, 2014; Kumar et al., 2015; Massaccesi et al., 2016; Zhao et al., 2017).

In the present study, we set out to investigate the inhibitory effects of DT-13 on human hormone-refractory prostate cancer cells and to elucidate the molecular mechanisms that account for the therapeutic effect. We have demonstrated that DT-13 inhibited proliferation and induced apoptosis in the path of mitochondrion in PC3 and DU145 cells. We have also found DT-13 could inhibit PC3 cells migration and invasion at low concentrations. Moreover, PI3K/Akt signaling pathway was proved to play an important role in the anticancer effect of DT-13 on prostate cancer.

MATERIALS AND METHODS

Reagents

DT-13 was purchased from Chengdu Push Bio-technology Co., Ltd. (Chengdu, China). MTT [3-(4,5-dimethyl-2-thiazolyl)-2,5-diphenyl-2-H-tetrazoliumbromide] was obtained from Amresco (Solon, OH, United States). Adriamycin (ADR) and z-VAD-FMK were from Selleck (London, ON, Canada). Hoechst 33342 and propidium iodide (PI) were purchased from Sigma-Aldrich (St. Louis, MO, United States). Antibodies against Akt, phospho-Akt (T308), phospho-PDK1 (Ser241), phospho-mTOR (Ser2448), phospho-p70S6k (Thr389), PI3K-p110 α , PI3K-p110 β , PARP, phospho-p38 (Thr180/Thr182), phospho-ERK1/2 (Thr202/Thr204), phospho-JNK (Thr183/Thr185), CytC, caspase-3, caspase-8, caspase-9, Integrin β 1, phospho-Integrin β 1 and β -actin were obtained from Cell Signaling Technology (Danvers, MA, United States). FITC Annexin-V apoptosis detection kit was obtained from BD Bioscience (San Jose, CA, United States). Mitochondrial membrane potential detection kit, mitochondrial isolation kit and 2',7'-Dichlorodihydrofluorescein diacetate (DCFH-DA) were purchased from Beyotime Biotech (Nantong, China).

Cell Culture

Human prostate cancer cell lines PC3 and DU145 were obtained from the cell bank of Chinese academy of sciences (Shanghai, China). All cells were cultured in RPMI 1640 medium supplemented with 10% fetal bovine serum (Biological Industries, Kibbutz Beit-Haemek, Israel), 10 μ g/ml streptomycin and 100 U/ml penicillin at 37°C in a humidified atmosphere containing 5% CO₂.

Cell Viability Assay

The effect of DT-13 on cell viability was determined by MTT assay as mentioned in our previous study (Zhou et al., 2016). In brief, PC3 and DU145 cells were seeded into 96-well plates separately at a density of 4×10^3 cells/200 μ l per well. Human peripheral blood mononuclear cells (PBMCs) were isolated from 15 ml of peripheral blood through density gradient centrifugation using Lymphoprep (DAKEWE, Shenzhen, China) and the suspensions of PBMCs were seeded into 96-well plate at the density of 8×10^3 cells/200 μ l per well. On the following day, different concentrations of DT-13 were added to each cell line. After 48 h treatment, 20 μ l MTT reagent was added to each well for additional 4 h incubation. Then the supernatant was removed and 150 μ l DMSO was added to dissolve the formazan crystals. The resulting absorbance at 490 nm was measured by using microplate reader iMark (Bio Rad, Hercules, CA, United States). IC₅₀ values were calculated based on the data generated from downward sloping dose-response curve by GraphPad Prism 5 Software (GraphPad Software, San Diego, CA, United States).

Flat Plate Colony Formation Assay

Flat plate colony formation assay was performed as we previously described, with a small modification (Chen et al., 2017). After treated with DT-13 (0, 2.5, 5, and 10 μ M) for 48 h, PC3

and DU145 cells were harvested and pipetted well to become single-cell suspension. After that, 4 ml of 10% FBS RPMI-1640 containing 0.6% agarose was injected into 60-mm dishes as the bottom layer, and 1×10^4 cells in 2 ml of 10% FBS RPMI-1640 and 0.3% agarose was put on the top. After incubation for 14 days, the colonies were fixed with 4% paraformaldehyde, and subsequently stained with crystal violet (0.5%) for 30 min. Colonies larger than 0.1 mm in diameter were counted using Image J software.

Cell Cycle Distribution Analysis

Cell cycle distribution was analyzed by PI labeling after the cells were treated with DT-13 as we previously described (Wang R. et al., 2016). Briefly, PC3 and DU145 cells were seeded into 6-well plates separately at a density of 4×10^5 cells/2 ml per well and treated with indicated concentrations of DT-13 (2.5, 5, and 10 μ M) for 48 h. Subsequently, both floating and adherent cells were collected, washed with cold PBS, fixed in ethanol (70%), and finally suspended in 50 μ g/ml of PI solution containing 0.5% Triton X-100 and 2% RNase A. Then the cells were placed in dark area for 30 min at 4°C and subjected to cell cycle analysis using BD FACS Verse flow cytometer (Becton Dickinson, Germany).

Annexin V/PI Staining Assay

Detection of cellular apoptosis was carried out by using the FITC Annexin-V apoptosis detection assay as reported by us previously (Wang Y. et al., 2016). Briefly, PC3 and DU145 cells were seeded into 6-well plates separately (4×10^5 cells/2 ml per well) and treated with DT-13 at indicated concentrations (2.5, 5, and 10 μ M). After incubation, cells were trypsinized, washed with ice-cold PBS, suspended in 50 μ l of 1 \times binding buffer, and stained with 2.5 μ l of FITC Annexin V and 2.5 μ l of PI for 15 min at 4°C in the dark. After a final dilution with 200 μ l of Annexin binding buffer, the samples were analyzed with BD FACS Verse flow cytometer (Becton Dickinson, Germany).

Hoechst Nuclear Staining

Hoechst 33342 has been used as a fluorescent nuclear staining reagent to identify apoptotic cells. PC3 and DU145 cells were placed on cover slips in 6-well plates at a density 4×10^5 cells/2 ml per well, followed by treatment with various concentration of DT-13 (0, 2.5, 5, and 10 μ M) and adriamycin (5 μ M) for 48 h. Afterward, the supernatant was removed and the cells were washed, fixed with formaldehyde, and incubated with pre-warmed cell culture medium containing Hoechst 33342 solution (1 μ g/ml) for 15 min. Fluorescent images were visualized and captured by a DMI3000B fluorescent microscope (Leica, Germany).

Assessment of Mitochondrial Membrane Potential (MMP)

The changes of MMP were estimated by using [5,5,6,6-Tetrachloro-1,1,3,3-tetraethylbenzimidazolylcarbocyanine iodide] (JC-1) probe as we previously described (Chen et al.,

2017). PC3 and DU145 cells were seeded into 6-well plates at a density of 4×10^5 cells/2 ml per well and incubated with 0, 2.5, 5, and 10 μ M of DT-13 for 48 h. Then the cells were collected and washed by cold PBS, followed by another 15 min exposure to 2 μ M of JC-1 at 37°C in darkness. The samples were suspended with 500 μ l of JC-1 staining buffer and the changes of MMP were analyzed by a FACS Verse flow cytometer (Becton Dickinson, Germany).

Measurement of Intracellular Reactive Oxygen Species (ROS) Levels

The fluorescent probe 2',7'-Dichlorodihydrofluorescein diacetate (DCFH-DA) was utilized to measure the changes of intracellular ROS levels as described by us previously (Wang R. et al., 2016). Briefly, PC3 and DU145 cells were seeded into 6-well plates separately at a density of 4×10^5 cells/2 ml per well, after incubation with indicated compounds for 24 h, cells were collected, washed with PBS for three times and incubated with 10 μ M of DCFH-DA in serum free medium for 20 min. Rosup, a reactive oxygen activator, was used as a positive control. After washing with PBS to remove the unconjugated probe, the samples were dispersed in 500 μ l of PBS and analyzed by flow cytometer (Becton Dickinson, Germany).

Wound Healing Assay

Wound healing assay was carried out to analyze the effect of DT-13 on cell migration as we reported previously, with a little modification (Zhao W. et al., 2013). Briefly, PC3 and DU145 cells were, respectively seeded into 12-well plates at a density of 2.5×10^5 cells/1 ml per well. After the cells reached 70–80% confluence, a 10 μ l pipette tip was used to scratch across the center of the monolayer cells. Then the cells was washed with PBS to remove the detached cells and replenished with fresh medium contained lower concentrations of DT-13 (0, 1, 2, and 4 μ M). After additional 24 h incubation, the migrated cells was monitored and imaged under the Olympus CKX41 microscope (Tokyo, Japan). Three images from three independent experiments were taken for quantitation.

Transwell Migration Assay

Transwell migration assay was conducted by using a Transwell Boyden Chamber (Corning, Corning, NY, United States), fitted with a polycarbonate membrane with pore size of 8 μ m as previously reported (Zhao W. et al., 2013). PC3 and DU145 cells were suspended in serum-free RPMI-1640 medium and plated into the upper chamber (5×10^5 cells/2 ml per well), while the lower chamber was filled with RPMI-1640 supplemented with 10% FBS. The same concentrations of DT-13 were added to both upper and lower compartments. Following 24 h incubation at 37°C, the cells that had migrated through the membrane were fixed with ethanol, stained with 0.5% eosin. Cells from the top side were removed with a cotton swab. The migrated cells were examined and counted by using the Olympus CKX41 microscope (Tokyo, Japan) at high power. Three images from three independent experiments were taken for quantitation.

Transwell Invasion Assay

Transwell invasion assay was used to examine the effect of DT-13 on invasive ability of PC3 cells as reported by us previously (Zhao W. et al., 2013). The transwell chamber was pretreated with matrigel (BD Biosciences, San Jose, MA, United States) and dried at room temperature. Other procedures are the same as for transwell migration assay, transwell invasion data were also obtained from the number of cells that had invaded across the membrane.

Gelatin Zymography Assay

The gelatin zymography was performed to detect MMP-2 and MMP-9 levels in PC3 cells. The cells (4×10^5 cells/2 ml per well) were seeded into 6-well plate, incubated with DT-13 (0, 1, 2, and 4 μ M) for 24 h, and then concentrated by Amicon Ultra-4 as we reported previously (Zhao W. et al., 2013). The protein samples were separated on 10% SDS-PAGE containing 0.1% gelatin by electrophoresis. Afterward, the gel was washed with 2.5% Triton X-100 and then incubated for 24 h at 37°C in reaction buffer (50 mM Tris-HCl, pH 7.5, 10 mM CaCl_2 , 0.01% NaN_3). Then the gel was stained with Coomassie Brilliant Blue R-250 (Merck, Darmstadt, Germany) in 10% acetic acid and 50% methanol and photographed by Bio-rad imager (Bio-rad ChemiDoc MP, United States).

Western Blot Analysis

PC3 and DU145 cells were seeded into 6-well plates separately at a density of 4×10^5 cells/2 ml per well. Cells were then treated with indicated concentrations of DT-13 and lysed in RIPA buffer for preparation of the whole cell lysate as we previously described (Wang R. et al., 2016). Equal amounts of protein were separated by 10–12% SDS-PAGE gels and then transferred electrophoretically to PVDF membranes. The blots were combined with primary antibodies (Akt, p-Akt, p-PDK1, p-mTOR, p-p70S6k, PI3K-p110 α , PI3K-p110 β , PARP, p-p38, p-ERK1/2, p-JNK, CytC, caspase-3, caspase-8, caspase-9, Integrin β 1, p-integrin β 1, and β -actin) followed by incubation with horseradish peroxidase-conjugated secondary antibodies. Immunoreactive bands were detected with ECL solution and digitalized by scanning.

Statistical Analysis

Data are presented as mean \pm standard deviation (SD) of three independent experiments. Student's *t*-test was carried out to determine significant differences among groups. The *p*-value < 0.05 was considered statistically significant. All of the statistical analysis was performed with GraphPad Prism 5 software.

RESULTS

DT-13 Inhibited Prostate Cancer Cells Proliferation *in vitro*

To investigate the *in vitro* anticancer activity of DT-13, we examined the effect of DT-13 on the proliferation of PC3 and

DU145 cell lines with MTT assay. After 48 h treatment, DT-13 inhibited PC3 and DU145 cell lines growth in a dose-dependent manner, with the IC_{50} values of 4.825 μ M and 5.102 μ M, respectively (Figure 1A). Besides, DT-13 showed far lower cytotoxic effect on human normal peripheral blood mononuclear cells (PBMC), with IC_{50} value of 127.8 μ M (Figure 1B). Next, soft agar colony formation assay was conducted to further evaluate the tumor growth inhibitory effect of DT-13. As shown in Figure 2, both number and size of the cell colonies were decreased after DT-13 treatment, indicating that DT-13 could inhibit the colony forming abilities of PC3 and DU145 cells. Together, these results suggested DT-13 had inhibiting potential of prostate cancer cells *in vitro*.

DT-13 Induced Apoptosis in Prostate Cancer Cells

To evaluate whether DT-13 inhibited cell proliferation by inducing apoptosis in PC3 and DU145 cells, Annexin V-FITC/PI staining assay was used to measure the population of apoptotic cells. As shown in Figures 3A,B, increase of apoptotic cells was observed following DT-13 treatment. The proportions of Annexin V staining cells in 0, 2.5, 5, and 10 μ M of DT-13 groups were 6.15, 6.26, 8.47, and 27.0 in PC3 cells and 1.74, 2.45, 10.8, and 18.2% in DU145 cells, indicating DT-13 induced early-phase apoptosis in both prostate cancer cell lines. More importantly, pretreatment with z-VAD-FMK, a Pan-caspase inhibitor, effectively blocked the effect of DT-13-induced apoptosis (Supplementary Figure S1A). Meanwhile, z-VAD-FMK treatment also significantly rescued cells viability after DT-13 treatment (Supplementary Figure S1B). Apoptosis is characterized by cellular shrinkage, nuclear condensation and fragmentation (Wang R. et al., 2016). Morphological assessment by Hoechst staining exhibited that chromatin condensation and nuclear shrinkage occurred in both DT-13 and ADR treated cells (Figure 3C), demonstrated the pro-apoptotic effect of DT-13 on PC3 and DU145 cells. In addition, to determine whether DT-13 can induce DNA damage, we measured the change of γ H2AX, the marker for DNA double strand breaks. As shown in Supplementary Figure S2, after expose to 10 μ M DT-13, the level of γ H2AX had no obvious change, suggesting DT-13 couldn't induce DNA damage in prostate cancer cells (Supplementary Figure S2). Taken together, these results indicated that DT-13 inhibited prostate cancer cells growth by inducing apoptosis.

DT-13 Did Not Cause Obvious Change in Cell Cycle Distribution

It is well established that cell cycle progress is crucial for cell proliferation, and treatment with chemical substances might cause cell senescence or apoptosis (Malumbres and Barbacid, 2009). The effect of DT-13 on cell cycle distribution was assessed by flow cytometry. DT-13 did not cause obvious change in cell cycle distribution. In PC3 cells, after treatment with 10 μ M DT-13, the cell population in G1, S and G2/M phases was 87.2, 3.90, and 8.53% respectively, while that for untreated cells

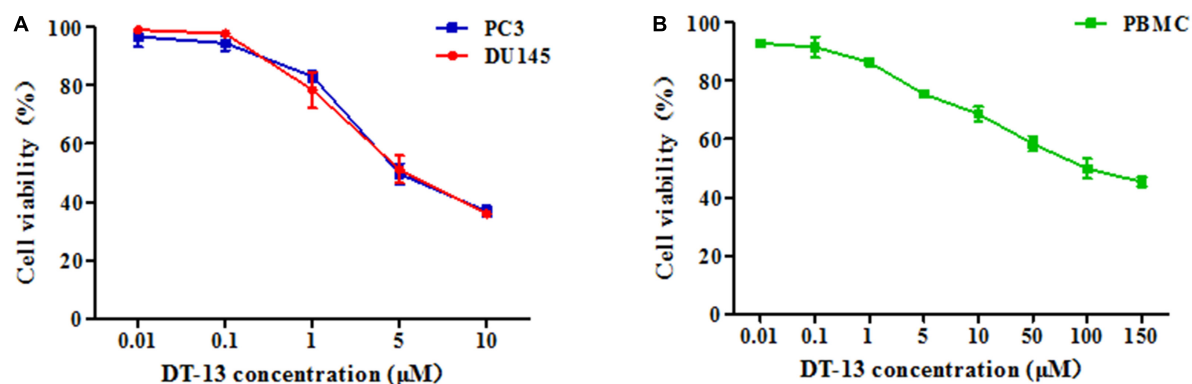


FIGURE 1 | Antiproliferative activities of DT-13 on prostate cancer cells and PBMC. Antiproliferative activities of indicated concentrations of DT-13 (0.01, 0.1, 1, 5, and 10 μM) toward **(A)** PC3, DU145, and **(B)** PBMC were determined by MTT assay. Data are presented as mean \pm SD, representative of three independent experiments.

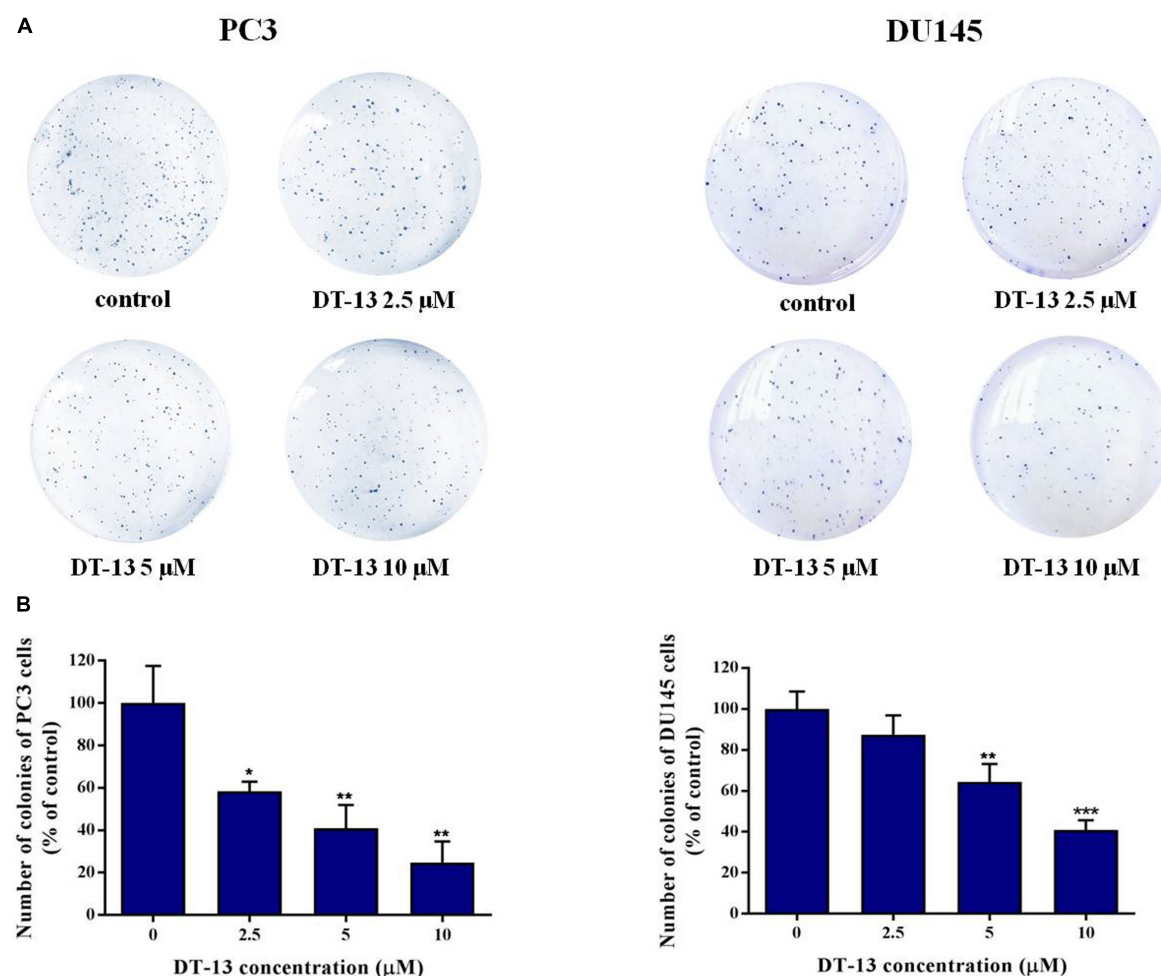


FIGURE 2 | Effect of DT-13 on colony formation capability of prostate cancer cells. **(A)** Clonogenic assay was carried out to assess the effect of DT-13 on the colony formation capability of PC3 and DU145 cells. After treatment with 0, 2.5, 5, and 10 μM of DT-13 for 48 h, cells were incubated in agarose plates for 14 days and then stained with crystal violet. **(B)** The histograms represent the number of colonies of PC3 and DU145 cells following treatment with DT-13, compared to those of control cells. Data are mean \pm SD ($n = 3$), representative of three independent experiments. * $P < 0.05$, ** $P < 0.01$, *** $P < 0.001$, compared with control.

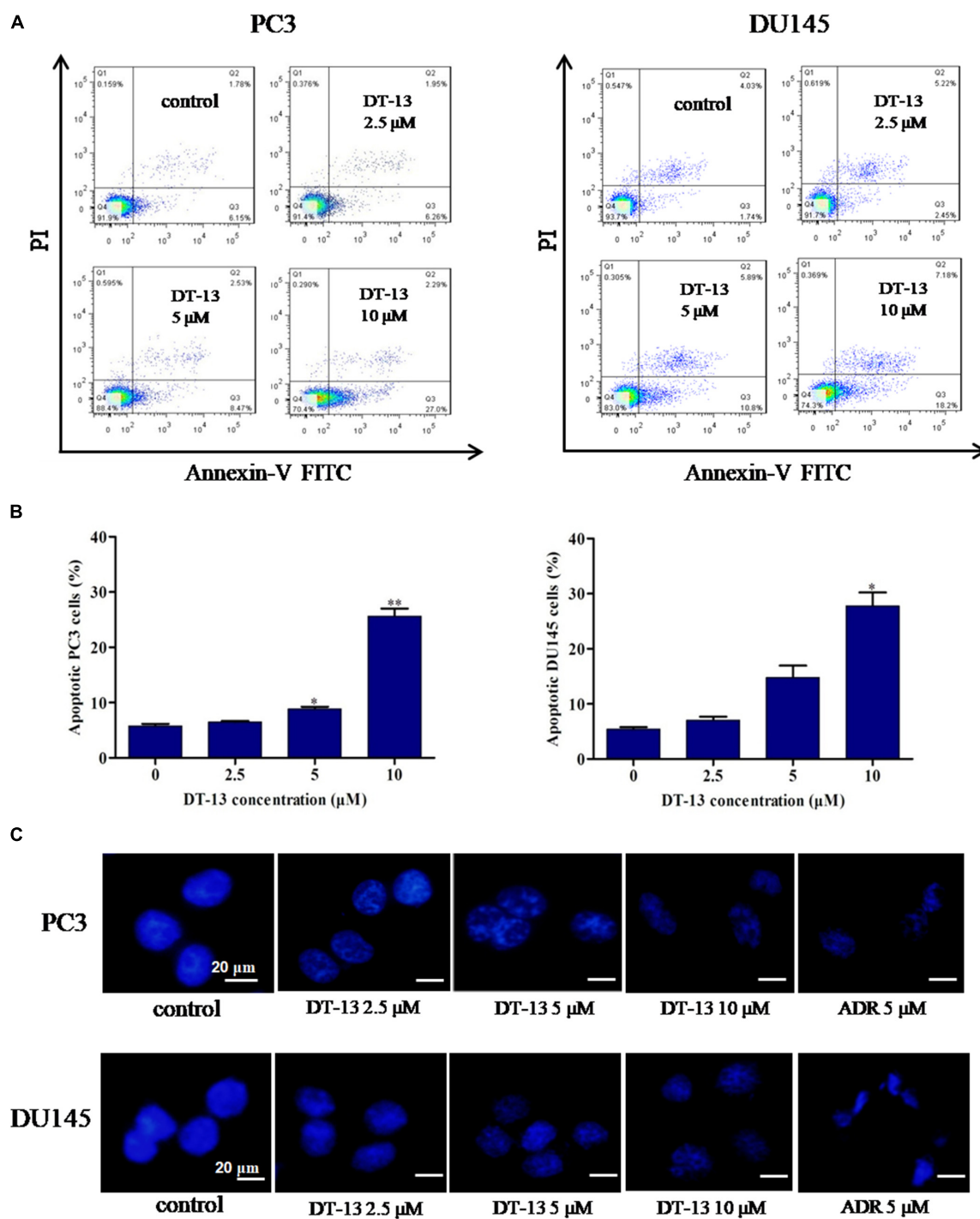


FIGURE 3 | DT-13 induced apoptosis in prostate cancer cells. **(A)** PC3 and DU145 cells were treated with DT-13 at 0, 2.5, 5, and 10 μ M for 48 h, stained with AnnexinV-FITC and PI, and then measured by flow cytometer. **(B)** The histograms show the percentage of apoptotic cells in PC3 and DU145 cells treated with indicated concentrations of DT-13 for 24 h. Data are mean \pm SD ($n = 3$), representative of three independent experiments. * $P < 0.05$, ** $P < 0.01$, compared with control. **(C)** PC3 and DU145 cells treated with different concentrations of DT-13 or 5 μ M Adriamycin (ADR) for 48 h, followed by staining with Hoechst 33342. Cytoplasmic shrinkage and nuclear fragmentation were observed under the fluorescence microscopy. Scale bar = 20 μ m.

was 82.5, 7.1, and 9.81%. In 10 μ M DT-13 treated DU145 cells, the cell population in G1, S and G2/M phases was 65.7, 4.91, and 24.8% respectively, while that for untreated cells was

64.5, 7.82, and 25.7%. The above results suggested DT-13 did not induce obvious growth arrest in PC3 and DU145 cells (Figures 4A,B).

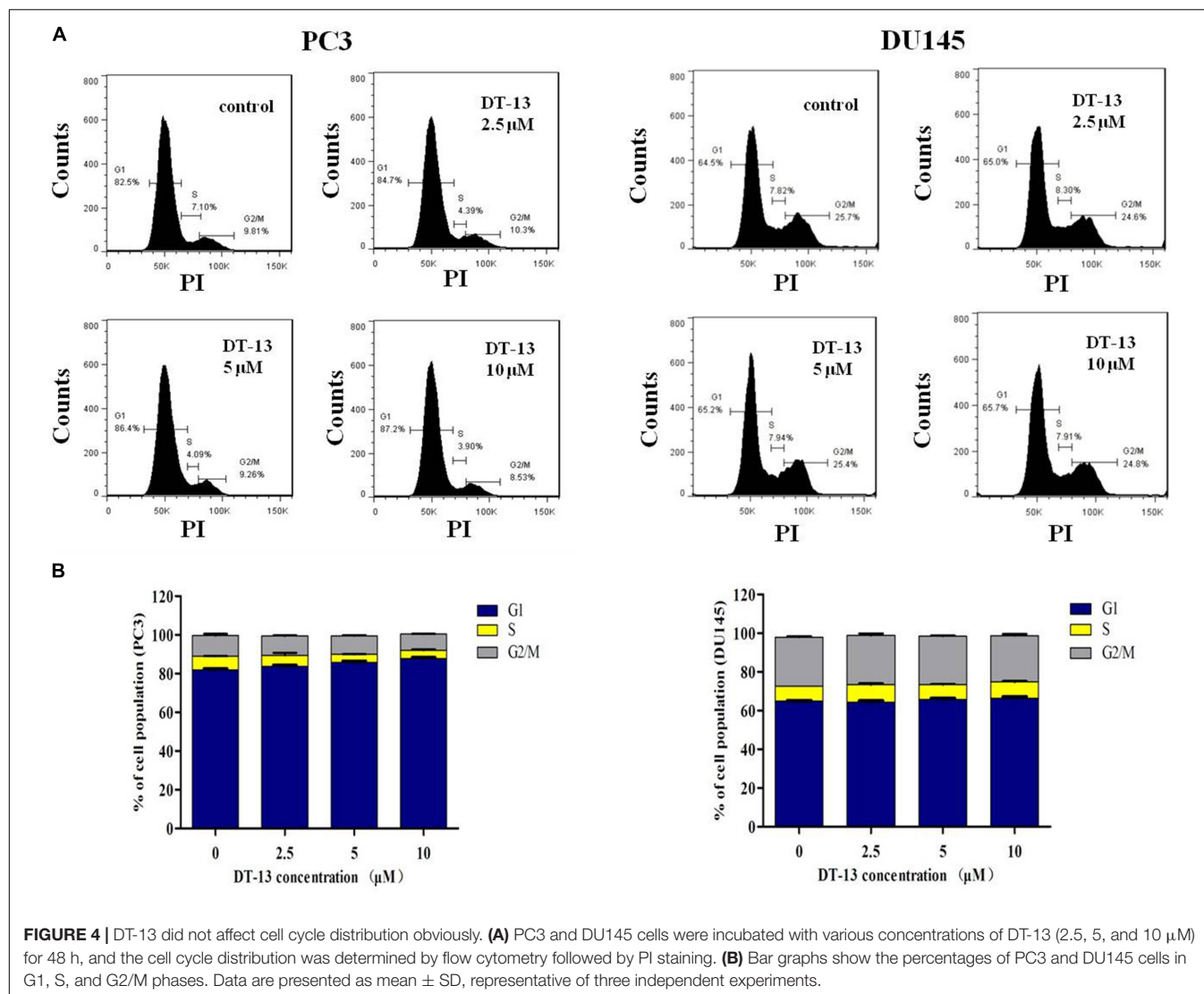
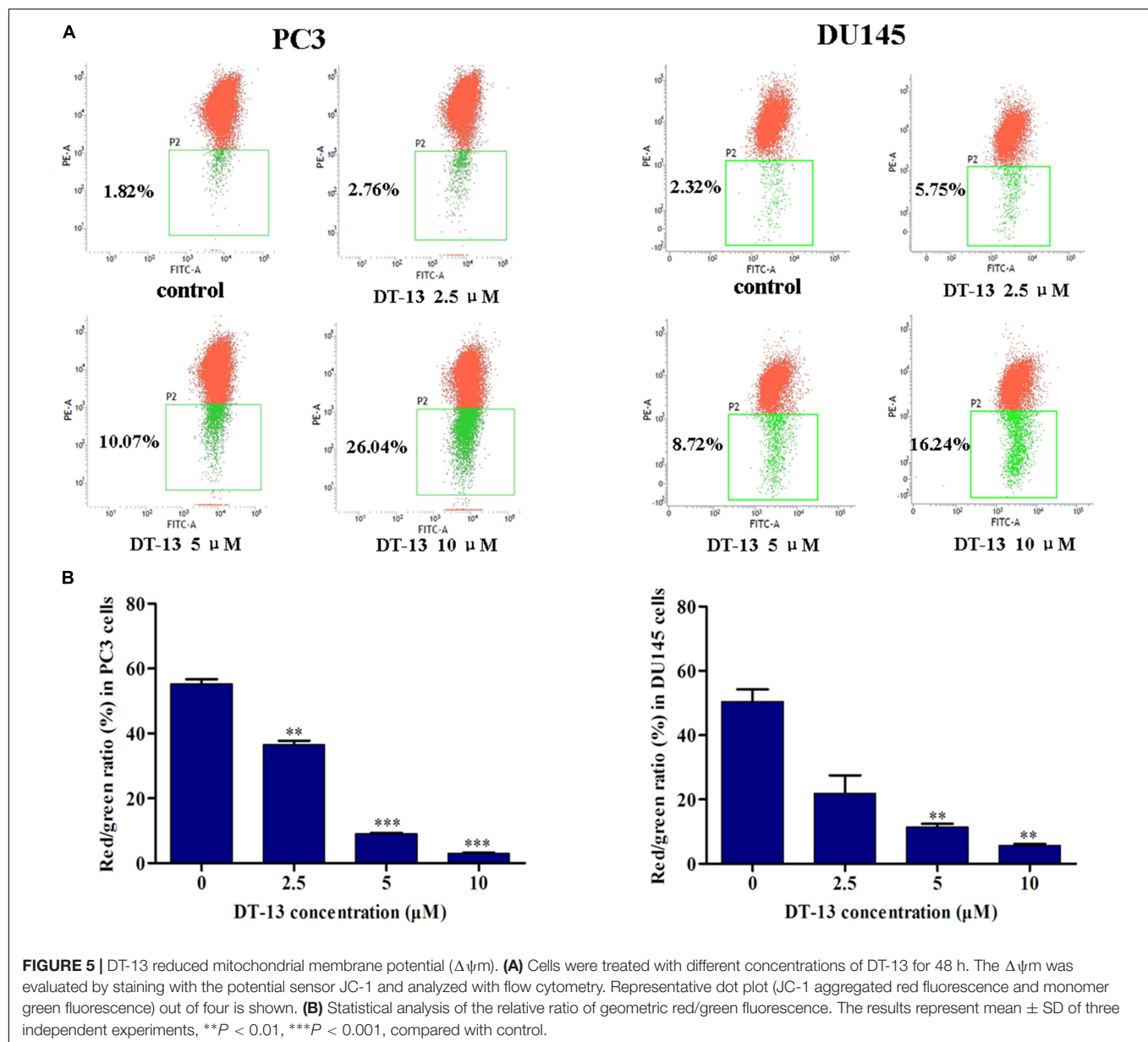


FIGURE 4 | DT-13 did not affect cell cycle distribution obviously. **(A)** PC3 and DU145 cells were incubated with various concentrations of DT-13 (2.5, 5, and 10 μ M) for 48 h, and the cell cycle distribution was determined by flow cytometry followed by PI staining. **(B)** Bar graphs show the percentages of PC3 and DU145 cells in G1, S, and G2/M phases. Data are presented as mean \pm SD, representative of three independent experiments.

DT-13 Promoted Apoptosis Through Mitochondrial Pathway

Mitochondria play an important role in keeping cells alive, and interruption of mitochondrial function will trigger apoptosis. Therein, the loss of MMP is an early sign of apoptosis occurrence (Kroemer et al., 1998). We explored the changes in MMP after DT-13 treatment using the membrane permeable fluorescent probe, JC-1. As shown in **Figure 5**, cells in green color indicated a decrease in mitochondrial membrane potential, while those in red color indicated the higher mitochondrial membrane potential. Accordingly, red/green rate decreased in a dose-dependent way in PC3 and DU145 cells after treatment with DT-13, suggesting DT-13 could reduce mitochondrial membrane potential in prostate cancer cells. The Bcl-2 family protein was known to affect cell apoptosis by activation or inactivation of mitochondrial outer membrane permeabilization pore, which is involved in regulation of Cytochrome c (Cyto c) release into cytosol to activate caspase cascades (Slee et al., 1999; Danial,

2007). Western blot analysis demonstrated that DT-13 increased the expressions of pro-apoptotic proteins Bax and Bad, and decreased the levels of anti-apoptotic protein Bcl-2 in PC3 and DU145 cells dose-dependently (**Figure 6A**). And the Bcl-2/Bax ratio apparently reduced after DT-13 treatment (**Figure 6B**). The expression level of Cyto c in mitochondria was down-regulated and that in the cytoplasm was up-regulated, suggesting DT-13 promoted Cyto c to release from mitochondria into cytosol (**Figure 6A**). Given that pro-caspase must undergo proteolytic activation to convert its active form to trigger apoptosis, we examined the effect of DT-13 on several key caspases and their cleaved form. As a result, the amount of cleaved caspase-9 and caspase-3 was increased in DT-13 treated cells, while that of the active caspase-8 was not detected, suggesting DT-13 might induce apoptosis through a mitochondrial-mediated intrinsic pathway. In addition, the cleavage of PARP as another sign of apoptosis was elevated after DT-13 treatment (**Figure 6A**). These results suggested that the apoptosis of PC3 and DU145 cells induced by DT-13 might be associated with the mitochondrial pathway.



DT-13 Had No Obvious Effect on ROS Production

It is well known that ROS plays important roles in modulation of cell apoptosis by changing the intracellular environment (Wu, 2006). We have investigated the effect of DT-13 on ROS level and found that compared with positive control, no obvious increase of ROS was detected in DT-13 treated cells (Supplementary Figure S3), indicating that DT-13 induced mitochondrial-initiated apoptosis might not be related to oxidative stress.

DT-13 Inhibited PC3 Cells Migration and Invasion

To explore the effect of DT-13 on cells migration and invasion, we performed a series of assays with DT-13 at non-cytotoxic

concentrations. In wound healing assay, 1, 2 and 4 μ M of DT-13 treatment for 24 h inhibited the migration of PC3 cells by 14.6, 33.5, and 52.6% respectively, compared to that for control cells, indicating that DT-13 inhibited PC3 cells migration in a dose-dependent manner (Figures 7A,B and Supplementary Figure S4). Nevertheless, DT-13 did not affect DU145 cells migration. We next used Transwell migration assay to further assess the anti-migration activity of DT-13. In accordance with the result in wound healing assay, DT-13 significantly inhibited the migration of PC3 rather than that of DU145 cells (Figures 7C,D). Subsequently, Transwell invasion assay was employed to investigate the effect of DT-13 on PC3 cells invasion capability. It was observed that following treatment with 1, 2 and 4 μ M of DT-13, the number of PC3 cells that had invaded through the membrane decreased to 80.1, 70.2, and

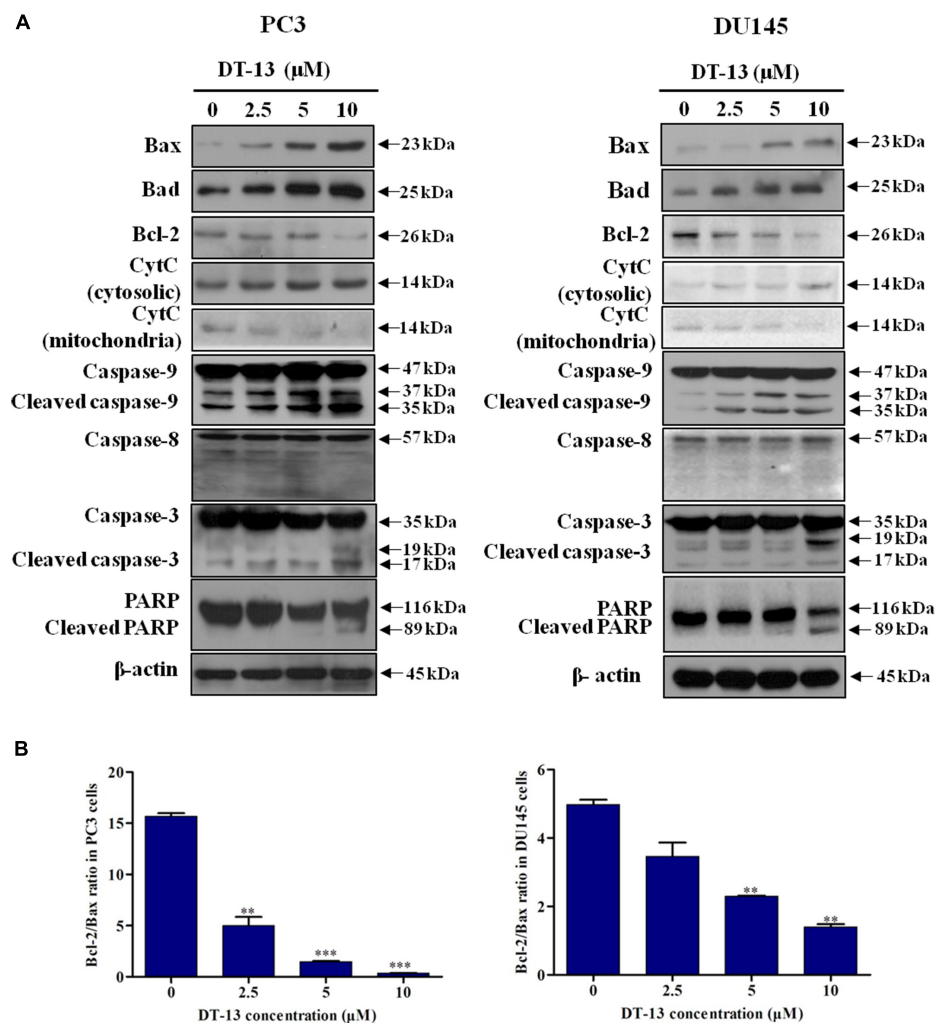


FIGURE 6 | Effect of DT-13 on the expression of apoptosis-related molecules in prostate cancer cells. **(A)** Western blot analysis of the expression of cell apoptosis-related proteins after DT-13 treatment. PC3 and DU145 cells were treated with 0, 2.5, 5, and 10 μ M of DT-13 for 48 h. The expression levels of Bax, Bad, Bcl-2, cytochrome c (CytC), Caspase-3, -8, -9, PARP, and cleaved Caspase-3, -8, -9, PARP were determined by western blot in both cell lines. **(B)** Bar graphs show the Bcl-2/Bax ratio in PC3 and DU145 cells. Data are mean \pm SD, representative of three independent experiments ($n = 3$), ** $P < 0.01$, *** $P < 0.001$, compared with control.

49.3%, respectively compared to that for control cells, indicating DT-13 was capable of blocking PC3 cells invasion (**Figures 7E,F**). In addition, we used z-VAD-FMK to assess if the inhibition of invasion/migration is independent of cell apoptosis in PC3 cells. As shown in **Supplementary Figures S5A–C**, pretreatment with z-VAD-FMK did not weaken the inhibitory effect of DT-13 on cell invasion and migration. Integrin β 1 as the downstream effector of PI3K, was reported to play a vital role in tumor migration and adhesion (Somanath et al., 2007). We have found that DT-13 inhibited the phosphorylation of Integrin β 1 in a dose-dependent manner (**Figure 7G**). Also, z-VAD-FMK treatment couldn't affect the reduction in phosphorylation of Integrin β 1 by DT-13 (**Supplementary Figure S5D**). The proteolytic activities of MMP-2 and MMP-9, which reflect the ability to degrade the components of extracellular matrix, were also decreased significantly after DT-13 treatment for 24 h (**Figure 7H**), further

proving the anti-metastatic activity of DT-13 on PC3 cells. To investigate the effect of DT-13 on EMT process in PC3 cells, we detected the protein expression of two EMT markers: Vimentin and E-cadherin in PC3 cells with or without DT-13 treatment. As expected, DT-13 treatment decreased expression of Vimentin and increased the expression of E-cadherin, suggesting DT-13 inhibited EMT process in PC3 cells (**Supplementary Figure S6**). Collectively, these results demonstrated that DT-13 could inhibit PC3 cell metastasis independent of cell apoptosis.

DT-13 Stimulated Apoptosis and Inhibited Metastasis Through Blocking PI3K/Akt Signaling Pathway

Several important cellular signaling pathways, such as PI3K/Akt pathway and MAPK pathway, are essential in regulating cell

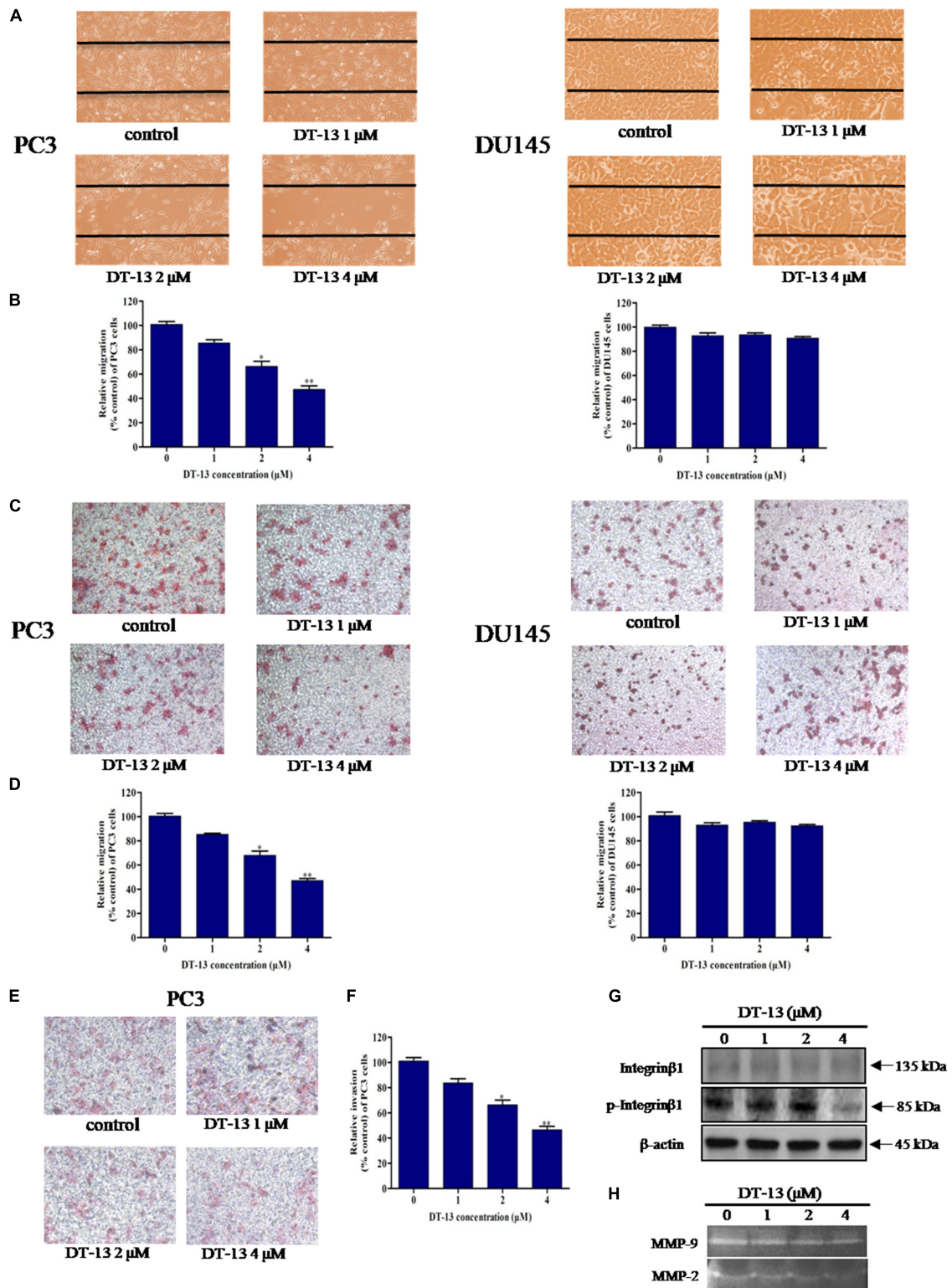


FIGURE 7 | DT-13 inhibited migration and invasion of prostate cancer PC3 cells. **(A)** Migration of prostate cancer cells with or without DT-13 treatment was determined using wound healing assay. Cells migrated to the wound area were photographed and counted by inverted microcopy. **(B)** Percentages of PC3 and DU145 cells migrated to the wound area following treatment with DT-13 relative to those of the control cells. Data are mean \pm SD, representative of three independent experiments ($n = 3$). $^*p < 0.05$, $^{**}p < 0.01$, compared with control. **(C)** Cells migration potential was assessed by Transwell migration assay.

(Continued)

FIGURE 7 | Continued

After treatment with DT-13 for 24 h, the cells migrated through the Transwell chamber membrane were measured. **(D)** Percentage of cells migrated after DT-13 treatment compared to those of control cells. Data are mean \pm SD, representative of three independent experiments ($n = 3$). * $p < 0.05$, ** $p < 0.01$, compared with control. **(E)** PC3 cells were subjected to a matrigel invasion assay with DT-13 treatment as indicated. PC3 cells invasion through the matrigel-coated chamber membrane were photographed and counted. **(F)** Percentage of PC3 cells invaded through the invasion chamber membrane after DT-13 treatment compared to those of control cells. Data are mean \pm SD, representative of three independent experiments ($n = 3$). * $p < 0.05$, ** $p < 0.01$, compared with control. **(G)** PC3 cells were exposed to the indicated concentrations of DT-13 for 24 h, then the expression level and phosphorylation level of Integrin $\beta 1$ was detected by Western blot. **(H)** PC3 cells were treated with the indicated concentrations of DT-13, and the MMP2/9 activity was determined by gelatin zymography assay.

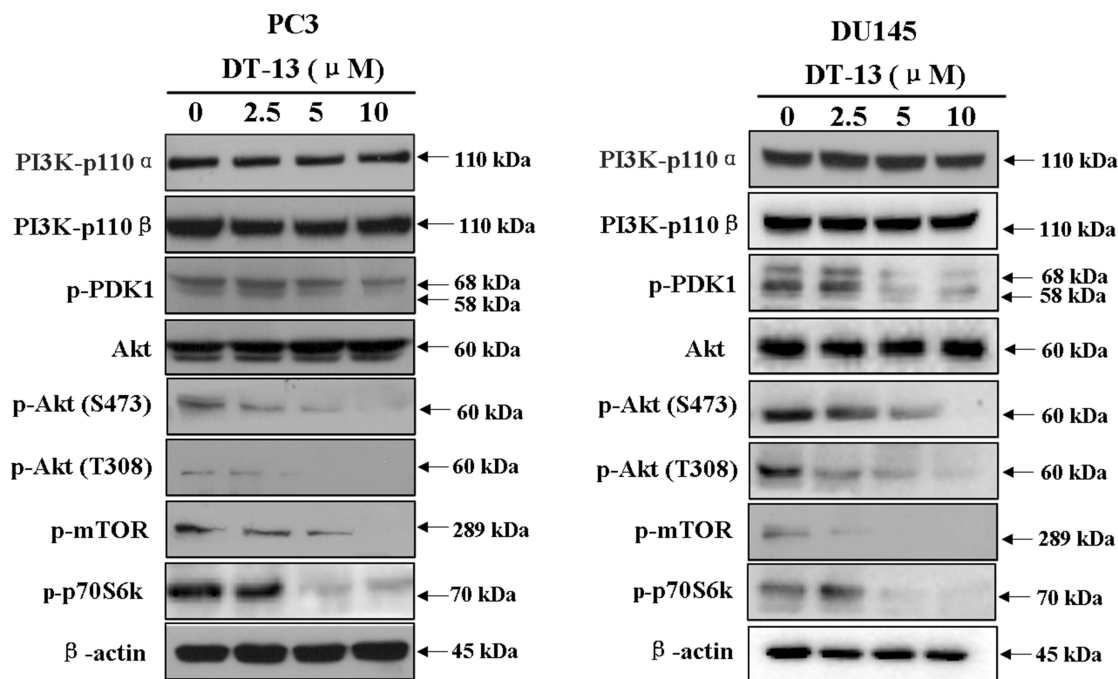


FIGURE 8 | Effect of DT-13 on PI3K/Akt pathway in prostate cancer cells. PC3 and DU145 cells were treated with 0, 2.5, 5, and 10 μ M of DT-13 for 48 h, then the cells were harvested, and the cell lysates were prepared to be available for western blot analysis for PI3K-p110 α , PI3K-p110 β , p-PDK1, p-Akt, Akt, p-mTOR and p-p70S6K.

growth, motility, apoptosis and metastasis (Kong and Yamori, 2009; Cargnello and Roux, 2011). Therefore, we investigated whether the effects of DT-13 on PC3 and DU145 cells were related to these two pathways. Firstly, we examined the activity of DT-13 on the key signaling molecules in PI3K/Akt pathway, and the results showed that DT-13 reduced the phosphorylation of Akt, mTOR, and p70S6K in a dose-dependent manner (Figure 8). Moreover, phosphorylation of PDK1, which is the effector of PI3K and the upstream activator of Akt was decreased. Meanwhile, there was no obvious change in the protein expression of PI3K-P110 α and PI3K-P110 β following DT-13 treatment. Additionally, ZSTK474, a specific PI3K inhibitor, was used as positive control to evaluate the effect of DT-13 on ROS production and ROS-activated proteins. As shown in Supplementary Figure S7A, no obvious increase of ROS was detected in either DT-13 or ZSTK474 treated prostate cancer cells. Also, the two compounds did not obviously decrease the phosphorylation of ROS activated proteins-ERK and p38 (Supplementary Figure S7B). Therefore, we can postulate that blockade of PI3K/Akt pathway might underlie the effect of DT-13 on apoptosis and migration in

prostate cancer cells. There are at least three distinct MAPK signaling molecules which mediate extracellular signals into the nucleus to turn on the responsive genes in mammalian cells, including ERK, JNK and p38 kinase (Cargnello and Roux, 2011). Here, we found the phosphorylation of p38, ERK and JNK in PC3 and DU145 cells was not affected by DT-13 (Supplementary Figure S8), suggesting the anticancer effect of DT-13 was not regulated by MAPK pathway. Taken together, DT-13 promoted apoptosis and suppressed metastasis in prostate cancer cells through down-regulating the PI3K/Akt signaling axis (Figure 9).

DISCUSSION

Natural products have been a rich source of lead compounds in drug discovery. More than half of commercialized anticancer drugs have been identified directly from natural sources, or indirectly by structural modification based on the natural lead compound (Gordaliza, 2007). Although a lot of anticancer agents have been successfully used in the control and treatment of cancer

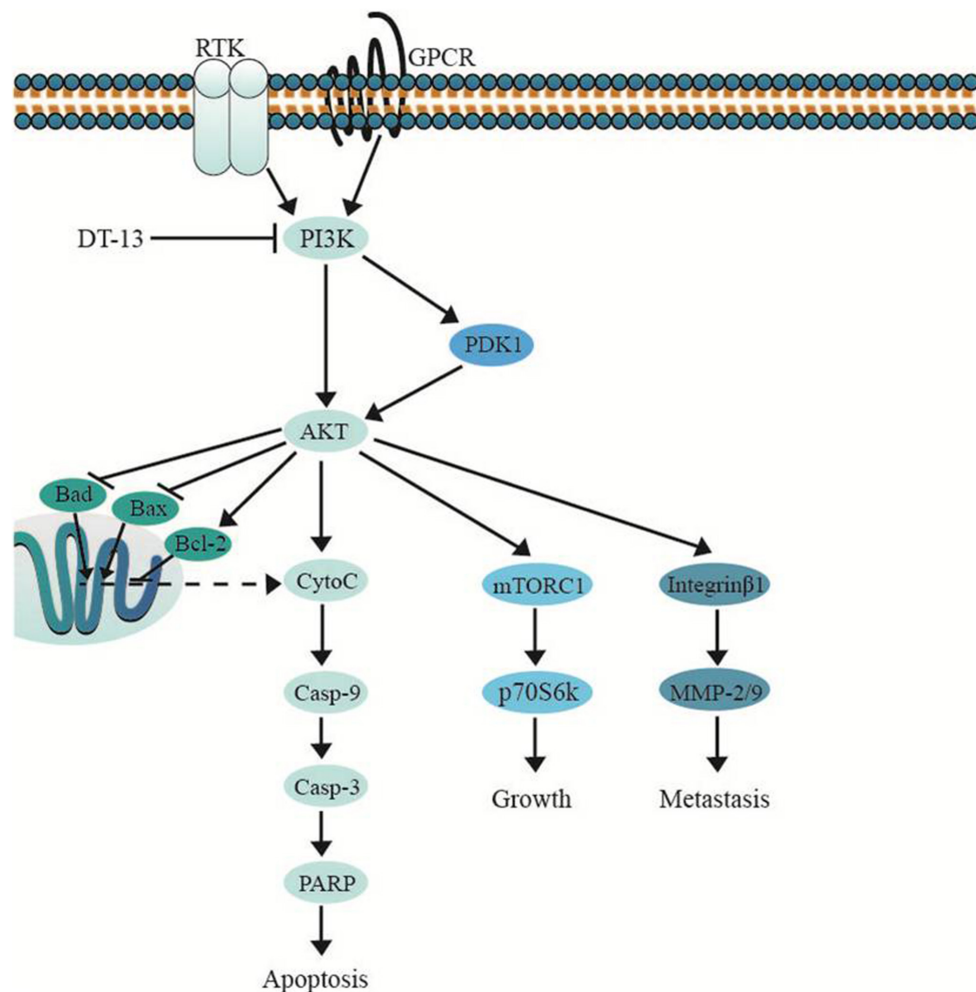


FIGURE 9 | DT-13 promoted mitochondrial apoptosis and inhibited metastasis via suppressing PI3K/Akt pathway.

progression, novel compounds are still needed. In this study, we have investigated the anti-cancer potential of the steroidal saponin DT-13 from *Liriope muscari* on prostate cancer cells. Previous study had shown the pro-apoptotic and anti-migration effect of DT-13 on lung cancer cells and gastric cancer cells. Also, Combination use of DT-13 and vinorelbine induced mitotic arrest in lung cancer NCI-H1299 cells (Zhang et al., 2012; Lin et al., 2014; Li et al., 2016, 2017a; Wei et al., 2016). However, the effect of DT-13 on prostate cancer and the underlying mechanism remain unexplored. Here, we report for the first time that DT-13 markedly inhibited proliferation and metastasis of human prostate cancer cells. We also demonstrated the potential antitumor mechanism of DT-13 involving apoptosis, migration, invasion, and PI3K/Akt pathway.

Apoptosis is an autonomic ordered programmed cell death that plays a critical role in the development and maintenance of homeostasis by eliminating damaged, aged or unnecessary cells. Impairment of this programmed cell death can result in tumorigenesis (Plati et al., 2011). Induction of apoptosis in cancer cells is known to be a key mechanism for many

chemotherapeutic agents (Grutter, 2000). In this study, we observed DT-13 suppressed PC3 and DU145 cells proliferation through inducing apoptosis. To date, two major apoptotic pathways have been reported: intrinsic and extrinsic pathway (Hassan et al., 2014). Within the intrinsic apoptotic pathway, the Bcl-2 protein family plays an important role in initiating apoptosis. As one family member, Bax is considered as a pro-apoptotic protein that can form a pore in the mitochondrial membrane to allow cytochrome C release from mitochondria into the cytoplasm to activate apoptosis. The anti-apoptotic Bcl-2 prevents the release of cytochrome C, and Bad could inactivate Bcl-2 via forming a heterodimer with it, thus allowing Bax-triggered apoptosis (Giam et al., 2008). In cytoplasm, cytochrome C binds to Apaf-1 and ATP, thus activates procaspase-9, and caspase-3, -6, and -7 to trigger cell death. Activation of caspase-3 also leads to the cleavage and inactivation of PARP, which is important in keeping cell stability and survival (Slee et al., 1999; Yu et al., 2006). Our results showed after DT-13 treatment, the expression of Bax, Bad, Cyto C (cytosolic), cleaved caspase-3, -9, PARP was up-regulated, the expression of Bcl-2 and Cyto C

(mitochondrial) was down-regulated, and the active caspase-8 (a sign of extrinsic pathway) was not detected, suggesting that intrinsic mitochondrial signaling pathway might be involved in DT-13-mediated cell death.

As prostate cancer cells commonly spread to lymph nodes and bones in the body, and the prognosis for patients with metastatic prostate cancer is very bad (Yu et al., 2006). So we next explored whether DT-13 had anti-metastasis activity on PC3 and DU145 cells. The results revealed that DT-13 obviously inhibited PC3 cells migration and invasion. Interestingly, DT-13 did not affect the metastasis of DU145 cells. It was reported that DU145 cells exhibits the characteristics of mesenchymal cells, and has stronger invasive potential than PC3 cells (van Bokhoven et al., 2003). We postulate that more powerful agent is required to suppress the metastasis of DU145 cells. To further explore the anti-metastasis mechanism of DT-13, we detected the effect of DT-13 on the phosphorylation of Integrin β 1 and the proteolytic capability of MMP-2/9. Enhanced expression of Integrin β 1 was observed in prostate tumor cells, which is correlated with worse outcomes of patients (Lee et al., 2013). Downregulation of Integrin β 1 could attenuate cell growth, migration, adhesion as well as angiogenesis (Howe and Addison, 2012). MMP-2/9 degrades extracellular matrix, which plays a critical role in cancer metastasis (Alaseem et al., 2017). Our result showed DT-13 could reduce the phosphorylation of Integrin β 1 and inhibit the proteolytic activities of MMP-2/9, which might in turn block the migration and invasion of PC3 cells.

At last, we investigated the molecular mechanism which might correlate with the above effects of DT-13. Previously reports showed DT-13 inhibited MDA-MB-435 cell adhesion and invasion by suppressing p38MAPK, and induced apoptosis through PI3K/Akt pathway in HUVEC (Zhang et al., 2012; Qiu et al., 2014). Therefore, the effect of DT-13 on PI3K/Akt and MAPK pathways was examined in PC3 and DU145 cells. The results showed the phosphorylation of PI3K downstream effectors including PDK-1, Akt, mTOR and p70S6K was inhibited in a dose-dependent manner, while the expression of PI3K-p110 α and -p110 β was not changed. Akt is known to phosphorylate CREB, which could promote the expression of Bcl-2. The pro-apoptotic proteins, such as Bad and Bax, were negatively regulated by Akt through direct phosphorylation (Du and Montminy, 1998). Akt also prevents cell death

by phosphorylation inactivation of Caspase-9 (Manning and Cantley, 2007). Therefore, the apoptosis induced by DT-13 might be attributed to the inhibition of Akt phosphorylation. On the aspect of cancer metastasis, it is well known that PI3K/Akt pathway plays a key role in cancer migration, invasion, and adhesion. Down-regulation of the phosphorylated Akt inhibits the proteolytic activity of MMP2/9 (Zhao W. et al., 2013). Akt phosphorylates Integrin β 1, which promotes tumor metastasis though intervention of extracellular matrix and the activity of MMPs (Somanath et al., 2007). Therefore, the anti-metastasis effect of DT-13 might be attributed to the inhibition of PI3K/Akt pathway. Moreover, DT-13 showed no effect on p38, ERK and JNK in PC3 and DU145 cells, suggesting the anticancer effect might not be related with MAPK pathway.

In summary, our findings demonstrate DT-13 can effectively induce apoptosis and inhibit metastasis in prostate cancer cells, the mechanism of which might be attributed to the blockade of PI3K/Akt signaling pathway. Since DT-13 showed weak cytotoxicity on normal cells, it is worthwhile to be further evaluated as an anticancer drug candidate for prostate cancer therapy.

AUTHOR CONTRIBUTIONS

ZW, YW, and SZ performed the experiments. YL, XP, and SZ analyzed the data. ZZ, YQ, and MJ prepared the figures. ZW and RW wrote the main manuscript. YZ and DK designed the experiments. All authors reviewed the manuscript.

FUNDING

This work was supported by grant from National Natural Science Foundation of China (81673464), and the grant for Major Project of Tianjin for New Drug Development (17ZXXYSY00050).

SUPPLEMENTARY MATERIAL

The Supplementary Material for this article can be found online at: <https://www.frontiersin.org/articles/10.3389/fphar.2018.01450/full#supplementary-material>

REFERENCES

- Alaseem, A., Alhazzani, K., Dondapati, P., Alobid, S., Bishayee, A., and Rathinavelu, A. (2017). Matrix metalloproteinases: a challenging paradigm of cancer management. *Semin. Cancer Biol.* doi: 10.1016/j.semcancer.2017.11.008 [Epub ahead of print].
- Cargnello, M., and Roux, P. P. (2011). Activation and function of the MAPKs and their substrates, the MAPK-activated protein kinases. *Microbiol. Mol. Biol. Rev.* 75, 50–83. doi: 10.1128/mmmbr.00031-10
- Center, M. M., Jemal, A., Lortet-Tieulent, J., Ward, E., Ferlay, J., Brawley, O., et al. (2012). International variation in prostate cancer incidence and mortality rates. *Eur. Urol.* 61, 1079–1092. doi: 10.1016/j.eururo.2012.02.054
- Chen, Y., Zhou, Q., Zhang, L., Zhong, Y., Fan, G., Zhang, Z., et al. (2017). Stelletin B induces apoptosis in human chronic myeloid leukemia cells via targeting PI3K and Stat5. *Oncotarget* 8, 28906–28921. doi: 10.18632/oncotarget.15957
- Cohen, R. B. (2014). Current challenges and clinical investigations of epidermal growth factor receptor (EGFR)- and ErbB family-targeted agents in the treatment of head and neck squamous cell carcinoma (HNSCC). *Cancer Treat. Rev.* 40, 567–577. doi: 10.1016/j.ctrv.2013.10.002
- Danial, N. N. (2007). BCL-2 family proteins: critical checkpoints of apoptotic cell death. *Clin. Cancer Res.* 13, 7254–7263. doi: 10.1158/1078-0432.ccr-07-1598
- Du, H., Liu, Y., Chen, X., Yu, X., Hou, X., Li, H., et al. (2018). DT-13 synergistically potentiates the sensitivity of gastric cancer cells to topotecan via cell cycle arrest in vitro and in vivo. *Eur. J. Pharmacol.* 818, 124–131. doi: 10.1016/j.ejphar.2017.10.014
- Du, K., and Montminy, M. (1998). CREB is a regulatory target for the protein kinase Akt/PKB. *J. Biol. Chem.* 273, 32377–32379.

- Giam, M., Huang, D. C., and Bouillet, P. (2008). BH3-only proteins and their roles in programmed cell death. *Oncogene* 27(Suppl. 1), S128–S136. doi: 10.1038/onc.2009.50
- Gordaliza, M. (2007). Natural products as leads to anticancer drugs. *Clin. Transl. Oncol.* 9, 767–776.
- Grutter, M. G. (2000). Caspases: key players in programmed cell death. *Curr. Opin. Struct. Biol.* 10, 649–655.
- Hassan, M., Watari, H., AbuAlmaaty, A., Ohba, Y., and Sakuragi, N. (2014). Apoptosis and molecular targeting therapy in cancer. *Biomed. Res. Int.* 2014:150845. doi: 10.1155/2014/150845
- Howe, G. A., and Addison, C. L. (2012). Beta1 integrin: an emerging player in the modulation of tumorigenesis and response to therapy. *Cell Adh. Migr.* 6, 71–77. doi: 10.4161/cam.20077
- Khan, G. J., Rizwan, M., Abbas, M., Naveed, M., Boyang, Y., Naeem, M. A., et al. (2018). Pharmacological effects and potential therapeutic targets of DT-13. *Biomed. Pharmacother.* 97, 255–263. doi: 10.1016/j.biopha.2017.10.101
- Kong, D., and Yamori, T. (2009). Advances in development of phosphatidylinositol 3-kinase inhibitors. *Curr. Med. Chem.* 16, 2839–2854.
- Kroemer, G., Dallaporta, B., and Resche-Rigon, M. (1998). The mitochondrial death/life regulator in apoptosis and necrosis. *Annu. Rev. Physiol.* 60, 619–642. doi: 10.1146/annurev.physiol.60.1.619
- Kumar, S., Guru, S. K., Pathania, A. S., Manda, S., Kumar, A., Bharate, S. B., et al. (2015). Faspaplysin induces caspase mediated crosstalk between apoptosis and autophagy through the inhibition of PI3K/AKT/mTOR signaling cascade in human leukemia HL-60 cells. *J. Cell. Biochem.* 116, 985–997. doi: 10.1002/jcb.25053
- Lawania, R. D., and Mishra, A. (2013). Anticancer potential of plants and natural products: a review. *J. Ethnopharmacol.* 01, 622–628.
- Lee, Y., Jin, J., Cheng, C., Huang, C., Song, J., Huang, M., et al. (2013). Targeting constitutively activated $\beta 1$ integrins inhibits prostate cancer metastasis. *Mol. Cancer Res.* 11, 405–417. doi: 10.3892/ol.2018.8076
- Li, H., Sun, L., de Carvalho, E. L., Li, X., Lv, X., Khan, G. J., et al. (2016). DT-13, a saponin monomer of dwarf lilyturf tuber, induces autophagy and potentiates anti-cancer effect of nutrient deprivation. *Eur. J. Pharmacol.* 781, 164–172. doi: 10.1016/j.ejphar.2016.04.016
- Li, H., Sun, L., Li, H., Lv, X., Semukunzi, H., Li, R., et al. (2017a). DT-13, a saponin monomer 13 of the *Dwarf lilyturf* tuber, synergized with vinorelbine to induce mitotic arrest via activation of ERK signaling pathway in NCI-H1299 cells. *Biomed. Pharmacother.* 89, 1277–1285. doi: 10.1016/j.biopha.2017.02.104
- Li, H., Sun, L., Li, H., Lv, X., Semukunzi, H., Li, R., et al. (2017b). DT-13 synergistically enhanced vinorelbine-mediated mitotic arrest through inhibition of FOXM1-BICD2 axis in non-small-cell lung cancer cells. *Cell Death Dis.* 8:e2810. doi: 10.1038/cddis.2017.218
- Lin, S. S., Fan, W., Sun, L., Li, F. F., Zhao, R. P., Zhang, L. Y., et al. (2014). The saponin DT-13 inhibits gastric cancer cell migration through down-regulation of CCR5-CCL5 axis. *Chin. J. Nat. Med.* 12, 833–840. doi: 10.1016/s1875-5364(14)60125-4
- Malumbres, M., and Barbacid, M. (2009). Cell cycle, CDKs and cancer: a changing paradigm. *Nat. Rev. Cancer* 9, 153–166. doi: 10.1038/nrc2602
- Manning, B. D., and Cantley, L. C. (2007). AKT/PKB signaling: navigating downstream. *Cell* 129, 1261–1274. doi: 10.1016/j.cell.2007.06.009
- Massacesi, C., Di Tomaso, E., Urban, P., Germa, C., Quadt, C., Trandafir, L., et al. (2016). PI3K inhibitors as new cancer therapeutics: implications for clinical trial design. *Onco Targets Ther.* 9, 203–210. doi: 10.2147/ott.s89967
- Perez-Gracia, J. L., Diez Caballero, F., Gurrpide, A., de Fata Chillon, F. R., and Villacampa, F. (2018). The role of chemotherapy in the treatment of hormone sensitive metastatic prostate cancer. *Arch. Esp. Urol.* 71, 276–280.
- Plati, J., Bucur, O., and Khosravi-Far, R. (2011). Apoptotic cell signaling in cancer progression and therapy. *Integr. Biol.* 3, 279–296. doi: 10.1039/c0ib00144a
- Qiu, C., Jozsef, L., Yu, B., and Yu, J. (2014). Saponin monomer 13 of dwarf lilyturf tuber (DT-13) protects serum withdrawal-induced apoptosis through PI3K/Akt in HUVEC. *Biochem. Biophys. Res. Commun.* 443, 74–79. doi: 10.1016/j.bbrc.2013.11.056
- Ren-Ping, Z., Sen-Sen, L., Yuan, S. T., Yu, B. Y., Bai, X. S., Sun, L., et al. (2014). DT-13, a saponin of dwarf lilyturf tuber, exhibits anti-cancer activity by down-regulating C-C chemokine receptor type 5 and vascular endothelial growth factor in MDA-MB-435 cells. *Chin. J. Nat. Med.* 12, 24–29. doi: 10.1016/s1875-5364(14)60005-4
- Siegel, R. L., Miller, K. D., and Jemal, A. (2018). Cancer statistics, 2018. *CA Cancer J. Clin.* 68, 7–30. doi: 10.3322/caac.21442
- Slee, E. A., Harte, M. T., Kluck, R. M., Wolf, B. B., Casiano, C. A., Newmeyer, D. D., et al. (1999). Ordering the cytochrome c-initiated caspase cascade: hierarchical activation of caspases-2, -3, -6, -7, -8, and -10 in a caspase-9-dependent manner. *J. Cell. Biol.* 144, 281–292.
- Somanath, P. R., Kandel, E. S., Hay, N., and Byzova, T. V. (2007). Akt1 signaling regulates integrin activation, matrix recognition, and fibronectin assembly. *J. Biol. Chem.* 282, 22964–22976. doi: 10.1074/jbc.M700241200
- van Bokhoven, A., Varella-Garcia, M., Korch, C., Johannes, W. U., Smith, E. E., Miller, H. L., et al. (2003). Molecular characterization of human prostate carcinoma cell lines. *Prostate* 57, 205–225. doi: 10.1002/pros.10290
- Wade, C. A., and Kyprianou, N. (2018). Profiling prostate cancer therapeutic resistance. *Int. J. Mol. Sci.* 19:E904. doi: 10.3390/ijms19030904
- Wang, R., Zhang, Q., Peng, X., Zhou, C., Zhong, Y., Chen, X., et al. (2016). Stelletin B induces G1 arrest, apoptosis and autophagy in human non-small cell lung cancer A549 cells via blocking PI3K/Akt/mTOR pathway. *Sci. Rep.* 6:27071. doi: 10.1038/srep27071
- Wang, Y., Liu, J., Qiu, Y., Jin, M., Chen, X., Fan, G., et al. (2016). ZSTK474, a specific class I phosphatidylinositol 3-kinase inhibitor, induces G1 arrest and autophagy in human breast cancer MCF-7 cells. *Oncotarget* 7, 19897–19909. doi: 10.18632/oncotarget.7658
- Wei, X. H., Lin, S. S., Liu, Y., Zhao, R. P., Khan, G. J., Du, H. Z., et al. (2016). DT-13 attenuates human lung cancer metastasis via regulating NMIIA activity under hypoxia condition. *Oncol. Rep.* 36, 991–999. doi: 10.3892/or.2016.4879
- Wu, W. S. (2006). The signaling mechanism of ROS in tumor progression. *Cancer Metastasis Rev.* 25, 695–705. doi: 10.1007/s10555-006-9037-8
- Yap, T. A., Bjerke, L., Clarke, P. A., and Workman, P. (2015). Drugging PI3K in cancer: refining targets and therapeutic strategies. *Curr. Opin. Pharmacol.* 23, 98–107. doi: 10.1016/j.coph.2015.05.016
- Yu, S. W., Andrabi, S. A., Wang, H., Kim, N. S., Poirier, G. G., Dawson, T. M., et al. (2006). Apoptosis-inducing factor mediates poly(ADP-ribose) (PAR) polymer-induced cell death. *Proc. Natl. Acad. Sci. U.S.A.* 103, 18314–18319. doi: 10.1073/pnas.0606528103
- Yu, X. W., Lin, S., Du, H. Z., Zhao, R. P., Feng, S. Y., Yu, B. Y., et al. (2016). Synergistic combination of DT-13 and topotecan inhibits human gastric cancer via myosin IIA-induced endocytosis of EGF receptor in vitro and in vivo. *Oncotarget* 7, 32990–33003. doi: 10.18632/oncotarget.8843
- Zhang, Y., Liu, J., Kou, J., Yu, J., and Yu, B. (2012). DT-13 suppresses MDA-MB-435 cell adhesion and invasion by inhibiting MMP-2/9 via the p38 MAPK pathway. *Mol. Med. Rep.* 6, 1121–1125. doi: 10.3892/mmr.2012.1047
- Zhao, R., Sun, L., Lin, S., Bai, X., Yu, B., Yuan, S., et al. (2013). The saponin monomer of dwarf lilyturf tuber, DT-13, inhibits angiogenesis under hypoxia and normoxia via multi-targeting activity. *Oncol. Rep.* 29, 1379–1386. doi: 10.3892/or.2013.2272
- Zhao, W., Guo, W., Zhou, Q., Ma, S. N., Wang, R., Qiu, Y., et al. (2013). In vitro antimetastatic effect of phosphatidylinositol 3-kinase inhibitor ZSTK474 on prostate cancer PC3 cells. *Int. J. Mol. Sci.* 14, 13577–13591. doi: 10.3390/ijms140713577
- Zhao, W., Qiu, Y., and Kong, D. (2017). Class I phosphatidylinositol 3-kinase inhibitors for cancer therapy. *Acta Pharm. Sin. B* 7, 27–37. doi: 10.1016/j.apsb.2016.07.006
- Zhou, Q., Chen, Y., Chen, X., Zhao, W., Zhong, Y., Wang, R., et al. (2016). In vitro antileukemia activity of ZSTK474 on K562 and multidrug resistant K562/A02 Cells. *Int. J. Biol. Sci.* 12, 631–638. doi: 10.7150/ijbs.14878

Conflict of Interest Statement: The authors declare that the research was conducted in the absence of any commercial or financial relationships that could be construed as a potential conflict of interest.

Copyright © 2018 Wang, Wang, Zhu, Liu, Peng, Zhang, Zhang, Qiu, Jin, Wang, Zhong and Kong. This is an open-access article distributed under the terms of the Creative Commons Attribution License (CC BY). The use, distribution or reproduction in other forums is permitted, provided the original author(s) and the copyright owner(s) are credited and that the original publication in this journal is cited, in accordance with accepted academic practice. No use, distribution or reproduction is permitted which does not comply with these terms.



MiR-3188 Inhibits Non-small Cell Lung Cancer Cell Proliferation Through FOXO1-Mediated mTOR-p-PI3K/AKT-c-JUN Signaling Pathway

Chunyan Wang*, Enqi Liu, Wen Li, Jue Cui and Tongxiang Li*

College of Food and Biology Engineering, Xuzhou Institute of Technology, Xuzhou, China

OPEN ACCESS

Edited by:

Dong-Hua Yang,
St. John's University, United States

Reviewed by:

Qisi Lu,
The Third Affiliated Hospital
of Southern Medical University, China
Haichang Li,
The Ohio State University,
United States

*Correspondence:

Chunyan Wang
cy_wang606@126.com
Tongxiang Li
1226048753@qq.com;
litxresearch@126.com

Specialty section:

This article was submitted to
Experimental Pharmacology
and Drug Discovery,
a section of the journal
Frontiers in Pharmacology

Received: 19 September 2018

Accepted: 05 November 2018

Published: 11 December 2018

Citation:

Wang C, Liu E, Li W, Cui J and
Li T (2018) MiR-3188 Inhibits
Non-small Cell Lung Cancer Cell
Proliferation Through
FOXO1-Mediated
mTOR-p-PI3K/AKT-c-JUN Signaling
Pathway. *Front. Pharmacol.* 9:1362.
doi: 10.3389/fphar.2018.01362

This study investigated the role of miR-3188 on the proliferation of non-small cell lung cancer cells and its relationship to FOXO1-modulated feedback loop. Two non-small cell lung cancer (NSCLC) cell lines A549 and H1299 were used. RNA silencing was achieved by lentiviral transfection. Cell proliferation was assessed by immunohistochemical staining of Ki67 and PCNA, Edu incorporation, and colony formation assay. Western blotting was used to examine expression of FOXO1, mTOR, p-mTOR, CCND1, p21, c-JUN, AKT, pAKT, PI3K, p-PI3K, and p27 proteins. It was found that miR-3188 reduced cell proliferation in NSCLC cells. Molecular analyses indicated that the effect of mammalian target of rapamycin (mTOR) was directly mediated by miR-3188, leading to p-PI3K/p-AKT/c-JUN inactivation. The inhibition of this signaling pathway further caused cell-cycle suppression. Moreover, FOXO1 was found to be involved in regulating the interaction of miR-3188 and mTOR through p-PI3K/p-AKT/c-JUN signaling pathway. Taken together, our study demonstrated that miR-3188 interacts with mTOR and FOXO1 to inhibit NSCLC cell proliferation through a mTOR-p-PI3K/AKT-c-JUN signaling pathway. Therefore, miR-3188 might be a potential target for the treatment of NSCLC.

Keywords: miR-3188, NSCLC, proliferation, mTOR, PI3K/AKT, c-JUN

INTRODUCTION

MicroRNAs (miRNAs or miRs) play important roles in development, cellular differentiation, proliferation, cell cycle control, and cell death (Bhaskaran and Mohan, 2014). They are critical in development and progression of various kinds of diseases including cancer (Hayes et al., 2014; Rupaimoole and Slack, 2017). Since it was found that the miRNA was involved in chronic lymphocytic leukemia, more and more miRNAs were identified to link with development and progression of cancers (Musilova and Mraz, 2015). It has been reported that miRNAs can regulate chemotherapeutic efficacy in multiple cancers (Magee et al., 2015; Mognato and Celotti, 2015). Hui-Ming Lin et al have discovered that miR-217 and miR-181b-5p significantly enhanced apoptosis in PC3 cells, indicating their therapeutic potential to improve taxane response in castration-resistant prostate cancer (CRPC) (Lin et al., 2018). Moreover, Bone marrow-derived mesenchymal stem/stromal cells (BM-MSCs)-derived exosomes promote colon cancer stem cell-like traits via miR-142-3p, suggesting multiple ways of miRNAs in regulating cancer progression

(Li and Li, 2018). As one of the original miRNAs discovered, the biological role of miR-3188 and its molecular mechanisms underlying cancer initiation and progression has been reported in nasopharyngeal carcinoma (Zhao et al., 2016). Additionally, miR-3188 suppression could inhibit proliferation of breast cancer cells through regulating p27 expression. However, how it works in non-small cell lung cancer remains unclear.

Forkhead box protein O1 (FOXO1) is a protein encoded by the FOXO1 gene. FOXO1 shuttles between nucleus and cytoplasm back and forth. AKT phosphorylates FOXO1 and leads to FOXO1 translocate from nucleus to cytoplasm (Hay, 2011; Tzivion et al., 2011). Phosphorylated FOXO1 induces cell proliferation, inhibits cell apoptosis, and increases cell invasion and metastasis. Moreover, it also promotes angiogenesis and reduces cell apoptosis in chemotherapy and radiotherapy (Dansen and Burgering, 2008; Zhang B. et al., 2015). AKT phosphorylation was induced by phospho-FOXO1 in NSCLC (Maekawa et al., 2009). However, the involvement of FOXO1 in inhibiting NSCLC cell proliferation is unrevealed.

PI3K/Akt/mTOR signaling pathway has been well characterized and recognized to play essential roles in lung cancer cell proliferation and survival. c-JUN was frequently overexpressed in NSCLC cells. miR-3188 was reported to suppress nasopharyngeal carcinoma cell growth through FOXO1-mediated mTOR-p-PI3K/AKT-c-JUN pathway. In this study, we investigated the interaction of miR-3188, mTOR, and FOXO1 in NSCLC cells. We hypothesized that miR-3188 also inhibit NSCLC cell proliferation via the same mTOR-p-PI3K/AKT-c-JUN signaling pathway. Indeed, we found miR-3188 expression was significantly higher in BEAS-2B cells than in NSCLC cells. miR-3188 mimics inhibited NSCLC cell growth both *in vitro* and *in vivo*. Overexpression of miR-3188 downregulated protein expression of mTOR and p-mTOR in NSCLC cells. And mTOR overexpression reverses inhibition of cell proliferation by miR-3188. More importantly, miR-3188 coordinates with FOXO1 through PI3K/AKT/c-JUN pathway. As such, miR-3188 may negatively modulate NSCLC cell growth by a FOXO1-modulating mTOR-p-PI3K/AKT-c-JUN signaling pathway. Our results suggested that miR3188 might be a potential therapeutic target for NSCLC treatment.

MATERIALS AND METHODS

Cell Culture and Synchronization

Two NSCLC cell lines (A549 and H1299) and a human lung epithelial BEAS-2B cell line were obtained from Shanghai Cell Bank of the Chinese Academy of Sciences. NSCLC cell lines were cultured in RPMI-1640 (Invitrogen, Carlsbad, United States) supplemented with 10% fetal calf serum (FCS; Hyclone, Invitrogen, Carlsbad, United States). BEAS-2B was cultured in defined Keratinocyte serum free medium (KSFM, Invitrogen Carlsbad, United States) supplemented with epidermal growth factor (Invitrogen, Carlsbad, United States). The cells were maintained at 37°C with 10% CO₂ in a humidified atmosphere.

In order to synchronize cells into G0 phase, NSCLC cells were starved with 0.1% FCS RPMI-1640 for 24–48 h. Cells were then further starved in serum free medium for another 48 h.

Cell Transfection

FOXO1, c-JUN and mTOR siRNA or miR-3188 mimics and related inhibitor were obtained from RiboBio Inc. (Guangzhou, China). The sequences of primers used for miR-3188 mimics were: Sense 5'AGAGGCUUUGUGCGGAUACGGGG3', Antisense 3'UCUCCGAAACACGCCUAUGCCCC5'. The sequences used for miR-3188 inhibitor was: 5'CCCCGUAUCCGCACAAAGCCUCU3'. mTOR and c-JUN plasmids were obtained from Biosense Technologies (Guangzhou, China). PI3K inhibitor Ly294002 was purchased from Sigma (St. Louis, United States). NSCLC cells were seeded onto a 6- or 96-well plate at 30–50% confluence before indicated transfection. Cells were transfected with plasmid, siRNA or miRNAs by using TurboFect siRNA Transfection Reagent (Fermentas, Vilnius, Lithuania) following the manufacturer's protocol. Cells were harvested 48–72 h later for further experiments.

Western Blotting

Cells were seeded into a 6-well plate and harvested when they reached 90–100% confluence. The detailed method was based on a previous publication (Zhang L. et al., 2015). Antibodies included anti-FOXO1 (2880, 1:1000, CST), mTOR (04-385, 1:1000, millipore), p-mTOR (2971, 1:1000, CST), CCND1 (ab134175, 1:1000, Abcam), p21 (ab109199, 1:1000, Abcam), c-JUN (9165, 1:500, CST), AKT (9272, 1:1000, CST), pAKT (Ser473, 9271, 1:1000, CST), PI3K (4292, 1:1000, CST), p-PI3K (Tyr458, 4228, 1:1000, CST), p27 (2552, 1:1000, CST), and β -actin (ab8227, 1:1000, Abcam). The signal was visualized by using the Western Lightning® ECL Pro Enhanced Chemiluminescence Substrate (PerkinElmer, United States) and exposed to X-ray film (Fujifilm, Japan).

Colony Formation Assay

For colony formation assay, 100 cells/well NSCLC cells were cultured in 6-well culture plates. Cells were incubated at 37°C for 2 weeks. Colonies were stained with hematoxylin solution after 2 times washing with PBS. Cell clusters include more than 50 cells were identified as colonies. Colony counting was performed using a microscope (IX83; Olympus).

EdU Incorporation Assay

EdU incorporation assay was performed as previously described (da Silva et al., 2013). Proliferating NSCLC cells were determined through the Cell-Light EdU Apollo 488 or 567 *in vitro* Imaging Kit (RiboBio, Guangzhou, China) based on the manufacturer's instruction. Briefly, NSCLC cells were incubated with 10 mM EdU for 2 h and then fixed with 4% paraformaldehyde. The fixed cells were permeabilized in 0.3% Triton X-100 for 5 min and stained with dyes accordingly. Cell nuclei were stained with DAPI (5 mg/ml) for 10 min. The number of EdU-positive cells was observed using a fluorescent Nikon microscope.

In vivo Tumorigenesis in Nude Mice

Mice (BALB/C, nu/nu, 6-weeks-old, female) were subcutaneously injected with A549 and H1299 cells ($5 \times 10^6/100 \mu\text{l}$) transfected with miR-3188, FOXO1 or the control ($n = 5$ per group). All mice were housed in a pathogen-free conditions with controlled temperature ($21 \pm 2^\circ\text{C}$) and 12 h light-dark cycle. Food and water were available freely for mice. Three weeks later, the mice were sacrificed and tumor tissues collected for immunohistochemical analysis.

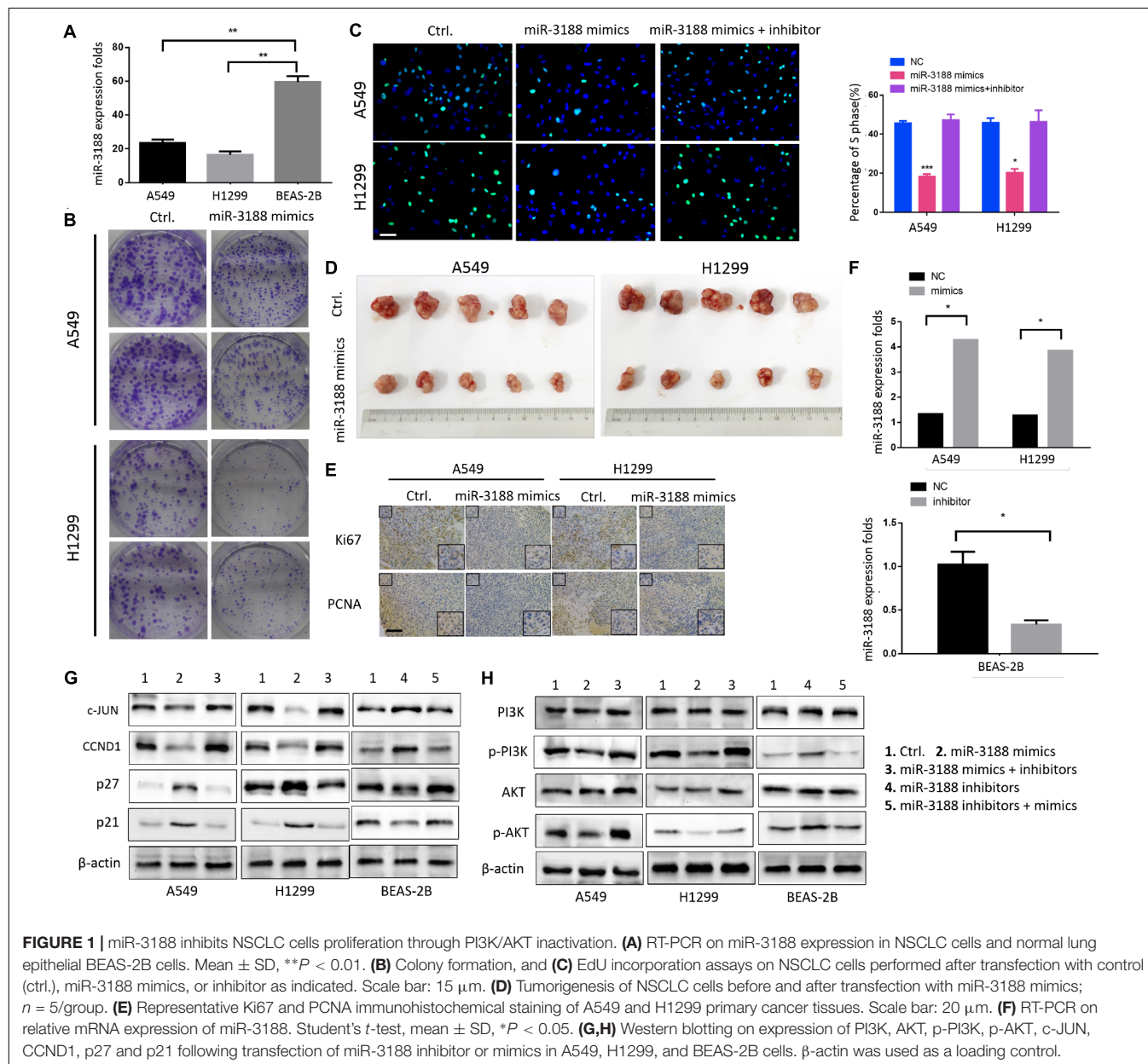
Immunohistochemical Staining

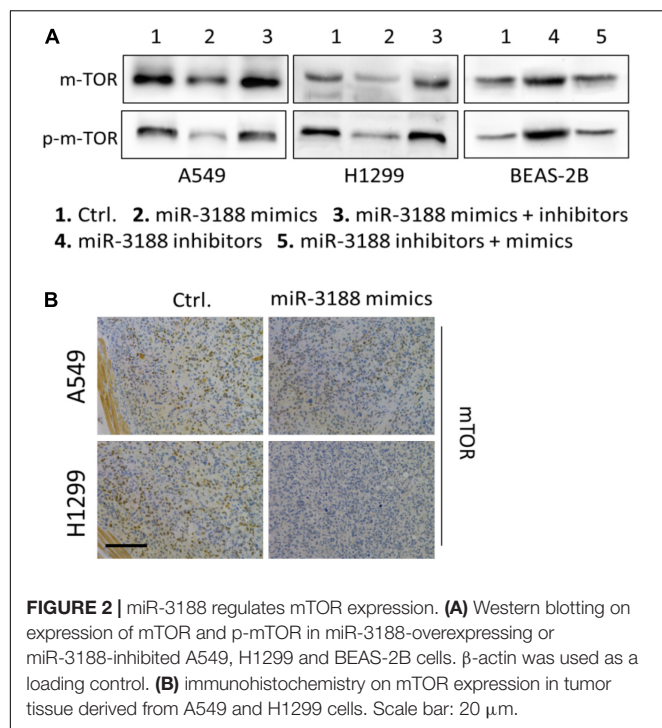
Paraffin sections obtained from animal model were used for immunohistochemical staining for FOXO1, mTOR, Ki67, PCNA, or c-JUN expression. The results of immunohistochemical

staining tissue sections were evaluated by two pathologists independently. The antibodies used were as follows: rabbit anti-FOXO1 (ab39670, 1:200, Abcam), anti-mTOR (04-385, 1:200, millipore), anti-PCNA (10205-2-AP, 1:50, PTG), anti-Ki67 (Ab16667, 1:50, Abcam), and anti-JUN (24909-1-AP, 1:200, PTG).

Statistical Analysis

Statistical analysis was performed using SPSS 21.0 software. Data are presented as mean \pm SD. Student's *t*-test was used to compare between two groups and one-way ANOVA (analysis of variance) analysis for multiple groups. All statistical tests were two-sided, and single, double and triple asterisks indicate statistical significance, * $P < 0.05$, ** $P < 0.01$, and *** $P < 0.001$.



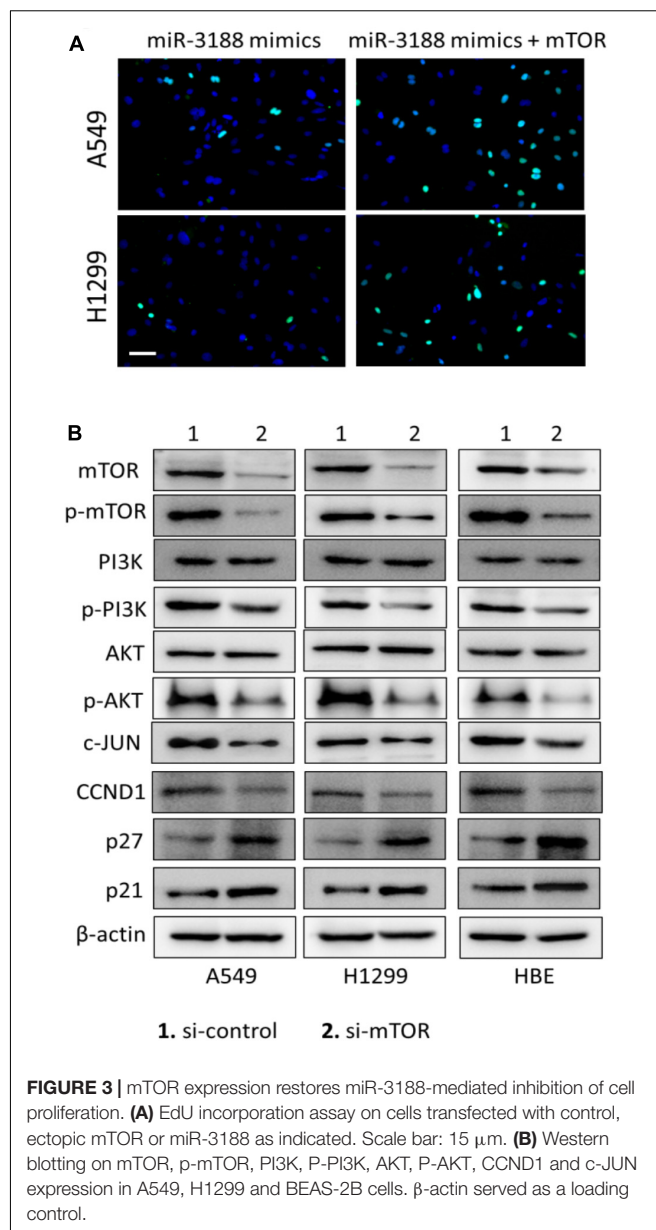


RESULTS

miR-3188 Suppresses NSCLC Cell Growth

To investigate the involvement of miR-3188 in NSCLC development, we first detected its expression in human lung epithelial BEAS-2B cells and NSCLC A549 and H1299 cells. It was found that miR-3188 is overexpressed in NSCLC cells but its expression is low in BEAS-2B cells (**Figure 1A**). To further identify its biological function in NSCLC, miR-3188 mimics or inhibitors were, respectively introduced into A549 and H1299, or BEAS-2B cells. More than twofold increase in miR-3188 expression was observed in A549 and H1299 cells treated with miR-3188 mimics compared with the control group by qRT-PCR analysis (Student's *t*-test, with $P < 0.05$ for both, **Figure 1F**). To examine the effect of miR-3188 expression on NSCLC cell growth *in vitro*, colony formation and Edu incorporation assay were performed. As expected, both A549 and H1299 cells transfected with miR-3188 mimics formed significantly less colonies (**Figure 1B**). Furthermore, the result of Edu incorporation assay shows that miR-3188 mimics efficiently decreased the number of cells in S phase, and this reduction was rescued by treating cells with miR-3188 inhibitor (**Figure 1C**). These results indicate that miR-3188 is capable of inhibiting cell proliferation and inducing G1/S transition in NSCLC cells.

Next, an *in vivo* tumor formation experiment was performed through subcutaneous injection of A549-miR-3188 and H1299-miR-3188 or control cells into nude mice. Three weeks later, it was found that tumor size of the mice injected with A549-miR-3188 and H1299-miR-3188 cells was smaller than that of control



cells (**Figure 1D**). Moreover, Ki67 and proliferating cell nuclear antigen (PCNA) expression were also lower in tumor tissues compared to that of control group (**Figure 1E**). These results suggest that miR-3188 inhibit tumorigenesis both *in vitro* and *in vivo*.

To investigate the mechanisms on how miR-3188 inhibits NSCLC cell proliferation, we performed Western blotting analysis on several biomarkers that regulate cell proliferation. It was found that miR-3188 overexpression reduced c-JUN and CCND1 expression, but increased expression of p27 and p21. miR-3188 inhibitors reverse the expression of these proteins (**Figure 1G**). Furthermore, p-PI3K and p-AKT expression reduced in miR-3188-overexpressing NSCLC cells (**Figure 1H**). These results indicate that phosphoinositide-3-kinase (PI3K)/AKT inactivation and c-JUN downregulation

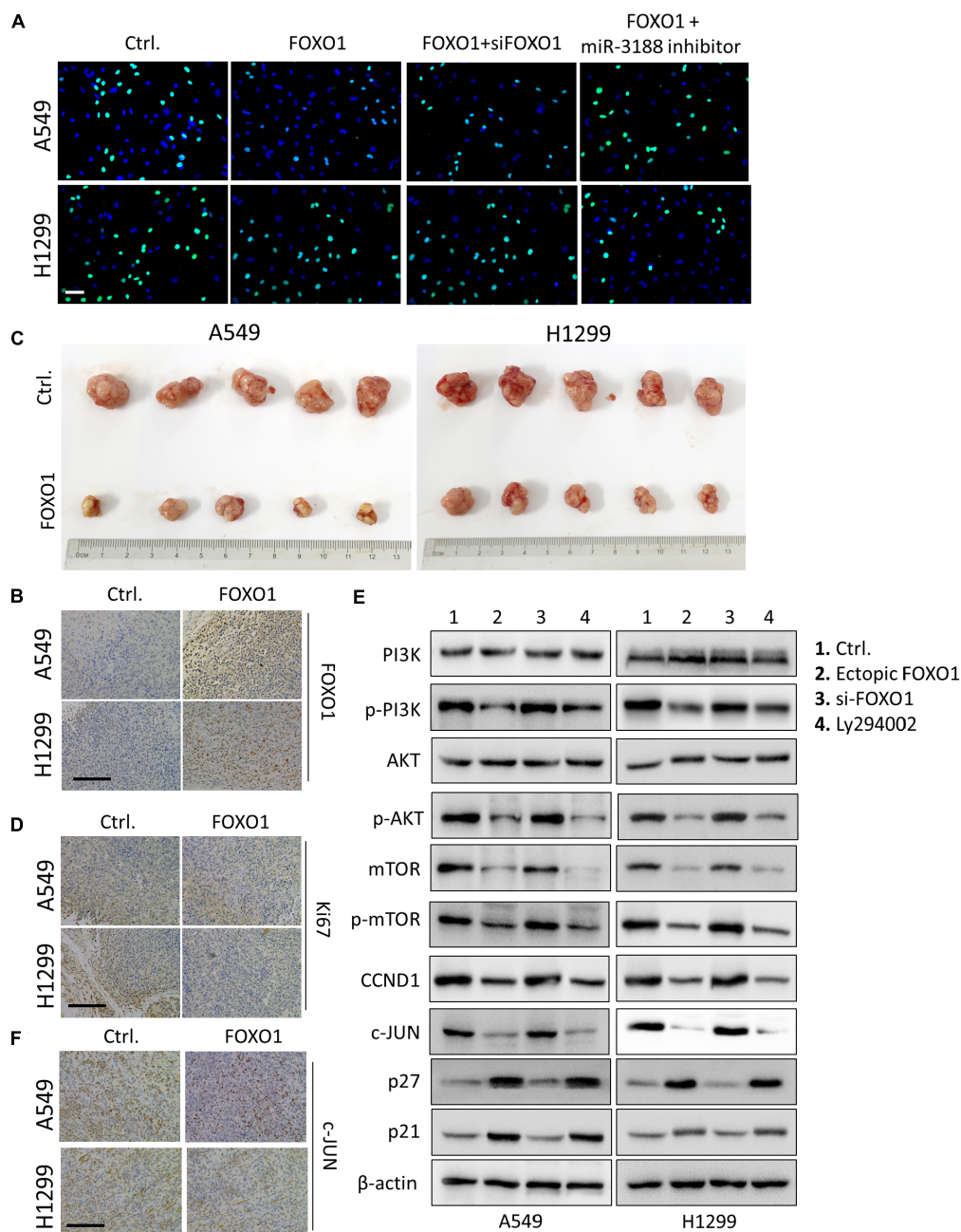


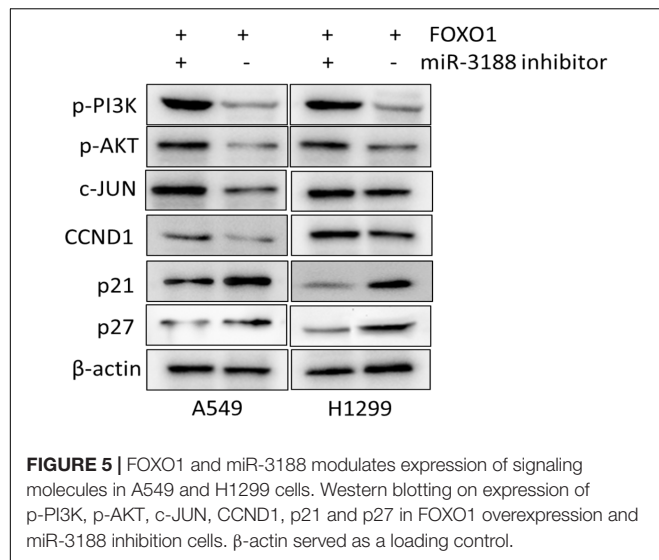
FIGURE 4 | FOXO1 inhibits NSCLC cells proliferation through PI3K/AKT pathway. **(A)** EdU incorporation assay on A549 and H1299 cells transfected with mock and/or FOXO1, siRNA as indicated. Scale bar: 15 μ m. **(B)** Immunohistochemical staining of FOXO1 in xenograft tumors. Scale bar: 15 μ m. **(C)** Reduced tumorigenicity in FOXO1 overexpressing A549 and H1299 cells; $n = 5$ /group. **(D)** Immunohistochemistry of Ki67 in xenograft tumors. Scale bar: 20 μ m. **(E)** Western blotting on PI3K, p-PI3K, AKT, p-AKT, mTOR, p-mTOR, c-JUN, CCND1, p27 and p21 expression in NSCLC cells transfected with control and FOXO1, siFOXO1 or Ly294002 as indicated. β -actin served as a loading control. **(F)** Immunohistochemical staining of c-JUN in FOXO1 overexpressing xenograft tumors. Scale bar: 20 μ m.

might be the mechanisms by which miR-3188 suppresses cell growth.

miR-3188 Targets mTOR

It has been reported that mTOR is a direct target of miR-3188 (Zhao et al., 2016). We found that overexpression of miR-3188

downregulated protein expression of mTOR and p-mTOR in NSCLC cells. In contrast, miR-3188 downregulation decreased mTOR and p-mTOR levels in BEAS-2B cells (**Figure 2A**). In mouse xenografts, immunohistochemistry in tumors from A549- and H1299-miR-3188 cells showed that mTOR expression was significantly downregulated (**Figure 2B**). Collectively, these



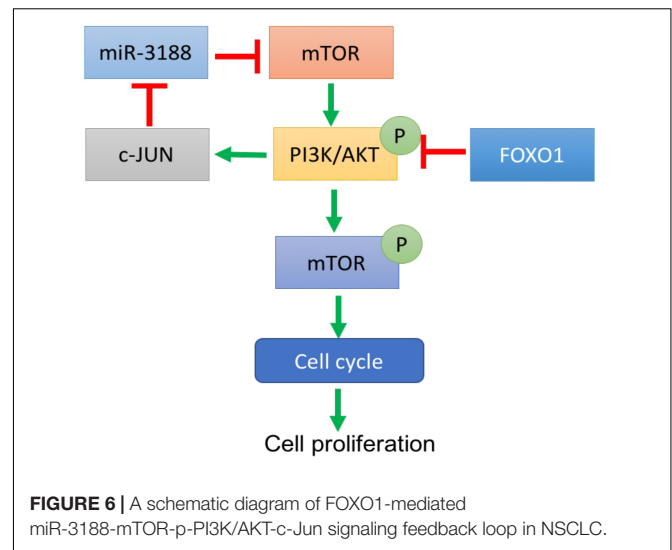
data suggest that miR-3188 might directly target mTOR and reduce its expression, leading to inhibition of proliferation and tumorigenesis of NSCLC cells.

mTOR Overexpression Reverses Inhibition of Cell Proliferation by miR-3188

EdU incorporation assay indicated that mTOR overexpression in transfected miR-3188-overexpressing NSCLC cells resulted in increasing cell growth (**Figure 3A**). In mTOR overexpression groups, more cells in phase S were observed in both A549- and H1299-miR-3188 cells, suggesting that mTOR overexpression can restore NSCLC cell proliferation which was inhibited by miR-3188. Also, we observed that mTOR knockdown by siRNA remarkably reduced the expression of mTOR, p-mTOR, p-PI3K, p-AKT, CCND1 and c-JUN, and enhanced expression of p27 and p21 (**Figure 3B**). These results further confirmed that miR-3188 suppresses cell growth by directly targeting mTOR.

FOXO1 Suppresses Cell Growth

It has been reported that FOXO1 induced PI3K/AKT signaling in gastric cancer. To evaluate the role of FOXO1 on NSCLC cell proliferation, we transfected a FOXO1 overexpressed lentiviral vector into NSCLC cells. FOXO1 markedly inhibited cell-cycle G1/S transition in NSCLC cells documented by EdU incorporation assay (**Figure 4A**). To further confirm that FOXO1 suppress NSCLC cell growth, *in vivo* tumorigenesis experiment was performed in nude mice. Successful overexpression of FOXO1 was confirmed by immunohistochemistry in A549 and H1299 tumors (**Figure 4B**). Tumor volumes were significantly smaller in tumors of FOXO1-overexpressing A549 and H1299 cells compared to control cells (**Figure 4C**). Ki67 expression in these tumors was also lower than that in controls (**Figure 4D**). These results indicate that FOXO1 negatively regulates tumor growth *in vivo*.



FOXO1 overexpression reduced the expression of p-PI3K, p-AKT, mTOR and p-mTOR. Moreover, we observed that overexpression of FOXO1 also downregulated expression of c-JUN and CCND1 and upregulated expression of p21 and p27. Indeed, FOXO1 knockdown by siRNA exhibited the opposite results as shown in **Figure 4E**. Additionally, the effect of FOXO1 on the expression of p-PI3K, p-AKT, mTOR, p-mTOR, c-JUN, CCND1, p21 and p27 was significantly reduced in cells treated with Ly294002, the specific PI3K inhibitor (**Figure 4E**).

It has been reported that miR-3188 expression was downregulated by c-JUN, which is a downstream regulator of the PI3K/AKT pathway. Immunohistochemical staining result in FOXO1-overexpressing tumor tissues of mice showed decreased expression of c-JUN (**Figure 4F**). These results indicate that FOXO1 may mediate NSCLC cell growth and cell-cycle progression through the PI3K/AKT/c-JUN signaling pathway.

miR-3188 Coordinates With FOXO1 Through PI3K/AKT/c-JUN Pathway

A previous study showed that miR-3188 is a positive modulator of FOXO1 (Zhao et al., 2016). miR-3188 inhibitor significantly rescue cell proliferation in Edu assay (**Figure 4A**). Expression of p-PI3K, p-AKT, c-JUN and CCND1 was enhanced, while expression of p27 and p21 were decreased in FOXO1-overexpressing NSCLC cells with miR-3188 inhibitor treatment, (**Figure 5**). These results indicate that miR-3188 coordinates with FOXO1 in suppressing NSCLC cell growth and support that the interaction of miR-3188 and FOXO1 is through PI3K/AKT/c-JUN signaling pathway (**Figure 6**).

DISCUSSION

miRNAs have been reported to be associated with various types of cancers (Liu and Gao, 2016; Zheng et al., 2017). However, the role of miR-3188 in NSCLC development has not been reported. In this study, we demonstrated that miR-3188 significantly

suppressed proliferation and G1/S cell-cycle transition in NSCLC cells as well as growth of tumor xenografts, indicating that miR-3188 might be a tumor suppressor in NSCLC.

It is well known that tumor cell proliferation is associated with cell-cycle progression (Collins et al., 1997). We found that miR-3188 regulate NSCLC tumorigenesis by affecting cell cycle. We also identified that the role of miR-3188 is associated with other key signaling molecules including mTOR, PI3K/AKT and c-JUN, that suppress cell cycle transition, thus inhibiting cell growth.

mTOR is an oncogene and constitutively activated PI3K/Akt signaling pathway was observed in almost every types of tumors (Populo et al., 2012; Xie et al., 2016; Wang et al., 2017) including NSCLC (Gridelli et al., 2008). It is well known that PI3K/Akt is involved in cell survival, growth, proliferation, repair, migration and angiogenesis (Lucas et al., 2010; Liu et al., 2014; Henderson et al., 2015). In cancer cells, activation of signaling pathway could be realized by gene mutation or upstream signaling molecules (Porta et al., 2014; Lien et al., 2016). It has been well documented that mTOR could form a negative feedback loop with PI3K/AKT (Efeyan and Sabatini, 2010; Rozengurt et al., 2014; Carneiro et al., 2015). In this study, we found that mTOR is one of the direct targets of miR-3188 and PI3K/AKT signaling was inhibited by miR-3188 overexpression. However, PI3K/AKT signaling activation was inhibited by mTOR in breast cancer (Khan et al., 2013; Paplomata and O'Regan, 2014), indicating differential effect of mTOR in different type of cancers. As such, c-JUN and p-mTOR that are PI3K/AKT downstream molecules increased in mTOR knockdown NSCLC cells, that was consistent with in miR-3188 overexpression cells. Furthermore, mTOR overexpression enhanced NSCLC cell proliferation suppressed by miR-3188. These results confirm that miR-3188 inhibits PI3K/AKT pathway by suppressing mTOR, leading to downregulation of c-JUN and p-mTOR.

c-JUN has been well known as a key player of cell proliferation (Shaulian and Karin, 2001), invasiveness and metastasis (Peng et al., 2016), and is one of the PI3K/AKT pathway downstream components (Cai et al., 2010; Zhang et al., 2014). Subsequent experiments confirmed that c-JUN negatively mediates miR-3188

expression indicating the formation of a complex miR-3188-mTOR-pPI3K/AKT-c-JUN loop in NSCLC.

It was reported that FOXO1 is a negative regulator in various types of cancers (Zhang et al., 2012; Hou et al., 2016). Consistent with previous reports, NSCLC cells in G1/S cell cycle transition and cell growth was significantly suppressed by FOXO1. In this study, FOXO1 overexpression inhibited PI3K/AKT signaling pathway mediated cell-cycle process in NSCLC cells. However, this finding is not consistent with that in gastric cancer (Park et al., 2014). In NSCLC cells, c-JUN, p-mTOR and total mTOR expression were downregulated. Similar to miR-3188, FOXO1 also inhibits NSCLC cell proliferation through suppressing PI3K/AKT mediated cell-cycle process.

We also found that miR-3188 failed to promote the expression of FOXO1, indicating that miR-3188 might be a downstream molecule of FOXO1. Through blocking mTOR-mediated p-PI3K/AKT/p-mTOR signaling activation, effect of miR-3188 was suppressed. In this case, FOXO1 lost its inhibitory effects on c-JUN and cell cycle and subsequently induced cell growth in NSCLC cells. Taken together, miR-3188 could be a downstream component of FOXO1 signaling.

In summary, our study supports that miR-3188 could form a negative feedback loop through mTOR/PI3K/AKT/c-JUN pathway. This pathway was regulated by FOXO1 which results in suppression of cell proliferation in NSCLC cells.

AUTHOR CONTRIBUTIONS

TL and CW conceived the project. CW, EL, WL, and JC performed experiments. CW, EL, WL, JC, and TL analyzed the results. TL and EL wrote the first draft. All authors revised the manuscript. TL edited and approved the manuscript.

FUNDING

This project was funded by the National Natural Science Foundation of P.R.China (No. 31401496) and by Jiangsu province key R&D projects of China (No. BE2016648).

REFERENCES

- Bhaskaran, M., and Mohan, M. (2014). MicroRNAs: history, biogenesis, and their evolving role in animal development and disease. *Vet. Pathol.* 51, 759–774. doi: 10.1177/0300985813502820
- Cai, T., Zuo, Z., Ding, J., Zhang, D., Li, J., and Huang, C. (2010). Abstract 4371: PI3K/Akt/JNK/c-Jun signaling pathway is a mediator for arsenite-induced cyclin D1 expression and cell growth in human bronchial epithelial cells. *Cancer Res.* 70. doi: 10.1158/1538-7445.AM10-4371
- Carneiro, B. A., Kaplan, J. B., Altman, J. K., Giles, F. J., and Platanius, L. C. (2015). Targeting mTOR signaling pathways and related negative feedback loops for the treatment of acute myeloid leukemia. *Cancer Biol. Ther.* 16, 648–656. doi: 10.1080/15384047.2015.1026510
- Collins, K., Jacks, T., and Pavletich, N. P. (1997). The cell cycle and cancer. *Proc. Natl. Acad. Sci. U.S.A.* 94, 2776–2778. doi: 10.1073/pnas.94.7.2776
- da Silva, M. S., Monteiro, J. P., Nunes, V. S., Vasconcelos, E. J., Perez, A. M., Freitas-Junior Lde, H., et al. (2013). Leishmania amazonensis promastigotes present two distinct modes of nucleus and kinetoplast segregation during cell cycle. *PLoS One* 8:e81397. doi: 10.1371/journal.pone.0081397
- Dansen, T. B., and Burgering, B. M. (2008). Unravelling the tumor-suppressive functions of FOXO proteins. *Trends Cell Biol.* 18, 421–429. doi: 10.1016/j.tcb.2008.07.004
- Efeyan, A., and Sabatini, D. M. (2010). mTOR and cancer: many loops in one pathway. *Curr. Opin. Cell Biol.* 22, 169–176. doi: 10.1016/j.ceb.2009.10.007
- Gridelli, C., Maione, P., and Rossi, A. (2008). The potential role of mTOR inhibitors in non-small cell lung cancer. *Oncologist* 13, 139–147. doi: 10.1634/theoncologist.2007-0171
- Hay, N. (2011). Interplay between FOXO, TOR, and Akt. *Biochim. Biophys. Acta* 1813, 1965–1970. doi: 10.1016/j.bbamcr.2011.03.013
- Hayes, J., Peruzzi, P. P., and Lawler, S. (2014). MicroRNAs in cancer: biomarkers, functions and therapy. *Trends Mol. Med.* 20, 460–469. doi: 10.1016/j.molmed.2014.06.005
- Henderson, V., Smith, B., Burton, L. J., Randle, D., Morris, M., and Otero-Marrah, V. A. (2015). Snail promotes cell migration through PI3K/AKT-dependent Rac1

- activation as well as PI3K/AKT-independent pathways during prostate cancer progression. *Cell Adh. Migr.* 9, 255–264. doi: 10.1080/19336918.2015.1013383
- Hou, L., Chen, J., Zheng, Y., and Wu, C. (2016). Critical role of miR-155/FoxO1/ROS axis in the regulation of non-small cell lung carcinomas. *Tumour Biol.* 37, 5185–5192. doi: 10.1007/s13277-015-4335-9
- Khan, K. H., Yap, T. A., Yan, L., and Cunningham, D. (2013). Targeting the PI3K-AKT-mTOR signaling network in cancer. *Chin. J. Cancer* 32, 253–265. doi: 10.5732/cjc.013.10057
- Li, H., and Li, F. (2018). Exosomes from BM-MSCs increase the population of CSCs via transfer of miR-142-3p. *Br. J. Cancer* 119, 744–755. doi: 10.1038/s41416-018-0254-z
- Lien, E. C., Lyssiotis, C. A., and Cantley, L. C. (2016). Metabolic reprogramming by the PI3K-Akt-mTOR pathway in cancer. *Recent Results Cancer Res.* 207, 39–72. doi: 10.1007/978-3-319-42118-6_3
- Lin, H. M., Nikolic, I., Yang, J., Castillo, L., Deng, N., Chan, C. L., et al. (2018). MicroRNAs as potential therapeutics to enhance chemosensitivity in advanced prostate cancer. *Sci. Rep.* 8:7820. doi: 10.1038/s41598-018-26050-y
- Liu, H. T., and Gao, P. (2016). The roles of microRNAs related with progression and metastasis in human cancers. *Tumor Biol.* 37, 15383–15397. doi: 10.1007/s13277-016-5436-9
- Liu, Q., Turner, K. M., Alfred Yung, W. K., Chen, K., and Zhang, W. (2014). Role of AKT signaling in DNA repair and clinical response to cancer therapy. *Neuro Oncol.* 16, 1313–1323. doi: 10.1093/neuonc/nou058
- Lucas, A., Kim, Y., Rivera-Pabon, O., Chae, S., Kim, D. H., and Kim, B. (2010). Targeting the PI3K/Akt cell survival pathway to induce cell death of HIV-1 infected macrophages with alkylphospholipid compounds. *PLoS One* 5:e13121. doi: 10.1371/journal.pone.0013121
- Maekawa, T., Maniwa, Y., Doi, T., Nishio, W., Yoshimura, M., Ohbayashi, C., et al. (2009). Expression and localization of FOXO1 in non-small cell lung cancer. *Oncol. Rep.* 22, 57–64.
- Magee, P., Shi, L., and Garofalo, M. (2015). Role of microRNAs in chemoresistance. *Ann. Transl. Med.* 3:332. doi: 10.3978/j.issn.2305-5839.2015.11.32
- Mognato, M., and Celotti, L. (2015). MicroRNAs used in combination with anti-cancer treatments can enhance therapy efficacy. *Mini Rev. Med. Chem.* 15, 1052–1062. doi: 10.2174/1389557515666150709115355
- Musilova, K., and Mraz, M. (2015). MicroRNAs in B-cell lymphomas: how a complex biology gets more complex. *Leukemia* 29, 1004–1017. doi: 10.1038/leu.2014.351
- Paplomata, E., and O'Regan, R. (2014). The PI3K/AKT/mTOR pathway in breast cancer: targets, trials and biomarkers. *Ther. Adv. Med. Oncol.* 6, 154–166. doi: 10.1177/1758834014530023
- Park, J., Ko, Y. S., Yoon, J., Kim, M. A., Park, J. W., Kim, W. H., et al. (2014). The forkhead transcription factor FOXO1 mediates cisplatin resistance in gastric cancer cells by activating phosphoinositide 3-kinase/Akt pathway. *Gastric Cancer* 17, 423–430. doi: 10.1007/s10120-013-0314-2
- Peng, Y., Zhang, P., Huang, X., Yan, Q., Wu, M., Xie, R., et al. (2016). Direct regulation of FOXK1 by C-jun promotes proliferation, invasion and metastasis in gastric cancer cells. *Cell Death Dis.* 7:e2480. doi: 10.1038/cddis.2016.225
- Populo, H., Lopes, J. M., and Soares, P. (2012). The mTOR signalling pathway in human cancer. *Int. J. Mol. Sci.* 13, 1886–1918. doi: 10.3390/ijms13021886
- Porta, C., Paglino, C., and Mosca, A. (2014). Targeting PI3K/Akt/mTOR signaling in cancer. *Front. Oncol.* 4:64. doi: 10.3389/fonc.2014.00064
- Rozengurt, E., Soares, H. P., and Sinnet-Smith, J. (2014). Suppression of feedback loops mediated by PI3K/mTOR induces multiple overactivation of compensatory pathways: an unintended consequence leading to drug resistance. *Mol. Cancer Ther.* 13, 2477–2488. doi: 10.1158/1535-7163.MCT-14-0330
- Rupaimoole, R., and Slack, F. J. (2017). MicroRNA therapeutics: towards a new era for the management of cancer and other diseases. *Nat. Rev. Drug Discov.* 16, 203–222. doi: 10.1038/nrd.2016.246
- Shaulian, E., and Karin, M. (2001). AP-1 in cell proliferation and survival. *Oncogene* 20, 2390–2400. doi: 10.1038/sj.onc.1204383
- Tzivion, G., Dobson, M., and Ramakrishnan, G. (2011). FoxO transcription factors; regulation by AKT and 14-3-3 proteins. *Biochim. Biophys. Acta* 1813, 1938–1945. doi: 10.1016/j.bbamcr.2011.06.002
- Wang, Z. Y., Valera, J. C., Zhao, X. F., Chen, Q. M., and Gutkind, J. S. (2017). mTOR co-targeting strategies for head and neck cancer therapy. *Cancer Metastasis Rev.* 36, 491–502. doi: 10.1007/s10555-017-9688-7
- Xie, J., Wang, X., and Proud, C. G. (2016). mTOR inhibitors in cancer therapy. *F1000Res.* 5:2078. doi: 10.12688/f1000research.9207.1
- Zhang, B., Gui, L. S., Zhao, X. L., Zhu, L. L., and Li, Q. W. (2015). FOXO1 is a tumor suppressor in cervical cancer. *Genetics Mol. Res.* 14, 6605–6616. doi: 10.4238/2015.June.18.3
- Zhang, L., Zhang, S., Yao, J., Lowery, F. J., Zhang, Q., Huang, W. C., et al. (2015). Microenvironment-induced PTEN loss by exosomal microRNA primes brain metastasis outgrowth. *Nature* 527, 100–104. doi: 10.1038/nature15376
- Zhang, E., Feng, X., Liu, F., Zhang, P., Liang, J., and Tang, X. (2014). Roles of PI3K/Akt and c-jun signaling pathways in human papillomavirus type 16 oncoprotein-induced HIF-1 α , VEGF, and IL-8 expression and in vitro angiogenesis in non-small cell lung cancer cells. *PLoS One* 9:e103440. doi: 10.1371/journal.pone.0103440
- Zhang, Y. R., Xing, Y. Q., Zhang, L., Mei, Y., Yamamoto, K., Mak, T. W., et al. (2012). Regulation of cell cycle progression by forkhead transcription factor FOXO3 through its binding partner DNA replication factor Cdt1. *Proc. Natl. Acad. Sci. U.S.A.* 109, 5717–5722. doi: 10.1073/pnas.1203210109
- Zhao, M., Luo, R., Liu, Y., Gao, L., Fu, Z., Fu, Q., et al. (2016). miR-3188 regulates nasopharyngeal carcinoma proliferation and chemosensitivity through a FOXO1-modulated positive feedback loop with mTOR-p-PI3K/AKT-c-JUN. *Nat. Commun.* 7:11309. doi: 10.1038/ncomms11309
- Zheng, Q., Chen, C., Guan, H., Kang, W., and Yu, C. (2017). Prognostic role of microRNAs in human gastrointestinal cancer: a systematic review and meta-analysis. *Oncotarget* 8, 46611–46623. doi: 10.18632/oncotarget.16679

Conflict of Interest Statement: The authors declare that the research was conducted in the absence of any commercial or financial relationships that could be construed as a potential conflict of interest.

Copyright © 2018 Wang, Liu, Li, Cui and Li. This is an open-access article distributed under the terms of the Creative Commons Attribution License (CC BY). The use, distribution or reproduction in other forums is permitted, provided the original author(s) and the copyright owner(s) are credited and that the original publication in this journal is cited, in accordance with accepted academic practice. No use, distribution or reproduction is permitted which does not comply with these terms.



Correlation Between C-MYC, BCL-2, and BCL-6 Protein Expression and Gene Translocation as Biomarkers in Diagnosis and Prognosis of Diffuse Large B-cell Lymphoma

YunXiang Zhang^{1*}, Hui Wang¹, Cuiai Ren¹, Hai Yu², Wenjia Fang^{3*}, Na Zhang¹, Sumei Gao¹ and Qian Hou¹

¹ Department of Pathology, Weifang People's Hospital, Weifang, China, ² Department of Pathology, Weifang Traditional Chinese Hospital, Weifang, China, ³ Department of Clinical Medicine, Nanchang University Medical College, Nanchang, China

OPEN ACCESS

Edited by:

Dong-Hua Yang,
St. John's University, United States

Reviewed by:

Xiaozhuo Liu,
University at Buffalo, United States
Ru Li,
Stony Brook University, United States

*Correspondence:

YunXiang Zhang
zhangbing199592@163.com
Wenjia Fang
fwjd2008@126.com

Specialty section:

This article was submitted to
Experimental Pharmacology and Drug
Discovery,
a section of the journal
Frontiers in Pharmacology

Received: 05 November 2018

Accepted: 07 December 2018

Published: 07 January 2019

Citation:

Zhang Y, Wang H, Ren C, Yu H,
Fang W, Zhang N, Gao S and Hou Q
(2019) Correlation Between C-MYC,
BCL-2, and BCL-6 Protein Expression
and Gene Translocation as Biomarkers
in Diagnosis and Prognosis of Diffuse
Large B-cell Lymphoma.
Front. Pharmacol. 9:1497.
doi: 10.3389/fphar.2018.01497

This study investigates the protein expression of C-MYC, BCL-2, and BCL-6 in diffuse large B-cell lymphoma (DLBCL) and their relationship with genetic abnormalities. A retrospective study of 42 cases on paraffin-embedded tissue specimens diagnosed with DLBCL was performed using immunohistochemistry (IHC) and fluorescence *in situ* hybridization (FISH). The expression of C-MYC, BCL-2, BCL-6 protein, and gene abnormalities in these tissue samples was analyzed. The relationship in genetic abnormalities and Ki-67, Hans classification, gender, and age was also evaluated. It was found that the positive rate of C-MYC expression was 47.6% (20/42), the rate of C-MYC gene abnormality was 26.2% (11/42), in which gene translocation accounted for 23.8% (10/42) and gene amplification 2.4% (1/42); C-MYC protein expression was positively correlated with C-MYC gene translocation ($\chi^2 = 11.813$; $P = 0.001$); C-MYC gene translocation was mainly found in germinal center B cell type ($\chi^2 = 4.029$; $P = 0.045$). The positive rate of BCL-2 protein expression was 85.71% (36/42), the positive rate of translocation was 42.86% (18/42) and the amplification rate was 26.19% (11/42); the overexpression of BCL-2 protein was correlated with the BCL-2 translocation ($\chi^2 = 3.407$; $P = 0.029$). The positive rate of BCL-6 protein expression was 45.24% (19/42), the positive rate of BCL-6 translocation was 14.29% (6/42) and the positive rate of BCL-6 amplification was 7.14% (3/42); the overexpression of BCL-6 protein was significantly correlated with BCL-6 translocation ($\chi^2 = 6.091$; $P = 0.014$). The Ki-67 index was significantly higher in C-MYC translocation cases than in non-C-MYC translocation cases ($\chi^2 = 4.492$; $P = 0.034$). Taken together, our results suggest that the protein expression of C-MYC, BCL-2, and BCL-6 are positively correlated with their gene translocation. Overexpression of C-MYC, BCL-2, BCL-6 protein suggests the possibility of translocation. Therefore, immunohistochemical detection of C-MYC, BCL-2, and BCL-6 are useful in diagnosis and prognosis of DLBCL.

Keywords: diffuse large B-cell lymphoma, C-MYC, BCL-2, BCL-6, gene translocation, gene amplification

INTRODUCTION

Diffuse large B-cell lymphoma (DLBCL) is a highly heterogeneous lymphoid hematopoietic malignancy which is one of the most common types of adult non-Hodgkin's lymphoma (NHL). The incidence of DLBCL is about 30% in Europe and the United States (Chung and Levens, 2005), while in China, it is as high as 40% of all lymphomas (Li et al., 2012). DLBCL can be divided into germinal center B cell type (GCB type) and non-germinal center B cell type (non-GCB type) based on Hans analysis (Hans et al., 2004). Hans criteria is based on the presence or absence of three biomarkers, CD10, BCL-6, and MUM-1 in immunohistochemical staining using antibodies against CD10, IRF4/MUM1, and BCL6. Those with the number of CD10 positive cells greater than 30%, as well as BCL6 positive belong to the germinal center B cell subtype, and the rest are judged as non-germinal center B cell subtype (Hans et al., 2004). Different types of lymphoma have differences in cell morphology, protein expression, genetic changes, and therapeutic responsiveness. Therefore, understanding the molecular characteristics of lymphoma are critical for individualized patient care.

In patients with DLBCL, anthracycline chemotherapy can achieve 70% of remission. However, only 50–60% of patients achieve long-term disease-free survival. Most of the unresolved patients are highly aggressive and have chemotherapy resistance to first-line regimens. The combination of rituximab and other chemotherapeutic drugs has greatly improved the response rate and prognosis of DLBCL patients. It would be greatly helpful to subgrouping DLBCL, to understand its pathogenesis and to guide clinical drug use.

In recent years, with the progress of molecular genetic research, it was understood that abnormal expression of some genes is directly correlated with the occurrence, development, treatment response and prognosis of DLBCL. Previous study indicated that some lymphoma is highly aggressive when it expressed C-MYC gene accompanied by expression of BCL-2 or BCL-6 genes (Valera et al., 2013). In 2016, the guidelines of the National Comprehensive Cancer Network (NCCN) recommended using FISH to detect gene abnormality, such as translocation in lymphoma cells.

A B-cell lymphoma with a combination of C-MYC and BCL-2 or BCL-6 translocations is called a Double-Hit lymphoma (DHL), and the one with three gene translocations is called a Triple-Hit lymphoma (THL) (Campo et al., 2011). In other words, DHL/THL refers to a B cell lymphoma with multiple activated oncogenes. C-MYC gene is the most common mutated gene in lymphomas. C-MYC and BCL-2 simultaneous translocation is the most common DHL, while C-MYC/BCL-6 DHL and C-MYC/BCL-2/BCL-6 THL are rare. The 2016 version of the WHO lymphoma classification suggests that C-MYC genetic alteration is one of the important diagnostic indicators of DLBCL, and defines DHL and THL as high-grade B-cell lymphoma (Arber et al., 2016). The understanding of DHL and THL is important because it may change the clinical management and prognosis of lymphomas. Therefore, further identifying the genetic abnormalities of C-MYC, BCL-2, and BCL-6 in DLBCL is

of great significance to guide clinical diagnosis and treatment of DLBCL.

In the present study, we use immunohistochemistry (IHC) and fluorescence *in situ* hybridization (FISH) to detect the expression and genetic abnormalities, particularly gene translocation and amplification of C-MYC, BCL-2, and BCL-6 genes in patients with DLBCL. We further analyze their correlation with clinical characteristics, to provide guidelines for using these biomarkers for diagnosing, guiding treatment and assessing prognosis of DLBCL.

MATERIALS AND METHODS

Patients and Specimens

This study was approved by the Ethics Committee of Weifang People's Hospital. A total of 67 cases of paraffin-embedded tissue specimens from patients who were diagnosed with DLBCL for the first time in the Department of Pathology, Weifang People's Hospital from January 2015 to October 2016 were collected. According to the diagnostic criteria of 2016 WHO classification of hematopoietic and lymphoid tissue tumors (Arber et al., 2016), two senior pathologists in the Department of Pathology of Weifang People's Hospital reviewed the cases, and 42 cases were eventually included in the study (25 patients were excluded due to incomplete clinical data and inaccurate classification). Complete pathological data and patients' informed consent were obtained. There were 26 males and 16 females with an average age of 58.9 ± 12.3 years old (range 43–80 years old). Specimens were from various sources: 27 cases of superficial lymph nodes, 6 cases of subcutaneous soft tissue, 6 cases of gastrointestinal tract, 1 case of mesentery and spleen, and 1 case of tonsil. Among these specimens, 16 cases were of GCB type and 26 cases of non-GCB type. Another 20 patients with reactive hyperplastic superficial lymph nodes were used as negative controls, including 12 males and 8 females, with an average age of 58.0 ± 10.5 (range 41–77 years). All specimens were fixed in 10% neutral formalin. Conventional paraffin embedding was performed. These specimens were assembled into a tissue microarray with the core diameter of 3 mm.

Immunohistochemistry

Immunohistochemistry was performed using Roche Benchmark XT Ventana automatic immunohistochemical staining instrument. The staining procedure was set up strictly according to the instructions for automatic immunohistochemical detection. A pair of positive and negative tissues was placed in each tissue microarray as required. BCL-2 and C-MYC rabbit anti-human monoclonal antibody (clone number EP36, and EP121), and BCL-6 mouse anti-human monoclonal antibody (clone number LN22) were purchased from Beijing Zhongshan Jinqiao Biotechnology Co., Ltd.

Fluorescence *in situ* Hybridization (FISH)

FISH detection was performed using $3\mu\text{m}$ paraffin tissue sections. C-MYC, BCL-2, and BCL-6 probes were purchased from Beijing Jinpui Company. The C-MYC normal signal is a yellow signal from fused red and green. The C-MYC gene

translocation is considered as positive when a yellow signal, a green signal, and a red signal, or two red signals or two green signals appear in the nucleus. The C-MYC gene amplification is interpreted as positive when three or more red-green fusions appeared as yellow signals were observed.

Analysis and determination of BCL-2 and BCL-6 test results: The BCL-2 and BCL-6 probes are a two-color fusion probe, and normally two red and two green signals are separated from each other. When a red signal, a green signal, and a red-green fused yellow signal or two yellow signals appear, it was interpreted as a positive BCL-2 or BCL-6 gene translocation. When three or more red or green signals appear in the nucleus, it was considered as positive BCL-2 or BCL-6 gene amplification.

Establishing the Staining Analyzing Threshold

Twenty non-lymphoma (reactive hyperplastic lymph nodes) tissue specimens were randomly selected as the control group. FISH detection of BCL-2, BCL-6, and C-MYC genes was performed. 200 cells per sample were analyzed and the number of cells, the mean percentage value and standard deviation of abnormal signals were calculated. The positive threshold was determined to be mean percentage \pm 3 standard deviation. The results were analyzed based on the threshold. The number of translocation and the number of abnormal amplified signal of cells in the lymphoma and non-lymphoma specimens were counted, and the average value was taken. The abnormality threshold was used to judge the detection result: the result was judged as negative if the percentage of abnormal signal cells was less than the threshold; the result was judged as positive if the percentage of abnormal signal cells was greater than the threshold. If the percentage of abnormal signal cells was equal to the threshold value, then the number of cells of the test sample was increased to obtain a final result.

Statistical Analysis

SPSS 20.0 software was applied for statistical analysis. The differences between the factors were analyzed by chi-square test. When the conditions of chi-square test cannot be met, Fisher's exact probability method was used. $P < 0.05$ was considered statistically significant.

RESULTS

The Morphology of DLBCL

Under the light microscope, DLBCL tumor tissue was seen as diffuse hyperplasia of large B lymphocytes that replaced normal lymph node structure. The morphology of these lymphocytes was atypical. The cell volume is more than twice as that of conventional cells, and nucleus of the tumor cells is mostly larger than that of normal lymphocytes (Figure 1).

Immunohistochemical Staining

BCL-6 and C-MYC positive staining were located in the nucleus, while BCL-2 positive staining was in the cytoplasm (Figure 2). According to previous reports, the staining could be judged as positive if the number of tumor cells positive for C-MYC \geq

40%, BCL-2 \geq 50%, or BCL-6 \geq 30% of tumor tissues (Hans et al., 2004; Horn et al., 2013). In our study, the positive rate of immunohistochemical staining of C-MYC, BCL-2, and BCL-6 protein was 47.6% (20/42), 85.71% (36/42), and 45.24% (19/42), respectively. Based on the Hans classification, the ratio of non-GCB type was 61.9% (26/42), which was higher than that of GCB type (38.1%, 16/42) in these 42 cases. The difference between GCB and non-GCB types was not statistically significant ($P > 0.05$). Similarly, there was no significant difference in the distribution of C-MYC, BCL-2, and BCL-6 protein expression in Hans classification, gender, and age (Table 1).

Among these 42 cases of DLBCL, 15 cases (35.71%, 15/42) were co-expressed with C-MYC and BCL-2 or BCL-6, 8 cases (19.05%, 8/42) were C-MYC and BCL-2 double positive expression, 7 patients (16.67%, 7/42) had C-MYC, BCL-2, and BCL-6 triple positive expression, and no cases of C-MYC and BCL-6 double expression were found. Although among these 15 cases of C-MYC, BCL-2, and BCL-6 protein co-expression, there were 10 cases of non-GCB type (38.46%, 10/26), 11 cases of men (42.31%, 11/26), 12 cases are \geq 50 years old (36.36%, 12/33), which made up a high proportion of Hans classification, gender, and age grouping, but these differences were not statistically significant (Table 1).

FISH Test

C-MYC Gene Abnormality

Among the 42 cases of DLBCL, C-MYC translocation was detected in 10 cases (23.8%) (Figure 3A). All of these cases were positive for C-MYC protein expression. No case of C-MYC translocation was found in negative C-MYC protein expression group. The difference between the positive and negative C-MYC translocation was statistically significant ($P = 0.001$, Table 2). There were 43.8% (7/16) of GCB type and 11.5% (3/26) of non-GCB type had C-MYC translocation, and the difference between the two groups had statistical significance ($P = 0.045$). Among the C-MYC translocation cases, 8 were male (8/26, 30.8%) and 2 were female (2/16); 10 patients with C-MYC translocation were \geq 50 years old (10/33, 30.30%). The difference of C-MYC translocation in different age and gender groups were not statistically significant ($P > 0.05$) (Table 2). These results suggested that C-MYC translocation was associated with C-MYC protein expression and GCB type, but not associated with age and gender.

Among the 42 cases of DLBCL, only one case (2.4%) of C-MYC amplification was detected (Figure 3B). There was no statistical significance concerning the differences in C-MYC amplification among C-MYC protein expression, Hans classification, gender, and age ($P > 0.05$, Table 2).

BCL-2 Gene Abnormality

In the FISH test, 18 cases of BCL-2 translocation were found (Figure 3C), all of which had positive BCL-2 protein expression, while no cases of BCL-2 translocation occurred in negative BCL-2 protein expression group. The difference in BCL-2 translocation between BCL-2 protein expression and non-BCL-2 protein expression groups was statistically significant ($P = 0.029$, Table 3). Among the cases of positive BCL-2 translocation, 7

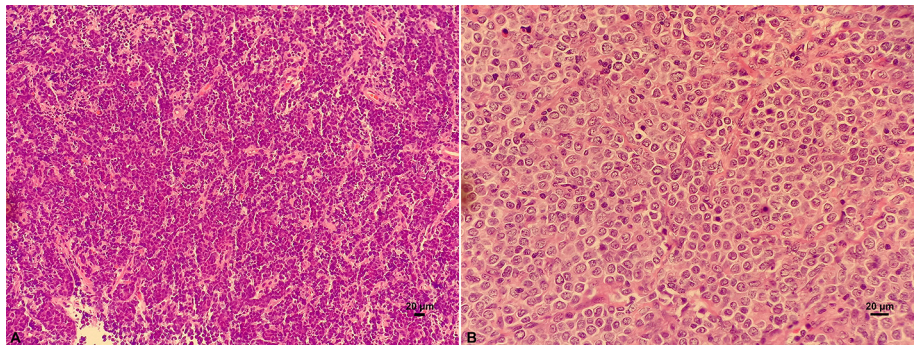


FIGURE 1 | HE staining on the structure of lymph nodes of DLBCL. **(A)** Diffuse hyperplasia of lymphocytes. **(B)** Higher magnification showing the morphology of atypical and blast DLBCL cells.

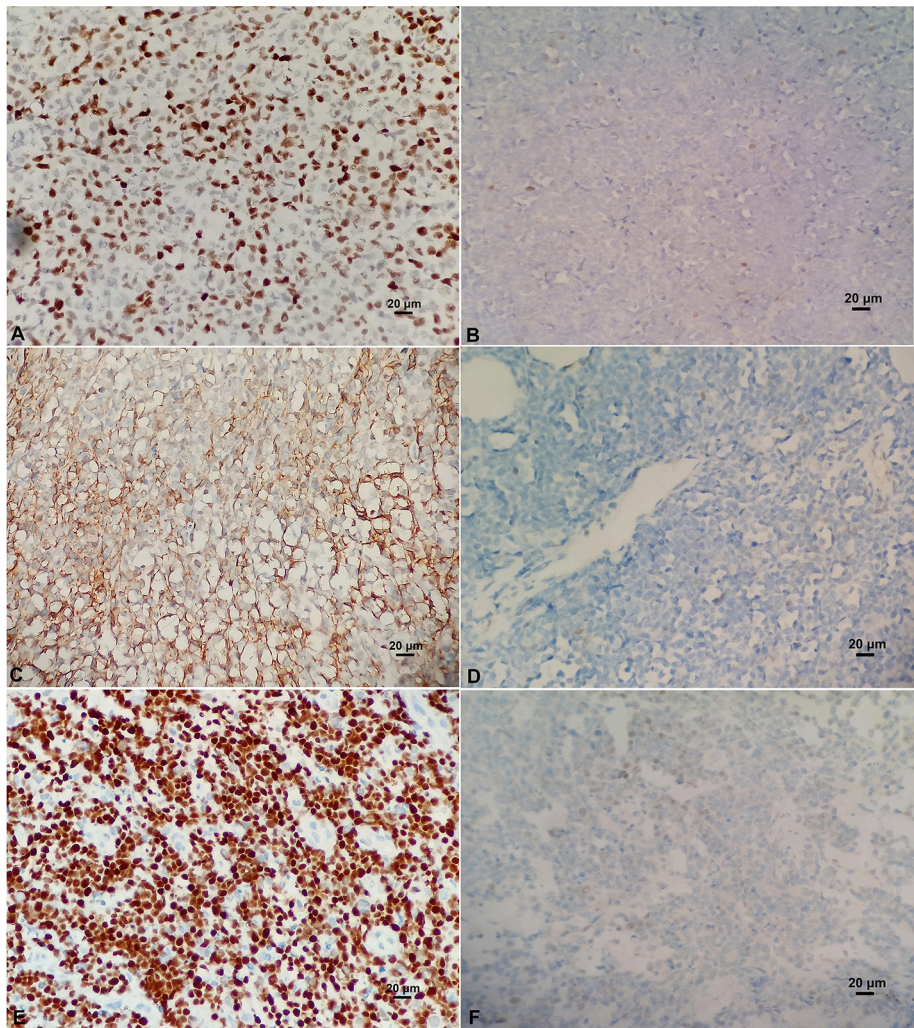


FIGURE 2 | **(A)** Positive C-MYC protein expression ($\times 400$). **(B)** Negative C-MYC protein expression ($\times 400$). **(C)** Positive BCL-2 protein expression ($\times 400$). **(D)** Negative BCL-2 protein expression ($\times 400$). **(E)** Positive BCL-6 protein expression ($\times 400$). **(F)** Negative BCL-6 protein expression ($\times 400$).

cases (7/16, 43.75%) were GCB and 11 cases (11/26, 42.31%) were non-GCB type. There was no significant difference between the two groups ($P = 0.927$, **Table 3**). There were 10 males (10/26,

38.46%) and 8 females (8/16, 50%); 13 cases (13/33, 39.39%) were ≥ 50 years old, and 5 cases were <50 years old (5/9, 55.56%). There was no significant difference in either age or gender for

TABLE 1 | Association of C-MYC, BCL-2, and BCL-6 protein expression and clinical characteristics.

		Hans typing		Gender		Age		Total cases
		GCB	Non-GCB	Male	Female	≥50 y	<50 y	
C-MYC expression	Positive	8	12	15	5	17	3	20
	Negative	8	14	11	11	16	6	22
			0.059		0.776		0.35	
χ^2								
P			0.808		0.096		0.554	
BCL-6 expression	Positive	12	24	21	15	27	9	36
	Negative	4	2	5	1	6	0	6
			1.216		0.59		0.713	
χ^2								
P			0.27		0.476		0.167	
BCL-2 expression	Positive	7	12	12	7	16	3	19
	Negative	9	14	14	9	17	6	23
			0.023		0.023		0.186	
χ^2								
P			0.879		0.879		0.666	
C-MYC/BCL-2 co-expression	Positive	5	10	11	4	12	3	15
	Negative	11	16	15	12	21	6	27
			0.224		1.292		0	
χ^2								
P			0.636		0.256		1	

BCL-2 gene translocation ($P > 0.05$, **Table 3**). These results suggested that BCL-2 translocation was associated with BCL-2 protein expression, but not associated with GCB type, age, and gender.

BCL-2 amplification was detected in 11 cases (26.19%) (**Figure 3D**). These cases were positive for BCL-2 protein expression. However, there was no correlation between BCL-2 protein expression and BCL-2 gene amplification ($P = 0.283$, **Table 3**), neither was there significant difference in BCL-2 amplification in Hans classification, gender, and age by statistical analysis ($P > 0.05$, **Table 3**).

BCL-6 Gene Abnormalities

Among these 42 cases of DLBCL, BCL-6 translocation was detected in 6 cases (14.29%) (**Figure 3E**), all of which were positive for BCL-6 protein expression, and BCL-6 translocation did not occur in negative BCL-6 protein expression group. The difference in BCL-6 translocation between positive and negative BCL-6 protein expression groups was statistically significant ($P = 0.014$, **Table 4**). BCL-6 translocation was found in 12.50% (2/16) GCB type and 15.38% (4/26) non-GCB type, and the difference between the two groups was not statistically significant ($P = 1.000$, **Table 4**). Although 6 patients with BCL-6 translocation were men and aged 50 years or older, there was no significant difference in either age or gender for BCL-6 translocation ($P > 0.05$, **Table 4**). These results suggested that BCL-6 translocation was associated with BCL-6 protein expression, but not associated with GCB type, age, or gender.

BCL-6 amplification was detected in 3 cases (7.14%) (**Figure 3F**), of which 1 case was positive for BCL-6 protein (5.26%, 1/19), and the other 2 cases were negative for BCL-6 protein (8.70%, 2/23). There was 1 case of GCB type (6.25%, 1/16) and 2 cases of non-GCB type (7.69%, 2/26); 1 case of male (3.85%,

1/26), 2 cases of female (12.50%, 2/16); 1 patient (3.03 %, 1/33) with age ≥ 50 years and 2 patients (22.22%, 2/9) with age < 50 years. There was no significant difference in BCL-6 amplification among BCL-6 protein expression, Hans classification, gender, or age ($P > 0.05$, **Table 4**).

Double-Hit Lymphomas (DHL)

Among these 42 cases of DLBCL, only 2 cases (4.76%) of DHL were detected, one had both C-MYC and BCL-2 translocation and is non-GCB type; the other was both C-MYC gene and BCL-6 gene translocation, and is GCB type. Although both cases of DHL are older than 50 years old with double expression of C-MYC and BCL-2 protein, meaning that they were dual expressor of lymphomas (DEL), analysis had suggested that there was no significant correlation between DHL and DEL, Hans classification, gender or age ($P > 0.05$, **Table 5**).

Ki-67 Proliferation Index and C-MYC, BCL-2, BCL-6 Gene Abnormalities

Ki-67 immunohistochemical staining was used to examine the proliferative ability of lymphoma tissues. The overexpression of Ki-67 in DLBCL indicates that the tumor is invasive, rapidly progress, and has poor clinical prognosis. The Ki-67 immunohistochemical staining was performed and intensity was quantified in all specimens (**Figure 4**). The cut-off value of Ki-67 positivity was set to 80 and 90%. According to group statistical analysis, 12 cases (28.57%, 12/42) had positive Ki-67 $\geq 90\%$, 25 cases (28.57%, 25/42) were Ki-67 $\geq 80\%$ in 42 cases of DLBCL. Six of Ten cases of C-MYC translocation cases were Ki-67 ≥ 90 , 60, and 18.75% (6/32) of non-C-MYC translocation cases were Ki-67 $\geq 90\%$. There were significant differences of Ki-67 positivity in C-MYC and non-C-MYC translocation cases ($P < 0.05$, **Table 6**). Ki-67 was 90 and 70% in 2 cases of DHL,

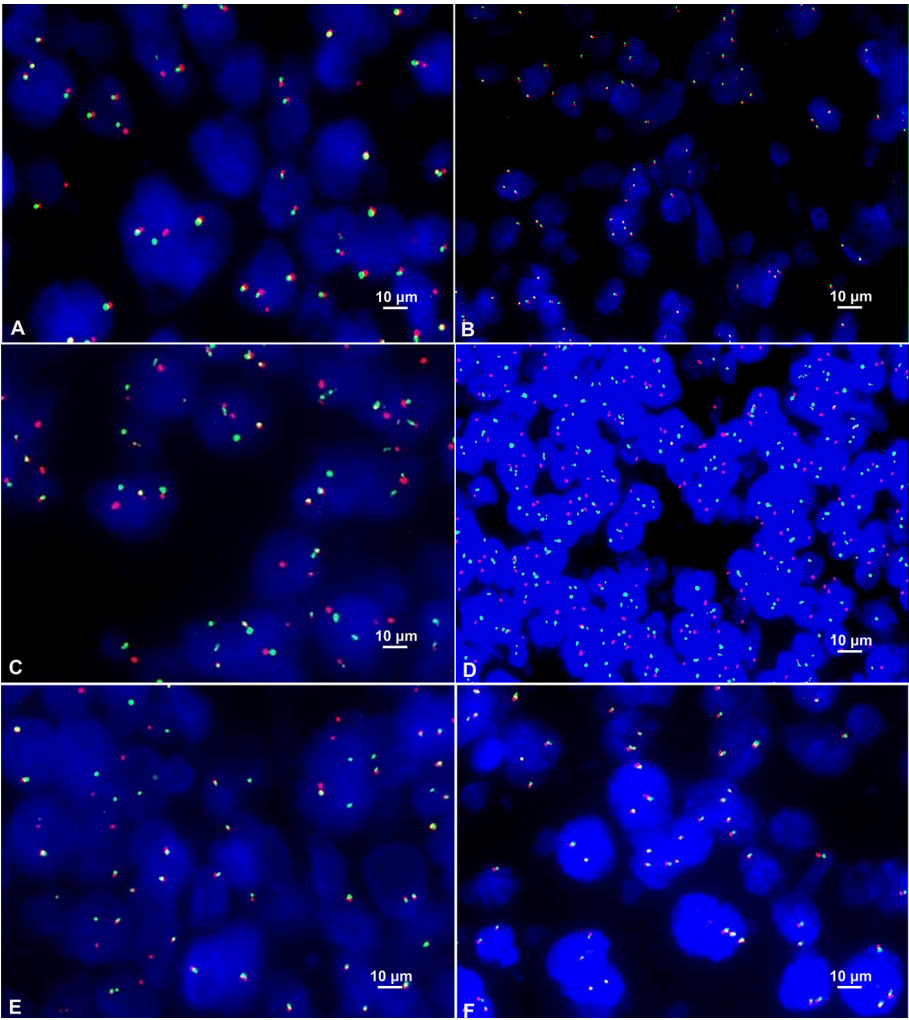


FIGURE 3 | (A) Positive C-MYC gene translocation showed 1 red signal, 1 green signal, and 1 red-green-fused yellow signal in the nucleus (FISH×1000). (B) Positive C-MYC gene amplification showed ≥3 red-green fused yellow signals in the nucleus (FISH×1000). (C) Positive BCL-2 gene translocation showed 1 red signal, 1 green signal and 1 red-green-fused yellow signal in the nucleus (FISH×1000). (D) Positive BCL-2 gene amplification showed ≥3 red or green signals in the nucleus (FISH×1000). (E) Positive BCL-6 gene translocation showed 1 red signal, 1 green signal and 1 red-green-fused yellow signal in the nucleus (FISH×1000). (F) Positive BCL-6 gene amplification showed ≥3 red-green-fused yellow signals in the nucleus (FISH×1000).

TABLE 2 | Association of C-MYC protein expression and gene translocation, amplification, and clinical characteristics.

Indicator		Total cases	C-MYC translocation		χ^2	P	C-MYC amplification		χ^2	P
			Positive	Negative			Positive	Negative		
C-MYC expression	Positive	20	10	10	11.813	0.001	0	20	0.000	1.000
	Negative	22	0	22			1	21		
Hans typing	GCB type	16	7	9	4.029	0.045	0	16	0.000	1.000
	Non-GCB type	26	3	23			1	25		
Gender	Male	26	8	18	0.954	0.329	0	26	0.000	0.381
	Female	16	2	14			1	15		
Age	≥50 years	33	10	23	2.104	0.147	1	32	0.000	1.000
	<50 years	9	0	9			0	9		

TABLE 3 | Association of BCL-2 protein expression, gene translocation, and amplification and clinical characteristics.

Indicator		Total cases	BCL-2 translocation		χ^2	P	BCL-2 amplification		χ^2	P
			Positive	Negative			Positive	Negative		
BCL-2 expression	Positive	36	18	18	3.407	0.029	11	25	1.155	0.283
	Negative	6	0	6			0	6		
Hans typing	GCB type	16	7	9	0.008	0.927	5	11	0.050	0.823
	Non-GCB type	26	11	15			6	20		
Gender	Male	26	10	16	0.538	0.463	6	20	0.050	0.823
	Female	16	8	8			5	11		
Age	≥50 years	33	13	20	0.239	0.625	8	25	0.015	0.903
	<50 years	9	5	4			3	6		
Total cases		42	18	24			11	31		
Total cases		42	10	32			1	41		

TABLE 4 | Association of BCL-6 protein expression, gene translocation and amplification, and clinical characteristics.

Indicator		Total cases	BCL-6 translocation		χ^2	P	BCL-6 amplification		χ^2	P
			Positive	Negative			Positive	Negative		
BCL-6 expression	Positive	19	6	13	6.091	0.014	1	18	0.000	1.000
	Negative	23	0	23			2	21		
Hans typing	GCB type	16	2	14	0.000	1.000	1	15	0.000	1.000
	Non-GCB type	26	4	22			2	24		
Gender	Male	26	6	20	2.629	0.105	1	25	0.194	0.659
	Female	16	0	16			2	14		
Age	≥50 years	33	6	27	0.713	0.398	1	32	0.000	0.111
	<50years	9	0	9			2	7		
Total cases		42	18	24			3	39		

TABLE 5 | The relationship between DHL and clinical characteristics.

Indicator		Total cases	DHL		χ^2	P
			Positive	Negative		
DEL	Positive	15	2	13	1.412	0.235
	Negative	27	0	27		
Hans typing	GCB type	16	1	15	0.000	1.000
	Non-GCB type	26	1	25		
Gender	Male	26	2	24	0.153	0.696
	Female	16	0	16		
Age	≥50 years	33	2	31	0.000	1.000
	<50 years	9	0	9		
Total cases		42	2	40		

and 90% in 1 case of C-MYC amplification. BCL-2 and BCL-6 translocation or amplification with overexpression of Ki-67 were analyzed, and it was found that there was no significant correlation in Ki-67 overexpression and C-MYC amplification ($P > 0.05$, **Table 6**). This result indicated that C-MYC translocation is more useful than C-MYC amplification in terms of diagnosis and prognosis of DLBCL.

DISCUSSION

Characteristics of Diffuse Large B-Cell Lymphoma

DLBCL is a highly heterogeneous and invasive lymphoma with various disease sites, immune-phenotypes, and clinical prognosis. Under a microscope, abnormal large B lymphocytes can be found and the widely distributed. The cell body of abnormal B lymphocytes was usually more than twice that of normal lymphocytes (Chinese and Society of Hematology et al., 2013).

FISH is a gold standard for detecting DHL. However, FISH is difficult to perform and takes long time to operate. Besides, the reagents are expensive. In contrast, it is convenient, rapid and low cost to detect the protein expression of corresponding genes by IHC. Therefore, IHC is commonly used in clinics to detect C-MYC, BCL-2, and BCL-6 protein expression in DLBCL. Green et al. (2012b) reported that in DLBCL, there was no significant difference in survival rate between DEL and DHL, suggesting that DEL has similar biological behaviors as DHL, and that “double expression” is also associated with poor prognosis of lymphoma. Swerdlow (2014) believe that although 70–80% of DHL or THL also shows “double expression,” DEL is not equivalent to and is more common than DHL, accounting for

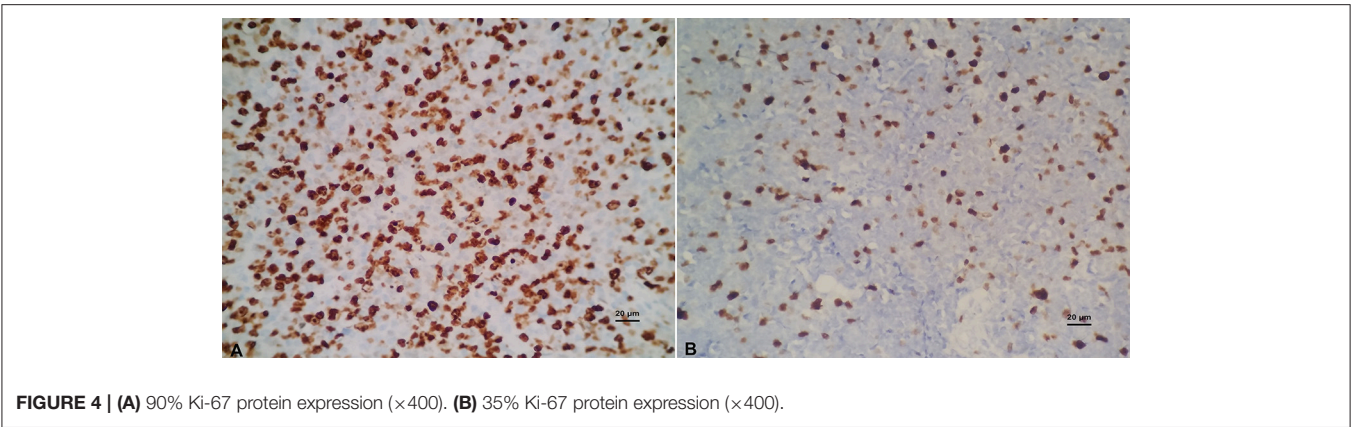


TABLE 6 | The relationship between Ki-67 and C-MYC BCL-2, and BCL-6 gene abnormalities.

Types of gene abnormalities		Total cases	Ki-67		χ^2	P	Ki-67		χ^2	P
			≥90% cases	<90% cases			≥80% cases	<80% cases		
C-MYC translocation	Positive	10	6	4	4.492	0.034	7	3	0.163	0.686
	Negative	32	6	26			18	14		
C-MYC amplification	Positive	1	1	0	0.230	0.631	1	0	0.000	1.000
	Negative	41	11	30			24	17		
BCL-2 translocation	Positive	18	3	15	2.188	0.139	9	9	1.186	0.276
	Negative	24	9	15			16	8		
BCL-2 amplification	Positive	11	1	10	1.629	0.202	5	6	0.561	0.454
	Negative	31	11	20			20	11		
BCL-6 translocation	Positive	6	1	5	0.044	0.834	5	1	0.696	0.404
	Negative	36	11	25			20	16		
BCL-6 amplification	Positive	3	1	2	0.000	1.000	1	2	0.122	0.727
	Negative	39	11	28			24	15		
Total cases		42	12	30			25	17		

18–33% of DLBCL (Green et al., 2012b; Valera et al., 2013), and only <20% of patients in DEL showed DHL (Green et al., 2012b).

The positive rate of C-MYC protein expression in this study was 47.6% (20/42), among which GCB type was 50% (8/16) and non-GCB type was 46.15% (12/26) according to the Hans typing method, and there was no significant difference between these two types. Among the 20 cases with positive C-MYC protein expression, males were 59.69% (15/26) and females were 31.25% (5/16); 51.52% (17/33) of patients were ≥50 years old and 33.33% (3/9) were <50 years old. Statistical analysis showed that, there was no significant difference in the expression of C-MYC protein related to age or gender of patients. These results were consistent with previous studies, in which the detection rate of C-MYC gene translocation in DLBCL is 2–16% (Smith et al., 2010; Aukema et al., 2011; Gouveia et al., 2012). In DLBCL, abnormalities in the C-MYC gene mainly include translocation and amplification, often occurred in the context of complex karyotypes, and have aggressive clinical behavior.

Biological Characteristics of C-MYC Gene Abnormality in DLBCL

Although immunohistochemical detection of C-MYC expression is not equivalent to C-MYC translocation, studies have shown that the expression of C-MYC in invasive B-cell lymphoma is associated with genetic abnormalities (Chisholm et al., 2015). Kluk et al. (2012) have shown that, when C-MYC protein expression ≥50%, the DLBCL can be identified as having the rearrangement of C-MYC gene. Green et al. proposed that if C-MYC protein expression ≥70%, the DLBCL is predicted to have translocation of C-MYC gene (Green et al., 2012a).

In addition to translocation, C-MYC gene abnormalities include amplification and mutation (Gurel et al., 2008; Leucci et al., 2008; Ruzinova et al., 2010). In the 42 cases of DLBCL in this study, only one case of C-MYC amplification (2.38%) was detected. At present, there are few reports on C-MYC amplification. Previous studies had suggested that DLBCL patients with C-MYC amplification have a relatively poor prognosis (Mossafa et al., 2006; Yoon et al., 2008; Stasik et al., 2010). The amplification rate of C-MYC gene by Stasik et al. (2010) was 38% (18/47), and C-MYC amplification was

correlated with its mRNA expression. However, a report from South Korea (Yoon et al., 2008) showed a C-MYC amplification rate of 7.1% (11/156), and multiple factors have suggested that C-MYC amplification is an independent prognostic factor for poor prognosis of DLBCL.

Biological Characteristics of BCL-2 Gene Abnormality in DLBCL

BCL-2 is detectable in approximately 50% of DLBCL and 75% of high-grade B-cell lymphomas, whose effect is to inhibit cell apoptosis and promote cell proliferation, which interacts with the action of C-MYC. BCL-2 also enhances the role of other oncogenes and induces lymphoma. BCL-2 protein accelerates the growth of lymphoma and promotes the resistance of tumor cells to chemical drugs.

The positive rate of BCL-2 protein expression in this study was 85.71% (36/42), and according to Hans typing method, 75% (12/16) of the cases were GCB and 92.31% (24/26) were non-GCB type. There was no significant difference between the types. Among the 36 cases with positive BCL-2 protein expression, males were 80.77% (21/26) and females were 93.75% (15/16), ≥ 50 years old were 81.82% (27/33); and < 50 years old were 100% (9/9). Statistically, there was no significant difference in the distribution of BCL-2 protein expression in age and gender.

Previous studies (Iqbal et al., 2004, 2006) reported that the incidence of BCL-2 translocation was 20–30%, and in the 42 cases of DLBCL in this study, 18 cases (42.86%) of BCL-2 were detected. One studies (Chen et al., 2010) showed that BCL-2 translocation mainly occurred in GCB type. Among the 18 cases of BCL-2 translocation that we have obtained, 7 cases were GCB type (7/16, 43.75%) and 11 cases were non-GCB type (11/26, 42.31%). Eighteen cases of BCL-2 translocation were positive for BCL-2 protein expression, while BCL-2 translocation did not occur in BCL-2 protein negative cases, suggesting that BCL-2 protein expression is prominently correlated with BCL-2 translocation.

Biological Characteristics of BCL-6 Gene Abnormality in DLBCL

BCL-6 is a nuclear transcriptional repressor. It was reported that BCL-6 gene mutation and chromosomal translocation are the basis of tumorigenesis. Abnormal expression of BCL-6 can directly regulate cell differentiation, proliferation and apoptosis to promote tumor growth and differentiation (Ci et al., 2008). BCL-6 can affect DLBCL by regulating B cell activation, differentiation, cell cycle, and apoptosis (Polo et al., 2004). In the study of Basso and Dalla Favera (Basso and Dalla-Favera, 2012), BCL-6 regulates the follicular germinal center response and inhibits C-MYC protein and BCL-2 protein expression in normal GCB cells. In addition, BCL-6 gene also regulates tumor growth by regulating the expression of other genes, such as signal transducers and activators of transcription (STAT) and B lymphocyte induced maturation protein-1 (Blimp-1) and others (Kusam et al., 2004).

The positive rate of BCL-6 protein expression in this study was 85.71% (19/42), among which, GCB type was 43.75%

(7/16), non-GCB type was 46.15% (12/26), and the detection rate of BCL-6 translocation was 14.29% (6/42). All 6 cases of BCL-6 translocation DLBCL have shown positive expression of BCL-6 protein. There was a correlation between BCL-6 gene translocation and protein expression in patients. In patients with negative BCL-6 protein expression, there was no BCL-6 translocation found. In this study, 6 DLBCL patients with BCL-6 translocation were males ≥ 50 years old, suggesting that DLBCL patients in middle-aged men have a relatively high BCL-6 translocation rate. Therefore, for patients with positive BCL-6 protein expression, there is a high probability of BCL-6 translocation.

The Proliferation Index Ki-67 and Abnormalities of C-MYC, BCL-2, and BCL-6 Genes

Studies (Mationg-Kalaw et al., 2012) have reported that when the proliferation index Ki-67 is $\geq 90\%$, the sensitivity of detecting DHL/THL in invasive B-cell lymphoma was 0.54; when Ki-67 $\geq 75\%$, it was 77%. Another study (Landsburg et al., 2014) set the cutoff value of Ki-67 to 80% and found no difference between DHL and non-DHL. In this study, we set Ki-67 with two cut-off values: ≥ 80 and $\geq 90\%$, and perform statistical analysis with C-MYC, BCL-2, BCL-6 translocation, and amplification. We found similar results with the previous studies (Mationg-Kalaw et al., 2012; Landsburg et al., 2014). Therefore, high Ki-67 proliferative index indicated a higher degree of malignancy in patients with C-MYC translocation in DLBCL.

DHL/THL and DEL/TEL

The poor prognosis caused by C-MYC translocation is mainly due to parallel BCL-2 or BCL-6 translocation (Johnson et al., 2009; Pedersen et al., 2012; Pillai et al., 2013). Studies have shown that the presence of C-MYC, BCL-2, or BCL-6 and TP53 gene alterations in DHL is important for pathogenesis and a poor prognosis of DHL (Aukema et al., 2011). Further studies (Gebauer et al., 2015) showed that there is a difference between C-MYC/BCL-2 translocation and C-MYC/BCL-6 translocation in DHL, and DHL of C-MYC/BCL-2 translocation shows frequent TP53 mutation, which rarely occurs in DHL of C-MYC/BCL-6 translocation.

Taken together, our results suggest that C-MYC, BCL-2, and BCL-6 gene translocations are correlated with their protein expression in DLBCL. Therefore, immunohistochemical staining of C-MYC, BCL-2, and BCL-6 proteins could be used for helping diagnosis and prognosis of DLBCL.

Because our sample sizes were small and our methods did not encompass all gene abnormalities, future study with a big sample size will be merited.

ETHICS STATEMENT

This study was approved the Ethics committee of Weifang People's Hospital.

AUTHOR CONTRIBUTIONS

YZ and WF conceived and designed the study. YZ, HW, and HY reviewed cases. CR and NZ collected cases. SG and WF performed statistical analyses. CR, WF, and QH performed experiments. YZ and WF wrote the manuscript. All authors read and revised the manuscript.

REFERENCES

- Arber, D. A., Orazi, A., Hasserjian, R., Thiele, J., Borowitz, M. J., Le Beau, M. M., et al. (2016). The 2016 revision to the World Health Organization classification of myeloid neoplasms and acute leukemia. *Blood* 127, 2391–2405. doi: 10.1182/blood-2016-03-643544
- Aukema, S. M., Siebert, R., Schuurin, E., van Imhoff, G. W., Kluin-Nelemans, H. C., Boerma, E. J., et al. (2011). Double-hit B-cell lymphomas. *Blood* 117, 2319–2331. doi: 10.1182/blood-2010-09-297879
- Basso, K., and Dalla-Favera, R. (2012). Roles of BCL6 in normal and transformed germinal center B cells. *Immunol. Rev.* 247, 172–183. doi: 10.1111/j.1600-065X.2012.01112.x
- Campo, E., Swerdlow, S. H., Harris, N. L., Pileri, S., Stein, H., and Jaffe, E. S. (2011). The 2008 WHO classification of lymphoid neoplasms and beyond: evolving concepts and practical applications. *Blood* 117, 5019–5032. doi: 10.1182/blood-2011-01-293050
- Chen, Y., Han, T., Iqbal, J., Irons, R., Chan, W. C., Zhu, X., et al. (2010). Diffuse large B-cell lymphoma in Chinese patients. *Am. J. Clin. Pathol.* 133, 305–313. doi: 10.1309/AJCP4H6ADGYDZMOA
- Chinese and Society of Hematology, Chinese Medical Association, Chinese Society of Lymphoma, and Chinese Anti-cancer Association (2013). Guidelines for the diagnosis and treatment of China's diffuse large B cell lymphoma by the Hematology Branch of Chinese Medical Association, China Anti-Cancer Association Lymphoma Professional Committee (2013 edition). *Chin. J. Hematol.* 34, 816–819. doi: 10.3760/cma.j.issn.0253-2727.2013.09.019
- Chisholm, K. M., Bangs, C. D., Bacchi, C. E., Molina-Kirsch, H., Cherry, A., and Natkunam, Y. (2015). Expression profiles of MYC protein and MYC gene rearrangement in lymphomas. *Am. J. Surg. Pathol.* 39, 294–303. doi: 10.1097/PAS.0000000000000365
- Chung, H. J., and Levens, D. (2005). *c-myc* expression: keep the noise down. *Molecules Cells* 20, 157–166.
- Ci, W., Polo, J. M., and Melnick, A. (2008). B-cell lymphoma 6 and themolecular pathogenesis of diffuse large B-cell lymphoma. *Curr. Opin. Hematol.* 15, 381–390. doi: 10.1097/MOH.0b013e328302c7df
- Gebauer, N., Bernard, V., Gebauer, W., Thorns, C., Feller, A. C., and Merz, H. (2015). TP53 mutations are frequent events in double-hit B-cell lymphomas with MYC and BCL2 but not MYC and BCL6 translocations. *Leuk. Lymphoma* 56, 179–185. doi: 10.3109/10428194.2014.907896
- Gouveia, G. R., Siqueira, S. A., Pereira, J. (2012). Pathophysiology and molecular aspects of diffuse large B-cell lymphoma. *Rev. Bras. Hematol. Hemoter.* 34, 447–451. doi: 10.5581/1516-8484.20120111
- Green, T. M., Nielsen, O., de Stricker, K., Xu-Monette, Z. Y., Young, K. H., and Moller, M. B. (2012a). High levels of nuclear MYC protein predict the presence of MYC rearrangement in diffuse large B-cell lymphoma. *Am. J. Surg. Pathol.* 36, 612–619. doi: 10.1097/PAS.0b013e318244e2ba
- Green, T. M., Young, K. H., Visco, C., Xu-Monette, Z. Y., Orazi, A., Go, R. S., et al. (2012b). Immunohistochemical double-hit score is a strong predictor of outcome in patients with diffuse large B-cell lymphoma treated with rituximab plus cyclophosphamide, doxorubicin, vincristine, and prednisone. *J. Clin. Oncol.* 30, 3460–3467. doi: 10.1200/JCO.2011.41.4342
- Gurel, B., Iwata, T., Koh, C. M., Jenkins, R. B., Lan, F., Van Dang, C., et al. (2008). Nuclear MYC protein overexpression is an early alteration in human prostate carcinogenesis. *Mod. Pathol.* 21, 1156–1167. doi: 10.1038/modpathol.2008.111

ACKNOWLEDGMENTS

The authors are grateful for the generous financial support from the Scientific and Technological Development Project of Shandong Province (2015GSF118168) and the Department of Science and Technology of Weifang City (20100220).

- Hans, C. P., Weisenburger, D. D., Greiner, T. C., Gascoyne, R. D., Delabie, J., Ott, G., et al. (2004). Confirmation of the molecular classification of diffuse large B-cell lymphoma by immunohistochemistry using a tissue microarray. *Blood* 103, 275–282. doi: 10.1182/blood-2003-05-1545
- Horn, H., Ziepert, M., Becher, C., Barth, T. F., Bernd, H. W., Feller, A. C., et al. (2013). MYC status in concert with BCL-2 and BCL-6 expression predicts outcome in diffuse large B-cell lymphoma. *Blood* 121, 2253–2263. doi: 10.1182/blood-2012-06-435842
- Iqbal, J., Neppalli, V. T., Wright, G., Dave, B. J., Horsman, D. E., Rosenwald, A., et al. (2006). BCL-2 expression is a prognostic marker for the activated B-cell-like type of diffuse large B-cell lymphoma. *J. Clin. Oncol.* 24, 961–968. doi: 10.1200/JCO.2005.03.4264
- Iqbal, J., Sanger, W. G., Horsman, D. E., Rosenwald, A., Pickering, D. L., Dave, B., et al. (2004). BCL-2 translocation defines a unique tumor subset within the germinal center B-cell-like diffuse large B-cell lymphoma. *Am. J. Pathol.* 165, 159–166. doi: 10.1016/S0002-9440(10)63284-1
- Johnson, N. A., Savage, K. J., Ludkovski, O., Ben-Neriah, S., Woods, R., Steidl, C., et al. (2009). Lymphomas with concurrent BCL2 and MYC translocations: the critical factors associated with survival. *Blood* 114, 2273–2279. doi: 10.1182/blood-2009-03-212191
- Kluk, M. J., Chapuy, B., Sinha, P., Roy, A., Dal Cin, P., Neuberg, D. S., et al. (2012). Immunohistochemical detection of MYC-driven diffuse large B-cell lymphomas. *PLoS ONE* 7:e33813. doi: 10.1371/journal.pone.0033813
- Kusam, S., Vasanwala, F. H., and Dent, A. L. (2004). Transcriptional repressor BCL-6 immortalizes germinal center-like B cells in the absence of p53 function. *Oncogene* 23, 839–844. doi: 10.1038/sj.onc.1207065
- Landsburg, D. J., Nasta, S. D., Svoboda, J., Morrisette, J. J., and Schuster, S. J. (2014). 'Double-Hit' cytogenetic status may not be predicted by baseline clinicopathological characteristics and is highly associated with overall survival in B cell lymphoma patients. *Br. J. Haematol.* 166, 369–374. doi: 10.1111/bjh.12901
- Leucci, E. M., Cocco, A., Onnis, A., De Falco, G., van Cleef, P., Bellan, C., et al. (2008). MYC translocation-negative classical Burkitt lymphoma cases: an alternative pathogenetic mechanism involving miRNA deregulation. *J. Pathol.* 216, 440–450. doi: 10.1002/path.2410
- Li, X., Li, G., and Gao, Z. (2012). Chinese lymphoma pathology research collaboration group. Chinese lymphoma subtype distribution: 10002 cases of multicenter cases in China. *Diagnostic Theory Practice* 11, 111–115. doi: 10.3969/j.issn.1671-2870.2012.02.006
- Mationg-Kalaw, E., Tan, L. H., Tay, K., Lim, S. T., Tang, T., Lee, Y. Y., et al. (2012). Does the proliferation fraction help identify mature B cell lymphomas with double and triple-hit translocations. *Histopathology* 61, 1214–1218. doi: 10.1111/j.1365-2559.2012.04351.x
- Mossafa, H., Damotte, D., Jenabian, A., Delarue, R., Vincenneau, A., Amouroux, I., et al. (2006). Non-Hodgkin's lymphomas with Burkitt-like cells are associated with C-MYC amplification and poor prognosis. *Leuk. Lymphoma* 547, 1885–1893. doi: 10.1080/10428190600687547
- Pedersen, M. O., Gang, A. O., Poulsen, T. S., Knudsen, H., Lauritzen, A. F., Nielsen, S. L., et al. (2012). Double-hit BCL2/MYC translocations in a consecutive cohort of patients with large B-cell lymphoma—a single centre's experience. *Eur. J. Haematol.* 89, 63–71. doi: 10.1111/j.1600-0609.2012.01787.x
- Pillai, R. K., Sathanoori, M., Van Oss, S. B., and Swerdlow, S. H. (2013). Double-hit B-cell lymphomas with BCL6 and MYC translocations are aggressive, frequently extranodal lymphomas distinct from BCL2 double-hit B-cell lymphomas. *Am. J. Surg. Pathol.* 37, 323–332. doi: 10.1097/PAS.0b013e31826cebad

- Polo, J. M., Dell'Oso, T., Ranuncolo, S. M., Cerchiatti, L., Beck, D., Da Silva, G. F., et al. (2004). Specific peptideinterference reveals BCL6 transcriptional and oncogenic mechanisms in b-cell lymphoma cells. *Nat Med.* 10, 1329–1335. doi: 10.1038/nm1134
- Ruzinova, M. B., Caron, T., and Rodig, S. J. (2010). Altered subcellular localization of C-MYC protein identifies aggressive B-cell lymphomas harboring a C-MYC translocation. *Am. J. Surg. Pathol.* 34, 882–891. doi: 10.1097/PAS.0b013e3181db83af
- Smith, S. M., Anastasi, J., Cohen, K. S., and Godley, L. A. (2010). The impact of MYC expression in lymphoma biology: beyond Burkitt lymphoma. *Blood Cells Mol. Dis.* 45, 317–323. doi: 10.1016/j.bcmd.2010.08.002
- Stasik, C. J., Nitta, H., Zhang, W., Mosher, C. H., Cook, J. R., Tubbs, R. R., et al. (2010). Increased MYC gene copy number correlates with increased mRNA levels in diffuse large B-cell lymphoma. *Haematologica* 95, 597–603. doi: 10.3324/haematol.2009.012864
- Swerdlow, S. H. (2014). Diagnosis of 'double hit' diffuse large B-cell lymphoma, and B-cell lymphoma, unclassifiable, with features intermediate between DLBCL, and Burkitt lymphoma: when, and how, FISH versus IHC. *Hematology Am. Soc. Hematol. Educ. Program* 2014, 90–99. doi: 10.1182/asheducation-2014.1.90
- Valera, A., López-Guillermo, A., Cardesa-Salzmann, T., Climent, F., González-Barca, E., Mercadal, S., et al. (2013). MYC protein expression and genetic alterations have prognostic impact in patients with diffuse large B-cell lymphoma treated with immunochemotherapy. *Haematologica* 98, 1554–1562. doi: 10.3324/haematol.2013.086173
- Yoon, S. O., Jeon, Y. K., Paik, J. H., Kim, W. Y., Kim, Y. A., Kim, J. E., et al. (2008). MYC translocation and an increased copy number predict poor prognosis in adult diffuse large B-cell lymphoma (DLBCL), especially in germinal centre-like B cell (GCB) type. *Histopathology* 53, 205–217. doi: 10.1111/j.1365-2559.2008.03076.x

Conflict of Interest Statement: The authors declare that the research was conducted in the absence of any commercial or financial relationships that could be construed as a potential conflict of interest.

Copyright © 2019 Zhang, Wang, Ren, Yu, Fang, Zhang, Gao and Hou. This is an open-access article distributed under the terms of the Creative Commons Attribution License (CC BY). The use, distribution or reproduction in other forums is permitted, provided the original author(s) and the copyright owner(s) are credited and that the original publication in this journal is cited, in accordance with accepted academic practice. No use, distribution or reproduction is permitted which does not comply with these terms.



Mutations Defining Patient Cohorts With Elevated PD-L1 Expression in Gastric Cancer

Otilia Menyhárt^{1,2}, Lőrinc Sándor Pongor^{1,2} and Balázs Györffy^{1,2*}

¹ 2nd Department of Pediatrics, Semmelweis University, Budapest, Hungary, ² MTA TTK Lendület Cancer Biomarker Research Group, Institute of Enzymology, Hungarian Academy of Sciences, Budapest, Hungary

OPEN ACCESS

Edited by:

Pascale Cohen,
Claude Bernard University Lyon 1,
France

Reviewed by:

Michele Caraglia,
Università degli Studi della Campania
Luigi Vanvitelli Caserta, Italy
Irina Pinchuk,
The University of Texas Medical
Branch at Galveston, United States

*Correspondence:

Balázs Györffy
gyorffy.balazs@ttk.mta.hu

Specialty section:

This article was submitted to
Experimental Pharmacology and Drug
Discovery,
a section of the journal
Frontiers in Pharmacology

Received: 13 October 2018

Accepted: 12 December 2018

Published: 08 January 2019

Citation:

Menyhárt O, Pongor LS and Györffy B
(2019) Mutations Defining Patient
Cohorts With Elevated PD-L1
Expression in Gastric Cancer.
Front. Pharmacol. 9:1522.
doi: 10.3389/fphar.2018.01522

The immunotherapy agent pembrolizumab has been approved for gastric cancer (GC) patients with recurrent or advanced disease who are PD-L1 positive. Mutations in the primary lesion may drive the expression of immune targets thereby priming the tumor to therapeutic sensitivity. In this study, we aimed to uncover mutations associated with elevated PD-L1 expression in GC patients. Data from 410 GC patients were available, including the mutational spectrum of 39,916 genes and expression values of 20,500 genes. PD-L1 gene expression was compared to the mutational status of each gene separately by using a Mann-Whitney *U*-test and a Receiver Operating Characteristic test. Only mutations with a prevalence over 5% were considered. Significance was accepted in cases of $p < 1E-05$ and a fold change over 1.44. Mutations in 209 genes were associated with increased PD-L1 expression. These mutations were enriched in genes related to microtubule-based movement ($p = 3.4E-4$), cell adhesion ($p = 4.9E-4$), response to DNA-damage ($p = 6.9E-4$), and double-strand break-repair ($p = 1.6E-3$). Mutations in *TTK* ($p = 8.8E-10$, AUC = 0.77), *COL7A1* ($p = 2.0E-9$, AUC = 0.74), *KIF15* ($p = 2.5E-9$, AUC = 0.75), and *BDP1* ($p = 3.3E-9$, AUC = 0.74) had the strongest link to elevated PD-L1 expression. Finally, we established a decision tree based on mutations in *PIK3CA*, *MEF2C*, *SLC11A1*, and *KIF15* capable to separate patient sub-cohorts with elevated PD-L1 expression. In summary, we identified mutations associated with elevated PD-L1 expression that facilitate the development of better prognostic biomarkers for GC, and might offer insight into the underlying tumor biology.

Keywords: immunotherapy, stomach cancer, immune checkpoint inhibitors, CD274, PIK3CA, TTK, KIF15

INTRODUCTION

Gastric cancer (GC) is the fifth most common cancer and the third leading cause of cancer-related mortality in both sexes worldwide with the highest mortality being observed in Eastern Asia, Central and Eastern Europe (Ferlay et al., 2015). Moreover, despite a steady decline in gastric cancer related mortality in the Western hemisphere (Malvezzi et al., 2010), population aging, a distinctive feature of developed countries, contributes once again to increasing trends (Menyhárt et al., 2018). Early diagnosis is difficult due to lack of symptoms, particularly in countries without active screening programs, while detection in an advanced stage limits survival prospects (Seeruttun et al., 2017). For advanced patients, standard treatment options based on combined chemotherapy regimens provide limited benefits, and the median overall survival is <12 months (Cunningham et al., 2010). In recent years, immune checkpoint inhibitors (ICI) have rapidly gained momentum in the treatment of advanced GCs and gastroesophageal junction cancers (GEJC) (Taieb et al., 2018).

The immune checkpoint receptor programmed cell death-1 (PD-1) is expressed on activated T cells and prevents overstimulation of immune responses (Francisco et al., 2010), while its ligand, PD-L1, is expressed on tumor infiltrating immune cells and tumor cells. The PD-1/PD-L1 pathway plays an active role in tumor immune evasion (Henick et al., 2014). Blocking their interaction resurrects T-cell-mediated anti-tumor immunity, providing a survival benefit in various advanced, refractory malignancies (Alsaab et al., 2017). The FDA granted accelerated approval to the anti-PD-1 monoclonal antibody pembrolizumab in 2017 as third line treatment for patients with recurrent, locally advanced or metastatic PD-L1-positive GC/GEJC (Fuchs et al., 2018). The anti-PD-1 agent nivolumab demonstrated survival benefits in refractory unresectable advanced or recurrent GC/GEJC, irrespective of PD-L1 expression status, leading to regulatory approval in Japan (Kang et al., 2017).

PD-1 and PD-L1 are expressed in up to 50% of GC/GEJC tumors and are usually associated with the poorest prognosis (Wu et al., 2015). PD-L1 expression is a potential predictive biomarker for the effectiveness of anti-PD-1 therapy: the objective response rate (ORR) to pembrolizumab monotherapy was 16% in PD-L1-positive vs. 6% in PD-L1-negative GC/GEJC patients. Responses were remarkably better when ICIs were administered as a first-line treatment: the ORR reached 36% in PD-L1-positive patients treated with pembrolizumab monotherapy (Fuchs et al., 2018).

PD-L1 status is typically detected by immunohistochemistry. Scoring methods, antibodies and cut-off values are different across clinical studies, making comparison difficult (Teng et al., 2018). Thus, additional biomarkers capable of identifying a subset of patients with elevated PD-L1 (CD274) expression as potential candidates for anti-PD-1 therapy are highly in demand.

Genetic alterations within tumors may influence immune system engagement eventually also impacting therapy response; in non-small cell lung cancer (NSCLC) cell lines *EGFR* mutations or *EML4-ALK* fusions activate the PD-1/PD-L1 pathway via PD-L1 upregulation, inducing immune escape (Akbay et al., 2013; Ota et al., 2015). Accordingly, anti-PD-L1 therapy induced higher ORRs in PD-L1-positive *EGFR* mutant patients (31%) compared to *EGFR* wild-type (22%) NSCLC patients (Peters et al., 2017). *KRAS* mutant advanced NSCLC patients with simultaneous *KEAP1/NFE2L2* mutations have reduced PD-L1 expression levels (Skoulidis et al., 2015), which eventually lead to decreased overall survival after the initiation of immune therapy (Arbour et al., 2018). In this study, our aim was to identify genetic alterations in GC that are associated with PD-L1 upregulation. These genes might serve as positive biomarkers capable of identifying responsive tumors. We also combined multiple genes with the goal of creating a decision tree to assist the selection of potentially eligible candidates for early anti-PD-1 therapy.

METHODS

Sequencing and Expression Database

Mutation and expression data were obtained from the TCGA repository (<https://portal.gdc.cancer.gov/>). Mutations identified

with the mutect2 algorithm were downloaded in VCF format. Variants were selected based on the mutect2 “PASS” status and filtered for mutations with at least 50× overall coverage and a minimum of 5 reads supporting the alteration. The remaining mutations were annotated using the *snpEff* (Cingolani et al., 2012) program using the GRCh38 human genome version. Only the canonical isoforms were selected in the database construction. The expression database was normalized using the DESeq2 (Varet et al., 2016) algorithm.

Classification Algorithm

Gene expression for PD-L1 was compared to the mutational status of each gene separately using a non-parametric Mann-Whitney U-test and a Receiver Operating Characteristic analysis. Only mutations with a prevalence over 5% were considered. Because of the high number of genes evaluated, statistical significance was only accepted in case of $p < 1e-05$ and a fold change (FC) difference over 1.44. In addition, sensitivity, specificity, and area under the curve (AUC) values were computed for each gene.

Gene ontology analysis for the frequently mutated genes was performed using the Database for Annotation, Visualization and Integrated Discovery (DAVID) Bioinformatics Resource 6.8 to determine the biological meanings of functionally related gene groups (Huang Da et al., 2009). Step-up multiple testing correction was executed for multiple hypothesis testing (Gyorffy et al., 2005).

Decision Tree

A decision tree was calculated using the conditional inference tree method (Hothorn et al., 2006; Hothorn and Zeileis, 2015). The algorithm uses statistics measuring the association between responses and covariates. In the analysis, we used the univariate distribution to determine the significance. We set the maximum depth to 3 for the tree, and at least 5% of the samples were needed to establish a terminal node during the tree generation. The displayed tree includes the branched decision pipeline and the expression range of PD-L1 in the designated patient cohorts.

RESULTS

Database Setup

Data from 438 patients diagnosed with gastric cancer were available from the TCGA repository (<https://cancergenome.nih.gov/>). Most patients were diagnosed in clinical stage III and with grade 3 disease. 64% of the patients were male and 69% of patients were 60 years of age or older, with a median age of 67 years. The average follow-up time was 9.86 months, and 20% of patients died during this period. Over 8% of the patients were identified with residual disease, while pathological complete response (pCR) following adjuvant therapy occurred in 32.4% of the patients (for details see **Supplemental Table 1**).

Mutations Associated With PD-L1 Expression

On average, 873 mutation events were identified per patient in our population based on the mutational profile of 39,916 genes.

The most frequently mutated genes, *PCDHA1-PCDHA4* and the tumor suppressor *TP53*, were mutated on average in every second patient.

The expression levels of 20,500 genes were investigated in our patient population. Data consisting of both the mutational spectrum and expression values for all genes were available for 410 GC patients. Mutations in 209 genes were associated with significantly increased PD-L1 expression (**Supplemental Table 2**). Mutations in *TTK* ($p = 8.83\text{E-}10$, AUC = 0.77), *COL7A1* ($p = 2\text{E-}9$, AUC = 0.74), *KIF15* ($p = 2.49\text{E-}9$, AUC = 0.75), and *BDP1* ($p = 3.26\text{E-}9$, AUC = 0.75) presented the strongest link to elevated PD-L1 expression (**Figure 1**).

We performed gene enrichment analysis to determine the biological functions of the most frequent mutations. According to the GO analysis, the significantly mutated genes were involved in microtubule-based movement ($p = 3.4\text{E-}4$), cell adhesion ($p = 4.9\text{E-}4$), response to DNA-damage ($p = 6.9\text{E-}4$), regulation of gene expression ($p = 1.5\text{E-}4$), and homologous recombination-dependent double-strand break repair ($p = 1.6\text{E-}3$) (**Supplemental Table 3**).

Mutation-Based Hierarchical Clustering

The mutational status of multiple critical genes may assist in the selection of even stronger candidates for ICI therapy. Based on hierarchical clustering of all significant genes with mutational prevalence >5% (when considering the mutation as a terminal node) and FC of at least 1.44, we constructed a decision tree to stratify patients with differential PD-L1 expression (**Figure 2**). The mutational status of *PIK3CA* was the best performing root node dividing patients into major subclasses. Both *PIK3CA* wild-type and mutant populations could be subdivided using additional mutations. Approximately 73% of all patients harbored wild-type alleles of both *PIK3CA* and *KIF15* that are associated with significantly lower overall PD-L1 expression, while *PIK3CA* wild-type patients with *KIF15* mutations (6%) showed significantly elevated PD-L1 expression ($p < 1\text{e-}03$). Patients with *PIK3CA* mutations (21%) could be stratified by two further genes. The presence of *MEF2C* ($p = 0.002$) or *SLC11A1* ($p < 0.001$) mutations (4%) was linked to PD-L1 upregulation, while PD-L1 expression was lower in subjects with the wild-type alleles of *SLC11A1* (17%). Altogether 10% of all patients harbored mutations associated with PD-L1 overexpression.

DISCUSSION

Genetic aberrations within tumors may alter PD-1/PD-L1 interactions by modulating the expression of immune markers (Skoulidis et al., 2015) potentially affecting therapy response (Arbour et al., 2018). We identified mutations of 209 genes associated with PD-L1 upregulation in GC that are involved in functions, such as microtubule-based movement, cell adhesion, gene expression regulation, response to DNA damage and double-strand break repair. Mutations in the *TTK*, *COL7A1*, *KIF15*, and *BDP1* genes present the strongest association with elevated PD-L1 expression. *TTK* frameshift mutations appear in microsatellite instability-high (MSI-H) subtypes of GC that

may alter cell cycle regulation (Ahn et al., 2009). Nonetheless, understanding the exact role of these genes in PD-L1 regulation requires further investigations.

To promote patient stratification, we created a decision tree capable of hypothetically prioritizing candidates for ICI therapy. The root node is set up by *PIK3CA*, while mutations involving *MEF2C*, *SLC11A1*, and *KIF15* provide additional sorting, all known to modulate various aspects of the immune system. *MEF2C* plays a role in immunity and leukemia development (Schuler et al., 2008), and was implicated as an oncogene in various hematological and solid cancers (Pon and Marra, 2016). *SLC11A1* encodes a transmembrane proton/divalent cation symporter, and participates in innate defense against pathogens by influencing macrophage activation (Archer et al., 2015). *KIF15* is involved in the maintenance of the mitotic spindle, and is upregulated in multiple solid malignancies (Scanlan et al., 2001; Wang et al., 2017). *KIF15* also inhibits the endocytic trafficking of $\alpha 2$ integrin, implicated in various immune diseases (De Fougerolles et al., 2000). Except for *PIK3CA*, the functional relationship between the described mutations, PD-L1 upregulation and GC outcome is yet unexplored.

Our findings are in keeping with previous reports showing that gastric tumors with high PD-L1 expression levels frequently harbor *PIK3CA* mutations (Cancer Genome Atlas Research Network, 2014). In fact, *PIK3CA* is among the most frequently mutated genes in GC, present in ~32% of hypermutated and 12% of non-hypermuted tumors (Cancer Genome Atlas Research Network, 2014; Cristescu et al., 2015). *PIK3CA* mutations are associated with more aggressive features, such as advanced T stage, poor differentiation and vascular invasion, especially in locoregional disease (Kim et al., 2017), and higher CD8⁺ T cell infiltration (Siemers et al., 2017). At the same time, *PIK3CA* mutations have not been directly linked to patient prognosis (Harada et al., 2016; Kim et al., 2017). In this study, we found diversity within the *PIK3CA* mutant population, as additional genes were required to stratify patients based on differential PD-L1 expression.

The PI3K/Akt-pathway is involved in the immune response against malignant cells (Dituri et al., 2011), and increases the expression of immune markers. Inhibiting PI3K in melanoma cells reduced (Jiang et al., 2013), and knockdown of PTEN in colorectal cancer cell lines increased the expression of PD-L1 (Song et al., 2013). The PI3K/Akt-pathway regulates PD-L1 expression on a cell- and tissue-dependent manner by either transcriptional or post-transcriptional mechanisms (Song et al., 2013).

PIK3CA mutations appear with high frequency in Epstein-Barr virus positive and MSI-high subtypes of GC (Cancer Genome Atlas Research Network, 2014; Cristescu et al., 2015), and *TTK* frameshift mutations are also relatively frequent in the latter (Ahn et al., 2009). These particular GC subtypes have been suggested to be the most promising candidates for immunotherapy (Cancer Genome Atlas Research Network, 2014; Cristescu et al., 2015). In a recent clinical trial, MSI-high patients treated with ICI reached higher ORRs compared to patients with non-MSI-high tumors. However, the prevalence of MSI-high cases reached only 4% in the study population (Fuchs et al., 2018).

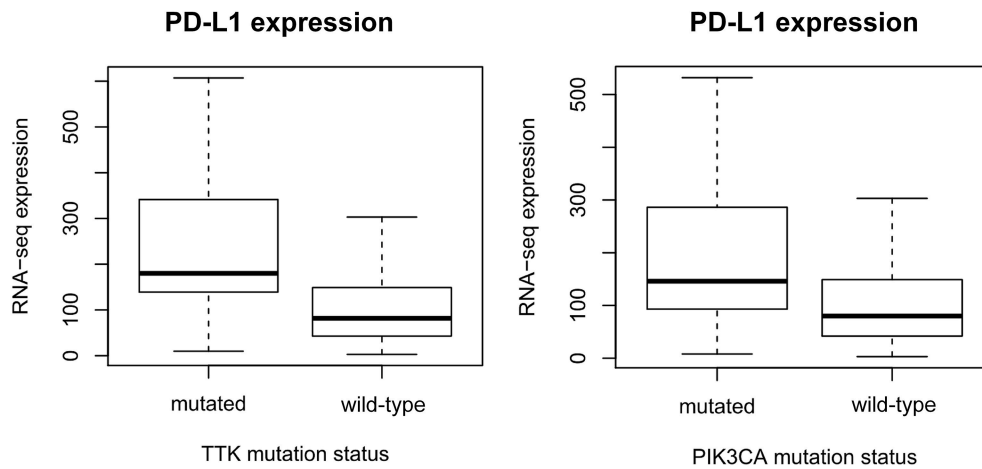


FIGURE 1 | Gene mutations defining higher PD-L1 expression. mRNA levels of PD-L1 (*CD274*) are significantly higher in *TTK* ($p = 8.8E-10$) and *PIK3CA* ($p = 1.7E-08$) mutant patients. The plots show Q1/Q2/Q3 within min-max range.

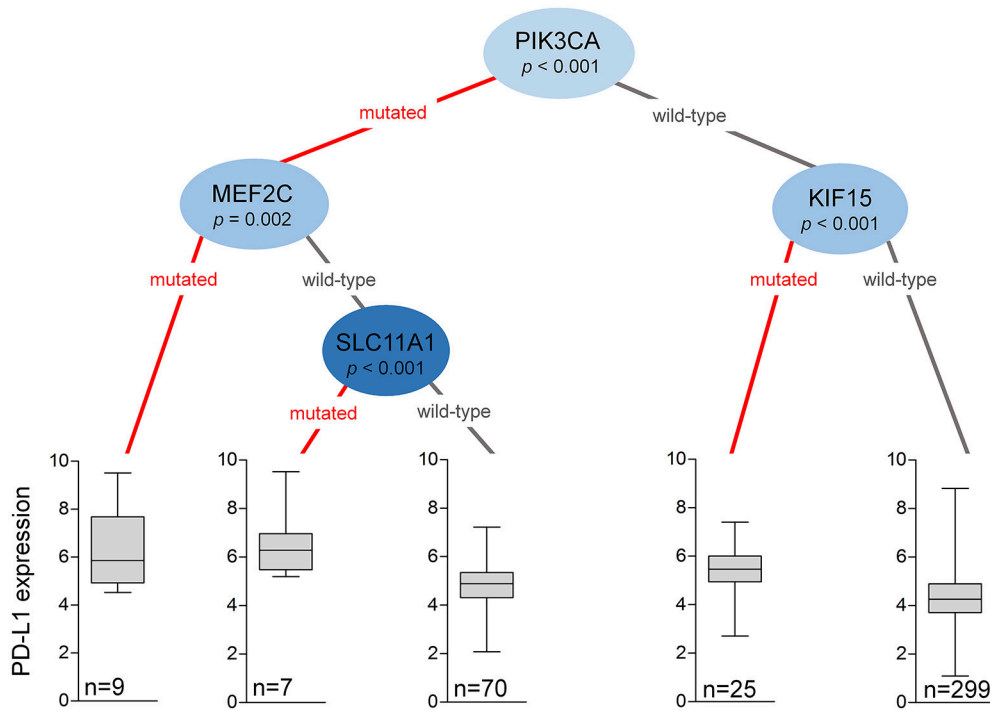


FIGURE 2 | Mutations in the *PIK3CA*, *MEF2C*, *SLC11A1*, and *KIF15* genes help to stratify patients into subcohorts with dissimilar PD-L1 (*CD274*) expression. The decision tree was generated by analyzing the mutational status of all genes simultaneously with a minimal threshold of having at least 5% of the patients in each node. The plots show Q1/Q2/Q3 within min-max range.

Future trials will be required to clarify the subgroup specific responses to anti-PD-1 therapy.

In summary, we present an approach to narrow the list of potentially eligible patients for early anti-PD-1 therapy, and provide a foundation for future studies to reveal functional implications of key mutations on PD-L1 regulation. Nevertheless, the observed associations do not infer functional relationships.

Our results facilitate the development of prognostic biomarkers for GC, and offer insight into the underlying tumor biology.

AUTHOR CONTRIBUTIONS

BG contributed to the conception and design of the study. LP organized the data acquisition and analysis. OM wrote the

first draft of the manuscript. LP and BG wrote sections of the manuscript. All authors contributed to manuscript revision, read and approved the submitted version.

FUNDING

The study was supported by the KH-129581 and the NVKP_16-1-2016-0037 grants of the National Research, Development and Innovation Office, Hungary. The use of the

computational infrastructure of Pázmány Péter University, provided within the National Bionics Program, is gratefully acknowledged.

SUPPLEMENTARY MATERIAL

The Supplementary Material for this article can be found online at: <https://www.frontiersin.org/articles/10.3389/fphar.2018.01522/full#supplementary-material>

REFERENCES

- Ahn, C. H., Kim, Y. R., Kim, S. S., Yoo, N. J., and Lee, S. H. (2009). Mutational analysis of TTK gene in gastric and colorectal cancers with microsatellite instability. *Cancer Res. Treat.* 41, 224–228. doi: 10.4143/crt.2009.41.4.224
- Akbay, E. A., Koyama, S., Carretero, J., Altan, A., Tchaicha, J. H., Christensen, C. L., et al. (2013). Activation of the PD-1 pathway contributes to immune escape in EGFR-driven lung tumors. *Cancer Discov.* 3, 1355–1363. doi: 10.1158/2159-8290.CD-13-0310
- Alsaab, H. O., Sau, S., Alzhrani, R., Tatiparti, K., Bhise, K., Kashaw, S. K., et al. (2017). PD-1 and PD-L1 checkpoint signaling inhibition for cancer immunotherapy: mechanism, combinations, and clinical outcome. *Front. Pharmacol.* 8:561. doi: 10.3389/fphar.2017.00561
- Arbour, K. C., Jordan, E., Kim, H. R., Dienstag, J., Yu, H. A., Sanchez-Vega, F., et al. (2018). Effects of co-occurring genomic alterations on outcomes in patients with KRAS-mutant non-small cell lung cancer. *Clin. Cancer Res.* 24, 334–340. doi: 10.1158/1078-0432.CCR-17-1841
- Archer, N. S., Nassif, N. T., and O'Brien, B. A. (2015). Genetic variants of SLC11A1 are associated with both autoimmune and infectious diseases: systematic review and meta-analysis. *Genes Immun.* 16, 275–283. doi: 10.1038/gene.2015.8
- Cancer Genome Atlas Research Network (2014). Comprehensive molecular characterization of gastric adenocarcinoma. *Nature* 513, 202–209. doi: 10.1038/nature13480
- Cingolani, P., Platts, A., Wang le, L., Coon, M., Nguyen, T., Wang, L., et al. (2012). A program for annotating and predicting the effects of single nucleotide polymorphisms, SnpEff: SNPs in the genome of *Drosophila melanogaster* strain w1118; iso-2; iso-3. *Fly* 6, 80–92. doi: 10.4161/fly.19695
- Cristescu, R., Lee, J., Nebozhyn, M., Kim, K. M., Ting, J. C., Wong, S. S., et al. (2015). Molecular analysis of gastric cancer identifies subtypes associated with distinct clinical outcomes. *Nat. Med.* 21, 449–456. doi: 10.1038/nm.3850
- Cunningham, D., Okines, A. F., and Ashley, S. (2010). Capecitabine and oxaliplatin for advanced esophagogastric cancer. *N. Engl. J. Med.* 362, 858–859. doi: 10.1056/NEJMc0911925
- de Fougerolles, A. R., Sprague, A. G., Nickerson-Nutter, C. L., Chi-Rosso, G., Rennert, P. D., Gardner, H., et al. (2000). Regulation of inflammation by collagen-binding integrins $\alpha 1 \beta 1$ and $\alpha 2 \beta 1$ in models of hypersensitivity and arthritis. *J. Clin. Invest.* 105, 721–729. doi: 10.1172/JCI7911
- Dituri, F., Mazzocca, A., Giannelli, G., and Antonaci, S. (2011). PI3K functions in cancer progression, anticancer immunity and immune evasion by tumors. *Clin. Dev. Immunol.* 2011:947858. doi: 10.1155/2011/947858
- Ferlay, J., Soerjomataram, I., Dikshit, R., Eser, S., Mathers, C., Rebelo, M., et al. (2015). Cancer incidence and mortality worldwide: sources, methods and major patterns in GLOBOCAN 2012. *Int. J. Cancer* 136, E359–E386. doi: 10.1002/ijc.29210
- Francisco, L. M., Sage, P. T., and Sharpe, A. H. (2010). The PD-1 pathway in tolerance and autoimmunity. *Immunol. Rev.* 236, 219–242. doi: 10.1111/j.1600-065X.2010.00923.x
- Fuchs, C. S., Doi, T., Jang, R. W., Muro, K., Satoh, T., Machado, M., et al. (2018). Safety and efficacy of pembrolizumab monotherapy in patients with previously treated advanced gastric and gastroesophageal junction cancer: phase 2 clinical KEYNOTE-059 trial. *JAMA Oncol.* 4:e180013. doi: 10.1001/jamaoncol.2018.0013
- Gyorffy, B., Gyorffy, A., and Tulassay, Z. (2005). The problem of multiple testing and solutions for genome-wide studies. *Orv. Hetil.* 146, 559–563.
- Harada, K., Baba, Y., Shigaki, H., Ishimoto, T., Miyake, K., Kosumi, K., et al. (2016). Prognostic and clinical impact of PIK3CA mutation in gastric cancer: pyrosequencing technology and literature review. *BMC Cancer* 16:400. doi: 10.1186/s12885-016-2422-y
- Henick, B. S., Herbst, R. S., and Goldberg, S. B. (2014). The PD-1 pathway as a therapeutic target to overcome immune escape mechanisms in cancer. *Expert Opin. Ther. Targets* 18, 1407–1420. doi: 10.1517/14728222.2014.955794
- Hothorn, T., Hornik, K., and Zeileis, A. (2006). Unbiased recursive partitioning: a conditional inference framework. *J. Comput. Graph. Stat.* 15, 651–674. doi: 10.1198/106186006X133933
- Hothorn, T., and Zeileis, A. (2015). *partykit: A Modular Toolkit for Recursive Partitioning in R*. Available online at: <http://jmlr.org/papers/v16/hothorn15a.html> (Accessed 16).
- Huang da, W., Sherman, B. T., and Lempicki, R. A. (2009). Systematic and integrative analysis of large gene lists using DAVID bioinformatics resources. *Nat. Protoc.* 4, 44–57. doi: 10.1038/nprot.2008.211
- Jiang, X., Zhou, J., Giobbie-Hurder, A., Wargo, J., and Hodi, F. S. (2013). The activation of MAPK in melanoma cells resistant to BRAF inhibition promotes PD-L1 expression that is reversible by MEK and PI3K inhibition. *Clin. Cancer Res.* 19, 598–609. doi: 10.1158/1078-0432.CCR-12-2731
- Kang, Y. K., Boku, N., Satoh, T., Ryu, M. H., Chao, Y., Kato, K., et al. (2017). Nivolumab in patients with advanced gastric or gastro-oesophageal junction cancer refractory to, or intolerant of, at least two previous chemotherapy regimens (ONO-4538-12, ATTRACTION-2): a randomised, double-blind, placebo-controlled, phase 3 trial. *Lancet* 390, 2461–2471. doi: 10.1016/S0140-6736(17)31827-5
- Kim, J. W., Lee, H. S., Nam, K. H., Ahn, S., Kim, J. W., Ahn, S. H., et al. (2017). PIK3CA mutations are associated with increased tumor aggressiveness and Akt activation in gastric cancer. *Oncotarget* 8, 90948–90958. doi: 10.18632/oncotarget.18770
- Malvezzi, M., Bonifazi, M., Bertuccio, P., Levi, F., La Vecchia, C., Decarli, A., et al. (2010). An age-period-cohort analysis of gastric cancer mortality from 1950 to 2007 in Europe. *Ann. Epidemiol.* 20, 898–905. doi: 10.1016/j.annepidem.2010.08.013
- Menyhárt, O., Fekete, J. T., and Gyorffy, B. (2018). Demographic shift disproportionately increases cancer burden in an aging nation: current and expected incidence and mortality in Hungary up to 2030. *Clin. Epidemiol.* 10, 1093–1108. doi: 10.2147/CLEP.S155063
- Ota, K., Azuma, K., Kawahara, A., Hattori, S., Iwama, E., Tanizaki, J., et al. (2015). Induction of PD-L1 expression by the EML4-ALK oncoprotein and downstream signaling pathways in non-small cell lung cancer. *Clin. Cancer Res.* 21, 4014–4021. doi: 10.1158/1078-0432.CCR-15-0016
- Peters, S., Gettinger, S., Johnson, M. L., Jänne, P. A., Garassino, M. C., Christoph, D., et al. (2017). Phase II trial of atezolizumab as first-line or subsequent therapy for patients with programmed death-ligand 1-selected advanced non-small-cell lung cancer (BIRCH). *J. Clin. Oncol.* 35, 2781–2789. doi: 10.1200/JCO.2016.71.9476
- Pon, J. R., and Marra, M. A. (2016). MEF2 transcription factors: developmental regulators and emerging cancer genes. *Oncotarget* 7, 2297–2312. doi: 10.18632/oncotarget.6223
- Scanlan, M. J., Gout, I., Gordon, C. M., Williamson, B., Stockert, E., Gure, A. O., et al. (2001). Humoral immunity to human breast cancer: antigen definition and quantitative analysis of mRNA expression. *Cancer Immun.* 1:4.

- Schüler, A., Schwieger, M., Engelmann, A., Weber, K., Horn, S., Müller, U., et al. (2008). The MADS transcription factor *Mef2c* is a pivotal modulator of myeloid cell fate. *Blood* 111, 4532–4541. doi: 10.1182/blood-2007-10-116343
- Seeruttun, S. R., Yuan, S., Qiu, H., Huang, Y., Li, Y., Liang, Y., et al. (2017). A comprehensive analysis comparing the eighth AJCC gastric cancer pathological classification to the seventh, sixth, and fifth editions. *Cancer Med.* 6, 2804–2813. doi: 10.1002/cam4.1230
- Siemers, N. O., Holloway, J. L., Chang, H., Chasalow, S. D., Ross-MacDonald, P. B., Voliva, C. F., et al. (2017). Genome-wide association analysis identifies genetic correlates of immune infiltrates in solid tumors. *PLoS ONE* 12:e0179726. doi: 10.1371/journal.pone.0179726
- Skoulidis, F., Byers, L. A., Diao, L., Papadimitrakopoulou, V. A., Tong, P., Izzo, J., et al. (2015). Co-occurring genomic alterations define major subsets of KRAS-mutant lung adenocarcinoma with distinct biology, immune profiles, and therapeutic vulnerabilities. *Cancer Discov.* 5, 860–877. doi: 10.1158/2159-8290.CD-14-1236
- Song, M., Chen, D., Lu, B., Wang, C., Zhang, J., Huang, L., et al. (2013). PTEN loss increases PD-L1 protein expression and affects the correlation between PD-L1 expression and clinical parameters in colorectal cancer. *PLoS ONE* 8:e65821. doi: 10.1371/journal.pone.0065821
- Taieb, J., Moehler, M., Boku, N., Ajani, J. A., Yañez Ruiz, E., Ryu, M. H., et al. (2018). Evolution of checkpoint inhibitors for the treatment of metastatic gastric cancers: current status and future perspectives. *Cancer Treat. Rev.* 66, 104–113. doi: 10.1016/j.ctrv.2018.04.004
- Teng, F., Meng, X., Kong, L., and Yu, J. (2018). Progress and challenges of predictive biomarkers of anti PD-1/PD-L1 immunotherapy: a systematic review. *Cancer Lett.* 414, 166–173. doi: 10.1016/j.canlet.2017.11.014
- Varet, H., Brillet-Guéguen, L., Coppée, J. Y., and Dillies, M. A. (2016). SARTools: a DESeq2- and EdgeR-based R pipeline for comprehensive differential analysis of RNA-seq data. *PLoS ONE* 11:e0157022. doi: 10.1371/journal.pone.0157022
- Wang, J., Guo, X., Xie, C., and Jiang, J. (2017). KIF15 promotes pancreatic cancer proliferation via the MEK–ERK signalling pathway. *Br. J. Cancer* 117, 245–255. doi: 10.1038/bjc.2017.165
- Wu, P., Wu, D., Li, L., Chai, Y., and Huang, J. (2015). PD-L1 and survival in solid tumors: a meta-analysis. *PLoS ONE* 10:e0131403. doi: 10.1371/journal.pone.0131403

Conflict of Interest Statement: The authors declare that the research was conducted in the absence of any commercial or financial relationships that could be construed as a potential conflict of interest.

Copyright © 2019 Menyhárt, Pongor and Györfy. This is an open-access article distributed under the terms of the Creative Commons Attribution License (CC BY). The use, distribution or reproduction in other forums is permitted, provided the original author(s) and the copyright owner(s) are credited and that the original publication in this journal is cited, in accordance with accepted academic practice. No use, distribution or reproduction is permitted which does not comply with these terms.



miR-26 Induces Apoptosis and Inhibits Autophagy in Non-small Cell Lung Cancer Cells by Suppressing TGF- β 1-JNK Signaling Pathway

Yi He[†], Hao Liu[†], Lianying Jiang[†], Bi Rui, Ju Mei* and Haibo Xiao*

Department of Cardiothoracic Surgery, School of Medicine, Xinhua Hospital, Shanghai Jiao Tong University, Shanghai, China

OPEN ACCESS

Edited by:

Dong-Hua Yang,
St. John's University, United States

Reviewed by:

Qisi Lu,
Third Affiliated Hospital, Southern
Medical University, China
Luca Vanella,
Università degli Studi di Catania, Italy

*Correspondence:

Ju Mei
meiju@xinhumed.com.cn
Haibo Xiao
xiaohaibo@xinhumed.com.cn

[†] These authors have contributed
equally to this work

Specialty section:

This article was submitted to
Experimental Pharmacology
and Drug Discovery,
a section of the journal
Frontiers in Pharmacology

Received: 31 August 2018

Accepted: 10 December 2018

Published: 09 January 2019

Citation:

He Y, Liu H, Jiang L, Rui B, Mei J
and Xiao H (2019) miR-26 Induces
Apoptosis and Inhibits Autophagy
in Non-small Cell Lung Cancer Cells
by Suppressing TGF- β 1-JNK
Signaling Pathway.
Front. Pharmacol. 9:1509.
doi: 10.3389/fphar.2018.01509

Non-small cell lung cancer (NSCLC) is one of the causes of cancer mortality worldwide. The role of miR-26 in the development and progression of NSCLC remains largely unknown. In this study we found an abnormal expression of miR-26 in human NSCLC tissues. It was found that miR-26 mimics induced cell apoptosis and promoted caspase-3, 9 activities in human NSCLC cells. The miR-26 inhibitor enhanced the expression of the light chain 3 (LC3) protein and the autophagy related genes in NSCLC cells. Moreover, miR-26 regulated apoptosis and autophagy by inhibiting TGF- β expression in a JNK dependent manner. In addition, miR-26 mimics induced cell apoptosis, was involved in the endoplasmic reticulum stress (ERS) signaling pathway. Down-regulation of the ERS, inhibited apoptosis which was induced by miR-26 mimics in NSCLC cells. In *in vivo* studies, TUNEL staining revealed that the number of TUNEL positive cells of the tumor tissue in the miR-26 treatment group, were significantly increased in comparison with the control group, while the number of TUNEL positive cells in the tumor tissue were remarkably decreased in the groups treated with miR-26, combined with the TGF- β 1 inhibitor or JNK inhibitor. Additionally, the immunoreactivity of TGF- β 1 in the cells treated with the miR-26 inhibitor, decreased in comparison to the control group. Our results indicated that miR-26 induced apoptosis and inhibited autophagy in human NSCLC cells through the TGF- β 1-JNK signaling pathway, suggesting that miR-26 could be a potential novel target for the treatment of NSCLC.

Keywords: NSCLC, miR-26, TGF- β , JNK, apoptosis, autophagy

INTRODUCTION

Lung cancer is the leading cause of cancer mortality in China (Hong et al., 2015; Zhang et al., 2017). Non-small cell lung cancer (NSCLC) accounts for nearly 85% of all types of lung cancers (Hutchinson, 2017). Currently, surgical resection is an effective treatment for NSCLC and can promotes a 5-year survival rate for NSCLC patients (Wu et al., 2017). However, because of distant metastasis as well as a shortage of effective chemotherapeutics, there is only a 10–15% 5-year survival rate for stage IIIA NSCLC (Ripley et al., 2016; Palka et al., 2017). Therefore, understanding

the underlying mechanisms of the progression of NSCLC, as well as novel therapeutic strategies, is critical in order to improve patients' survival time.

MicroRNA (miRNA) is a class of small non-coding RNAs, which regulates gene expression by binding to mRNA (Williams et al., 2016). It is well known that miRNA participates in numerous biological processes of various human diseases, including cancer (Jing et al., 2015; Singh and Sen, 2017). miR-26, a functional miRNA, has been investigated in various human cancers (Kwon et al., 2015; Deng et al., 2017; Jin et al., 2017; Li et al., 2017). A previous study reported that the expression of miR-26 was down-regulated in bladder cancer (Lin et al., 2013). In addition, miR-26 was found to be down-regulated in breast cancer tissues and cell lines. Up-regulation of miR-26 expression mediated apoptosis through endogenous and exogenous pathways by directly binding to the 3'-UTR of MTDH and EZH2 (Zhang et al., 2011). However, the expression and effect of miR-26 in NSCLC is still obscure. A transforming growth factor (TGF- β), a multifunctional cytokine, can induce cell apoptosis and autophagy in various human diseases (Jiang et al., 2016). A previous study showed that the TGF- β induced autophagy and apoptosis by regulating the expression of Disabled-2 (Xu et al., 2012). JNK, a protein kinase of the MAPK family, plays a critical role in the biological process of the apoptosis and autophagy of cancer cells (Díaz et al., 2017; Lu et al., 2017). A recent study has demonstrated that the TGF- β induced autophagy and apoptosis in hepatocellular carcinoma and mammary carcinoma cells, through mediating the JNK pathways (Kiyono et al., 2009). However, the role of the TGF- β on NSCLC and whether there is a crosstalk between the TGF- β and JNK in NSCLC, remains unknown. ERS, a fundamental property of all cells, is critical in regulating cell growth and apoptosis (Liu et al., 2017; Song et al., 2017). A previous study revealed that ERS induced cell apoptosis, by arresting cells at the G1 phase (Thinon et al., 2016). Additionally, ERS could re-establish cellular homeostasis by serving as a checkpoint molecule (Verfaillie et al., 2013). ER stress-inducing agents exhibited increased cell apoptosis in Perk^{-/-} mouse embryonic fibroblasts (Gupta et al., 2012).

In this study, we explored the role and molecular mechanism of miR-26 on the development and progression of NSCLC. We examined how miR-26 mimics or inhibitors, regulate cell apoptosis and autophagy, and related signaling pathways in NSCLC both *in vitro* and *in vivo*. We found that miR-26 induced cell apoptosis and inhibited autophagy by targeting the TGF- β expression in a JNK dependent manner in human NSCLC cells. Moreover, miR-26 regulated cell apoptosis was involved in ER stress in human NSCLC cells. Down-regulation of ERS inhibited cell apoptosis, regulated by miR-26 mimics. Our results provided a potential therapeutic strategy for improving NSCLC treatment.

MATERIALS AND METHODS

Patients and Tissue Samples

This study was approved by the Human Research Ethics Committee of Xin Hua Hospital (NO: 2015-035). The NSCLC

tissues and adjacent non-tumor lung tissues were obtained from six patients who underwent the primary surgical resection of NSCLC at the Xin Hua Hospital (Shanghai). All participants provided written informed consent. The samples contained well-documented clinicopathological information, including age, gender, tumor size and location, tumor differentiation, invasion depth, lymph node metastasis, distant metastasis, tumor stage, and follow-up data. Tissues were immediately frozen in liquid nitrogen after resection and stored at -80°C . Both NSCLC tissues and the adjacent non-tumor lung tissues were confirmed by a pathological examination.

Reagents

The synthetic miR-26 mimics, miR-26 inhibitor oligonucleotides, as well as the control inhibitor oligonucleotides, were purchased from Sangon Biotech (Shanghai, China). The TGF- β 1 inhibitor was purchased from Sigma (St. Louis, MO, United States). The TGF- β 1 was obtained from R&D Systems (Minneapolis, MN, United States). The JNK inhibitor and Lipofectamine 2000, were purchased from Invitrogen (Carlsbad, CA, United States). The Apoptosis Detection Kit was acquired from BioLegend (San Diego, CA, United States).

Cell Culture

The NSCLC cell lines A549, H1703, and 801D were purchased from the Shanghai Institute of Chinese Academy of Sciences (Shanghai, China). All cells were maintained in RPMI-1640 and supplemented with a 10% inactivated fetal bovine serum (Gibco, Grand Island, NY, United States), 100 U/mL penicillin and 100 $\mu\text{g/mL}$ streptomycin (Gibco) in a humid environment at 37°C with 95% air and 5% CO_2 .

Plasmid Construction and Transfection

The sequence of the JNK was designed to be amplified and cloned into a pCDNA3.1 expression vector (Invitrogen). Transfection was performed using the Lipofectamine 2000 reagent. Briefly, cells were inoculated into 6-well plates and a plasmid and liposomal transfection reagent was added to the cells.

Lentivirus-Mediated siRNA Knockdown

The lentiviral expression systems were purchased from System Biosciences (SBI, Mountain View, CA, United States). Oligonucleotides of siRNA for Chop, ATF-4, Bip, XBP-1, and the control were obtained from Sangon Biotech (Shanghai). After co-transfection, the virus media was harvested. Cells were infected for 72 h with a lentivirus containing Chop, ATF-4, Bip, XBP-1, and control siRNA.

Caspase Activity

The activation of caspase-3, 9 was detected with a caspase activity assay. Briefly, cells in 96-well plates were treated with the miR-26 inhibitor or the control inhibitor. After incubation for 24 h, 20 μL of lysis buffer was added to each well. The cell lysate was incubated with 5 μL of a chromogenic substrate at room temperature in the dark for 20 min. The results were measured with a plate reader at 560 nm light length.

Quantitative Real-Time PCR

A TRIzol reagent (Invitrogen, Carlsbad, CA, United States) was used to extract the total RNA. The complementary DNA samples were subjected to denaturing at 95°C for 10 s, annealing at 55°C for 15 s, and extension at 72°C for 30 s, for 45 cycles using a High Capacity cDNA Reverse Transcription Kit (Applied Biosystems Inc.). The following primer pairs were used (Table 1): Chop, ATF-4, Bip, XBP-1, DR5, BECLIN1, ATG5, ATG7, DAPK, and GAPDH. Relative gene expressions were quantified by real-time PCR, using the SYBR Premix Ex Taq™ II (TaKaRa Bio, Dalian, China) on a Lightcycler 480 RealTime PCR System (Roche Diagnostics, Meylan, France).

Western Blotting

Protein was resolved by an SDS-PAGE. Subsequently, gel-separated proteins were blotted. The membranes were probed with primary antibodies LC3, TGF-β1 (Abcam, Cambridge, MA, United States) and Bcl, Bax, BECLIN1, ATG5, ATG7, DAPK, JNK, Chop, ATF-4, Bip, and XBP-1 antibodies (Cell Signaling Technology, Beverly, MA, United States) were diluted according to the manufacturer's instructions. The membranes were then probed with horseradish peroxidase-conjugating (HRP) secondary antibody (1:10000; GE Healthcare, Tokyo, Japan). The proteins in the blots were visualized using the ECL plus system (Amersham Pharmacia Biotech, Buckinghamshire, United Kingdom) to capture the images.

In situ Hybridization (ISH) Staining

The slides were cut from paraffin-embedded tissue to evaluate the miRNA-26 expression by ISH. In brief, the slides were incubated at 60°C for 1 h, deparaffinized in xylene, and rehydrated with graded alcohol washes. Slides were washed and digested, then hybridized at 55°C for 2 h with 50 nmol/L locked

nucleic acid -modified digoxigenin-labeled probes for miRNA-26 (Boster, Wuhan, China). Slides were placed in a blocking solution for 1 h at room temperature. An antibody signal was detected with a 4-nitro-blue tetrazolium and 5-bromo-4-chloro-3'-indolylphosphate substrate (Roche, Mannheim, Germany).

Flow Cytometry

To detect cell apoptosis, transfected or treated cells were double stained with an annexin V-FITC/7-amino-actinomycin D (7-AAD) kit (Beckman Coulter) according to the manufacturer's protocol. The stained cells were immediately analyzed by flow cytometry on the FACS calibur (BD Biosciences, CA, United States).

Cell Cycle Analysis

The cell cycle was assessed using the GENMED Universal periodic flow cytometry kit (Genmed Scientifics Inc., United States). Cells were seeded in 6-well plates and incubated with the miR-26 mimics at 37°C for 48 h in a humidified chamber containing 5% CO₂.

Luciferase Reporter Assays

The promoter of the TGF-β1 was amplified and cloned into a pGL 3.0 luciferase reporter plasmid. Cells were then transfected with the pRL-CMV renilla luciferase reporter and the pGL 3.0 luciferase reporter plasmid. The activities of the luciferases were detected using a dual luciferase reporter assay system (Promega).

Xenograft Nude Mouse Model

The Specific-pathogen-free (SPF)-grade nude mice (4–6 weeks of age) were obtained from the Model Animal Research Center of Nanjing University (Nanjing, Jiangsu, China), and housed with a pathogen-free fodder, equipment, and environment. The control, miR-26 inhibitor, miR-26 inhibitor + TGF-β1 inhibitor, miR-26 inhibitor + JNK inhibitor treated A549 cells were subcutaneously injected at the inguinal region of the nude mice, in a SPF-grade ultraclean work station. Using the vernier calipers, tumor diameters were measured every 2 days after 2 weeks to calculate the tumor volume: TV (mm³) = d² × D/2, where d and D represent the shortest and the longest diameters, respectively. The mice were sacrificed 30 days after the cell implantation, and the tumors were extracted.

Histopathological Analyses

Lungs cancer tissues were obtained from the sacrificed mice. The tissues were embedded in paraffin and sets of different consecutive 5-um-thick sections were acquired using an automatic microtome (SLEE Medical GmbH, Germany). The set of slides were processed for immunohistochemical staining using an anti-TGF-β1 antibody (1:100, Abcam).

TUNEL Staining

After the mice were sacrificed, the lung cancer tissues were embedded, sectioned, and deparaffinized. The sections were incubated with proteinase K for 1 h at room temperature.

TABLE 1 | Primers used for PCR amplification.

CHOP	Forward primer, 5'-GAACCTGAGGAGAAGAGTGTTCAC-3' Reverse primer, 5'-AGTGACTCAGCTGCCATCTCTGT-3'
ATF-4	Forward primer, 5'-CTGGAGAGAAGATGGTAGCAGCAA-3' Reverse primer, 5'-GCCCTCTTCTTCTGGCGGTA-3'
Bip	Forward primer, 5'-CCAACTGTTACAATCAAGGTC-3' Reverse primer, 5'-ACGAGGAGCAGGAGGAAT-3'
XBP-1	Forward primer, 5'-TGCTGAGTCCGCAGCAGGTG-3' Reverse primer, 5'-GCTGGCAGGCTCTGGGGAAG-3'
DR5	Forward primer, 5'-TCAAAGGACACGGCAGAGCCTGTGCCA-3' Reverse primer, 5'-GGGAGCCGCTCATGAGGAAGTTGG-3'
BECLIN1	Forward primer, 5'-ACCGTGTACCATCCAGGAA-3' Reverse primer, 5'-GAAGCTGTTGGCACTTTCTGT-3'
ATG5	Forward primer, 5'-AGCAACTCTGGATGGGATTG-3' Reverse primer, 5'-CACTGCAGAGGTGTTTCCAA-3'
ATG7	Forward primer, 5'-ACCCAGAAGAAGCTGAACGA-3' Reverse primer, 5'-AGACAGAGGGCAGGATAGCA-3'
DAPK	Forward primer, 5'-TCTACCAGCCACGGGACTTC-3' Reverse primer, 5'-GCTGGCCTGTGAGTAGACGT-3'
GAPDH	Forward primer, 5'-TGGAAGGACTCATGACCACA-3' Reverse primer, 5'-TTCAGCTCAGGGATGACCTT-3'

Sections were then treated with 2% H_2O_2 in distilled water for 30 min at room temperature. After the enzymatic reaction, sections were washed with PBS and incubated with anti-digoxigenin peroxidase conjugate for 30 min at room temperature in a humidified chamber. Sections were stained with diaminobenzine and counterstained with hematoxylin and observed under a light microscope.

Statistical Analysis

The data were analyzed using the SPSS 17.0 software (SPSS Inc., Chicago, IL, United States). The comparison between the two groups was analyzed by an unpaired Student's *t*-test and multiple comparisons were compared by a one-way ANOVA analysis of variance followed by a Dunnett's test. Statistical significance was defined as $P < 0.05$.

RESULTS

miR-26 Induced Apoptosis in NSCLC Cells

The *in situ* hybridization of miR-26 in adjacent non-tumor lung or NSCLC tissues was performed and the representative result is shown in **Figures 1A,B**. The expression level of miR-26 in NSCLC patients was relatively lower than the expression in adjacent non-tumor lung tissues (**Figure 1C**). In order to examine the effect of miR-26 on apoptosis in NSCLC cells,

flow cytometry was performed in A549 cells after treatment with miR-26 mimics at a final concentration of 20 nM. In comparison with the non-treatment counterparts, miR-26 mimics treatment significantly increased the number of apoptotic cells (**Figures 2A,B**). Furthermore, we examined the activities of caspase-3 and caspase-9 in A549 cells. The results revealed that miR-26 mimics treatment significantly increased the activities of caspase-3 and caspase-9 in A549 cells, compared with the non-treatment counterparts (**Figures 2C–E**). The expression apoptosis related proteins was also examined and the results showed that Bcl was obviously decreased, while Bax was obviously increased following miR-26 mimics treatment in A549 cells (**Figure 2F**). In addition, to examine whether miR-26 mimics induces cell cycle arrest, we performed a flow cytometry analysis to investigate the cell cycle distribution after miR-26 mimics treatment. The result showed that the proportion of the cell cycle arrest in the G0/G1 phase and G2/M phase, obviously increased when treated with miR-26 mimics (**Figure 2G**). These results suggest that miR-26 induced apoptosis and the cell cycle arrest in NSCLC cells.

miR-26 Down-Regulation Induced Autophagy in NSCLC Cells

To understand the effect of miR-26 on the autophagy of NSCLC cells, we examined the expression of autophagy related molecules using Western blotting and RT-PCR in A549 cells. In comparison with the non-treatment counterparts, 50 nM

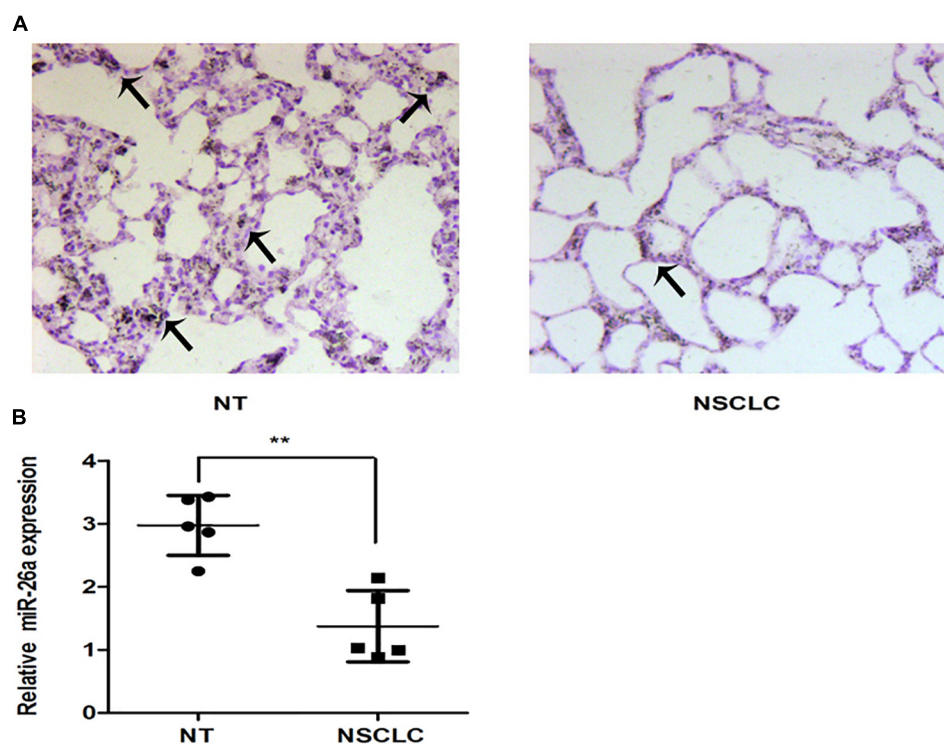


FIGURE 1 | The expression of miR-26 in non-small cell lung cancer. **(A)** The representative results of ISH staining in normal tissues and lung cancer tissues. **(B)** The miR-26 expression was detected in normal tissues and lung cancer tissues. Arrows represented the positive cells.

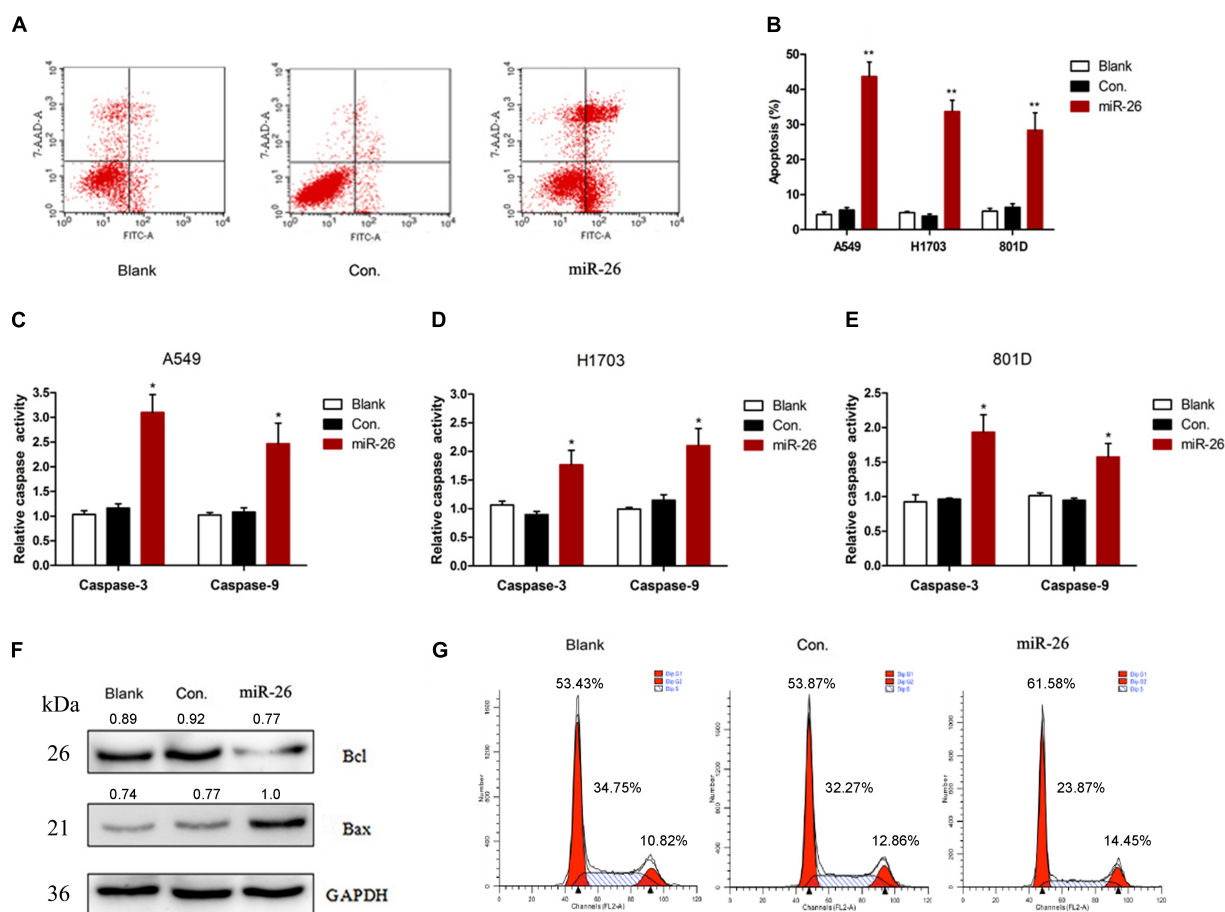


FIGURE 2 | miR-26 induced cell apoptosis in non-small cell lung cancer cells. **(A,B)** Flow cytometry showed that miR-26 increased cell apoptosis in A549 cells. **(C–E)** Caspase activity assay showed increased Caspase-3 and caspase-9 activities after treatment with miR-26 in A549 cells. **(F)** Western blot showed a decreased expression of the Bcl protein and an increased expression of the Bax protein following miR-26 treatment in A549 cells. **(G)** miR-26 caused cell cycle arrest in A549 cells. * $P < 0.05$ vs. Blank, ** $P < 0.01$ vs. Blank.

of miR-26 inhibitor treatment significantly increased the protein expression of LC3 (**Figure 3A**). In addition, miR-26 inhibitor treatment also increased the protein expression of BECLIN1, ATG5, ATG7, and DAPK compared with the non-treatment counterparts (**Figure 3B**). Moreover, the mRNA expression of BECLIN1, ATG5, ATG7, and DAPK increased in the miR-26 inhibitor treatment group compared with the non-treatment counterparts in A549 cells (**Figure 3C**).

TGF- β 1 Was a Direct Target of miR-26 in A549 Cells

To verify whether miR-26 directly targets TGF- β 1, we constructed luciferase-reporter plasmids containing the wt or mutant 3'-UTR segments of TGF- β 1. The wt or mutant reporter plasmid was co-transfected into A549 cells along with the miR-26 or control. miR-26 significantly decreased the relative luciferase activity when co-transfected with the wt reporter plasmid. However, the mutant reporter plasmid reversed the miR-26 mediated decrease in luciferase

activity (**Figure 4B**). The protein expression of TGF- β 1 was significantly decreased following miR-26 treatment in A549 cells (**Figure 4A**), consistently. These findings suggest that miR-26 suppressed TGF- β 1 by directly binding to the 3'-UTR of TGF- β 1.

miR-26 Down-Regulation Regulated the TGF- β 1 Signaling Pathway in a JNK-Dependent Manner in A549 Cells

We assessed whether down-regulation of miR-26 affected JNK protein expression in A549 cells. Cells were treated with the miR-26 inhibitor, the TGF- β 1 or TGF- β 1 inhibitor. The increased JNK protein expression was detected in the miR-26 inhibitor treatment, which was further enhanced with TGF- β 1 transfection. However, the TGF- β 1 inhibitor notably reversed the increase of JNK protein expression induced by the miR-26 inhibitor (**Figure 5A**). We further tested the apoptosis in cells treated by miR-26 mimics and TGF- β 1, JNK, or TGF- β 1 inhibitor and JNK inhibitor. The

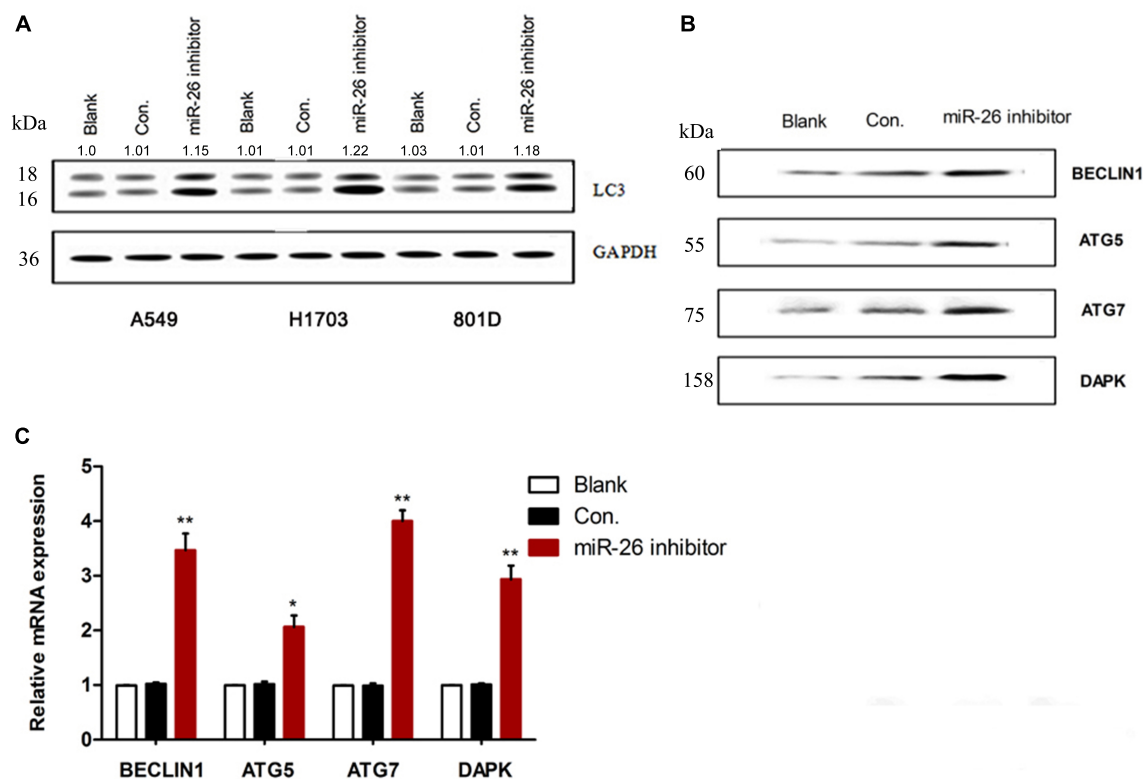


FIGURE 3 | miR-26 inhibitor induced autophagy in non-small cell lung cancer cells. **(A)** Western blotting showed an increased expression of the LC3 protein following miR-26 inhibitor treatment in NSCLC cells. **(B,C)** Western blot and RT-PCR showed an increased expression of autophagy related protein molecules and mRNA of BECLIN1, ATG5, ATG7, and DAPK following miR-26 inhibitor treatment in A549 cells. * $P < 0.05$ vs. Blank, ** $P < 0.01$ vs. Blank.

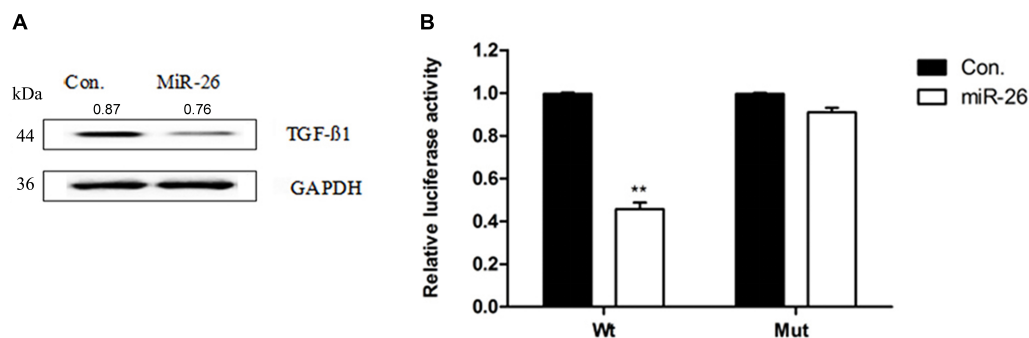


FIGURE 4 | miR-26 inhibited TGF-β1 in non-small cell lung cancer cells. **(A)** Western blotting showed a decreased expression of the TGF-β1 protein following miR-26 treatment in A549 cells. **(B)** luciferase reporter assay revealed increased ASPP2 3'UTR luciferase activity in mutant A549 cells. ** $P < 0.01$ VS Con.

results revealed that TGF-β1 or JNK treatment significantly decreased cell apoptosis induced by miR-26 mimics. Whereas, TGF-β1 inhibitor or the JNK inhibitor combined with miR-26 mimics treatment significantly increased apoptosis of A549 cells compared with the miR-26 mimics treatment alone (Figures 5B,D). Moreover, the protein expression of LC3 was notably increased in the TGF-β1 or JNK combined miR-26 inhibitor, while decreased in the TGF-β1 inhibitor or JNK inhibitor combined with the miR-26

inhibitor, compared with the miR-26 inhibitor treatment alone (Figures 5C,E).

miR-26 Regulated Autophagy and Apoptosis Were Related to ERS Signaling

We examined whether ERS signaling was involved in miR-26 regulated autophagy and apoptosis in NSCLC cells. It was found that the protein expression of Chop, ATF-4, Bip, and XBP-1 were

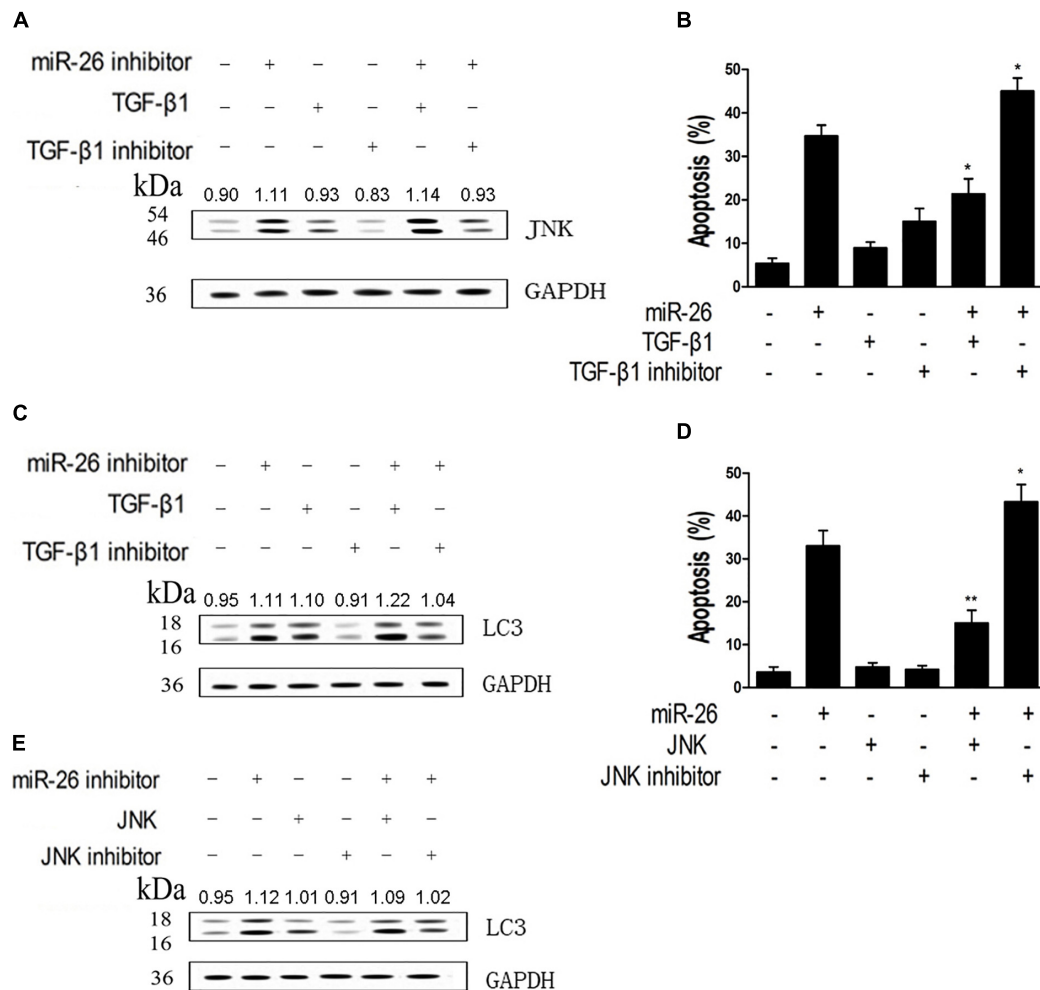


FIGURE 5 | miR-26 inhibitor induced autophagy and apoptosis by targeting TGF-β1 in a JNK-dependent manner. **(A)** Western blot on the protein expression of JNK following treatment with the miR-26 inhibitor combined with the TGF-β1 or TGF-β1 inhibitor in A549 cells. **(B)** Flow cytometry on cell apoptosis in A549 cells treated with miR-26 followed by treatment with the TGF-β1 or TGF-β1 inhibitor. **(C)** Western blot on the protein expression of LC3 following treatment with the iR-26 inhibitor combined with the TGF-β1 or TGF-β1 inhibitor in A549 cells. **(D)** Flow cytometry on cell apoptosis in A549 cells treated with the miR-26 and the JNK or JNK inhibitor. **(E)** Western blot on the protein expression of LC3 following treatment with the miR-26 inhibitor combined with the JNK or JNK inhibitor in A549 cells.

* $P < 0.05$ VS miR-26 group, ** $P < 0.01$ VS miR-26 group.

up-regulated after treatment with miR-26 mimics (**Figure 6A**). We down-regulated Chop, ATF-4, Bip, and XBP-1 with siRNA transfection and the efficiency of the transfection was confirmed by a real-time PCR (**Figure 6B**). Furthermore, the apoptosis in cells treated with miR-26 mimics and Chop, ATF-4, Bip, and XBP-1 siRNA was detected. The results showed that miR-26 mimics combined with Bip, XBP-1, and Chop siRNA significantly decreased apoptosis of A549 cells (**Figure 6E**). The mRNA expression of DR5 was significantly decreased following siRNA of Chop, Bip, and XBP-1 combined with the miR-26 mimics treatment (**Figure 6C**). Consistently, the protein expression of Bcl was notably increased, while the Bax expression decreased following siRNA of Chop, Bip, and XBP-1 combined with the miR-26 mimics treatment (**Figure 6D**). However, the protein expression of LC3 was not obviously changed following siRNA of Bip, ATF-4, and XBP-1 combined with the miR-26 inhibitor

treatment, except for the Chop siRNA treatment (**Figure 6G**). In addition, the mRNA expression of BECLIN1 did not change following siRNA of Bip, ATF-4, and XBP-1 combined with the miR-26 inhibitor treatment except for the Chop siRNA treatment (**Figure 6F**).

miR-26 Inhibited NSCLC Growth *in vivo*

The effect of miR-26 on NSCLC growth was investigated *in vivo*. The tumor volume was measured in mouse xenografts treated with miR-26 combined with the TGF-β1 inhibitor or JNK inhibitor. The results showed that miR-26 significantly decreased the tumor volume compared with the control (**Figure 7A**). The protein expression of JNK, LC3 increased following the miR-26 inhibitor treatment, while treatment with the miR-26 inhibitor combined with the TGF-β1 inhibitor or JNK inhibitor reversed the protein expression of JNK and LC3 compared

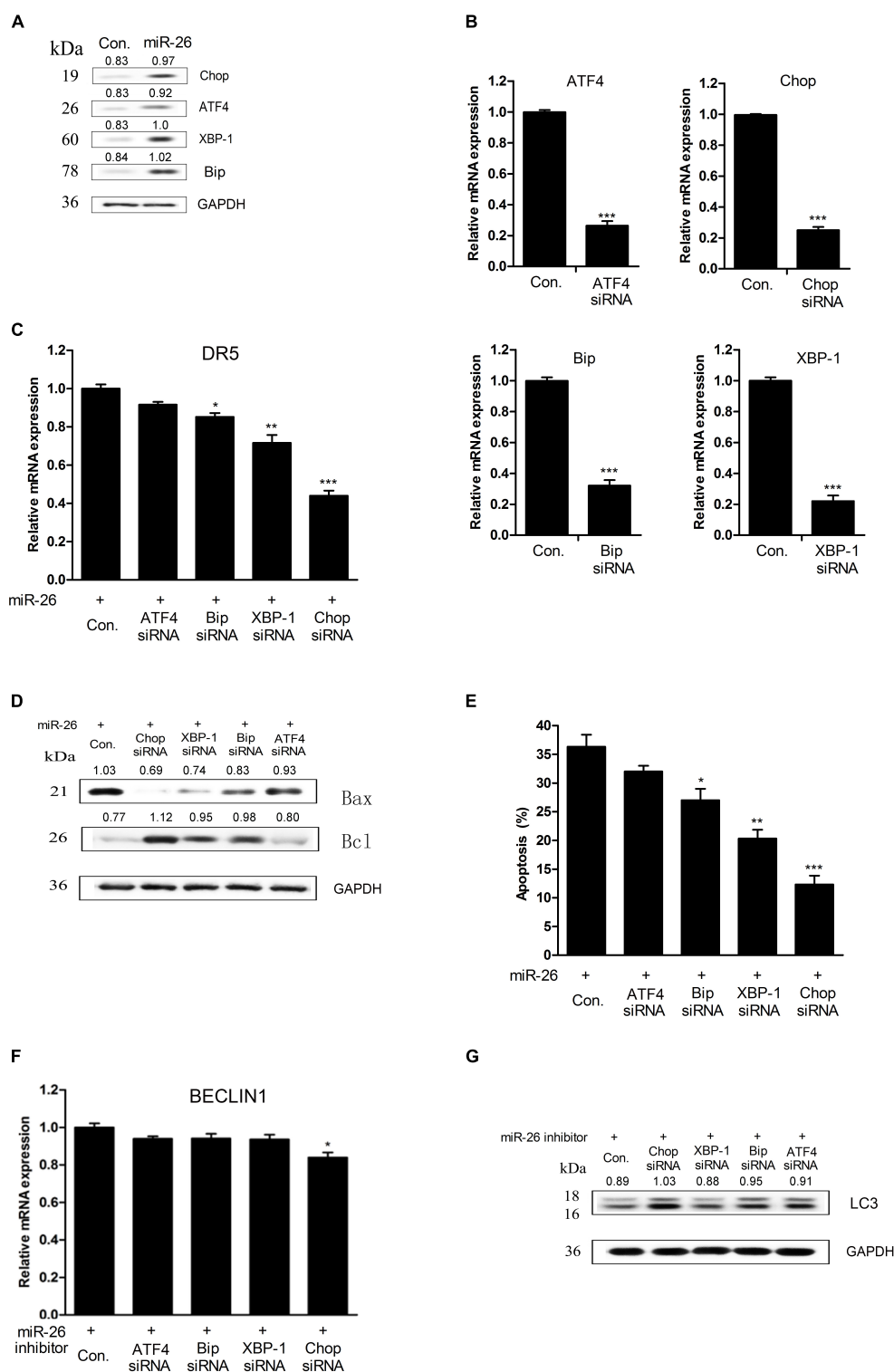
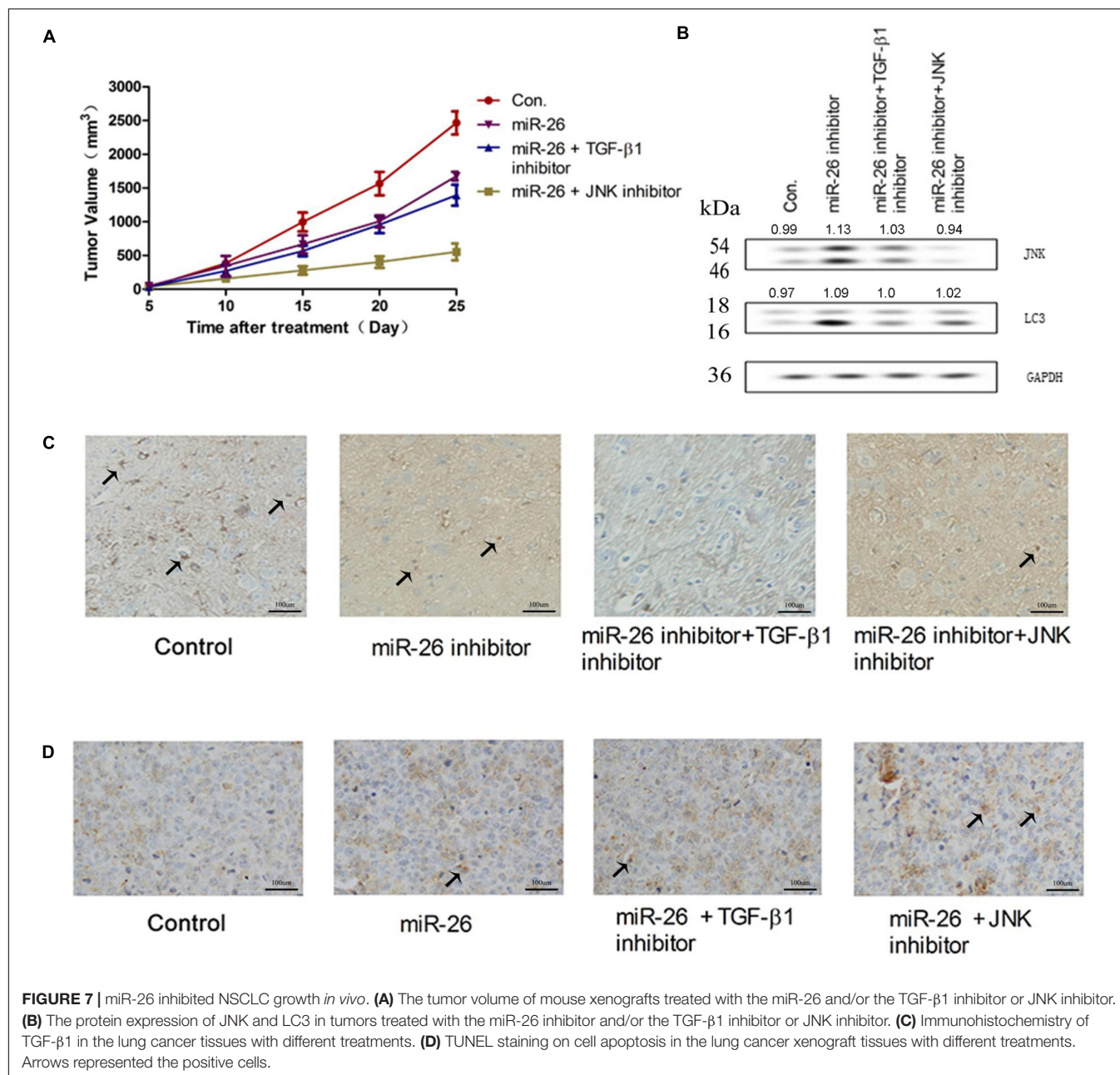


FIGURE 6 | miR-26 regulated autophagy and apoptosis were correlated with ERS signaling. **(A)** Western blot on the protein expression of Chop, ATF-4, Bip, and XBP-1 following miR-26 treatment in A549 cells. **(B)** RT-PCR on the mRNA expression of Chop, ATF-4, Bip, and XBP-1 following treatment with a siRNA of Chop, ATF-4, Bip, and XBP-1. **(C)** The mRNA expression of DR5 following a siRNA of Chop, ATF-4, Bip, and XBP-1 combined with the miR-26 treatment. **(D)** Western blot on the protein expression of Bcl and Bax following a siRNA of Chop, ATF-4, Bip, and XBP-1 combined with the miR-26 treatment. **(E)** Flow cytometry on cell apoptosis detected following a siRNA of Chop, ATF-4, Bip and XBP-1 combined with miR-26 treatment. **(F)** RT-PCR on the mRNA expression of BECLIN1 detected following a siRNA of Chop, ATF-4, Bip, and XBP-1 combined with miR-26 inhibitor treatment. **(G)** Western blot on the protein expression of LC3 detected following a siRNA of Chop, ATF-4, Bip, and XBP-1 combined with the miR-26 inhibitor treatment. * $P < 0.05$ VS Con., ** $P < 0.01$ VS Con., *** $P < 0.001$ VS Con.



with the miR-26 inhibitor treatment alone (Figure 7B). To determine the role of miR-26 in cell apoptosis *in vivo*, a TUNEL assay was performed on tumor xenograft tissues. The results showed that TUNEL positive cells of the tumor tissue in the miR-26 treatment group, significantly increased in comparison with the control group, while the number of TUNEL positive cells of the tumor tissue remarkably decreased in the groups of the miR-26 combined with the TGF-β1 inhibitor or JNK inhibitor (Figure 7D). In addition, representative results of the immunohistochemical staining of TGF-β1 in the lung cancer tissues are shown in Figure 7C. The results showed that the immunoreactivity of TGF-β1 in the miR-26 inhibitor group decreased in comparison to the control group. Moreover, TGF-β1

intensity significantly attenuated after treatment with the miR-26 inhibitor combined with the TGF-β1 inhibitor in the lung cancer tissues.

DISCUSSION

This study showed that TGF-β was negatively regulated by miR-26 at the post-transcriptional level in human NSCLC cells. miR-26 induced cell apoptosis and inhibited cell autophagy through the down-regulation of TGF-β in a JNK dependent manner in human NSCLC cells. In addition, miR-26 mimics induced cell apoptosis was associated with ER stress signaling in human

NSCLC cells. Down-regulation of ERS led to the inhibition of apoptosis induced by miR-26 mimics.

miR-26 is one of the most significant miRNAs involved in human malignancy. Aberrant expression of miR-26 was found in various types of cancers including esophageal squamous cancer, colorectal cancer and breast cancer (Liu et al., 2015; Li et al., 2017; López-Urrutia et al., 2017). Our study demonstrated that miR-26 expression was lower in NSCLC tissues than in non-tumor tissues. A previous study demonstrated that miR-26 promoted apoptosis of the hepatocellular carcinoma cells through inhibiting autophagy (Johnston et al., 2016). Our study showed that miR-26 mimics induced cell apoptosis in NSCLC cells and promoted caspase-3, 9 activities in NSCLC cells. Interestingly, the miR-26 inhibitor enhanced the protein expression of LC3 and autophagy related genes in NSCLC cells.

TGF- β , a multifunctional cytokine, was involved in various biological processes, including development, cell apoptosis, proliferation, and autophagy through the interaction with several signaling pathways (Katz et al., 2013; Chen et al., 2016; Gratchev, 2017; Ramu et al., 2017). A previous study showed that gramine treatment diminished angiogenesis and induced cell apoptosis by modulating TGF- β signals in hamster buccal pouch (HBP) carcinogenesis (Liu et al., 2016). Many studies have demonstrated that TGF- β induced autophagy in hepatocellular carcinoma cells and mammary carcinoma cells (Sureshbabu et al., 2016; Ren et al., 2017). In this study, we found that miR-26 significantly suppressed TGF- β protein expression and TGF- β activation. TGF- β could down-regulate apolipoprotein M expression through a JNK pathway in the HepG2 cells (Song et al., 2017). In this study, we observed that the miR-26 inhibitor induced autophagy, while the miR-26 induced cell apoptosis by inhibiting TGF- β expression in a JNK-dependent manner. A recent study revealed that the crosstalk of autophagy and

apoptosis was involved in the dual role of autophagy under ER Stress (Li et al., 2016). Our results identified that miR-26 mimics enhanced expression of ERS related proteins. Down-regulation of ERS inhibited the apoptosis induced by miR-26 mimics in A549 cells. Interestingly, Down-regulation of ERS failed to affect cell autophagy induced by the miR-26 inhibitor. These results demonstrated that the ERS signaling pathway was associated with miR-26 regulated apoptosis in NSCLC cells.

In conclusion, this study demonstrated that miR-26 induced cell apoptosis and inhibited cell autophagy of NSCLC, through inhibiting TGF- β expression in a JNK dependent manner, both *in vitro* and *in vivo*. Moreover, miR-26 mimics induced cell apoptosis was associated with ER stress in human NSCLC cells. Down-regulation of ERS could reverse the apoptosis induced by miR-26 mimics. Our results provided a novel potential therapeutic target for treatment of NSCLC.

AUTHOR CONTRIBUTIONS

YH, HL, and LJ carried out the studies, participated in the experimental design, statistical analysis, and drafted the manuscript. BR participated in the sample collection and statistical analysis. JM and HX conceived the study, participated in its design and coordination, and helped to draft the manuscript. All authors read and approved the final manuscript.

FUNDING

This work was supported by the National Natural Science Foundation of China (No. 30901467).

REFERENCES

- Chen, J. L., Colgan, T. D., Walton, K. L., Gregorevic, P., and Harrison, C. A. (2016). The TGF-beta signaling network in muscle development, adaptation and disease. *Adv. Exp. Med. Biol.* 900, 97–131. doi: 10.1007/978-3-319-27511-6_5
- Deng, M., Zhang, R., He, Z., Qiu, Q., Lu, X., Yin, J., et al. (2017). TET-mediated sequestration of miR-26 drives EZH2 expression and gastric carcinogenesis. *Cancer Res.* 77, 6069–6082. doi: 10.1158/0008-5472.CAN-16-2964
- Díaz, M., González, R., Plano, D., Palop, J. A., Sanmartín, C., and Encío, I. (2017). A diphenyldiselenide derivative induces autophagy via JNK in HTB-54 lung cancer cells. *J. Cell. Mol. Med.* 22, 289–301. doi: 10.1111/jcmm.13318
- Gratchev, A. (2017). TGF-beta signalling in tumour associated macrophages. *Immunobiology* 222, 75–81. doi: 10.1016/j.imbio.2015.11.016
- Gupta, S., Giricz, Z., Natoni, A., Donnelly, N., Deegan, S., Szegezdi, E., et al. (2012). NOXA contributes to the sensitivity of PERK-deficient cells to ER stress. *FEBS Lett.* 586, 4023–4030. doi: 10.1016/j.febslet.2012.10.002
- Hong, Q. Y., Wu, G. M., Qian, G. S., Hu, C. P., Zhou, J. Y., Chen, L. A., et al. (2015). Prevention and management of lung cancer in China. *Cancer* 121, 3080–3088. doi: 10.1002/cncr.29584
- Hutchinson, L. (2017). Targeted therapies: defining the best-in-class in NSCLC. *Nat. Rev. Clin. Oncol.* 14:457. doi: 10.1038/nrclinonc.2017.99
- Jiang, Y., Woosley, A. N., Sivalingam, N., Natarajan, S., and Howe, P. H. (2016). Cathepsin-B-mediated cleavage of disabled-2 regulates TGF-beta-induced autophagy. *Nat. Cell Biol.* 18, 851–863. doi: 10.1038/ncb3388
- Jin, F., Wang, Y., Li, M., Zhu, Y., Liang, H., Wang, C., et al. (2017). MiR-26 enhances chemosensitivity and promotes apoptosis of hepatocellular carcinoma cells through inhibiting autophagy. *Cell Death Dis.* 8:e2540. doi: 10.1038/cddis.2016.461
- Jing, D., Hao, J., Shen, Y., Tang, G., Li, M. L., Huang, S. H., et al. (2015). The role of microRNAs in bone remodeling. *Int. J. Oral Sci.* 7, 131–143. doi: 10.1038/ijos.2015.22
- Johnston, C. J., Smyth, D. J., Dresser, D. W., and Maizels, R. M. (2016). TGF-beta in tolerance, development and regulation of immunity. *Cell. Immunol.* 299, 14–22. doi: 10.1016/j.cellimm.2015.10.006
- Katz, L. H., Li, Y., Chen, J. S., Munoz, N. M., Majumdar, A., Chen, J., et al. (2013). Targeting TGF-beta signaling in cancer. *Expert Opin. Ther. Targets* 17, 743–760. doi: 10.1517/14728222.2013.782287
- Kiyono, K., Suzuki, H. I., Matsuyama, H., Morishita, Y., Komuro, A., Kano, M. R., et al. (2009). Autophagy is activated by TGF-beta and potentiates TGF-beta-mediated growth inhibition in human hepatocellular carcinoma cells. *Cancer Res.* 69, 8844–8852. doi: 10.1158/0008-5472.CAN-08-4401
- Kwon, Y., Kim, Y., Eom, S., Kim, M., Park, D., Kim, H., et al. (2015). MicroRNA-26a/-26b-COX-2-MIP-2 loop regulates allergic inflammation and allergic inflammation-promoted enhanced tumorigenic and metastatic potential of cancer cells. *J. Biol. Chem.* 290, 14245–14266. doi: 10.1074/jbc.M115.645580
- Li, J., Liang, Y., Lv, H., Meng, H., Xiong, G., Guan, X., et al. (2017). miR-26a and miR-26b inhibit esophageal squamous cancer cell proliferation through suppression of c-MYC pathway. *Gene* 625, 1–9. doi: 10.1016/j.gene.2017.05.001
- Li, X., Zhu, F., Jiang, J., Sun, C., Zhong, Q., Shen, M., et al. (2016). Simultaneous inhibition of the ubiquitin-proteasome system and autophagy

- enhances apoptosis induced by ER stress aggravators in human pancreatic cancer cells. *Autophagy* 12, 1521–1537. doi: 10.1080/15548627.2016.1191722
- Lin, Y., Chen, H., Hu, Z., Mao, Y., Xu, X., Zhu, Y., et al. (2013). miR-26a inhibits proliferation and motility in bladder cancer by targeting HMGA1. *FEBS Lett.* 587, 2467. doi: 10.1016/j.febslet.2013.06.021
- Liu, F. L., Mo, E. P., Yang, L., Du, J., Wang, H. S., Zhang, H., et al. (2016). Autophagy is involved in TGF-beta1-induced protective mechanisms and formation of cancer-associated fibroblasts phenotype in tumor microenvironment. *Oncotarget* 7, 4122–4141. doi: 10.18632/oncotarget.6702
- Liu, P., Tang, H., Chen, B., He, Z., Deng, M., Wu, M., et al. (2015). miR-26a suppresses tumour proliferation and metastasis by targeting metadherin in triple negative breast cancer. *Cancer Lett.* 357, 384–392. doi: 10.1016/j.canlet.2014.11.050
- Liu, Y., Zhu, H., Yan, X., Gu, H., Gu, Z., and Liu, F. (2017). Endoplasmic reticulum stress participates in the progress of senescence and apoptosis of osteoarthritis chondrocytes. *Biochem. Biophys. Res. Commun.* 491, 368–373. doi: 10.1016/j.bbrc.2017.07.094
- López-Urrutia, E., Coronel-Hernández, J., García-Castillo, V., Contreras-Romero, C., Martínez-Gutiérrez, A., Estrada-Galicia, D., et al. (2017). MiR-26a downregulates retinoblastoma in colorectal cancer. *Tumour Biol.* 39:1010428317695945. doi: 10.1177/1010428317695945
- Lu, Z., Miao, Y., Muhammad, I., Tian, E., Hu, W., Wang, J., et al. (2017). Colistin-induced autophagy and apoptosis involves the JNK-Bcl2-Bax signaling pathway and JNK-p53-ROS positive feedback loop in PC-12 cells. *Chem. Biol. Interact.* 277, 62–73. doi: 10.1016/j.cbi.2017.08.011
- Palka, M., Sanchez, A., Córdoba, M., Nuevo, G. D., De Ugarte, A. V., Cantos, B., et al. (2017). Cisplatin plus vinorelbine as induction treatment in stage IIIA non-small cell lung cancer. *Oncol. Lett.* 13, 1647–1654. doi: 10.3892/ol.2017.5620
- Ramu, A., Kathiresan, S., and Ali Ahmed, B. (2017). Gramine inhibits angiogenesis and induces apoptosis via modulation of TGF-beta signalling in 7,12 dimethylbenz[a]anthracene (DMBA) induced hamster buccal pouch carcinoma. *Phytomedicine* 33, 69–76. doi: 10.1016/j.phymed.2017.05.008
- Ren, K., Mo, Z. C., Liu, X., Tang, Z. L., Jiang, Y., Peng, X. S., et al. (2017). TGF-beta Down-regulates apolipoprotein M expression through the TAK-1-JNK-c-jun pathway in HepG2 cells. *Lipids* 52, 109–117. doi: 10.1007/s11745-016-4227-9
- Ripley, R. T., Suzuki, K., Tan, K. S., Adusumilli, P. S., Huang, J., Park, B. J., et al. (2016). Postinduction positron emission tomography assessment of N2 nodes is not associated with ypN2 disease or overall survival in stage IIIA non-small cell lung cancer. *J. Thorac. Cardiovasc. Surg.* 151, 969–977. doi: 10.1016/j.jtcvs.2015.09.127
- Singh, A., and Sen, D. (2017). MicroRNAs in Parkinson's disease. *Exp. Brain Res.* 235, 2359–2374. doi: 10.1007/s00221-017-4989-1
- Song, S., Tan, J., Miao, Y., Li, M., and Zhang, Q. (2017). Crosstalk of autophagy and apoptosis: involvement of the dual role of autophagy under ER stress. *J. Cell. Physiol.* 232, 2977–2984. doi: 10.1002/jcp.25785
- Sureshbabu, A., Muhsin, S. A., and Choi, M. E. (2016). TGF-beta signaling in the kidney: profibrotic and protective effects. *Am. J. Physiol. Renal Physiol.* 310, F596–F606. doi: 10.1152/ajprenal.00365.2015
- Thinon, E., Morales-Sanfrutos, J., Mann, D. J., and Tate, E. W. (2016). N-Myristoyltransferase inhibition induces ER-stress, cell cycle arrest, and apoptosis in cancer cells. *ACS Chem. Biol.* 11, 2165–2176. doi: 10.1021/acschembio.6b00371
- Verfaillie, T., Garg, A. D., and Agostinis, P. (2013). Targeting ER stress induced apoptosis and inflammation in cancer. *Cancer Lett.* 332, 249–264. doi: 10.1016/j.canlet.2010.07.016
- Williams, M., Cheng, Y. Y., Blenkiron, C., and Reid, G. (2016). Exploring mechanisms of MicroRNA downregulation in cancer. *Microna* 6, 2–16. doi: 10.2174/2211536605666161208154633
- Wu, A. J., Garay, E., Foster, A., Hsu, M., Zhang, Z., Chaff, J. E., et al. (2017). Definitive radiotherapy for local recurrence of NSCLC after surgery. *Clin. Lung Cancer* 18, e161–e168. doi: 10.1016/j.clcc.2017.01.014
- Xu, Y., Yang, S., Huang, J., Ruan, S., Zheng, Z., and Lin, J. (2012). TGF-beta 1 induces autophagy and promotes apoptosis in renal tubular epithelial cells. *Int. J. Mol. Med.* 29, 781–790. doi: 10.3892/ijmm.2012.911
- Zhang, B., Liu, X. X., He, J. R., Zhou, C. X., Guo, M., He, M., et al. (2011). Pathologically decreased miR-26a antagonizes apoptosis and facilitates carcinogenesis by targeting MTDH and EZH2 in breast cancer. *Carcinogenesis* 32, 2–9. doi: 10.1093/carcin/bgq209
- Zhang, X., Liu, S., Liu, Y., Du, J., Fu, W., Zhao, X., et al. (2017). Economic burden for lung cancer survivors in urban China. *Int. J. Environ. Res. Public Health* 14, E308. doi: 10.3390/ijerph14030308

Conflict of Interest Statement: The authors declare that the research was conducted in the absence of any commercial or financial relationships that could be construed as a potential conflict of interest.

Copyright © 2019 He, Liu, Jiang, Rui, Mei and Xiao. This is an open-access article distributed under the terms of the Creative Commons Attribution License (CC BY). The use, distribution or reproduction in other forums is permitted, provided the original author(s) and the copyright owner(s) are credited and that the original publication in this journal is cited, in accordance with accepted academic practice. No use, distribution or reproduction is permitted which does not comply with these terms.



The Prognostic and Therapeutic Value of PD-L1 in Glioma

Ruo Qiao Chen¹, Feng Liu^{1,2}, Xin Yao Qiu^{1,2*} and Xiao Qian Chen^{1,2*}

¹ School of Basic Medicine, Tongji Medical College, Huazhong University of Science and Technology, Wuhan, China,

² Department of Pathophysiology, School of Basic Medicine, Tongji Medical College, Huazhong University of Science and Technology, Wuhan, China

OPEN ACCESS

Edited by:

Dong-Hua Yang,
St. John's University, United States

Reviewed by:

Md. Areeful Haque,
University Kebangsaan Malaysia,
Malaysia
Chenran Wang,
University of Cincinnati, United States

*Correspondence:

Xin Yao Qiu
qiu.xinyao1991@outlook.com
Xiao Qian Chen
chenxq@mails.tjmu.edu.cn

Specialty section:

This article was submitted to
Experimental Pharmacology and Drug
Discovery,
a section of the journal
Frontiers in Pharmacology

Received: 13 October 2018

Accepted: 10 December 2018

Published: 09 January 2019

Citation:

Chen RQ, Liu F, Qiu XY and Chen XQ
(2019) The Prognostic and
Therapeutic Value of PD-L1 in Glioma.
Front. Pharmacol. 9:1503.
doi: 10.3389/fphar.2018.01503

Glioma is the most common type of primary brain tumors. After standard treatment regimen (surgical section, radiotherapy and chemotherapy), the average survival time remains merely around 14 months for glioblastoma (grade IV glioma). Recent immune therapy targeting to the immune inhibitory checkpoint axis, i.e., programmed cell death protein 1 (PD-1) and its ligand PD-L1 (i.e., CD274 or B7-H1), has achieved breakthrough in many cancers but still not in glioma. PD-L1 is considered a major prognostic biomarker for immune therapy in many cancers, with anti-PD-1 or anti-PD-L1 antibodies being used. However, the expression and subcellular distribution of PD-L1 in glioma cells exhibits great variance in different studies, severely impairing PD-L1's value as therapeutic and prognostic biomarker in glioma. The role of PD-L1 in modulating immune therapy is complicated. In addition, endogenous PD-L1 plays tumorigenic roles in glioma development. In this review, we summarize PD-L1 mRNA expression and protein levels detected by using different methods and antibodies in human glioma tissues in all literatures, and we evaluate the prognostic value of PD-L1 in glioma. We also summarize the relationships between PD-L1 and immune cell infiltration in glioma. The mechanisms regulating PD-L1 expression and the oncogenic roles of endogenous PD-L1 are discussed. Further, the therapeutic results of using anti-PD-1/PD-L1 antibodies or PD-L1 knockdown are summarized and evaluated. In summary, current results support that PD-L1 is not only a prognostic biomarker of immune therapy, but also a potential therapeutic target for glioma.

Keywords: glioma, PD-L1, immune response, tumor infiltrating lymphocytes, Ras

INTRODUCTION

Glioma, predominantly derived from glial cells, is the most common type of primary tumors in the human brain. Pathologically, glioma is categorized into grade I-IV according to World Health Organization (WHO) criteria, in which grade I-II are considered low-grade glioma (LGG) while grade III-IV are high-grade glioma (HGG). WHO grade IV glioma, also called glioblastoma or glioblastoma multiforme (GBM), is characterized by its tissue ischemic necrosis, strong invasiveness and microvascular proliferation. After conventional surgery, radiation therapy and chemotherapy, GBM patients have a 5-year survival rate of around 9.8% and a median survival time of 14 months (Stupp et al., 2005, 2009; Tran and Rosenthal, 2010). Currently, there is still no effective clinical therapy for primary or recurrent GBM. Recently, immune therapies targeting to the inhibitory immune checkpoint axis signaling, mainly PD-1/PD-L1 pairs, are

revolutionary. Blocking PD-1/PD-L1 pathway by antibodies achieved clinical cure in advanced melanoma including its brain metastasis (Wolchok et al., 2017; Long et al., 2018), opening a new era of cancer therapies. Pembrolizumab and Nivolumab, the most commonly used monoclonal PD-1 antibodies approved by USFDA, have been widely used for melanoma as well as non-small cell lung cancer (Robert et al., 2015; Reck et al., 2016). Currently, many other cancers such as renal carcinoma, colorectal cancer, lymphoma, head and neck carcinoma, bladder cancer, hepatocellular carcinoma and metastatic colorectal cancer are also approved for PD-1/PD-L1-targeting therapy (Ansell et al., 2015; Le et al., 2015; Ferris et al., 2016; Bellmunt et al., 2017; Motzer et al., 2018; Overman et al., 2018). The predictive markers in PD-1/PD-L1 antibody therapy are mainly the number of cytotoxic T-lymphocytes inside tumor tissues and the expression level of PD-L1 in cancer cells (Chen et al., 2016). Clinical trials of PD-1/PD-L1 antibody immunotherapy for glioma are relatively delayed, largely remaining on phase II (e.g., NCT01952769, Pidilizumab) and phase III (e.g., NCT02017717, Nivolumab) (Filley et al., 2017; Maxwell et al., 2017). Till now, there is still no reliable predictive marker for targeting inhibitory immune checkpoint in glioma. Meanwhile, unlike other solid tumors, the relationship between PD-L1 and T-lymphocyte infiltration in glioma, as well as therapeutic effects of PD-1/PD-L1 antibodies remains largely elusive, which probably reflect the specificities of cellular and structural microenvironment in the brain (Huang et al., 2017). Here, we summarize major recent results: (1) PD-L1 expression/subcellular distribution in glioma tissues; (2) The correlation between PD-L1 level and survival time of glioma patients; (3) The relationship between PD-L1 and immune cell infiltration; (4) The mechanism controlling PD-L1 expression and its intracellular oncogenic role; (5) The therapeutic effects of PD-1 antibodies in patients and PD-L1 antibodies in animals.

THE EXPRESSION AND SUBCELLULAR DISTRIBUTION OF PD-L1 IN HUMAN GLIOMA TISSUES

PD-1 and PD-L1 are two major negative regulatory molecules at the immune checkpoint axis. PD-1 (i.e., CD279), a cell surface receptor belonging to the extended CD28/cytotoxic T-lymphocyte-associated protein 4 (CTLA-4) family of T cell regulators (Shinohara et al., 1994), is predominantly expressed on activated T cells, B cells, and macrophages (Agata et al., 1996). PD-L1 and PD-L2, both PD-1 ligands, belongs to the B7 family. PD-L1 protein is widely expressed in almost all tumor cells as well as many normal cells, while PD-L2 is mainly expressed in dendritic cells and a few tumor cell lines. Crucially, PD-L1 can be upregulated in cancer cells upon interferon- γ (IFN- γ) stimulation and some activated immune cells (e.g., macrophages, dendritic cells) (Dong et al., 1999), indicating the major regulator role of PD-L1 in cancer tissues. PD-L1 binds not only to PD-1 but also other costimulatory molecules such as CD28, CD80, and CTLA-4, whereas PD-L2 binds mainly to PD-1 (Said et al., 2010), suggesting that PD-L1 has wider and

more complicated mechanisms for regulating immune responses. The binding of PD-L1 to PD-1 delivers strong inhibitory signals to suppress the proliferation, activation and infiltration of cytotoxic T-lymphocytes (CTL) (Dong et al., 2002), which was proved to be the major negative regulation of CTL in cancer microenvironment (Dong et al., 2002; Alsaab et al., 2017; Wang et al., 2018). Since PD-L1 level in cancer cells is considered to be a major predictive marker of PD-1/PD-L1 antibody response (Sanmamed and Chen, 2018), it is of primary importance to analyze the expression and subcellular distribution of PD-L1 in glioma tissues.

In previous studies, flow cytometry (FCM) detected PD-L1 expression in 12 glioma cell lines (Wintterle et al., 2003), most primary cultures of glioma cells (6/8) (Wilmotte et al., 2005) and glioma cells from a great number of human glioma specimens (Berghoff et al., 2015), demonstrating the presence of PD-L1 on cell surface of most glioma cells. In addition, many results of immunohistochemistry (IHC) show much higher PD-L1 protein expression in human glioma tissues than that in their surrounding or distant normal tissues (Berghoff et al., 2015; Wang and Wang, 2017). However, PD-L1 levels in human glioma tissues detected by different laboratories vary greatly (Table 1). It is worth noting that 11 different PD-L1 antibodies have been utilized in IHC, and each PD-L1 antibody showed distinct PD-L1 expression and subcellular distribution pattern in glioma cells, indicating the intriguing role of PD-L1 in glioma.

First of all, the most widely used PD-L1 antibody Clone 5H1 can detect both diffuse/fibrillary PD-L1 intracellularly and on cell surface (Wintterle et al., 2003; Berghoff et al., 2015; Bellmunt et al., 2017). In two experiments involving 9 GBM and 1 grade III mixed glioma specimens, PD-L1 protein was detected in all glioma samples and areas with PD-L1⁺-cells accounted for 50–90% of the specimens (Wintterle et al., 2003). In another study containing 174 human glioma specimens, Clone 5H1 showed that 70.1% of all specimens was diffuse/fibrillary PD-L1-positive (>25% of the tumor cells was PD-L1⁺), and 40.8% of all specimens was PD-L1⁺ on cell membranes (Berghoff et al., 2017). Whereas, in a study containing 135 glioma specimens, only 34.8% of all glioma specimens were PD-L1⁺ (Berghoff et al., 2015). Moreover, most glioma specimens (82.9%) exhibited a diffuse/fibrillary distribution pattern of PD-L1, while membranous distribution of PD-L1 in tumor cells covered >5% merely (Berghoff et al., 2015). In short, the employment of Clone 5H1 receives high positive rates of PD-L1 in human glioma tissues (>30%).

When using PD-L1 antibody SP142, the percentage of PD-L1⁺ samples decreases greatly. In all three studies involving large numbers of specimens, the detected rates of PD-L1 were <20%: 1. PD-L1 was positive in 19% of all 1035 GBM specimens ($\geq 2+$ and $\geq 5\%$) (Xiu et al., 2016); 2. PD-L1 was positive in only 6.1% of all 347 glioma specimens (staining of PD-L1 on tumor cell membranes >1+) (Garber et al., 2016); 3. PD-L1 was positive in only 8.1% of all 327 glioma specimens (staining of PD-L1 on tumor cell membranes >1+) (Hodges et al., 2017).

Furthermore, Nduom et al. (2016) compared several PD-L1 antibodies including Abcam ab58810, Abcam clone EPR1161, Clone 7G11, and Clone 5H1 antibodies. They found that

TABLE 1 | The expression of PD-L1 in human glioma tissues.

Materials	PD-L1 antibody	Criteria for IHC positive	Expression rate of PD-L1	Other results	Reference
TMA: 1035 GBM specimens (grade IV tumors with gliosarcoma were not included)	SP142	<5% or $\geq 2+$ or $\geq 2+$ and $\geq 5\%$	PD-L1 positive in 19% of all specimens		Xiu et al., 2016
233 GBM specimens; WHO (II, 15.6%; WHO III 13.6%; gliosarcomas 3.7%)	SP142	PD-L1 expression detected on cell membranes	PD-L1 positive in 6.1% (21/345) of all glioma specimens, and in 35.0% (57/163) of all GBM specimens	High expression of PD-L1 in WHO IV GBM specimens, while low expression in IDH-mutant glioma specimens	Garber et al., 2016
327 glioma specimens (grade I-IV); 198 GBM specimens	SP142	PD-L1 expression detected on cell membranes	PD-L1 positive in 8.1% (24/295) of all glioma specimens, and in 10.1% (19/189) of all GBM specimens	Low expression of PD-L1 in IDH-mutant glioma specimens	Hodges et al., 2017
117 newly diagnose glioblastoma specimens, 18 recurrent glioblastoma specimens	Clone 5H1	Membranous PD-L1 expression: PD-L1 detected on >5% of the tumor cell membranes;	PD-L1 positive in 37.6% (44/117) of newly diagnosed glioblastoma specimens and 16.7% (3/18) of recurrent glioblastoma specimens;		Berghoff et al., 2015
		Diffuse/fibrillary PD-L1 expression: PD-L1 detected in non-necrotic areas	PD-L1 expression in 84.6% (99/117) of newly diagnosed glioblastoma specimens and 72.2% (13/18) of recurrent glioblastoma specimens.		
43 WHO II/III (39 IDH-mutant, 4 IDH-wild type) glioma specimens; 14 GBM with IDH-mutant specimen; 117 GBM with IDH-wild type specimens	Clone 5H1	Membranous PD-L1 expression: PD-L1 detected on >1% of the tumor cell membranes;	Positive expression in 56.2% (68/121) of IDH-wild type glioma and 5.7% (3/53) of IDH-mutant glioma;	A significant negative correlation between PD-L1 expression and IDH-mutant status ($P < 0.001$)	Berghoff et al., 2017
		Diffuse/fibrillary PD-L1 expression: PD-L1 detected in >25% of all non-necrotic areas	Positive expression in 84.3% (102/121) of IDH-wild type glioma and 37.3% (20/53) of IDH-mutant glioma.		
9 GBM specimens; 1 mixed glioma (WHO III) specimen	Clone 5H1	PD-L1 expression was divided into 4 levels: <25%; 25–50%; 50–75% and >75%	PD-L1 expression in all 10 specimens (with a positive rate of 50–90%)		Witterle et al., 2003
TMA: 99 GBM specimens	EPR1161	Compact brown particles shown on cell membranes	60.6% of the specimens with >1% PD-L1 expression; 38.3% of the specimens with >5% PD-L1 expression		Nduom et al., 2016
TMA: 229 glioma specimens (WHO I–IV)	Rabbit polyclonal antibody anti-PD-L1	>5% of tumor cell with membrane or cytoplasm PD-L1 expression	49.2, 53.7, and 68.6% of grade II, III and IV gliomas with positive PD-L1 expression respectively	No significant correlation between PD-L1 expression and WHO levels ($P = 0.327$)	Zeng et al., 2016
54 brain tumor specimens, 1 epilepsy specimen	clone MIH1 eBioscience	Positive signals detected in glioma cells	Positive expression of PD-L1 in 85.2% (46/54) of all brain tumor specimens and 19/19 GBM specimens	The positive expression rate of PD-L1 in GBM specimens higher than that in other brain tumor specimens	Wilmotte et al., 2005
64 glioma specimens (grade I–IV)	ab58810, Abcam	Positive signals detected in >5% of all tumor cells (membrane or cytoplasm)	PD-L1 positive in 78.12% (50/64) of all specimens, 60.87% (14/23) of the LGG specimens and 87.80% (36/41) of the HGG specimens	A significant positive correlation between PD-L1 expression and WHO levels ($P = 0.013$)	Xue et al., 2017a

(Continued)

TABLE 1 | Continued

Materials	PD-L1 antibody	Criteria for IHC positive	Expression rate of PD-L1	Other results	Reference
Initial and secondary resected tumor specimens from 16 GBM patients (excision time within 2 years after the first operation)	28–8, Abcam	PD-L1 in tumor cells was graded as “–” (absence of staining), “+” (up to 25% of cells stained), “++” (25–50% of cells stained) or “+++” (more than 50% of cells stained)	Initial resected tumor specimens median: ++; secondary resected tumor specimens median: ++	No difference between the expression of PD-L1 in initial and secondary resected tumor ($P = 0.187$)	Miyazaki et al., 2017
TMA: 54 GBM specimens	Cell Marque, Rocklin, CA, USA	PD-L1 expression detected in >5% of all tumor cell membranes	PD-L1 positive in 31.5% of all GBM specimens		Han et al., 2017
Initial and secondary resected tumor specimens from 64 GBM	E1LRN, Cell Signaling	Diffuse/fibrillary PD-L1 expression in 75% of all specimens; Cytoplasmic PD-L1 expression in 20% of all specimens; membranous PD-L1 expression in 5% of all specimens	PD-L1 expression level in secondary resected GBM specimens reduced 66.71% compared to that in initial resected GBM specimens ($p = 0.0045$)		Heynckes et al., 2017
62 malignant brainstem glioma specimens	ab205921, Abcam, Cambridge, UK	Unknown	PD-L1 expression in 59.7% (37/62) of all specimens		Zhang et al., 2017
TMA: 115 GBM specimens	E1LRN, Cell Signaling	Positive signals detected in >5% of tumor cells (either membrane or cytoplasm)	PD-L1 positive in 32.2% (37/115) of all GBM specimens	PD-L1 expression was significantly associated with IDH-mutant status ($P = 0.008$)	Lee et al., 2018

TMA, tissue microarray; GBM, glioblastoma multiforme; IDH-mutant, isocitrate dehydrogenase-mutant.

PD-L1 antibody EPR1161 showed relatively satisfying results of membranous PD-L1. The specificity of EPR1161 antibody to PD-L1 was confirmed by several positive controls (e.g., human placenta, tonsil tissues and PD-L1-overexpressed HEK 293 cells). EPR1161 antibody detection was used to analyze PD-L1 expression on a tissue microarray containing 99 GBM specimens. Only tumor cells showed positive PD-L1 signals on cell membranes: 60.6% of all specimens contained >1% PD-L1⁺-glioma cells, 38.3% contained >5% PD-L1⁺-glioma cells, 17% contained >25% PD-L1⁺-glioma cells and 5.32% contained >50% PD-L1⁺-glioma cells. These results indicate that a more comprehensive evaluation of PD-L1 expression in glioma is desirable.

Importantly, several recent studies reported that expression levels of PD-L1 are positively correlated with glioma grades (Garber et al., 2016; Wang et al., 2016; Xue et al., 2017a; Zhang et al., 2017). Xue et al. (2017a) reported that the PD-L1 expression levels positively correlated with the grades of gliomas. Wang et al. (2016) and Zhang et al. (2017) reported that PD-L1 expression was much higher in GBM compared to grade II and III gliomas. Garber et al. (2016) found that the high expression level of PD-L1 (IHC) was positively associated with only grade IV gliomas, though high PD-L1 expression could also be detected in other grades of gliomas.

Moreover, PD-L1 expression is associated with glioma genotypes. For instance, in different grades of gliomas, all PD-L1 expression in isocitrate dehydrogenase (IDH)-mutant gliomas was significantly lower than that in IDH-wild type (Wang et al., 2016). In fact, the methylation level of PD-L1 promoter in IDH-mutant glioma was higher than that in IDH-wild type glioma, and PD-L1 expression negatively correlated with PD-L1 promoter methylation level (Berghoff et al., 2017; Röver et al., 2018). Additionally, low PD-L1 levels (IHC) were observed in proneural and glioma CpG island methylator phenotype (G-CIMP) subtypes, while high PD-L1 expression was detected in mesenchymal subtype (Berghoff et al., 2015).

In brief, the expression patterns of PD-L1 in specimens are mainly influenced by the following factors: (1) The selected PD-L1 antibodies: if the antibody can detect both membranous and cytoplasmic PD-L1, the percentage of PD-L1-positive specimens rises remarkably [e.g., Clone 5H1 (Winterle et al., 2003; Berghoff et al., 2015, 2017), Clone MIH1 eBioscience (Wilmotte et al., 2005), ab58810 Abcam (Xue et al., 2017a), E1LRN Cell Signaling (Heynckes et al., 2017), ab205921 Abcam (Zhang et al., 2017), and E1LRN Cell Signaling (Lee et al., 2018)]; if the antibody detects only membranous PD-L1, the percentage of PD-L1-positive specimens is low (e.g., SP142, EPR1161) (Garber et al., 2016; Nduom et al., 2016). (2) The PD-L1-positive criteria: if membranous PD-L1 is used as criteria, low PD-L1-positive percentage appears; while if cytoplasmic PD-L1 (either diffuse or fibrillary pattern) serves as criteria, much higher PD-L1-positive percentage can be obtained. (3) The constitution of illness cases: the expression of PD-L1 is considerably increased in GBM specimens, but decreased in recurrent glioma specimens (Berghoff et al., 2015) as well as IDH-mutant glioma specimens. (4) The stability of PD-L1 on glioma cell membranes: PD-L1 can be detected at various cellular components such as cell

membrane, cytoplasm or vesicles. It is conceivable that the recycling pattern and turnover rate of PD-L1 in glioma cells can affect PD-L1 detection.

THE PROGNOSTIC VALUE OF PD-L1 IN GLIOMA PATIENTS

Many studies investigated the correlation between PD-L1 expression levels and prognosis of glioma patients. In brief, more than half of literatures reported a negative correlation between PD-L1 and the prognosis of glioma patients. However, others reported that PD-L1 was not correlated with the prognosis of glioma (Table 2). Basing on The Cancer Genome Atlas (TCGA) and Chinese Glioma Genome Atlas (CGGA) database analysis and meta-analysis, in two studies involving 976 and 1,052 glioma patients respectively, high PD-L1 mRNA expression level was found to be associated with significantly shorter overall survival (OS) of glioma patients (Wang et al., 2016; Xue et al., 2017b). Various other studies basing on IHC results reported similar relationship (Liu et al., 2013; Nduom et al., 2016; Han et al., 2017; Lee et al., 2018; Pratt et al., 2018). Whereas in several other IHC analyses as well as a TCGA database analysis involving 444 GBM patients, no significant relationship was found between PD-L1 expression and glioma patients' OS (Berghoff et al., 2015; Zeng et al., 2016; Miyazaki et al., 2017). This is probably due to their relatively small scale of glioma samples.

In addition to case number, PD-L1⁺-cellular components in glioma microenvironment may also be an important factor affecting the prognostic value of PD-L1. Several studies reported that PD-L1 in glioma microenvironment is contributed mainly by tumor-infiltrating myeloid cells (TIM, including macrophages and T-regulatory cells) rather than tumor cells themselves (Mirghorbani et al., 2013; Antonios et al., 2017). The increase of PD-L1⁺ TIM surrounding glioma cells is associated with strong immune inhibition (Liu et al., 2008; Mirghorbani et al., 2013; Hosseini et al., 2015). Jan et al. (2018) found that lower PD-L1 level in glioma cells is associated with neither abating immune inhibition nor better prognosis of glioma, which is probably linked with elevated PD-L1⁺ TIM in glioma microenvironment.

Constitution of illness cases and limited human glioma tissue may also influence the evaluation of PD-L1 as a prognostic marker. For instance, the following factors can be taken into account: (1) The glioma type. Pratt et al. (2018) reported that there was no significant correlation between PD-L1 expression and OS ($P = 0.135$) of all glioma patients, while among recurrent, non-G-CIMP (IDH-wild type) patients, the PD-L1 expression was negatively associated with the OS ($P = 0.023$). This evidence suggests that PD-L1 expression may have prognostic values in specific subtypes of gliomas. Future studies may focus on analyzing the relationships between PD-1 and other molecular markers of glioma. (2) The way of resection. In a study involving initial and secondary resected glioma specimens from 16 GBM patients, PD-1 but not PD-L1 expression was positively associated with long progression-free survival (PFS) ($P = 0.029$) in initial resected specimens. After secondary surgery, PD-1 expression was negatively associated with survival time following

recurrence ($P = 0.030$) (Miyazaki et al., 2017). (3) The time of patients' survival. In Zeng's study (Zeng et al., 2016) involving 229 glioma specimens of grade I-IV, no significant correlation between PD-L1 and OS was found in all gliomas, but further analysis revealed a negative correlation between PD-L1 and OS ($P = 0.018$) if OS > 12 months is set a criterion in grade IV glioma only. While for those whose OS are <12 months, PD-L1 expression was not significantly associated with patients' OS, suggesting that PD-L1 is more favorable for the prediction of long-time survival patients (Zeng et al., 2016).

Although less studied, PD-1 expression level was also reported to be inversely associated with prognosis of GBM patients (Wang et al., 2016). In addition, PD-1 but not PD-L1 methylation was found to be positively associated with the OS of LGG patients (Röver et al., 2018). What is more, Bloch et al. (2017) reported that lower PD-L1 expression on peripheral myeloid cells is a primary independent predictor of survival in GBM patients ($n=46$) receiving autologous heat-shock protein vaccine (Prophage) after surgical resection followed by standard radiation and chemotherapy. The evaluation of PD-L1 expression on peripheral blood cells has great practical applications in predicting patients' survival time and their responses to PD-1/PD-1 antibody therapy. Clearly, the predicting value of PD-L1 or PD-1 in glioma will be increased with accumulating data. In addition, the search of other biomarkers is also important (Xue et al., 2017c).

PD-L1 MODULATING IMMUNE CELL INFILTRATION IN GLIOMA MICROENVIRONMENT

As is well-known, the engagement of PD-1 and PD-L1 promotes apoptosis of PD-1⁺ CTL. In various types of cancers including glioma, PD-L1 plays a major inhibitory role in modulating infiltration of immune cells, such as CTL, tumor infiltrating lymphocytes (TIL) and regulatory T-lymphocytes (Treg) (Taube et al., 2012; Dong et al., 2017). Thus it is the rationale to hypothesize that inhibiting PD-1/PD-L1 signaling promotes the antitumoral activity of TIL. Indeed, this hypothesis has been widely demonstrated in various cancer models including glioma (Taube et al., 2012; Antonios et al., 2016; Dong et al., 2017) and proved to be clinically effective in several cancers such as melanoma and non-small cell lung cancer. In fact, the relationships between PD-L1⁺ cancer cells and PD-1⁺ immune cells (mainly TIL) in tumor environment are complicated. For example, TIL secrete large amounts of cytokines (e.g., IFN- γ) to strongly upregulate PD-L1 expression in melanoma cells, which in turn triggers TIL themselves' inhibition (Taube et al., 2012). In most cancers, the upregulation of PD-L1 in tumor cells appears to be associated with increased TIL (Antonios et al., 2016).

PD-L1 plays opposite regulatory roles in functions of CTL and Treg in various cancers. Early studies considered that the interaction of PD-L1/tumor cells and PD-1/CTL may form a temporal "PD-L1/PD-1 shield" to prevent CTL-mediated tumor cell lysis (Hirano et al., 2005). In this model, it is supposed that CTL lose their ability to control tumor growth

TABLE 2 | The relationship between PD-L1 expression and prognosis of glioma patients.

Materials	PD-L1 antibody	Correlation with prognosis	Reference
Data of 149 GBM patients from TCGA		TCGA database analysis: for PD-L1 and PD-1, high expression associated with significantly shorter survival (Kaplan-Meier, $P = 0.023$ and $P = 0.028$, respectively); high expression of both PD-L1 and PD-1 negatively correlates with prognosis of patients ($P = 0.0031$)	Nduom et al., 2016
976 glioma specimens' data from CGGA and TCGA		CGGA database analysis: negative correlation between PD-L1 expression and the OS of glioma patients ($P < 0.001$) or GBM patients ($P = 0.0253$); TCGA database analysis: negative correlation between PD-L1 expression and the OS of glioma patients ($P < 0.001$) or GBM patients ($P = 0.043$)	Wang et al., 2016
TMA: 229 glioma specimens (grade I-IV)	Rabbit polyclonal antibody	No significant correlation between PD-L1 expression and patients' OS; univariate analysis: negative correlation between PD-L1 expression and prognosis of patients whose OS > 12 months ($P = 0.018$); multivariate analysis: no significant relation between PD-L1 expression and poor OS, but a strong tendency toward significance.	Zeng et al., 2016
117 newly diagnosed glioma specimens, 18 recurrent glioma specimens	Clone 5H1	No significant correlation between PD-L1 expression and patients' OS ($P = 0.724$)	Berghoff et al., 2015
Initial and secondary resected glioma specimens from 16 GBM patients (time of resection within 2 years after the first operation)	28-8, Abcam	No significant correlation between PD-L1/PD-1 expression and patients' PFS or OS in initial resected specimens; PD-1 high expression significantly associated with long progression-free survival ($P = 0.029$) and short survival after recurrence ($P = 0.030$) in secondary resected specimens	Miyazaki et al., 2017
TMA: 54 GBM specimens	Cell Marque, Rocklin, CA, USA	Negative correlation between PD-L1 expression and patients' OS (multivariate analysis: $P = 0.007$; univariate analysis: $P = 0.024$; Kaplan-Meier survival analysis: $P = 0.017$); no significant correlation between PD-L1 expression and patients' PFS ($P = 0.14$)	Han et al., 2017
TMA: 115 GBM specimens	E1L3N, Cell signaling	Kaplan-Meier analysis: PD-L1 expression in tumor cells significantly associated with poor overall survival (OS) ($P = 0.017$)	Lee et al., 2018
TMA: 99 GBM specimens	EPR1161	Significant negative correlation between PD-L1 expression and patients' OS ($P = 0.086$)	Nduom et al., 2016
Gene methylation data of 419 LGG patients from TCGA		Positive correlation between PD-1 methylation and patients' OS ($P = 0.001$); no significant correlation between PD-L1 methylation and the prognosis of patients	Röver et al., 2018
Data of 1,052 glioma patients from 4 previous studies		Meta analysis: pooled result: high PD-L1 expression associated with worse OS in glioma patients ($P = 0.032$); subgroup analysis: high PD-L1 expression in glioblastoma (GBM) associated with worse OS ($P = 0.030$); index subgroup analysis: neither PD-L1 protein ($P = 0.068$) nor gene ($P = 0.322$) significantly associated with OS	Xue et al., 2017b
Specimens from 17 GBM patients	MIH5	PD-L1 expression in tumors negatively associated with GBM patient survival ($P = 0.001$)	Liu et al., 2013
TMA: 183 tumor patient tissues (102 IDH-wild type diffuse gliomas);		NIH cohort glioblastoma and NIH cohort recurrent glioblastoma (IDH-wildtype): PD-L1 negatively associated with patients' OS ($P < 0.001$ and $P = 0.015$, respectively);	Pratt et al., 2018
Data of 444 GBM and 12 recurrent, non-G-CIMP (IDH-wild type) samples from TCGA		TCGA database analysis: in all glioblastoma, no significant correlation between PD-L1 expression and patients' OS ($P = 0.135$); in recurrent, non-G-CIMP (IDH-wild type), PD-L1 expression negatively associated with patients' OS ($P = 0.023$)	
Data of 47 GBM patient samples from a previous clinical study		GBM tumor cells expressing PD-L1 nor not does not affect the OS and PFS of ADCTA group or reference group patients (ADCTA group OS $P = 0.086$ and PFS $P = 0.239$; reference group OS $P = 0.376$ and PFS $P = 0.421$)	Jan et al., 2018

TABT, tumor-adjacent brain tissue; LGG, low-grade glioma.

but remain intact. Later, it was discovered that the PD-1/PD-L1 interaction increases indoleamine 2,3-dioxygenase (IDO) in melanoma microenvironment, which exhausts T cells of essential tryptophan and suppresses their metabolites, thus leading to CTL inhibition and Treg elevation (Dong et al., 2017). Moreover, PD-L1 inhibits chemokine production (e.g., CCL2-5 and CXCL9-10) that is crucial for recruitment of CTL, preventing the influx of CTL into tumor microenvironment (Gajewski et al., 2013). The roles of PD-1/PD-L1 pathway in inducing CTL exhaustion and Treg augment in tumor microenvironment have been verified in various cancer models (Dong et al., 2017; Jan et al., 2018).

PD-L1 in gliomas shows similar effects on CTL and Treg as in other cancers. Early studies demonstrated that PD-L1 expressed by glioma cells inhibits T-lymphocyte functions and induces apoptosis of tumor-specific T-lymphocytes mainly via decreasing cytokines production (e.g., IFN- γ , IL-2 and IL-10) (Winterle et al., 2003; Ahn et al., 2013). However, more recent studies revealed that PD-L1/PD-1 pathway inhibits CTL functions primarily via TIMs in glioma microenvironment (Antonios et al., 2017). The upregulation of PD-L1 in circulating monocytes and tumor-infiltrative macrophages in gliomas is associated with its cytotoxicity to T cells (Bloch et al., 2013). What is more, PD-L1 induces and maintains Treg in glioma. The elevation of PD-L1⁺ peripheral blood cells was associated with an increased Treg fraction in GBM patients (DiDomenico et al., 2018). Moreover, PD-L1 co-stimulation resulted in greater Treg expansion and improved preservation of the Treg phenotype, indicating that PD-L1 may expand and maintain immunosuppressive Treg. The increase of Treg is associated with decreased survival in glioma patients (DiDomenico et al., 2018). Until now, the exact relationships among PD-L1 and infiltrating immune cells in gliomas are far from clear. A major difficulty may be the very limited brain tissues obtained from glioma patients. Accurate information requires data accumulation from large quantity of human glioma samples.

THE REGULATORY MECHANISMS OF PD-L1 EXPRESSION AND SECRETION

In gliomas, the tumor suppressor phosphatase and tension homology deleted on chromosome 10 (PTEN), a major negative regulator of Akt activation, plays a vital role in regulating PD-L1 protein expression. PTEN mutation or homozygous deletion (in 36% of glioma) is highly associated with PD-L1 expression in gliomas. Activation of PI3K-Akt-mTOR-S6K1 cascade facilitates PD-L1 transcript into polysome so that PD-L1 translation increases (Parsa et al., 2007). Co-activation of Ras and Akt in glioma cells further elevated PD-L1 translation by recruiting polysome. PTEN loss in glioma causes Akt activation, thus induces PD-L1 protein via its translational regulatory mechanisms. On the contrary, the restoration of PTEN function reduces PD-L1 expression in gliomas. In addition to PTEN mutation, cytokines such as interferons may also induce PD-L1 via PI3K-Akt-mTOR-S6K1-mediated translational regulation (D'Arrigo et al., 2017).

Recently, microRNA-34a (miR-34a) and the PD-L1 co-chaperone FKBP51 binding protein 5 (spliced FKBP51) are also reported to be associated with PD-L1 expression in gliomas. MiR-34a functions as a tumor suppressor via modulating epidermal growth factor receptor (EGFR) or PD-L1 translation directly in glioma. miR-34a overexpression attenuated PD-L1-induced chemoresistance in glioma cells, supporting that miR-34a is a negative regulator of PD-L1 signaling (Wang and Wang, 2017). FKBP51s works as a co-chaperone with isomerase activity. FKBP51s abundantly exists in glioma and increases membranous PD-L1 by catalyzing the protein folding required for subsequent glycosylation. FKBP51s silencing significantly decreases PD-L1 on U251 cell surface. Moreover, FKBP51s is required for PD-L1 maturation in endoplasmic reticulum (ER), supporting that the FKBP51s functions as an important PD-L1 molecular chaperone (D'Arrigo et al., 2017).

IFN- γ is likely to be the strongest PD-L1 inducer in various cancers. It is reported that PD-L1 upregulation in melanoma tumor microenvironment depends on CTL-secreted IFN- γ rather than cancer cells themselves (Gajewski et al., 2013; Spranger et al., 2013; Dong et al., 2017). Some immunogenic tumors (e.g., metastatic colorectal cancer with high-level microsatellite instability, MSI-H-CRC) attract TIL, which produce IFN- γ and upregulate PD-L1 in tumor epithelial cells (Gatalica et al., 2014). In this way TIL can actually trigger their own inhibition by secreting cytokines that drive tumor PD-L1 expression (Taube et al., 2012). In gliomas, both monocytic and granulocytic myeloid-derived suppressor cells may contribute largely to PD-L1 upregulation inside the tumors, as infiltrated CTL were few (Dubinski et al., 2016).

IFN- γ relies on the activation of cyclin-dependent kinase 5 (Cdk5) to induce PD-L1 expression (Dorand et al., 2016). Loss of Cdk5 activity in many cancers results in persistent overexpression of the interferon regulatory factors IRF2 and IRF2BP2, two PD-L1 transcriptional repressors that negatively regulate PD-L1 expression in tumor cells. The persistent interferon regulatory factor 2 (IRF2) and IRF2-binding protein 2 (IRF2BP2) overexpression lasts for up to 48 hours after IFN- γ exposure in Cdk5-deficient medulloblastoma cells. Furthermore, disrupting Cdk5 in rhabdomyosarcoma also led to IFN- γ -induced PD-L1 ineffectiveness, supporting a general role of Cdk5 in PD-L1 regulation in cancer cells. Thus, Cdk5 is a key enzyme linked to IFN- γ and PD-L1 upregulation (Dorand et al., 2016).

IL-10 may serve as a vital cytokine upregulating PD-L1 expression in circulating monocytes and tumor-infiltrative macrophages in an autocrine/paracrine pattern in gliomas. Previous studies reported that glioma cells could stimulate monocytes and glioma-associated macrophages to produce IL-10, which in turn significantly increases PD-L1 expression in monocytes and tumor-infiltrative macrophages (Bloch et al., 2013).

Most recently, a novel mechanism of PD-L1-induced immune suppression is discovered, i.e., the interaction between interferon- γ -induced exosomal PD-L1 and PD-1 on peripheral T-cells (Chen et al., 2018). In metastatic melanomas cells, extracellular vesicles (mainly exosomes) with PD-L1 on exosome surface are secreted into tumor microenvironment and body

circulation. IFN- γ exacerbates PD-L1's release in melanoma exosomes, suppressing nearby and remote CD8⁺-T cell functions and facilitating tumor growth. Such evidence suggests that circulating exosomal PD-L1 may be a more practical and dynamic monitoring-marker for predicting host responses to immune therapy. The regulatory mechanisms of PD-L1 expression and secretion are summarized in **Figure 1**. The precise understanding of detailed PD-L1 regulatory mechanisms may provide insight in developing novel immunotherapeutic strategy for glioma.

THE ONCOGENIC ROLES OF ENDOGENOUS PD-L1 AS A SIGNALING PROTEIN

PD-L1 contains an extracellular immunoglobulin domain, a transmembrane domain (TM), and a short

intracellular/cytoplasmic domain (30 aa), indicating its probability in controlling cell-intrinsic signaling (**Figure 2**). Earliest evidence of its intrinsic signaling activities was reported (Azuma et al., 2008). PD-L1 confers tumor resistance to CTL lysis, depending on its intracellular domain (Azuma et al., 2008). Similarly, Gato-Cañas et al. (2017) discovered that PD-L1 cell-intrinsic signaling protects cancer cells from IFN-induced cytotoxicity and accelerates tumor progression. They further identified three conserved motifs (i.e., RMLDVEKC, DTSSK and QFEET) in the intracellular domain of PD-L1 after aligning it in 10 mammalian species, revealing the functions of these motifs. By inhibiting signal transducers and activators of transcription 3 (STAT3) phosphorylation, RMLDVEKC motif of PD-L1 was required for cancer cells to withstand the IFN-induced apoptosis, while DTSSK motif counteracts the RMLDVEKC motif's function (Gato-Cañas et al., 2017). The evidence together demonstrates that PD-L1 confers resistance toward pro-apoptotic stimuli,

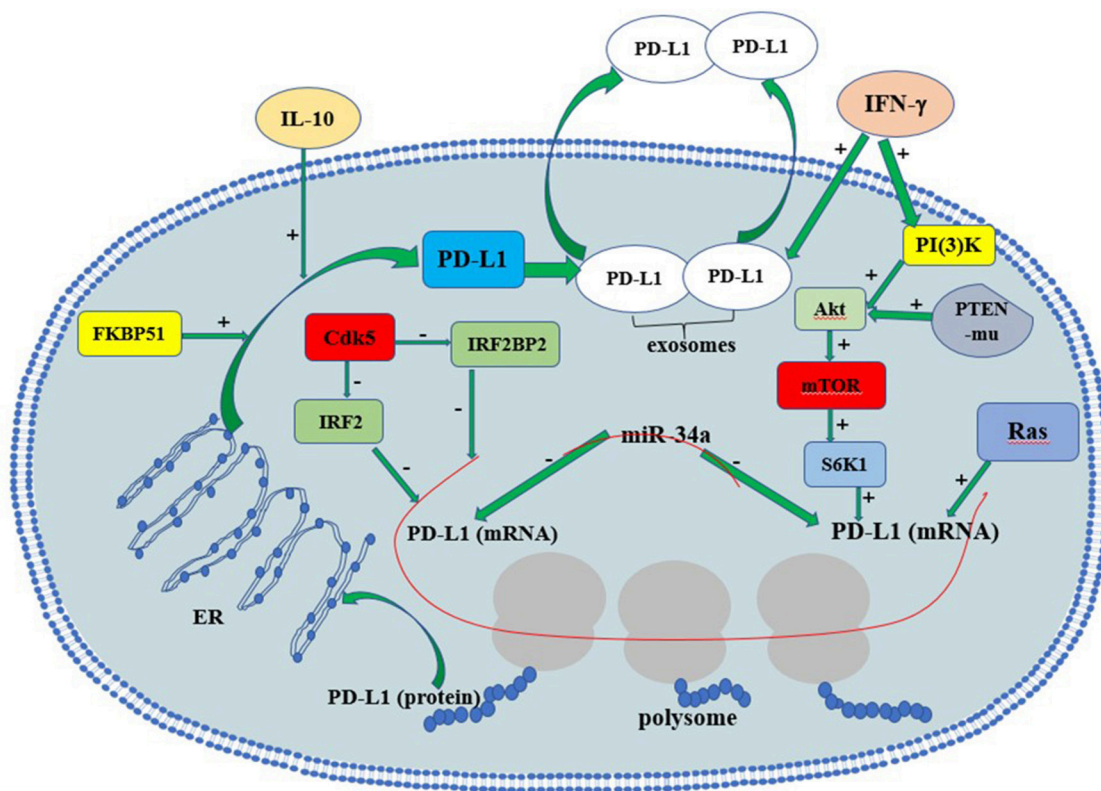


FIGURE 1 | The regulation of PD-L1 expression in glioma cells. Red line indicates RNAs. PTEN-mu, PTEN-mutant; ER, endoplasmic reticulum.

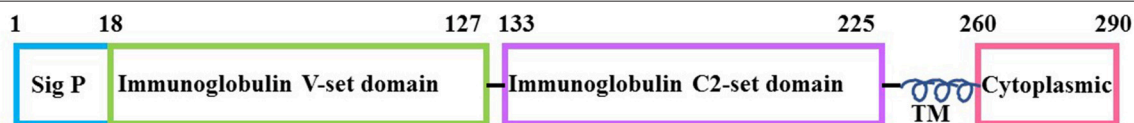


FIGURE 2 | The structure of PD-L1 protein molecule. The numbers represent the amino acid. Sig P, signal peptide; it directs PD-L1 toward cell membrane; TM, transmembrane domain; Cytoplasmic: the cytoplasmic or intracellular domain of PD-L1. The intracellular domain contains several conserved motifs: RMLDVEKC, DTSSK and QFEET.

such as IFN and CTL lysis, depending on its intracellular domain.

More direct evidence was provided by Chang et al. (2015). Tumor cells and T cells compete for nutrient such as glucose in tumor microenvironment, and predominant glucose consumption by tumors metabolically restricts T cell functions (e.g., reduction of mTOR activity/glycolytic capacity/IFN- γ production). *In vitro* and *in vivo* studies demonstrated that checkpoint blockade antibodies against PD-L1 restore glucose in tumor microenvironment, permitting T cell glycolysis and IFN- γ production. Further, *in vitro* studies showed that both PD-L1 antibodies and PD-L1 knockdown in tumor cells impaired sarcoma cell glycolysis and inhibited intracellular Akt/mTOR signaling, indicating the role of PD-L1 in modulating intracellular signaling pathway. Moreover, PD-L1 antibody treatment induces membranous PD-L1 internalization, implying that it is membranous PD-L1 rather than cytoplasmic PD-L1 that is involved in Akt/mTOR signaling in tumor cells (Chang et al., 2015). PD-L1 knockdown significantly decreases tumor volume of ovarian cancer and melanoma in immune-competent mice (Clark et al., 2016). PD-L1 knockout in murine medulloblastoma cells significantly reduced tumor incidence (30% of the mice inoculated with medulloblastoma cells remained tumor-free for more than 4 weeks) (Dorand et al., 2016). Recently, several teams reported that independent of immune function, PD-L1 regulated cell growth, proliferation, apoptosis, autophagy, migration and invasion in various cancers including ovarian cancer, melanoma, and pancreatic cancer via modulating PI3K/Akt/mTOR signaling pathway (Clark et al., 2016; Zhao et al., 2017). Additionally, PD-L1 promotes self-renewal and tumorigenicity of malignant melanoma initiating cells (Zheng et al., 2017), as well as embryonic stem cell transcriptional factors octamer-binding transcription factor 4 (OCT4) and Nanog expression dependent on PI3K/Akt activation and B lymphoma Mo-MLV insertion region 1 homolog (BMI1) expression in PI3K/Akt independent manner in breast cancer stem cells (Almozyan et al., 2017). Both evidence suggest the tumor-intrinsic role of PD-L1 in modulating signal transduction and the PD-L1's oncogenic/ tumorigenic role in certain cancers.

Specifically, in gliomas, PD-L1 expression was reported to be significant positively correlated to vascular endothelial growth factor (VEGF) and Ki-67 levels, detected by IHC with 64 patient specimens (Xue et al., 2017a). Our recent research reported that PD-L1 overexpression promoted and PD-L1 knockout/knockdown dampened glioma growth both *in vitro* and *in vivo* (Qiu et al., 2018). Further, transcriptome sequencing demonstrated that PD-L1 overexpression in glioma cell line significantly altered gene expression panel, suggesting PD-L1's cell-intrinsic roles. We have identified the intracellular interactions between PD-L1 and H-Ras, which further led to Ras/Erk activation, resulting in promoted glioma cell epithelial mesenchymal transition (EMT), migration and invasion. It is worth mentioning that PD-L1 knockdown almost abrogated the glioma xenografts formation in nude mice. This result suggests that the reduction of endogenous PD-L1 may be more effective than the employment of PD-L1 antibody, as the former inhibits both PD-1/PD-L1 axis signaling and oncogenic effects of PD-L1

(Qiu et al., 2018). It may also suggest an important glioma therapeutic strategy by drugs. Indeed, in glioma cells from the C57/GL261 orthotopic glioma model, we found that repaglinide significantly reduced PD-L1 expression, which correlates with the increase of TIL and the increase of survival time of mice (Xiao et al., 2017). These evidence suggest that targeting glioma PD-L1 directly by drugs or RNA interference might be an effective therapy for glioma. The functional roles of intrinsic PD-L1 as an oncogenic signaling molecule are summarized in Figure 3.

THE EFFECTS OF PD-1/PD-L1 TARGETING-THERAPY IN GLIOMA

Most clinical studies of PD-1/PD-L1 inhibition remain recruiting and inconclusive (Filley et al., 2017; Maxwell et al., 2017; Shergalis et al., 2018). Several studies reported that glioma or GBM patients may benefit from PD-1 antibody therapy. Reiss et al. reported that 24 HGG patients receiving pembrolizumab had a median PFS of 1.4 months and a median OS of 4 months with few serious toxicities (Reiss et al., 2017). Omuro et al. reported that nivolumab treatment on 3 in all 30 patients achieved partial responses, and 8 in all 40 patients with nivolumab treatment stayed stable for over 12 weeks (Omuro et al., 2018). Recently, Kline et al. reported that nivolumab in combination with reirradiation ($n = 8$) slightly prolonged OS of recurrent diffuse intrinsic pontine glioma in children compared to reirradiation alone ($n = 4$) (22.9 vs. 20.4 months since diagnosis; 6.8 vs. 6.0 months since reirradiation) in a retrospective study (Kline et al., 2018). All patients receiving reirradiation with or without nivolumab tolerated the therapy without severe acute or late toxicity. In a retrospective study of recurrent HGG among adult patients ($n = 31$), Kurz et al. reported that the median PFS showed no difference between patients receiving nivolumab (3.8 months) and pembrolizumab (2.3 months). The median survival time from date of first anti-PD-1 dose was 6.6 months ($n = 31$) (Kurz et al., 2018). In another retrospective study of recurrent HGG ($n = 50$), Mantica et al. reported a median PFS of 4.3 months and a median OS of 6.5 months after receiving nivolumab

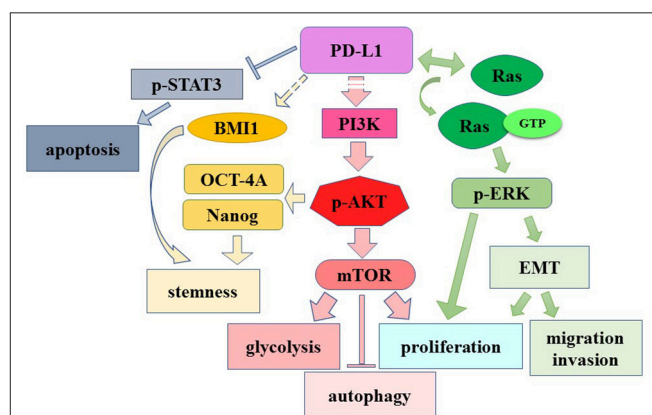


FIGURE 3 | The role of cell-intrinsic PD-L1 in modulating signaling pathway. Dashed lines: unknown mechanisms. →, induction or activation; ⇌, binding.

TABLE 3 | The therapeutic effects of PD-1 antibody in glioma patients.

Glioma type	Antibody	Time to progression		Survival		References
		Months	P-value	Months	P-value	
HGG	Pembrolizumab (<i>n</i> = 24)	1.4	range 0.2–9.4	4	range 0.5–13.8	Reiss et al., 2017
DIPG	reRT with Nivolumab vs. reRT (<i>n</i> = 31)	4.2 vs. 4.1	0.90	22.9 vs. 20.4	0.44	Kline et al., 2018
HGG	Nivolumab with Bevacizumab (<i>n</i> = 50)	4.3	95% CI (3.5–5.3)	6.5	95% CI (6.0–8.8)	Mantica et al., 2018
GBM	Nivolumab (<i>n</i> = 11) vs. Pembrolizumab (<i>n</i> = 19)	3.8 vs. 2.3	0.08	10.9 vs. 5.3	0.2	Kurz et al., 2018
GBM	Nivo3 (<i>n</i> = 10) vs. Nivo1+Ipi3 (<i>n</i> = 10) vs. Nivo3+Ipi1 (<i>n</i> = 20)	1.9 vs. 1.5 vs. 2.1	95% CI (1.3–4.6); (0.5–2.8); (1.4–2.8)	10.4 vs. 9.2 vs. 7.3	95% CI (4.1–22.8; 3.9–12.7; 4.7; 12.9)	Omuro et al., 2018
GBM	Pembrolizumab (<i>n</i> = 10)			2.6 Media OS from start of PBZ	range 0.4–11.6	Blumenthal et al., 2016
GBM (bMMRD)	Nivolumab (<i>n</i> = 2)			>9		Bouffet et al., 2016
GBM	Nivolumab (<i>n</i> = 1)			>24		Roth et al., 2017

reRT, reirradiation; Nivo3, nivolumab 3 mg/kg every 2 weeks; Nivo1+Ipi3, nivolumab 1 mg/kg + ipilimumab 3 mg/kg every 3 weeks for 4 doses, then nivolumab 3 mg/kg every 2 weeks; Nivo3+Ipi1, nivolumab 3 mg/kg + ipilimumab 1 mg/kg every 3 weeks for 4 doses, then nivolumab 3 mg/kg Q2W every 2 weeks.

alone or in combination with bevacizumab (*n* = 43). In a subset of patients, disease stabilization appeared in heavily pre-treated recurrent HGG (Mantica et al., 2018).

There are case reports showing that PD-1 antibody therapy have evident therapeutic effects on GBM patients. Patrick et al. reported a 60-year-old GBM patient receiving nivolumab treatment for almost 2 years after standard radiotherapy and temozolomide therapy, and magnetic resonance imaging (MRI) revealed a continuous shrinking of the tumor (Roth et al., 2017). Bouffet et al. also reported that 2 young recurrent GBM patients receiving nivolumab treatment achieved 5 and 9 month-relieve with a MRI-detected shrinkage of GBM lesions (Bouffet et al., 2016). In addition, pembrolizumab treatment increases lymphocyte infiltration in resected metastatic spinal lesion, indicating that checkpoint PD1/PD-L1 blockade may result in immune activation in central nervous system (Johanns et al., 2016). In another case of an adult GBM patient, a severe hepatitis was found to be associated with nivolumab therapy, which may impair its therapeutic effect (Simonelli et al., 2016). The therapeutic effects of PD-1 antibody in glioma are summarized in **Table 3**.

Until now, there has been no report of PD-L1 antibody therapy in glioma, however, animal studies support that PD-L1 antibody may also be effective in treatments of gliomas. Wainwright et al. reported that administration of PD-L1 antibody (clone 10F.9G2) had a long-term survival effect on mice/GL261 glioma model (60%, *n* = 10) (Wainwright et al., 2014). This effect was completely abolished in Rag1^{-/-} mice (lack functional T and B cells), implying that the therapeutic effect of PD-L1 antibody depends on immune response of glioma. However, PD-L1 antibody is unable to enhance animal survival time in a more aggressive B16-F10-derived intracranial melanoma, indicating a selective function of PD-L1 antibody in brain tumors. Reardon et al. also reported that PD-L1

antibody (339.6A2) had a long-term survival effect (25%, *n* = 8) in mice/GL261 glioma model, although slightly less potent compared to that of PD-1 antibody (Reardon et al., 2016). What is more, Saha et al. reported that administration of PD-L1 antibody (rat clone 10F.9G2) alone showed better therapeutic effects than PD-1 antibody alone, and it significantly increased mean survival time (42 days, *n* = 7; 25% increase) as compared to its mock (33.5 days, *n* = 6) in a glioma stem cell-derived glioma model (Saha et al., 2017).

PD-L1 antibody had cumulative therapeutic effects on C57 mice/GL261 orthotopic glioma when in combination with other drugs or CTLA4 antibody. Earlier supplement of methyltryptophan but not temozolomide together with PD-L1 antibody greatly enhances the long-term survival of mice bearing GL261-orthotopic glioma (Wainwright et al., 2014). Zhai et al. reported that PD-L1 in combination with CTLA4 antibodies significantly increased survival time of mice/GL261 intracranial glioma model (Zhai et al., 2017). Jiang et al. reported that intratumoral injection of oncolytic adenovirus (Delta-24-RGD expressing the immune costimulator OX40 ligand) followed by PD-L1 antibody (Bio X Cell) injection greatly improved the long-term survival rate of C57/GL261 model mice (85%), compared to viruses (28%) or antibodies (15%) injection alone (Jiang et al., 2017). Moreover, most of the survived mice (*n* = 5/6) were long-term survived after re-implantation GL261 cells in their contralateral hemispheres (rechallenge), indicating that the combination treatment induced developments of an immune memory which prevented tumor growth at a distant site. The actual therapeutic effect of PD-L1 antibody in glioma patients remains to be verified by clinical studies.

In summary, present data of clinical studies suggest that the overall effect of PD-1 antibody therapy in glioma is limited. However, its efficacy is much improved in some subtypes of glioma. The combination of immune therapy including

PD-1/PD-L1 antibodies and molecular targeted anti-tumor drugs may be a future direction of glioma therapy.

CONCLUSION

The positive rate and subcellular distribution of PD-L1 in glioma cells depend on the antibody that is used. The selection of a proper PD-L1 antibody is important in order to obtain positive results. PD-L1 is mainly upregulated in HGG and negatively correlated with the survival time of patients. Further analysis of the relationships between PD-L1 expression and other glioma molecular markers is worthy. Both positive (e.g., IFN- γ , IL-10) and negative (e.g., miR-34a, PTEN) signals are involved in the regulation of PD-L1 expression in gliomas. Comprehensive understanding of those regulatory mechanisms is beneficial for the modification of immunotherapy strategy. PD-L1 is not only associated with decreased CTL and increased Treg in glioma lesions, but also has intrinsic oncogenic roles by interacting with Ras. Intrinsic PD-L1 as well as its related signaling pathways may be also served as therapeutic targets. PD-1 antibody has limited therapeutic effects on glioma patients, while PD-L1 experimentally shows therapeutic effects in animal glioma-models. The improvement of PD-1/PD-L1 antibody-based immunotherapy relies largely on increasing clinical

data. The combination of PD-1/PD-L1 antibodies with other molecule-targeted anti-cancer drugs is prospective.

AUTHOR CONTRIBUTIONS

RC: researched literature, wrote the manuscript and contributed to discussion; FL: researched literature and wrote the manuscript; XQ: researched literature, wrote the manuscript and modified the manuscript; XC: designed, wrote, reviewed, edited the manuscript, and contributed to discussion.

FUNDING

This work was supported by grants from the National Nature Science Foundation of China (Grant No. 81471386, 81672504) and the Fundamental Research Funds for the Central Universities, HUST (Grant No. 2017KFYXJ048) to XC. We declare all sources of funding received for the research being submitted.

ACKNOWLEDGMENTS

We thank Hong Qiu for her help in graphic drawing.

REFERENCES

- Agata, Y., Kawasaki, A., Nishimura, H., Ishida, Y., Tsubata, T., Yagita, H., et al. (1996). Expression of the PD-1 antigen on the surface of stimulated mouse T and B lymphocytes. *Int. Immunol.* 8, 765–772. doi: 10.1093/intimm/8.5.765
- Ahn, B. J., Pollack, I. F., and Okada, H. (2013). Immune-checkpoint blockade and active immunotherapy for glioma. *Cancers (Basel)* 5, 1379–1412. doi: 10.3390/cancers5041379
- Almozyan, S., Colak, D., Mansour, F., Alaiya, A., Al-Harazi, O., Qattan, A., et al. (2017). PD-L1 promotes OCT4 and Nanog expression in breast cancer stem cells by sustaining PI3K/AKT pathway activation. *Int. J. Cancer* 141, 1402–1412. doi: 10.1002/ijc.30834
- Alsaab, H. O., Sau, S., Alzhrani, R., Tatiparti, K., Bhise, K., Kashaw, S. K., et al. (2017). PD-1 and PD-L1 checkpoint signaling inhibition for cancer immunotherapy: mechanism, combinations, and clinical outcome. *Front. Pharmacol.* 8:561. doi: 10.3389/fphar.2017.00561
- Ansell, S. M., Lesokhin, A. M., Borrello, I., Halwani, A., Scott, E. C., Gutierrez, M., et al. (2015). PD-1 blockade with nivolumab in relapsed or refractory Hodgkin's Lymphoma. *N. Engl. J. Med.* 372, 311–319. doi: 10.1056/NEJMoa1411087
- Antonios, J. P., Soto, H., Everson, R. G., Moughon, D., Orpilla, J. R., Shin, N. P., et al. (2017). Immunosuppressive tumor-infiltrating myeloid cells mediate adaptive immune resistance via a PD-1/PD-L1 mechanism in glioblastoma. *Neuro-Oncol.* 19, 796–807. doi: 10.1093/neuonc/now287
- Antonios, J. P., Soto, H., Everson, R. G., Orpilla, J., Moughon, D., Shin, N., et al. (2016). PD-1 blockade enhances the vaccination-induced immune response in glioma. *JCI Insight* 1:e87059. doi: 10.1172/jci.insight.87059
- Azuma, T., Yao, S., Zhu, G., Flies, A. S., Flies, S. J., and Chen, L. (2008). B7-H1 is a ubiquitous antiapoptotic receptor on cancer cells. *Blood* 111, 3635–3643. doi: 10.1182/blood-2007-11-123141
- Bellmunt, J., de Wit, R., Vaughn, D. J., Fradet, Y., Lee, J. L., Fong, L., et al. (2017). Pembrolizumab as second-line therapy for advanced urothelial carcinoma. *N. Engl. J. Med.* 376, 1015–1026. doi: 10.1056/NEJMoa1613683
- Berghoff, A. S., Kiesel, B., Widhalm, G., Rajky, O., Ricken, G., Wöhrer, A., et al. (2015). Programmed death ligand 1 expression and tumor-infiltrating lymphocytes in glioblastoma. *Neuro-Oncol.* 17, 1064–1075. doi: 10.1093/neuonc/nou307
- Berghoff, A. S., Kiesel, B., Widhalm, G., Wilhelm, D., Rajky, O., Kurscheid, S., et al. (2017). Correlation of immune phenotype with IDH mutation in diffuse glioma. *Neuro-Oncol.* 19, 1460–1468. doi: 10.1093/neuonc/now054
- Bloch, O., Crane, C. A., Kaur, R., Safaei, M., Rutkowski, M. J., and Parsa, A. T. (2013). Gliomas promote immunosuppression through induction of B7-H1 expression in tumor-associated macrophages. *Clin. Cancer Res.* 19, 3165–3175. doi: 10.1158/1078-0432.CCR-12-3314
- Bloch, O., Lim, M., Sughrue, M. E., Komotar, R. J., Abrahams, J. M., O'Rourke, D. M., et al. (2017). Autologous heat shock protein peptide vaccination for newly diagnosed glioblastoma: impact of peripheral PD-L1 expression on response to therapy. *Clin. Cancer Res.* 23, 3575–3584. doi: 10.1158/1078-0432.CCR-16-1369
- Blumenthal, D. T., Yalon, M., Vainer, G. W., Lossos, A., Yust, S., Tzach, L., et al. (2016). Pembrolizumab: first experience with recurrent primary central nervous system (CNS) tumors. *J. Neuro Oncol.* 129, 453–460. doi: 10.1007/s11060-016-2190-1
- Bouffet, E., Larouche, V., Campbell, B. B., Merico, D., de Borja, R., Aronson, M., et al. (2016). Immune checkpoint inhibition for hypermutant glioblastoma multiforme resulting from germline biallelic mismatch repair deficiency. *J. Clin. Oncol.* 34, 2206–2211. doi: 10.1200/JCO.2016.66.6552
- Chang, C. H., Qiu, J., O'Sullivan, D., Buck, M. D., Noguchi, T., Curtis, J. D., et al. (2015). Metabolic competition in the tumor microenvironment is a driver of cancer progression. *Cell* 162, 1229–1241. doi: 10.1016/j.cell.2015.08.016
- Chen, G., Huang, A. C., Zhang, W., Zhang, G., Wu, M., Xu, W., et al. (2018). Exosomal PD-L1 contributes to immunosuppression and is associated with anti-PD-1 response. *Nature* 560, 382–386. doi: 10.1038/s41586-018-0392-8
- Chen, P. L., Roh, W., Reuben, A., Cooper, Z. A., Spencer, C. N., Prieto, P. A., et al. (2016). Analysis of immune signatures in longitudinal tumor samples yields insight into biomarkers of response and mechanisms of resistance to immune checkpoint blockade. *Cancer Discov.* 6, 827–837. doi: 10.1158/2159-8290.CD-15-1545
- Clark, C. A., Gupta, H. B., Sareddy, G., Pandeswara, S., Lao, S., Yuan, B., et al. (2016). Tumor-Intrinsic PD-L1 signals regulate cell growth, pathogenesis, and autophagy in ovarian cancer and melanoma. *Cancer Res.* 76, 6964–6974. doi: 10.1158/0008-5472.CAN-16-0258
- D'Arrigo, P., Russo, M., Rea, A., Tufano, M., Guadagno, E., Del Basso De Caro, M. L., et al. (2017). A regulatory role for the co-chaperone

- FKBP51s in PD-L1 expression in glioma. *Oncotarget* 8, 68291–68304. doi: 10.18632/oncotarget.19309
- DiDomenico, J., Lamanò, J. B., Oyon, D., Li, Y., Veliceasa, D., Kaur, G., et al. (2018). The immune checkpoint protein PD-L1 induces and maintains regulatory T cells in glioblastoma. *Oncoimmunology* 7:e1448329. doi: 10.1080/2162402X.2018.1448329
- Dong, H., Strome, S. E., Salomao, D. R., Tamura, H., Hirano, F., Flies, D. B., et al. (2002). Tumor-associated B7-H1 promotes T-cell apoptosis: a potential mechanism of immune evasion. *Nat. Med.* 8, 793–800. doi: 10.1038/nm730
- Dong, H., Zhu, G., Tamada, K., and Chen, L. (1999). B7-H1, a third member of the B7 family, co-stimulates T-cell proliferation and interleukin-10 secretion. *Nat. Med.* 5, 1365–1369. doi: 10.1038/70932
- Dong, Y., Sun, Q., and Zhang, X. (2017). PD-1 and its ligands are important immune checkpoints in cancer. *Oncotarget* 8, 2171–2186. doi: 10.18632/oncotarget.13895
- Dorand, R. D., Nthale, J., Myers, J. T., Barkauskas, D. S., Avril, S., Chirieleison, S. M., et al. (2016). Cdk5 disruption attenuates tumor PD-L1 expression and promotes antitumor immunity. *Science* 353, 399–403. doi: 10.1126/science.aae0477
- Dubinski, D., Wölfer, J., Hasselblatt, M., Schneider-Hohendorf, T., Bogdahn, U., Stummer, W., et al. (2016). CD4⁺ T effector memory cell dysfunction is associated with the accumulation of granulocytic myeloid-derived suppressor cells in glioblastoma patients. *Neuro-oncology* 18, 807–818. doi: 10.1093/neuonc/nov280
- Ferris, R. L., Blumenschein, G. Jr., Fayette, J., Guigay, J., Colevas, A. D., Licitra, L., et al. (2016). Nivolumab for recurrent squamous-cell carcinoma of the head and neck. *N. Engl. J. Med.* 375, 1856–1867. doi: 10.1056/NEJMoa1602252
- Filley, A. C., Henriquez, M., and Dey, M. (2017). Recurrent glioma clinical trial, CheckMate-143: the game is not over yet. *Oncotarget* 8, 91779–91794. doi: 10.18632/oncotarget.21586
- Gajewski, T. F., Schreiber, H., and Fu, Y. X. (2013). Innate and adaptive immune cells in the tumor microenvironment. *Nat. Immunol.* 14, 1014–1022. doi: 10.1038/ni.2703
- Garber, S. T., Hashimoto, Y., Weathers, S. P., Xiu, J., Gatalica, Z., Verhaak, R. G., et al. (2016). Immune checkpoint blockade as a potential therapeutic target: surveying CNS malignancies. *Neuro-Oncol.* 18, 1357–1366. doi: 10.1093/neuonc/nov132
- Gatalica, Z., Snyder, C., Maney, T., Ghazalpour, A., Holterman, D. A., Xiao, N., et al. (2014). Programmed cell death 1 (PD-1) and its ligand (PD-L1) in common cancers and their correlation with molecular cancer type. *Cancer Epidemiol. Biomarkers Prev.* 23, 2965–2970. doi: 10.1158/1055-9965.EPI-14-0654
- Gato-Cañas, M., Zuazo, M., Arasanz, H., Ibañez-Vea, M., Lorenzo, L., Fernandez-Hinojal, G., et al. (2017). PDL1 signals through conserved sequence motifs to overcome interferon-mediated cytotoxicity. *Cell Rep.* 20, 1818–1829. doi: 10.1016/j.celrep.2017.07.075
- Han, J., Hong, Y., and Lee, Y. S. (2017). PD-L1 expression and combined status of PD-L1/PD-1-positive tumor infiltrating mononuclear cell density predict prognosis in glioblastoma patients. *J. Pathol. Transl. Med.* 51, 40–48. doi: 10.4132/jptm.2016.08.31
- Heynckes, S., Gaebelein, A., Haaker, G., Grauvogel, J., Franco, P., Mader, I., et al. (2017). Expression differences of programmed death ligand 1 in *de-novo* and recurrent glioblastoma multiforme. *Oncotarget* 8, 74170–74177. doi: 10.18632/oncotarget.18819
- Hirano, F., Kaneko, K., Tamura, H., Dong, H., Wang, S., Ichikawa, M., et al. (2005). Blockade of B7-H1 and PD-1 by monoclonal antibodies potentiates cancer therapeutic immunity. *Cancer Res.* 65, 1089–1096.
- Hodges, T. R., Ott, M., Xiu, J., Gatalica, Z., Swensen, J., Zhou, S., et al. (2017). Mutational burden, immune checkpoint expression, and mismatch repair in glioma: implications for immune checkpoint immunotherapy. *Neuro-Oncol.* 19, 1047–1057. doi: 10.1093/neuonc/nox026
- Hosseini, M., Yousefifard, M., Aziznejad, H., and Nasirinezhad, F. (2015). The effect of bone marrow-derived mesenchymal stem cell transplantation on allodynia and hyperalgesia in neuropathic animals: a systematic review with meta-analysis. *Biol. Blood Marrow Transplant.* 21, 1537–1544. doi: 10.1016/j.bbmt.2015.05.008
- Huang, J., Liu, F., Liu, Z., Tang, H., Wu, H., Gong, Q., et al. (2017). Immune checkpoint in glioblastoma: promising and challenging. *Front. Pharmacol.* 8:242. doi: 10.3389/fphar.2017.00242
- Jan, C. I., Tsai, W. C., Harn, H. J., Shyu, W. C., Liu, M. C., Lu, H. M., et al. (2018). Predictors of response to autologous dendritic cell therapy in glioblastoma multiforme. *Front. Immunol.* 9:727. doi: 10.3389/fimmu.2018.00727
- Jiang, H., Rivera-Molina, Y., Gomez-Manzano, C., Clise-Dwyer, K., Bover, L., Vence, L. M., et al. (2017). Oncolytic adenovirus and tumor-targeting immune modulatory therapy improve autologous cancer vaccination. *Cancer Res.* 77, 3894–3907. doi: 10.1158/0008-5472.CAN-17-0468
- Johanns, T. M., Miller, C. A., Dorward, I. G., Tsen, C., Chang, E., Perry, A., et al. (2016). Immunogenomics of hypermutated glioblastoma: a patient with germline POLE deficiency treated with checkpoint blockade immunotherapy. *Cancer Discov.* 6, 1230–1236. doi: 10.1158/2159-8290.CD-16-0575
- Kline, C., Liu, S. J., Duriseti, S., Banerjee, A., Nicolaides, T., Raber, S., et al. (2018). Reirradiation and PD-1 inhibition with nivolumab for the treatment of recurrent diffuse intrinsic pontine glioma: a single-institution experience. *J. Neurooncol.* 140, 629–638. doi: 10.1007/s11060-018-2991-5
- Kurz, S. C., Cabrera, L. P., Hastie, D., Huang, R., Unadkat, P., Rinne, M., et al. (2018). PD-1 inhibition has only limited clinical benefit in patients with recurrent high-grade glioma. *Neurology* 91, e1355–e1359. doi: 10.1212/WNL.0000000000006283
- Le, D. T., Uram, J. N., Wang, H., Bartlett, B. R., Kemberling, H., Eyring, A. D., et al. (2015). PD-1 blockade in tumors with mismatch-repair deficiency. *N. Engl. J. Med.* 372, 2509–2520. doi: 10.1056/NEJMoa1500596
- Lee, K. S., Lee, K., Yun, S., Moon, S., Park, Y., Han, J. H., et al. (2018). Prognostic relevance of programmed cell death ligand 1 expression in glioblastoma. *J. Neurooncol.* 136, 453–461. doi: 10.1007/s11060-017-2675-6
- Liu, Y., Carlsson, R., Ambjørn, M., Hasan, M., Badn, W., Darabi, A., et al. (2013). PD-L1 expression by neurons nearby tumors indicates better prognosis in glioblastoma patients. *J. Neurosci.* 33, 14231–14245. doi: 10.1523/JNEUROSCI.5812-12.2013
- Liu, Y., Zeng, B., Zhang, Z., Zhang, Y., and Yang, R. (2008). B7-H1 on myeloid-derived suppressor cells in immune suppression by a mouse model of ovarian cancer. *Clin. Immunol.* 129, 471–481. doi: 10.1016/j.clim.2008.07.030
- Long, G. V., Atkinson, V., Lo, S., Sandhu, S., Guminski, A. D., Brown, M. P., et al. (2018). Combination nivolumab and ipilimumab or nivolumab alone in melanoma brain metastases: a multicentre randomised phase 2 study. *Lancet Oncol.* 19, 672–681. doi: 10.1016/S1470-2045(18)30139-6
- Mantica, M., Pritchard, A., Lieberman, F., and Drappatz, J. (2018). Retrospective study of nivolumab for patients with recurrent high grade gliomas. *J. Neurooncol.* 139, 625–631. doi: 10.1007/s11060-018-2907-4
- Maxwell, R., Jackson, C. M., and Lim, M. (2017). Clinical trials investigating immune checkpoint blockade in glioblastoma. *Curr. Treat. Options Oncol.* 18:51. doi: 10.1007/s11864-017-0492-y
- Mirghorbani, M., Van Gool, S., and Rezaei, N. (2013). Myeloid-derived suppressor cells in glioma. *Expert Rev. Neurother.* 13, 1395–1406. doi: 10.1586/14737175.2013.857603
- Miyazaki, T., Ishikawa, E., Matsuda, M., Akutsu, H., Osuka, S., Sakamoto, N., et al. (2017). Assessment of PD-1 positive cells on initial and secondary resected tumor specimens of newly diagnosed glioblastoma and its implications on patient outcome. *J. Neurooncol.* 133, 277–285. doi: 10.1007/s11060-017-2451-7
- Motzer, R. J., Tannir, N. M., McDermott, D. F., Frontera, O. A., Melichar, B., Choueiri, T. K., et al. (2018). Nivolumab plus ipilimumab versus sunitinib in advanced renal-cell carcinoma. *N. Engl. J. Med.* 378, 1277–1290. doi: 10.1056/NEJMoa1712126
- Nduom, E. K., Wei, J., Yaghi, N. K., Huang, N., Kong, L. Y., Gabrusiewicz, K., et al. (2016). PD-L1 expression and prognostic impact in glioblastoma. *Neuro-Oncol.* 18, 195–205. doi: 10.1093/neuonc/nov172
- Omuro, A., Vlahovic, G., Lim, M., Sahebjam, S., Baehring, J., Cloughesy, T., et al. (2018). Nivolumab with or without ipilimumab in patients with recurrent glioblastoma: results from exploratory phase I cohorts of CheckMate 143. *Neuro-Oncol.* 20, 674–686. doi: 10.1093/neuonc/nox208
- Overman, M. J., Lonardi, S., Wong, K. Y. M., Lenz, H. J., Gelsomino, F., Aglietta, M., et al. (2018). Durable clinical benefit with nivolumab plus ipilimumab in DNA mismatch repair-deficient/microsatellite instability-high metastatic colorectal cancer. *J. Clin. Oncol.* 36, 773–779. doi: 10.1200/JCO.2017.76.9901
- Parsa, A. T., Waldron, J. S., Panner, A., Crane, C. A., Parney, I. F., Barry, J. J., et al. (2007). Loss of tumor suppressor PTEN function increases B7-H1 expression and immunoresistance in glioma. *Nat. Med.* 13, 84–88. doi: 10.1038/nm1517
- Pratt, D., Dominah, G., Lobel, G., Obungu, A., Lynes, J., Sanchez, V., et al. (2018). Programmed death ligand 1 is a negative prognostic marker

- in recurrent isocitrate dehydrogenase-wildtype glioblastoma. *Neurosurgery* doi: 10.1093/neuros/nyy268. [Epub ahead of print].
- Qiu, X. Y., Hu, D. X., Chen, W. Q., Chen, R. Q., Qian, S. R., Li, C. Y., et al. (2018). PD-L1 confers glioblastoma multiforme malignancy via Ras binding and Ras/Erk/EMT activation. *Biochim. Biophys. Acta Mol. Basis. Dis.* 1864(5 Pt A), 1754–1769. doi: 10.1016/j.bbdis.2018.03.002
- Reardon, D. A., Gokhale, P. C., Klein, S. R., Ligon, K. L., Rodig, S. J., Ramkissoon, S. H., et al. (2016). Glioblastoma eradication following immune checkpoint blockade in an orthotopic, immunocompetent model. *Cancer Immunol Res* 4, 124–135. doi: 10.1158/2326-6066.CIR-15-0151
- Reck, M., Rodríguez-Abreu, D., Robinson, A. G., Hui, R., Csoszi, T., Fülöp, A., et al. (2016). Pembrolizumab versus chemotherapy for PD-L1-positive non-small-cell lung cancer. *N. Engl. J. Med.* 375, 1823–1833. doi: 10.1056/NEJMoa1606774
- Reiss, S. N., Yerram, P., Modelevsky, L., and Grommes, C. (2017). Retrospective review of safety and efficacy of programmed cell death-1 inhibitors in refractory high grade gliomas. *J. Immunother. Cancer* 5, 99. doi: 10.1186/s40425-017-0302-x
- Robert, C., Schachter, J., Long, G. V., Arance, A., Grob, J. J., Mortier, L., et al. (2015). Pembrolizumab versus ipilimumab in advanced melanoma. *N. Engl. J. Med.* 372, 2521–2532. doi: 10.1056/NEJMoa1503093
- Roth, P., Valavanis, A., and Weller, M. (2017). Long-term control and partial remission after initial pseudoprogression of glioblastoma by anti-PD-1 treatment with nivolumab. *Neuro-Oncol.* 19, 454–456. doi: 10.1093/neuonc/now265
- Röver, L. K., Gevensleben, H., Dietrich, J., Bootz, F., Landsberg, J., Goltz, D., et al. (2018). PD-1 (PDCD1) promoter methylation is a prognostic factor in patients with diffuse lower-grade gliomas harboring isocitrate dehydrogenase (IDH) mutations. *EBioMedicine* 28, 97–104. doi: 10.1016/j.ebiom.2018.01.016
- Saha, D., Martuza, R. L., and Rabkin, S. D. (2017). Macrophage polarization contributes to glioblastoma eradication by combination immunovirotherapy and immune checkpoint blockade. *Cancer Cell* 32, 253–267. doi: 10.1016/j.ccell.2017.07.006
- Said, E. A., Dupuy, F. P., Trautmann, L., Zhang, Y., Shi, Y., El-Far, M., et al. (2010). Programmed death-1-induced interleukin-10 production by monocytes impairs CD4+ T cell activation during HIV infection. *Nat. Med.* 16, 452–459. doi: 10.1038/nm.2106
- Sanmamed, M. F., and Chen, L. (2018). A paradigm shift in cancer immunotherapy: from enhancement to normalization. *Cell* 175, 313–326. doi: 10.1016/j.cell.2018.09.035
- Shergalis, A., Bankhead, A. III., Luesakul, U., Muangsin, N., and Neamati, N. (2018). Current challenges and opportunities in treating glioblastoma. *Pharmacol. Rev.* 70, 412–445. doi: 10.1124/pr.117.014944
- Shinohara, T., Taniwaki, M., Ishida, Y., Kawaichi, M., and Honjo, T. (1994). Structure and chromosomal localization of the human PD-1 gene (PDCD1). *Genomics* 23, 704–706. doi: 10.1006/geno.1994.1562
- Simonelli, M., Di Tommaso, L., Baretta, M., and Santoro, A. (2016). Pathological characterization of nivolumab-related liver injury in a patient with glioblastoma. *Immunotherapy* 8, 1363–1369. doi: 10.2217/imt-2016-0057
- Spranger, S., Spaepen, R. M., Zha, Y., Williams, J., Meng, Y., Ha, T. T., et al. (2013). Up-regulation of PD-L1, IDO, and T(regs) in the melanoma tumor microenvironment is driven by CD8+ T cells. *Sci. Transl. Med.* 5, 200ra116. doi: 10.1126/scitranslmed.3006504
- Stupp, R., Hegi, M. E., Mason, W. P., van den Bent, M. J., Taphoorn, M. J., Janzer, R. C., et al. (2009). Effects of radiotherapy with concomitant and adjuvant temozolomide versus radiotherapy alone on survival in glioblastoma in a randomised phase III study: 5-year analysis of the EORTC-NCIC trial. *Lancet Oncol.* 10, 459–466. doi: 10.1016/S1470-2045(09)70025-7
- Stupp, R., Mason, W. P., van den Bent, M. J., Weller, M., Fisher, B., Taphoorn, M. J., et al. (2005). Radiotherapy plus concomitant and adjuvant temozolomide for glioblastoma. *N. Engl. J. Med.* 352, 987–996. doi: 10.1056/NEJMoa043330
- Taube, J. M., Anders, R. A., Young, G. D., Xu, H., Sharma, R., McMiller, T. L., et al. (2012). Colocalization of inflammatory response with B7-h1 expression in human melanocytic lesions supports an adaptive resistance mechanism of immune escape. *Sci. Transl. Med.* 4, 127ra137. doi: 10.1126/scitranslmed.3003689
- Tran, B., and Rosenthal, M. A. (2010). Survival comparison between glioblastoma multiforme and other incurable cancers. *J. Clin. Neurosci.* 17, 417–421. doi: 10.1016/j.jocn.2009.09.004
- Wainwright, D. A., Chang, A. L., Dey, M., Balyasnikova, I. V., Kim, C. K., Tobias, A., et al. (2014). Durable therapeutic efficacy utilizing combinatorial blockade against IDO, CTLA-4, and PD-L1 in mice with brain tumors. *Clin. Cancer Res.* 20, 5290–5301. doi: 10.1158/1078-0432.CCR-14-0514
- Wang, Y., Wang, H., Yao, H., Li, C., Fang, J. Y., and Xu, J. (2018). Regulation of PD-L1: emerging routes for targeting tumor immune evasion. *Front. Pharmacol.* 9:536. doi: 10.3389/fphar.2018.00536
- Wang, Y., and Wang, L. (2017). miR-34a attenuates glioma cells progression and chemoresistance via targeting PD-L1. *Biotechnol. Lett.* 39, 1485–1492. doi: 10.1007/s10529-017-2397-z
- Wang, Z., Zhang, C., Liu, X., Wang, Z., Sun, L., Li, G., et al. (2016). Molecular and clinical characterization of PD-L1 expression at transcriptional level via 976 samples of brain glioma. *Oncoimmunology* 5:e1196310. doi: 10.1080/2162402X.2016.1196310
- Wilmotte, R., Burkhardt, K., Kindler, V., Belkouch, M. C., Dussex, G., Tribolet, N., et al. (2005). B7-homolog 1 expression by human glioma: a new mechanism of immune evasion. *Neuroreport* 16, 1081–1085. doi: 10.1097/00001756-200507130-00010
- Wintterle, S., Schreiner, B., Mitsdoerffer, M., Schneider, D., Chen, L., Meyermann, R., et al. (2003). Expression of the B7-related molecule B7-H1 by glioma cells: a potential mechanism of immune paralysis. *Cancer Res.* 63, 7462–7467.
- Wolchok, J. D., Chiarion-Sileni, V., Gonzalez, R., Rutkowski, P., Grob, J. J., Cowey, C. L., et al. (2017). Overall survival with combined nivolumab and ipilimumab in advanced melanoma. *N. Engl. J. Med.* 377, 1345–1356. doi: 10.1056/NEJMoa1709684
- Xiao, Z. X., Chen, R. Q., Hu, D. X., Xie, X. Q., Yu, S. B., and Chen, X. Q. (2017). Identification of repaglinide as a therapeutic drug for glioblastoma multiforme. *Biochem. Biophys. Res. Commun.* 488, 33–39. doi: 10.1016/j.bbrc.2017.04.157
- Xiu, J., Piccioni, D., Juarez, T., Pingle, S. C., Hu, J., Rudnick, J., et al. (2016). Multi-platform molecular profiling of a large cohort of glioblastomas reveals potential therapeutic strategies. *Oncotarget* 7, 21556–21569. doi: 10.18632/oncotarget.7722
- Xue, S., Hu, M., Iyer, V., and Yu, J. (2017c). Blocking the PD-1/PD-L1 pathway in glioma: a potential new treatment strategy. *J. Hematol. Oncol.* 10, 81. doi: 10.1186/s13045-017-0455-6
- Xue, S., Hu, M., Li, P., Ma, J., Xie, L., Teng, F., et al. (2017a). Relationship between expression of PD-L1 and tumor angiogenesis, proliferation, and invasion in glioma. *Oncotarget* 8, 49702–49712. doi: 10.18632/oncotarget.17922
- Xue, S., Song, G., and Yu, J. (2017b). The prognostic significance of PD-L1 expression in patients with glioma: a meta-analysis. *Sci. Rep.* 7, 4231. doi: 10.1038/s41598-017-04023-x
- Zeng, J., Zhang, X. K., Chen, H. D., Zhong, Z. H., Wu, Q. L., and Lin, S. X. (2016). Expression of programmed cell death-ligand 1 and its correlation with clinical outcomes in gliomas. *Oncotarget* 7, 8944–8955. doi: 10.18632/oncotarget.6884
- Zhai, L., Ladomersky, E., Dostal, C. R., Lauing, K. L., Swoap, K., Billingham, L. K., et al. (2017). Non-tumor cell IDO1 predominantly contributes to enzyme activity and response to CTLA-4/PD-L1 inhibition in mouse glioblastoma. *Brain Behav. Immun.* 62, 24–29. doi: 10.1016/j.bbi.2017.01.022
- Zhang, Y., Pan, C., Wang, J., Cao, J., Liu, Y., Wang, Y., et al. (2017). Genetic and immune features of resectable malignant brainstem gliomas. *Oncotarget* 8, 82571–82582. doi: 10.18632/oncotarget.19653
- Zhao, L., Li, C., Liu, F., Zhao, Y., Liu, J., Hua, Y., et al. (2017). A blockade of PD-L1 produced antitumor and antimetastatic effects in an orthotopic mouse pancreatic cancer model via the PI3K/Akt/mTOR signaling pathway. *Onco. Targets. Ther.* 10, 2115–2126. doi: 10.2147/OTT.S130481
- Zheng, F., Dang, J., Zha, H., Zhang, B., Lin, M., and Cheng, F. (2017). PD-L1 Promotes self-renewal and tumorigenicity of malignant melanoma initiating cells. *Biomed Res. Int.* 2017, 1293201. doi: 10.1155/2017/1293201

Conflict of Interest Statement: The authors declare that the research was conducted in the absence of any commercial or financial relationships that could be construed as a potential conflict of interest.

Copyright © 2019 Chen, Liu, Qiu and Chen. This is an open-access article distributed under the terms of the Creative Commons Attribution License (CC BY). The use, distribution or reproduction in other forums is permitted, provided the original author(s) and the copyright owner(s) are credited and that the original publication in this journal is cited, in accordance with accepted academic practice. No use, distribution or reproduction is permitted which does not comply with these terms.



Y₆, an Epigallocatechin Gallate Derivative, Reverses ABCG2-Mediated Mitoxantrone Resistance

Rui-Qiang Zhao^{1,2,3†}, Yan Wen^{3,4†}, Pranav Gupta³, Zi-Ning Lei³, Chao-Yun Cai³, Gang Liang⁵, Dong-Hua Yang³, Zhe-Sheng Chen^{3*} and Yu-An Xie^{1*}

¹ The Affiliated Tumor Hospital of Guangxi Medical University, Nanning, China, ² Department of Biochemistry and Molecular Biology, School of Preclinical Medicine, Guangxi Medical University, Nanning, China, ³ Department of Pharmaceutical Sciences, College of Pharmacy and Health Sciences, St. John's University, Queens, NY, United States, ⁴ Department of Pharmacy, The First Affiliated Hospital of Guangxi Medical University, Nanning, China, ⁵ College of Pharmacy, Guangxi Medical University, Nanning, China

OPEN ACCESS

Edited by:

Salvatore Salomone,
Università degli Studi di Catania, Italy

Reviewed by:

Jun Lin,
Stony Brook University, United States
Ian Kerr,
The University of Nottingham,
United Kingdom
Kenneth K. W. To,
The Chinese University of Hong Kong,
China

*Correspondence:

Zhe-Sheng Chen
chenz@stjohns.edu
Yu-An Xie
gxxya@allyun.com

[†] These authors have contributed
equally to this work

Specialty section:

This article was submitted to
Experimental Pharmacology
and Drug Discovery,
a section of the journal
Frontiers in Pharmacology

Received: 05 September 2018

Accepted: 18 December 2018

Published: 10 January 2019

Citation:

Zhao R-Q, Wen Y, Gupta P,
Lei Z-N, Cai C-Y, Liang G, Yang D-H,
Chen Z-S and Xie Y-A (2019) Y₆, an
Epigallocatechin Gallate Derivative,
Reverses ABCG2-Mediated
Mitoxantrone Resistance.
Front. Pharmacol. 9:1545.
doi: 10.3389/fphar.2018.01545

Multidrug resistance is reported to be related to the transmembrane transportation of chemotherapeutic drugs by adenosine triphosphate-binding cassette (ABC) transporters. ABC subfamily G member 2 (ABCG2) is a member of the ABC transporter superfamily proteins, which have been implicated as a key contributor to the development of multidrug resistance in cancers. A new epigallocatechin gallate derivative, Y₆ was synthesized in our group. Our previous study revealed that Y₆ increased the sensitivity of drug-resistant cells to doxorubicin, which was associated with down-regulation of P-glycoprotein expression. In this study, we further determine whether Y₆ could reverse ABCG2-mediated multidrug resistance. Results showed that, at non-toxic concentrations, Y₆ significantly sensitized drug-selected non-small cell lung cancer cell line NCI-H460/MX20 to substrate anticancer drugs mitoxantrone, SN-38, and topotecan, and also sensitized ABCG2-transfected cell line HEK293/ABCG2-482-R2 to mitoxantrone and SN-38. Further study demonstrated that Y₆ significantly increased the accumulation of [³H]-mitoxantrone in NCI-H460/MX20 cells by inhibiting the transport activity of ABCG2, without altering the expression levels and the subcellular localization of ABCG2. Furthermore, Y₆ stimulated the adenosine triphosphatase activity with a concentration-dependent pattern under 20 μM in membranes overexpressing ABCG2. In addition, Y₆ exhibited a strong interaction with the human ABCG2 transporter protein. Our findings indicate that Y₆ may potentially be a novel reversal agent in ABCG2-positive drug-resistant cancers.

Keywords: epigallocatechin gallate (EGCG), 5, 3', 4', 3'', 4'', 5''-6-O-ethyl-EGCG (Y₆), ABC transporter, ABCG2, multidrug resistance

INTRODUCTION

Multidrug resistance (MDR) to chemotherapeutic drugs could be found in various types of cancer cells (Fletcher et al., 2010). A wide range of structurally different chemotherapeutic drugs have been shown to be substrates of ATP-binding cassette (ABC) transporter proteins. Powered by the energy from ATP hydrolysis, ABC-transporters have become a significant impediment in cancer therapy.

In total, 48 different ABC transporters were identified in the human genome, divided to seven subfamilies (ABCA-ABCG) due to structural similarities. Among all subfamilies, P-glycoprotein (P-gp/ABCB1) and breast cancer resistance protein (BCRP/ABCG2) are major transporters in MDR (Sodani et al., 2012).

ABCG2 is also known as mitoxantrone resistance-associated protein (MXR) or placenta-specific ATP-binding cassette transporter (ABCP) (Miyake et al., 1999; Dean and Allikmets, 2001). The ABCG2 protein has a molecular weight of 72-kDa. It is a half transporter with one nucleotide binding domain (NBD) and one transmembrane domain (TMD) and functions in the form of homodimer or an oligomer (Taylor et al., 2017). ABCG2 transporter is specifically distributed in the plasma membrane. Normally, it is highly expressed in the colon epithelium, the apical surface of small intestines, the canalicular membrane of liver and bile duct, cortical tubules of the kidney and prostate epithelium, and at the luminal surfaces of microvessel endothelium of human brain (Maliepaard et al., 2001; Fetsch et al., 2006). Such distribution results in alteration of the absorption, distribution, metabolism, and elimination of drugs since ABCG2 performs compound transmembrane transport on secretory surfaces of organs. ABCG2 could transport a variety of anti-neoplastic drugs such as mitoxantrone, topotecan, irinotecan, doxorubicin, daunorubicin, 9-aminocamptothecin, and epirubicin as its substrates (Doyle and Ross, 2003).

A mutation at position 482 (Arg or R) of ABCG2 produces a distinct substrate preference (Chen et al., 2003), which results in different drug-binding and drug-efflux capacity of the transporter (Honjo et al., 2001; Pozza et al., 2006; Dai et al., 2009). For example, after Arg at position 482 was replaced by threonine (Thr or T) or glycine (Gly or G), the substrate specificity was changed in both mutant and wild-type variants. Mitoxantrone and major nucleoside inhibitors are common substrates of wild-type and mutant ABCG2, while daunorubicin is the substrate of mutant Gly and Thr variants and is not a substrate of the wild-type ABCG2 (Ejendal and Hrycyna, 2002; Mao and Unadkat, 2005; Ejendal et al., 2006).

Multidrug resistance in acute myeloid leukemia (AML), non-small cell lung cancer (NSCLC), colon carcinoma and breast cancer were also reported to be strongly correlated with the overexpression of ABCG2 (Steinbach et al., 2002; van den Heuvel-Eibrink et al., 2002; Nakanishi and Ross, 2012). Notably, ABCG2 is overexpressed only in subpopulations of AML specimens (Abbott et al., 2002; Suvannasankha et al., 2004). The overexpression of ABCG2 in these subpopulations of stem cells was also reported among other tumors such as neuroblastomas, Ewing sarcomas, breast cancer, small cell lung cancer, and glioblastomas (Hirschmann-Jax et al., 2004). These stem cells with overexpression of ABCG2 may play an important role in resistance to chemotherapeutic drugs.

As one of the MDR reversal modulators, epigallocatechin gallate (EGCG) was revealed to down-regulate P-gp and BCRP in a tamoxifen resistant cancer cell line (Farabegoli et al., 2010). Furthermore, EGCG (Figure 1A) was reported to significantly

inhibit proliferation of a drug-resistant cancer cell line, BEL-7404/DOX, *in vitro* when co-administered with doxorubicin (Liang et al., 2010). However, the application of EGCG was limited due to an unstable chemical profile that could be subjected to rapid oxidation and short duration of action because of multiple phenolic hydroxyl groups (Lee et al., 2002). Inspired by the structure of EGCG, we synthesized Y₆ (Figure 1B), an ethylation product of EGCG. Y₆ has been evaluated as a reversal agent that specifically reverses ABC transporter-mediated MDR *in vitro* (Wen et al., 2017). In this study, we determined the potential effect of Y₆ as a reversal agent that re-sensitizes ABCG2-mediated MDR *in vitro*.

MATERIALS AND METHODS

Reagents

Y₆ (purity 96.87%) was synthesized in our research group and was made in a 10 mM stock solution in dimethylsulfoxide (DMSO). Dulbecco's modified Eagle's medium (DMEM), penicillin/streptomycin, trypsin 0.25%, fetal bovine serum (FBS) and bovine calf serum were purchased from Hyclone (GE Healthcare Life Science, Pittsburgh, PA, United States). Mitoxantrone, SN-38, topotecan, and cisplatin were products from Sigma-Aldrich (St. Louis, MO, United States). Fumitremorgin C (FTC) was provided by Dr. Susan E. Bates from NIH (Bethesda, MD, United States). [³H]-Mitoxantrone was purchased from Moravsek Biochemicals, Inc. (Brea, CA, United States). Mouse monoclonal ABCG2 antibody and mouse monoclonal β -actin antibody were purchased from Gene Tex, Inc. (Irvine, CA, United States). Goat anti-mouse IgG secondary antibody conjugated with Alexa Fluor 488 and 4',6-diamidino-2-phenylindole (DAPI) were purchased from Thermo Fisher Scientific, Inc. (Rockford, IL, United States). The ATPase assay kit and membrane vesicles were purchased from BD Biosciences (San Jose, CA, United States). PBS and trypsin were purchased from Bosterbio (Pleasanton, CA, United States). RIPA lysis buffer, protein loading buffer, BCA protein assay kit, SDS-PAGE gel preparation kit, protein marker, western transfer buffer, SDS-PAGE running buffer, primary/secondary antibody dilution buffer were purchased from Sigma-Aldrich (St. Louis, MO, United States).

Cell Lines and Cell Culture

Non-small cell lung cancer cell line NCI-H460 and its mitoxantrone-selected ABCG2-overexpressing NCI-H460/MX20 cells were used in the ABCG2 reversal study. NCI-H460/MX20 cells were cultured in a medium containing 20 nM of mitoxantrone. HEK293/pcDNA3.1 and wild-type HEK293/ABCG2-482-R2 were established by transfecting HEK293 cells with either an empty pcDNA3.1 vector or a vector containing full length ABCG2 with Arg at position 482. HEK293/ABCG2-482-R2 cells were cultured in a medium containing 2 mg/mL of G418. All the cell lines were maintained in DMEM containing 10% (v/v) FBS and

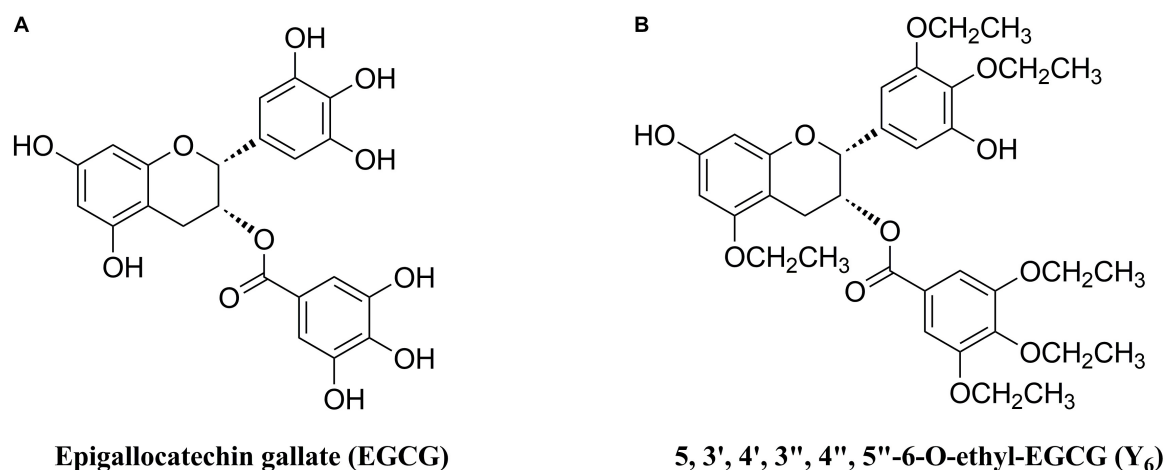


FIGURE 1 | Chemical structures of (A) EGCG and (B) Y₆.

1% (v/v) penicillin/streptomycin in a constant temperature incubator containing 5% CO₂ at 37°C.

Cytotoxicity by MTT Assay

The viability of NCI-H460 and NCI-H460/MX20 cells or HEK293/pcDNA3.1 and HEK293/ABCG2-482-R2 cells to chemotherapeutic drugs was measured for the ABCG2 reversal study using the MTT assay. Cells (5000 cells per well) were seeded into 96-well microplates with 160 µL per well and cultured overnight. Mitoxantrone, SN-38, topotecan, and cisplatin were diluted with PBS to a series of various concentrations and added to designated wells (20 µL per well) with or without the reversal agents (Y₆ and FTC) (20 µL per well). Cells were incubated for 72 h at 37°C. Then, 20 µL of MTT solution (4 mg/mL, in PBS) was added into each well and incubated for 4 h at 37°C in dark. Then the supernatant medium was discarded and 100 µL of DMSO was added to each well for formazan dissolution. Finally, the light absorbance at 490 nm was measured using the OPSYS microplate reader (Dynex Technology, Chantilly, VA, United States). FTC was used as positive reversal agent of ABCG2.

Western Blotting Analysis

NCI-H460/MX20 cells were treated with or without Y₆ for 72 h with different drug concentrations (5, 10, 15 µM). In addition, NCI-H460/MX20 cells were also treated with or without 10 µM of Y₆ for different time periods (24, 48, 72 h). Then cells were collected and lysed in ice-cold lysis buffer containing 50 mM Tris (pH 7.4), 150 mM NaCl, 1% Triton X-100, 0.1% SDS, 1 mM EDTA, and 1× phosphatase inhibitor cocktail on ice for 20 min. Cell lysates were centrifuged at 4°C at 13,000 rpm/min for 10 min. Subsequently, the supernatant was collected in Eppendorf tubes and protein concentrations were determined by bicinchoninic acid (BCATM)-based protein assay (Thermo Scientific, Rockford, IL, United States). Equal amount of protein was loaded and separated by SDS-polyacrylamide gel electrophoresis and

transferred to a polyvinylidene fluoride (PVDF) membrane through electrophoresis. The PVDF membrane was submerged in 5% skim milk for 1 h, and then was incubated with primary monoclonal antibodies (ABCG2 at 1:500 dilution or β-actin at 1:1000 dilution) overnight at 4°C. After the membrane was washed with the TBST buffer, the membrane was incubated with HRP (horseradish peroxidase)-conjugated secondary antibody (1:1000 dilution) at room temperature for 2 h. The washing with TBST buffer, the membrane was exposed to Infrared Imaging System to visualize the bands.

Immunofluorescence of ABCG2

Equal amounts of NCI-H460 and NCI-H460/MX20 cells were seeded in sterile coated 24-well plates and were cultured overnight. NCI-H460/MX20 cells were treated with or without 10 µM of Y₆ for different time periods (24, 48, 72 h). Then the cells were fixed in 4% paraformaldehyde for 15 min, permeabilized by 0.25% Triton X-100 for 15 min and then blocked with 6% BSA for 1 h. Cells were further incubated with mouse monoclonal antibody against ABCG2 (1:200) overnight, and then were submerged in Alexa Fluor 488 conjugated secondary antibody (1:2000) solution in the dark for 2 h to localize ABCG2. 2-(4-aminophenyl)-6-indolecarbamide dihydrochloride (DAPI) solution was used to counterstain the nuclei in dark. Images were taken with an inverted IX70 microscope (Olympus, Center Valley, PA, United States) following our previous protocol (Guo et al., 2014).

[³H]-Mitoxantrone Accumulation Assay

The accumulation of [³H]-mitoxantrone in NCI-H460 and NCI-H460/MX20 was measured in the presence or absence of inhibitors (FTC or Y₆). The cells (5 × 10⁶) in each centrifuge tube were trypsinized, resuspended, and pre-incubated with PBS, Y₆ (5 and 10 µM), or FTC (5 µM) for 2 h at 37°C. After the cell suspension was centrifuged at 1500 rpm/min for 5 min, the supernatant was discarded. Subsequently, cells were

resuspended in medium containing 0.1 μM [^3H]-mitoxantrone at 37°C for 2 h in the presence or absence of inhibitors following above treatment. Cells were washed three times with ice-cold PBS. Then, cells were placed in 5 ml scintillation liquid and their radioactivity was measured in the Packard TRI-CARB 1900CA liquid scintillation analyzer (Packard Instrument, Downers Grove, IL, United States) (Sun et al., 2012; Patel et al., 2013). FTC was used as the positive reversal agent of ABCG2.

[^3H]-Mitoxantrone Efflux Assay

Mitoxantrone drug efflux in NCI-H460 or NCI-H460/MX20 was measured. The cells were pretreated with PBS, Y₆ (5 and 10 μM) or FTC (5 μM) for 2 h at 37°C. Then radioactive substrate [^3H]-mitoxantrone was added and the cells were further incubated for 2 h. Cell suspension was centrifuged at 1500 rpm/min for 5 min and the supernatant was discarded. The cells were re-supplemented with fresh medium with or without a reversal agent. After 0, 30, 60, and 120 min, the aliquots of cells were removed and washed three times with ice-cold PBS immediately. Radioactivity was then measured as described in the accumulation assay above.

ABCG2 ATPase Assay

The vanadate-sensitive ATPase activity of ABCG2 was performed by an ATPase assay kit from BD Biosciences (San Jose, CA, United States) as previously described (Zhang et al., 2016). Briefly, the ABCG2 membrane vesicles were incubated in ATPase buffer with or without vanadate for 5 min at 37°C. Y₆ was then added to the assay buffer in concentration gradient (0–40 μM). The mixtures were incubated for 5 min at 37°C. Then Mg-ATP solution was added to assay buffer and was incubated for 20 min at 37°C. The mixture was added with 100 μL of 5% SDS solution and then its light absorption was detected at 880 nm using a spectrophotometer.

Molecular Docking of Y₆ With ABCG2 Model

Molecular modeling was performed with Maestro v11.1 (Schroëdinger, LLC, New York, NY, United States 2017) software (Zhang et al., 2017). The protein preparation of wild-type human ABCG2 (PDB ID: 6FFC) (Jackson et al., 2018) was essentially performed and the grid (30 Å) was generated by selecting the same binding pocket as the two substrates (MZ29) in TMD. After that, the structure of Y₆ was built and prepared. Compound Y₆ with best-scored conformation was obtained through Glide XP docking then was used to generate receptor grid for induced-fit docking (IFD). The IFD protocol with default parameters was performed and the docking score (kcal/mol) was obtained.

Statistical Analysis

The data were analyzed using a *t*-test method. All values represent the mean \pm standard deviation SD of three independent experiments performed in triplicate. The priori *p*-value for significance was *p* < 0.05.

RESULTS

Y₆ Sensitized ABCG2-Overexpressing Cells to Chemotherapeutic Drugs

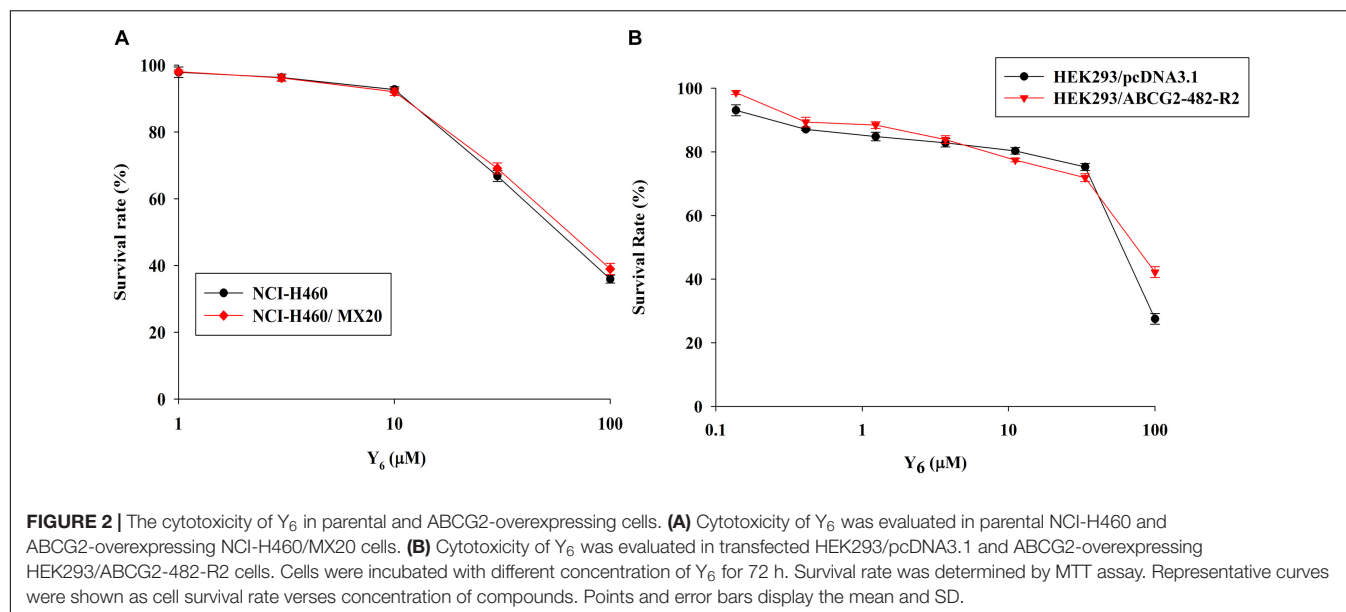
In order to investigate the reversal effects of Y₆ on drug-resistant cells, we first examined the sensitivity of ABCG2-overexpressing cells to Y₆. Based on the results from the cytotoxicity assay, two non-toxic concentrations of Y₆ (5.0 and 10.0 μM) were selected for further experimentation (Figures 2A,B).

In the sensitization experiment, mitoxantrone-selected NCI-H460/MX20 cells showed a much higher IC₅₀ value to ABCG2 substrates (mitoxantrone, SN-38, and topotecan) than that in parental NCI-H460 cells. Y₆ at both 5.0 and 10.0 μM were able to significantly increase the sensitivity of NCI-H460/MX20 cells to mitoxantrone, SN-38, and topotecan. A significant reduction in IC₅₀ values was observed with the treatment of Y₆ in NCI-H460/MX20 cells as shown in Table 1. Meanwhile, no significant changes in IC₅₀ values were observed in parental NCI-H460 cells. Similarly, Y₆ also increased the sensitivity of transfected HEK293/ABCG2-482-R2 cells, which had a much higher IC₅₀ value to ABCG2 substrates than that in parental HEK293/pcDNA3.1 cells. Significant decrease in IC₅₀ values of mitoxantrone and SN-38 was observed

TABLE 1 | Reversal effects of Y₆ to NCI-H460 and NCI-H460/MX20 cell lines.

Compounds	IC ₅₀ \pm SD ^a (nM)			
	NCI-H460	(RF) ^b	NCI-H460/MX20	(RF)
Mitoxantrone	45.11 \pm 1.79	1.0	2670.33 \pm 105.10	59.2
+ Y ₆ 5.0 μM	34.99 \pm 4.33	0.8	1268.67 \pm 87.85	28.1*
+ Y ₆ 10.0 μM	35.69 \pm 5.67	0.8	414.16 \pm 6.86	9.2*
+ FTC 5.0 μM	27.51 \pm 2.67	0.6	532.04 \pm 19.04	11.8*
SN-38	446.21 \pm 41.04	1.0	10614.67 \pm 775.84	23.8
+ Y ₆ 5.0 μM	377.84 \pm 22.25	0.8	1831.67 \pm 116.62	4.1*
+ Y ₆ 10.0 μM	310.97 \pm 30.29	0.7	944.61 \pm 28.50	2.1*
+ FTC 5.0 μM	221.18 \pm 17.71	0.5	1048.89 \pm 57.92	2.4*
Topotecan	174.39 \pm 8.92	1.0	9041.33 \pm 535.04	51.8
+ Y ₆ 5.0 μM	60.85 \pm 4.55	0.3	1205.67 \pm 40.02	6.9*
+ Y ₆ 10.0 μM	57.78 \pm 4.83	0.3	406.49 \pm 5.97	2.3*
+ FTC 5.0 μM	61.98 \pm 5.18	0.4	629.64 \pm 26.71	3.6*
Compounds	IC ₅₀ \pm SD (μM)			
	NCI-H460	(RF)	NCI-H460/MX20	(RF)
Cisplatin	1.98 \pm 0.07	1.0	1.77 \pm 0.15	0.9
+ Y ₆ 5.0 μM	1.60 \pm 0.07	0.8	1.88 \pm 0.13	0.9
+ Y ₆ 10.0 μM	1.85 \pm 0.16	0.9	1.85 \pm 0.13	0.9
+ FTC 5.0 μM	1.85 \pm 0.03	0.9	1.77 \pm 0.03	0.9

^aIC₅₀ values are represented as mean \pm SD of three independent experiments performed in triplicate; ^bValues represent the resistance fold (RF) calculated by dividing IC₅₀ values of anticancer drug in NCI-H460 and NCI-H460/MX20 cells in presence or absence of reversal agent by the IC₅₀ value of NCI-H460 cells without reversal agent. **p* < 0.05 versus no reversal agent group.



in Y₆-present treatment of transfected HEK293/ABCG2-482-R2 cells as compared to Y₆-absent treatment, and no significant change was observed in HEK293/pcDNA3.1 cells as shown in **Table 2**. Uniformly, the efficacy of Y₆ showed a concentration-dependent pattern. Cisplatin, which is not a

substrate of ABCG2, was used as a negative control. FTC at 5.0 μM was used as a positive control to evaluate the effects of Y₆.

Based on the above results, it appeared that Y₆ could significantly reverse ABCG2-mediated MDR in both NCI-H460/MX20 and HEK293/ABCG2-482-R2 cells.

TABLE 2 | Reversal effects of Y₆ to HEK293/pcDNA3.1 and HEK293/ABCG2-482-R2 cell lines.

Compounds	IC ₅₀ ± SD ^a (nM)			
	HEK293/ pcDNA3.1	(RF) ^b	HEK293/ ABCG2-482-R2	(RF)
Mitoxantrone	76.06 ± 4.14	1.0	662.90 ± 45.40	8.7
+ Y ₆ 5.0 μM	67.91 ± 5.44	0.9	184.22 ± 11.47	2.4*
+ Y ₆ 10.0 μM	41.05 ± 4.24	0.5	84.31 ± 3.02	1.1*
+ FTC 5.0 μM	67.39 ± 7.37	0.9	94.77 ± 3.87	1.2*
SN-38	61.92 ± 1.41	1.0	571.30 ± 31.80	9.2
+ Y ₆ 5.0 μM	62.32 ± 2.59	1.0	152.24 ± 13.88	2.5*
+ Y ₆ 10.0 μM	56.64 ± 7.25	0.9	79.23 ± 7.14	1.3*
+ FTC 5.0 μM	57.41 ± 4.11	0.9	80.09 ± 7.07	1.3*

Compounds	IC ₅₀ ± SD (μM)			
	HEK293/pcDNA3.1	(RF)	HEK293/ ABCG2-482-R2	(RF)
Cisplatin	1.80 ± 0.03	1.0	1.57 ± 0.10	0.9
+ Y ₆ 5.0 μM	1.81 ± 0.02	1.0	1.75 ± 0.01	1.0
+ Y ₆ 10.0 μM	1.80 ± 0.11	1.0	1.53 ± 0.12	0.9
+ FTC 5.0 μM	1.84 ± 0.05	1.0	1.69 ± 0.10	0.9

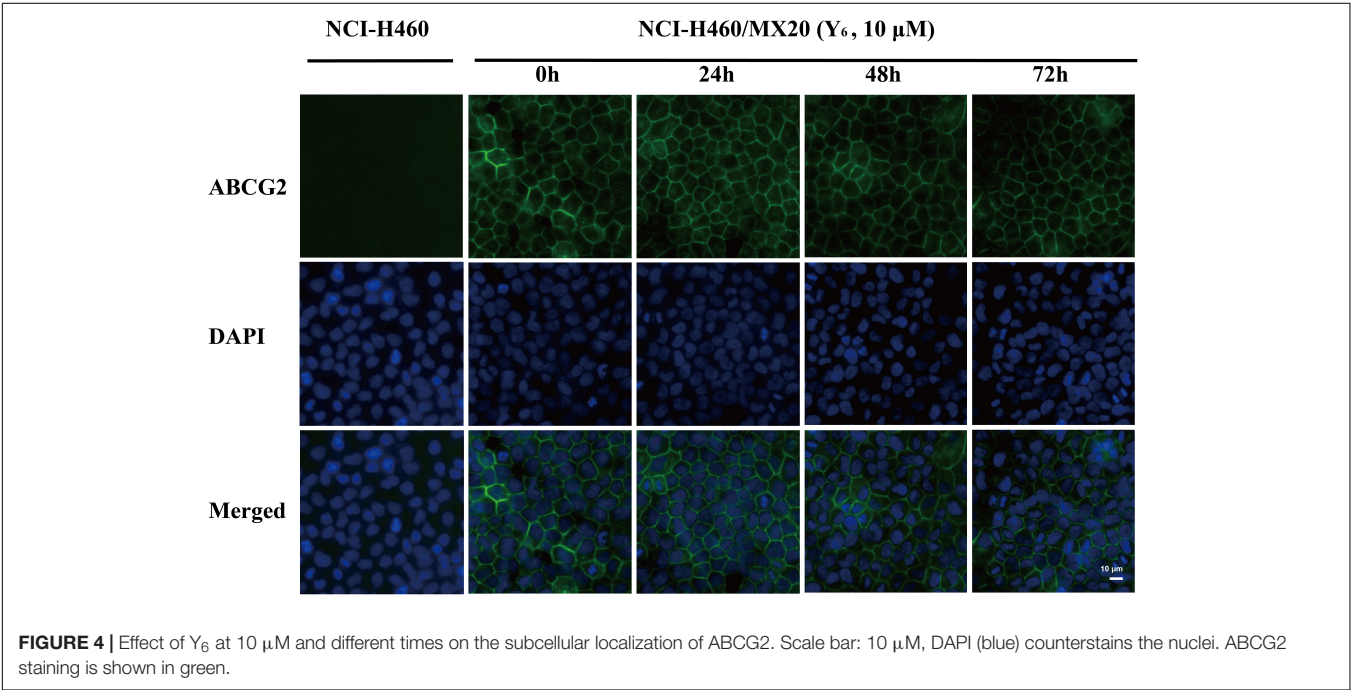
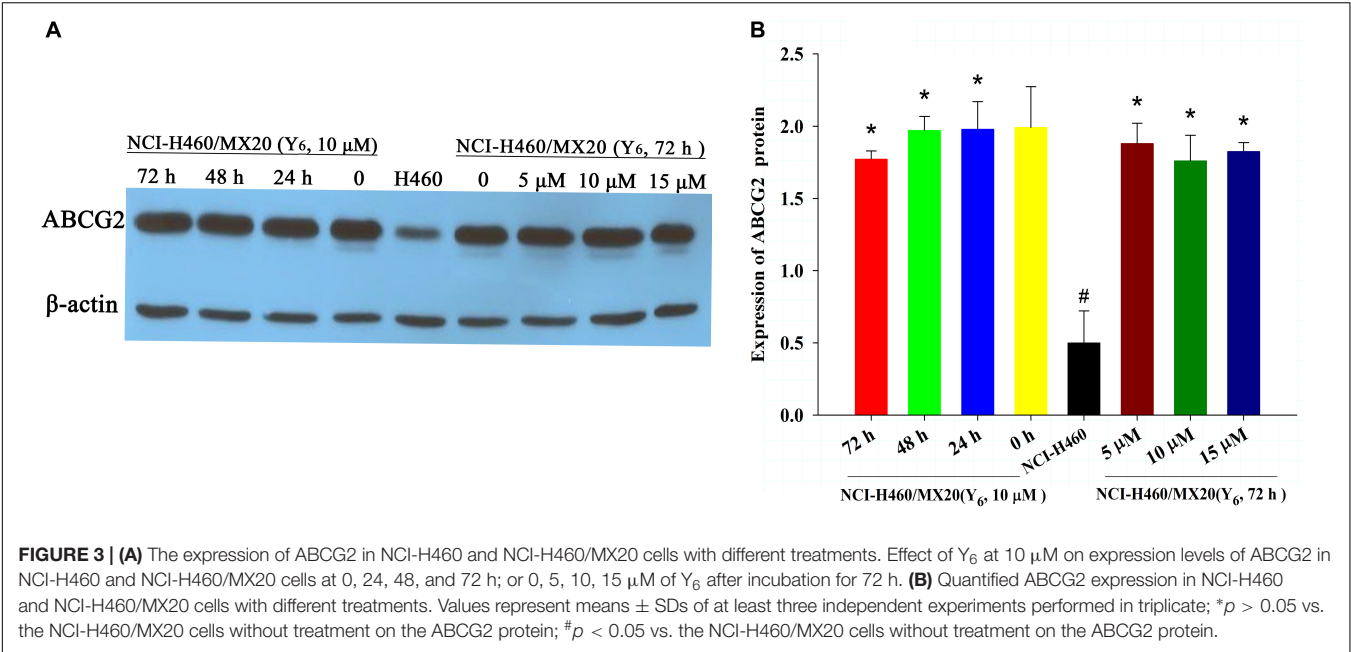
^aIC₅₀ values are represented as mean ± SD of three independent experiments performed in triplicate; ^bRF calculated by dividing IC₅₀ values of anticancer drug in HEK293/pcDNA3.1 and HEK293/ABCG2-482-R2 cells in presence or absence of reversal agent by the IC₅₀ value of HEK293/pcDNA3.1 cells without reversal agent. **p* < 0.05 versus no reversal agent group.

Y₆ Had No Effect on the Protein Expression of ABCG2 in NCI-H460/MX20 Cells

To determine the reversal mechanism of Y₆ on ABCG2-mediated MDR in cancer cells, Western blot analysis was performed using the parental NCI-H460 cells and the drug-selective NCI-H460/MX20 cells. NCI-H460/MX20 cells were incubated with either different concentrations of Y₆ (0, 5, 10, 15 μM for 72 h) or different incubation time (0, 24, 48, 72 h at 10 μM). No significant changes were observed in the expression level of ABCG2 protein in NCI-H460/MX20 cells treated with Y₆ compared to Y₆-absent treatment group (**Figures 3A,B**). The results indicated that the MDR reversal mechanism of Y₆ was not relative to the expression level of ABCG2.

Y₆ Did Not Alter the Subcellular Localization of ABCG2 in NCI-H460/MX20 Cells

As a transmembrane protein, ABCG2 could also be affected by protein localization. Thus, effect of Y₆ on ABCG2 protein cellular localization was determined with immunofluorescence assay. As is shown in **Figure 4**, Y₆ did not trigger the internalization of ABCG2 in NCI-H460/MX20 cells after incubating with 10 μM of Y₆ for 0, 24, 48, and 72 h. The results indicated that the MDR reversal mechanism of Y₆ was not induced by altering the localization of ABCG2.



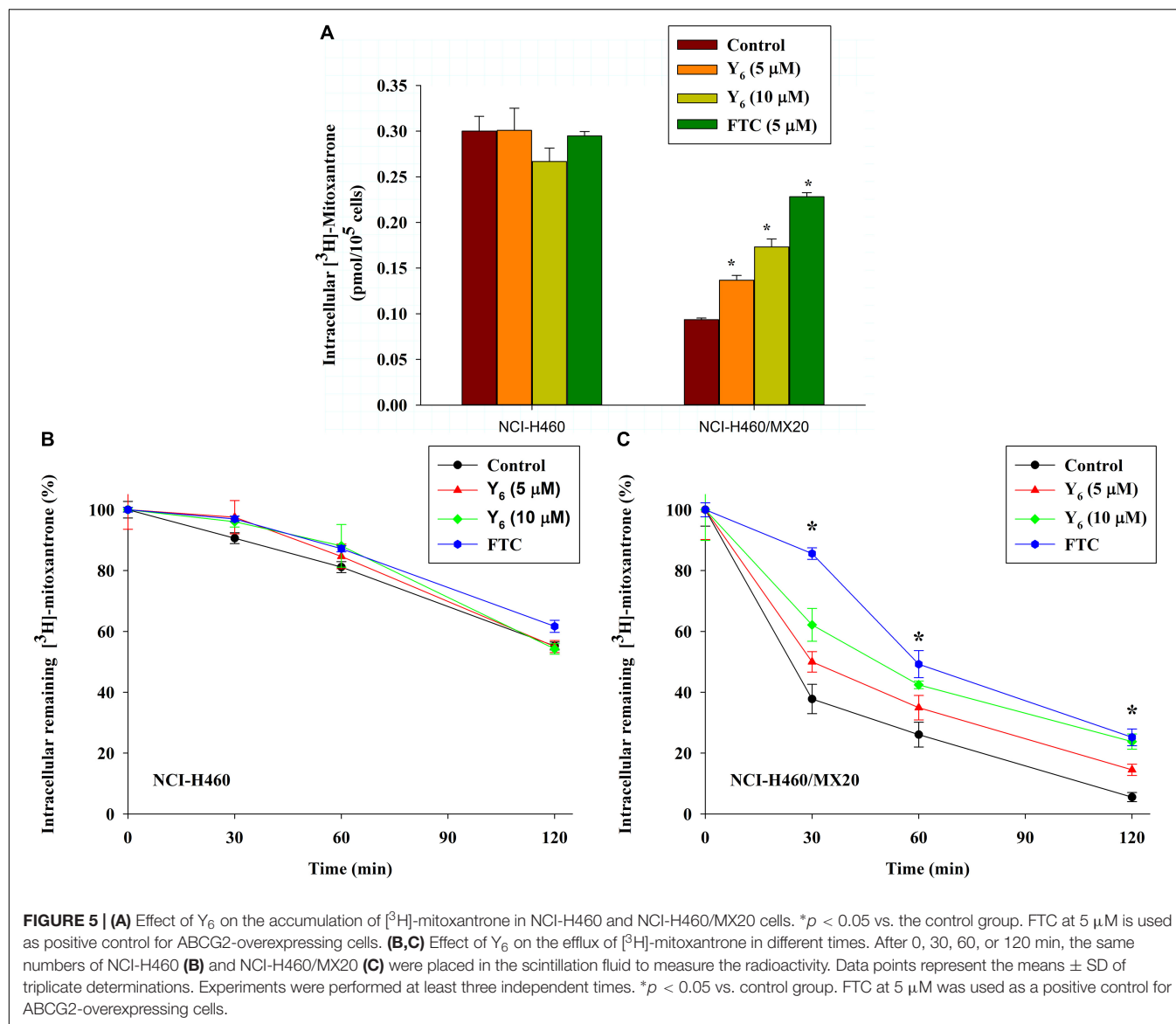
Effect of Y₆ on the Intracellular Accumulation of [³H]-Mitoxantrone

To further investigate the mechanism of reversal effect, we studied the intracellular accumulation of [³H]-mitoxantrone in NCI-H460/MX20 cells treated by Y₆. We found that the intracellular accumulation of [³H]-mitoxantrone was significantly increased in NCI-H460/MX20 cells treated with 5.0 and 10 μ M of Y₆ (Figure 5A). The accumulation increased with increasing concentrations of Y₆. However, Y₆ did not show a significant effect on the intracellular accumulation of

[³H]-mitoxantrone in parental NCI-H460 cells. The results showed that Y₆ has comparable effects to FTC (5 μ M). It could be concluded that Y₆ significantly increased intracellular concentrations of chemotherapeutic drugs in NCI-H460/MX20 cells and increased cytotoxicity in ABCG2-overexpressing cells.

Effect of Y₆ on the [³H]-Mitoxantrone Efflux Time-Course

The ABCG2 transporter is known to induce antitumor drug resistance by pumping out drugs and lowering their intracellular

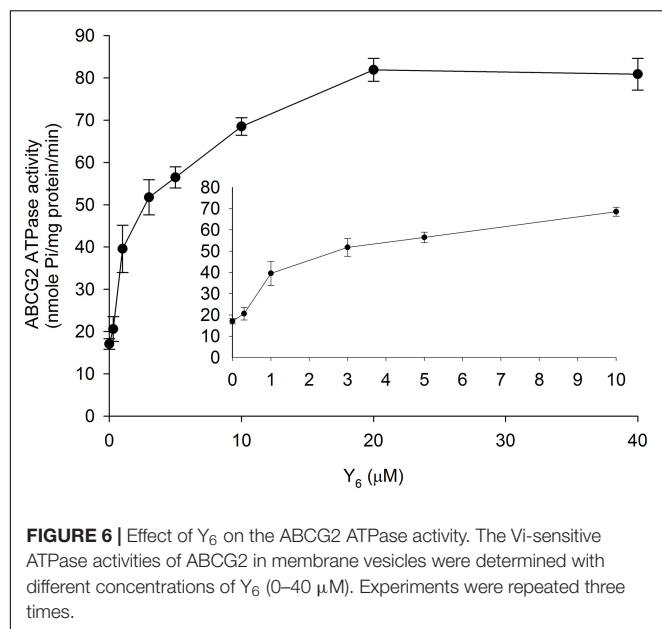


concentration. To further measure if the drug accumulation was relative with Y₆ inhibiting ABCG2-mediated drug efflux, we performed a time-course efflux of [³H]-mitoxantrone with or without Y₆ at different time points. After removing [³H]-mitoxantrone from the culture medium, efflux occurred in NCI-H460 and NCI-H460/MX20 cells as shown in **Figures 5B,C**. After NCI-H460/MX20 cells were incubated for 30 min, about 50, 38, and 62% normalized loss of [³H]-mitoxantrone occurred in Y₆-treated (5, 10 μM) groups and the control group, respectively. About 65, 58, and 73% normalized loss of [³H]-mitoxantrone, respectively, occurred with or without Y₆ after incubating for 60 min; furthermore, NCI-H460/MX20 cells lost about 86, 76, and 94% normalized [³H]-mitoxantrone, respectively, after incubating for 120 min. Meanwhile, 10 μM of Y₆ retained more [³H]-mitoxantrone in NCI-H460/MX20 cells than 5 μM of Y₆ (**Figure 5C**). Efflux pattern of NCI-H460 cells were not significantly altered by Y₆ (**Figure 5B**). The results showed

that Y₆ inhibited the efflux of [³H]-mitoxantrone in NCI-H460/MX20 cells and the retention amount in cells followed a Y₆-concentration-dependent pattern.

Effect of Y₆ on the ABCG2 ATP Hydrolysis

The ABCG2 transporter could transport substrates across the membrane by utilizing energy derived from ATP hydrolysis. To evaluate the effect of Y₆ on the ABCG2 ATP hydrolysis, we measured ATPase activity in the presence of Y₆ at a series of concentrations ranging from 0 to 40 μM. Results showed that Y₆ stimulated the ATPase activity of ABCG2 at concentrations ranging from 0 to 20 μM. No further increase in ATPase activity occurred when the concentration of Y₆ was above 20 μM (**Figure 6**), which could indicate that Y₆ stimulates the ATPase activity of ABCG2 by acting on the drug-substrate-binding site.



Docking Analysis of Y₆ With Human ABCG2 Model

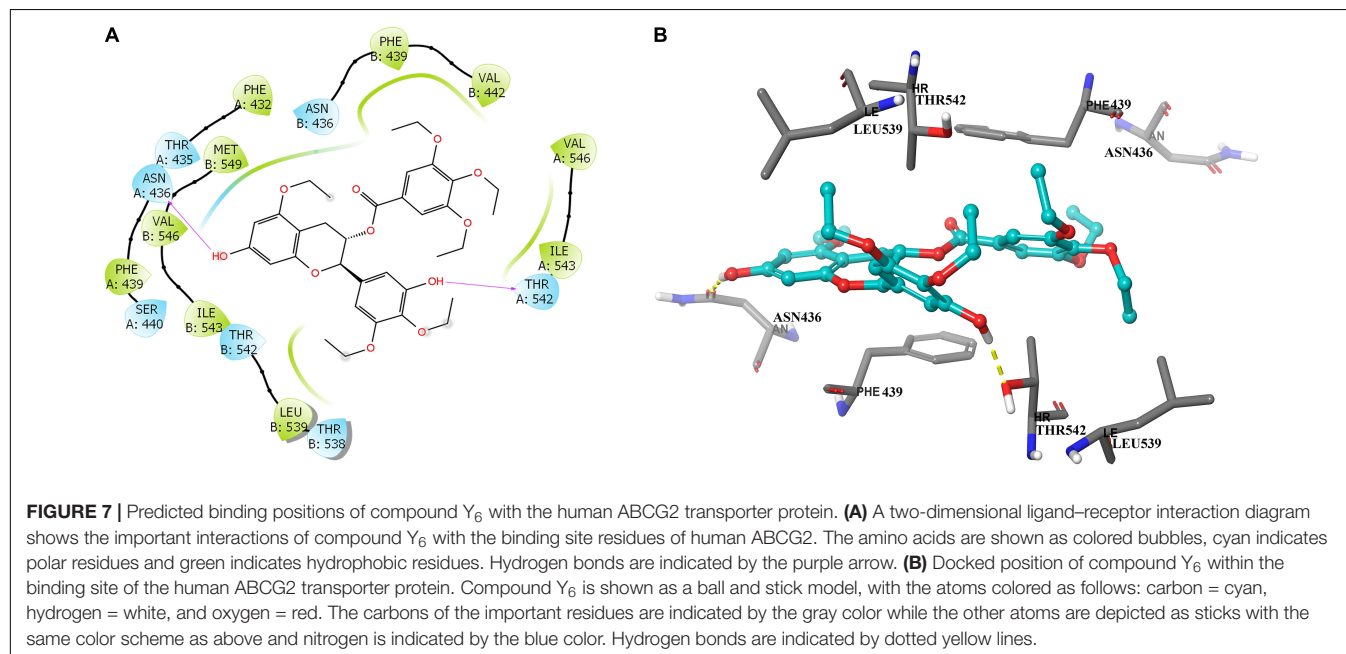
To further learn if Y₆ have direct interactions with the ABCG2 transporter, we performed a molecular docking simulation. A two-dimensional ligand-receptor interaction diagram of the best-scored induced-fit docked position of Y₆ within the drug-binding cavity of human ABCG2 is shown in **Figure 7A**, while the three-dimensional ligand-receptor interaction diagram is shown in **Figure 7B**. The 7-hydroxy group in the chroman ring of compound Y₆ forms a hydrogen bonding with Asn436 ($-\text{OH} \cdots \text{O}=\text{C}-\text{Asn436}$), while the hydroxy group in the

3,4-diethoxy-5-hydroxyphenyl group forms a hydrogen bonding with Thr542 ($-\text{OH} \cdots \text{OH}-\text{Thr542}$). Moreover, compounds Y₆ was stabilized into a hydrophilic pocket formed by residues Phe432, Phe439, Val442, Leu539, Ile543, Val546, and Met549 of the ABCG2 protein. From the results, compound Y₆ had a strong interaction (-11.448 kcal/mol) with the human ABCG2 transporter protein.

DISCUSSION

In recent years, the studied reversal agents which acted on ABC transporter family mostly targeted ABCB1, and very few targeted ABCG2. FTC was one of the ABCG2 reversal agents that was widely used in ABCG2-mediated MDR research. FTC was a toxin obtained from *Aspergillus fumigatus*, which could inhibit ABCG2 activity at a low concentration without much effect on the functions of ABCB1 and ABCC1. However, its use was limited in clinical patients because of its central nervous system neurotoxicity, although FTC was a classic ABCG2 reversal agent in experiments (Rabindran et al., 1998). Therefore, to look for more safe and effective ABCG2 reversal agents, we performed research on Y₆ and evaluated its reversal effect on ABCG2-overexpressing cells. Our previously published study indicated that Y₆ could reverse ABCB1-mediated multidrug resistance by down-regulating ABCB1 protein expression level and changing its function in ABCB1-overexpressing cells (Wen et al., 2017). In this study, we performed the experiments on ABCG2-overexpressing cells and found that Y₆ was also effective in inhibiting ABCG2-mediated drug resistance at non-toxic concentrations.

In our experiments, mitoxantrone-selected MDR cells, NCI-H460/MX20, and their parental cells, as well as ABCG2-overexpressing transfected cells, HEK293/ABCG2-482-R2, and their parental cells were used to determine cytotoxicity and



reversal effect of Y₆. Results showed that Y₆ significantly sensitized NCI-H460/MX20 and HEK293/ABCG2-482-R2 to mitoxantrone, SN-38, or topotecan (Tables 1, 2). However, Y₆ did not increase the cytotoxic effect of cisplatin, which is not a substrate for the ABCG2 transporter. The results implied that Y₆ could reverse ABCG2-mediated drug resistance in ABCG2-overexpressed cells.

ABCG2 played an important role in protecting tumor cells from cytotoxic damage of antineoplastic drugs (Polgar et al., 2008). One of the most prominent MDR mechanisms is ABCG2 overexpression. The overexpression of ABCG2 can produce MDR to antineoplastic drugs as shown in many studies (Sargent et al., 2001; Ho et al., 2008). Susceptibility to drugs could be increased with absence of ABCG2 as shown in the *bcrp1* (−/−) knockout mice studies (Kanzaki et al., 2001; Jonker et al., 2002). Increased ABCG2 expression was also correlated with complete remission, overall survival, relapse-free survival and disease-free survival (Suvannasankha et al., 2004; Damiani et al., 2006; van den Heuvel-Eibrink et al., 2007). To find out the possible mechanism of Y₆ in reversing ABCG2-mediated drug resistance, we measured its effect on the expression of ABCG2. In our previous study, Y₆ could down-regulate the expression of ABCB1 transporter in the reverse resistance experiment (Wen et al., 2017). In this study, the expression of ABCG2 transporter was not changed by Y₆ with different concentrations and incubated time (Figure 3). Y₆ also did not alter the subcellular localization of ABCG2 in NCI-H460/MX20 cells with different incubated times compared to untreated control (Figure 4). The results indicated that the MDR reversal mechanism of Y₆ was not relative with the expression level and subcellular localization of ABCG2.

A decreased concentration of intracellular chemotherapeutic drug was a major cause of MDR in cancer cells. In order to further understand the reversal mechanism of Y₆, we conducted a radiolabeled [³H]-mitoxantrone accumulation and efflux study to evaluate the intracellular drug level. ABCG2 is characterized as a part of self-defense systems and function as an efflux pump to transfer the toxic endogenous molecules and xenobiotics, including many cancer chemotherapies, out of the cell (Nakanishi and Ross, 2012). Mitoxantrone is one of ABCG2 substrates as confirmed in studies (Ozvegy et al., 2001; Nakanishi et al., 2003). Cellular resistance to mitoxantrone conferred by ABCG2 could lead to increased efflux and a low level intracellular accumulation of mitoxantrone (Doyle et al., 1998; Miyake et al., 1999; Nakanishi et al., 2003; Robey et al., 2003). Our results showed that NCI-H460/MX20 cells had lower level intracellular accumulation of [³H]-mitoxantrone than parental NCI-H460 cells. Y₆ could increase the accumulation of [³H]-mitoxantrone compared to untreated control in the NCI-H460/MX20 cells, and the accumulation followed a Y₆-concentration-dependent pattern (Figure 5A). Subsequently, an efflux assay was performed to determine whether the accumulation increase was relative to the inhibition of ABCG2 function by Y₆. The results showed that ABCG2-mediated [³H]-mitoxantrone efflux was suppressed by Y₆ and the efflux amount showed a negative correlation with the concentration of Y₆ (Figures 5B,C). ABCG2 transfer function was inhibited by Y₆.

To further understand the interaction of Y₆ with ABCG2, an ATPase assay using ABCG2 overexpressed membranes and molecular docking simulation using human ABCG2 model were performed. ABC transporters could use energy from the hydrolysis of ATP to transport their substrates across the membrane (Borths et al., 2002; Locher, 2004; Locher and Borths, 2004). It was observed in the study that Y₆ could stimulate ATPase ability of ABCG2 in a dose-dependent pattern at concentrations ranging from 0 to 20 μM, and then leveled off when Y₆ concentration was above 20 μM (Figure 6). Moreover, the docking analysis of Y₆ to human ABCG2 model further revealed that Y₆ had a strong direct interaction with ABCG2 (Figure 7). Thus, we can confer that Y₆ stimulates the ATPase ability of ABCG2 by acting on the drug-substrate-binding site.

CONCLUSION

The study demonstrated that Y₆ could reverse ABCG2-mediated MDR *in vitro*. The mechanisms of Y₆ in reversing MDR is related with the inhibition efflux function of ABCG2 by being a typical competitive substrate of ABCG2, while not relative to down-regulating the ABCG2 expression or altering subcellular localization of ABCG2. Thus, Y₆ is expected to be a potential ABCG2-mediated resistance reversal agent with multiple targets.

AUTHOR CONTRIBUTIONS

Y-AX, Z-SC, and GL contributed to experiment design. R-QZ, YW, PG, Z-NL, and C-YC performed the experiments. R-QZ and YW analyzed the data and wrote the initial draft of manuscript. D-HY reviewed the manuscript. Z-SC and YW obtained the funding.

FUNDING

This work was supported by the Open Project of Guangxi Colleges and Universities Key Laboratory of Biological Molecular Medicine Research (Grant No. GXBMR201602), the Young and Middle-aged Teachers Foundation Ability Enhancement Project of Guangxi Colleges and Universities (Grant No. 2018KY0102), the National Natural Science Foundation of China (Grant No. 81160532), and NIH (Grant No. 1R15CA143701).

ACKNOWLEDGMENTS

We are thankful to Drs. Susan E. Bates and Robert W. Robey (NIH, Bethesda, MD, United States) for providing us HEK293/pcDNA3.1 (parental), HEK293/ABCG2-482-R2, NCI-H460, and NCI-H460/MX20 cell lines. We thank Dr. Tanaji T. Talele (St. John's University, New York, NY, United States) for providing the computational resources for molecular modeling, and Dr. Yangmin Chen for reviewing and editing the paper.

REFERENCES

- Abbott, B. L., Colapietro, A. M., Barnes, Y., Marini, F., Andreeff, M., and Sorrentino, B. P. (2002). Low levels of ABCG2 expression in adult AML blast samples. *Blood* 100, 4594–4601. doi: 10.1182/blood-2002-01-0271
- Borths, E. L., Locher, K. P., Lee, A. T., and Rees, D. C. (2002). The structure of *Escherichia coli* BtuF and binding to its cognate ATP binding cassette transporter. *Proc. Natl. Acad. Sci. U.S.A.* 99, 16642–16647. doi: 10.1073/pnas.262659699
- Chen, Z. S., Robey, R. W., Belinsky, M. G., Shchaveleva, I., Ren, X. Q., Sugimoto, Y., et al. (2003). Transport of methotrexate, methotrexate polyglutamates, and 17 β -estradiol 17-(β -D-glucuronide) by ABCG2: effects of acquired mutations at R482 on methotrexate transport. *Cancer Res.* 63, 4048–4054.
- Dai, C. L., Liang, Y. J., Wang, Y. S., Tiwari, A. K., Yan, Y. Y., Wang, F., et al. (2009). Sensitization of ABCG2-overexpressing cells to conventional chemotherapeutic agent by sunitinib was associated with inhibiting the function of ABCG2. *Cancer Lett.* 279, 74–83. doi: 10.1016/j.canlet.2009.01.027
- Damiani, D., Tiribelli, M., Calistri, E., Geromin, A., Chiarvesio, A., Michelutti, A., et al. (2006). The prognostic value of P-glycoprotein (ABCB) and breast cancer resistance protein (ABCG2) in adults with de novo acute myeloid leukemia with normal karyotype. *Haematologica* 91, 825–828.
- Dean, M., and Allikmets, R. (2001). Complete characterization of the human ABC gene family. *J. Bioenerg. Biomembr.* 33, 475–479. doi: 10.1023/A:1012823120935
- Doyle, L., and Ross, D. D. (2003). Multidrug resistance mediated by the breast cancer resistance protein BCRP (ABCG2). *Oncogene* 22, 7340–7358. doi: 10.1038/sj.onc.1206938
- Doyle, L. A., Yang, W., Abruzzo, L. V., Krogmann, T., Gao, Y., Rishi, A. K., et al. (1998). A multidrug resistance transporter from human MCF-7 breast cancer cells. *Proc. Natl. Acad. Sci. U.S.A.* 95, 15665–15670. doi: 10.1073/pnas.95.26.15665
- Ejendal, K. F., Diop, N. K., Schweiger, L. C., and Hrycyna, C. A. (2006). The nature of amino acid 482 of human ABCG2 affects substrate transport and ATP hydrolysis but not substrate binding. *Protein Sci.* 15, 1597–1607. doi: 10.1110/ps.051998406
- Ejendal, K. F., and Hrycyna, C. A. (2002). Multidrug resistance and cancer: the role of the human ABC transporter ABCG2. *Curr. Protein Pept. Sci.* 3, 503–511. doi: 10.2174/138920302380521
- Farabegoli, F., Papi, A., Bartolini, G., Ostan, R., and Orlandi, M. (2010). (-)-Epigallocatechin-3-gallate downregulates Pg-P and BCRP in a tamoxifen resistant MCF-7 cell line. *Phytomedicine* 17, 356–362. doi: 10.1016/j.phymed.2010.01.001
- Fetsch, P. A., Abati, A., Litman, T., Morisaki, K., Honjo, Y., Mittal, K., et al. (2006). Localization of the ABCG2 mitoxantrone resistance-associated protein in normal tissues. *Cancer Lett.* 235, 84–92. doi: 10.1016/j.canlet.2005.04.024
- Fletcher, J. I., Haber, M., Henderson, M. J., and Norris, M. D. (2010). ABC transporters in cancer: more than just drug efflux pumps. *Nat. Rev. Cancer* 10, 147–156. doi: 10.1038/nrc2789
- Guo, H. Q., Zhang, G. N., Wang, Y. J., Zhang, Y. K., Sodani, K., Talele, T. T., et al. (2014). β -Elemene, a compound derived from *Rhizoma zedoariae*, reverses multidrug resistance mediated by the ABCB1 transporter. *Oncol. Rep.* 31, 858–866. doi: 10.3892/or.2013.2870
- Hirschmann-Jax, C., Foster, A. E., Wulf, G. G., Nuchtern, J. G., Jax, T. W., Gobel, U., et al. (2004). A distinct "side population" of cells with high drug efflux capacity in human tumor cells. *Proc. Natl. Acad. Sci. U.S.A.* 101, 14228–14233. doi: 10.1073/pnas.0400067101
- Ho, M. M., Hogge, D. E., and Ling, V. (2008). MDR1 and BCRP1 expression in leukemic progenitors correlates with chemotherapy response in acute myeloid leukemia. *Exp. Hematol.* 36, 433–442. doi: 10.1016/j.exphem.2007.11.014
- Honjo, Y., Hrycyna, C. A., Yan, Q. W., Medina-Perez, W. Y., Robey, R. W., van de Laar, A., et al. (2001). Acquired mutations in the MXR/BCRP/ABCP gene alter substrate specificity in MXR/BCRP/ABCP-overexpressing cells. *Cancer Res.* 61, 6635–6639.
- Jackson, S. M., Manolaridis, I., Kowal, J., Zechner, M., Taylor, N., Bause, M., et al. (2018). Structural basis of small-molecule inhibition of human multidrug transporter ABCG2. *Nat. Struct. Mol. Biol.* 25, 333–340. doi: 10.1038/s41594-018-0049-1
- Jonker, J. W., Buitelaar, M., Wagenaar, E., Van Der Valk, M. A., Scheffer, G. L., Scheper, R. J., et al. (2002). The breast cancer resistance protein protects against a major chlorophyll-derived dietary phototoxin and protoporphyria. *Proc. Natl. Acad. Sci. U.S.A.* 99, 15649–15654. doi: 10.1073/pnas.202607599
- Kanzaki, A., Toi, M., Nakayama, K., Bando, H., Mutoh, M., Uchida, T., et al. (2001). Expression of multidrug resistance-related transporters in human breast carcinoma. *Jpn. J. Cancer Res.* 92, 452–458. doi: 10.1111/j.1349-7006.2001.tb01115.x
- Lee, M. J., Maliakal, P., Chen, L., Meng, X., Bondoc, F. Y., Prabhu, S., et al. (2002). Pharmacokinetics of tea catechins after ingestion of green tea and (-)-epigallocatechin-3-gallate by humans: formation of different metabolites and individual variability. *Cancer Epidemiol. Biomarkers Prev.* 11, 1025–1032.
- Liang, G., Tang, A., Lin, X., Li, L., Zhang, S., Huang, Z., et al. (2010). Green tea catechins augment the antitumor activity of doxorubicin in an in vivo mouse model for chemoresistant liver cancer. *Int. J. Oncol.* 37, 111–123.
- Locher, K. P. (2004). Structure and mechanism of ABC transporters. *Curr. Opin. Struct. Biol.* 14, 426–431. doi: 10.1016/j.sbi.2004.06.005
- Locher, K. P., and Borths, E. (2004). ABC transporter architecture and mechanism: implications from the crystal structures of BtuCD and BtuF. *FEBS Lett.* 564, 264–268. doi: 10.1016/S0014-5793(04)00289-3
- Maliepaard, M., Scheffer, G. L., Faneyte, I. F., van Gastelen, M. A., Pijnenborg, A. C., Schinkel, A. H., et al. (2001). Subcellular localization and distribution of the breast cancer resistance protein transporter in normal human tissues. *Cancer Res.* 61, 3458–3464.
- Mao, Q., and Unadkat, J. D. (2005). Role of the breast cancer resistance protein (ABCG2) in drug transport. *AAPS J.* 7, E118–E133. doi: 10.1208/aapsj070112
- Miyake, K., Mickle, L., Litman, T., Zhan, Z., Robey, R., Cristensen, B., et al. (1999). Molecular cloning of cDNAs which are highly overexpressed in mitoxantrone-resistant cells: demonstration of homology to ABC transport genes. *Cancer Res.* 59, 8–13.
- Nakanishi, T., Doyle, L. A., Hassel, B., Wei, Y., Bauer, K. S., Wu, S., et al. (2003). Functional characterization of human breast cancer resistance protein (BCRP, ABCG2) expressed in the oocytes of *Xenopus laevis*. *Mol. Pharmacol.* 64, 1452–1462. doi: 10.1124/mol.64.6.1452
- Nakanishi, T., and Ross, D. D. (2012). Breast cancer resistance protein (BCRP/ABCG2): its role in multidrug resistance and regulation of its gene expression. *Chin. J. Cancer* 31, 73–99. doi: 10.5732/cjc.011.10320
- Ozvegy, C., Litman, T., Szakacs, G., Nagy, Z., Bates, S., Varadi, A., et al. (2001). Functional characterization of the human multidrug transporter, ABCG2, expressed in insect cells. *Biochem. Biophys. Res. Commun.* 285, 111–117. doi: 10.1006/bbrc.2001.5130
- Patel, A., Tiwari, A. K., Chufan, E. E., Sodani, K., Anreddy, N., Singh, S., et al. (2013). PD173074, a selective FGFR inhibitor, reverses ABCB1-mediated drug resistance in cancer cells. *Cancer Chemother. Pharmacol.* 72, 189–199. doi: 10.1007/s00280-013-2184-z
- Polgar, O., Robey, R. W., and Bates, S. E. (2008). ABCG2: structure, function and role in drug response. *Expert Opin. Drug Metab. Toxicol.* 4, 1–15. doi: 10.1517/17425255.4.1.1
- Pozza, A., Perez-Victoria, J. M., Sardo, A., Ahmed-Belkacem, A., and Di Pietro, A. (2006). Purification of breast cancer resistance protein ABCG2 and role of arginine-482. *Cell. Mol. Life Sci.* 63, 1912–1922. doi: 10.1007/s00018-006-6159-7
- Rabindran, S. K., He, H., Singh, M., Brown, E., Collins, K. I., Annable, T., et al. (1998). Reversal of a novel multidrug resistance mechanism in human colon carcinoma cells by fumitremorgin C. *Cancer Res.* 58, 5850–5858.
- Robey, R. W., Honjo, Y., Morisaki, K., Nadjem, T. A., Runge, S., Risbood, M., et al. (2003). Mutations at amino-acid 482 in the ABCG2 gene affect substrate and antagonist specificity. *Br. J. Cancer* 89, 1971–1978. doi: 10.1038/sj.bjc.6601370
- Sargent, J. M., Williamson, C. J., Maliepaard, M., Elgie, A. W., Scheper, R. J., and Taylor, C. G. (2001). Breast cancer resistance protein expression and resistance to daunorubicin in blast cells from patients with acute myeloid leukaemia. *Br. J. Haematol.* 115, 257–262. doi: 10.1046/j.1365-2141.2001.03122.x
- Sodani, K., Patel, A., Kathawala, R. J., and Chen, Z. S. (2012). Multidrug resistance associated proteins in multidrug resistance. *Chin. J. Cancer* 31, 58–72. doi: 10.5732/cjc.011.10329
- Steinbach, D., Sell, W., Voigt, A., Hermann, J., Zintl, F., and Sauerbrey, A. (2002). BCRP gene expression is associated with a poor response to remission induction therapy in childhood acute myeloid leukemia. *Leukemia* 16, 1443–1447. doi: 10.1038/sj.leu.2402541

- Sun, Y. L., Kathawala, R. J., Singh, S., Zheng, K., Talele, T. T., Jiang, W. Q., et al. (2012). Zafirlukast antagonizes ATP-binding cassette subfamily G member 2-mediated multidrug resistance. *Anticancer Drugs* 23, 865–873. doi: 10.1097/CAD.0b013e328354a196
- Suvannasankha, A., Minderman, H., O'Loughlin, K. L., Nakanishi, T., Ford, L. A., Greco, W. R., et al. (2004). Breast cancer resistance protein (BCRP/MXR/ABCG2) in adult acute lymphoblastic leukaemia: frequent expression and possible correlation with shorter disease-free survival. *Br. J. Haematol.* 127, 392–398. doi: 10.1111/j.1365-2141.2004.05211.x
- Taylor, N., Manolaridis, I., Jackson, S. M., Kowal, J., Stahlberg, H., and Locher, K. P. (2017). Structure of the human multidrug transporter ABCG2. *Nature* 546, 504–509. doi: 10.1038/nature22345
- van den Heuvel-Eibrink, M. M., van der Holt, B., Burnett, A. K., Knauf, W. U., Fey, M. F., Verhoef, G. E., et al. (2007). CD34-related coexpression of MDR1 and BCRP indicates a clinically resistant phenotype in patients with acute myeloid leukemia (AML) of older age. *Ann. Hematol.* 86, 329–337. doi: 10.1007/s00277-007-0269-7
- van den Heuvel-Eibrink, M. M., Wiemer, E. A., Prins, A., Meijerink, J. P., Vossebeld, P. J., van der Holt, B., et al. (2002). Increased expression of the breast cancer resistance protein (BCRP) in relapsed or refractory acute myeloid leukemia (AML). *Leukemia* 16, 833–839. doi: 10.1038/sj.leu.2402496
- Wen, Y., Zhao, R. Q., Zhang, Y. K., Gupta, P., Fu, L. X., Tang, A. Z., et al. (2017). Effect of Y6, an epigallocatechin gallate derivative, on reversing doxorubicin drug resistance in human hepatocellular carcinoma cells. *Oncotarget* 8, 29760–29770. doi: 10.18632/oncotarget.15964
- Zhang, Y. K., Zhang, G. N., Wang, Y. J., Patel, B. A., Talele, T. T., Yang, D. H., et al. (2016). Bafetinib (INNO-406) reverses multidrug resistance by inhibiting the efflux function of ABCB1 and ABCG2 transporters. *Sci. Rep.* 6:25694. doi: 10.1038/srep25694
- Zhang, Y. K., Zhang, X. Y., Zhang, G. N., Wang, Y. J., Xu, H., Zhang, D., et al. (2017). Selective reversal of BCRP-mediated MDR by VEGFR-2 inhibitor ZM323881. *Biochem. Pharmacol.* 132, 29–37. doi: 10.1016/j.bcp.2017.02.019

Conflict of Interest Statement: The authors declare that the research was conducted in the absence of any commercial or financial relationships that could be construed as a potential conflict of interest.

Copyright © 2019 Zhao, Wen, Gupta, Lei, Cai, Liang, Yang, Chen and Xie. This is an open-access article distributed under the terms of the Creative Commons Attribution License (CC BY). The use, distribution or reproduction in other forums is permitted, provided the original author(s) and the copyright owner(s) are credited and that the original publication in this journal is cited, in accordance with accepted academic practice. No use, distribution or reproduction is permitted which does not comply with these terms.



MicroRNA-181a Functions as an Oncogene in Gastric Cancer by Targeting Caprin-1

Qiang Lu^{1†}, Yanchun Chen^{2,3†}, Dan Sun¹, Shukun Wang¹, Kang Ding¹, Meiyi Liu⁴, Yan Zhang⁴, Yujuan Miao⁴, Huancai Liu⁵ and Fenghua Zhou^{1,3*}

¹ Department of Pathology, Weifang Medical University, Weifang, China, ² Department of Histology and Embryology, Weifang Medical University, Weifang, China, ³ Neurological Disorders and Regenerative Repair Key Laboratory, Weifang Medical University, Weifang, China, ⁴ Department of Bioscience and Technology, Weifang Medical University, Weifang, China, ⁵ Department of Joint Surgery, Affiliated Hospital of Weifang Medical University, Weifang, China

OPEN ACCESS

Edited by:

Dong-Hua Yang,
St. John's University, United States

Reviewed by:

Ji-Ye Yin,
Central South University, China
Honglin Jiang,
University of California,
San Francisco, United States

*Correspondence:

Fenghua Zhou
zhoufh@wfmuc.edu.cn

[†] These authors have contributed
equally to this work

Specialty section:

This article was submitted to
Experimental Pharmacology
and Drug Discovery,
a section of the journal
Frontiers in Pharmacology

Received: 18 November 2018

Accepted: 24 December 2018

Published: 10 January 2019

Citation:

Lu Q, Chen Y, Sun D, Wang S,
Ding K, Liu M, Zhang Y, Miao Y, Liu H
and Zhou F (2019) MicroRNA-181a
Functions as an Oncogene in Gastric
Cancer by Targeting Caprin-1.
Front. Pharmacol. 9:1565.
doi: 10.3389/fphar.2018.01565

MicroRNA-181a (miRNA-181a) is a multifaceted miRNA implicated in various cellular processes, particularly in cell fate determination and cellular invasion. It is frequently expressed aberrantly in human tumors and shows opposing functions in different types of cancers. In this study, we found that miRNA-181a is overexpressed in Gastric cancer (GC) tissues. Clinical and pathological analyses revealed that the expression of miRNA-181a is correlated with tumor size, lymph node metastasis, distant metastasis, and TNM stage. Kaplan-Meier analysis indicated that overexpression of miRNA-181a is associated with poor overall survival of patients with GC. Moreover, miRNA-181a is overexpressed in GC cells, and downregulation of miRNA-181a induced cell apoptosis and suppressed the proliferation, invasion, and metastasis of GC cells both *in vitro* and *in vivo*. Target prediction and luciferase reporter assay showed that caprin-1 was a direct target of miRNA-181a. Downregulation of caprin-1 expression resulted in a converse change with miRNA-181a in GC. Spearman's correlation test confirmed that the expression of miRNA-181a expression was inversely correlated with that of caprin-1 in GC cells. Furthermore, the expression of caprin-1 increased after downregulation of miRNA-181a in the GC cells. Caprin-1 siRNA can rescue the oncogenic effect of miRNA-181a on GC cell proliferation, apoptosis, migration, and invasion. These findings suggest that miRNA-181a directly inhibits caprin-1 and promotes GC development. miRNA-181a could be a target for anticancer drug development.

Keywords: miRNA-181a, oncogene, gastric cancer, caprin-1, metastasis

INTRODUCTION

Gastric cancer (GC) is the fifth cause of cancer incidence and the third cause of cancer-related death worldwide (Kim et al., 2018). Although surgery and chemotherapy have improved considerably in the past few decades, the 5-year survival rates of patients with advanced or metastatic GC have remained low, usually ranging from 5 to 20%, and the median overall survival of the patients is less than 1 year (Docrat et al., 2018). A better understanding of the molecular mechanism underlying tumor progression and metastasis may contribute to the design of novel therapeutic target of GC.

MicroRNAs (miRNAs) are a novel class of 20–22 nt-long small non-coding RNAs that control the stability and translation of target genes (Bellazzo et al., 2018). Thus far, more than 1800 human miRNAs have been identified, and most of them are involved in the regulation of virtually all biological processes (Xia et al., 2015). In tumors, miRNAs affect every step of carcinogenesis, including proliferation, apoptosis, migration, and metastasis (Bracken et al., 2016). Emerging evidence has shown that various miRNAs contribute to the tumorigenesis and progression of GC. For instance, miR-506 suppresses GC angiogenesis and epithelial-to-mesenchymal transition (EMT) by targeting ETS1 (Li et al., 2015). MiR-616-3p promotes angiogenesis and EMT in GC through the PTEN/AKT/mTOR pathway (Wu et al., 2018). MiR-422a expression is downregulated and involved in metabolic reprogramming by PDK2 in GC (He et al., 2018). However, the function of miRNA-181a in GC remains to be validated.

In the present study, we demonstrated that miRNA-181a expression is upregulated and caprin-1 expression is downregulated in GC tissues and cell lines. The ectopic expression of miRNA-181a promoted the proliferation, invasion, and migration of GC cells and inhibited apoptosis *in vitro* and *in vivo*. Furthermore, we identified caprin-1 as the direct target gene of miRNA-181a in GC.

MATERIALS AND METHODS

Patient Samples and Cell Culture

Ninety human GC and thirty adjacent non-tumor tissue samples were obtained from the Affiliated Hospital of Weifang Medical University. The samples were obtained through surgical resection. Pathological diagnosis was evaluated according to the World Health Organization classification system. The samples were classified as adenocarcinoma ($n = 90$). The experiments were approved by the Ethics Committee of the Affiliated Hospital of Weifang Medical University, and all the patients gave written informed consent. The samples were collected in accordance with the approved guidelines. None of the patients received chemotherapy or radiotherapy before sample collection. Four GC cell lines (MKN45, SGC-7901, MGC803, and BGC-823), normal gastric epithelial cell line GES-1, and 293T cells were obtained from the American Type Culture Collection and cultured at 37 °C in DMEM supplemented with 10% fetal bovine serum (Hyclone, United States) in an atmosphere containing 5% CO₂.

Quantitative RT-PCR

Total RNA was isolated from the tissue and cell samples with TRIzol reagent (Life Technologies, Carlsbad, CA, United States). The amount of RNA was quantified with an ND-1000 spectrophotometer (Nano-drop 3000c, Thermo Scientific, MA, United States). To detect the mRNA levels of miRNA-181a and caprin-1, we performed qRT-PCR according to the manufacturer's instructions as previously described (Zhou et al., 2013, 2018). The following primers (Sangon Biotech, China) were used in reverse transcription: (miRNA-181a), 5'-GTCGTATCCAGTGCAGGGTCCGAGGTATTTCGCACTGGATA

CGACACTCAC-3', (U6), 5'-CGCTTCACGAATTTGCGTGT CAT-3'. The following primers (Sangon Biotech, China) were used for PCR: miRNA-181a sense, 5'-GCGGCGGA ACATTCAACGCTGTC-3', miRNA-181a antisense, 5'-ATCCA GTGCAGGGTCCGAGG-3'; U6 sense, 5'-GCTTCGGCAGCA CATATACTAAAAT-3', U6 antisense, 5'-CGCTTCACGAATT TCGTGTTCAT-3'. Caprin-1 sense, 5'-AGGCTGGGACAA GTAAACCTT-3', Caprin-1 antisense, 5'-TCATTAGCAGGAG GGAATGG-3'; β -actin sense, 5'-TGACGTGGACATCCGCA AAG-3', β -actin antisense, 5'-CTGGAAGGTGGACAGCGAGG-3'. Endogenous U6 expression was used as the control for miRNA-181a, whereas endogenous β -actin expression served as the control for caprin-1. The differences in the relative expression levels of miRNA-181a and caprin-1 were calculated using the $2^{-\Delta\Delta C_t}$ method.

Immunohistochemistry and Evaluation Criteria

The expression of caprin-1 in the human GC samples and adjacent non-tumor tissues were determined by immunohistochemistry (IHC). The tissues were fixed in 4% paraformaldehyde, embedded in paraffin, and sliced into consecutive tissue sections. Then, the tissue sections were deparaffinized, dehydrated, and heated in citrate buffer (pH 6.0) for antigen retrieval. To block the non-specific bindings of the first antibody, we added 1% bovine serum onto the slides for 20 min at 37°C. The tissue sections were then incubated with caprin-1 polyclonal antibody (1:100; Fitzgerald, United Kingdom). Finally, the sections were visualized with a DAB kit (ZSGB-bio, China) and counterstained with hematoxylin (ZSGB-bio, Beijing, China). We omitted primary antibody and added phosphate buffered saline (PBS) to the sections as negative controls. The sections were photographed with an optical microscope (Olympus, Tokyo, Japan) and then analyzed with the Image-ProPlus6.0 analytic system (IPP6.0).

Western Blot Analysis

Western blot analysis was performed according to a standard method described previously. A polyclonal caprin-1 antibody (1:1000; Fitzgerald) was used. Mouse monoclonal antibody GAPDH (1:2000; Proteintech Group, Chicago) was used as loading control. The density of the caprin-1 protein band was quantified after it was normalized to the density of the GAPDH band in the same sample during Western blot analysis. The procedures were performed in duplicate.

Cell Transfection

SGC-7901 cells, which presented the highest miRNA-181a expression level in the four GC cell lines, were transfected with RFP-miRNA-181a (control-miRNA-181a-down or miRNA-181a-down) plasmid (GenechemBiotech, Shanghai, China) or cotransfected with RFP-miRNA-181a plasmid and siRNA-caprin-1 (RIBOBIO, China). The transfection was performed with Lipofectamine 3000 (Life Technologies, Carlsbad, CA, United States) according to the manufacturer's instructions. Stable transfectants were selected, incubated with 600 μ g/mL

of G418 after 48 h of transfection. All the procedures were performed in triplicate.

Reporter Vector Construction and Luciferase Reporter Assay

HEK293T cells were used in the luciferase reporter assay. The putative miRNA-181a binding sites in the 3'UTR of caprin-1 were subcloned into a pMIR-report vector (Ambion, Austin, TX, United States), named caprin-1-WT. The primer sequences used for the amplification of caprin-1 3'-UTR were 5'-GAGGAGTTGTGTTTGTGGAC-3' (forward) and 5'-GCGAGGTCCGAAGACTCATTT-3' (reverse). Efficient insertion was confirmed by sequencing. Mutant caprin-1 3'-UTR bearing a substitution of six nucleotides (GAAUGU to CTTTAT) in the miRNA-181a target sequence was named caprin-1-Mut. The MiRNA-181a precursor and negative control (miR-con) were purchased from GenechemBiotech (Shanghai, China). Luciferase activities were determined with Promega dual-luciferase reporter system. All the assays were performed in triplicate.

Cell Proliferation Assay

Human GC cell proliferation index was measured with Cell Counting Kit-8 (CCK-8) assay (Beyotime Institute of Biotechnology, Jiangsu, China) and 5-ethynyl-2-deoxyuridine (EdU) incorporation assay (RIBOBIO, China) kits according to the manufacturers' instructions. In the CCK-8 assay, the cells were cultured in a 96-well plate. CCK-8 was added into the medium and incubated at 37°C for 4 h. Absorbance (OD) was measured at 450 nm at 24, 48, 72, and 96 h after transfection. EdU incorporation assay was performed as previously described (Wang et al., 2017). The percentage of EdU-positive cells was calculated from five random fields, and all experiments were repeated five times.

Cell Apoptosis Assays

The apoptosis of cells was measured with a Cell-Light™ EdUTP Apollo®488 TUNEL cell detection kit (RIBOBIO, China). Approximately 5×10^4 cells were seeded into each well of the 96-well plates and was examined 48 h after transfection. Cells were fixed with 4% paraformaldehyde (pH 7.4) for 20 min. After being washed with PBS solution for three times, the samples were incubated with 50 μ L of reaction buffer (TdT Enzyme 5 μ L+Labeling Safe Buffer 45 μ L) for 60 min at 37°C. The labeling procedure was stopped by washing the samples with 2% BSA solution three times. The TUNEL incorporation rate was expressed as the ratio between the EdUTP-positive and total Hoechst 33342-positive cells. The percentage of the EdUTP-positive cells was calculated from five random fields, and all the experiments were repeated five times.

Transwell Migration and Invasion Assays

Transwell migration and invasion assays were performed according to a standard method (Wang et al., 2017). The images of the invaded or migrated cells were photographed, and the

cells were counted in five random fields. The average number of cells were obtained from three independent experiments and quantified by the PPI software (Media Cybernetics, United States).

In vivo Proliferation and Metastasis Assays

A mouse xenograft model was established in 4-week-old male NU/NU nude mice (Beijing HFK Bioscience Co., Ltd, Beijing, China) in accordance with the institutional guidelines. The mice were manipulated and housed according to the protocols approved by the Ethics Committee of Weifang Medical University.

The miRNA-181a-silenced SGC-7901 cells and their parallel control cells were used for the *in vivo* proliferation and metastasis assay. For the cell proliferation assay, 1×10^6 SGC-7901 cells were suspended in 200 μ L of PBS and then injected subcutaneously of each nude mice (three mice per group). The tumors were observed every 7 days. The mice were euthanized after 5 weeks, and the subcutaneous tumors were isolated, measured, and calculated with the following formula: length \times (width)² \times 1/2. The tumors were collected for the detection of miRNA-181a and caprin-1 by qRT-PCR and Western blot analysis. For tumor metastasis assay, 5×10^6 SGC-7901 cells in 200 μ L of PBS were injected into the tail veins of the NU/NU nude mice (four for each group). The mice were euthanized after 12 weeks, and the entire lung tissues were isolated. The tissue was cut into sections and then stained with hematoxylin and eosin for micrometastasis detection.

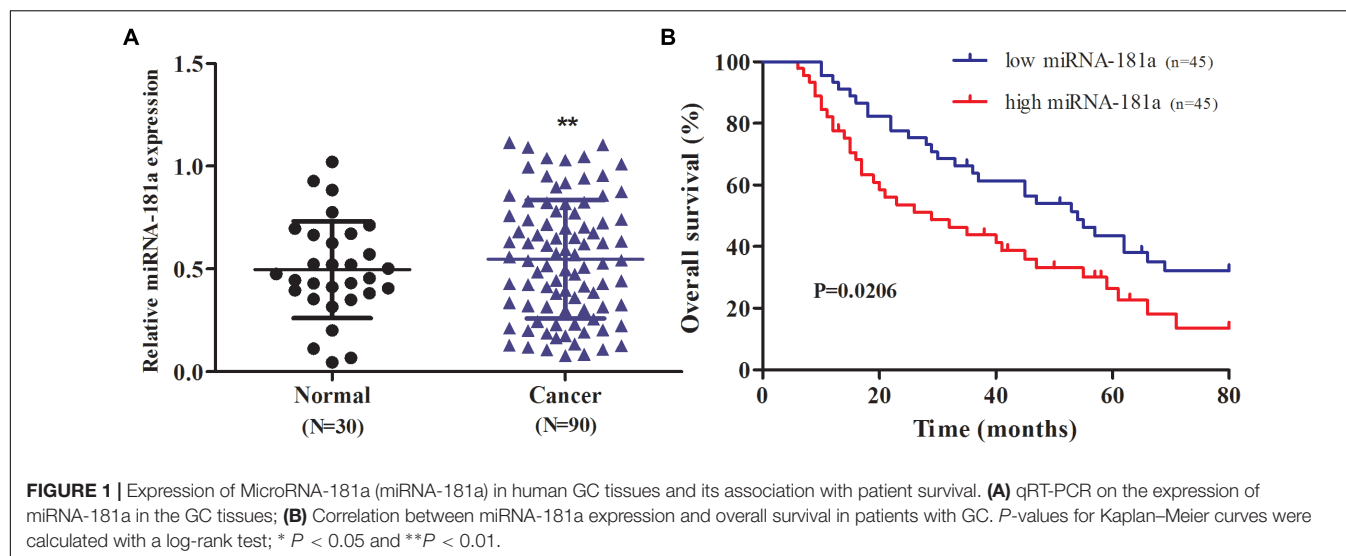
Statistical Analysis

All the data were presented as means \pm standard deviation. Statistical analyses were performed with GraphPad Prism5 (San Diego, CA, United States). The differences in the expression of miRNA-181a and caprin-1 in the GC tissues and GC cell lines were assessed by Student's *t*-test and analysis of variance. The association of miRNA-181a expression with clinicopathological parameters was analyzed with Chi-squared and Fisher's exact tests. The correlation between the miRNA-181a and caprin-1 expression was tested by Spearman's correlation. The Kaplan-Meier method was used for the analysis of the survival curve, and the differences were determined by the log-rank test. $P < 0.05$ was considered statistically significant.

RESULTS

Overexpression of miRNA-181a in GC Tissues Was Associated With Poor Patient Survival

To define the role of miRNA-181a in GC, we evaluated the expression of miRNA-181a in the GC tissues through qRT-PCR. The expression of miRNA-181a was significantly higher in the GC tissues in contrast to that in the adjacent non-tumor tissues (Figure 1A; $P < 0.01$). To determine the relationship



between expression of miRNA-181a and clinicopathological features, we divided the 90 patients with GC into two groups according to their median miRNA-181a level, namely, the high miRNA-181a expression group (above the median level) and low miRNA-181a expression group (below the median level). Clinicopathological analysis revealed that the high expression of miRNA-181a correlates with larger tumor size, more lymph node and distant metastasis, and high TNM stage (Table 1). To further determine the role of miRNA-181a in GC development, we performed follow-ups on all the patients and determined their overall survival after surgery. Kaplan–Meier survival indicated that the overall survival of patients with high miRNA-181a expression was significantly lower than that of low miRNA-181a expression ($P = 0.0206$; Figure 1B).

Down-Regulation of miRNA-181a Inhibited the Proliferation, Migration, Invasion and Enhanced Apoptosis of SGC7901 Cells

To confirm the results of the human GC samples, we assessed the miRNA-181a level in GC cells using qRT-PCR. Results showed that miRNA-181a level was higher in the GC cells than in the normal gastric epithelial GES-1 cell. The metastatic GC SGC7901 cell had the highest level of miRNA-181a (Figure 2A). To examine whether miRNA-181a can affect the biological characteristics of GC, we down-regulated the expression of miRNA-181a in the SGC7901 by miRNA-181a-down plasmid transfection. qRT-PCR was performed to assess the transfection efficiency. It was found that the relative expression of miRNA-181a was significantly lower in the miRNA-181a-down plasmid transfected SGC7901 cells than in the negative control group (Figure 2B). The effects of miRNA-181a on cell proliferation and apoptosis were assessed through CCK-8, EDU, and TUNEL incorporation assays. The result indicated that downregulation of miRNA-181a inhibited proliferation and

enhanced apoptosis of the SGC7901 cells (Figures 2C–E). To investigate the role of miRNA-181a on the migration and invasion of SGC7901 cells, we performed transwell invasion and

TABLE 1 | Clinicopathologic characteristics of GC associated with miRNA-181a expression.

Characteristics	MiRNA-181a expression		Median	p-value
	High (Number)	Low (Number)		
Age(years)				
≥60	18	34	0.5250	0.2849
<60	11	27	0.5485	
Gender				
male	19	35	0.55	0.4613
female	10	26	0.5215	
Tumor size(cm)				
<5	9	34	0.474	0.0283*
>5	20	27	0.631	
Differentiation status				
well	4	11	0.474	0.8806
moderate	15	30	0.575	
poor	10	20	0.525	
TNM stage				
I+II	8	34	0.399	0.0141*
III+IV	21	27	0.651	
Lauren's classification				
Intestinal	18	32	0.554	0.3912
Diffuse	11	29	0.5345	
Distant metastasis				
Negative	22	56	0.512	0.0376*
Positive	7	5	0.762	
Lymph node metastasis				
negative	8	34	0.3745	0.0124*
positive	21	27	0.637	

* $P < 0.05$.

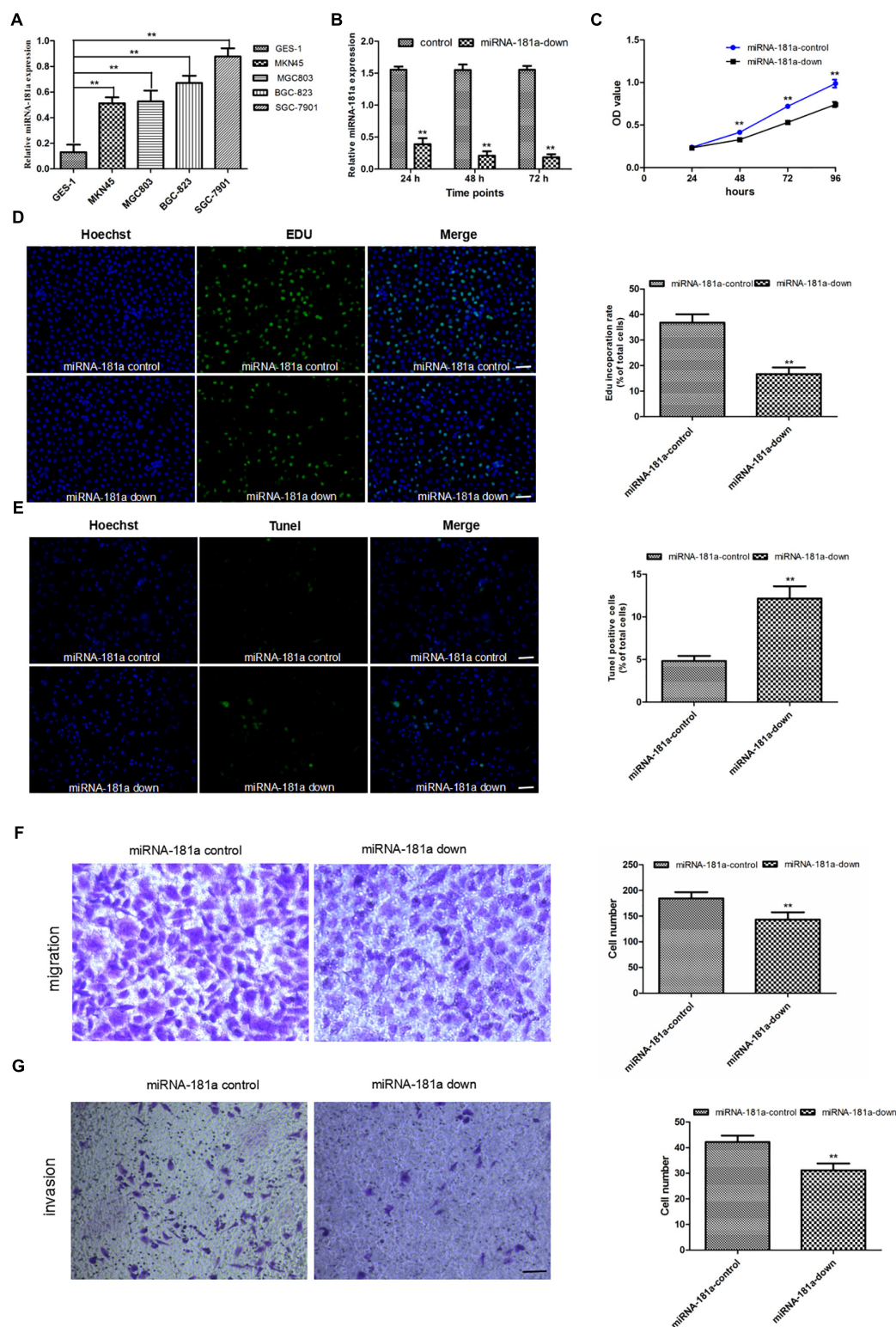


FIGURE 2 | Downregulation of miRNA-181a inhibited the proliferation, invasion, and metastasis, as well as enhanced the apoptosis of the SGC7901 cells.

(A) MiRNA-181a expression increased in the GC cell lines as detected by qRT-PCR; **(B)** Relative miRNA-181a expression decreased in the SGC7901 cells transfected with siRNA miRNA-181a; **(C–D)** Cell proliferation was inhibited in the miRNA-181a downregulated SGC7901 cells, as indicated by the CCK-8 (24, 48, 72, and 96 h) and EDU (48 h) assay, bar = 100 μ m; **(E)** Cell apoptosis was enhanced by EdUTP TUNEL Cell Detection Kit in the SGC7901 cells (48 h), bar = 100 μ m; **(F–G)** Transwell migration and invasion were inhibited in the SGC7901 cells (48 h), bar = 50 μ m; * $P < 0.05$ and ** $P < 0.01$.

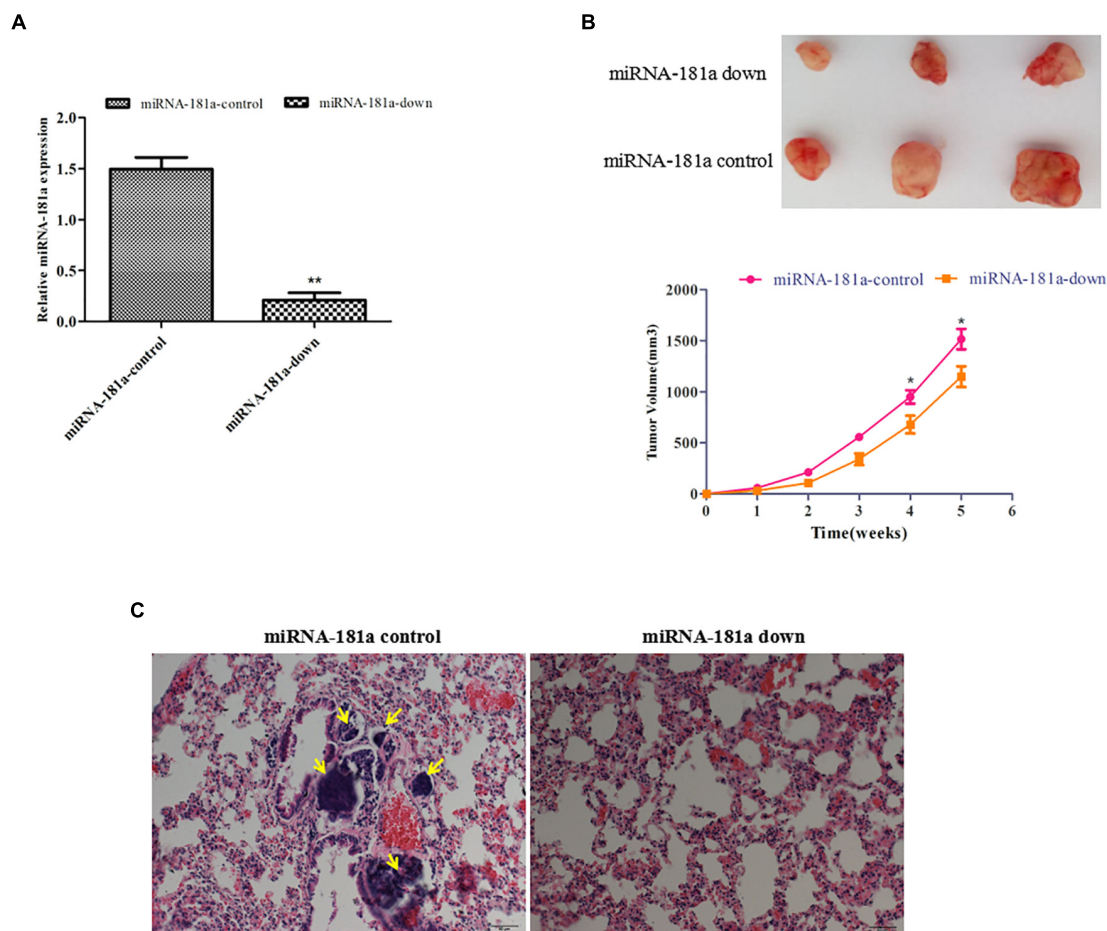


FIGURE 3 | Downregulation of miRNA-181a suppressed GC growth and lung metastasis *in vivo*. **(A)** qRT-PCR on the expression of miRNA-181a; **(B)** The average size of subcutaneous tumors decreased in miRNA-181a downregulated group; **(C)** Metastasis to the lungs observed in the NC group, whereas no metastatic locus was found in the miRNA-181a downregulated group after 12 weeks, bar = 100 μ m; * P < 0.05 and ** P < 0.01.

migration assays 48 h after transfection with miRNA-181a or negative control. The results showed that downregulation of miRNA-181a inhibited migration and invasion of the SGC7901 cells (Figures 2F,G).

Downregulation of miRNA-181a Suppressed GC Growth and Lung Metastasis *in vivo*

To determine whether miRNA-181a inhibits growth and metastasis *in vivo*, SGC7901 cells expressing ectopic miRNA-181a were injected subcutaneously or into tail veins of the nude mice. As shown in Figure 3A, tumors of different sizes formed in the left abdominal subcutaneous tissues after 5 weeks. The average size of the tumors decreased, and miRNA-181a expression markedly decreased, as shown by qRT-PCR, in the miRNA-181a downregulated group, in contrast to those in the NC group (Figures 3A,B). Furthermore, tumor metastasis to the lungs was found in two of the four injected mice in the NC group, whereas no metastatic locus was observed in the miRNA-181a downregulated group after 12 weeks (Figure 3C). Overall,

downregulation of miRNA-181a significantly inhibited tumor growth and metastasis in the mouse xenografts.

Caprin-1 Was Downregulated in the GC Tissue and Was a Target of miRNA-181a in GC

To explore the molecular mechanism underlying miRNA-181a in GC, caprin-1 was predicted bioinformatically as a putative target of miRNA-181a through TargetScan database (Figure 4A). To explore whether miRNA-181a targets caprin-1, dual luciferase assay was performed to determine the 3'-UTR of caprin-1 mRNA. The HEK293T cells transfected with miRNA-181a precursor and caprin-1-WT plasmid showed reduced luciferase activity in contrast to those transfected with the miRNA-181a precursor or caprin-1-Mut plasmid (Figure 4B). Furthermore, the caprin-1 mRNA and protein levels in the GC tissues were examined through qRT-PCR and Western blot analysis. As shown in Figures 4C,D, caprin-1 mRNA and protein levels were significantly lower in the GC tissues than in those in the adjacent non-tumor tissues (P < 0.01). IHC analysis of paraffin-embedded

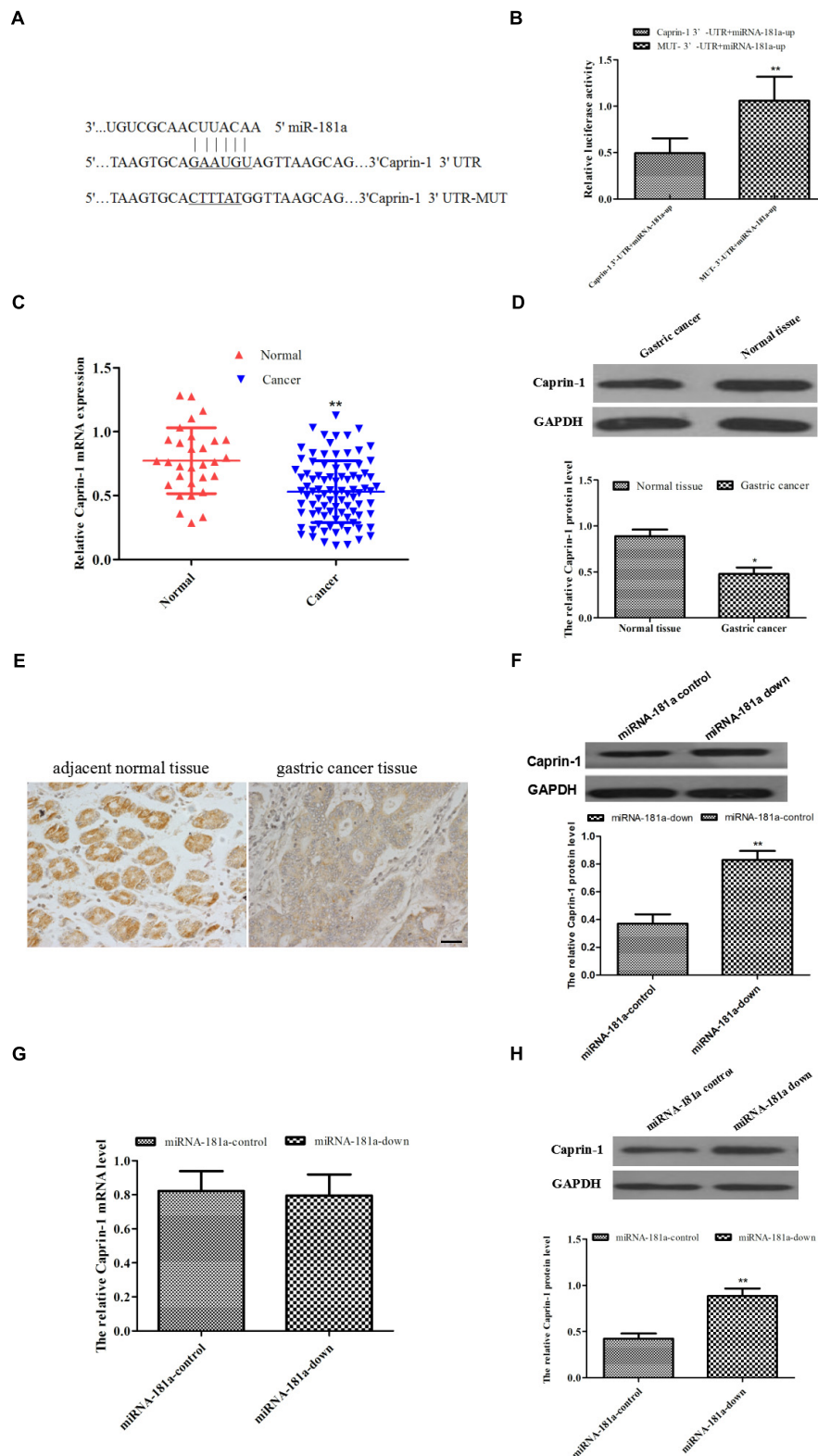


FIGURE 4 | Caprin-1 was downregulated in the GC tissue and was a target of miRNA-181a in GC. **(A)** Binding sites of miRNA-181a to 3'-UTR and mut-3'-UTR of caprin-1 mRNA; **(B)** Luciferase activity of HEK293T cells transfected with miRNA-181a precursor and caprin-1-WT plasmid; **(C)** Caprin-1 mRNA decreased in the GC tissues; **(D)** Caprin-1 protein decreased in the GC tissues; **(E)** IHC analysis on expression of caprin-1, bar = 50 μ m; **(F)** Protein of Caprin-1 in the SGC7901 cells after transfection with miRNA-181a downregulated plasmid; **(G)** mRNA level of caprin-1 in the SGC7901 cells after transfection with miRNA-181a downregulated plasmid; **(H)** Caprin-1 protein level increased in the subcutaneous tumors in xenografts; * $P < 0.05$ and ** $P < 0.01$.

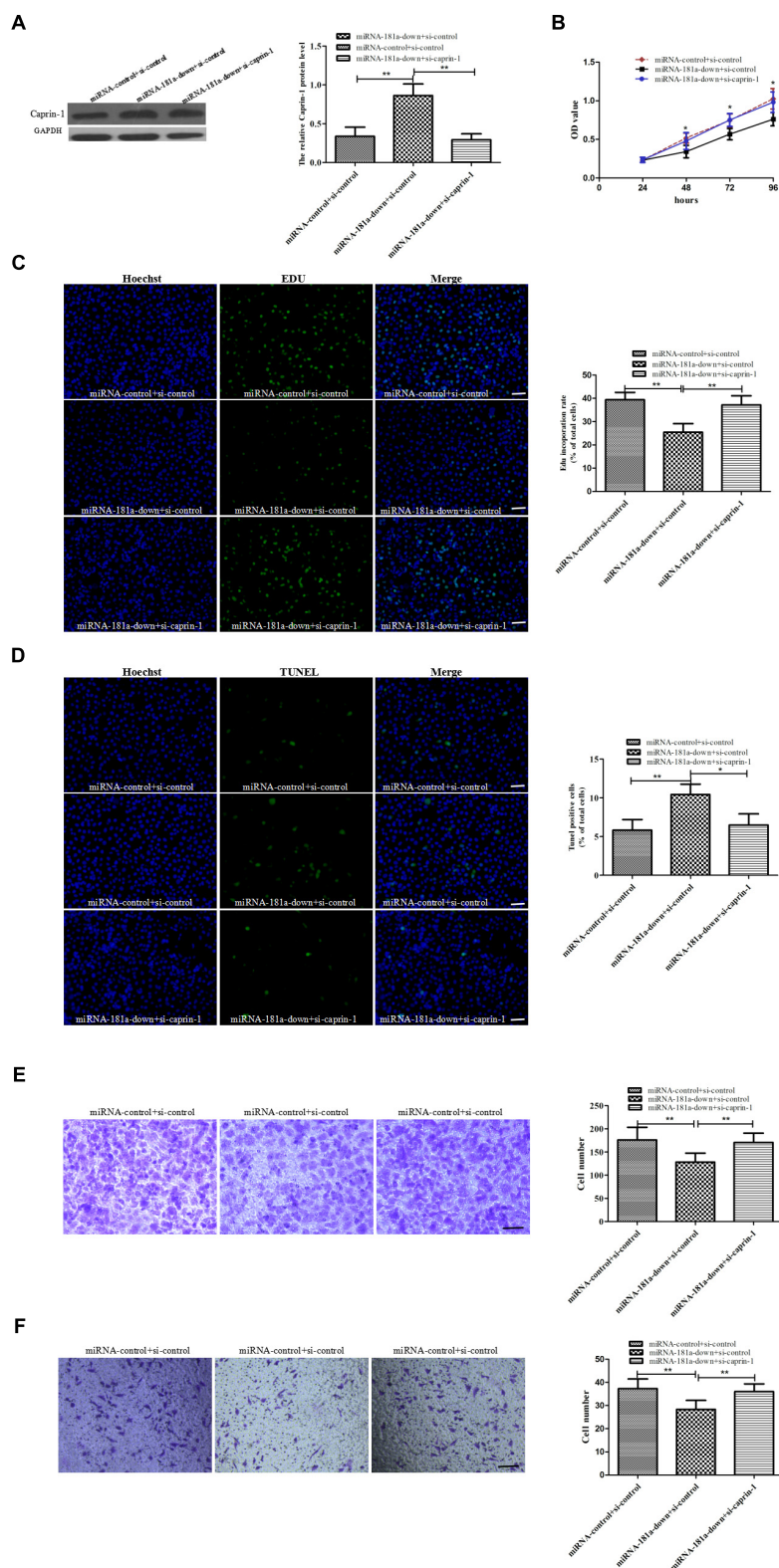


FIGURE 5 | Caprin-1 silence rescues the oncogenic effect of miRNA-181a on GC cell **(A)** Caprin-1 expression decreased in the SGC7901 cells cotransfected with siRNA caprin-1 and miRNA-181a downregulated plasmid detected by Western blot analysis; **(B–C)** Cell proliferation was reversed in the co-transfected SGC7901 cells, as indicated by the CCK-8 (24, 48, 72, and 96 h) and EdU (48 h) assays, bar = 100 μ m; **(D)** Cell apoptosis inhibited by EdUTP TUNEL Cell Detection in the co-transfected SGC7901 cells (48 h); **(E–F)** Transwell migration and invasion detected in the co-transfected SGC7901 cells (48 h); * $P < 0.05$ and ** $P < 0.01$.

tissues revealed that the positive expression of caprin-1 was significantly lower in GC tissues compared with that in the adjacent non-tumor tissues [23.33% (21/90) vs. 66.67% (20/30)] (Figure 4E). We further verified the expression of miRNA-181a was inversely correlated with the expression of caprin-1 with Spearman's correlation test ($n = 90$, $r = -0.7284$). The mRNA and protein levels of caprin-1 were determined after knocking down of miRNA-181a expression in the SGC7901 cells. We found that the protein level of caprin-1 increased, whereas the mRNA level of caprin-1 remained unchanged in the SGC7901 cells (Figures 4F,G). The caprin-1 protein level increased in the subcutaneous tumors of the xenografts (Figure 4H). These results demonstrated that miRNA-181a downregulates caprin-1 expression by binding to the caprin-1 3'-UTR.

Caprin-1 siRNA Rescued miRNA-181a Oncogenic Effects in GC Cells

To determine the role of caprin-1 in the oncogenic effects of miRNA-181a in GC, we performed rescue experiment. SGC7901 cells were co-transfected with miRNA-181a-knock-down plasmid or miRNA-181a-control plasmid and siRNA-caprin-1. It was found that the upregulation of Caprin-1 by miRNA-181a was counteracted by caprin-1 siRNA in GC cell as verified by Western blot analysis (Figure 5A). Cell proliferation, apoptosis, migration, and invasion assays were performed after cotransfection. As expected, caprin-1 siRNA reversed the oncogenic effects of miRNA-181a on GC cells (Figures 5B–F). These results demonstrated that the oncogenic effect of miRNA-181a was achieved at least in part by targeting caprin-1 in GC.

DISCUSSION

MiRNAs are involved in tumor initiation and metastasis (Chowdhury et al., 2018; Lin et al., 2018; Wang et al., 2018). MiRNA-181a has been identified as a multifaceted molecular regulator in different human tumors, and it may be a useful target for treatments of tumors (Wei et al., 2014; Zhang et al., 2014; Brockhausen et al., 2015; Zhu et al., 2016). Although miRNA-181a acts as a tumor suppressor in glioma (Shi et al., 2008), it is often regarded as an oncogene in other tumors, including neuroblastoma, hepatocellular carcinoma, breast cancer, and colorectal cancer (Schulte et al., 2010; Pichler et al., 2014).

In this study, we found that miRNA-181a was upregulated in GC tissues and in patients with lymph node metastasis, and the expression of miRNA-181a was correlated with tumor size, lymph node involvement, distant metastasis, and TNM stage. The cumulative survival rate of patients with high miRNA-181a expression was significantly lower than those with low miRNA-181a expression. These results showed that miRNA-181a was associated with the development and progression of human GC. Moreover, the expression of miRNA-181a was higher in a panel of GC cells compared to that of normal gastric epithelial cells. The highest expression of miRNA-181a was observed in the metastatic GC SGC7901 cells. Downregulation of miRNA-181a inhibited the growth, invasion, and migration but enhanced the apoptosis of

the SGC7901 cells. Downregulation of miRNA-181a considerably inhibited tumor growth and metastasis in the mouse xenografts *in vivo*. These results suggested that miRNA-181a contributed to the development and progression of GC both *in vivo* and *in vitro*.

Caprin-1 is an RNA-binding protein that plays critical roles in human cancers. It promotes osteosarcoma tumor growth and lung metastasis in mice (Sabile et al., 2013) and regulates the proliferation and invasion of human breast cancer cells (Gong et al., 2013). Upregulation of caprin-1 is associated with poor prognosis in hepatocellular carcinoma (Tan et al., 2017). However, the expression patterns and biological functions of caprin-1 in GC have not been established.

MiRNAs control gene expression at the post-transcriptional and translational levels by binding to complementary sequences in the 3'-UTRs of target mRNAs (Li et al., 2018). We explored the underlying mechanisms and the correlations between miRNA-181a and caprin-1 in GC cells. Caprin-1 was predicted bioinformatically as a putative target of miRNA-181a. Dual luciferase assay demonstrated that miRNA-181a targets caprin-1 by binding to the 3'-UTR of caprin-1 mRNA. MiRNA-181a expression was negatively correlated with caprin-1 expression in the GC tissues. Furthermore, the protein level of caprin-1 after knocking down of miRNA-181a in the SGC7901 cells showed a converse change with miRNA-181a, and caprin-1 knockdown reversed the oncogenic effect of miRNA-181a on GC cell proliferation, apoptosis, migration, and invasion. These results indicated that miRNA-181a functions as an oncogene in gastric tumorigenesis at least in part by targeting caprin-1 in GC.

Taken together, our data showed an interesting correlation between miRNA-181a and caprin-1 in GC. The upregulation of miRNA-181a and downregulation of caprin-1 were observed in the GC tissues and GC cell lines. MiRNA-181a enhanced the proliferation, migration, and invasion of GC cells and suppressed apoptosis by downregulating caprin-1, particularly by binding to the 3'UTR mRNA. MiRNA therapeutics is a growing field and has potential application in GC treatment. We highlighted the interaction between miRNA-181a and caprin-1 in GC development, which may provide a target for the exploration of novel therapeutic strategies for GC treatment.

AUTHOR CONTRIBUTIONS

QL and YC participated in most of the experiments, such as cell biology and molecular biology experiments. DS, YM, and KD performed CCK-8, Dual luciferase, EDU, and TUNEL incorporation assays. ML and YZ performed animal studies. SW and HL performed transwell assay. QL and DS directed data analysis. FZ designed the project.

FUNDING

This work was supported by Natural Science Foundation of Shandong Province (ZR2016HL20 and ZR2016HM60).

REFERENCES

- Bellazzo, A., Di Minin, G., Valentino, E., Sicari, D., Torre, D., Marchionni, L., et al. (2018). Cell-autonomous and cell non-autonomous downregulation of tumor suppressor DAB2IP by microRNA-149-3p promotes aggressiveness of cancer cells. *Cell Death Differ.* 25, 1224–1238. doi: 10.1038/s41418-018-0088-5
- Bracken, C. P., Scott, H. S., and Goodall, G. J. (2016). A network-biology perspective of microRNA function and dysfunction in cancer. *Nat. Rev. Genet.* 17, 719–732. doi: 10.1038/nrg.2016.134
- Brockhausen, J., Tay, S. S., Grzelak, C. A., Bertolino, P., Bowen, D. G., D'Avigdor, W. M., et al. (2015). miR-181a mediates TGF-beta-induced hepatocyte EMT and is dysregulated in cirrhosis and hepatocellular cancer. *Liver Int.* 35, 240–253. doi: 10.1111/liv.12517
- Chowdhury, S. M., Lee, T., Bachawal, S. V., Devulapally, R., Abou-Elkacem, L., Yeung, T. A., et al. (2018). Longitudinal assessment of ultrasound-guided complementary microRNA therapy of hepatocellular carcinoma. *J. Control Release* 281, 19–28. doi: 10.1016/j.jconrel.2018.05.009
- Docrat, T. F., Nagiah, S., Krishnan, A., Naidoo, D. B., and Chuturgoon, A. A. (2018). Atorvastatin induces MicroRNA-145 expression in HEPG2 cells via regulation of the PI3K/AKT signalling pathway. *Chem. Biol. Interact.* 287, 32–40. doi: 10.1016/j.cbi.2018.04.005
- Gong, B., Hu, H., Chen, J., Cao, S., Yu, J., Xue, J., et al. (2013). Caprin-1 is a novel microRNA-223 target for regulating the proliferation and invasion of human breast cancer cells. *Biomed. Pharmacother.* 67, 629–636. doi: 10.1016/j.biopha.2013.06.006
- He, Z., Li, Z., Zhang, X., Yin, K., Wang, W., Xu, Z., et al. (2018). MiR-422a regulates cellular metabolism and malignancy by targeting pyruvate dehydrogenase kinase 2 in gastric cancer. *Cell Death Dis.* 9:505. doi: 10.1038/s41419-018-0564-3
- Kim, H., Keum, N., Giovannucci, E. L., Fuchs, C. S., and Bao, Y. (2018). Garlic intake and gastric cancer risk: results from two large prospective US cohort studies. *Int. J. Cancer* 143, 1047–1053. doi: 10.1002/ijc.31396
- Li, Q., Xia, S., Yin, Y., Guo, Y., Chen, F., and Jin, P. (2018). miR-5591-5p regulates the effect of ADSCs in repairing diabetic wound via targeting AGEs/AGER/JNK signaling axis. *Cell Death Dis.* 9:566. doi: 10.1038/s41419-018-0615-9
- Li, Z., Liu, Z., Dong, S., Zhang, J., Tan, J., Wang, Y., et al. (2015). miR-506 inhibits epithelial-to-mesenchymal transition and angiogenesis in gastric cancer. *Am. J. Pathol.* 185, 2412–2420. doi: 10.1016/j.ajpath.2015.05.017
- Lin, H. M., Nikolic, I., Yang, J., Castillo, L., Deng, N., Chan, C. L., et al. (2018). MicroRNAs as potential therapeutics to enhance chemosensitivity in advanced prostate cancer. *Sci. Rep.* 8:7820. doi: 10.1038/s41598-018-26050-y
- Pichler, M., Winter, E., Ress, A. L., Bauernhofer, T., Gerger, A., Kiesslich, T., et al. (2014). miR-181a is associated with poor clinical outcome in patients with colorectal cancer treated with EGFR inhibitor. *J. Clin. Pathol.* 67, 198–203. doi: 10.1136/jclinpath-2013-201904
- Sabile, A. A., Arlt, M. J., Muff, R., Husmann, K., Hess, D., Bertz, J., et al. (2013). Caprin-1, a novel Cyr61-interacting protein, promotes osteosarcoma tumor growth and lung metastasis in mice. *Biochim. Biophys. Acta* 1832, 1173–1182. doi: 10.1016/j.bbdis.2013.03.014
- Schulte, J. H., Marschall, T., Martin, M., Rosenstiel, P., Mestdagh, P., Schlierf, S., et al. (2010). Deep sequencing reveals differential expression of microRNAs in favorable versus unfavorable neuroblastoma. *Nucleic Acids Res.* 38, 5919–5928. doi: 10.1093/nar/gkq342
- Shi, L., Cheng, Z., Zhang, J., Li, R., Zhao, P., Fu, Z., et al. (2008). hsa-mir-181a and hsa-mir-181b function as tumor suppressors in human glioma cells. *Brain Res.* 1236, 185–193. doi: 10.1016/j.brainres.2008.07.085
- Tan, N., Dai, L., Liu, X., Pan, G., Chen, H., Huang, J., et al. (2017). Upregulation of caprin1 expression is associated with poor prognosis in hepatocellular carcinoma. *Pathol. Res. Pract.* 213, 1563–1567. doi: 10.1016/j.prp.2017.07.014
- Wang, Q., Liu, H., Wang, Q., Zhou, F., Liu, Y., Zhang, Y., et al. (2017). Involvement of c-Fos in cell proliferation, migration, and invasion in osteosarcoma cells accompanied by altered expression of Wnt2 and Fzd9. *PLoS One* 12:e0180558. doi: 10.1371/journal.pone.0180558
- Wang, Y., Zeng, X., Wang, N., Zhao, W., Zhang, X., Teng, S., et al. (2018). Long noncoding RNA DANCR, working as a competitive endogenous RNA, promotes ROCK1-mediated proliferation and metastasis via decoying of miR-335-5p and miR-1972 in osteosarcoma. *Mol. Cancer* 17:89. doi: 10.1186/s12943-018-0837-6
- Wei, Z., Cui, L., Mei, Z., Liu, M., and Zhang, D. (2014). miR-181a mediates metabolic shift in colon cancer cells via the PTEN/AKT pathway. *FEBS Lett.* 588, 1773–1779. doi: 10.1016/j.febslet.2014.03.037
- Wu, Z. H., Lin, C., Liu, C. C., Jiang, W. W., Huang, M. Z., Liu, X., et al. (2018). MiR-616-3p promotes angiogenesis and EMT in gastric cancer via the PTEN/AKT/mTOR pathway. *Biochem. Biophys. Res. Commun.* 501, 1068–1073. doi: 10.1016/j.bbrc.2018.05.109
- Xia, W., Chen, Q., Wang, J., Mao, Q., Dong, G., Shi, R., et al. (2015). DNA methylation mediated silencing of microRNA-145 is a potential prognostic marker in patients with lung adenocarcinoma. *Sci. Rep.* 5:16901. doi: 10.1038/srep16901
- Zhang, X., Nie, Y., Li, X., Wu, G., Huang, Q., Cao, J., et al. (2014). MicroRNA-181a functions as an oncomir in gastric cancer by targeting the tumour suppressor gene ATM. *Pathol. Oncol. Res.* 20, 381–389. doi: 10.1007/s12253-013-9707-0
- Zhou, F., Guan, Y., Chen, Y., Zhang, C., Yu, L., Gao, H., et al. (2013). miRNA-9 expression is upregulated in the spinal cord of G93A-SOD1 transgenic mice. *Int. J. Clin. Exp. Pathol.* 6, 1826–1838.
- Zhou, F., Zhang, C., Guan, Y., Chen, Y., Lu, Q., Jie, L., et al. (2018). Screening the expression characteristics of several miRNAs in G93A-SOD1 transgenic mouse: altered expression of miRNA-124 is associated with astrocyte differentiation by targeting Sox2 and Sox9. *J. Neurochem.* 145, 51–67. doi: 10.1111/jnc.14229
- Zhu, Z. J., Huang, P., Chong, Y. X., Kang, L. X., Huang, X., Zhu, Z. X., et al. (2016). MicroRNA-181a promotes proliferation and inhibits apoptosis by suppressing CFIm25 in osteosarcoma. *Mol. Med. Rep.* 14, 4271–4278. doi: 10.3892/mmr.2016.5741

Conflict of Interest Statement: The authors declare that the research was conducted in the absence of any commercial or financial relationships that could be construed as a potential conflict of interest.

Copyright © 2019 Lu, Chen, Sun, Wang, Ding, Liu, Zhang, Miao, Liu and Zhou. This is an open-access article distributed under the terms of the Creative Commons Attribution License (CC BY). The use, distribution or reproduction in other forums is permitted, provided the original author(s) and the copyright owner(s) are credited and that the original publication in this journal is cited, in accordance with accepted academic practice. No use, distribution or reproduction is permitted which does not comply with these terms.



Evaluating *ZNF217* mRNA Expression Levels as a Predictor of Response to Endocrine Therapy in ER+ Breast Cancer

Julie A. Vendrell¹, Jérôme Solassol^{2,3}, Balázs Györfy^{4,5}, Paul Vilquin², Marta Jarlier⁶, Caterina F. Donini¹, Laurent Gamba², Thierry Maudelonde², Philippe Rouanet⁷ and Pascale A. Cohen^{1*}

¹ Univ Lyon, Université Claude Bernard Lyon 1, INSERM U1052, CNRS 5286, Centre Léon Bérard, Centre de Recherche en Cancérologie de Lyon, Lyon, France, ² Département de Pathologie et Oncobiologie, Laboratoire de Biologie des Tumeurs Solides, CHU Montpellier, University of Montpellier, Montpellier, France, ³ Institut de Recherche en Cancérologie de Montpellier (IRCM), INSERM U1194, University Montpellier, Montpellier, France, ⁴ 2nd Department of Paediatrics, Semmelweis University, Budapest, Hungary, ⁵ MTA TTK Lendület Cancer Biomarker Research Group, Institute of Enzymology, Budapest, Hungary, ⁶ Biometrics Unit, Institut du Cancer de Montpellier, University of Montpellier, Montpellier, France, ⁷ Département de Chirurgie Oncologique, Institut du Cancer de Montpellier, University of Montpellier, Montpellier, France

OPEN ACCESS

Edited by:

Dagmar Meyer zu Heringdorf,
Goethe-Universität Frankfurt am Main,
Germany

Reviewed by:

Juntaro Matsuzaki,
National Cancer Centre, Japan
Francesco Calazza,
University of California,
San Francisco, United States

*Correspondence:

Pascale A. Cohen
pascale.cohen@univ-lyon1.fr

Specialty section:

This article was submitted to
Experimental Pharmacology
and Drug Discovery,
a section of the journal
Frontiers in Pharmacology

Received: 15 October 2018

Accepted: 31 December 2018

Published: 25 January 2019

Citation:

Vendrell JA, Solassol J, Györfy B, Vilquin P, Jarlier M, Donini CF, Gamba L, Maudelonde T, Rouanet P and Cohen PA (2019) Evaluating *ZNF217* mRNA Expression Levels as a Predictor of Response to Endocrine Therapy in ER+ Breast Cancer. *Front. Pharmacol.* 9:1581. doi: 10.3389/fphar.2018.01581

ZNF217 is a candidate oncogene with a wide variety of deleterious functions in breast cancer. Here, we aimed at investigating in a pilot prospective study the association between *ZNF217* mRNA expression levels and the clinical response to neoadjuvant endocrine therapy (ET) in postmenopausal ER-positive (ER+) breast cancer patients. Core surgical biopsy samples before treatment initiation and post-treatment were obtained from 68 patients, and Ki-67 values measured by immunohistochemistry (IHC) were used to identify responders ($n = 59$) and non-responders ($n = 9$) after 4 months of ET. We report for the first time that high *ZNF217* mRNA expression level measured by RT-qPCR in the initial tumor samples (pre-treatment) is associated with poor response to neoadjuvant ET. Indeed, the clinical positive response rate in patients with low *ZNF217* expression levels was significantly higher than that in those with high *ZNF217* expression levels ($P = 0.027$). Additionally, a retrospective analysis evaluating *ZNF217* expression levels in primary breast tumor of ER+/HER2-/LN0 breast cancer patients treated with adjuvant ET enabled the identification of poorer responders prone to earlier relapse ($P = 0.013$), while *ZNF217* did not retain any prognostic value in the ER+/HER2-/LN0 breast cancer patients who did not receive any treatment. Altogether, these data suggest that *ZNF217* expression might be predictive of clinical response to ET.

Keywords: breast cancer, *ZNF217*, endocrine therapy, clinical response, predictive biomarker

Abbreviations: ER+, ER α -positive; ER α , estrogen receptor alpha; ET, endocrine therapy; HR, hormone receptor; IHC, immunohistochemistry; LN0, no invaded lymph nodes; PR, progesterone receptor; RFS, relapse-free survival; RT-qPCR, real-time quantitative PCR.

INTRODUCTION

In recent years, studies investigating neoadjuvant therapies have emerged improving both patient management by providing a means of performing less extensive surgery and our understanding of tumor biology and response to treatment (for review, Charehbili et al., 2014). Neoadjuvant ET is administered to HR-positive postmenopausal patients, as recommended by the 15th St. Gallen International Breast Cancer Conference (Morigi, 2017). The main advantage of such a preoperative systemic ET is the prospect of downsizing and downstaging large tumors, thus facilitating breast-conserving surgical interventions. Despite the use of standard biomarkers, the heterogeneity of response to therapy still represents a challenge to clinicians in terms of selecting the most suitable neoadjuvant therapy. Thus, there is an urgent need to discover predictive biomarkers capable to identify patients who will respond to neoadjuvant ET.

We previously described that high expression levels of *ZNF217*, a candidate oncogene, are associated with poor prognosis, shorter RFS in breast cancer (Vendrell et al., 2012; Bellanger et al., 2017). A functional crosstalk exists between *ZNF217* and ER signaling (Nguyen et al., 2014), representing a potential mechanism to escape ET. Most interestingly, high *ZNF217* expression levels confer resistance to ET in ER+ breast cancer cell lines, and *ZNF217* expression silencing is associated with reversion of such resistance (Nguyen et al., 2014). Furthermore, a decrease in Ki-67 levels during neoadjuvant ET (considered alone or as part of a Preoperative Endocrine Prognostic Index) was shown to predict response to ET (Dowsett et al., 2005, 2007; Ellis et al., 2011, 2017; Iwamoto et al., 2017). The aim of this pilot study is to investigate the predictive value of *ZNF217* mRNA levels for response to neoadjuvant ET in patients with ER+ breast cancer.

MATERIALS AND METHODS

Study Design

This was a prospective neoadjuvant ET study on breast cancers expressing the estrogen receptor (ER+) and having a clinical size exceeding 2 cm (T2). This study has been approved by the local ethics committee (Institut du Cancer de Montpellier, France). Patients were informed that their data could be used for research; all the patients signed an informed consent form and the study was conducted in accordance with the Declaration of Helsinki principles. A total of 111 patients were treated for 4 months with neoadjuvant ET (letrozole 2.5 mg/day or tamoxifen 20 mg/day), before being subjected to resection surgery (see **Supplementary Material**). The response to treatment was evaluated by monitoring the evolution of a biological marker of proliferation (Ki-67) before (initial tumor) and after 4 months of ET. Investigation of *ZNF217* mRNA expression levels was also conducted in the initial breast tumor and in the post-treatment tumor samples.

Sample Collection

Three micro-biopsies were collected per patient: one for histopathological diagnosis and the other two were frozen in liquid nitrogen until further use. These tissues were later used for RNA extraction and *ZNF217* mRNA expression analysis, respecting post-therapeutic medical diagnostic requirements. Moreover, IHC examination was carried out to assess the statuses of ER, PR, HER2, and Ki-67. Ki-67 IHC values were measured pre- and post-treatment for each patient and used to discriminate between responders and non-responders (Dowsett et al., 2007). Patients displaying a $\Delta\text{Ki-67}$ (Ki-67 IHC value post-treatment – Ki-67 IHC value pre-treatment) ≤ 0 were designated to be responders, while patients with $\Delta\text{Ki-67} > 0$ were non-responders.

RNA Extraction and Real-Time Quantitative PCR (RT-qPCR)

Total RNA was extracted from frozen biopsies using the RNeasy Mini Kit (Qiagen, Hilden, Germany). After checking RNA quality, 68 tumor samples were deemed suitable for expression analysis (59 responders and nine non-responders) (**Supplementary Table 1**). Reverse-transcription and RT-qPCR measurements were performed as described in the **Supplementary Material**. A P -value of ≤ 0.05 was considered to be statistically significant (StatgraphicsTM Software). ROC-AUC was investigated using the SPSSTM Software.

The Kaplan-Meier Plotter (KMP) Breast Cancer Cohort

The KMP cohort investigation resulted from a meta-analysis of gene-expression profiles from 2,978 primary breast cancer specimens who had not received any therapy before surgery and with known adjuvant therapy and clinical follow-up (Gyorffy and Schafer, 2009). The SPSSTM Software was used to assess the prognostic value of *ZNF217* or *Ki-67* mRNA expression (univariate analysis). Data were divided into two groups with either high or low expression values according to the median value. Candidate prognostic factors for RFS with a 0.1 significance level in univariate analysis were entered in a multivariate Cox model, and a backward selection procedure was used to determine independent prognostic markers.

RESULTS

ZNF217 mRNA expression levels were not correlated with Ki-67 values, neither in the initial breast tumor (pre-treatment) ($r = -0.169$, $P = 0.17$), nor in the post-treatment samples ($r = -0.026$, $P = 0.83$), nor with the $\Delta\text{Ki-67}$ values ($r = -0.136$, $P = 0.26$), thus ruling out that investigating *ZNF217* expression levels was merely a surrogate markers of Ki-67 expression (Spearman test).

In responders ($n = 59$) and in non-responders ($n = 9$), *ZNF217* expression was associated with response to neoadjuvant ET, since *ZNF217* mRNA expression levels tended to be significantly higher ($P = 0.05$) in the initial breast tumor in patients who did not respond to neoadjuvant ET (median = 5.98) than those who did (median = 3.01) (**Figure 1A**).

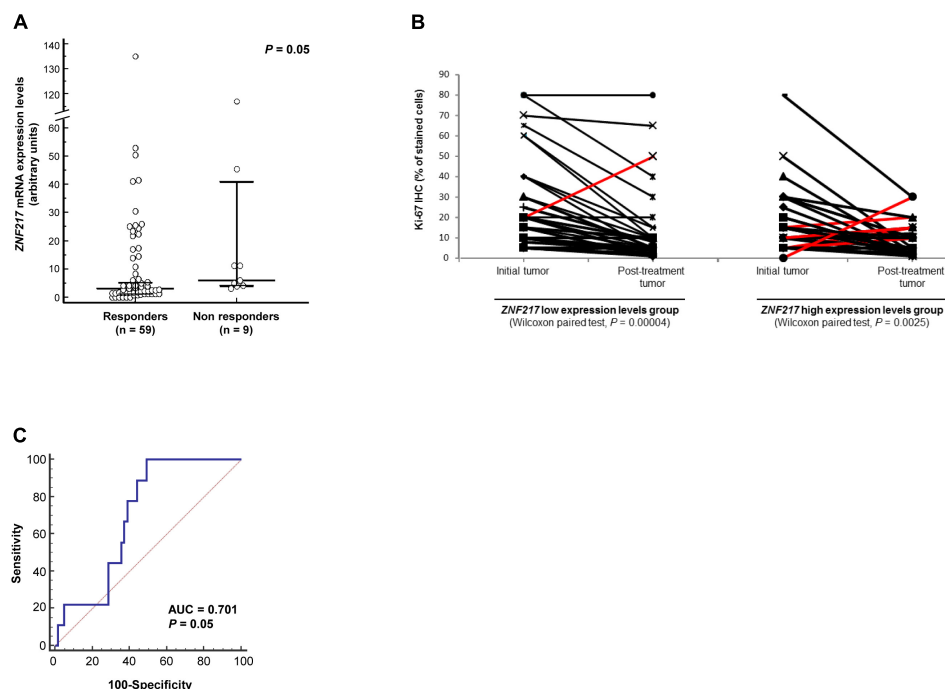


FIGURE 1 | High *ZNF217* mRNA expression levels are associated with poor neoadjuvant ET response. **(A)** Dot plot representing *ZNF217* mRNA expression levels in the initial breast tumors of responders or non-responders. Medians and 95% confidence intervals are shown for each group. **(B)** Changes in the Ki-67 expression for patients in the initial tumor and post-treatment tumor according to the mRNA expression levels of *ZNF217*. Red lines correspond to the non-responders (displaying increased Δ Ki-67). **(C)** Receiver operating characteristic (ROC) curve for *ZNF217* mRNA expression levels. AUC, area under curve.

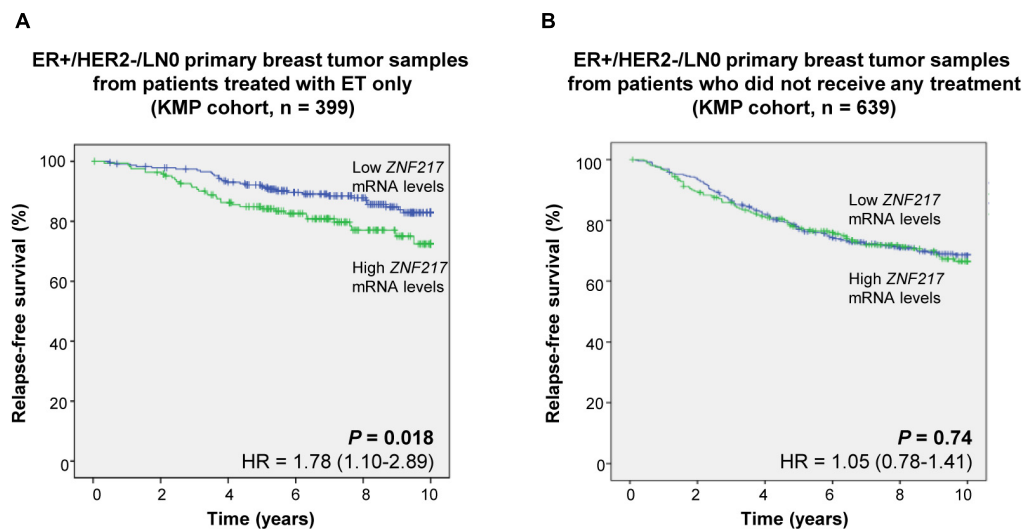


FIGURE 2 | High *ZNF217* mRNA expression levels are associated with earlier relapse for patients treated with ET only. Kaplan-Meier analyses for relapse-free survival (RFS) are shown for ER+/HER2-/LN0 breast cancer patients **(A)** treated with adjuvant ET only and **(B)** who did not receive any treatment.

Fisher's exact test was used to investigate the association between the dichotomized clinical response measures and the *ZNF217* molecular marker. The 68 patients were separated in two groups, based on the median *ZNF217* expression value. The positive clinical response rate in the low *ZNF217* expression level group was significantly higher ($P = 0.027$) than that in

the high *ZNF217* expression level group, with high *ZNF217* expression levels being associated with the absence of response to neoadjuvant ET (**Supplementary Table 2**).

The *ZNF217* low and high expression level groups were comparable in terms of Ki-67 values in the initial tumor (pre-treatment) ($P = 0.20$, data not shown). Changes in Ki-67

for individual patients before and after neoadjuvant ET response are shown in **Figure 1B**. In the *ZNF217* low expression levels group (Wilcoxon signed-rank test, $P < 0.00004$), only one patient was ET-resistant (displaying increased Ki-67 level), while 33/34 patients were responders (**Figure 1B**). In the *ZNF217* high expression level group (Wilcoxon signed-rank test, $P < 0.0025$), eight patients displayed an increase in Ki-67 (ET-resistant patients), whereas 26 patients were responders (**Figure 1B**).

Although our study is exploratory with a limited sample size ($n = 68$) and with limited relapse events ($n = 9$), we assessed the predictive power of *ZNF217* expression level for response to ET. The AUC was 0.701 (95% confidence interval: 0.563–0.838, $P = 0.05$), which represents a good/moderate discriminatory accuracy for a model including few events ($n = 9$) (**Figure 1C**). Based on the ROC curve, the discriminating sensitivity and specificity were 100 and 51%, respectively.

A number of studies have suggested that post-treatment biomarkers (such as Ki-67 and ER) could have a better prognostic value than pre-treatment biomarkers, and investigating biomarkers in post-treatment samples is thus of interest (Dowsett et al., 2007; Ellis et al., 2008; Chia et al., 2010). In post-treatment tumor samples, no differences in *ZNF217* expression levels were observed between responders and non-responders ($P = 0.4$, Mann-Whitney test, data not shown), suggesting that assessing *ZNF217* expression levels in the initial tumor before ET is the most informative.

To support our finding, we then hypothesized that if *ZNF217* expression retains any predictive value for ET response in the neoadjuvant setting, then, the biomarker value of *ZNF217* would be different between ER+ breast cancer patients treated with adjuvant ET only and patients who did not received any treatment. We thus performed a retrospective analysis of gene-expression array data from 2,978 breast cancer patients (KMP cohort). In this cohort, we have previously demonstrated that high levels of *ZNF217* mRNA expression levels were strongly and significantly associated with shorter RFS ($P < 10^{-9}$, Nguyen et al., 2014). Strikingly, when considering the ER+/HER2-/LN0 patients, high *ZNF217* mRNA levels were predictive of earlier relapse for patients treated with adjuvant ET only ($n = 399$, $P = 0.018$, univariate analysis), but not for non-treated patients ($n = 639$, $P = 0.74$, univariate analysis) (**Figure 2**). In ER+/HER2-/LN0 patients, *ZNF217*, and Ki-67 mRNA expression levels were not correlated ($r = -0.07$, $P = 0.14$, Spearman test). Since Ki-67 mRNA levels were almost significantly correlated with RFS in this cohort ($P = 0.094$, univariate analysis), the two factors were entered in a multivariate Cox model, and both persisted in the model showing that they are independent biomarkers ($P < 0.1$). A signature associating *ZNF217* and Ki-67 mRNA levels displayed a prognostic value with regards to RFS ($P = 0.01$, univariate analysis). Interestingly, this signature was identified as the best fit for predicting clinical outcome of ET-treated patients (likelihood = 741.46), compared to the models integrating *ZNF217* mRNA levels (likelihood = 746.65, $P = 0.023$) or Ki-67 mRNA levels (likelihood = 749.24, $P = 0.005$) only. Our data support that *ZNF217* is a predictive biomarker for response to ET, and that, in the ER+/HER2-/LN0 cohort, the signature including

both *ZNF217*/Ki-67 mRNA levels had the best predictive value.

DISCUSSION

Short-term pre-operative trials with specific groups of patients have proven to be highly promising in identifying biomarkers predictive for the efficacy of targeted anti-cancer therapies (Marous et al., 2015). Early evidence of endocrine drug effectiveness can be obtained in the pre-operative (neoadjuvant) setting by profiling baseline and on-treatment biopsy samples using the window-of-opportunity. This predictive evidence acquired during short-term neoadjuvant therapy can help in identifying individual patients who will potentially benefit from long-term adjuvant treatment enabling personalized approaches. Short-term reduction in Ki-67 is predictive of clinical response to ET (Dowsett et al., 2005, 2007; Ellis et al., 2011, 2017; Iwamoto et al., 2017). However, controversy remains regarding the reproducibility of Ki-67 measurements and international efforts are ongoing to standardize and validate Ki-67 by IHC (Polley et al., 2015; Rimm et al., 2018). An additional obstacle derives from intra-tumor heterogeneity of Ki-67 (Focke et al., 2016). Altogether, there is an urgent need for further biomarkers that might increase the accuracy of prediction of response to ET.

In a previous study, proliferation-associated genes, including cyclins, mini chromosome maintenance genes and mitotic spindle-associated genes were shown to be predictive of response to ET after 2 weeks but not before treatment (Turnbull et al., 2015). A four-gene signature measuring two genes pre-treatment and two genes after 2 weeks of treatment was shown to predict response to neoadjuvant ET in ER+ patients (Turnbull et al., 2015). The genes that predicted response to ET included two pre-treatment genes associated with immune response and apoptosis and two genes measured after 2 weeks of treatment, which were associated with proliferation. Altogether, these data suggest that transcriptomic changes that develop during treatment are representative of the drug's mechanism of action, suggesting that suppression of proliferation is the main driver of response.

In the present pilot study, the clinical sample size used is small and included only nine non-responders. Nevertheless, we found that *ZNF217* expression levels are predictive of neoadjuvant ET response in ER+ breast cancer. *ZNF217* expression levels are not associated with Ki-67 values, neither in the initial nor in the treated tumor, ruling out that *ZNF217* could only be a surrogate marker of cell proliferation. Of utmost interest is that the predictive value of *ZNF217* expression levels seems to reside in the initial tumor and is not the reflection of transcriptional changes following ET in the treated tumors. This is the first pilot prospective study conducted in the neoadjuvant setting to relate *ZNF217* expression levels with treatment efficacy, thus suggesting that aside from its prognostic value in luminal breast cancers (Vendrell et al., 2012; Nguyen et al., 2014), *ZNF217* expression may also be predictive of response to ET. In this exploratory study, it is difficult to estimate the accuracy of *ZNF217* mRNA

levels for predicting response to ET, due to the low numbers of non-responders (9 out of 68). However, while obtained in a small cohort, our preliminary data are encouraging and need to be extended to a larger cohort for validation.

Interestingly, evaluating *ZNF217* expression levels in the primary breast tumor of ER+/HER2-/LN0 breast cancer patients treated by adjuvant ET led to the identification of poorer responders prone to earlier relapse, while in ER+/HER2-/LN0 breast cancer patients who did not receive any treatment the association between *ZNF217* expression and RFS was not significant. Previous studies reported multi-gene genomic assays predicting response to neoadjuvant ET (Turnbull et al., 2015; Iwata et al., 2018), and we speculate that these coupling with the *ZNF217* biomarker might improve their predictive performance. Indeed, we herein demonstrated in the ER+/HER2-/LN0 cohort that combining *ZNF217* and *Ki-67* expression levels was more performant at predicting relapse under ET, than each of these biomarkers taken individually.

Altogether, these data support the idea that in the luminal breast cancer subclass, *ZNF217* expression levels relate to ET response and provide a novel candidate biomarker. Finally, there are several ongoing trials investigating the combination of ET and other targeted therapies to prevent/reverse endocrine resistance. The PI3K/mTOR pathway, CDK4/6, HDAC, and immune checkpoints are the most promising and widely investigated targets (Rugo et al., 2016). Further studies are needed to delineate whether the ER+/*ZNF217*_{high} breast cancer subpopulation might benefit from combining ET with another therapy.

REFERENCES

- Bellanger, A., Donini, C. F., Vendrell, J. A., Lavaud, J., Machuca-Gayet, I., Ruel, M., et al. (2017). The critical role of the *ZNF217* oncogene in promoting breast cancer metastasis to the bone. *J. Pathol.* 242, 73–89. doi: 10.1002/path.4882
- Charehbili, A., Fontein, D. B., Kroep, J. R., Liefers, G. J., Mieog, J. S., Nortier, J. W., et al. (2014). Neoadjuvant hormonal therapy for endocrine sensitive breast cancer: a systematic review. *Cancer Treat. Rev.* 40, 86–92. doi: 10.1016/j.ctrv.2013.06.001
- Chia, Y. H., Ellis, M. J., and Ma, C. X. (2010). Neoadjuvant endocrine therapy in primary breast cancer: indications and use as a research tool. *Br. J. Cancer* 103, 759–764. doi: 10.1038/sj.bjc.6605845
- Dowsett, M., Smith, I. E., Ebbs, S. R., Dixon, J. M., Skene, A., A'Hern, R., et al. (2007). Prognostic value of Ki67 expression after short-term presurgical endocrine therapy for primary breast cancer. *J. Natl. Cancer Inst.* 99, 167–170. doi: 10.1093/jnci/djk020
- Dowsett, M., Smith, I. E., Ebbs, S. R., Dixon, J. M., Skene, A., Griffith, C., et al. (2005). Short-term changes in Ki-67 during neoadjuvant treatment of primary breast cancer with anastrozole or tamoxifen alone or combined correlate with recurrence-free survival. *Clin. Cancer Res.* 11, 951s–958s.
- Ellis, M. J., Suman, V. J., Hoog, J., Goncalves, R., Sanati, S., Creighton, C. J., et al. (2017). Ki67 proliferation index as a tool for chemotherapy decisions during and after neoadjuvant aromatase inhibitor treatment of breast cancer: results from the american college of surgeons oncology group Z1031 trial (Alliance). *J. Clin. Oncol.* 35, 1061–1069. doi: 10.1200/JCO.2016.69.4406
- Ellis, M. J., Suman, V. J., Hoog, J., Lin, L., Snider, J., Prat, A., et al. (2011). Randomized phase II neoadjuvant comparison between letrozole, anastrozole, and exemestane for postmenopausal women with estrogen receptor-rich stage 2 to 3 breast cancer: clinical and biomarker outcomes and predictive value of

AUTHOR CONTRIBUTIONS

PR and TM designed and supervised the neoadjuvant clinical trial. JV, PV, and LG performed the experiments. JV, PV, and CD performed the RT-qPCR data analysis. MJ performed the clinical data analysis. JV and BG performed the retrospective *in silico* analysis. PR, TM, and PC conceived and supervised the study. JV, JS, TM, and PC wrote the manuscript.

FUNDING

Charge-free waiver (PC was associate editor of the “Novel Targets and Biomarkers in Solid Tumors” research topic, agreement with the Editor). PC was supported by the French Ligue contre le cancer (committees 42 and 71). BG was supported by the KH-129581 and the NVKP_16-1-2016-0037 grants of the National Research, Development and Innovation Office, Hungary.

ACKNOWLEDGMENTS

We thank Dr. B. Manship for critical reading of the manuscript.

SUPPLEMENTARY MATERIAL

The Supplementary Material for this article can be found online at: <https://www.frontiersin.org/articles/10.3389/fphar.2018.01581/full#supplementary-material>

- the baseline PAM50-based intrinsic subtype-ACOSOG Z1031. *J. Clin. Oncol.* 29, 2342–2349. doi: 10.1200/JCO.2010.31.6950
- Ellis, M. J., Tao, Y., Luo, J., A'Hern, R., Evans, D. B., Bhatnagar, A. S., et al. (2008). Outcome prediction for estrogen receptor-positive breast cancer based on postneoadjuvant endocrine therapy tumor characteristics. *J. Natl. Cancer Inst.* 100, 1380–1388. doi: 10.1093/jnci/djn309
- Focke, C. M., Decker, T., and van Diest, P. J. (2016). Intratumoral heterogeneity of Ki67 expression in early breast cancers exceeds variability between individual tumours. *Histopathology* 69, 849–861. doi: 10.1111/his.13007
- Gyorffy, B., and Schafer, R. (2009). Meta-analysis of gene expression profiles related to relapse-free survival in 1,079 breast cancer patients. *Breast Cancer Res. Treat.* 118, 433–441. doi: 10.1007/s10549-008-0242-8
- Iwamoto, T., Katagiri, T., Niikura, N., Miyoshi, Y., Kochi, M., Nogami, T., et al. (2017). Immunohistochemical Ki67 after short-term hormone therapy identifies low-risk breast cancers as reliably as genomic markers. *Oncotarget* 8, 26122–26128. doi: 10.18632/oncotarget.15385
- Iwata, H., Masuda, N., Yamamoto, Y., Fujisawa, T., Toyama, T., Kashiwaba, M., et al. (2018). Validation of the 21-gene test as a predictor of clinical response to neoadjuvant hormonal therapy for ER+, HER2-negative breast cancer: the TransNEOS study. *Breast Cancer Res. Treat.* doi: 10.1007/s10549-018-4964-y [Epub ahead of print].
- Marous, M., Bieche, I., Paoletti, X., Alt, M., Razak, A. R., Stathis, A., et al. (2015). Designs of preoperative biomarkers trials in oncology: a systematic review of the literature. *Ann. Oncol.* 26, 2419–2428. doi: 10.1093/annonc/mdv378
- Morigi, C. (2017). Highlights from the 15th St Gallen International Breast Cancer Conference 15-18 March, 2017, Vienna: tailored treatments for patients with early breast cancer. *Ecancermedicalscience* 11:732. doi: 10.3332/ecancer.2017.732
- Nguyen, N. T., Vendrell, J. A., Poulard, C., Gyorffy, B., Goddard-Leon, S., Bieche, I., et al. (2014). A functional interplay between *ZNF217* and estrogen receptor

- alpha exists in luminal breast cancers. *Mol. Oncol.* 8, 1441–1457. doi: 10.1016/j.molonc.2014.05.013
- Polley, M. Y., Leung, S. C., Gao, D., Mastropasqua, M. G., Zabaglo, L. A., Bartlett, J. M., et al. (2015). An international study to increase concordance in Ki67 scoring. *Mod. Pathol.* 28, 778–786. doi: 10.1038/modpathol.2015.38
- Rimm, D. L., Leung, S. C. Y., McShane, L. M., Bai, Y., Bane, A. L., Bartlett, J. M. S., et al. (2018). An international multicenter study to evaluate reproducibility of automated scoring for assessment of Ki67 in breast cancer. *Mod. Pathol.* 32, 59–69. doi: 10.1038/s41379-018-0109-4
- Rugo, H. S., Vidula, N., and Ma, C. (2016). Improving response to hormone therapy in breast cancer: new targets, new therapeutic options. *Am. Soc. Clin. Oncol. Educ. Book* 35, e40–e54. doi: 10.14694/EDBK_159198
- Turnbull, A. K., Arthur, L. M., Renshaw, L., Larionov, A. A., Kay, C., Dunbier, A. K., et al. (2015). Accurate prediction and validation of response to endocrine therapy in breast cancer. *J. Clin. Oncol.* 33, 2270–2278. doi: 10.1200/JCO.2014.57.8963
- Vendrell, J. A., Thollet, A., Nguyen, N. T., Ghayad, S. E., Vinot, S., Bieche, I., et al. (2012). ZNF217 is a marker of poor prognosis in breast cancer that drives epithelial-mesenchymal transition and invasion. *Cancer Res.* 72, 3593–3606. doi: 10.1158/0008-5472.CAN-11-3095
- Conflict of Interest Statement:** The authors declare that the research was conducted in the absence of any commercial or financial relationships that could be construed as a potential conflict of interest.

Copyright © 2019 Vendrell, Solassol, Györfy, Vilquin, Jarlier, Donini, Gamba, Maudelonde, Rouanet and Cohen. This is an open-access article distributed under the terms of the Creative Commons Attribution License (CC BY). The use, distribution or reproduction in other forums is permitted, provided the original author(s) and the copyright owner(s) are credited and that the original publication in this journal is cited, in accordance with accepted academic practice. No use, distribution or reproduction is permitted which does not comply with these terms.



Upregulation of lncRNA NR_046683 Serves as a Prognostic Biomarker and Potential Drug Target for Multiple Myeloma

Hang Dong^{1†}, Siyi Jiang^{2†}, Yunfeng Fu¹, Yanwei Luo¹, Rong Gui^{1*} and Jing Liu^{2*}

¹ Department of Blood Transfusion, The Third Xiangya Hospital of Central South University, Changsha, China, ² Department of Hematology, The Third Xiangya Hospital of Central South University, Changsha, China

OPEN ACCESS

Edited by:

Salvatore Salomone,
Università degli Studi di Catania, Italy

Reviewed by:

Shanchun Guo,
Xavier University of Louisiana,
United States
Hua Yang,
Third Military Medical University,
China

*Correspondence:

Rong Gui
aguirong@163.com
Jing Liu
jiliuliuyswq@126.com

[†] These authors have contributed
equally to this work

Specialty section:

This article was submitted to
Experimental Pharmacology
and Drug Discovery,
a section of the journal
Frontiers in Pharmacology

Received: 18 November 2018

Accepted: 14 January 2019

Published: 31 January 2019

Citation:

Dong H, Jiang S, Fu Y, Luo Y,
Gui R and Liu J (2019) Upregulation
of lncRNA NR_046683 Serves as
a Prognostic Biomarker and Potential
Drug Target for Multiple Myeloma.
Front. Pharmacol. 10:45.
doi: 10.3389/fphar.2019.00045

Aim: To investigate the prognostic value of lncRNA NR_046683 in multiple myeloma (MM).

Methods: High-throughput lncRNA array was combined with bioinformatics techniques to screen differentially expressed lncRNA in MM. qRT-PCR was adopted to determine the expression of target lncRNAs in MM patients and controls.

Results: It was found for the first time that lncRNA NR_046683 is closely related to the prognosis of MM. It was also detected in tumor cell lines KM3, U266, especially in drug-resistant cell lines KM3/BTZ and MM1R. The NR_046683 expression differed significantly in patients of different MM subtypes and staging. Moreover, the overexpression of NR-046683 is closely related to β_2 -microglobulin. We also found that the overexpression of NR-046683 correlates to chromosomal aberrations, such as del(13q14), gain 1q21, and t(4;14).

Conclusion: lncRNA NR_046683 can serve as a novel biomarker for potential drug target and prognostic prediction in MM.

Keywords: lncRNA, NR_046683, multiple myeloma, prognostic factor, drug target

INTRODUCTION

Multiple myeloma (MM) is a hematologic malignancy caused by the proliferation of plasma cells in bone marrows. MM is the second most common cancer of blood system after non-Hodgkin lymphoma, and is associated with the signs and symptoms of bone pain, pathologic fractures, hypercalcemia, anemia, and renal failure (Chen W. C. et al., 2017; Cowan et al., 2018). MM usually develops from monoclonal gammopathy of under determined significance (MGUS) (Weiss et al., 2009; Kyle and Rajkumar, 2010). The development from MGUS to MM is accompanied by genetic variations such as cytogenetic aberrations, primary or secondary chromosomal translocation and oncogene activation. Understanding these genetic variations is of high importance for prognostic and response prediction.

Non-coding RNAs (ncRNAs) are defined as RNA molecules that do not encode proteins, but recent evidence has proven that peptides/proteins encoded by ncRNAs do indeed exist and may have an important role in regulating tumor energy metabolism, epithelial to mesenchymal transition of cancer cells (Zhu et al., 2018). These peptides/proteins represent promising drug

targets for fighting against tumor growth or biomarkers for predicting the prognosis of cancer patients. Depending on length, ncRNAs are divided into short and long ncRNAs (lncRNAs). lncRNAs are usually longer than 200 nt and highly conservative during mammal evolution (including human). lncRNAs are involved in many biological processes, such as gene transcription regulation, maintenance of genomic integrity, X-chromosome inactivation, genomic imprinting, cell differentiation and development. lncRNAs are known to be abnormally expressed in cancer tissues and involved in carcinogenesis or tumor suppression (Poliseno et al., 2010; Hung and Chang, 2014). The human lncRNA catalog has been constantly expanding in recent years. The largest database of lncRNAs transcripts contains over 90,000 human lncRNA genes (e.g., 51, 382 LNCipedia v5.0; 96, 308 Noncode v5.0) (Volders et al., 2015; Fang et al., 2018). Although, the working mechanism of most lncRNAs remains unclear, the dysregulation of different lncRNAs contributes to the development and metastasis of different tumors, such as breast cancer, gastric cancer, hematologic cancer, and lung cancer (Chen J. S. et al., 2016; Rodriguez-Malave and Rao, 2016; Alvarez-Dominguez and Lodish, 2017; Cai et al., 2017; Fu et al., 2018).

The latest bioinformatics technique was used in combination with high-throughput lncRNA database of a small sample size to identify lncRNAs. These lncRNAs influenced the therapeutic response and efficacy of MM. Real-time quantitative polymerase chain reaction (qRT-PCR) was adopted to determine the expression of target lncRNAs in plasma cells from the bone marrows of MM patients and controls. lncRNA-mRNA co-expression network was established by combining with medical history of patients. It was then analyzed whether or not the expression of target lncRNAs could be used to predict the prognosis of MM. This was of high clinical significance to identify effective biomarkers and new treatment targets for MM.

MATERIALS AND METHODS

Clinical Data

From January 2012 to January 2018, 86 cases (53 males and 33 females) with MM treated at the Third Xiangya Hospital of Central South University were recruited. Their bone marrow samples and clinical data were collected. The median age of MM onset was 55 years old (44–78 years). All included cases had complete clinical and pathological data (Table 1). All MM cases were diagnosed according to the diagnostic criteria developed by International Myeloma Working Group (IMWG) (Rajkumar et al., 2011). Given the lack of bone marrow samples from normal donors, the sample variation was reduced by selecting 30 cases with iron deficiency anemia (IDA) as controls, and their bone marrow samples were collected. The sample collection was approved by the hospital's ethics committee (approval number: 2016121) and the informed consents were signed by all cases.

RNA Extraction

Total RNA extraction was performed from bone marrow samples of MM and IDA patients. Prior to use, RNA samples were

TABLE 1 | Characteristics of study population.

Clinical characteristics	MM patients	Value
Sex	Male	53 (62%)
	Female	33 (38%)
Age (yr)		Median 55 (range: 44–78)
International staging system	Stage 1	16 (19%)
	Stage 2	33 (38%)
	Stage 3	37 (43%)
Durie-Salmon stage	Stage 1	40 (47%)
	Stage 2	20 (23%)
	Stage 3	26 (30%)
Isotype	IgG	43 (50%)
	IgA	22 (26%)
	Light chain	12 (14%)
	Unclassified	9 (10%)
Percentage of myeloma cells in BM	<40%	57 (66%)
	≥ 40%	29 (34%)
Bone disease	No	7 (8%)
	Yes	79 (92%)
Renal insufficiency	No	67 (78%)
	Yes	19 (22%)
Cytogenetic abnormality	No	29 (34%)
	Yes	57 (66%)
Hemoglobin (g/dl)		101.18 ± 26.11
Platelet count ($\times 10^9/L$)		169.29 ± 88.43
Neutrophil ($\times 10^9/L$)		2.81 ± 1.96
Albumin (g/L)		34.21 ± 6.46
Globulin (g/L)		32.90 ± 22.40
LDH (IU/L)		265.23 ± 161.23
β_2 -MG ($\mu g/ml$)		5.35 ± 3.88
Creatinine ($\mu mol/L$)		106.18 ± 122.22
Serum Calcium (mmol/L)		2.21 ± 0.20

MM, multiple myeloma; BM, bone marrow; LDH, lactate dehydrogenase; β_2 -MG, β_2 -microglobulin.

stored at $-80^\circ C$. NanoDrop ND-1000 was used to determine RNA concentration and activity. RNA integrity was assessed by denaturing gel electrophoresis.

Result Analysis of High-Throughput lncRNA Array and Differential Expression

Labeling and array hybridization were performed using Agilent One-Color Microarray-Based Gene Expression Protocol (Agilent Technology). rRNA was removed from total RNA using mRNA-ONLY TM, Eukaryotic mRNA Isolation Kit (Epicenter). Each sample was amplified and transcribed into fluorescent-labeled cRNA. The labeled cRNAs were purified

TABLE 2 | Primers designed for qRT-PCR validation of candidate lncRNAs.

	Primer	Tm (°C)
β-actin	F:5' GTGGCCGAGGACTTTGATTG3' R:5' CCTGTAACAACGCATCTCATATT 3'	60
NR_104063	F:5' AAGCAAAAGTGCAGAAAACCAT 3' R:5' CTGAGTGACCTGTTGCCTGAA 3'	60
T283430	F:5' AGAAATGGGATACCAAAGGAGT 3' R:5' TCCTCTCTATCCTTCAGCACAT 3'	60
NR_046683	F:5' GATGTGATGCCTGAAGATGTG 3' R:5' TTCTGTGCTGCCAGTTGTG 3'	60
uc021pbg.1	F:5' CTACCTGAGCCAGTTCTCCTAA 3' R:5' GGGTTCCTCATCGGTGTAAT 3'	60

using RNeasy Mini Kit (Qiagen), and NanoDrop ND-1000 was used to determine its concentration and activity. Microarray hybridization was performed (Arraystar Human lncRNA Array V4.0). Microarray images were generated using Agilent Feature Extraction (v11.0.1.1), and the original data were read. Quantile normalization was performed on the original data using GeneSpring GX v12.1 (Agilent Technologies) with data processing. Differentially expressed lncRNA were identified based on fold change and *p* value. The fold-change threshold

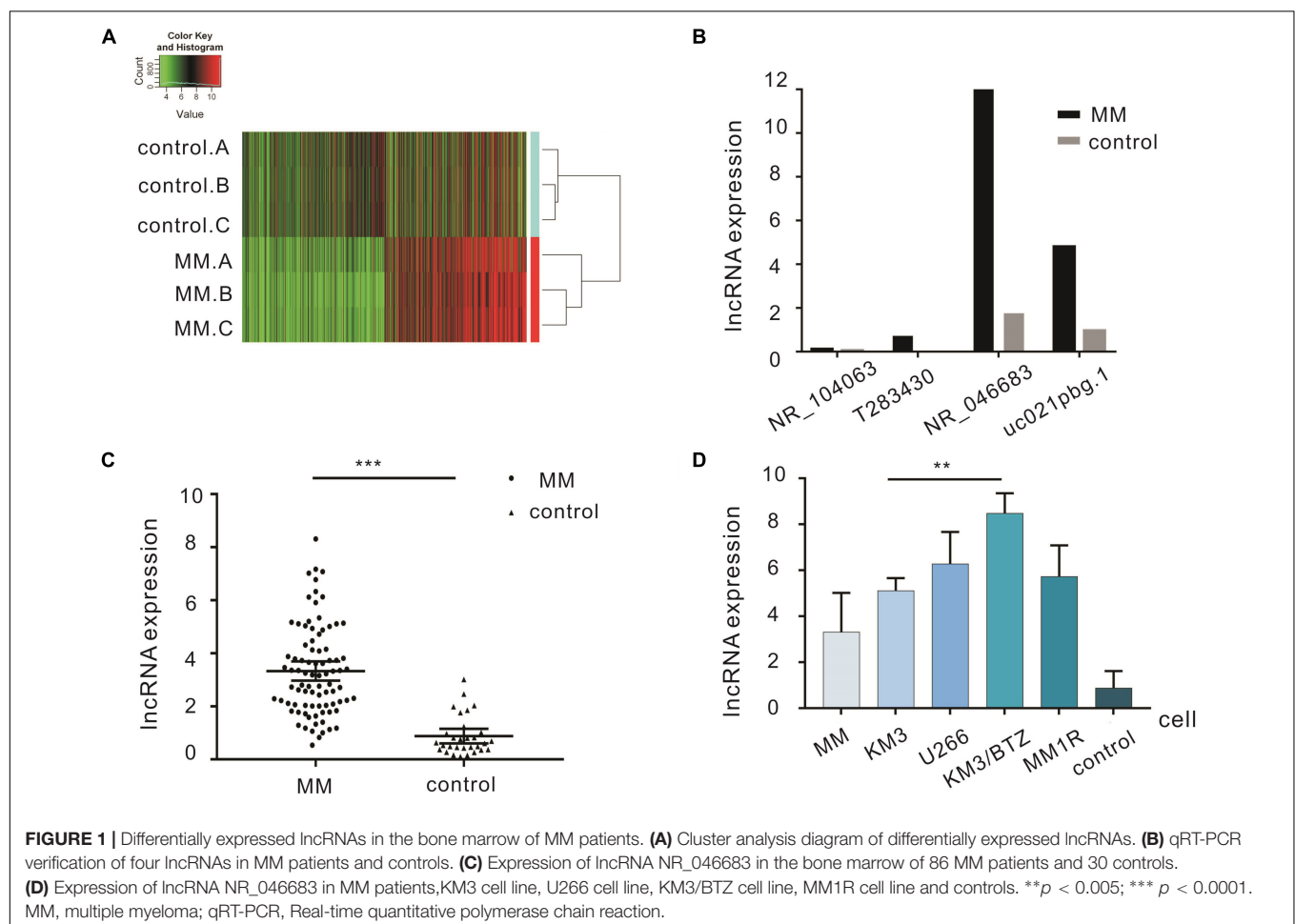
for upregulated and downregulated genes was >2.0 with $p < 0.05$.

Verification by Quantitative RT-PCR

RNA was reversely transcribed into cDNA using SuperScript III Reverse Transcriptase (Invitrogen, Grand Island, NY, United States). qRT-PCR (Arraystar) was performed using ViiA 7 Real-time PCR System (Applied Biosystems) and 2 × PCR Master Mix. The reaction conditions were as follows: incubation at 95°C for 10 min, 95°C 10 s and 60°C 1 min, a total of 40 cycles. β-actin was taken as internal reference and the expression of target lncRNAs was normalized based on β-actin. ΔCt value indicated the lncRNA expression level. Primers for each gene are shown in Table 2.

Functional Analysis of lncRNA

The correlations between differentially expressed lncRNAs and mRNAs were determined. The lncRNA-mRNA co-expression network was established based on the normalized signal intensity of lncRNAs and mRNA. Using Pearson's correlation coefficient ≥ 0.7 , mRNA and encoding genes were determined. Then the lncRNA-mRNA co-expression network was established according to mRNA/lncRNA expression correlation using



Cytoscape (The Cytoscape Consortium, San Diego, CA, United States) (Pujana et al., 2007). GO analysis was conducted using Kyoto Encyclopedia of Genes and Genomes (Zhao et al., 2015; Chen R. et al., 2016). GO analysis was also used to determine the biological functions of the adjacent protein-coding genes of the target lncRNAs.

Statistical Analysis

Statistical analyses were performed using SPSS 20.0 software. The relative expression of target lncRNAs in bone marrow samples from MM and IDA patients was compared by using the Mann-Whitney test. Multiple intergroup comparisons were performed using Kruskal-Wallis H test. Kaplan-Meier survival curve was plotted, and log-rank test was used to detect significant difference in the survival of two groups. The Chi-square test was adopted to analyze the relationship between upregulated and downregulated lncRNAs and chromosomal aberrations. $p < 0.05$ indicated significant difference.

RESULTS

Differentially Expressed lncRNAs in the Bone Marrow of MM Patients

From 3 cases of MM and 3 cases of IDA diagnosed preliminarily, high-throughput lncRNA array was used and thousands of differentially expressed lncRNAs were detected. There were 1489 upregulated lncRNAs and 1661 downregulated lncRNAs (Figure 1A). qRT-PCR was performed to verify the 4 most significantly upregulated lncRNAs in 20 MM cases and 10 IDA cases. NR_046683 was most significantly upregulated (Figure 1B), so the expression of lncRNA NR_046683 was further detected in 66 MM patients (Figure 1C). At the same time, we detected its expression in cell lines KM3, U266, KM3/BTZ, and MM1R. The results showed that it was highly expressed in drug-resistant strains (Figure 1D). The results indicated that lncRNA NR_046683 is a reliable biomarker and potential drug target for MM diagnosis.

Relationship Between lncRNA NR_104063 Expression and Clinicopathological Features of MM Patients

The correlation between lncRNA expression and clinicopathological factors (e.g., age, gender, subtype, and staging) was determined (Table 3). The results showed that lncRNA NR_046683 correlated to the subtype ($H = 18.2$, $p < 0.001$) and ISS staging of MM ($H = 12.982$, $p = 0.002$), but not to age, gender or DS staging.

Clinical Significance of lncRNA Expression of MM Patients

Based on the above results, the correlation between lncRNA NR_046683 expression in bone marrow and serum β_2 M, albumin, λ light chain and κ light chain levels was determined in

TABLE 3 | Correlations between the relative expression of lncRNA NR_046683 and clinicopathologic features in 86 MM patients.

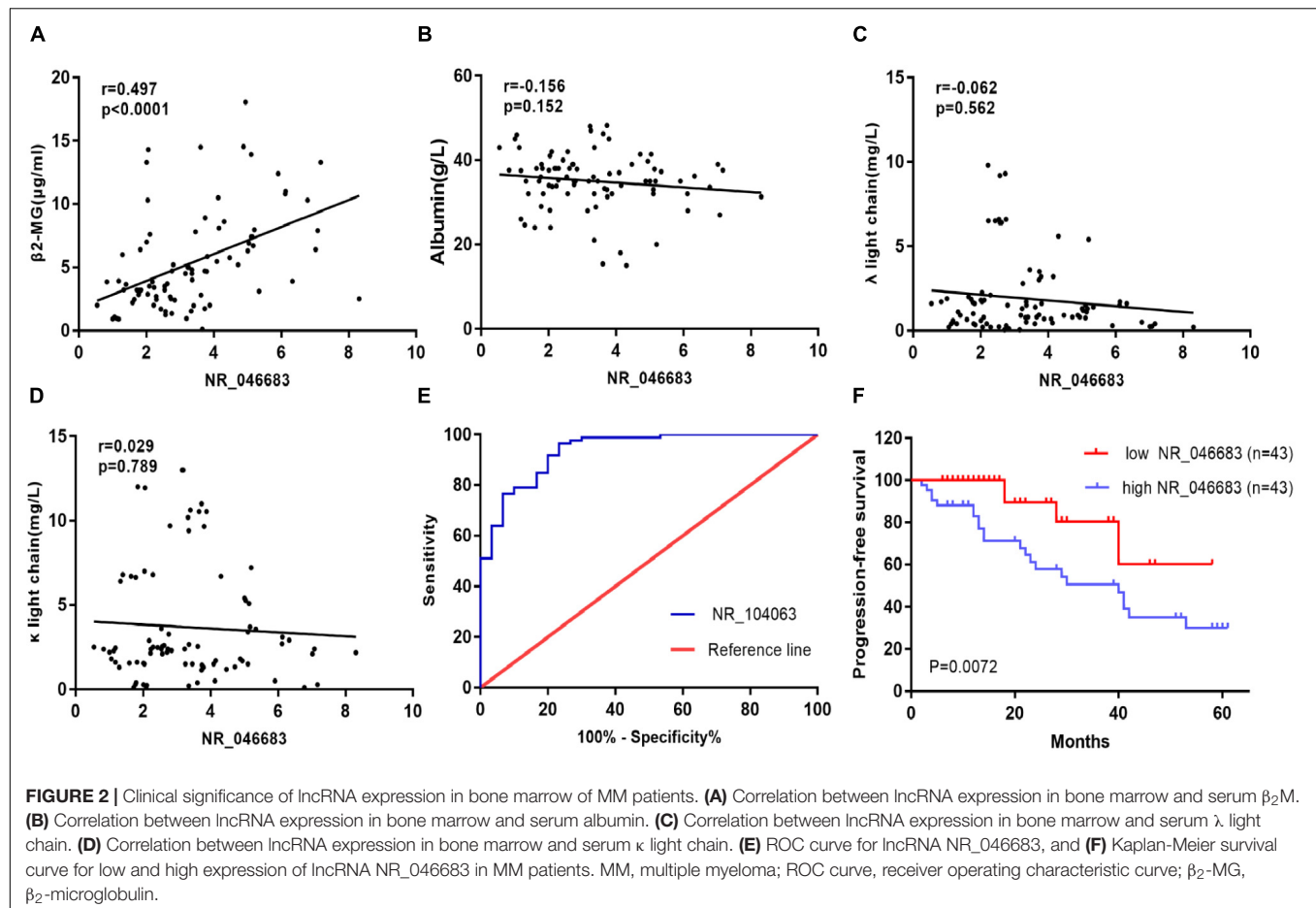
Clinicopathologic features	Cases	NR_046683 relative expression (Mean \pm SD)	U/H value	P value
Age (yr)			U = 1120	0.205
<60	48	2.80 \pm 1.22		
≥ 60	38	3.96 \pm 2.00		
Sex			U = 602.5	0.174
Male	53	3.60 \pm 1.54		
Female	33	2.89 \pm 1.83		
Isotype			H = 18.2	0.000*
IgG	43	2.98 \pm 1.64		
IgA	22	3.79 \pm 1.25		
Light chain	12	4.64 \pm 2.00		
Unclassified	9	1.86 \pm 0.65		
International staging system			H = 12.982	0.002*
Stage 1	16	2.45 \pm 1.65		
Stage 2	33	3.03 \pm 1.59		
Stage 3	37	3.98 \pm 1.58		
Durie-Salmon stage			H = 1.9	0.387
Stage 1	40	3.26 \pm 1.63		
Stage 2	23	2.76 \pm 0.61		
Stage 3	26	3.88 \pm 2.18		
Cytogenetic abnormality			U = 1154	0.003*
Yes	57	2.66 \pm 1.68		
No	29	3.67 \pm 1.61		

SD, standard deviation; U value, Mann-Whitney test; H value, Kruskal-Wallis H-test. * $p < 0.05$.

86 MM patients. The relative expression of NR_046683 correlated positively to β_2 M levels ($r = 0.497$, $p < 0.001$), but not to albumin, λ light chain or κ light chain levels ($r = -0.156$, $p = 0.152$; $r = -0.062$, $p = 0.562$; $r = 0.029$, $p = 0.789$) (Figures 2A–D). The estimated ROC curves were compared between the MM group and control group (Figure 2E), and the sensitivity and specificity on NR_046683 were evaluated. The AUC value was 0.9376 (95%CI 0.8899–0.9853). The correlation between lncRNA and prognosis of MM patients was analyzed (Figure 2F). None of the 86 MM patients dropped out during the follow-up. Using the median expression of NR_046683 in the bone marrows of MM patients, the patients were divided into high and low lncRNA expression groups. The prognostic value of lncRNA for MM was determined based on progression-free survival (PFS).

Correlation Between lncRNA Expression and Cytogenetic Variation

Using the median expression of lncRNA NR_046683, the patients were divided into low and high expression groups, and the correlation to chromosomal aberrations was assessed using the chi-square test. The over expression of lncRNA NR_046683 was found to be correlated to chromosomal aberrations, such as gain 1q2 ($p = 0.0096$), del. 13q14 ($P = 0.0288$) and $t(4; 14)$ ($p = 0.0266$), but not to hyperdiploid ($p = 0.3722$) (Table 4).



Functional Analysis of lncRNA

lncRNAs targeted by miRNAs were used for the prediction of target genes and the subsequent functional analysis. lncRNA NR_046683 was selected to establish the lncRNA-mRNA co-expression network (Figure 3A). A total of 76 mRNAs was

correlated to lncRNA NR_046683, including ROR2, MTBP and ATP2C2, which are tumor-related protein-coding genes. GO analysis indicated that the genes of lncRNA NR_046683 were mainly involved in the activation of leukocyte activation, bone marrow white blood cells, bone marrow cell activation and immune response (Figure 3B).

TABLE 4 | Cytogenetic aberration status distribution between low/high NR_046683 expression groups of MM patients.

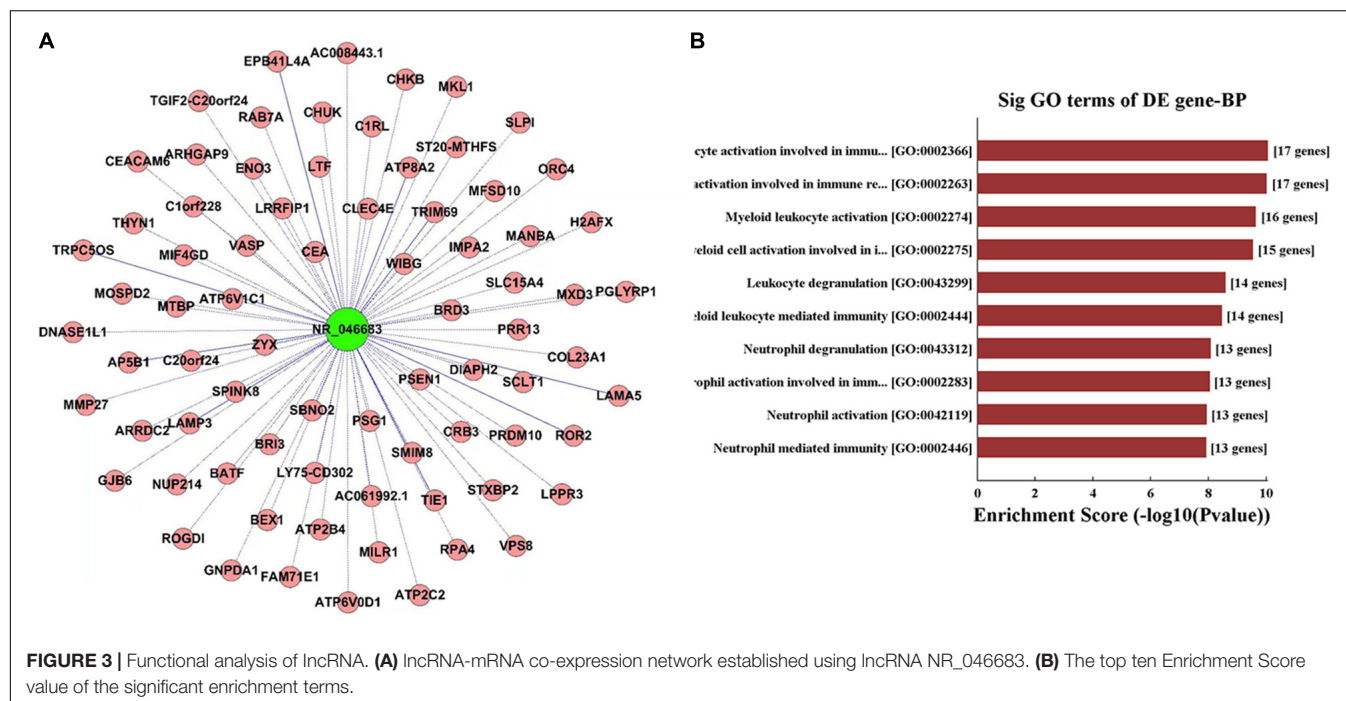
Group	Low NR_046683	High NR_046683	P value
del (13q14)			$P = 0.0288^*$
Positive	30.2% (13/43)	53.5% (23/43)	
Negative	69.8% (30/43)	46.5% (20/43)	
gain 1q21			$P = 0.0096^*$
Positive	34.9% (15/43)	62.8% (27/43)	
Negative	65.1% (28/43)	37.2% (16/43)	
t(4;14)			$P = 0.0266^*$
Positive	9.3% (4/43)	28.9% (12/43)	
Negative	90.7% (39/43)	72.1% (31/43)	
Hyperdiploidy			$P = 0.3722$
Positive	41.9% (18/43)	32.6% (14/43)	
Negative	58.1% (25/43)	67.4% (29/43)	

MM: multiple myeloma; * $p < 0.05$.

DISCUSSION

MM is a highly heterogenous clonal disease with complex molecular biological characteristics that leads to renal injury, anemia and bone destruction. Along with microenvironmental changes, abnormalities in biomarkers and cytogenetics may already be present before the presentation of symptoms appear (Chen R. et al., 2017; Cowan et al., 2018). Therefore, the search for new indicators for early clinical diagnosis, therapeutic response and prognostic prediction is an urgent issue.

Recent evidences have demonstrated that lncRNA has a key role in the pathogenesis of tumors. lncRNAs can be used for cancer diagnosis, classification, and prognostic evaluation, along with acting as a potential drug target (Huarte, 2015). Previous studies mainly focus on the effect of known lncRNAs on MM. For example, metastasis-associated lung



adenocarcinoma transcript 1 (MALAT-1) is overexpressed in some solid tumors (Tripathi et al., 2010; Yang et al., 2013). Cho, S. F. et al. proved the overexpression of MALAT1 of newly diagnosed MM, suggesting that MALAT1 was an eligible biomarker for early progression. lncRNA PDIA3P is found to play an important role in oral squamous cell carcinoma and hepatocellular carcinoma (Kong et al., 2017; Sun et al., 2017). Yang et al. (2018) clarified the potential regulatory mechanism of lncRNA PDIA3P in the pentose phosphate pathway in MM. Moreover, potential targets of metabolic regulation and drug resistance were identified for MM.

For the first time, we combined high-throughput lncRNA array with bioinformatics technique and found an overexpression of lncRNA NR-046683 in bone marrows of MM patients. This result was then verified by using qRT-PCR in large samples ($n = 86$). Combining with the clinicopathological features of MM patients, we found that the NR-046683 expression differed significantly in patients with different MM subtypes and staging. In addition, the overexpression of NR-046683 was closely related to the concentration of β_2 -microglobulin. β_2 -microglobulin has been clinically validated and recognized by most doctors. It is a meaningful indicator closely related to multiple myeloma (Avet-Loiseau et al., 2007). By verifying the relationship between our newly discovered molecules and these indicators, lnc NR-046683 can be used as a biomarker for diagnosis and prognostic prediction in MM.

Chromosomal aberrations are considered relevant to the diagnosis, progression and prognostic prediction of MM (Kumar et al., 2012). In the present study, an overexpression of NR-046683 correlated to the gain 1q21, del. 13q14, and $t(4; 14)$,

all of which are associated with a poor prognosis of MM (Nemec et al., 2012). To some extent, an overexpression of NR-046683 is correlated to disease progression and predicted poor prognosis. In addition, an analysis of lncRNA-mRNA co-expression indicated that lncRNA is related to ROR2 and MTBP genes (Bi et al., 2015; Debebe and Rathmell, 2015; Lu et al., 2015), which are tumor-associated protein-coding genes. It is implied that lncRNA NR_046683 is possibly involved in the regulation of biological behaviors of tumor cells. Using GO analysis, lncRNA NR_046683-associated mRNA was involved in the activation of bone marrow white blood cells and immune response. This implied that lncRNA NR_046683 may potentially promote MM development and progression by regulating proliferation and apoptosis of bone marrow white blood cells.

The accuracy of bioinformatics technique was verified based on big sample data, indicating that NR-046683 is a candidate target for the treatment of MM. However, the present study is a single-center small-sample-size experiment, from which the results had limitations in guiding clinical treatment (Luo et al., 2018). In the future, the sample size should be enlarged. Understanding the biological features of lncRNA NR-046683 and its involvement in the pathophysiological process of MM is crucial for treatment.

Analysis on lncRNA-mRNA co-expression and GO analysis provides theoretical basis for further investigation. Linkage of lncRNA NR-046683 to mRNA suggests that the lncRNA might provide a potential drug target for small molecule or antibody approaches in controlling the activity of the gene product. As lncRNAs are novel targets with often undefined mechanisms, it is critical to find therapeutic targets for drug discovery during disease progression.

To conclude, lncRNA NR-046683 can serve as a novel biomarker for potential drug target and prognostic prediction in MM.

DATA AVAILABILITY STATEMENT

The datasets generated for this study can be found in Arraystar Human LncRNA Array V4.0, <https://www.arraystar.com/human-lncrna-expression-array-v4-0/>.

ETHICS STATEMENT

Ethical approval for this study was obtained from the Ethics Committee of the Third Xiangya Hospital of Central South University (No. 2016121).

REFERENCES

- Alvarez-Dominguez, J. R., and Lodish, H. F. (2017). Emerging mechanisms of long noncoding RNA function during normal and malignant hematopoiesis. *Blood* 130, 1965–1975. doi: 10.1182/blood-2017-06-788695
- Avet-Loiseau, H., Attal, M., Moreau, P., Charbonnel, C., Garban, F., Hulin, C., et al. (2007). Genetic abnormalities and survival in multiple myeloma: the experience of the intergroupe francophone du myelome. *Blood* 109, 3489–3495. doi: 10.1182/blood-2006-08-040410
- Bi, Q., Ranjan, A., Fan, R., Agarwal, N., Welch, D. R., Weinman, S. A., et al. (2015). MTBP inhibits migration and metastasis of hepatocellular carcinoma. *Clin. Exp. Metastasis* 32, 301–311. doi: 10.1007/s10585-015-9706-5
- Cai, C., Huo, Q., Wang, X., Chen, B., and Yang, Q. (2017). SNHG16 contributes to breast cancer cell migration by competitively binding miR-98 with E2F5. *Biochem. Biophys. Res. Commun.* 485, 272–278. doi: 10.1016/j.bbrc.2017.02.094
- Chen, J. S., Wang, Y. F., Zhang, X. Q., Lv, J. M., Li, Y., Liu, X. X., et al. (2016). H19 serves as a diagnostic biomarker and up-regulation of H19 expression contributes to poor prognosis in patients with gastric cancer. *Neoplasma* 63, 223–230. doi: 10.4149/207_150821N454
- Chen, R., Liu, L., Xiao, M., Wang, F., and Lin, X. (2016). Microarray expression profile analysis of long noncoding RNAs in premature brain injury: a novel point of view. *Neuroscience* 319, 123–133. doi: 10.1016/j.neuroscience.2016.01.033
- Chen, R., Zhang, X., Gao, C., Luan, C., Wang, Y., and Chen, B. (2017). Treatment and prognostic factors for survival in newly diagnosed multiple myeloma patients with bortezomib and dexamethasone regimen: a single Chinese center retrospective study. *Cancer Manag. Res.* 9, 373–380. doi: 10.2147/CMAR.S144405
- Chen, W. C., Kanate, A. S., Craig, M., Petros, W. P., and Hazlehurst, L. A. (2017). Emerging combination therapies for the management of multiple myeloma: the role of elotuzumab. *Cancer Manag. Res.* 9, 307–314. doi: 10.2147/CMAR.S117477
- Cowan, A. J., Allen, C., Barac, A., Basaleem, H., Bensenor, I., Curado, M. P., et al. (2018). Global burden of multiple myeloma: a systematic analysis for the global burden of disease study 2016. *JAMA Oncol.* 4, 1221–1227. doi: 10.1001/jamaoncol.2018.2128
- Debebe, Z., and Rathmell, W. K. (2015). Ror2 as a therapeutic target in cancer. *Pharmacol. Ther.* 150, 143–148. doi: 10.1016/j.pharmthera.2015.01.010
- Fang, S., Zhang, L., Guo, J., Niu, Y., Wu, Y., Li, H., et al. (2018). NONCODEV5: a comprehensive annotation database for long non-coding RNAs. *Nucleic Acids Res.* 46, D308–D314. doi: 10.1093/nar/gkx1107
- Fu, Y., Li, C., Luo, Y., Li, L., Liu, J., and Gui, R. (2018). Silencing of long non-coding RNA MIAT sensitizes lung cancer cells to gefitinib by epigenetically regulating miR-34a. *Front. Pharmacol.* 9:82. doi: 10.3389/fphar.2018.00082
- Huarte, M. (2015). The emerging role of lncRNAs in cancer. *Nat. Med.* 21, 1253–1261. doi: 10.1038/nm.3981

AUTHOR CONTRIBUTIONS

HD and SJ designed and performed the study. HD, RG, and JL wrote the manuscript with inputs from all authors. YF and YL performed the analytic calculations and statistical analysis. All authors provided critical feedback and helped to shape the research, analysis, and manuscript.

FUNDING

This study was supported by Hunan Provincial Natural Science Foundation of China (Grant No. 2017JJ3463) and the Graduate Self-Exploration and Innovation Project of Central South University of China (Grant No. 2018zzts941).

- Hung, T., and Chang, H. Y. (2014). Long noncoding RNA in genome regulation. *RNA Biol.* 7, 582–585. doi: 10.4161/rna.7.5.13216
- Kong, Y., Zhang, L., Huang, Y., He, T., Zhang, L., Zhao, X., et al. (2017). Pseudogene PDIA3P1 promotes cell proliferation, migration and invasion, and suppresses apoptosis in hepatocellular carcinoma by regulating the p53 pathway. *Cancer Lett.* 407, 76–83. doi: 10.1016/j.canlet.2017.07.031
- Kumar, S., Fonseca, R., Ketterling, R. P., Dispenzieri, A., Lacy, M. Q., Gertz, M. A., et al. (2012). Trisomies in multiple myeloma: impact on survival in patients with high-risk cytogenetics. *Blood* 119, 2100–2105. doi: 10.1182/blood-2011-11-390658
- Kyle, R. A., and Rajkumar, S. V. (2010). Monoclonal gammopathy of undetermined significance and smoldering multiple myeloma. *Curr. Hematol. Malig. Rep.* 5, 62–69. doi: 10.1007/s11899-010-0047-9
- Lu, S., Zhou, W., Wei, H., He, L., and Li, L. (2015). MTBP Promotes the invasion and metastasis of hepatocellular carcinoma by enhancing the mdm2-mediated degradation of E-Cadherin. *Dig. Dis. Sci.* 60, 3681–3690. doi: 10.1007/s10620-015-3824-4
- Luo, X. W., Du, X. Q., Li, J. L., Liu, X. P., and Meng, X. Y. (2018). Treatment options for refractory/relapsed multiple myeloma: an updated evidence synthesis by network meta-analysis. *Cancer Manag. Res.* 10, 2817–2823. doi: 10.2147/CMAR.S166640
- Nemec, P., Zemanova, Z., Kuglik, P., Michalova, K., Tajtlova, J., Kaisarova, P., et al. (2012). Complex karyotype and translocation t(4;14) define patients with high-risk newly diagnosed multiple myeloma: results of CMG2002 trial. *Leuk. Lymphoma* 53, 920–927. doi: 10.3109/10428194.2011.634042
- Poliseno, L., Salmena, L., Zhang, J., Carver, B., Haveman, W. J., and Pandolfi, P. P. (2010). A coding-independent function of gene and pseudogene mRNAs regulates tumour biology. *Nature* 465, 1033–1038. doi: 10.1038/nature09144
- Pujana, M. A., Han, J. D., Starita, L. M., Stevens, K. N., Tewari, M., Ahn, J. S., et al. (2007). Network modeling links breast cancer susceptibility and centrosome dysfunction. *Nat. Genet.* 39, 1338–1349. doi: 10.1038/ng.2007.2
- Rajkumar, S. V., Harousseau, J. L., Durie, B., Anderson, K. C., Dimopoulos, M., Kyle, R., et al. (2011). Consensus recommendations for the uniform reporting of clinical trials: report of the international myeloma workshop consensus panel 1. *Blood* 117, 4691–4695. doi: 10.1182/blood-2010-10-299487
- Rodriguez-Malave, N. I., and Rao, D. S. (2016). Long noncoding RNAs in hematopoietic malignancies. *Brief Funct. Genomics* 15, 227–238. doi: 10.1093/bfgp/rlv047
- Sun, C. C., Zhang, L., Li, G., Li, S. J., Chen, Z. L., Fu, Y. F., et al. (2017). The lncRNA PDIA3P interacts with mir-185-5p to modulate oral squamous cell carcinoma progression by targeting cyclin D2. *Mol. Ther. Nucleic Acids* 9, 100–110. doi: 10.1016/j.omtn.2017.08.015
- Tripathi, V., Ellis, J. D., Shen, Z., Song, D. Y., Pan, Q., Watt, A. T., et al. (2010). The nuclear-retained noncoding RNA MALAT1 regulates alternative splicing

- by modulating SR splicing factor phosphorylation. *Mol. Cell.* 39, 925–938. doi: 10.1016/j.molcel.2010.08.011
- Volders, P. J., Verheggen, K., Menschaert, G., Vandepoele, K., Martens, L., Vandesompele, J., et al. (2015). An update on LNCipedia: a database for annotated human lncRNA sequences. *Nucleic Acids Res.* 43, D174–D180. doi: 10.1093/nar/gku1060
- Weiss, B. M., Abadie, J., Verma, P., Howard, R. S., and Kuehl, W. M. (2009). A monoclonal gammopathy precedes multiple myeloma in most patients. *Blood* 113, 5418–5422. doi: 10.1182/blood-2008-12-195008
- Yang, F., Yi, F., Han, X., Du, Q., and Liang, Z. (2013). MALAT-1 interacts with hnRNP C in cell cycle regulation. *FEBS Lett.* 587, 3175–3181. doi: 10.1016/j.febslet.2013.07.048
- Yang, X., Ye, H., He, M., Zhou, X., Sun, N., Guo, W., et al. (2018). lncRNA PDIA3P interacts with c-Myc to regulate cell proliferation via induction of pentose phosphate pathway in multiple myeloma. *Biochem. Biophys. Res. Commun.* 498, 207–213. doi: 10.1016/j.bbrc.2018.02.211
- Zhao, Z., Bai, J., Wu, A., Wang, Y., Zhang, J., Wang, Z., et al. (2015). Co-lncRNA: investigating the lncRNA combinatorial effects in go annotations and kegg pathways based on human RNA-Seq data. *Database* 2015, bav082. doi: 10.1093/database/bav082
- Zhu, S., Wang, J., He, Y., Meng, N., and Yan, G. R. (2018). Peptides/proteins encoded by non-coding RNA: a novel resource bank for drug targets and biomarkers. *Front. Pharmacol.* 9:1295. doi: 10.3389/fphar.2018.01295
- Conflict of Interest Statement:** The authors declare that the research was conducted in the absence of any commercial or financial relationships that could be construed as a potential conflict of interest.
- Copyright © 2019 Dong, Jiang, Fu, Luo, Gui and Liu. This is an open-access article distributed under the terms of the Creative Commons Attribution License (CC BY). The use, distribution or reproduction in other forums is permitted, provided the original author(s) and the copyright owner(s) are credited and that the original publication in this journal is cited, in accordance with accepted academic practice. No use, distribution or reproduction is permitted which does not comply with these terms.



Research Progress on PARP14 as a Drug Target

Wei Qin[†], Hong-Jie Wu[†], Lu-Qi Cao, Hui-Jin Li, Chun-Xia He, Dong Zhao, Lu Xing, Peng-Quan Li, Xi Jin and Hui-Ling Cao*

Shaanxi Key Laboratory of Ischemic Cardiovascular Disease, Shaanxi Key Laboratory of Brain disorders, Institute of Basic and Translational Medicine, Xi'an Medical University, Xi'an, China

OPEN ACCESS

Edited by:

Dong-Hua Yang,
St. John's University, United States

Reviewed by:

Bashir M. Rezk,
Southern University at New Orleans,
United States
Laura Calza,
University of Bologna, Italy

*Correspondence:

Hui-Ling Cao
caohuiling_jzs@xmu.edu.cn

[†]These authors have contributed
equally to this work

Specialty section:

This article was submitted to
Experimental Pharmacology and Drug
Discovery,
a section of the journal
Frontiers in Pharmacology

Received: 26 November 2018

Accepted: 11 February 2019

Published: 05 March 2019

Citation:

Qin W, Wu H-J, Cao L-Q, Li H-J, He
C-X, Zhao D, Xing L, Li P-Q, Jin X and
Cao H-L (2019) Research Progress on
PARP14 as a Drug Target.
Front. Pharmacol. 10:172.
doi: 10.3389/fphar.2019.00172

Poly-adenosine diphosphate-ribose polymerase (PARP) implements posttranslational mono- or poly-ADP-ribosylation modification of target proteins. Among the known 18 members in the enormous family of PARP enzymes, several investigations about PARP1, PARP2, and PARP5a/5b have been launched in the past few decades; more specifically, PARP14 is gradually emerging as a promising drug target. An intact PARP14 (also named ARTD8 or BAL2) is constructed by macro1, macro2, macro3, WWE, and the catalytic domain. PARP14 takes advantage of nicotinamide adenine dinucleotide (NAD⁺) as a metabolic substrate to conduct mono-ADP-ribosylation modification on target proteins, taking part in cellular responses and signaling pathways in the immune system. Therefore, PARP14 has been considered a fascinating target for treatment of tumors and allergic inflammation. More importantly, PARP14 could be a potential target for a chemosensitizer based on the theory of synthetic lethality and its unique role in homologous recombination DNA repair. This review first gives a brief introduction on several representative PARP members. Subsequently, current literatures are presented to reveal the molecular mechanisms of PARP14 as a novel drug target for cancers (e.g., diffuse large B-cell lymphoma, multiple myeloma, prostate cancer, and hepatocellular carcinoma) and allergic inflammatory. Finally, potential PARP inhibitor-associated adverse effects are discussed. The review could be a meaningful reference for innovative drug or chemosensitizer discovery targeting to PARP14.

Keywords: PARP14, drug target, cancer, atherosclerosis, allergic inflammation, molecular mechanism

INTRODUCTION

The poly-adenosine diphosphate-ribose polymerase (PARP) enzyme family catalyzes protein posttranslational ribosylation modification and utilizes nicotinamide adenine dinucleotide (NAD⁺) as a substrate to perform mono- or poly-ADP-ribosylation modification on target proteins (Amé et al., 2004; Vyas et al., 2014). Notably, the PARP family is also known as the ADP-ribosyltransferase Diphtheria-toxin like (ARTD) family, which is based on its enzymatic reaction and structural features (Hottiger et al., 2010). Another alias that describes some of its members is B-Aggressive lymphoma (BAL) proteins, in that some of PARP candidates are homologous with BAL proteins that were encoded by genes that were first discovered in diffuse large B-cell lymphoma (DLBCL) (Aguirre et al., 2005). For simplicity, this review will refer to the traditional name of PARP family.

PARP was first identified in 1963 (Chambon et al., 1963) and currently there are 18 members classified in different subgroups of the PARP family (Vyas et al., 2013). Interestingly, there is low amino acid sequence homology among its family members. Their N-termini have obvious variability in their domains and functional motifs, including regulatory motifs, the zinc finger, and ubiquitin-binding domains. However, most candidates have a similar conserved C-terminal catalytic domain. Representative members such as PARP1, PARP2, and PARP5a/5b have been investigated intensively, whereas studies on PARP14 are currently rare. As a mono-ADP-ribosyltransferase, PARP14 (ARTD8/BAL2) includes 1,801 amino acids and it mainly consists of macro1-3, WWE and the catalytic domain. Except the self-evident importance of the catalytic domain, the unique macro domains can engage in biological metabolism through binding mono (ADP-ribose). PARP14 can modify mono-ADP-ribosylation on target proteins, and thus elicit cellular responses. In fact, interest in PARP14 has grown in recent years as a potential drug target for tumors and allergic inflammation.

Because of its functions in ADP-ribosylation, PARP plays a key role in different processes of metabolism, such as DNA repair, transcription regulation and even pathogenesis of diseases. Remarkably, in tumor cells, PARP inhibitors can treat cancer by aggravating DNA damage from error-prone repair, inducing unstable genome that leads to the programmed death of cancer cells. Therefore, PARP has been a promising anticancer drug target for breast, ovarian, and prostate cancers. Many inhibitors in preclinical and clinical trials target both PARP1 and PARP2. In the Protein Data Bank (PDB), there are now 43 PARP1 or PARP1/2 inhibitors being released (<http://www.rcsb.org/pdb/>, 2019.01.31). Among them, a dozen PARP1/2 inhibitors are in clinical trials and four inhibitors (olaparib, rucaparib, niraparib, and talazoparib) have been approved by the US food and drug administration (FDA) for the treatment of breast cancer and ovarian cancer with breast cancer susceptibility gene 1/2 (*BRCA1/2*) genetic deficiency, fallopian tube carcinoma and peritoneal carcinoma (Gunderson and Moore, 2015; Dockery et al., 2017; Scott, 2017; Hoy, 2018).

Although more and more novel inhibitors are being evaluated in preclinical and clinical trials, there are two possible issues of vital concern in the application of PARP as a drug target. The first is the possibility of these inhibitors to function while bypassing PARP. For instance, minocycline, a potent PARP1 inhibitor, can protect against allergen-induced asthma by the means of controlling the T cell receptor (TCR)-nuclear factor κ B (NF- κ B)-trans-acting T-cell-specific transcription factor (GATA3)-interleukin-4 (IL-4) axis, without a direct modulation of PARP1 activity (Naura et al., 2013). Another thought-provoking proposal is the repurposing of PARP inhibitor such as olaparib for the treatment of other kinds of tumors beyond *BRCA*-deficient cancers. There is evidence that PARP1 regulates estrogen-dependent breast cancer cell growth through the modulation of the estrogen receptor (ER)-insulin-like growth factor 1 receptor (IGF-1R)-Na(+)/H(+) exchange regulatory cofactor NHE-RF3 (PDZK1) axis. Thus, PARP inhibitors may be powerful weapons for the therapy of ER-positive cancers (Kim et al., 2015).

As we briefly introduce the PARP family, highlight the number of recent literatures that elucidate the molecular mechanisms of PARP14 as a drug target for cancers and immunological diseases, and detail the potential toxicity for consideration, we hope this review becomes a significant reference in the development of a new drug or a chemosensitizer and further research concerning PARP14.

STRUCTURE AND FUNCTION OF THE PARP MEMBERS

PARPs perform posttranslational mono-/poly-ADP-ribosylation modification on target proteins, which include PARPs themselves (Amé et al., 2004). The negatively charged linear or branched chains of poly (ADP-ribose) on target proteins change the biochemical properties of these macromolecules, leading to the alteration of their structures and functions (Gagne et al., 2008). Activated PARP breaks down NAD⁺ into nicotinamide and ADP-ribose, and connects 50–200 ADP-ribose units to the target proteins via covalent bonds (Altmeyer et al., 2009). At sites of DNA damage, poly-ADP ribosylation PARP recruits various enzymes to initiate DNA repair, and to promote the growth and proliferation of cells (Satoh and Lindahl, 1992). Notably, the continuous activities of poly-ADP ribosylation may block rebinding of PARP to damaged DNA fragments, resulting in a pause of the repair process. To eliminate unintended effects, poly (ADP-ribose) glycohydrolase (PARG) cleaves the long poly (ADP-ribose) chains into short chains to recover the DNA damage repair activity of PARP (Satoh et al., 1994).

PARP1 and PARP2 have been amply studied for many years. PARP1 consists of three domains, including a DNA-binding domain, an auto-modification domain and a catalytic domain (Kameshita et al., 1984; Thomas and Tulin, 2013). The DNA-binding domain is composed of three zinc finger motifs involved in the recognition of damaged DNA regions. In addition, it contains a signal to facilitate PARP1 localization in the nucleus (Decker et al., 2000). When a catalytic process is completed, the auto-modification domain is responsible for protein dissociation from DNA substrate via the posttranslational modification on PARP1 (Altmeyer et al., 2009). Furthermore, a specific region within this domain, called the breast cancer-associated 1 C-terminal domain (BRCT), may mediate the binding activity between PARP1 and other partner molecules (Masson et al., 1998). The catalytic domain binds NAD⁺ to achieve poly-ADP ribosylation on target proteins, which is also the target of drug design (Langelier et al., 2011). PARP2 and PARP1 have similar structures, with 69% homology. The main difference is that PARP2 lacks an N-terminal DNA-binding domain. It has been speculated that several residues in the N-terminal domain of PARP2 may be capable of binding target DNA fragments and are involved in nuclear localization activity (Oliver et al., 2004). Due to their indispensable role in DNA repair and cellular metabolism, PARP1 and PARP2 are attractive anticancer targets. For instance, as the first PARP inhibitor, olaparib (Lynparza) was approved by the US FDA in 2014 as monotherapy for *BRCA*-mutant advanced ovarian cancer. In December 2016, the

US FDA granted accelerated approval of rucaparib (Rubraca) for the therapy of previously treated BRCA-deficient ovarian cancer. Only 1 year later, niraparib (Zejula) was approved by the US FDA for the treatment of epithelial ovarian, fallopian tube, and primary peritoneal cancer. In October 2018, talazoparib (Talzenna) was approved for use as an oral PARP inhibitor by the US FDA for the treatment of BRCA-deficient, human epidermal growth factor receptor 2 (HER2)-negative, locally advanced or metastatic breast cancer (Gunderson and Moore, 2015; Dockery et al., 2017; Scott, 2017; Hoy, 2018).

PARP5a and PARP5b, also known as tankyrase 1 and tankyrase 2, may be other potential drug targets. There is a high level of homology between PARP5b and PARP5a (~85%), with the notable discrepancy being that there is no His-Pro-Ser motif in PARP5b. PARP5a/5b comprises of an ankyrin repeat domain, an oligomerization domain, and a catalytic domain (Morrone et al., 2012). The N-terminal of PARP5a contains a His-Pro-Ser motif, which has functional similarity to mitogen-activated protein kinase (MAPK). The enzymatic activity of PARP5a is markedly enhanced by the phosphorylation of this motif, activated by insulin stimulation, which indicates that PARP5a is a potential target in insulin signal transduction (De Rycker et al., 2003). Moreover, in the C-terminal region of PARP5a, the oligomerization domain (known as the sterile alpha motif, SAM) plays a crucial role during the process of PARP oligomerization and interaction with other target proteins (DaRosa et al., 2016).

Compared with PARP1, the domains of PARP14 are relatively simple. Full-length PARP14 is composed of five primary domains: macro1 (791–978), macro2 (1003–1190), macro3 (1216–1387), WWE (1523–1601), and a catalytic domain (1605–1801) (Forst et al., 2013). There are two contiguous RNA recognition motif (RRM) domains in front of the N-terminus, required for RNA recognition (Schweiker et al., 2018). From the determined crystal structures and solution structure (WWE) of these domains, it has been found that all three macro domains are very similar to some extent, with several β -sheets and 2–3 α -helices on each side (Figure 1). More importantly, three consecutive macro domains (containing 180 amino acids) are engaged in ADP-ribose binding on the N-terminus, which can specifically recognize mono (ADP-ribose) rather than poly (ADP-ribose) (Feijs et al., 2013; Forst et al., 2013). Based on this function of macro domains, cofactor proteins might be linked by this bridge to form complicated functional complexes in biological metabolism. The WWE domain is particularly involved in protein-protein interactions in ubiquitination and is composed of three conserved residues (Trp-Trp-Glu) between the macro domains and the C-terminal catalytic domain (Aravind, 2001). The catalytic domain is involved in the mono-ADP-ribosylation modification of target proteins, which include PARP14 itself. Intriguingly, on account of special macro and catalytic domains, PARP14 is integrated with an executor, as well as a reader of ADP-ribosylation at the same time. In 2012, the first complex crystal structure of the catalytic domain and its inhibitor, 3-aminobenzamide (3AB), was determined, which laid the structural basis for drug discovery associated with this domain (Wahlberg et al., 2012). Plenty of literature indicated that PARP14 is not only related to cancers but also to other diseases,

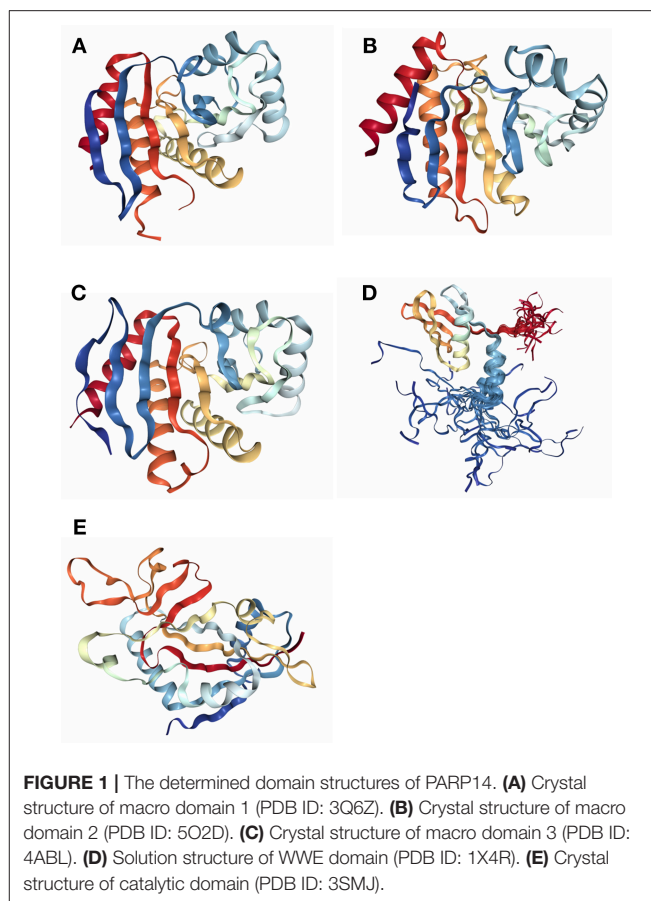


FIGURE 1 | The determined domain structures of PARP14. **(A)** Crystal structure of macro domain 1 (PDB ID: 3Q6Z). **(B)** Crystal structure of macro domain 2 (PDB ID: 5O2D). **(C)** Crystal structure of macro domain 3 (PDB ID: 4ABL). **(D)** Solution structure of WWE domain (PDB ID: 1X4R). **(E)** Crystal structure of catalytic domain (PDB ID: 3SMJ).

such as atherosclerosis and allergic inflammation. As a result, PARP14 has great potential as a new drug target for the treatment of diverse diseases.

THE CLASSICAL MECHANISM OF PARP14 AS A DRUG TARGET

PARP14 can cleave one NAD^+ molecule into one ADP ribose and nicotinamide, and then transfer the mono (ADP-ribose) unit onto target proteins. Based on this particular biochemical reaction in cells, PARP14 has been regarded as an arrestive drug target for anticancer and anti-inflammatory therapy. But questions remain on how to achieve this intention and regarding the exact molecular mechanism behind this hypothesis. Until recent years, only one convincing mechanism has been discovered to illustrate the critical role of PARP14 in cellular signal pathway.

Signal transducer and activator of transcription 6 (STAT6) plays a key positive role in the regulation of IL-4-dependent gene activation. PARP14 acts as a molecular switch that controls gene transcription, beginning with STAT6-mediated IL-4 dependent gene transcription activation (Goenka et al., 2007; Mehrotra et al., 2011). At first, PARP14 was deemed a collaborator to STAT6 (CoaSt6) because of its ability to facilitate IL-4-dependent transcription, and the macro domains

of PARP14 could enhance IL-4-induced gene expression by cooperation with STAT6 (Goenka and Boothby, 2006). In the absence of IL-4, PARP14 initially binds histone deacetylases 2 and 3 (HDAC2 and HDAC3), as well as IL-4 responsive promoters, to maintain gene silence. Upon IL-4 stimulation, STAT6 is activated to bind its target genes, which induces the catalytic activation of PARP14. Active PARP14 accomplishes mono-ADP-ribosylation on HDAC2, HDAC3 and itself, which allows PARP14 and HDACs to dissociate from IL-4-responsive promoters, in order to recruit nuclear receptor coactivator 1 and 3 (NCoA1 and NCoA3) and p300 to bind IL-4-responsive promoters. Next, histones are acetylated, and this starts a specific downstream gene transcription (Goenka and Boothby, 2006; Goenka et al., 2007; Mehrotra et al., 2011), as shown in **Figure 2**. Both the inactive mutant of PARP14 and inhibition of its activity using inhibitor 3AB block IL-4-dependent transcription from target promoters *in vivo* (Goenka et al., 2007).

In some tumor cells, cytokine IL-4 can act as a pro-survival signal factor and activate downstream STAT6 to begin responsive gene transcription for anti-apoptotic activity. Beyond the IL-4-STAT6 signaling pathway, there are some distinct and more

complicated modes of communication among PARP14 and other cell factors implicated in physiological metabolism, exemplifying the complexity of disease pathogenesis. PARP14 could be a profound drug target as more knowledge beyond its classical mechanism is revealed.

NEW DRUG TARGET PARP14

New Drug Target for Cancer

According to the classical mechanism mentioned above, as the transcriptional switch for STAT6-dependent gene expression, PARP14 takes advantage of mono-ADP-ribosyltransferase activity to mediate transcription of target genes involved in growth and proliferation of tumor cells (Goenka and Boothby, 2006; Goenka et al., 2007; Mehrotra et al., 2011). PARP14 could be a possible therapeutic target for cancers such as DLBCL. However, the pathogenesis of other types of cancers including multiple myeloma (MM), prostate cancer (PCa) and hepatocellular carcinoma (HCC) are not consistent with the classical mechanism. PARP14 would perform intricate roles in the development and progression of these tumors.

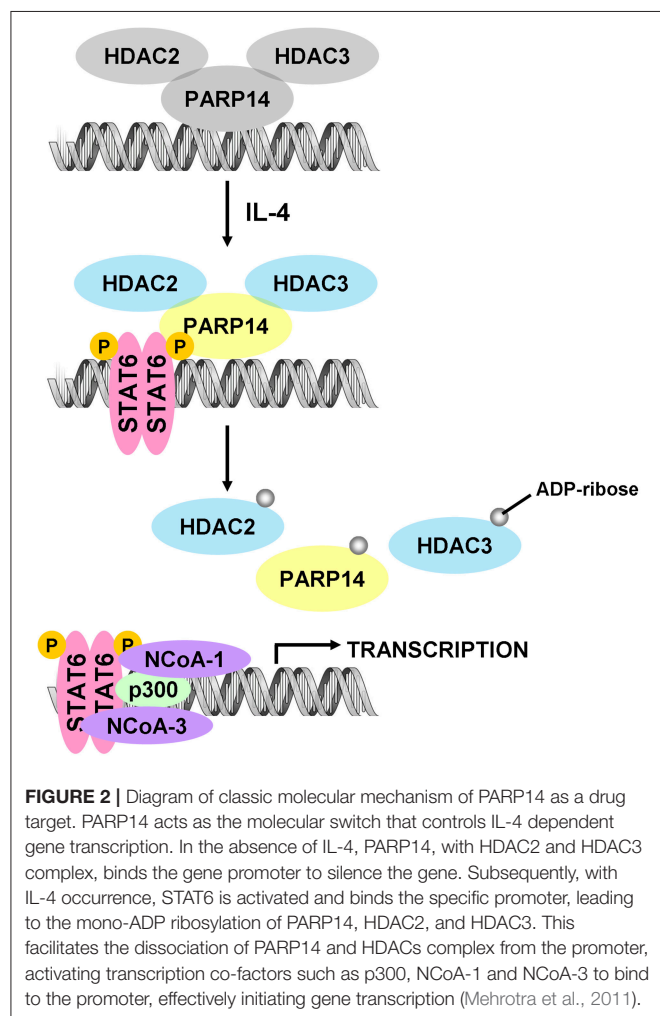
New Drug Target for Diffuse Large B-Cell Lymphoma (DLBCL)

DLBCL is a lymphoid malignancy of B cells, which are responsible for producing antibodies. As an aggressive tumor, DLBCL can arise in any part of the body, with typical symptoms including rapidly growing masses located in multiple lymph nodes. It was indicated that PARP14 is overexpressed in some subtypes of DLBCL cell lines (Camicia et al., 2013). PARP14, as a coregulator of STAT6, regulates STAT6-dependent gene expression in B cells to facilitate B-cell survival and proliferation against the adverse conditions of irradiation and growth factor deficiency, in order to avoid apoptosis (Goenka et al., 2007; Cho et al., 2009). Based on the aforementioned, classical mechanism, PARP14 can modulate the IL-4-STAT6 signaling pathway to enhance several downstream gene expressions, allowing DLBCL tumor cell survival. There are two remarkable factors (Pim-1 and Mcl-1) induced in the process of regulation to protect DLBCL against apoptosis. Moreover, as a cofactor of transcription, PARP14 can prevent cell death by inhibiting the activity of caspase-3 in the context of IL-4 induction (Cho et al., 2009).

Another typical example of the role of PARP14 in B lymphomagenesis is that IL-4 enhances glycolysis and glucose oxidation to promote the growth and proliferation of B cells. Furthermore, PARP14 accelerates lymphoma growth and, conversely, PARP14 deficiency prohibits c-Myc-induced B-lymphoid oncogenesis in a mice model. The results showed that PARP14 (mediated by IL-4) is a key component of the pro-survival signaling pathway for lymphoma (Cho et al., 2011). Therefore, PARP14 has garnered more attention as a drug target for anti-DLBCL therapy.

New Drug Target for Multiple Myeloma (MM)

MM, as the second most common hematologic malignancy, is characterized by the abnormal cloning and proliferation of plasma cells. Unfortunately, MM currently remains incurable



(Raab et al., 2009; Rajkumar, 2011). There are no obvious initial symptoms. However, symptoms such as bone pain, frequent infections, and anemia may occur with disease progression. There are several signaling pathways involved in the occurrence and progression of human cancers. An important pathway is MAPK, which participates in the regulation of cell survival (Geest and Coffey, 2009). As a key part of this signaling pathway, the Jun N-terminal kinase (JNK) signaling pathway plays an important role in cell proliferation and apoptosis via the phosphorylation of target proteins, which is involved in tumorigenesis (Bogoyevitch and Kobe, 2006).

The JNK2-PARP14-JNK1 axis is extraordinarily vital to the fate of malignant MM cells (Barbarulo et al., 2013). JNK1 and JNK2 are two crucial members from among the JNK proteins, and the nuclear activity of JNK2 is continuously active, resulting in the protective effect and prolonged life span of MM cells, which mainly rely on the blockade of JNK1-associated apoptosis. Recent findings demonstrated that PARP14 is overexpressed in over 80% of MM cell lines. Intriguingly, JNK2 may regulate PARP14 expression in an indirect manner at the transcriptional or post-transcriptional level, which is beneficial to the survival of myeloma cells. This pro-survival function is extremely dependent on PARP14 as a mediator. As a novel downstream target of JNK2, PARP14 can facilitate MM cell survival by binding and inhibiting the kinase activity of JNK1. The suppression of JNK1 catalytic activity is achieved through the binding of JNK1 and PARP14, with the assistance of the C-terminal region of PARP14, which impedes JNK1-dependent apoptosis. One reasonable hypothesis is that the WWE domain of PARP14 related to the protein-protein interactions may be engaged in this binding process. Nevertheless, whether the PARP14 catalytic activity is indispensable in blocking JNK1 kinase activity remains unknown. Additionally, inhibition of PARP14, using the chemical inhibitor PJ34, makes MM cells much more sensitive to antimyeloma drugs (Barbarulo et al., 2013). The results may shed new light on PARP14 as an anti-MM drug target.

New Drug Target for Prostate Cancer (PCa)

Recent studies provide new clues about the fascinating functions of PARP14 in PCa progression (Bachmann et al., 2014). PCa is a common malignancy in men worldwide, with the tendency to metastasize from the prostate to other parts of the body. Investigations on metastatic PCa (mPCa) cell lines have revealed that PARP14, together with deltex-3-like E3 ubiquitin ligase (DTX3L) and PARP9, promoted mPCa cell survival and proliferation by forming complexes, which implies that the catalytic activity of PARP14 is indispensable for the survival of mPCa cells. To be specific, in mPCa cells, overexpression of DTX3L, PARP14, and PARP9 are constitutive in the context of interferon γ (IFN γ)-STAT1 signaling increasing. DTX3L binds to the catalytic domain of PARP9 (Takeyama et al., 2003). In mPCa cells, DTX3L can form a strong endogenous complex with PARP14 and PARP9. Interestingly, both DTX3L and PARP9 can interact with PARP14 tightly, which means that DTX3L, PARP9, and PARP14 can form complexes with each other. However, the mechanisms behind these interactions are quite distinct. Particularly, the formation of complexes

between DTX3L and PARP9 or PARP14 are independent from ADP-ribosylation. On the contrary, the interaction between PARP9 and PARP14 strongly relies on mono-ADP-ribosylation. Whether the interaction between PARP9 and PARP14 is regulated by their macro domains, requires further investigation. The study indicated that the interaction between PARP10 and PARP14 is regulated by the macro domains, which would give some inspiring clues (Feijs et al., 2013; Forst et al., 2013).

Furthermore, studies also indicated that DTX3L and PARP9 regulate proliferation of mPCa cells in a STAT1-dependent manner by the inhibition of interferon regulatory factor 1 (IRF1) expression. More importantly, there is crosstalk between PARP14-STAT6 and DTX3L/PARP9-STAT1 signaling pathways to achieve the goal of mPCa cell survival (Bachmann et al., 2014). Thus, the combined inhibition of PARP14 together with other protein factors may provide an effective strategy to improve the traditional treatment of PCa.

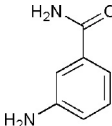
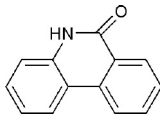
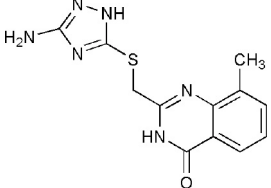
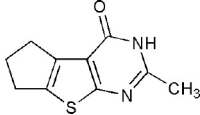
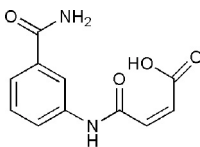
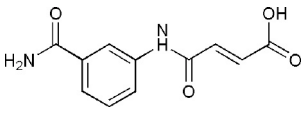
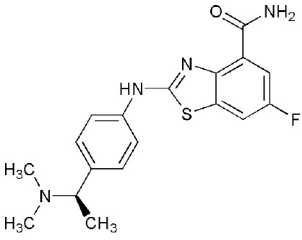
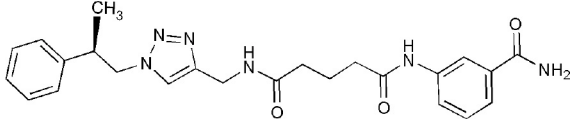
New Drug Target for Hepatocellular Carcinoma (HCC)

A study concerning aerobic glycolysis (the Warburg effect) in HCC showed an amazing connection between cell survival and apoptosis (Iansante et al., 2015). HCC is not only the most common type of primary liver cancer but is also the most common cause of death from liver cirrhosis in adults. It is well-known that the rapid proliferation of cancer cells (including HCC cells) always utilizes aerobic glycolysis to provide energy for growth. In HCC and cirrhotic livers, there is an obvious up-regulation of PARP14 expression correlated with glycolytic gene expression, which clearly predicts the vital role of PARP14 in HCC cell growth and survival. Not surprisingly, the Warburg effect is severely hampered with the knockdown of PARP14. So, what is the molecular mechanism behind this shadow?

Generally, PARP14 causes impairment of the JNK1-dependent phosphorylation of pyruvate kinase M2 (PKM2) in HCC cells. As a mediator of aerobic glycolysis in tumor cells, PKM2 can translocate to the nucleus, interacting with transcription factors such as hypoxia-inducible factor (HIF) 1 α and Myc to enhance glycolytic gene expression (Yang et al., 2012). Moreover, Tyr105 residue of PKM2 can be directly phosphorylated by the tyrosine kinase fibroblast growth factor receptor-1 (FGFR1) to inactivate PKM2, resulting in a transfer of glycolytic intermediates in biosynthetic pathways (Hitosugi et al., 2009).

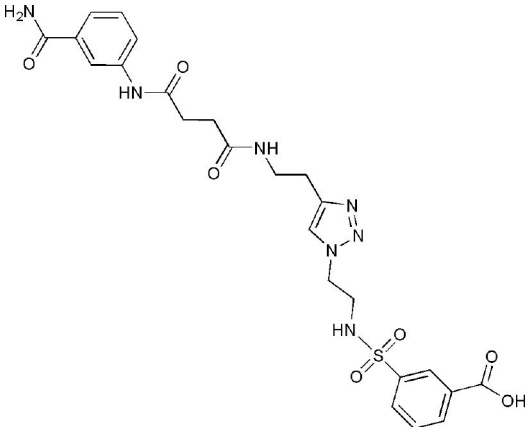
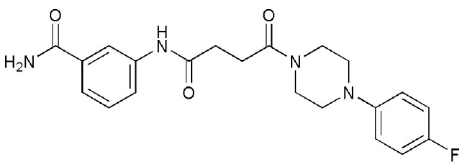
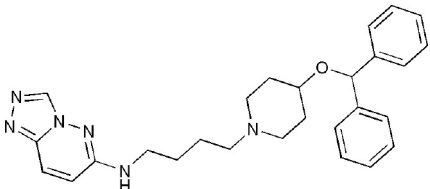
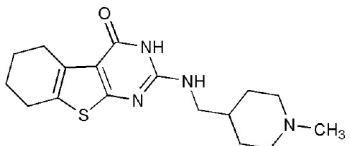
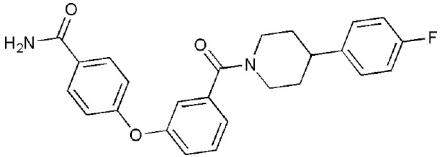
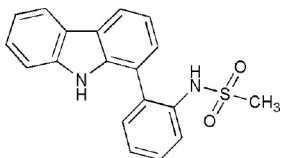
In HCC cells, PARP14 being a pro-survival protein can firstly impede the serine/threonine kinase activity of pro-apoptosis protein JNK1, which is an upstream regulator of PKM2. This leads to the subsequent inhibition of the nuclear function of downstream PKM2, which promotes tumor cell survival. Notably, JNK1 can directly activate PKM2 by phosphorylating at the Thr365 residue, which is crucial for the catalytic activity of PKM2. In other words, the low activity of PKM2 is suitable for the aerobic glycolysis that promotes HCC cell survival by accumulating antioxidants. In contrast, in the absence of PARP14, PKM2 is phosphorylated by active JNK1, leading to the conversion of glucose to pyruvate, which enhances cell apoptosis. In addition, the inhibition of

TABLE 1 | PARP14 ligands and their crystal structures available in PDB.

PDB ID	Ligand	Target domain	Structure
3GOY	3-aminobenzamide	Catalytic domain	
3SE2	phenanthridin-6(5H)-one	Catalytic domain	
3SMI	2-[[[(3-amino-1H-1,2,4-triazol-5-yl)sulfanyl]methyl]-8-methylquinazolin-4(3H)-one	Catalytic domain	
3SMJ	2-methyl-3,5,6,7-tetrahydro-4H-cyclopenta[4,5]thieno[2,3-d]pyrimidin-4-one	Catalytic domain	
4F1L	(2Z)-4-[(3-carbamoylphenyl)amino]-4-oxobut-2-enoic acid	Catalytic domain	
4F1Q	(2E)-4-[(3-carbamoylphenyl)amino]-4-oxobut-2-enoic acid	Catalytic domain	
4PY4	2-[(4-[(1R)-1-(dimethylamino)ethyl]phenyl)amino]-6-fluoro-1,3-benzothiazole-4-carboxamide	Catalytic domain	
5LXP	~[N]'--(3-aminocarbonylphenyl)-~[N]-[[1-[(2~)-2-phenylpropyl]-1,2,3-triazol-4-yl]methyl]pentanediamide	Catalytic domain	

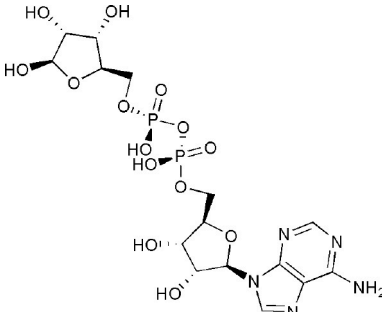
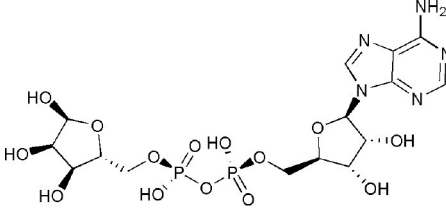
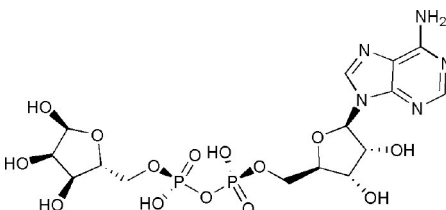
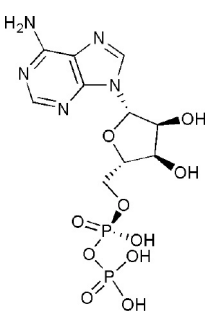
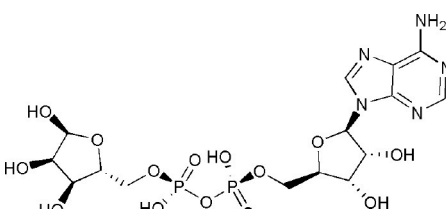
(Continued)

TABLE 1 | Continued

PDB ID	Ligand	Target domain	Structure
5LYH	3-[2-[4-[2-[(3-aminocarbonylphenyl)amino]-4-oxidanylidenebutanoyl]amino]ethyl]-1,2,3-triazol-1-yl]ethylsulfamoyl]benzoic acid	Catalytic domain	
5NQE	3-[[4-[4-(4-fluorophenyl)piperazin-1-yl]-4-oxidanylidenebutanoyl]amino]benzamide	Catalytic domain	
5V7T	N-{4-[4-(diphenylmethoxy)piperidin-1-yl]butyl}[1,2,4]triazolo[4,3-b]pyridazin-6-amine	Catalytic domain	
5V7W	2-[[[(1-methylpiperidin-4-yl)methyl]amino]-5,6,7,8-tetrahydro[1]benzothieno[2,3-d]pyrimidin-4(3H)-one	Catalytic domain	
6G0W	4-[3-[4-(4-fluorophenyl)piperidin-1-yl]carbonylphenoxy]benzamide	Catalytic domain	
5O2D	~-[2-(9~-carbazol-1-yl)phenyl]methanesulfonamide	Macro domain 2	

(Continued)

TABLE 1 | Continued

PDB ID	Ligand	Target domain	Structure
3Q6Z	adenosine-5-diphosphoribose	Macro domain 1	
3Q71	adenosine-5-diphosphoribose	Macro domain 2	
3VFQ	adenosine-5-diphosphoribose	Macro domain 1/2	
4D86	adenosine-5-diphosphate	Macro domain 1/2	
4ABK	adenosine-5-diphosphoribose	Macro domain 3	

PARP14 via inhibitor PJ34 can make HCC cells sensitive to anti-HCC drugs (Iansante et al., 2015). However, whether phosphorylation of PKM2 could cause conformational changes of the binding site for its substrates (phosphoenolpyruvate and ADP) or alteration of enzymatic function requires further

investigation. The study revealed that the PARP14-JNK1-PKM2 regulatory axis plays a significant role in the aerobic glycolysis and cellular metabolism of HCC cells. Hence, the development of PARP14 inhibitors may be an effective strategy for HCC treatment.

PARP14 Could Be a New Drug Target for Chemosensitizer

As a traditional pharmacological theory, synthetic lethality means that an expression defect of only one gene cannot lead to cell death, but the combined expression defects of two or more genes could cause cell death. This theory has been successfully applied to molecular targeted cancer therapy.

For instance, *BRCA1* and *BRCA2* are crucial for the repair of double-stranded DNA (dsDNA) damage in homologous recombination repair pathway. Thus, *BRCA1* or *BRCA2* deficiency could lead to serious mistakes in the DNA repair process, which results in breast cancer. PARP1 performs a key role in repairing single-stranded DNA (ssDNA) damage. The application of PARP1 inhibitors to block the activity of this enzyme would cause double strand DNA breaks. In breast cancer cells with *BRCA1/2* mutations, the administration of PARP1 inhibitors would largely destroy the repair of damaged DNA by blocking the homologous recombination repair pathway, eventually leading to cell death. Thus far, the US FDA has approved four PARP inhibitors, olaparib, rucaparib, niraparib, and talazoparib. These PARP inhibitors are outstanding examples of clinically approved chemosensitizers that utilize the synthetic lethality concept (Lord and Ashworth, 2017).

Furthermore, there is evidence showing a novel role for PARP14 in homologous recombination DNA repair. Through interaction with proliferating cell nuclear antigen (PCNA), PARP14 promoted the replication of DNA even through damaged sites to maintain genomic stability. This study indicates that PARP14 inhibition and other undiscovered gene mutations beyond *BRCA1/2* deficiency might hamper the homologous recombination repair pathway, making cancer cells more susceptible to DNA lesions (Nicolae et al., 2015). In fact, the inhibition of PARP14 using inhibitor PJ34 made MM and HCC cells much more sensitive to anti-MM or anti-HCC drugs (Barbarulo et al., 2013; Iansante et al., 2015). The synthetic lethality of PARP14 inhibitors along with an identified genetic defect in the DNA repair process would make PARP14 a remarkable target for chemosensitizer design, which means the combination of PARP14 inhibitors and anticancer drugs causing DNA damage activity can amplify the cancer cell killing effect. Consequently, PARP14 could be a momentous drug target not only as an anticancer drug but also as a chemosensitizer.

New Drug Target For Atherosclerosis

Atherosclerosis (AS), as an independent risk factor for cardiovascular diseases, is a disease characterized by the narrowing of arteries due to plaque accumulation. AS progression over time results in coronary artery disease, stroke, or kidney problems. AS is an autoimmune disease in which an immune response plays a crucial role in its occurrence and development. Studies indicated that PARP14 might regulate post-transcription in macrophages to influence the expression of tissue factor, which plays a pivotal role in AS development (Iqbal et al., 2014). AS plaques are infiltrated by a large number of T helper (Th) cells, among which Th17 cells and its cytokine IL-17 play an important role in AS formation. IL-17 promotes macrophage accumulation in plaques and the release of

cytokines such as tumor necrosis factor α (TNF- α), IL-6, vascular cell adhesion molecule 1 (VCAM-1) and chemokine C-C motif ligand 5 (CCL5) (Erbel et al., 2011). Furthermore, the cytokine-activated vascular endothelial cells induce their apoptosis, which exacerbates inflammation in the vessel and promotes plaque formation (Zhu et al., 2011). Astonishingly, *in vitro*, PARP14 can regulate Th17 cell growth and differentiation as well as IL-17 secretion, to affect AS progression (Mehrotra et al., 2015). However, one recent literature illustrated that inactive PARP14 induced pro-inflammatory genes and suppressed anti-inflammatory gene expression. Moreover, a deficiency of PARP14 in hematopoietic cells worsened the inflammatory response of acute and chronic arterial damage in mice (Iwata et al., 2016). Thus, the accurate role of PARP14 in relation to AS progression is unknown and remains an urgent question to answer before taking advantage of PARP14 as a newborn drug target for AS therapy.

New Drug Target for Allergic Inflammation

Epithelial cells of the airways and the esophagus, and keratinocytes secrete numerous cytokines in response to environmental allergens, leading to the activation of immune processes. This long-term and repeated physiological reaction causes allergic inflammatory diseases such as asthma and eosinophilic esophagitis (EoE).

Asthma is a common chronic inflammatory disease of the airways. Symptoms include wheezing, shortness of breath and coughing, which are a consequence of airway obstruction and airway hyperresponsiveness (AHR). The occurrence and progression of allergic airway diseases (AAD) is closely related to many components of the immune system, including T cells and cytokines (Broide et al., 2011). Studies on a murine model of AAD showed that *Parp14*^{-/-} mice had improved lung pathology, and the inhibition of PARP14 catalytic activity using inhibitor PJ34 attenuated the severity of lung inflammation and AHR. In addition, PARP14 promoted Th2 differentiation *in vitro* by controlling the process of STAT6 binding to *Gata3* promoter (Mehrotra et al., 2013). It was also shown that PARP14 influences the induction of IL-21, which promotes Th17 differentiation through binding target DNA (Riley et al., 2013). Cytokine IL-17A, produced by Th17, is positively correlated with airway resistance in the progression of asthma (Alcorn et al., 2010). PARP14 deficiency and inhibition of its activity by PJ34 decreased Th17 cell numbers in a model of allergic airway inflammation. Moreover, the deficiency of PARP14 in mice impaired T follicular helper (Tfh) development, which plays a key role in allergic responses (Crotty, 2014). All of these changes in Th17 and Tfh development were regulated by PARP14 through controlling the activation of STAT3 via phosphorylation (Mehrotra et al., 2015).

EoE, also known as allergic esophagitis, is an allergic inflammatory condition of the esophagus that is characterized by difficulty swallowing, food impaction, and vomiting (Blanchard et al., 2005). STAT6 regulates the expression of eotaxin-3/CCL26 to produce the accumulation of eosinophil in EoE patients (Kagami et al., 2005; Blanchard et al., 2006; Niranjan et al., 2013). Remarkably, there is an obvious increase in both PARP14 and eotaxin-3 expression, due to the binding of STAT6

with eotaxin-3 promoter in esophageal biopsies from children. The blockade of PARP14 catalytic activity, to a large extent, diminishes eotaxin-3 expression in human esophageal epithelial cells (Krishnamurthy et al., 2014).

INHIBITORS OF PARP14 DOMAINS

Currently, twenty-two structures concerning PARP14 have been released in the PDB. Among them, there are three single domain structures and nineteen complex crystal structures of PARP14 domains binding to ligands. The single domain structures include two solution structures, WWE domain (PDB ID, 1X4R) and RRM domain (PDB ID, 1X5P), and one crystal structure, macro domain 3 (PDB ID, 4ABL). Among nineteen complex crystal structures, there are five endogenous ligands such as ADP and ADP-ribose: one structure for macro domain 1 (PDB ID, 3Q6Z), one structure for macro domain 2 (PDB ID, 3Q71), two structures for macro domain 1/2 (PDB ID, 3VFQ, 4D86) and one structure for macro domain 3 (PDB ID, 4ABK). The ligands of other fourteen structures are small molecular inhibitors: one structure for macro domain 2 (PDB ID, 5O2D) and thirteen structures for the catalytic domain (PDB ID, 3GOY, 3SE2, 3SMI, 3SMJ, 4F1L, 4F1Q, 4PY4, 5LXP, 5LYH, 5NQE, 5V7T, 5V7W, 6G0W) (<http://www.rcsb.org/>, 2019.01.31) (Andersson et al., 2012; Wahlberg et al., 2012; Forst et al., 2013; Peng et al., 2017; Schuller et al., 2017; Upton et al., 2017; Yoneyama-Hirozane et al., 2017; Holeczek et al., 2018; Moustakim et al., 2018). All the PARP14 ligands released in the PDB are summarized in **Table 1**. There is only one inhibitor aimed at macro domain 2 of PARP14, while thirteen inhibitors are designed to target the catalytic domain of this enzyme (**Table 1**). Among the released inhibitors, there are several potent candidates showing remarkable water solubility or favorable selectivity for PARP14 as sub-micromolar inhibitors (Andersson et al., 2012; Peng et al., 2017; Upton et al., 2017). In addition, the macro domains 2 and 3 of PARP14 has been proven to possess outstanding selectivity for ADP-ribose binding function, which indicates that these domains might be potential therapeutic targets for selective inhibition (Forst et al., 2013; Schuller et al., 2017; Moustakim et al., 2018; Schweiker et al., 2018). By taking advantage of the information, researchers could design novel, highly selective inhibitors targeting to the catalytic domain or macro domains of PARP14 to block its enzymatic activities. An obstacle to be aware of is the high conservation of the catalytic domain across PARP family members, which may interfere with designing selective PARP14 inhibitors that do not impact other PARP candidates. In this context, choosing macro or even WWE domains as targets can shed a new light on a possible solution (Schweiker et al., 2018).

Another problem arising in treatment of diseases is the related toxicities of PARP inhibitors. Firstly, many *in vitro* studies illustrated that PARP inhibitors could severely influence chromosomal stability, thereby causing DNA injury and damage of chromosomal integrity, which can manifest dramatic genotoxicity in different cell lines (Berger et al., 2018). Therefore, one must consider the potential genotoxic effects when utilizing PARP inhibitors such as olaparib or veliparib for non-cancer indications.

Albeit no clinical trial data of PARP14 inhibitors has been reported yet, the available evidence from tests of PARP1/2 inhibitors could be reference for consideration. For instance, the associated toxicities of olaparib, niraparib, and rucaparib manifested in distinct physiological reactions in the phase III clinical trials. The typical toxic effects include hematological toxicities (anemia, neutropenia, and thrombocytopenia), gastrointestinal toxicities (nausea, constipation, vomiting, diarrhea, abdominal pain, dyspepsia, and dysgeusia), renal adverse events and fatigue. Additional unique and severe side effects pertaining to this class of drugs include neurological toxicities (headache and insomnia), respiratory toxicities (dyspnea, cough, nasopharyngitis, and upper respiratory tract infection), musculoskeletal toxicities (arthralgia and back pain), cutaneous toxicities (photosensitivity reactions, pruritus, rash, peripheral edema, and urticaria), cardiovascular toxicities (hypertension, tachycardia, and palpitations) and secondary malignancies (myelodysplastic syndrome and acute myeloid leukemia) (LaFargue et al., 2019). There is also a large amount of overlapping toxicities when PARP inhibitors are studied in doublet and triplet combination trials with antiangiogenic drugs, PI3K drugs, immunotherapy, and chemotherapy. As a result, the adverse effects of PARP inhibitors should be treated cautiously with relevant management strategies to attain maximal clinical benefit for patients (LaFargue et al., 2019).

As demonstrated by the associated adverse effects of currently approved PARP inhibitors, selectivity of inhibitors targeting PARP14 becomes more important in avoiding toxicity. This should be carefully considered in the process of designing new drugs or clinical trials concerning PARP14.

AUTHOR CONTRIBUTIONS

WQ and H-JW are responsible for the review writing and reference analysis. L-QC, H-JL, C-XH, and DZ focus on the reference review and analysis. LX, P-QL, and XJ devote themselves to the reference collection. H-LC commits herself to the manuscript revise and polish. All authors have contributed significantly.

FUNDING

This work was supported by the National Natural Science Foundation of China (No. 31700699); the Key Program of Shaanxi Provincial Science and Technology Department (No. 2017ZDXM-SF-029); the Key Program of Shaanxi Provincial Education Department (No. 17JS118, No. 18JS102, No. 17JK0669); Shaanxi Provincial Research Center for the Project of Prevention and Treatment of Respiratory Diseases (No. 2016HXXF07); the Talents Program of Xi'an Medical University (No. 2015RCYJ01, No. 2016DOC12, No. 2016DXS1-27).

ACKNOWLEDGMENTS

We thank Prof. Da-Chuan Yin, Prof. Qi-Bing Mei, and Prof. Jian-Hua He for improving and polishing of the manuscript.

REFERENCES

- Aguiar, R. C., Takeyama, K., He, C., Kreinbrink, K., and Shipp, M. A. (2005). B-aggressive lymphoma family proteins have unique domains that modulate transcription and exhibit poly(ADP-ribose) polymerase activity. *J. Biol. Chem.* 280, 33756–33765. doi: 10.1074/jbc.M505408200
- Alcorn, J. F., Crowe, C. R., and Kolls, J. K. (2010). TH17 cells in asthma and COPD. *Annu. Rev. Physiol.* 72, 495–516. doi: 10.1146/annurev-physiol-021909-135926
- Altmeyer, M., Messner, S., Hassa, P. O., Fey, M., and Hottiger, M. O. (2009). Molecular mechanism of poly(ADP-ribosyl)ation by PARP1 and identification of lysine residues as ADP-ribose acceptor sites. *Nucleic Acids Res.* 37, 3723–3738. doi: 10.1093/nar/gkp229
- Amé, J. C., Spenlehauer, C., and de Murcia, G. (2004). The PARP superfamily. *Bioessays* 26, 882–893. doi: 10.1002/bies.20085
- Andersson, C. D., Karlberg, T., Ekblad, T., Lindgren, A. E., Thorsell, A. G., Spjut, S., et al. (2012). Discovery of ligands for ADP-ribosyltransferases via docking-based virtual screening. *J. Med. Chem.* 55, 7706–7718. doi: 10.1021/jm300746d
- Aravind, L. (2001). The WWE domain: a common interaction module in protein ubiquitination and ADP ribosylation. *Trends Biochem. Sci.* 26, 273–275. doi: 10.1016/S0968-0004(01)01787-X
- Bachmann, S. B., Frommel, S. C., Camicia, R., Winkler, H. C., Santoro, R., and Hassa, P. O. (2014). DTX3L and ARTD9 inhibit IRF1 expression and mediate in cooperation with ARTD8 survival and proliferation of metastatic prostate cancer cells. *Mol. Cancer* 13:125. doi: 10.1186/1476-4598-13-125
- Barbarulo, A., Iansante, V., Chaidos, A., Naresh, K., Rahemtulla, A., Franzoso, G., et al. (2013). Poly(ADP-ribose) polymerase family member 14 (PARP14) is a novel effector of the JNK2-dependent pro-survival signal in multiple myeloma. *Oncogene* 32, 4231–4242. doi: 10.1038/ncr.2012.448
- Berger, N. A., Besson, V. C., Boulares, A. H., Bürkle, A., Chiarugi, A., Clark, R. S., et al. (2018). Opportunities for the repurposing of PARP inhibitors for the therapy of non-oncological diseases. *Br. J. Pharmacol.* 175, 192–222. doi: 10.1111/bph.13748
- Blanchard, C., Durual, S., Estienne, M., Emami, S., Vasseur, S., and Cuber, J. C. (2005). Eotaxin-3/CCL26 gene expression in intestinal epithelial cells is up-regulated by interleukin-4 and interleukin-13 via the signal transducer and activator of transcription 6. *Int. J. Biochem. Cell Biol.* 37, 2559–2573. doi: 10.1016/j.biocel.2005.06.010
- Blanchard, C., Wang, N., Stringer, K. F., Mishra, A., Fulkerson, P. C., Abonia, J. P., et al. (2006). Eotaxin-3 and a uniquely conserved gene-expression profile in eosinophilic esophagitis. *J. Clin. Invest.* 116, 536–547. doi: 10.1172/JCI26679
- Bogoyevitch, M. A., and Kobe, B. (2006). Uses for JNK: the many and varied substrates of the c-Jun N-terminal kinases. *Microbiol. Mol. Biol. Rev.* 70, 1061–1095. doi: 10.1128/MMBR.00025-06
- Broide, D. H., Finkelman, F., Bochner, B. S., and Rothenberg, M. E. (2011). Advances in mechanisms of asthma, allergy, and immunology in 2010. *J. Allergy Clin. Immunol.* 127, 689–695. doi: 10.1016/j.jaci.2011.01.027
- Camicia, R., Bachmann, S. B., Winkler, H. C., Beer, M., Tinguely, M., Haralambieva, E., et al. (2013). BAL1/ARTD9 represses the anti-proliferative and pro-apoptotic IFN γ -STAT1-IRF1-p53 axis in diffuse large B-cell lymphoma. *J. Cell Sci.* 126(Pt 9), 1969–1980. doi: 10.1242/jcs.118174
- Chambon, P., Weill, J. D., and Mandel, P. (1963). Nicotinamide mononucleotide activation of new DNA-dependent polyadenylic acid synthesizing nuclear enzyme. *Biochem. Biophys. Res. Commun.* 11, 39–43. doi: 10.1016/0006-291X(63)90024-X
- Cho, S. H., Ahn, A. K., Bhargava, P., Lee, C. H., Eischen, C. M., McGuinness, O., et al. (2011). Glycolytic rate and lymphomagenesis depend on PARP14, an ADP ribosyltransferase of the B aggressive lymphoma (BAL) family. *Proc. Natl. Acad. Sci. U.S.A.* 108, 15972–15977. doi: 10.1073/pnas.1017082108
- Cho, S. H., Goenka, S., Hentinen, T., Gudapati, P., Reinikainen, A., Eischen, C. M., et al. (2009). PARP-14, a member of the B aggressive lymphoma family, transduces survival signals in primary B cells. *Blood* 113, 2416–2425. doi: 10.1182/blood-2008-03-144121
- Crotty, S. (2014). T follicular helper cell differentiation, function, and roles in disease. *Immunity* 41, 529–542. doi: 10.1016/j.immuni.2014.10.004
- DaRosa, P. A., Ovchinnikov, S., Xu, W., and Kleivit, R. E. (2016). Structural insights into SAM domain-mediated tankyrase oligomerization. *Protein Sci.* 25, 1744–1752. doi: 10.1002/pro.2968
- De Rycker, M., Venkatesan, R. N., Wei, C., and Price, C. M. (2003). Vertebrate tankyrase domain structure and sterile alpha motif (SAM)-mediated multimerization. *Biochem. J.* 372(Pt 1), 87–96. doi: 10.1042/bj20021450
- Decker, P., Isenberg, D., and Muller, S. (2000). Inhibition of caspase-3-mediated poly(ADP-ribose) polymerase (PARP) apoptotic cleavage by human PARP autoantibodies and effect on cells undergoing apoptosis. *J. Biol. Chem.* 275, 9043–9046. doi: 10.1074/jbc.275.12.9043
- Dockery, L. E., Gunderson, C. C., and Moore, K. N. (2017). Rucaparib: the past, present, and future of a newly approved PARP inhibitor for ovarian cancer. *Oncol. Targets. Ther.* 10, 3029–3037. doi: 10.2147/OTT.S114714
- Erbel, C., Dengler, T. J., Wangler, S., Lasitschka, F., Bea, F., Wambsgans, N., et al. (2011). Expression of IL-17A in human atherosclerotic lesions is associated with increased inflammation and plaque vulnerability. *Basic Res. Cardiol.* 106, 125–134. doi: 10.1007/s00395-010-0135-y
- Feijs, K. L., Forst, A. H., Verheugd, P., and Lüscher, B. (2013). Macrodomein-containing proteins: regulating new intracellular functions of mono(ADP-ribosyl)ation. *Nat. Rev. Mol. Cell Biol.* 14, 443–451. doi: 10.1038/nrm3601
- Forst, A. H., Karlberg, T., Herzog, N., Thorsell, A. G., Gross, A., Feijs, K. L., et al. (2013). Recognition of mono-ADP-ribosylated ARTD10 substrates by ARTD8 macrodomains. *Structure* 21, 462–475. doi: 10.1016/j.str.2012.12.019
- Gagne, J. P., Isabelle, M., Lo, K. S., Bourassa, S., Hendzel, M. J., Dawson, V. L., et al. (2008). Proteome-wide identification of poly(ADP-ribose) binding proteins and poly(ADP-ribose)-associated protein complexes. *Nucleic Acids Res.* 36, 6959–6976. doi: 10.1093/nar/gkn771
- Geest, C. R., and Coffey, P. J. (2009). MAPK signaling pathways in the regulation of hematopoiesis. *J. Leukoc. Biol.* 86, 237–250. doi: 10.1189/jlb.0209097
- Goenka, S., and Boothby, M. (2006). Selective potentiation of Stat-dependent gene expression by collaborator of Stat6 (Coast6), a transcriptional cofactor. *Proc. Natl. Acad. Sci. U.S.A.* 103, 4210–4215. doi: 10.1073/pnas.0506981103
- Goenka, S., Cho, S. H., and Boothby, M. (2007). Collaborator of Stat6 (Coast6)-associated poly(ADP-ribose) polymerase activity modulates Stat6-dependent gene transcription. *J. Biol. Chem.* 282, 18732–18739. doi: 10.1074/jbc.M611283200
- Gunderson, C. C., and Moore, K. N. (2015). Olaparib: an oral PARP-1 and PARP-2 inhibitor with promising activity in ovarian cancer. *Fut. Oncol.* 11, 747–757. doi: 10.2217/fon.14.313
- Hitosugi, T., Kang, S., Vander Heiden, M. G., Chung, T. W., Elf, S., Lythgoe, K., et al. (2009). Tyrosine phosphorylation inhibits PKM2 to promote the Warburg effect and tumor growth. *Sci. Signal.* 2:ra73. doi: 10.1126/scisignal.2000431
- Holecchek, J., Lease, R., Thorsell, A. G., Karlberg, T., McCadden, C., Grant, R., et al. (2018). Design, synthesis and evaluation of potent and selective inhibitors of mono-(ADP-ribosyl)transferases PARP10 and PARP14. *Bioorg. Med. Chem. Lett.* 28, 2050–2054. doi: 10.1016/j.bmcl.2018.04.056
- Hottiger, M. O., Hassa, P. O., Lüscher, B., Schüler, H., and Koch-Nolte, F. (2010). Toward a unified nomenclature for mammalian ADP-ribosyltransferases. *Trends Biochem. Sci.* 35, 208–219. doi: 10.1016/j.tibs.2009.12.003
- Hoy, S. M. (2018). Talazoparib: first global approval. *Drugs* 78, 1939–1946. doi: 10.1007/s40265-018-1026-z
- Iansante, V., Choy, P. M., Fung, S. W., Liu, Y., Chai, J. G., Dyson, J., et al. (2015). PARP14 promotes the Warburg effect in hepatocellular carcinoma by inhibiting JNK1-dependent PKM2 phosphorylation and activation. *Nat. Commun.* 6:7882. doi: 10.1038/ncomms8882
- Iqbal, M. B., Johns, M., Cao, J., Liu, Y., Yu, S. C., Hyde, G. D., et al. (2014). PARP-14 combines with tristetraprolin in the selective posttranscriptional control of macrophage tissue factor expression. *Blood* 124, 3646–3655. doi: 10.1182/blood-2014-07-588046
- Iwata, H., Goettsch, C., Sharma, A., Ricchiuto, P., Goh, W. W., Halu, A., et al. (2016). PARP9 and PARP14 cross-regulate macrophage activation via STAT1 ADP-ribosylation. *Nat. Commun.* 7:12849. doi: 10.1038/ncomms12849
- Kagami, S., Saeki, H., Komine, M., Kakinuma, T., Tsunemi, Y., Nakamura, K., et al. (2005). Interleukin-4 and interleukin-13 enhance CCL26 production in a human keratinocyte cell line, HaCaT cells. *Clin. Exp. Immunol.* 141, 459–466. doi: 10.1111/j.1365-2249.2005.02875.x
- Kameshita, I., Matsuda, Z., Taniguchi, T., and Shizuta, Y. (1984). Poly (ADP-Ribose) synthetase. Separation and identification of three proteolytic fragments as the substrate-binding domain, the DNA-binding domain, and the automodification domain. *J. Biol. Chem.* 259, 4770–4776.

- Kim, H., Tarhuni, A., Abd Elmageed, Z. Y., and Boulares, A. H. (2015). Poly(ADP-ribose) polymerase as a novel regulator of 17 β -estradiol-induced cell growth through a control of the estrogen receptor/IGF-1 receptor/PDZK1 axis. *J. Transl. Med.* 13:233. doi: 10.1186/s12967-015-0589-7
- Krishnamurthy, P., Sherrill, J. D., Parashette, K., Goenka, S., Rothenberg, M. E., Gupta, S., et al. (2014). Correlation of increased PARP14 and CCL26 expression in biopsies from children with eosinophilic esophagitis. *J. Allergy Clin. Immunol.* 133, 577–580. doi: 10.1016/j.jaci.2013.09.031
- LaFargue, C. J., Dal Molin, G. Z., Sood, A. K., and Coleman, R. L. (2019). Exploring and comparing adverse events between PARP inhibitors. *Lancet Oncol.* 20, e15–e28. doi: 10.1016/S1470-2045(18)30786-1
- Langelier, M. F., Planck, J. L., Roy, S., and Pascal, J. M. (2011). Crystal structures of poly(ADP-ribose) polymerase-1 (PARP-1) zinc fingers bound to DNA: structural and functional insights into DNA-dependent PARP-1 activity. *J. Biol. Chem.* 286, 10690–10701. doi: 10.1074/jbc.M110.202507
- Lord, C. J., and Ashworth, A. (2017). PARP inhibitors: synthetic lethality in the clinic. *Science* 355, 1152–1158. doi: 10.1126/science.aam7344
- Masson, M., Niedergang, C., Schreiber, V., Muller, S., Menissier-de Murcia, J., and de Murcia, G. (1998). XRCC1 is specifically associated with poly(ADP-ribose) polymerase and negatively regulates its activity following DNA damage. *Mol. Cell. Biol.* 18, 3563–3571. doi: 10.1128/MCB.18.6.3563
- Mehrotra, P., Hollenbeck, A., Riley, J. P., Li, F., Patel, R. J., Akhtar, N., et al. (2013). Poly (ADP-ribose) polymerase 14 and its enzyme activity regulates T(H)2 differentiation and allergic airway disease. *J. Allergy Clin. Immunol.* 131, 521–531.e1–12. doi: 10.1016/j.jaci.2012.06.015
- Mehrotra, P., Krishnamurthy, P., Sun, J., Goenka, S., and Kaplan, M. H. (2015). Poly-ADP-ribosyl polymerase-14 promotes T helper 17 and follicular T helper development. *Immunology* 146, 537–546. doi: 10.1111/imm.12515
- Mehrotra, P., Riley, J. P., Patel, R., Li, F., Voss, L., and Goenka, S. (2011). PARP-14 functions as a transcriptional switch for Stat6-dependent gene activation. *J. Biol. Chem.* 286, 1767–1776. doi: 10.1074/jbc.M110.157768
- Morrone, S., Cheng, Z., Moon, R. T., Cong, F., and Xu, W. (2012). Crystal structure of a Tankyrase-Axin complex and its implications for Axin turnover and Tankyrase substrate recruitment. *Proc. Natl. Acad. Sci. U.S.A.* 109, 1500–1505. doi: 10.1073/pnas.1116618109
- Moustakim, M., Riedel, K., Schuller, M., Gehring, A. P., Monteiro, O. P., Martin, S. P., et al. (2018). Discovery of a novel allosteric inhibitor scaffold for polyadenosine-diphosphate-ribose polymerase 14 (PARP14) macrodomain 2. *Bioorg. Med. Chem.* 26, 2965–2972. doi: 10.1016/j.bmc.2018.03.020
- Naura, A. S., Kim, H., Ju, J., Rodriguez, P. C., Jordan, J., Catling, A. D., et al. (2013). Minocycline blocks asthma-associated inflammation in part by interfering with the T cell receptor-nuclear factor kappaB-GATA-3-IL-4 axis without a prominent effect on poly(ADP-ribose) polymerase. *J. Biol. Chem.* 288, 1458–1468. doi: 10.1074/jbc.M112.419580
- Nicolae, C. M., Aho, E. R., Choe, K. N., Constantin, D., Hu, H. J., Lee, D., et al. (2015). A novel role for the mono-ADP-ribosyltransferase PARP14/ARTD8 in promoting homologous recombination and protecting against replication stress. *Nucleic Acids Res.* 43, 3143–3153. doi: 10.1093/nar/gkv147
- Niranjan, R., Rayapudi, M., Mishra, A., Dutt, P., Dynda, S., and Mishra, A. (2013). Pathogenesis of allergen-induced eosinophilic esophagitis is independent of interleukin (IL)-13. *Immunol. Cell Biol.* 91, 408–415. doi: 10.1038/icb.2013.21
- Oliver, A. W., Ame, J. C., Roe, S. M., Good, V., de Murcia, G., and Pearl, L. H. (2004). Crystal structure of the catalytic fragment of murine poly(ADP-ribose) polymerase-2. *Nucleic Acids Res.* 32, 456–464. doi: 10.1093/nar/gkh215
- Peng, B., Thorsell, A. G., Karlberg, T., Schüler, H., and Yao, S. Q. (2017). Small molecule microarray based discovery of PARP14 inhibitors. *Angew. Chem. Int. Ed Engl.* 56, 248–253. doi: 10.1002/anie.201609655
- Raab, M. S., Podar, K., Breitkreutz, I., Richardson, P. G., and Anderson, K. C. (2009). Multiple myeloma. *Lancet* 374, 324–339. doi: 10.1016/S0140-6736(09)60221-X
- Rajkumar, S. V. (2011). Treatment of multiple myeloma. *Nat. Rev. Clin. Oncol.* 8, 479–491. doi: 10.1038/nrclinonc.2011.63
- Riley, J. P., Kulkarni, A., Mehrotra, P., Koh, B., Perumal, N. B., Kaplan, M. H., et al. (2013). PARP-14 binds specific DNA sequences to promote Th2 cell gene expression. *PLoS ONE* 8:e83127. doi: 10.1371/journal.pone.0083127
- Satoh, M. S., and Lindahl, T. (1992). Role of poly(ADP-ribose) formation in DNA repair. *Nature* 356, 356–358. doi: 10.1038/356356a0
- Satoh, M. S., Poirier, G. G., and Lindahl, T. (1994). Dual function for poly(ADP-ribose) synthesis in response to DNA strand breakage. *Biochemistry* 33, 7099–7106. doi: 10.1021/bi00189a012
- Schuller, M., Riedel, K., Gibbs-Seymour, I., Uth, K., Sieg, C., Gehring, A. P., et al. (2017). Discovery of a selective allosteric inhibitor targeting macrodomain 2 of polyadenosine-diphosphate-ribose polymerase 14. *ACS Chem. Biol.* 12, 2866–2874. doi: 10.1021/acscchembio.7b00445
- Schweiker, S. S., Tauber, A. L., Sherry, M. E., and Levison, S. M. (2018). Structure, function and inhibition of poly(ADP-ribose)polymerase, member 14 (PARP14). *Mini Rev. Med. Chem.* 18, 1659–1669. doi: 10.2174/1389557518666180816111749
- Scott, L. J. (2017). Niraparib: first global approval. *Drugs* 77, 1029–1034. doi: 10.1007/s40265-017-0752-y
- Takeyama, K., Aguiar, R. C., Gu, L., He, C., Freeman, G. J., Kutok, J. L., et al. (2003). The BAL-binding protein BBAP and related Deltex family members exhibit ubiquitin-protein isopeptide ligase activity. *J. Biol. Chem.* 278, 21930–21937. doi: 10.1074/jbc.M301157200
- Thomas, C., and Tulin, A. V. (2013). Poly-ADP-ribose polymerase: machinery for nuclear processes. *Mol. Aspects Med.* 34, 1124–1137. doi: 10.1016/j.mam.2013.04.001
- Upton, K., Meyers, M., Thorsell, A. G., Karlberg, T., Holechek, J., Lease, R., et al. (2017). Design and synthesis of potent inhibitors of the mono(ADP-ribosyl)transferase, PARP14. *Bioorg. Med. Chem. Lett.* 27, 2907–2911. doi: 10.1016/j.bmc.2017.04.089
- Vyas, S., Chesarone-Cataldo, M., Todorova, T., Huang, Y. H., and Chang, P. (2013). A systematic analysis of the PARP protein family identifies new functions critical for cell physiology. *Nat. Commun.* 4:2240. doi: 10.1038/ncomms3240
- Vyas, S., Matic, I., Uchima, L., Rood, J., Zaja, R., Hay, R. T., et al. (2014). Family-wide analysis of poly(ADP-ribose) polymerase activity. *Nat. Commun.* 5:4426. doi: 10.1038/ncomms5426
- Wahlberg, E., Karlberg, T., Kouznetsova, E., Markova, N., Macchiarulo, A., Thorsell, A. G., et al. (2012). Family-wide chemical profiling and structural analysis of PARP and tankyrase inhibitors. *Nat. Biotechnol.* 30, 283–288. doi: 10.1038/nbt.2121
- Yang, W., Zheng, Y., Xia, Y., Ji, H., Chen, X., Guo, F., et al. (2012). ERK1/2-dependent phosphorylation and nuclear translocation of PKM2 promotes the Warburg effect. *Nat. Cell Biol.* 14, 1295–1304. doi: 10.1038/ncb2629
- Yoneyama-Hirozane, M., Matsumoto, S. I., Toyoda, Y., Saikatendu, K. S., Zama, Y., Yonemori, K., et al. (2017). Identification of PARP14 inhibitors using novel methods for detecting auto-ribosylation. *Biochem. Biophys. Res. Commun.* 486, 626–631. doi: 10.1016/j.bbrc.2017.03.052
- Zhu, F., Wang, Q., Guo, C., Wang, X., Cao, X., Shi, Y., et al. (2011). IL-17 induces apoptosis of vascular endothelial cells: a potential mechanism for human acute coronary syndrome. *Clin. Immunol.* 141, 152–160. doi: 10.1016/j.clim.2011.07.003

Conflict of Interest Statement: The authors declare that the research was conducted in the absence of any commercial or financial relationships that could be construed as a potential conflict of interest.

Copyright © 2019 Qin, Wu, Cao, Li, He, Zhao, Xing, Li, Jin and Cao. This is an open-access article distributed under the terms of the Creative Commons Attribution License (CC BY). The use, distribution or reproduction in other forums is permitted, provided the original author(s) and the copyright owner(s) are credited and that the original publication in this journal is cited, in accordance with accepted academic practice. No use, distribution or reproduction is permitted which does not comply with these terms.



Sphingomyelin Synthase 1 (SMS1) Downregulation Is Associated With Sphingolipid Reprogramming and a Worse Prognosis in Melanoma

Fatima Bilal^{1,2,3,4}, Anne Montfort^{1,2,4}, Julia Gilhodes⁵, Virginie Garcia^{1,2}, Joëlle Riond^{1,2}, Stéphane Carpentier^{1,2,4}, Thomas Filleron⁵, Céline Colacios^{1,2,4}, Thierry Levade^{1,2,4,6}, Ahmad Daher³, Nicolas Meyer^{1,4,5}, Nathalie Andrieu-Abadie^{1,2} and Bruno Ségui^{1,2,4*}

¹ INSERM UMR 1037, CRCT, Toulouse, France, ² Equipe Labellisée Ligue Contre Le Cancer, Toulouse, France, ³ Ecole Doctorale de Sciences et Technologies, Université Libanaise, Beirut, Lebanon, ⁴ Université Toulouse III – Paul Sabatier, Toulouse, France, ⁵ Institut Universitaire du Cancer, Toulouse, France, ⁶ Laboratoire de Biochimie, CHU Purpan, Institut Fédératif de Biologie, Toulouse, France

OPEN ACCESS

Edited by:

Pascale Cohen,
Université Claude Bernard Lyon 1,
France

Reviewed by:

Paola Giussani,
University of Milan, Italy
Youssef Zeidan,
American University of Beirut,
Lebanon
Liana C. Silva,
Universidade de Lisboa, Portugal

*Correspondence:

Bruno Ségui
bruno.segui@inserm.fr

Specialty section:

This article was submitted to
Experimental Pharmacology
and Drug Discovery,
a section of the journal
Frontiers in Pharmacology

Received: 19 November 2018

Accepted: 08 April 2019

Published: 30 April 2019

Citation:

Bilal F, Montfort A, Gilhodes J, Garcia V, Riond J, Carpentier S, Filleron T, Colacios C, Levade T, Daher A, Meyer N, Andrieu-Abadie N and Ségui B (2019) Sphingomyelin Synthase 1 (SMS1) Downregulation Is Associated With Sphingolipid Reprogramming and a Worse Prognosis in Melanoma. *Front. Pharmacol.* 10:443. doi: 10.3389/fphar.2019.00443

Sphingolipid (SL) metabolism alterations have been frequently reported in cancer including in melanoma, a bad-prognosis skin cancer. In normal cells, *de novo* synthesized ceramide is mainly converted to sphingomyelin (SM), the most abundant SL, by sphingomyelin synthase 1 (SMS1) and, albeit to a lesser extent, SMS2, encoded by the *SGMS1* and *SGMS2* genes, respectively. Alternatively, ceramide can be converted to glucosylceramide (GlcCer) by the GlcCer synthase (GCS), encoded by the *UGCG* gene. Herein, we provide evidence for the first time that SMS1 is frequently downregulated in various solid cancers, more particularly in melanoma. Accordingly, various human melanoma cells displayed a SL metabolism signature associated with (i) a robust and a low expression of *UGCG* and *SGMS1/2*, respectively, (ii) higher *in situ* enzyme activity of GCS than SMS, and (iii) higher intracellular levels of GlcCer than SM. SMS1 was expressed at low levels in most of the human melanoma biopsies. In addition, several mutations and increased CpG island methylation in the *SGMS1* gene were identified that likely affect SMS1 expression. Finally, low SMS1 expression was associated with a worse prognosis in metastatic melanoma patients. Collectively, our study indicates that SMS1 downregulation in melanoma enhances GlcCer synthesis, triggering an imbalance in the SM/GlcCer homeostasis, which likely contributes to melanoma progression. Evaluating SMS1 expression level in tumor samples might serve as a biomarker to predict clinical outcome in advanced melanoma patients.

Keywords: sphingolipids, ceramide, glucosylceramide, prognosis biomarker, cancer

INTRODUCTION

Melanoma is the most dangerous and deadliest form of skin cancers. Despite emerging targeted therapies and immunotherapies, most of the patients do not respond optimally, and/or develop acquired resistance (Eroglu and Ribas, 2016; Sharma et al., 2017).

Sphingolipids (SL) are bioactive molecules that play key roles in plasma membrane homeostasis and dynamics as well as in many cellular processes including cell death and proliferation as

well as cancer progression (Hannun, 1996; Hannun and Obeid, 2002; Ogretmen and Hannun, 2004; Segui et al., 2006). In melanoma, numerous studies have documented alterations in SL metabolism (Colie et al., 2009; Sorli et al., 2013; Albinet et al., 2014; Mrad et al., 2016; Leclerc et al., 2018). Glucosylceramide synthase (GCS), which converts ceramide to glucosylceramide (GlcCer), is involved in melanoma progression in mice (Deng et al., 2002; Weiss et al., 2003). To the best of our knowledge, sphingomyelin synthases SMS1 and SMS2 (encoded by the *SGMS1* and *SGMS2* genes), which metabolize ceramide into sphingomyelin (SM) (Huitema et al., 2004; Yamaoka et al., 2004), the most abundant SL in mammalian cells (Lafont et al., 2010), have not been analyzed in melanoma.

Herein, we show that SMS1 downregulation (i) occurs frequently in melanoma, (ii) is associated with SL reprogramming, and (iii) constitutes a worse prognosis biomarker in metastatic melanoma.

MATERIALS AND METHODS

Macroarray Experiment

Cancer Profiling array II (#631777) including patient-derived cDNA tumor and non-tumor samples was purchased from BD Biosciences Clontech. Human samples were collected in accordance with all applicable laws and regulations in an ethical manner. Membrane was successively hybridized according to the manufacturer's instructions with SMS1 and ubiquitin ³²P-labeled probes generated using a random nonamer primer labeling procedure (# RPN1604, Amersham Biosciences). The membrane was exposed to an intensifying screen that was developed using PhosphorImager and Image Quant software.

SGMS1, *SGMS2*, and *UGCG* Expression and Mutations in Human Melanoma

SGMS1, *SGMS2*, and *UGCG* expression was evaluated from Oncomine database (Haqq et al., 2005; Talantov et al., 2005; Riker et al., 2008) and the cancer genome atlas (TCGA) melanoma (Cancer Genome Atlas Network, 2015). TCGA genomic and clinical data were downloaded from the UCSC cancer genome browser project¹. The analysis population consisted of 342 patients with distant metastasis for whom RNAseq and clinical data overlap. All survival times were calculated from the date of specimen procurement and were estimated by the Kaplan Meier method with 95% confidence intervals (CI). Univariate analyses were performed using Cox proportional hazards model. Alternatively, *SGMS1*, *SGMS2*, and *UGCG* mutation analyses in human melanoma were assessed on cBioportal² (Cerami et al., 2012; Gao et al., 2013).

SGMS1 Methylation Analysis

The correlation between *SGMS1* expression and methylation status of *SGMS1* CpGs in metastatic patient samples was analyzed using the TCGA melanoma RNA-seq and DNA methylation

Illumina datasets. For each analyzed CpG, the rho values, indicating the Spearman's rank correlation coefficients between the CpG methylation and the *SGMS1* expression, are reported. The organization of the *SGMS1* locus is depicted in **Figure 2A** as previously described (Vladychenskaya et al., 2004).

Melanoma Cell Lines

Human melanoma cell lines (M249, SKMEL28, A375, WM9, WM35, WM115, WM266, WM793, WM1346, COLO829, and G361) were from ATCC or Wistar institute.

Determination of *in situ* SMS and GCS Activities

1×10^6 melanoma cells were incubated with 2.5 μ M C6-NBD-ceramide (Sigma) solubilized in ethanol and SMS and GCS activities were measured as previously described (Lafont et al., 2010; Bilal et al., 2017a).

Analysis of Sphingolipids

Sphingolipids were analyzed from 1.10^6 melanoma cells by liquid chromatography/mass spectrometry (LC/MS) as previously described (Bilal et al., 2017b).

qRT-PCR Analysis

Total RNA was reverse-transcribed using 1 μ g of input RNA and random primers (SuperScript II, Invitrogen). qRT-PCR reactions were performed in duplicate on StepOne apparatus (Applied Biosystems) using SYBR Green (QuantiTect, Qiagen) as fluorescent detection dye. Results were quantified and mRNA expression for each target gene (*UGCG*, *SGMS1*, or *SGMS2*) was determined by normalization to reference genes (β -actin and GAPDH) using the Δ Ct method. Primers for *UGCG* and reference genes were from Qiagen. Primers for *SGMS1* and *SGMS2* were from Sigma (Lafont et al., 2010).

Statistics and Reproducibility

Statistical significance of differences between groups was evaluated using the Graph-Pad Prism 7 software. For multiple comparisons, an Anova test was used. Wilcoxon test was used in **Figure 1B**. Differences were considered to be statistically significant when $p < 0.05$ (* $p < 0.05$; ** $p < 0.01$; *** $p < 0.001$).

RESULTS

SMS1 Downregulation in Melanoma Is Associated With SL Metabolism Reprogramming

We initially performed a macroarray to evaluate the expression of SMS1 in matched tumor and non-tumor samples from the same patients (**Figure 1A**). The data analysis with a threshold of 1.5 showed that, whereas SMS1 was up-regulated in 11% of tumor samples, it was down-regulated in 46% of tumor samples (**Supplementary Table 1**). As a matter of fact, SMS1 was most frequently down-regulated in vulva (5 out of 5), testis (9 out of 10), and skin (9 out of 10) cancers, including melanoma (6

¹<https://genome-cancer.ucsc.edu>

²<http://www.cbioportal.org/>

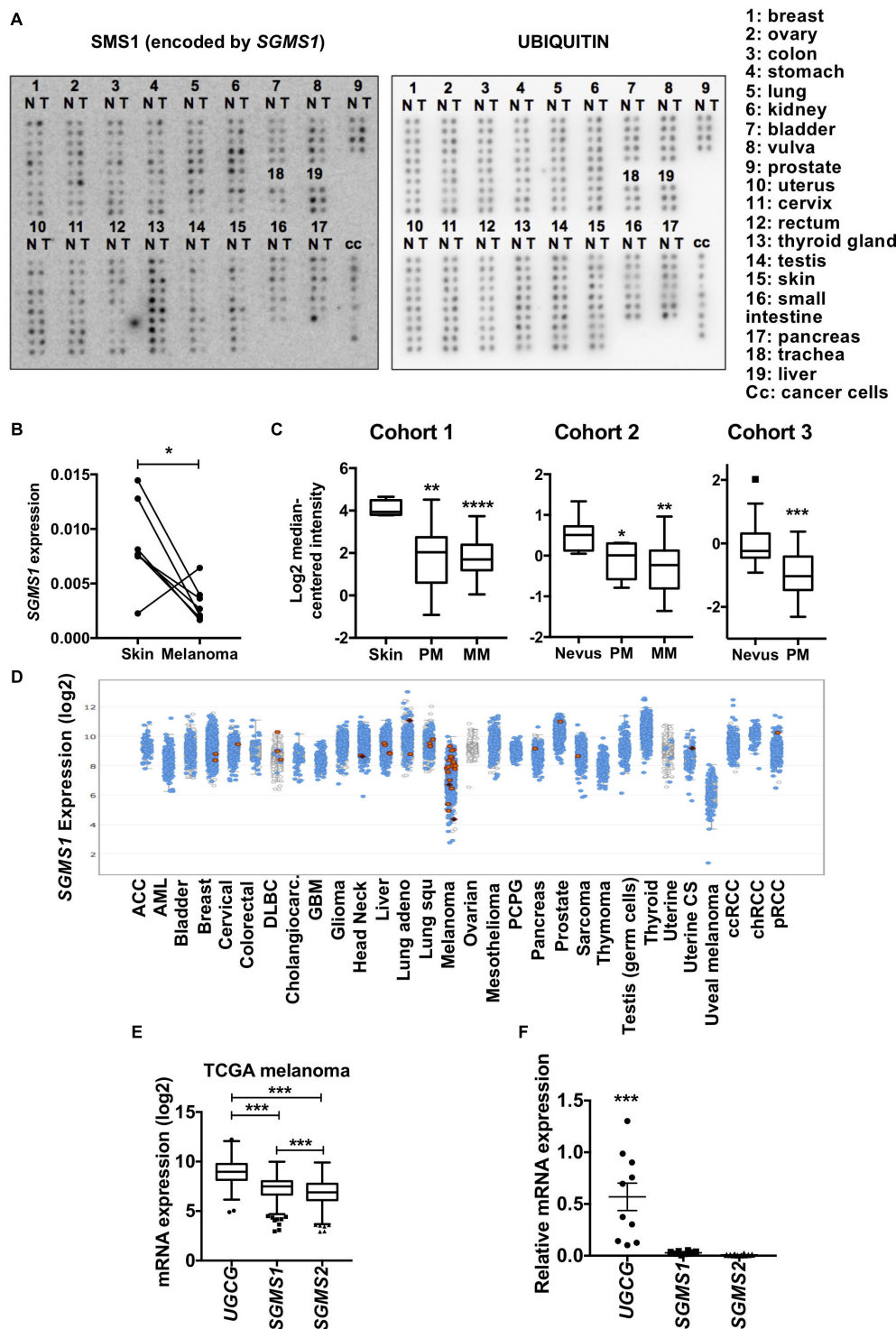


FIGURE 1 | Sphingomyelin synthase 1 (SMS1) is frequently downregulated in melanoma. **(A)** cDNA samples isolated from normal (N) and tumor (T) tissues from the same patient were compared. Expression of *SGMS1* (left panel) and ubiquitin (right panel). **(B)** The *SGMS1* expression was normalized to ubiquitin and expressed for each pair in normal skin and melanoma samples. **(C)** *SGMS1* expression was analyzed in 3 different cohorts from Oncomine in normal Skin ($n = 4$), primary (PM; $n = 14$), and metastatic (MM; $n = 39$) melanoma (Ricker's cohort) (left panel); in nevus ($n = 9$), primary (PM; $n = 6$), and metastatic (MM; $n = 19$) melanoma (Haqq's cohort) (middle panel); in nevus ($n = 18$) and primary melanoma (PM; $n = 45$) (Talantov's cohort) (right panel). **(D)** The expression of *SGMS1* was analyzed in various cancer type cohorts from cBioportal. **(E)** The expression of *UGCG*, *SGMS1*, and *SGMS2* was analyzed in melanoma samples from the TCGA metastatic melanoma patients ($n = 342$). **(F)** A set of melanoma cell lines ($n = 10$) was analyzed for the expression of *UGCG*, *SGMS1*, and *SGMS2* by RT-qPCR ($n = 10$). Data from at least two independent experiments are means \pm SEM. * $p < 0.05$, ** $p < 0.01$, *** $p < 0.001$, and **** $p < 0.0001$.

out of 7) (Figure 1B and Supplementary Table 1). Accordingly, our transcriptomic analysis in 3 different cohorts from published database indicates that *SGMS1* was downregulated in primary and metastatic human melanoma as compared to normal skin and nevus (Figure 1C; Haqq et al., 2005; Talantov et al., 2005; Riker et al., 2008). In contrast, the expression of *SGMS2* and *UGCG*, encoding SMS2 and GCS, respectively, remained unchanged (Supplementary Figure 1A). We next evaluated the expression of *SGMS1* in various cancer types from the TCGA database. Strikingly, melanoma exhibited the lowest expression of *SGMS1* (Figure 1D). Moreover, melanoma expressed *SGMS2* at rather low levels, while expressing *UGCG* at high levels (Supplementary Figure 1B). In metastatic melanoma from the TCGA, the expression of *UGCG* was significantly higher than

that of *SGMS1* and *SGMS2* (Figure 1E). Accordingly, melanoma cells exhibited low *SGMS1* and *SGMS2* expression, while they expressed *UGCG* at higher levels (Figure 1F).

We next evaluated the SL metabolism signature in human melanoma cell lines. Whereas four melanoma cell lines exhibited a higher proportion of SM, six were enriched in GlcCer (Figure 2A). Accordingly, *in situ* enzyme activity was significantly higher for GCS than for SMS in the cell lines with high GlcCer proportion only (Figure 2B). Consequently, endogenous intracellular levels of GlcCer were greater than SM and other SL species as evaluated by mass spectrometry for those six melanoma cell lines (Figure 2A and Supplementary Table 2). Of note, neither the mutation status (Bairoch, 2018) nor the origin of the melanoma cell lines (i.e., from radial or vertical

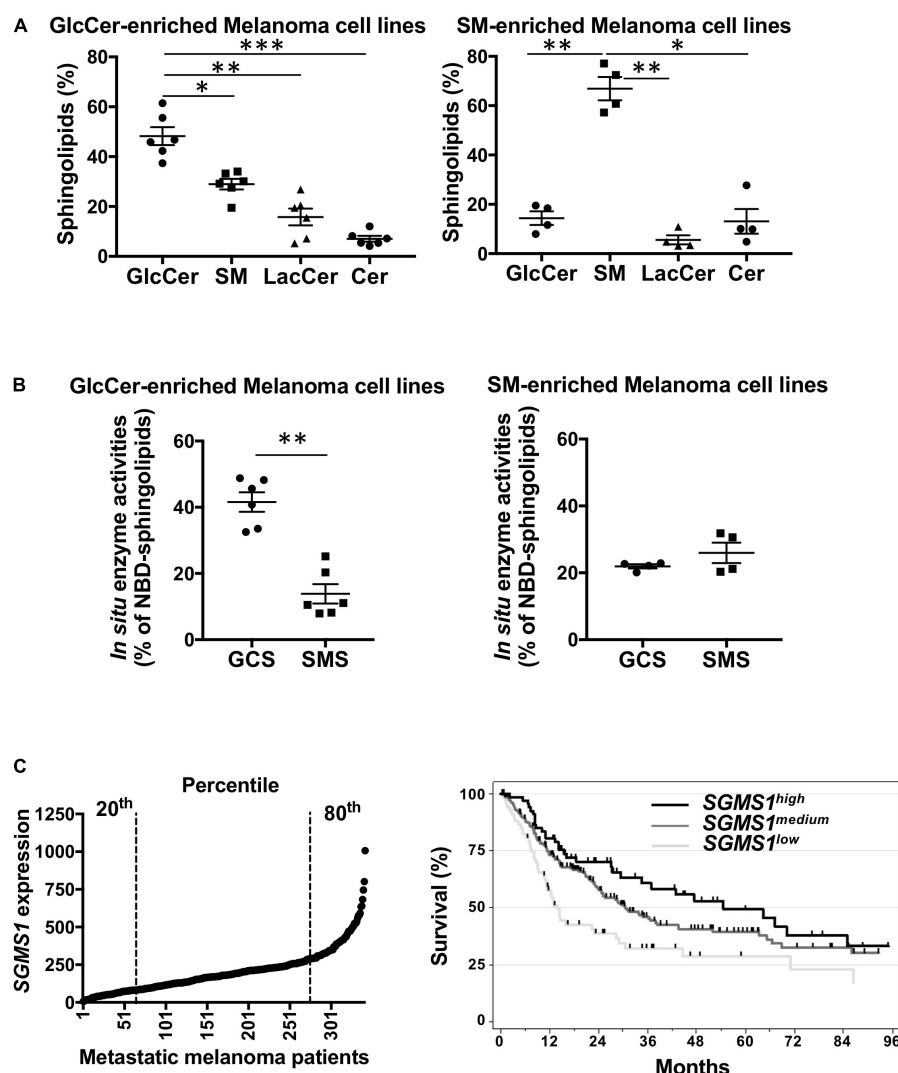


FIGURE 2 | Spingomyelin synthase 1 downregulation is associated with a worse prognosis in advanced melanoma patients. (A,B) A set of melanoma cell lines ($n = 10$) was analyzed for SLs by mass spectrometry (A) and GCS and SMS enzyme activities (B). Data from one experiment representative of three independent experiments are means \pm SEM. (C) *SGMS1* expression in melanoma samples from the TCGA melanoma cohort ($n = 342$) (left panel) and overall survival of patients exhibiting low ($n = 68$), medium ($n = 206$), and high ($n = 68$) *SGMS1* expression (right panel). Cox model: *SGMS1*^{low} (Reference), *SGMS1*^{medium}: HR = 0.62 [95% CI = 0.44; 0.88] $p = 0.007$; *SGMS1*^{high}: HR = 0.48 [95% CI 0.31; 0.76] $p = 0.002$. * $p < 0.05$, ** $p < 0.01$, and *** $p < 0.001$.

growth phase or metastasis) were associated with a specific SL signature (**Supplementary Table 3**).

SMS1 Downregulation in Human Melanoma Is Associated With a Worse Prognosis

To get insight into the molecular mechanisms that may account for SMS1 downregulation and/or inhibition of enzyme activity, we evaluated *SGMS1* mutation and methylation status in the public databases of melanoma. Whereas *SGMS2* and *UGCG* were mutated with low frequency, *SGMS1* exhibited a higher mutation rate in the coding sequence (**Supplementary Figure 2**). Most of the mutations were missense mutations and some of them affected residues in the catalytic domain (**Supplementary Figure 2** and **Supplementary Table 4**). In the TCGA melanoma cohort, 7.7% of the 287 sequenced samples were mutated (16 missense mutations, 2 non-sense mutations and 4 deep deletions). One of the non-sense mutations (W309*) was also found in one specimen from another melanoma cohort (**Supplementary Table 4**). The other non-sense mutation (R387*) was also found in colorectal carcinoma, sarcoma and uterus carcinoma (data not shown).

To delineate the effect of DNA methylation on the regulation of *SGMS1* expression, we analyzed the TCGA metastatic melanomas. Among the 50 *SGMS1* Illumina 450K probes with workable data, the DNA methylation level of 33 probes displayed a significant correlation with expression. Ten probes out of the 14 located in the CpG island 1 and its shores, as well as 3 out of the 3 in the CpG island 2 and its shores, both containing putative promoter sequences, were inversely correlated with the expression level. In contrast, 13 CpG out of the 16 located outside CpG islands and shores were positively correlated with the expression (**Supplementary Figures 3A,B**). Thus, hypermethylation of CpG islands and hypomethylation events in open sea were significantly associated with the decrease in *SGMS1* expression, indicating the regulation of SMS1 expression in metastatic melanoma might rely, at least partly, on DNA methylation of the *SGMS1* locus.

Finally, the clinical outcome in metastatic melanoma patients exhibiting low (20th percentile, medium (between the 20th and 80th percentile), high (80th percentile) *SGMS1*, *SGMS2*, and *UGCG* expression was analyzed in the TCGA cohort. Whereas *UGCG* and *SGMS2* expression did not impact on overall survival (**Supplementary Figure 4**), low *SGMS1* expression was statistically associated with shortened overall survival (**Figure 2C**).

Collectively, our data indicate that melanoma exhibit a SL metabolism reprogramming associated with SMS1 downregulation, which constitutes a worse-prognosis biomarker.

DISCUSSION

Herein, we provide evidence for the first time that melanoma exhibit SL metabolism changes associated with SMS1 downregulation, not only decreasing SM synthesis but also

promoting the synthesis of GlcCer, which facilitates tumor progression in mouse melanoma models (Deng et al., 2002; Weiss et al., 2003). Interestingly, a recent study indicates the formation of an heterocomplex between SMS1 and GCS in mammalian cells, which enhances and reduces SM, and GlcCer synthesis, respectively (Hayashi et al., 2018). SMS1 downregulation may limit the formation of such a complex, promoting GlcCer synthesis in melanoma. Since *de novo* synthesized ceramide is the substrate of both SMS1 and GCS in the Golgi, downregulation of SMS1 likely increases the ceramide pool available for GCS to produce GlcCer.

Strikingly, low SMS1 expression is associated with a worse prognosis in metastatic melanoma, suggesting that reduced SM synthesis likely contributes to melanoma progression. SMS1 down-regulation, which occurs in primary melanoma, is likely an early event in melanomagenesis. Several mutations affecting the coding sequence of *SGMS1* probably contribute to the decreased SMS1 expression. In the TCGA melanoma cohort, 5 out of 16 missense mutations and 1 non-sense mutation were associated with shallow deletions. Moreover, 4 deep deletions were identified as well as 17 CpG located on the two CpG islands and their shores, the methylation of which was correlated with *SGMS1* downregulation in metastatic melanoma. SMS1 expression and activity are likely regulated by translational and post-translational mechanisms such as recently described in Bcr-Abl-expressing leukemia cells (Moorthi et al., 2018). Whereas key driver mutations have been identified in melanoma (Hodis et al., 2012), we found no correlation between mutation status and SL signature.

Ceramide clearance catalysed by GCS plays a role in multidrug resistance of cancer cell lines (Lavie et al., 1997; Liu et al., 2004; Sun et al., 2006; Liu et al., 2010). However, our team provided genetic evidence that GCS is unlikely a critical enzyme to confer melanoma resistance to chemotherapy in a mouse melanoma model (Veldman et al., 2003). Because SLs are key components of the plasma membrane, modulating various signaling pathways (Hannun, 1996; Hannun and Obeid, 2002), future experiments will address whether or not SM/GlcCer homeostasis alterations in melanoma impair the efficacy of emerging therapies such as targeted therapies and immunotherapies. Finally, it remains to evaluate whether low SMS1 expression in melanoma samples is a valuable biomarker to predict the resistance of patients to emerging therapies.

ETHICS STATEMENT

As clearly stated in the manuscript, the results shown here are part based upon data generated by the TCGA Research Network. In addition, we have analyzed data from the oncomine database. We have performed a macroarray to evaluate the expression of SMS1 in matched tumor and non-tumor samples from the same patients by using the Cancer Profiling array II (Clontech #631777) membrane.

AUTHOR CONTRIBUTIONS

FB, VG, and SC performed the experiments. JG and JR performed the methylation analyses. JG and TF performed the bio-statistical analyses of the TCGA melanoma. AM, CC, TL, AD, NM, and NA-A edited the manuscript. SB designed and supervised the study and wrote the manuscript.

FUNDING

The results shown here are part based upon data generated by the TCGA Research Network: <http://cancergenome.nih.gov/>. This work was supported by Ligue Nationale Contre le

Cancer, INSERM Transfert, ROTARY Toulouse clubs, Fondation Toulouse Cancer Santé, INSERM, and Paul Sabatier University (Toulouse III). BF has been co-funded by the “Association de Spécialisation et d’Orientation Scientifique” and the “Plateforme de Recherche et d’Analyse en Sciences de l’Environnement (PRASE)” (Lebanon).

SUPPLEMENTARY MATERIAL

The Supplementary Material for this article can be found online at: <https://www.frontiersin.org/articles/10.3389/fphar.2019.00443/full#supplementary-material>

REFERENCES

- Albinet, V., Bats, M. L., Huwiler, A., Rochaix, P., Chevreau, C., Segui, B., et al. (2014). Dual role of sphingosine kinase-1 in promoting the differentiation of dermal fibroblasts and the dissemination of melanoma cells. *Oncogene* 33, 3364–3373. doi: 10.1038/onc.2013.303
- Bairoch, A. (2018). The cellosaurus, a cell-line knowledge resource. *J. Biomol. Tech.* 29, 25–38. doi: 10.7171/jbt.18-2902-002
- Bilal, F., Peres, M., Andrieu-Abadie, N., Levade, T., Badran, B., Daher, A., et al. (2017a). Method to measure sphingomyelin synthase activity changes in response to CD95L. *Methods Mol. Biol.* 1557, 207–212. doi: 10.1007/978-1-4939-6780-3_19
- Bilal, F., Peres, M., Le Faouder, P., Dupuy, A., Bertrand-Michel, J., Andrieu-Abadie, N., et al. (2017b). Liquid chromatography-high resolution mass spectrometry method to study sphingolipid metabolism changes in response to CD95L. *Methods Mol. Biol.* 1557, 213–217. doi: 10.1007/978-1-4939-6780-3_20
- Cancer Genome Atlas Network (2015). Genomic classification of cutaneous melanoma. *Cell* 161, 1681–1696. doi: 10.1016/j.cell.2015.05.044
- Cerami, E., Gao, J., Dogrusoz, U., Gross, B. E., Sumer, S. O., Aksoy, B. A., et al. (2012). The cBio cancer genomics portal: an open platform for exploring multidimensional cancer genomics data. *Cancer Discov.* 2, 401–404. doi: 10.1158/2159-8290.CD-12-0095
- Colie, S., Van Veldhoven, P. P., Kedjouar, B., Bedia, C., Albinet, V., Sorli, S. C., et al. (2009). Disruption of sphingosine 1-phosphate lyase confers resistance to chemotherapy and promotes oncogenesis through Bcl-2/Bcl-xL upregulation. *Cancer Res.* 69, 9346–9353. doi: 10.1158/0008-5472.CAN-09-2198
- Deng, W., Li, R., Guerrero, M., Liu, Y., and Ladisch, S. (2002). Transfection of glucosylceramide synthase antisense inhibits mouse melanoma formation. *Glycobiology* 12, 145–152. doi: 10.1093/glycob/12.3.145
- Eroglu, Z., and Ribas, A. (2016). Combination therapy with BRAF and MEK inhibitors for melanoma: latest evidence and place in therapy. *Ther. Adv. Med. Oncol.* 8, 48–56. doi: 10.1177/1758834015616934
- Gao, J., Aksoy, B. A., Dogrusoz, U., Dresdner, G., Gross, B., Sumer, S. O., et al. (2013). Integrative analysis of complex cancer genomics and clinical profiles using the cBioPortal. *Sci. Signal.* 6:11. doi: 10.1126/scisignal.2004088
- Hannun, Y. A. (1996). Functions of ceramide in coordinating cellular responses to stress. *Science* 274, 1855–1859. doi: 10.1126/science.274.5294.1855
- Hannun, Y. A., and Obeid, L. M. (2002). The Ceramide-centric universe of lipid-mediated cell regulation: stress encounters of the lipid kind. *J. Biol. Chem.* 277, 25847–25850. doi: 10.1074/jbc.r200008200
- Haqq, C., Nosrati, M., Sudilovsky, D., Crothers, J., Khodabakhsh, D., Pulliam, B. L., et al. (2005). The gene expression signatures of melanoma progression. *Proc. Natl. Acad. Sci. U.S.A.* 102, 6092–6097.
- Hayashi, Y., Nemoto-Sasaki, Y., Matsumoto, N., Hama, K., Tanikawa, T., Oka, S., et al. (2018). Complex formation of sphingomyelin synthase 1 with glucosylceramide synthase increases sphingomyelin and decreases glucosylceramide levels. *J. Biol. Chem.* 293, 17505–17522. doi: 10.1074/jbc.RA118.002048
- Hodis, E., Watson, I. R., Kryukov, G. V., Arol, S. T., Imielinski, M., Theurillat, J. P., et al. (2012). A landscape of driver mutations in melanoma. *Cell* 150, 251–263.
- Huitema, K., Van Den Dikkenberg, J., Brouwers, J. F., and Holthuis, J. C. (2004). Identification of a family of animal sphingomyelin synthases. *EMBO J.* 23, 33–44. doi: 10.1038/sj.emboj.7600034
- Lafont, E., Milhas, D., Carpentier, S., Garcia, V., Jin, Z. X., Umehara, H., et al. (2010). Caspase-mediated inhibition of sphingomyelin synthesis is involved in FasL-triggered cell death. *Cell Death Differ.* 17, 642–654. doi: 10.1038/cdd.2009.130
- Lavie, Y., Cao, H., Volner, A., Lucci, A., Han, T. Y., Geffen, V., et al. (1997). Agents that reverse multidrug resistance, tamoxifen, verapamil, and cyclosporin A, block glycosphingolipid metabolism by inhibiting ceramide glycosylation in human cancer cells. *J. Biol. Chem.* 272, 1682–1687. doi: 10.1074/jbc.272.3.1682
- Leclerc, J., Garandeau, D., Pandiani, C., Gaudel, C., Bille, K., Nottet, N., et al. (2018). Lysosomal acid ceramidase Asah1 controls the transition between invasive and proliferative phenotype in melanoma cells. *Oncogene* 38, 1282–1295. doi: 10.1038/s41388-018-0500-0
- Liu, Y. Y., Gupta, V., Patwardhan, G. A., Bhinge, K., Zhao, Y., Bao, J., et al. (2010). Glucosylceramide synthase upregulates MDR1 expression in the regulation of cancer drug resistance through cSrc and beta-catenin signaling. *Mol. Cancer* 9:145. doi: 10.1186/1476-4598-9-145
- Liu, Y. Y., Han, T. Y., Yu, J. Y., Bitterman, A., Le, A., Giuliano, A. E., et al. (2004). Oligonucleotides blocking glucosylceramide synthase expression selectively reverse drug resistance in cancer cells. *J. Lipid Res.* 45, 933–940. doi: 10.1194/jlr.m300486-jlr200
- Moorthi, S., Burns, T. A., Yu, G. Q., and Luberto, C. (2018). Bcr-Abl regulation of sphingomyelin synthase 1 reveals a novel oncogenic-driven mechanism of protein up-regulation. *FASEB J.* 32, 4270–4283. doi: 10.1096/fj.201701016R
- Mrad, M., Imbert, C., Garcia, V., Rambow, F., Therville, N., Carpentier, S., et al. (2016). Downregulation of sphingosine kinase-1 induces protective tumor immunity by promoting M1 macrophage response in melanoma. *Oncotarget* 7, 71873–71886. doi: 10.18632/oncotarget.12380
- Ogretmen, B., and Hannun, Y. A. (2004). Biologically active sphingolipids in cancer pathogenesis and treatment. *Nat. Rev. Cancer* 4, 604–616. doi: 10.1038/nrc1411
- Riker, A. I., Enkemann, S. A., Fodstad, O., Liu, S., Ren, S., Morris, C., et al. (2008). The gene expression profiles of primary and metastatic melanoma yields a transition point of tumor progression and metastasis. *BMC Med. Genomics* 1:13. doi: 10.1186/1755-8794-1-13
- Segui, B., Andrieu-Abadie, N., Jaffrezou, J. P., Benoist, H., and Levade, T. (2006). Sphingolipids as modulators of cancer cell death: potential therapeutic targets. *Biochim. Biophys. Acta* 1758, 2104–2120. doi: 10.1016/j.bbame.2006.05.024
- Sharma, P., Hu-Lieskovan, S., Wargo, J. A., and Ribas, A. (2017). Primary, adaptive, and acquired resistance to cancer immunotherapy. *Cell* 168, 707–723. doi: 10.1016/j.cell.2017.01.017
- Sorli, S. C., Colie, S., Albinet, V., Dubrac, A., Touriol, C., Guilbaud, N., et al. (2013). The nonlysosomal beta-glucosidase GBA2 promotes endoplasmic reticulum stress and impairs tumorigenicity of human melanoma cells. *FASEB J.* 27, 489–498. doi: 10.1096/fj.12-215152

- Sun, Y. L., Zhou, G. Y., Li, K. N., Gao, P., Zhang, Q. H., Zhen, J. H., et al. (2006). Suppression of glucosylceramide synthase by RNA interference reverses multidrug resistance in human breast cancer cells. *Neoplasma* 53, 1–8.
- Talantov, D., Mazumder, A., Yu, J. X., Briggs, T., Jiang, Y., Backus, J., et al. (2005). Novel genes associated with malignant melanoma but not benign melanocytic lesions. *Clin. Cancer Res.* 11, 7234–7242. doi: 10.1158/1078-0432.ccr-05-0683
- Veldman, R. J., Mita, A., Cuvillier, O., Garcia, V., Klappe, K., Medin, J. A., et al. (2003). The absence of functional glucosylceramide synthase does not sensitize melanoma cells for anticancer drugs. *FASEB J.* 17, 1144–1146. doi: 10.1096/fj.02-1053fje
- Vladychenskaya, I. P., Dergunova, L. V., Dmitrieva, V. G., and Limborska, S. A. (2004). Human gene MOB: structure specification and aspects of transcriptional activity. *Gene* 338, 257–265. doi: 10.1016/j.gene.2004.06.003
- Weiss, M., Hettmer, S., Smith, P., and Ladisch, S. (2003). Inhibition of melanoma tumor growth by a novel inhibitor of glucosylceramide synthase. *Cancer Res.* 63, 3654–3658.
- Yamaoka, S., Miyaji, M., Kitano, T., Umehara, H., and Okazaki, T. (2004). Expression cloning of a human CDNA restoring sphingomyelin synthesis and cell growth in sphingomyelin synthase-defective lymphoid cells. *J. Biol. Chem.* 279, 18688–18693. doi: 10.1074/jbc.m401205200
- Conflict of Interest Statement:** NM has worked as an investigator and/or consultant and/or speaker for: BMS, MSD, Amgen, Roche, GSK, Novartis, and Pierre Fabre. BS has worked as an investigator for BMS. The authors disclose they are in the process applying for a patent based upon these findings.
- The remaining authors declare that the research was conducted in the absence of any commercial or financial relationships that could be construed as a potential conflict of interest.

Copyright © 2019 Bilal, Montfort, Gilhodes, Garcia, Riond, Carpentier, Filleron, Colacios, Levade, Daher, Meyer, Andrieu-Abadie and Ségui. This is an open-access article distributed under the terms of the Creative Commons Attribution License (CC BY). The use, distribution or reproduction in other forums is permitted, provided the original author(s) and the copyright owner(s) are credited and that the original publication in this journal is cited, in accordance with accepted academic practice. No use, distribution or reproduction is permitted which does not comply with these terms.



DDR1 and MT1-MMP Expression Levels Are Determinant for Triggering BIK-Mediated Apoptosis by 3D Type I Collagen Matrix in Invasive Basal-Like Breast Carcinoma Cells

Charles Saby¹, Guillaume Collin¹, Maha Sinane¹, Emilie Buache¹, Laurence Van Gulick¹, Frédéric Saltel², Erik Maquoi^{3†} and Hamid Morjani^{1*†}

OPEN ACCESS

Edited by:

Salvatore Salomone,
Università degli Studi di Catania, Italy

Reviewed by:

Hailin Tang,
Sun Yat-sen University Cancer Center
(SYSUCC), China
Jiange Qiu,
Zhengzhou University, China

*Correspondence:

Hamid Morjani
hamid.morjani@univ-reims.fr

[†]EM and HM are co-senior
authors of this work

Specialty section:

This article was submitted to
Experimental Pharmacology and
Drug Discovery,
a section of the journal
Frontiers in Pharmacology

Received: 19 January 2019

Accepted: 11 April 2019

Published: 03 May 2019

Citation:

Saby C, Collin G, Sinane M,
Buache E, Van Gulick L, Saltel F,
Maquoi E and Morjani H (2019)
DDR1 and MT1-MMP Expression
Levels Are Determinant for Triggering
BIK-Mediated Apoptosis by
3D Type I Collagen Matrix in Invasive
Basal-Like Breast Carcinoma Cells.
Front. Pharmacol. 10:462.
doi: 10.3389/fphar.2019.00462

Type I collagen is the major adhesive component in breast interstitial stroma, which represents the first barrier against tumor cell invasion after basement-membrane degradation. Among cellular receptors, type I collagen is able to activate discoidin domain receptors DDR1 and DDR2. We have previously shown that in 3D collagen matrix, DDR1 plays a key role as it promotes cell growth suppression and apoptosis through the upregulation of the pro-apoptotic mediator BIK in noninvasive luminal-like breast carcinoma cells. We have also shown that MT1-MMP is able to rescue these cells and protect them against the effects induced by collagen/DDR1/BIK axis. Our data suggested that the protective effect of MT1-MMP might be mediated through the degradation of type I collagen and/or DDR1 cleavage. Decreased DDR1 expression has been associated with the epithelial to mesenchymal transition process in breast cancer, and its overexpression in aggressive basal-like breast cancer cells reduces their invasiveness in 3D cultures and *in vivo*. In the present work, we propose to study the role of MT1-MMP in the resistance against collagen-induced apoptosis in basal-like breast carcinoma MDA-MB-231 cells. We aimed to investigate whether MT1-MMP depletion is able to restore apoptosis mediated by collagen/DDR1/BIK axis and to verify if such depletion is able to restore full-length DDR1 expression and phosphorylation. ShRNA strategy against MT1-MMP mRNA was able to partially restore full length DDR1 expression and phosphorylation. This was accompanied by a decrease in cell growth and an upregulation of BIK expression. This suggested that MT1-MMP expression in basal-like breast carcinoma cells, in addition to a low basal level of DDR1 expression, protects these cells against collagen-induced apoptosis via DDR1 cleavage. Since DDR1 was moderately expressed in MDA-MB-231 cells, we then investigated whether overexpression of DDR1 could be able to increase its ability to suppress cell growth and to induce apoptosis. Data showed that

overexpression of DDR1 induced a decrease in cell growth and an increase in BIK expression, suggesting that moderate expression level of full length DDR1 in basal-like breast carcinoma provides them with a capacity to resist to collagen-induced cell growth suppression and apoptosis. Finally, the combined overexpression of DDR1 and depletion of MT1-MMP in MDA-MB-231 cells synergistically increased collagen-induced cell growth suppression and apoptosis to a level similar to that observed in luminal breast carcinoma. Taken together, our data suggest that during the acquisition of mesenchymal features, the low level of DDR1 expression should be considered as an important biomarker in the prognosis of basal-like breast carcinoma, conferring them a high rate of cell growth and resistance to BIK-mediated apoptosis induced by the stromal collagen.

Keywords: type I collagen, MT1-MMP, DDR1, apoptosis, breast carcinoma

INTRODUCTION

The extracellular matrix plays an important role in the regulation of tumor progression (Pickup et al., 2014). Type I collagen is the major adhesive component in breast tumors and represents the first barrier against tumor cells after basement-membrane degradation (Mouw et al., 2014). Among cellular receptors, type I collagen is able to activate integrins ($\alpha1\beta1$, $\alpha2\beta1$, $\alpha10\beta1$, and $\alpha11\beta1$) (Humphries et al., 2006; Leitingner, 2011) and discoidin domain receptors DDR1 and DDR2 (Vogel et al., 1997; Leitingner, 2011; Carafoli and Hohenester, 2013; Fu et al., 2013b). DDRs belong to the receptor tyrosine kinase family and play important roles in physiological and pathological conditions (Borza and Pozzi, 2013; Leitingner, 2014).

DDR1 and DDR2 have been demonstrated to predominantly regulate tumor progression (Valiathan et al., 2012). In addition to their oncogenic function, it has also been reported that these receptors can play a role of tumor suppressor (Rammal et al., 2016; Henriët et al., 2018). For example, in 3D collagen matrix, DDR2 is able to suppress tumor cell growth (Wall et al., 2005; Iwai et al., 2013; Saby et al., 2016; Terashima et al., 2016). DDR1 is also a key factor in collagen-induced apoptosis in noninvasive luminal-like breast carcinoma cells. In this case, apoptosis is mostly characterized by the expression of the pro-apoptotic mediator BIK (Assent et al., 2015; Saby et al., 2018). In addition to a high level of DDR1 expression, the luminal-like breast carcinoma cells are characterized by a low expression level of MT1-MMP (Maquoi et al., 2012). However, in invasive basal-like breast carcinoma cells, DDR1 has been described to promote linear invadosomes and tumor invasion (Juin et al., 2014). At the opposite of the luminal-like breast carcinoma cells, the basal-like ones express low levels of DDR1 and a high level of MT1-MMP (Maquoi et al., 2012; Croissant et al., 2018). In some of the basal-like breast carcinoma cells, it has been reported that the low level of DDR1 expression could be compensated by an increase in DDR2 expression (Toy et al., 2015). This low level of DDR1 is yet sufficient to promote tumor invasion in a kinase-independent manner (Juin et al., 2014). Interestingly, studies have shown that a low DDR1 expression is correlated with poor relapse-free

survival, confirming its controversial role in tumor progression (Ford et al., 2007; Takai et al., 2018). Concerning the role of MT1-MMP in the regulation of collagen-induced apoptosis, we and others have previously shown that when expressed by luminal-like breast carcinoma, this metalloproteinase protects cells against collagen-induced apoptosis (Maquoi et al., 2012; Albrechtsen et al., 2013; Saby et al., 2018). These studies supported a model in which MT1-MMP inactivates the collagen/DDR1/BIK apoptosis signaling pathway through the degradation of collagen (Amar et al., 2017) and/or the cleavage of DDR1 (Fu et al., 2013a).

Basal-like breast cancers are among the most aggressive and deadly breast cancer subtypes, displaying a high metastatic ability associated with mesenchymal features. These mesenchymal features are acquired as a consequence of an epithelial to mesenchymal transition (EMT). This process is classically characterized by the dedifferentiation from an epithelial to mesenchymal phenotype, marked by the decreased expression of E-cadherin and increased expression of vimentin, as well as expression of cellular proteases such as MT1-MMP. Decreased DDR1 expression has been associated with the EMT process in breast cancer, and its overexpression in aggressive basal-like breast cancer cells reduces their invasiveness in 3D cultures and *in vivo*, supporting an anti-migratory function of DDR1 in this cancer (Koh et al., 2015). In a previous study, we have examined this correlation in multiple breast cancer cell lines, by analyzing expression levels of E-cadherin, vimentin, DDR1, DDR2, MT1-MMP, and BIK mRNAs in 58 breast cancer cell lines (Saby et al., 2018). High DDR1 expression was clearly observed in the E-cadherin-high and vimentin-low epithelial cell lines. In contrast, the more mesenchymal breast cancer cell lines (E-cadherin-low and vimentin-high) were characterized by a weak DDR1 level, a high MT1-MMP, and a low BIK expression (Saby et al., 2018). We have then suggested that the acquisition of mesenchymal features including the downregulation of DDR1 and the overexpression of collagenolytic proteinases such as MT1-MMP provide breast carcinoma cells with an increased capacity to resist to apoptosis induced by 3D collagen matrix. More recently, DDR1 ablation

in vivo was reported to confer a basal-like phenotype to luminal-like breast carcinoma population and to increase their metastatic potential (Takai et al., 2018).

Treatment of the basal-like breast carcinoma MDA-MB-231 cells with BB-94, a synthetic broad spectrum MMP inhibitor, was shown to restore a collagen-induced apoptosis (Maquoi et al., 2012). Likewise, a specific depletion of MT1-MMP using a siRNA strategy increased the number of apoptotic bodies in these cells. However, the potential contribution of the collagen/DDR1/BIK axis was not investigated (Albrechtsen et al., 2013).

In the present work, we aim at studying the contribution of MT1-MMP in the resistance of basal-like breast carcinoma cells against collagen-induced apoptosis. Whether MT1-MMP silencing is able to restore apoptosis induced through the collagen/DDR1/BIK axis, as well as to restore full length DDR1 expression and phosphorylation, will be investigated. Since DDR1 is moderately expressed in basal-like breast carcinoma cells, we propose to explore whether overexpression of DDR1 could restore apoptosis. Finally, we will test whether the simultaneous silencing of MT1-MMP and overexpression of DDR1 in basal-like breast carcinoma cells are able to restore apoptosis to a level similar to that observed in luminal-like breast carcinoma cells. Our data suggest that, in addition to the known markers related to mesenchymal features (basal-like), the concomitant overexpression of MT1-MMP and downregulation of DDR1 expression should be considered as important biomarkers in the prognosis of breast carcinomas.

MATERIALS AND METHODS

Cell Culture

The human breast adenocarcinoma cell lines MCF-7 (HTB-22) and MDA-MB-231 (HTB-26) were purchased from the American Type Culture Collection (ATCC). MCF-7 cells stably transfected with the full-length MT1-MMP vector (MCF-7 MT1-MMP) and MCF-7 cells transfected with the empty vector (MCF-7 VEC) were obtained as previously described (Maquoi et al., 2012). MCF-7 and MDA-MB-231 cell lines were cultured in DMEM (4.5 g/l glucose) with Glutamax I (PAN-Biotech, p04-04500) supplemented with 10% fetal bovine serum (Dominique Dutscher, S1810-500) and 1% penicillin-streptomycin (Invitrogen, 15140). Cultures were maintained at 37°C in a humidified atmosphere containing 5% CO₂ (v/v). Cells were routinely passaged at preconfluency using 0.05% trypsin, 0.53 mM EDTA (Invitrogen, 25300) and screened for the absence of mycoplasma using PCR methods.

Preparation and Characterization of Type I Collagen

Fibrillar native type I collagen was extracted from tail tendons of 2-month-old rats and prepared as already described (Garnotel et al., 2000). Briefly, type I collagen was extracted from tail tendons of Wistar rats (Janvier) using 0.5-M acetic acid

at 4°C, in the presence of protease inhibitors. Then, type I collagen was specifically precipitated with NaCl 0.7 M and centrifuged. The precipitate was then re-suspended in 18 mM acetic acid, and salts used during the precipitation step were eliminated by dialysis against distilled water for 1 week at 4°C. Finally, the collagen was characterized as described in our previous work, before use (Saby et al., 2016, 2018).

Plastic and 3D Cell Culture

Type I collagen effect on breast adenocarcinoma cells growth was studied in 24-well plates. For plastic condition, cells were seeded at a density of 3×10^4 cells/well (1 ml/well). For 3D cell culture, 3×10^4 cells were resuspended in 100-μl fetal bovine serum and mixed with a solution containing 100 μl of 10X culture medium DMEM (Gibco, 52100), 100 μl NaHCO₃ (0.44 M), 100 μl H₂O, 90 μl NaOH 0.1 M, 10 μl glutamine 200 mM and 500 μl collagen 3 mg/ml. Then, 1 ml/well of this solution was deposited in 24-well plates, and gels were polymerized at 37°C during 30 min. Finally, 1 ml of complete culture medium was added on top of each gel and the plates were incubated at 37°C. After 5 days, the covering medium was removed, and cell populated gels were digested with collagenase P (2 mg/ml – Roche, 11213873001). Viability and cellular density of this suspension were determined by phase contrast microscopy using Kova® Glasstic® Slides (Kova International Inc, 87144). In some 3D culture experiments, cells were treated with DDR1 pharmacological inhibitors nilotinib (Selleckchem, No.S1033), at 100 nM.

Vectors, Transfection, and Infection

DDR1-GFP overexpression was performed with pLVX-CMV-DDR1-GFP. DDR1-GFP lentiviral particles were generated through co-transfection of 293 T cells with pCMV ΔR8.91 (gag-pol) and pHCMVG-VSVG (env) expression constructs using the FuGene 6 transfection reagent (Promega) according to the manufacturer's recommendations. Three days after transfection, the viral supernatant mixed with fresh medium (1 of 4) and hexadimethrine bromide at 8 μg/ml (Sigma) was used to infect MDA-MB-231 cells. Infected cells were selected using puromycin (Invivogen) at 1 μg/ml.

MT1-MMP knock-down was achieved with MMP-14-specific shRNAs (Buache et al., 2014). shRNA MMP-14 retroviral particles were generated through co-transfection of 293 T cells with pCL-Ampho expression constructs using the FuGene 6 transfection reagent (Promega) according to the manufacturer's recommendations. Three days after transfection, the viral supernatant mixed with fresh medium (1 of 4) and hexadimethrine bromide at 8 μg/ml (Sigma) was used to infect MDA-MB-231 cells. Infected cells were selected using puromycin (Invivogen) at 1 μg/ml.

Reverse Transcription and Real-Time Quantitative PCR

Total RNA was isolated with a phenol-chloroform extraction method, using RNA Extracol (EURx). Then, 1 μg of total RNA

was converted to cDNA by reverse transcription using the Maxima First Strand cDNA Synthesis kit (Thermo Fisher Scientific) according to the manufacturer's recommendations. Real-time PCR was performed using a Maxima SYBR GREEN/ROX qPCR Master Mix (Thermo Fisher Scientific, #KO222) on the Stratagene Mx3005P qPCR detection system (Agilent Technologies). Polymerase chain reaction conditions were 15 min at +95°C, followed by 35 cycles each consisting of 15 s at +95°C (denaturation) and 30 s at +60°C (annealing/extension). Results were standardized to the eEF1A1 gene expression by calculating ΔC_t using the formula $\Delta C_t = (C_t \text{ gene of interest} - C_t \text{ eEF1A1})$. Gene expression was represented as $2^{-\Delta C_t}$. The following primers were used: BIK forward primer: 5'-aggacctggaccctatggag-3' and reverse primer: 5'-ccctgatgtcctcagttggg-3'; eEF1A1 forward primer: 5'-ctggagccaagtgtcaatgcc-3' and reverse primer: 5'-ccgggtttgagaacaccagtc-3'.

Quantification of Annexin V Positive Cells

Cells were cultured in type I collagen 3D matrices as described in "plastic and 3D cell culture". After 36 hours, 1×10^5 cells were harvested for each condition using collagenase P at 2 mg/ml, washed twice with PBS and analyzed using the Muse® Annexin V and Dead Cell Assay Kit, Millipore, MCH100105, according to the manufacturer's instructions.

Western Blotting

Cells were cultured in type I collagen 3D matrices or plastic as described in the "plastic and 3D cell culture". After 5 days, cells were harvested using collagenase P at 2 mg/ml for 3D matrices, washed twice with PBS, and lysed with RadioImmuno Precipitation Assay (RIPA) buffer (Thermo Fisher Scientific, 89900), supplemented with Halt™ Protease and Phosphatase Inhibitor Cocktail 1X (Thermo Scientific, 78442). For plastic conditions, cells were directly washed and lysed without the use of collagenase P. Cell lysates were sonicated and clarified by centrifugation at $14\,000 \times g$ at 4°C for 15 min. Then, total protein content was estimated by bicinchoninic acid (BCA) assay method (Thermo Scientific, 23227), and proteins were separated by SDS-PAGE and transferred to a nitrocellulose membrane. Membranes were blocked with Tris Buffered Saline (TBS) (0.02 M Tris-HCl, 0.137 M NaCl, pH 7.6) containing 0.1% Tween (TBS-T) and 5% Bovine Serum Albumin (BSA) at room temperature during 1 hour and incubated overnight at 4°C with anti-DDR1 (Cell Signaling Technology, #5583), anti-phospho DDR1 (Tyr 792) (Cell Signaling Technology, #11994), anti-GAPDH antibodies (Cell Signaling Technology, #5174), and anti-MT1-MMP, obtained from Dr. Tomasetto C. L (IGBMC, Illkirch, France) (Buache et al., 2014). Membranes were washed with TBS-T and incubated with peroxidase conjugated anti-rabbit secondary antibody (Cell Signaling Technology, #7074) at room temperature for 1 h. Chemiluminescent detection was performed by using an ECL Prime Kit (GE Healthcare, RPN2236). Electrophoretic images were analyzed with ImageJ software.

Expression Level of EMT Marker in Breast Cancer Cell Lines

The expression levels of E-cadherin, vimentin, DDR1, DDR2, $\alpha 2$ integrin, $\alpha 11$ integrin, COL1A1, MT1-MMP, BIK, estrogen receptor α , progesterone receptor, and HER2 mRNAs in 58 breast cancer cell lines were obtained by interrogating the Broad-Novartis Cancer Cell Line Encyclopedia (CCLE) database.

Correlation Analyses Between DDR1 and BIK mRNA Levels in Breast Cancer

Correlations analysis between DDR1 and BIK mRNA levels were performed by interrogating gene expression data sets contained at cBioPortal¹ and Breast Cancer Gene-Expression Miner (bc-GenExMiner)². bc-GenExMiner contains 36 datasets including 5861 breast cancer patients (Jézéquel et al., 2012). cBioPortal was used to explore the TCGA breast cohort (Ciriello et al., 2015).

KM Plotter Database Analysis

Kaplan–Meier curves were generated with the Kaplan–Meier plotter website (<http://kmplot.com>), using a database of public microarray datasets (Györfy et al., 2010). Automatic cut-off scores were selected during queries, and relapse-free survival (RFS) was selected. Number of cases, hazard ratios (HRs), 95% confidence intervals, and *p*-values were extracted from the KM plotter webpage. The analyses were performed with the mean expression of the 4 DDR1 Affymetrix probes (1007_s_at, 207169_x_at, 208779_x_at, and 210749_x_at).

Statistical Analyses

Data are presented as mean \pm standard error of the mean (SEM) from three independent experiments. Statistical significance was assessed with Student's *t* test, or with one-way ANOVA, followed by Tukey's multiple comparison test. *p* < 0.05 was considered as significant (**p* < 0.05; ***p* < 0.01; ****p* < 0.001).

RESULTS

MCF-7 and MDA-MB-231 Cells Present Different Expression Profiles for EMT Markers

The human breast adenocarcinoma cell lines MCF-7 and MDA-MB-231 cells display different phenotypes. While the noninvasive luminal-like MCF-7 cells present typical epithelial features, the invasive basal-like MDA-MB-231 cells present a more mesenchymal phenotype (Maquoi et al., 2012). The expression levels of E-cadherin, vimentin, DDR1, DDR2, $\alpha 2$ integrin, $\alpha 11$ integrin, COL1A1, MT1-MMP, BIK, estrogen receptor α , progesterone receptor, and HER2 mRNAs in 58 breast cancer cell lines were analyzed *in silico*, by using the Broad-Novartis Cancer Cell Line Encyclopedia (CCLE)

¹www.cbioportal.org

²www.bcgenex.centregauducheau.fr

database. As shown in **Figure 1**, the 58 breast cancer cell lines segregate into two distinct groups. The first one includes cells with a relatively high level of E-cadherin, DDR1, BIK, and a low level of MT1-MMP, vimentin, DDR2, $\alpha 2$ integrin, $\alpha 11$ integrin, and COL1A1 and is essentially composed of cells with an epithelial phenotype like the MCF-7 cells, which are estrogen receptor α and progesterone receptor positive. The second group is represented by cells with a low level of E-cadherin, DDR1, and BIK and a high level of MT1-MMP, vimentin, and other markers. This group is composed by cells with mesenchymal features like the MDA-MB-231 triple negative cells. These data show that in addition to the switch of classical EMT markers expression, there is a concomitant

switch of DDR1 and BIK expression between the epithelial and mesenchymal breast cancer cells.

DDR1 Is More Expressed in Luminal Breast Adenocarcinomas Than in the Basal Ones

DDR1 expression level was analyzed in a cohort of TCGA breast cancer patients. As shown in **Figure 2A**, basal-like breast tumors express significantly lower levels of DDR1 mRNA when compared to luminal A and B tumors. DDR1 expression was then studied in a cohort of 3,951 breast tumors from patients where relapse free survival (RFS) was assessed. As shown in **Figure 2B**, high DDR1 expression is associated with a better

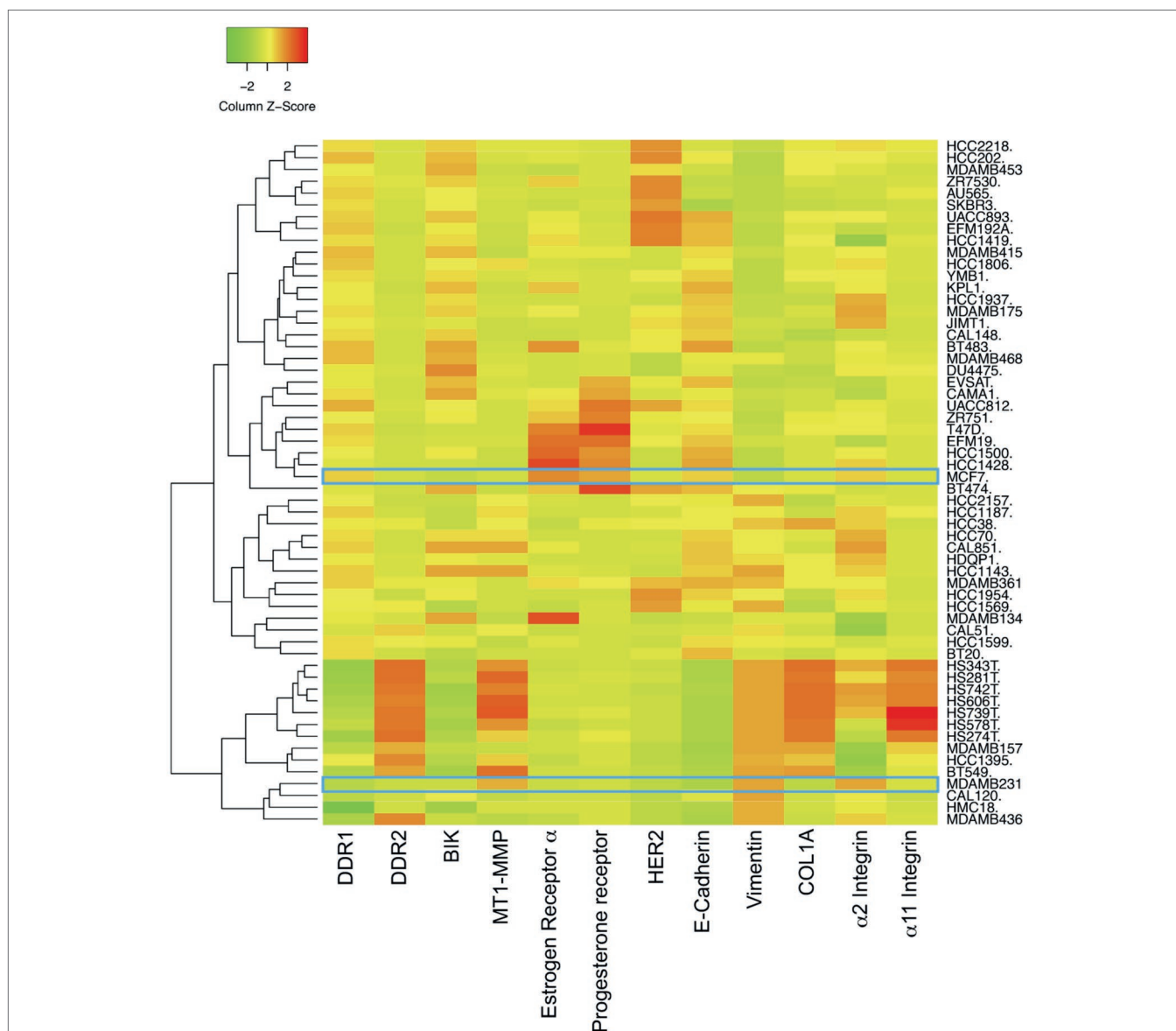


FIGURE 1 | Expression of DDR1, BIK and MT1-MMP in basal and luminal breast cancer cell lines. Heat map depicting the relative expression of E-cadherin (CDH1, luminal marker), vimentin (VIM, basal marker), DDR1, DDR2, $\alpha 2$ integrin, $\alpha 11$ integrin, αv integrin, COL1A1, MT1-MMP, and BIK in 58 breast cancer cell lines.

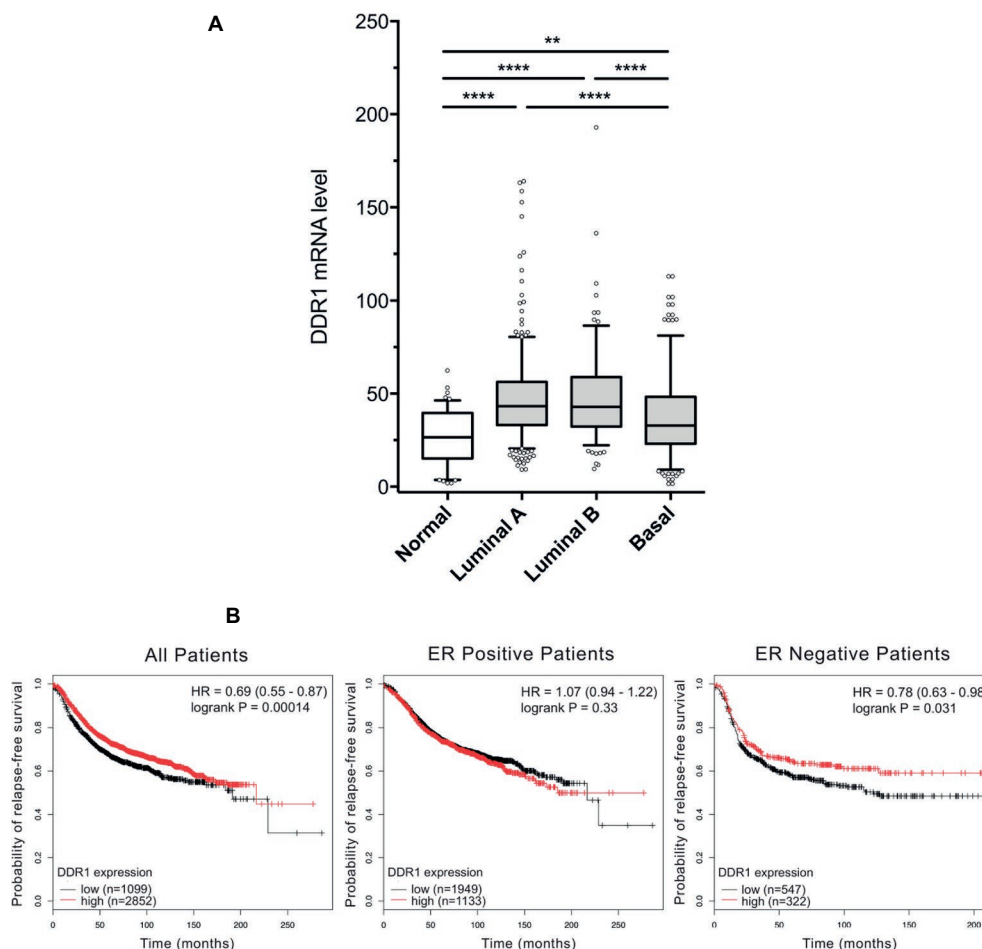


FIGURE 2 | DDR1 expression in breast cancer and the associated correlation with prognosis in ER negative tumors. **(A)** Box-and-whisker plots comparing the expression level of DDR1 among normal, luminal A, luminal B, and basal subtypes. Shaded rectangles represent interquartile range; line in the middle of each rectangle represents median value. Lines extending from the interquartile range mark the 5th and 95th percentile values, and the individual open circles represent values that are either above the 95th percentile or below the 5th percentile for each distribution. **, $p < 0.01$; ****, $p < 0.0001$. **(B)** Kaplan-Meier representation of relapse-free survival (RFS) probability over time for breast cancer patients irrespective of the ER status, ER positive and ER negative patients with high or low DDR1 expression.

RFS probability in the total patient population ($HR = 0.69$, $p = 0.00014$) and in estrogen receptor negative tumors ($HR = 0.78$, $p = 0.031$) but not in the estrogen receptor positive tumors ($HR = 1.07$, $p = 0.33$). In contrast, DDR1 expression level was not associated with an altered RFS probability when patients were stratified according to the expression of progesterone receptor, HER2, tumor grades, or intrinsic subtypes (data not shown).

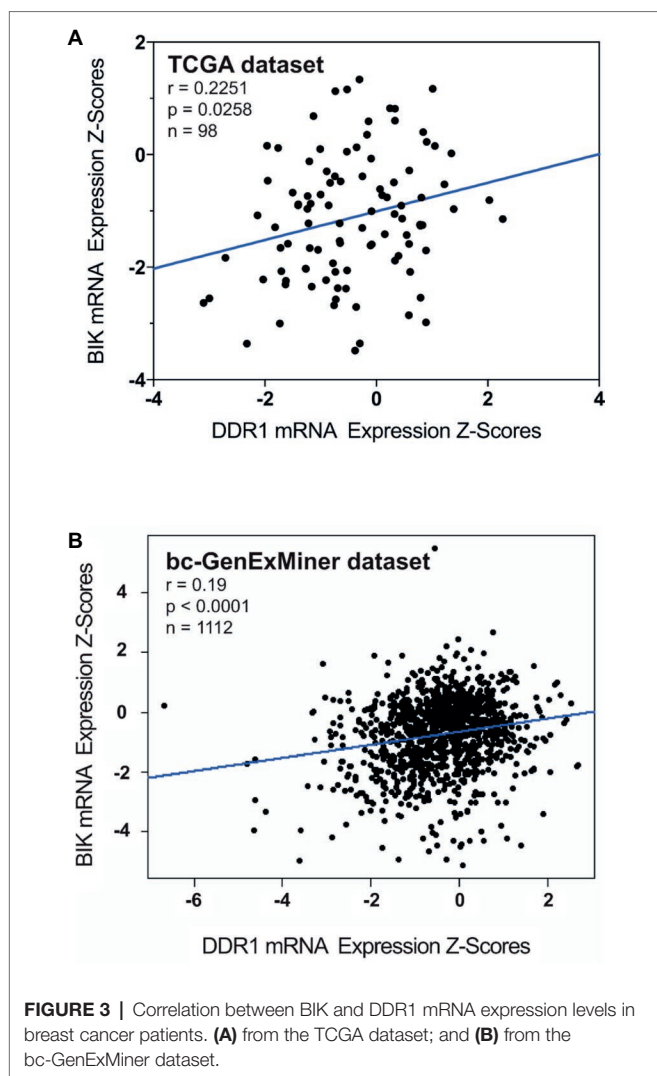
BIK and DDR1 mRNA Levels Are Positively Correlated in Basal-Like Breast Tumors

Correlation between BIK and DDR1 mRNA expression levels was analyzed using published genomic data from two dataset of breast cancer patients, the TCGA and the bc-GenExMiner (Jézéquel et al., 2012). As shown in **Figure 3A**, the expression level of apoptosis marker BIK was positively correlated to that of DDR1 in basal-like breast tumors ($r = 0.2251$, $p = 0.0258$). The same results were obtained with the bc-GenExMiner dataset

that shows a positive correlation between BIK and DDR1 mRNA expression ($r = 0.19$, $p < 0.0001$; **Figure 3B**).

MCF-7 and MDA-MB-231 Cells Express Different Levels of DDR1 and MT1-MMP

DDR1 has the unique ability among the tyrosine kinase receptors to be activated only by type I collagen in its fibrillary state. We have previously shown that DDR1 was able to initiate apoptosis in luminal-like breast carcinoma MCF-7 cells embedded in 3D type I collagen matrices (Assent et al., 2015; Saby et al., 2018). We have also shown that MT1-MMP, the primary enzyme used by stromal and cancer cells to cleave and migrate through fibrillar collagen, plays a crucial role in the regulation of cell growth and survival in 3D type I collagen matrices. Here, DDR1 and MT1-MMP protein expression levels were compared by western blot analysis in MDA-MB-231 and MCF-7 cells. In agreement with *in silico* transcriptomic data (**Figure 1**), MCF-7 cells express a high level of DDR1 and a low level of



MT1-MMP, whereas an opposite expression profile was observed in MDA-MB-231 cells (**Figures 4A,B**).

3D Type I Collagen Matrices Promote Apoptosis in MCF-7 Cells

Since 3D type I collagen matrices are known to induce apoptosis in luminal-like breast carcinoma cell lines, thus regulating tumor cell growth, we first compared the growth of MCF-7 and MDA-MB-231 cell lines, cultivated for 5 days in two different experimental settings: (i) plated on plastic (used as a control) or (ii) suspended within a 3D native type I collagen gel. MCF-7 cells exhibited a significantly lower cell growth in 3D collagen when compared to 2D plastic condition, whereas MDA-MB-231 cells showed a similar cell growth in the two culture conditions (**Figure 4C**). Since it has been shown that type I collagen/DDR1 axis was able to induce apoptosis in MCF-7 cells (Assent et al., 2015; Saby et al., 2018), we then compared apoptosis between MCF-7 and MDA-MB-231 cells. As shown in **Figure 4D**, 3D collagen strongly increased apoptosis in MCF-7 cells as evidenced by annexin V staining, whereas

it failed to modulate apoptosis in MDA-MB-231 cells. These data demonstrate that the luminal and basal-like breast carcinoma cell lines exhibit a different behavior in a 3D type I collagen environment.

MT1-MMP Overexpression in MCF-7 Cells Induces a Cleavage of DDR1 and Promotes Cell Growth

Previous works have shown that MT1-MMP was able to cleave DDR1 (Fu et al., 2013a; Assent et al., 2015), and that depletion of MT1-MMP was able to increase apoptosis in basal-like breast cancer cells (Albrechtsen et al., 2013). Here, we investigated whether MT1-MMP is involved in the cleavage of DDR1 providing cell protection against the cell growth suppressor and pro-apoptotic effects of type I collagen/DDR1/BIK signaling pathways. To this end, MCF-7 cells that are lacking endogenous MT1-MMP were transfected with a full-length MT1-MMP expression vector (MCF-7 MT1-MMP) or an empty vector (MCF-7 VEC), as already described (Maquoi et al., 2012; Saby et al., 2018). In MCF-7 MT1-MMP cells, MT1-MMP is expressed as a 60-kDa mature form and a 43-kDa autoproteolytic degradation product (**Figure 5A**). In those cells, DDR1 expression was analyzed by western blotting. As shown in **Figure 5B**, MCF-7 MT1-MMP cells present both the full length DDR1 and a lower molecular weight form which corresponds to a cleaved membrane-anchored c-terminal fragment (Fu et al., 2013a), whereas MCF-7 VEC cells present only the full length DDR1. These data confirmed the previously reported efficient cleavage of DDR1 by MT1-MMP (Fu et al., 2013a; Assent et al., 2015). We then studied the effect of MT1-MMP overexpression on MCF-7 cells growth and apoptosis. As shown in **Figures 5C,D**, MCF-7 MT1-MMP exhibited a higher cell growth and a lower apoptosis rate.

MT1-MMP Depletion in MDA-MB-231 Cells Induces an Increase in Full Length DDR1 Expression and Promotes Cell Apoptosis

Since MT1-MMP is involved in DDR1 cleavage, partially protecting cells from the type I collagen induced apoptosis observed in the luminal breast cancer cell line MCF-7, we then investigated the effect of MT1-MMP depletion on DDR1 expression profile in the basal-like cell line MDA-MB-231. Albrechtsen et al. showed that the depletion of MT1-MMP using a siRNA strategy in MDA-MB-231 cells was able to increase the number of apoptotic bodies. However, the potential implication of the collagen/DDR1/BIK axis in this apoptotic process was not characterized (Albrechtsen et al., 2013). To that purpose, MDA-MB-231 cells were stably transfected with a shRNA directed against MT1-MMP. As shown in **Figure 6A**, MDA-MB-231 shMT1-MMP cells exhibit a lower level of MT1-MMP when compared to shCtrl transfected cells. By using western blotting, we then compared DDR1 expression and phosphorylation in shCtrl and shMT1-MMP MDA-MB-231 cells. **Figure 6B** shows that the full length DDR1 is more expressed in MDA-MB-231 shMT1-MMP cells than in MDA-MB-231 shCtrl cells. Also, the analysis of DDR1

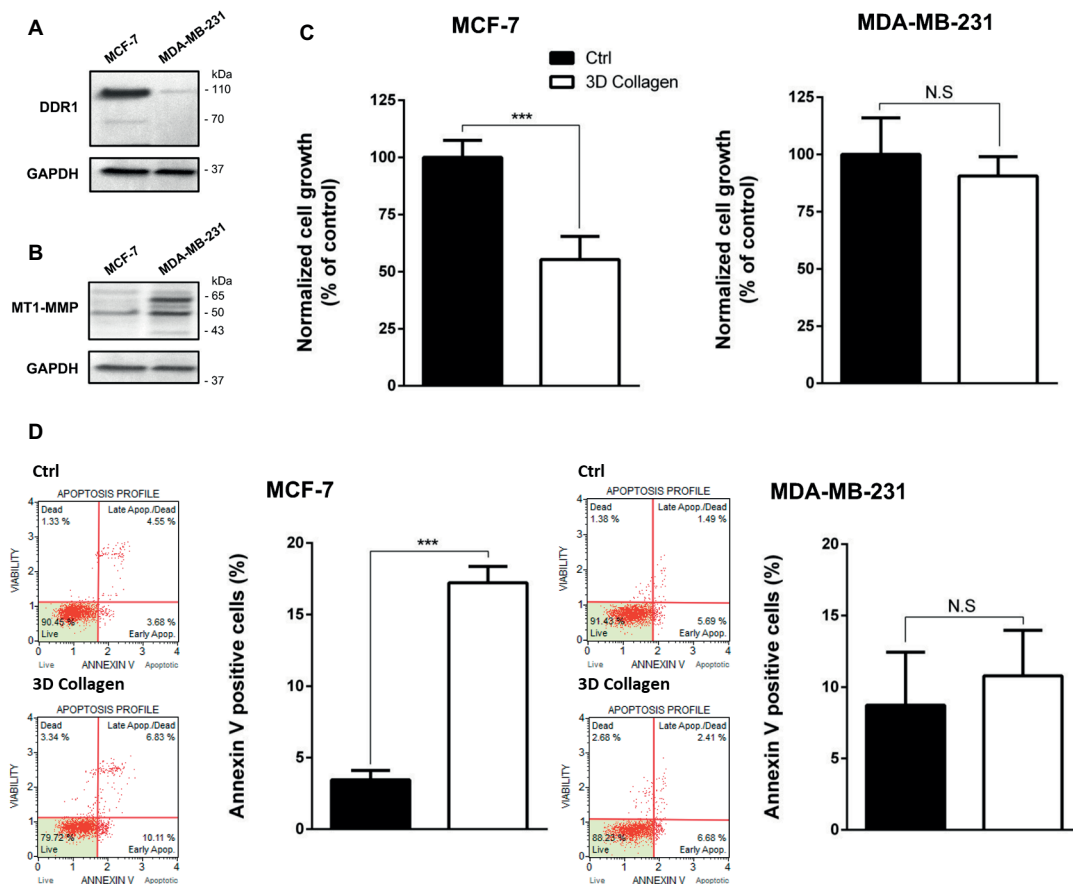


FIGURE 4 | Effect of type I collagen on the growth of MCF-7 luminal breast cancer cells and MDA-MB-231 basal-like breast cancer cells. **(A)** DDR1 protein expression was evaluated using Western Blotting. GAPDH was used as a loading control. **(B)** MT1-MMP protein expression was evaluated using Western Blotting. GAPDH was used as a loading control. **(C,D)** MCF7 (left panel) and MDA-MB-231 (right panel) cells were seeded on plastic or in 3D type I collagen matrices. After 5 days of culture, viable cell density was evaluated by phase contrast microscopy **(C)** and after 36 h of culture, apoptosis was quantified using the Muse[®] annexin V and dead cell assay kit **(D)**. Values represent the mean \pm S.D. of three independent experiments (** $p < 0.001$, N.S. = not significant).

phosphorylation in both conditions shows a 1.34-fold increase in pDDR1/DDR1 ratio in MDA-MB-231 shMT1-MMP cells compared to shCtrl cells. We then analyzed cell growth and apoptosis in both cell lines. As shown in **Figure 6C**, MDA-MB-231 shMT1-MMP cells exhibit a lower cell growth after 5 days in 3D collagen matrices than shCtrl cells. This is linked with a higher apoptosis rate in cells silenced for MT1-MMP, as revealed in **Figures 6D,E**, which show an increase in both the number of annexin V positive cells and the mRNA level of the pro-apoptotic mediator BIK.

DDR1 Overexpression in MDA-MB-231 Cells Increases Apoptosis

We have previously shown that in MCF-7 cells, the decreased growth was induced by 3D type I collagen and was dependent on DDR1-induced apoptosis (Assent et al., 2015; Saby et al., 2018). Since MDA-MB-231 cells slightly express DDR1, we assume that the weak expression of this receptor is a key parameter explaining why type I collagen fails to impair

growth and survival of these basal-like breast carcinoma cells. To address this hypothesis, MDA-MB-231 cells were transfected with a full-length DDR1-GFP expression vector (MDA-MB-231 DDR1-GFP) or an empty vector (MDA-MB-231 VEC-GFP), and cell growth and apoptosis were evaluated. As shown in **Figure 7A**, MDA-MB-231 DDR1-GFP expressed a high level of both full-length (140 kDa) and cleaved (70 kDa) DDR1-GFP, whereas MDA-MB-231 VEC-GFP only expresses low level of wild-type full length DDR1 (110 kDa). MDA-MB-231 DDR1-GFP and VEC-GFP were then seeded in 3D type I collagen matrices, and cell growth was quantified after 5 days. As shown in **Figure 7B**, DDR1 overexpression decreases MDA-MB-231 cell growth. Apoptosis was also evaluated by quantifying the expression of the proapoptotic BIK mRNA. As observed in **Figure 7C**, BIK is more expressed in MDA-MB-231 DDR1-GFP cells than in MDA-MB-231 VEC-GFP. Since DDR1 phosphorylation was affected by MT1-MMP expression status (**Figure 6B**), we measured the impact of nilotinib (100 nM), a receptor tyrosine kinase inhibitor with high potency against DDR1, on BIK expression. **Figure 7C** shows

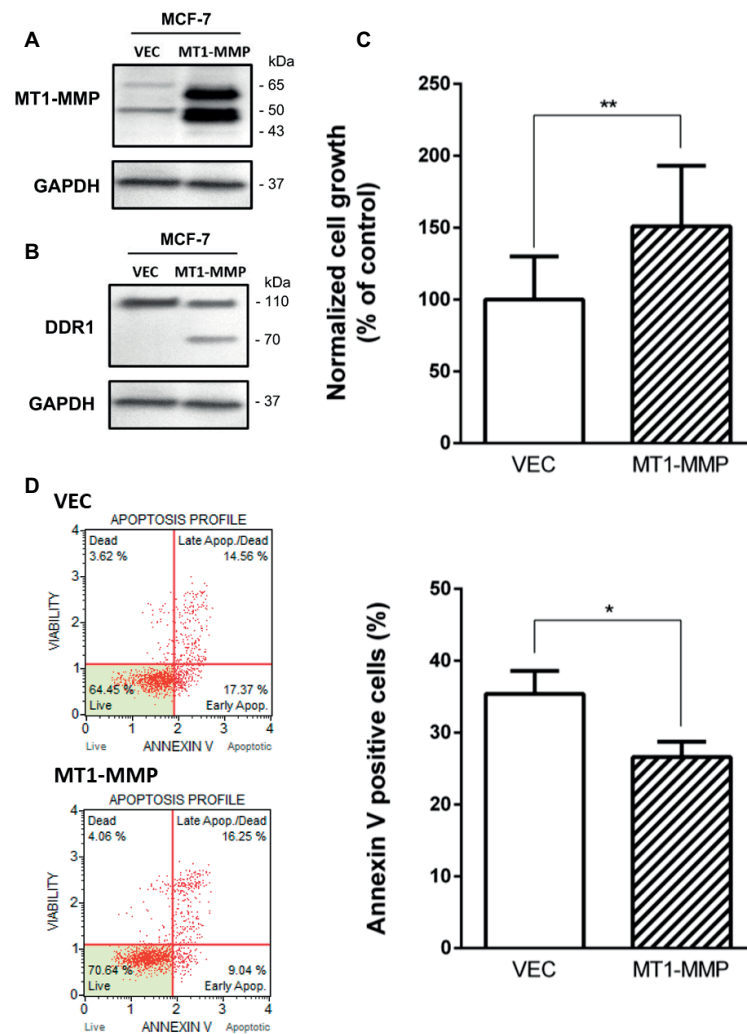


FIGURE 5 | Effect of MT1-MMP expression on type I collagen-induced growth reduction and apoptosis in MCF-7. **(A)** Western blot analysis of ectopically expressed MT1-MMP in MCF-7. GAPDH was used as a loading control. **(B)** Western blot analysis showing the cleavage of DDR1 in MCF7 ectopically expressing MT1-MMP. GAPDH was used as a loading control. **(C,D)** MCF-7 VEC (empty vector) and MCF-7 MT1-MMP (full length MT1-MMP expression vector) cells were seeded in type I collagen 3D matrices. After 5 days of culture, viable cell density was evaluated by phase contrast microscopy **(C)** and after 36 h of culture, apoptosis was quantified using the Muse[®] annexin V and dead cell assay kit **(D)**. Values represent the mean \pm S.D. of three independent experiments (* $p < 0.05$, ** $p < 0.01$).

that nilotinib was able to significantly decrease BIK expression in both MDA-MB-231 VEC-GFP and MDA-MB-231 DDR1-GFP cells. Taken together, these data suggest that collagen-induced apoptosis is BIK dependent and relies on DDR1 phosphorylation.

DDR1 Overexpression Coupled With MT1-MMP Depletion in MDA-MB-231 Cells Increases Cell Apoptosis

Since both DDR1 overexpression and MT1-MMP depletion were able individually to increase apoptosis in MDA-MB-231 cells, we hypothesized that the double transfection of DDR1 and shMT1-MMP in these cells could synergize to decrease

cell growth and increase collagen-induced apoptosis to a level similar to that observed in luminal-like breast carcinoma cells. To this end, MDA-MB-231 cells overexpressing DDR1-GFP (MDA-MB-231 DDR1-GFP) were transfected with shRNA against MT1-MMP. As shown in **Figure 8A**, MT1-MMP depletion in these cells increases by 1.44-fold the expression of full length DDR1, when compared with MDA-MB-231 DDR1-GFP shCtrl cells. Then, cell growth and apoptosis in 3D collagen matrix were studied. As shown in **Figure 8B**, MDA-MB-231 DDR1-GFP exhibits a lower cell growth when MT1-MMP is depleted (MT1-MMP shRNA). This reduction is associated with a concomitant increase in apoptosis, as reflected by the increased number of annexin V positive cells (**Figure 8C**). We then studied the expression of the pro-apoptotic

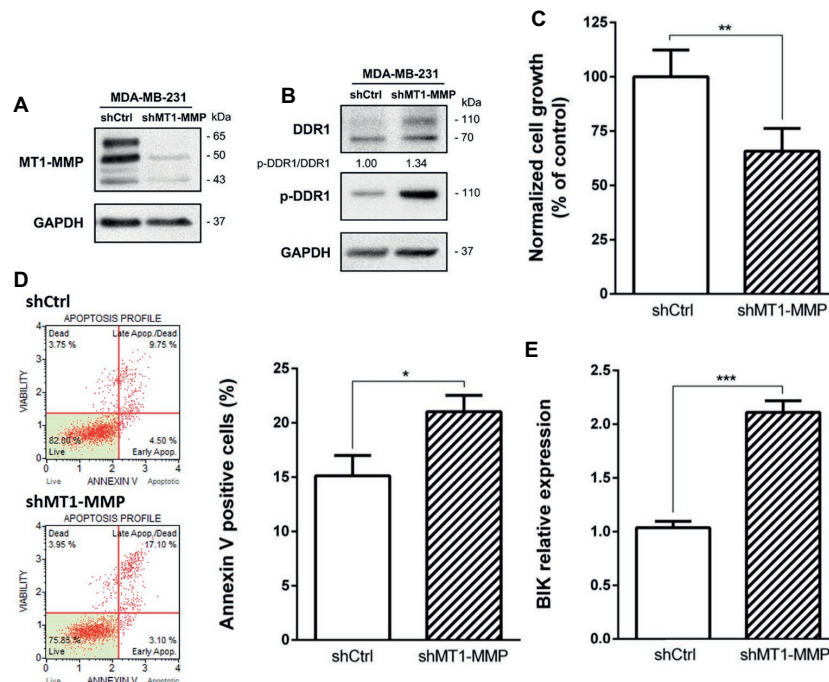


FIGURE 6 | Effect of MT1-MMP silencing in MDA-MB-231 on cell growth and survival in 3D type I collagen matrices. **(A)** Western blot analysis confirming efficient knock down of MT1-MMP in MDA-MB-231 shMT1-MMP. GAPDH was used as a loading control. **(B–E)** MDA-MB-231 shCtrl and MDA-MB-231 shMT1-MMP cells were embedded in 3D type I collagen matrices. After 36 h of culture, cell extracts were analyzed for tyrosine phosphorylation of DDR1 and total DDR1 by Western blotting. GAPDH was used as a loading control **(B)**. After 5 days of culture, viable cell density was evaluated by phase contrast microscopy **(C)**. After 36 h of culture, apoptosis was quantified using the Muse[®] annexin V and dead cell assay kit **(D)** and BIK expression was measured by RT-PCR **(E)**. Values represent the mean \pm S.D. of three independent experiments (* p < 0.05; ** p < 0.01; *** p < 0.001).

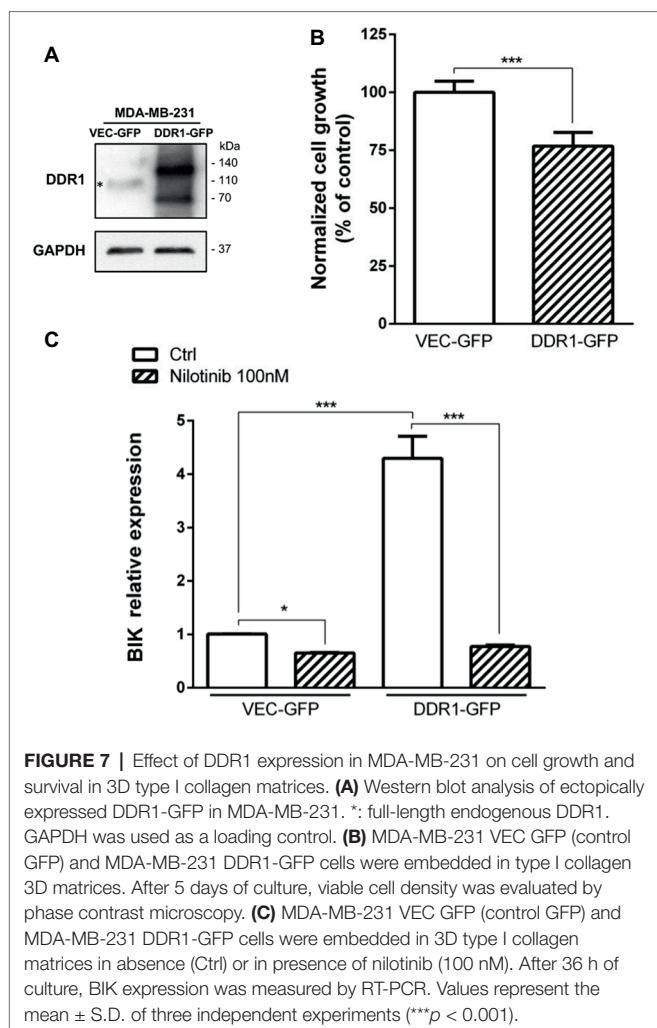
mediator BIK in those cells (**Figure 8D**). The data confirmed the previous results, with an increase in BIK mRNA expression in MDA-MB-231 DDR1-GFP treated with MT1-MMP shRNA compared to shCtrl. More importantly, **Figure 8D** showed that compared to MDA-MB-231 VEC-GFP, MDA-MB-231 DDR1-GFP cells exhibit about 6-fold increase in BIK mRNA level when MT1-MMP is depleted. Taken together, these data suggest that in basal-like breast carcinoma MDA-MB-231 cells, DDR1 activity and shMT1-MMP are able to synergize and increase collagen-induced apoptosis.

DISCUSSION

The extracellular matrix (ECM) represents an important component of the stromal microenvironment and functions as a master regulator of tumor behavior. In fact, the ECM plays key roles in major steps of cancer progression including cell proliferation, plasticity, survival and metastasis (Quail and Joyce, 2013; Pickup et al., 2014). Among ECM components, a complex network of adhesive proteins, including collagens, proteoglycans and glycoproteins, is able to regulate these different functions. These macromolecules are secreted by stromal cells and can be cleaved by several proteases including matrix metalloproteinases (MMPs), leading to the remodeling of the ECM (Bonnans et al., 2014).

The collagen superfamily is the major component of this ECM, particularly type I collagen which is the most abundant in several organs such as breast, lung, and skin (Mouw et al., 2014). In addition to its contribution to the architectural properties of the tissues, type I collagen is able to induce different cellular signaling pathways, which regulate several functions of tumor cells (Leitinger, 2011). Among type I collagen receptors, integrin heterodimers $\alpha 1 \beta 1$, $\alpha 2 \beta 1$, $\alpha 10 \beta 1$, and $\alpha 11 \beta 1$ are the most well known (Humphries et al., 2006). Recently, discoidin domain receptors have drawn special attention in the cross-talk between members of the collagen family, especially type I collagen and tumor cells. The particularity of these receptors is to be the only collagen receptors that possess a tyrosine kinase (RTK) activity. In addition, these receptors are characterized by a delayed and relatively long activation period (2 and 18 h, respectively) (Vogel et al., 1997; Fu et al., 2013b; Leitinger, 2014).

During tumor progression, especially after the degradation of the basement membrane, type I collagen is the major adhesive ECM protein encountered by invasive cancer cells, especially in breast carcinoma (Egeblad et al., 2010). We have previously shown that in 3D type I collagen matrix, DDR1 triggers a BIK-mediated apoptosis in poorly invasive luminal-like breast carcinomas cell lines (Assent et al., 2015; Saby et al., 2018). However, type I collagen failed to do so in the invasive basal-like MDA-MB-231 breast carcinoma cell line (Maquoi et al., 2012). This cell line is representative of aggressive breast cancer models, displaying a



high metastatic ability associated with mesenchymal features. The expression of the membrane-anchored MT1-MMP, a major collagenolytic MMP, by the basal-like cancer cells has been largely described as a crucial step to promote the invasion process (Poincloux et al., 2009; Castro-Castro et al., 2016). Since the fibrillar organization of type I collagen is crucial for DDR1 activation (Vogel et al., 1997), the MT1-MMP-mediated degradation of type I collagen has been hypothesized to protect cancer cells from type I collagen-induced apoptosis. In accordance with this hypothesis, the enforced expression of MT1-MMP in luminal-like breast carcinoma cells abrogates the BIK-mediated apoptosis, suggesting that the degradation of type I collagen could be responsible of a lower DDR1 activation and thus a decreased apoptosis (Assent et al., 2015). A similar impairment of BIK-mediated apoptosis was also observed when these cells were exposed to aged type I collagen (Saby et al., 2018), which is characterized by an altered fibrillar organization (Aït-Belkacem et al., 2012).

However, MT1-MMP is also known to cleave DDR1, thereby reducing its activation (Fu et al., 2013a; Assent et al., 2015). As a consequence, MT1-MMP might also abrogate BIK-mediated apoptosis by negatively regulating the level of activated DDR1. To address this point and in order to study tumor cells harboring

endogenous MT1-MMP, we investigated whether basal-like MDA-MB-231 breast carcinoma cells present a low level of DDR1 expression. As expected and at the opposite of the luminal-like MCF-7 breast cancer cells, MDA-MB-231 cells expressed MT1-MMP at a high level and DDR1 at a very low level (Figures 4A,B). Interestingly, we show that for Estrogen Receptor (ER) negative breast cancer patients, a low DDR1 expression is associated with a worse relapse-free survival (Figure 2B). It is worth noting that the mRNA level of the pro-apoptotic mediator BIK was positively correlated to that of DDR1 in human basal-like breast tumors (Figure 3). This suggests that tumors with high levels of DDR1 might be more sensitive to the BIK-mediated apoptotic pathway triggered by fibrillar type I collagen. It is important to state that the low level of DDR1 expression observed in most basal-like breast cancer cell lines is compensated by an upregulation of DDR2, with the noticeable exception of the MDA-MB-231 cells (Figure 1; Saby et al., 2018). This compensatory mechanism has been previously reported in invasive breast carcinoma from patients in which DDR1 and DDR2 were coordinately and inversely deregulated. In these patients, a DDR1 (Low)/DDR2 (High) expression profile has been associated with a significantly worse overall survival (Toy et al., 2015).

As shown in Figures 1, 4, DDR1 and MT1-MMP exhibit opposite expression patterns in MCF-7 and MDA-MB-231 cells. Previous works have reported that the DDR1 promoter region contains a p53 regulatory element and that wild-type p53 is able to induce DDR1 expression (Sakuma et al., 1996; Ongusaha et al., 2003). Interestingly, several studies that have investigated the mutational status of p53 in breast carcinoma have reported a wild type and mutated forms of p53 in MCF-7 and MDA-MB-231 cells, respectively (Lacroix et al., 2006; Muller and Vousden, 2014). Another possibility to explain this differential expression pattern of DDR1 between these two types of breast carcinoma could be related to a CpG methylation of the *DDR1* promoter during epithelial-mesenchymal transition (Chung et al., 2017).

Analysis of cell growth and apoptosis in MCF-7 cells showed that 3D collagen decreases cell growth by inducing apoptosis, whereas it failed to induce the same effects in MDA-MB-231 cells (Figures 4C,D). We then proposed to first verify whether enforced expression of MT1-MMP in MCF-7 cells was able to induce a protection against DDR1-mediated cell growth suppression and apoptosis. Accordingly, the enforced expression of MT1-MMP induced the cleavage of DDR1, thereby decreasing the abundance of the full length form of this receptor (Figures 5A,B). Interestingly, this cleavage was associated with an increase in cell growth and a decrease in apoptosis (Figures 5C,D).

We then investigated whether an endogenously expressed MT1-MMP is able to protect the basal-like MDA-MB-231 cells against BIK-mediated apoptosis and to regulate the level of DDR1. As shown in Figure 6, MT1-MMP depletion increased both full-length DDR1 expression and activation. As a direct consequence of this activation, the ability of type I collagen to suppress cell growth and to increase apoptosis was restored as evidenced by the increase in both annexin V staining and BIK expression (Figures 6C–E). This agrees with the positive correlation observed between DDR1 and BIK expression in human basal-like breast tumors (Figure 3). These results suggest

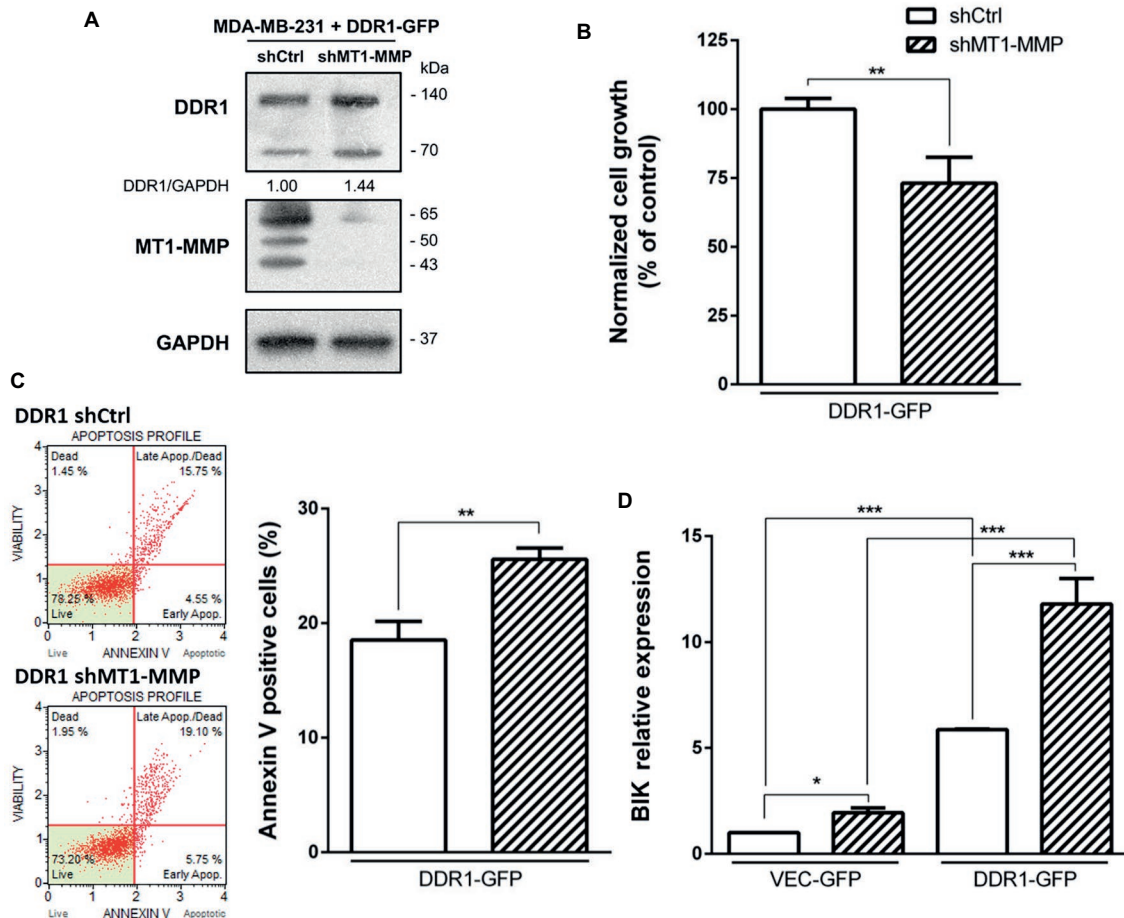


FIGURE 8 | Effect of MT1-MMP silencing in MDA-MB-231 DDR1-GFP on cell growth and survival in 3D type I collagen matrices. **(A)** Western blot analysis confirming efficient knock down of MT1-MMP in MDA-MB-231 DDR1-GFP. GAPDH was used as a loading control. **(B,C)** MDA-MB-231 DDR1-GFP shCtrl and MDA-MB-231 DDR1-GFP shMT1-MMP cells were seeded in 3D type I collagen matrices. After 5 days of culture, viable cell density was evaluated by phase contrast microscopy **(B)**. After 36 h of culture, apoptosis was quantified using the Muse[®] annexin V and dead cell assay kit **(C)**. **(D)** MDA-MB-231 DDR1-GFP shCtrl and MDA-MB-231 DDR1-GFP shMT1-MMP cells were embedded in 3D type I collagen matrices in absence (Ctrl) or in presence of nilotinib (100 nM). After 36 h of culture, BIK expression was measured by RT-PCR. Values represent the mean \pm S.D. of three independent experiments (* p < 0.05, ** p < 0.01, *** p < 0.001).

that in MDA-MB-231 cells, the ability of type I collagen to suppress cell growth and to increase apoptosis is prevented by the conjunction of an intrinsically low level of DDR1 expression and a high MT1-MMP-dependent capacity to shed the extracellular domain of this receptor. Nevertheless, an association between a low or absent DDR1 expression with basal-like phenotype and worse relapse-free survival remains controversial. Recently, DDR1 knock-down in luminal-type MMTV-PyMT mammary tumor mouse model was shown to give rise to tumors displaying basal-type characteristics, a faster growth, and enhanced lung metastasis (Takai et al., 2018). This work suggested that DDR1 loss, by compromising cell adhesion and providing a cell growth advantage, contributes to the basal-like phenotype and consequently increases both the aggressiveness and metastatic potential of breast carcinomas. However, despite its low expression level in MDA-MB-231 cells, DDR1 was reported recently to induce the formation of linear invadosomes and to play an important role in proteolysis-based cell invasion in a

collagen-rich environment (Juin et al., 2014; Moreau and Saltel, 2015; Di Martino et al., 2016). In this model, DDR1 depletion blocked cell invasion and, unexpectedly, its kinase activity was not required for invadosome formation (Juin et al., 2014).

We then investigated whether an increased DDR1 expression could sensitize the MDA-MB-231 cells toward the type I collagen-induced and BIK-mediated apoptosis. As shown in **Figure 7C**, enforced DDR1 expression significantly increased BIK expression in cells exposed to 3D collagen. This is in agreement with the positive correlation observed between DDR1 and BIK expression in basal-like tumors (**Figure 3**). To determine whether DDR1 kinase activity was required for this process, we treated MDA-MB-231 cells with its kinase function inhibitor nilotinib at a sub-toxic concentration. By using DDR1 and DDR2 gatekeeper mutations, we and others have previously demonstrated that nilotinib was able to inhibit specifically DDR1 and DDR2 (Beauchamp et al., 2014; Saby et al., 2016; Jeitany et al., 2018). By inhibiting DDR1 kinase function in

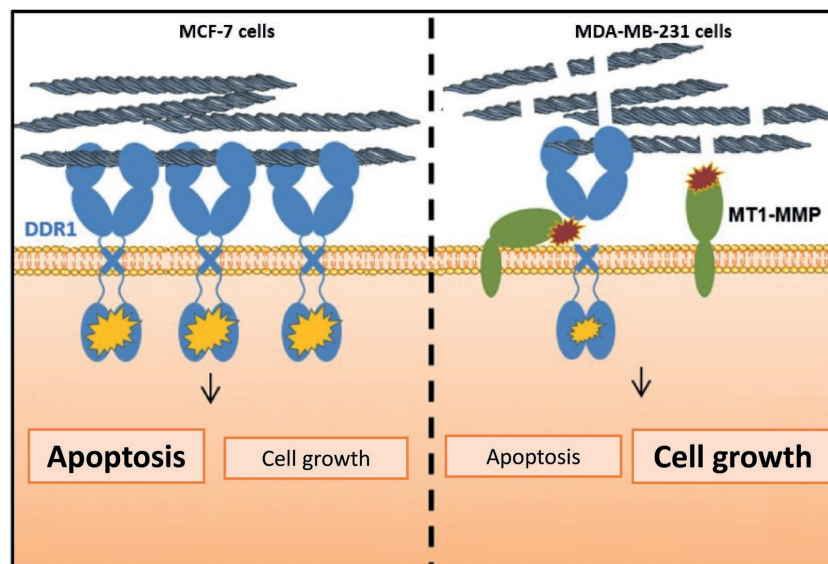


FIGURE 9 | Proposed model highlighting the importance of MT1-MMP and DDR1 expression balance in the regulation of cell growth and survival in breast cancer cells cultivated in 3D type I collagen matrix.

MDA-MB-231 cells overexpressing DDR1, nilotinib was able to clearly prevent the upregulation of BIK mRNA (**Figure 7C**). Finally, in order to obtain expression levels of both DDR1 and MT1-MMP close to those observed in the luminal-like cell lines, DDR1 was overexpressed, and MT1-MMP was depleted in MDA-MB-231 cells. Under these settings, MT1-MMP depletion was able to further increase the expression of the full-length form of DDR1 (**Figure 8A**). This led to a decrease in cell growth that was associated with a significant increase in BIK-mediated apoptosis (**Figures 8B,D**). Collectively, these data reveal that both DDR1 and MT1-MMP represent key factors, in addition to the other mesenchymal markers, contributing to the aggressive phenotype in invasive breast carcinoma tumors.

In conclusion, and in agreement with the other studies (Ford et al., 2007; Koh et al., 2015; Toy et al., 2015; Takai et al., 2018), our data suggest that during the acquisition of mesenchymal features, the level of full-length DDR1 expression should be considered, in addition to the other markers, as an important biomarker in the prognosis of aggressive breast carcinomas. As summarized in **Figure 9**, the regulation of cell proliferation and apoptosis by the collagen/DDR1 axis involves a differential activation of DDR1 signaling pathway and thus BIK expression. In the case of the basal-like breast carcinoma cells, collagen proteolysis

by MT1-MMP, the low expression of DDR1, and its cleavage by MT1-MMP could contribute to cell survival in the interstitial microenvironment. However, although our *in vitro* data suggest that low level of DDR1 expression should be considered as an additional important biomarker in the prognosis of breast carcinoma, these data need to be confirmed in future animal studies.

Finally, it is important to keep in mind that despite its low expression level in the aggressive breast carcinomas, DDR1 plays also a crucial role in the proteolysis-based cell invasion of a collagen-rich stroma (Juin et al., 2014).

AUTHOR CONTRIBUTIONS

All authors listed have made a substantial, direct and intellectual contribution to the work, and approved it for publication.

FUNDING

This work was supported by grants from Ligue Contre le Cancer 2016 and 2018 (CCIR Grand-Est). EM is a Research Associate from the Fund for Scientific Research—FNRS (Belgium).

REFERENCES

- Ait-Belkacem, D., Guilbert, M., Roche, M., Duboisset, J., Ferrand, P., Sockalingum, G., et al. (2012). Microscopic structural study of collagen aging in isolated fibrils using polarized second harmonic generation. *J. Biomed. Opt.* 17, 080506–080501. doi: 10.1117/1.JBO.17.8.080506
- Albrechtsen, R., Kveiborg, M., Stautz, D., Vikeså, J., Noer, J. B., Kotzsh, A., et al. (2013). ADAM12 redistributes and activates MMP-14, resulting in gelatin degradation, reduced apoptosis and increased tumor growth. *J. Cell Sci.* 126, 4707–4720. doi: 10.1242/jcs.129510
- Amar, S., Smith, L., and Fields, G. B. (2017). Matrix metalloproteinase collagenolysis in health and disease. *Biochim. Biophys. Acta, Mol. Cell Res.* 1864, 1940–1951. doi: 10.1016/j.bbamcr.2017.04.015
- Assent, D., Bourgot, I., Hennuy, B., Geurts, P., Noël, A., Foidart, J. M., et al. (2015). A membrane-type-1 matrix metalloproteinase (MT1-MMP)-discoidin domain receptor 1 axis regulates collagen-induced apoptosis in breast cancer cells. *PLoS One* 10:e0116006. doi: 10.1371/journal.pone.0116006
- Beauchamp, E. M., Woods, B. A., Dulak, A. M., Tan, L., Xu, C., Gray, N. S., et al. (2014). Acquired resistance to dasatinib in lung cancer cell lines

- conferred by DDR2 gatekeeper mutation and NF1 loss. *Mol. Cancer Ther.* 13, 475–482. doi: 10.1158/1535-7163.MCT-13-0817
- Bonnans, C., Chou, J., and Werb, Z. (2014). Remodelling the extracellular matrix in development and disease. *Nat. Rev. Mol. Cell Biol.* 15, 786–801. doi: 10.1038/nrm3904
- Borza, C. M., and Pozzi, A. (2013). Discoidin domain receptors in disease. *Matrix Biol.* 34, 185–192. doi: 10.1016/j.matbio.2013.12.002
- Buache, E., Thai, R., Wendling, C., Alpy, F., Page, A., Chenard, M. P., et al. (2014). Functional relationship between matrix metalloproteinase-11 and matrix metalloproteinase-14. *Cancer Med.* 3, 1197–1210. doi: 10.1002/cam4.290
- Carafoli, F., and Hohenester, E. (2013). Collagen recognition and transmembrane signalling by discoidin domain receptors. *Biochim. Biophys. Acta* 1834, 2187–2194. doi: 10.1016/j.bbapap.2012.10.014
- Castro-Castro, A., Marchesin, V., Monteiro, P., Lodillinsky, C., Rossé, C., and Chavrier, P. (2016). Cellular and molecular mechanisms of MT1-MMP-dependent cancer cell invasion. *Annu. Rev. Cell Dev. Biol.* 32, 555–576. doi: 10.1146/annurev-cellbio-111315-125227
- Chung, V. Y., Tan, T. Z., Huang, R. L., Lai, H. C., and Huang, R. Y. (2017). Loss of discoidin domain receptor 1 (DDR1) via CpG methylation during EMT in epithelial ovarian cancer. *Gene* 635, 9–15. doi: 10.1016/j.gene.2017.09.001
- Ciriello, G., Gatz, M. L., Beck, A. H., Wilkerson, M. D., Rhie, S. K., Pastore, A., et al. (2015). Comprehensive molecular portraits of invasive lobular breast cancer. *Cell* 163, 506–519. doi: 10.1016/j.cell.2015.09.033
- Croissant, C., Tuariihiiono, A., Bacou, M., Souleyreau, W., Sala, M., Henriët, E., et al. (2018). DDR1 and DDR2 physical interaction leads to signaling interconnection but with possible distinct functions. *Cell Adhes. Migr.* 12, 324–334. doi: 10.1080/19336918.2018.1460012
- Di Martino, J., Henriët, E., Ezzoukhy, Z., Goetz, J. G., Moreau, V., and Saltel, F. (2016). The microenvironment controls invadosome plasticity. *J. Cell Sci.* 129, 1759–1768. doi: 10.1242/jcs.182329
- Egeblad, M., Rasch, M. G., and Weaver, V. M. (2010). Dynamic interplay between the collagen scaffold and tumor evolution. *Curr. Opin. Cell Biol.* 22, 697–706. doi: 10.1016/j.ccb.2010.08.015
- Ford, C. E., Lau, S. K., Zhu, C. Q., Andersson, T., Tsao, M. S., and Vogel, W. F. (2007). Expression and mutation analysis of the discoidin domain receptors 1 and 2 in non-small cell lung carcinoma. *Br. J. Cancer* 96, 808–814. doi: 10.1038/sj.bjc.6603614
- Fu, H. L., Sohail, A., Valiathan, R. R., Wasinski, B. D., Kumarasiri, M., Mahasen, K. V., et al. (2013a). Shedding of discoidin domain receptor 1 by membrane-type matrix metalloproteinases. *J. Biol. Chem.* 288, 12114–12129. doi: 10.1074/jbc.M112.409599
- Fu, H. L., Valiathan, R. R., Arkwright, R., Sohail, A., Mihai, C., Kumarasiri, M., et al. (2013b). Discoidin domain receptors: unique receptor tyrosine kinases in collagen-mediated signaling. *J. Biol. Chem.* 288, 7430–7437. doi: 10.1074/jbc.R112.444158
- Garnotel, R., Rittie, L., Poitevin, S., Monboisse, J. C., Nguyen, P., Potron, G., et al. (2000). Human blood monocytes interact with type I collagen through alpha x beta 2 integrin (CD11c-CD18, gp150-95). *J. Immunol.* 164, 5928–5934. doi: 10.4049/jimmunol.164.11.5928
- Györfy, B., Lanczky, A., Eklund, A. C., Denkert, C., Budczies, J., Li, Q., et al. (2010). An online survival analysis tool to rapidly assess the effect of 22,277 genes on breast cancer prognosis using microarray data of 1,809 patients. *Breast Cancer Res. Treat.* 123, 725–731.
- Henriët, E., Sala, M., Abou Hammoud, A., Tuariihiiono, A., Di Martino, J., Ros, M., et al. (2018). Multitasking discoidin domain receptors are involved in several and specific hallmarks of cancer. *Cell Adhes. Migr.* 12, 363–377. doi: 10.1080/19336918.2018.1465156
- Humphries, J. D., Byron, A., and Humphries, M. J. (2006). Integrin ligands at a glance. *J. Cell Sci.* 19(Pt 119), 3901–3903. doi: 10.1242/jcs.03098
- Iwai, L. K., Payne, L. S., Luczynski, M. T., Chang, F., Xu, H., Clinton, R. W., et al. (2013). Phosphoproteomics of collagen receptor networks reveals SHP-2 phosphorylation downstream of wild-type DDR2 and its lung cancer mutants. *Biochem. J.* 454, 501–513. doi: 10.1042/BJ20121750
- Jeitany, M., Leroy, C., Tosti, P., Lafitte, M., Le Guet, J., Simon, V., et al. (2018). Inhibition of DDR1-BCR signalling by nilotinib as a new therapeutic strategy for metastatic colorectal cancer. *EMBO Mol. Med.* 10:e7918. doi: 10.15252/emmm.201707918
- Jézéquel, P., Campone, M., Gouraud, W., Guerin-Charbonnel, C., Leux, C., Ricolleau, G., et al. (2012). Bc-GenExMiner: an easy-to-use online platform for gene prognostic analyses in breast cancer. *Breast Cancer Res. Treat.* 131, 765–775. doi: 10.1007/s10549-011-1457-7
- Juin, A., Di Martino, J., Leitinger, B., Henriët, E., Gary, A. S., Paysan, L., et al. (2014). Discoidin domain receptor 1 controls linear invadosome formation via a Cdc42-tuba pathway. *J. Cell Biol.* 207, 517–533. doi: 10.1083/jcb.201404079
- Koh, M., Woo, Y., Valiathan, R. R., Jung, H. Y., Park, S. Y., Kim, Y. N., et al. (2015). Discoidin domain receptor 1 is a novel transcriptional target of ZEB1 in breast epithelial cells undergoing H-Ras-induced epithelial to mesenchymal transition. *Int. J. Cancer* 136, E508–E520. doi: 10.1002/ijc.29154
- Lacroix, M., Toillon, R. A., and Leclercq, G. (2006). p53 and breast cancer, an update. *Endocr. Relat. Cancer* 13, 293–325. doi: 10.1677/erc.1.01172
- Leitinger, B. (2011). Transmembrane collagen receptors. *Annu. Rev. Cell Dev. Biol.* 27, 265–290. doi: 10.1146/annurev-cellbio-092910-154013
- Leitinger, B. (2014). Discoidin domain receptor functions in physiological and pathological conditions. *Int. Rev. Cell Mol. Biol.* 310, 39–87. doi: 10.1016/B978-0-12-800180-6.00002-5
- Maquoi, E., Assent, D., Detilleux, J., Pequeux, C., Foidart, J. M., and Noël, A. (2012). MT1-MMP protects breast carcinoma cells against type I collagen-induced apoptosis. *Oncogene* 31, 480–493. doi: 10.1038/onc.2011.249
- Moreau, V., and Saltel, F. (2015). Type I collagen fibrils and discoidin domain receptor 1 set invadosomes straight. *Mol. Cell Oncol.* 2:e1004963. doi: 10.1080/23723556.2015.1004963
- Mouw, J. K., Ou, G., and Weaver, V. M. (2014). Extracellular matrix assembly: a multiscale deconstruction. *Nat. Rev. Mol. Cell Biol.* 15, 771–785. doi: 10.1038/nrm3902
- Muller, P. A., and Vousden, K. H. (2014). Mutant p53 in cancer: new functions and therapeutic opportunities. *Cancer Cell* 25, 304–317. doi: 10.1016/j.ccr.2014.01.021
- Ongusaha, P. P., Kim, J. I., Fang, L., Wong, T. W., Yancopoulos, G. D., Aaronson, S. A., et al. (2003). p53 induction and activation of DDR1 kinase counteract p53-mediated apoptosis and influence p53 regulation through a positive feedback loop. *EMBO J.* 22, 1289–1301. doi: 10.1093/emboj/cdg129
- Pickup, M. W., Mouw, J. K., and Weaver, V. M. (2014). The extracellular matrix modulates the hallmarks of cancer. *EMBO Rep.* 15, 1243–1253. doi: 10.15252/embr.201439246
- Poincloux, R., Lizárraga, F., and Chavrier, P. (2009). Matrix invasion by tumour cells: a focus on MT1-MMP trafficking to invadopodia. *J. Cell Sci.* 17(Pt 122), 3015–3024. doi: 10.1242/jcs.034561
- Quail, D. F., and Joyce, J. A. (2013). Microenvironmental regulation of tumor progression and metastasis. *Nat. Med.* 19, 1423–1437. doi: 10.1038/nm.3394
- Rammal, H., Saby, C., Magnien, K., Van-Gulick, L., Garnotel, R., Buache, E., et al. (2016). Discoidin domain receptors: potential actors and targets in cancer. *Front. Pharmacol.* 7:55. doi: 10.3389/fphar.2016.00055
- Saby, C., Buache, E., Brassart-Pasco, S., El Btaouri, H., Courageot, M. P., Van Gulick, L., et al. (2016). Type I collagen aging impairs discoidin domain receptor 2-mediated tumor cell growth suppression. *Oncotarget* 7, 24908–24927. doi: 10.18632/oncotarget.8795
- Saby, C., Rammal, H., Magnien, K., Buache, E., Brassart-Pasco, S., Van-Gulick, L., et al. (2018). Age-related modifications of type I collagen impair DDR1-induced apoptosis in non-invasive breast carcinoma cells. *Cell Adhes. Migr.* 12, 335–347. doi: 10.1080/19336918.2018.1472182
- Sakuma, S., Saya, H., Tada, M., Nakao, M., Fujiwara, T., Roth, J. A., et al. (1996). Receptor protein tyrosine kinase DDR is up-regulated by p53 protein. *FEBS Lett.* 398, 165–169. doi: 10.1016/S0014-5793(96)01234-3
- Takai, K., Drain, A. P., Lawson, D. A., Littlepage, L. E., Karpuz, M., Kessenbrock, K., et al. (2018). Discoidin domain receptor 1 (DDR1) ablation promotes tissue fibrosis and hypoxia to induce aggressive basal-like breast cancers. *Genes Dev.* 32, 244–257. doi: 10.1101/gad.301366.117
- Terashima, M., Togashi, Y., Sato, K., Mizuuchi, H., Sakai, K., Suda, K., et al. (2016). Functional analyses of mutations in receptor tyrosine kinase genes in non-small cell lung cancer: double-edged sword of DDR2. *Clin. Cancer Res.* 22, 3663–3671. doi: 10.1158/1078-0432.CCR-15-2093
- Toy, K. A., Valiathan, R. R., Núñez, F., Kidwell, K. M., Gonzalez, M. E., Fridman, R., et al. (2015). Tyrosine kinase discoidin domain receptors DDR1

- and DDR2 are coordinately deregulated in triple-negative breast cancer. *Breast Cancer Res. Treat.* 150, 9–18. doi: 10.1007/s10549-015-3285-7
- Valiathan, R. R., Marco, M., Leitinger, B., Kleer, C. G., and Fridman, R. (2012). Discoidin domain receptor tyrosine kinases: new players in cancer progression. *Cancer Metastasis Rev.* 31, 295–321. doi: 10.1007/s10555-012-9346-z
- Vogel, W., Gish, G. D., Alves, F., and Pawson, T. (1997). The discoidin domain receptor tyrosine kinases are activated by collagen. *Mol. Cell* 1, 13–23. doi: 10.1016/S1097-2765(00)80003-9
- Wall, S. J., Werner, E., Werb, Z., and DeClerck, Y. A. (2005). Discoidin domain receptor 2 mediates tumor cell cycle arrest induced by fibrillar collagen. *J. Biol. Chem.* 280, 40187–40194. doi: 10.1074/jbc.M508226200

Conflict of Interest Statement: The authors declare that the research was conducted in the absence of any commercial or financial relationships that could be construed as a potential conflict of interest.

Copyright © 2019 Saby, Collin, Sinane, Buache, Van Gulick, Saltel, Maquoi and Morjani. This is an open-access article distributed under the terms of the Creative Commons Attribution License (CC BY). The use, distribution or reproduction in other forums is permitted, provided the original author(s) and the copyright owner(s) are credited and that the original publication in this journal is cited, in accordance with accepted academic practice. No use, distribution or reproduction is permitted which does not comply with these terms.



The ZNF217 Biomarker Predicts Low- and High-Risk Oncotype DX[®] Recurrence Score in ER-Positive Invasive Breast Cancers

Pascale A. Cohen^{1,2*}, Olivier Loudig³, Christina Liu³, Joseph Albanese⁴ and Susan Fineberg⁴

¹ Univ Lyon, Université Claude Bernard Lyon 1, INSERM U1052, CNRS 5286, Centre de Recherche en Cancérologie de Lyon, Lyon, France, ² Department of Anatomy and Structural Biology, Albert Einstein College of Medicine, Bronx, NY, United States, ³ Center for Discovery and Innovation, Hackensack University Medical Center (HUMC), Nutley, NJ, United States, ⁴ Department of Pathology, Montefiore Medical Center and the Albert Einstein College of Medicine, Bronx, NY, United States

We assessed mRNA and protein expression levels of the ZNF217 oncogene in 17 clinical FFPE ER-positive invasive breast cancer specimens with known (low or high) Oncotype DX[®] Recurrence Scores. This study shows that mRNA or nuclear protein levels of the ZNF217 significantly correlate with Oncotype DX[®] Recurrence Score.

OPEN ACCESS

Edited by:

Luciano Saso,
Sapienza University of Rome, Italy

Reviewed by:

Massimo Libra,
Università degli Studi di Catania, Italy
Massimiliano Berretta,
Centro di Riferimento Oncologico di
Aviano (IRCCS), Italy

*Correspondence:

Pascale A. Cohen
pascale.cohen@univ-lyon1.fr

Specialty section:

This article was submitted to
Experimental Pharmacology and Drug
Discovery,
a section of the journal
Frontiers in Pharmacology

Received: 19 November 2018

Accepted: 25 April 2019

Published: 28 May 2019

Citation:

Cohen PA, Loudig O, Liu C,
Albanese J and Fineberg S (2019) The
ZNF217 Biomarker Predicts Low- and
High-Risk Oncotype DX[®] Recurrence
Score in ER-Positive Invasive Breast
Cancers. *Front. Pharmacol.* 10:524.
doi: 10.3389/fphar.2019.00524

Keywords: breast cancer, estrogen-receptor positive, ZNF217, expression, Oncotype DX[®], biomarker

REPORT

Breast cancer (BC) is the most frequent cancer among women. Expression of Estrogen Receptor α (ER α) is found in 60–80% of BC patients, and allows an accurate prediction of response to endocrine therapy (ET). However, between 10 and 50% of ER⁺ BC treated patients will later relapse. Thus, a more precise method for stratifying patients based on their prognosis and for predicting their response to therapy remains needed.

The Oncotype DX[®] (ODX) genomic assay tests for the expression of 21 genes and calculates a Recurrence Score (RS), which predicts the risk of distant disease recurrence in ER⁺ BC. A high RS value indicates a poor prognosis and a higher probability of distant recurrence at 10 years in patients treated with adjuvant ET (Paik et al., 2004). We have shown that high expression levels of the ZNF217 oncogenic transcription factor are associated with poor prognosis, recurrent distant metastases and can predict response to ET in ER⁺ BC (Vendrell et al., 2012; Nguyen et al., 2014). This novel snapshot report investigates the correlation between ZNF217 expression levels (protein or mRNA) and ODX RS.

After approval by the Institutional Review Board, the pathology database of the Montefiore Medical Center (NY, USA) was searched to identify ER⁺ BC cases with: (i) low-risk (<18) or high-risk (>31) ODX RS; (ii) sufficient tissue for both ZNF217 immunohistochemistry (IHC) (Nguyen et al., 2014) and ZNF217 RTQ-PCR (Loudig et al., 2007; Kotorashvili et al., 2012; Vendrell et al., 2012) investigations. Seventeen FFPE clinical specimens were selected (**Figure 1A**). After ZNF217 IHC analysis, the percentage of positive staining of tumor nuclei was estimated (range: 0–80%). ZNF217 mRNA levels ranged from 0.5 to 22.5 (arbitrary units) and the mean value was used as a cutoff. **Figure 1** illustrates that: (i) all the clinical specimens with low-risk ODX RS displayed

Abbreviations: BC, Breast Cancer; ER α , Estrogen receptor α ; ER⁺, Estrogen receptor α -positive; ET, endocrine therapy; ODX, Oncotype DX[®]; RS, Recurrence Score; FFPE, Formalin-Fixed, Paraffin-Embedded; IHC, immunohistochemistry; RTQ-PCR, real-time quantitative polymerase chain reaction.

A	Oncotype DX® Recurrence Score		<i>P value</i> ¹
	Low risk (RS <10)	High risk (RS ≥ or = 31)	
Nuclear ZNF217 IHC staining			
< 5% of stained breast tumor cells	7 (41.2%)	4 (23.5 %)	0.01
≥ or equal to 5% of stained breast tumor cells	0 (0%)	6 (35.3%)	
ZNF217 mRNA levels			
Low levels (< 4)	7 (41.2%)	5 (29.4%)	0.04
High levels (≥ 4)	0 (0%)	5 (29.4%)	
Combination of ZNF217 IHC staining and ZNF217 mRNA levels			
Low ZNF217 IHC staining (< to 5% of breast tumor cells) and Low ZNF217 mRNA levels (< 4)	7 (41.2%)	2 (11.7%)	0.002
High ZNF217 IHC staining (≥ or equal to 5% of breast tumor cells) and/or High ZNF217 mRNA levels (≥ 4)	0	8 (47.1%)	

¹*P* (Fisher's exact test) was considered significant when *P* < 0.05 (SPSS Statistics software)

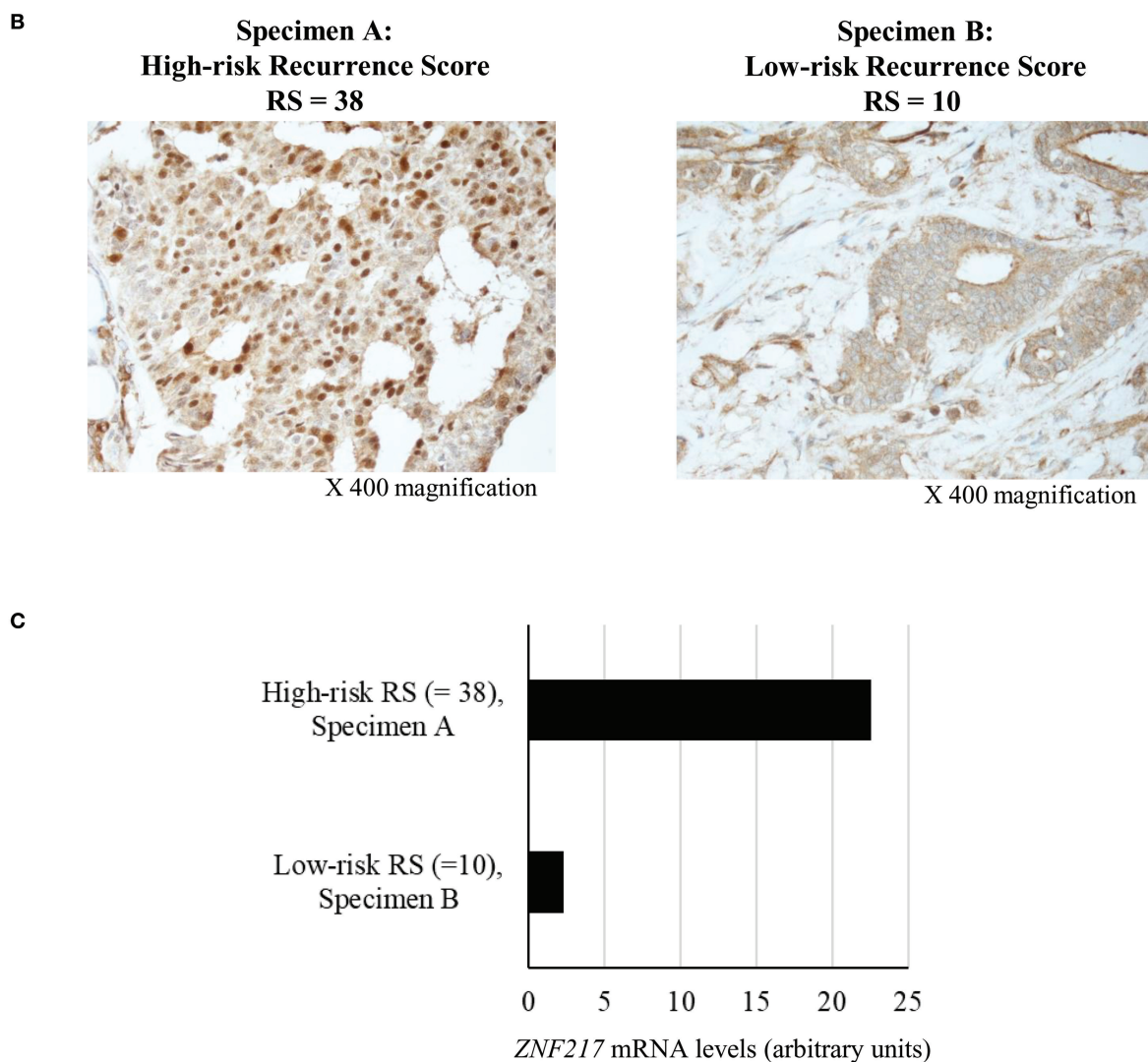


FIGURE 1 | (A) ZNF217 predicts low- and high-risk Oncotype DX® Recurrence Score. **(B)** Illustrative examples of ZNF217 IHC staining in two representative ER⁺ invasive breast carcinoma tumor samples with high-risk Oncotype DX® Recurrence Score with positive nuclear staining (specimen A) or low-risk Oncotype DX® Recurrence Score without nuclear staining (specimen B). **(C)** RTQ-PCR assessment of ZNF217 mRNA levels (arbitrary units) in specimen A and specimen B.

low *ZNF217* mRNA levels (<4) or low percentage of IHC stained nuclei (<5%); (ii) *ZNF217* nuclear staining and *ZNF217* mRNA levels were significantly associated with ODX RS; (iii) combining both IHC analysis and *ZNF217* mRNA levels allowed the stratification of the samples with a better accuracy, with 100 and 80%, respectively, of low-risk ODX RS and high-risk ODX RS correctly classified and significantly association with *ZNF217* expression levels ($P = 0.002$). Strikingly, two high ODX RS specimens displaying the highest *ZNF217* mRNA levels (9.2 and 22.5) also displayed the highest *ZNF217* IHC staining (70–80%) and pejorative clinical record (T2 with invaded nodes and recurrent breast cancer, respectively).

Altogether, while these exploratory results were obtained in a small cohort, our preliminary data indicate a correlation between *ZNF217* expression levels and ODX RS. This is in agreement with previous observations that both *ZNF217* expression levels and the ODX RS are prognostic and predictive of ET response in ER⁺ BC. Supporting recent observations indicate that *ZNF217* expression levels also predict neoadjuvant ET response in these patients (Vendrell et al., 2018). However, it is necessary to extend our study to a larger cohort including low-, high- but also intermediate- ODX RS specimens to investigate whether assessing *ZNF217* levels (alone or in combination with

ODX) could provide additional information to the current well-established ODX genomic assay.

ETHICS STATEMENT

The protocol was approved by the Institutional Review Board, Montefiore Medical Center and Albert Einstein College of Medicine (NY, USA).

AUTHOR CONTRIBUTIONS

PC and SF conceived the study. SF supervised and analyzed the IHC experiments performed by JA. OL supervised and analyzed the RTQ-PCR experiments performed by CL. PC and SF co-analyzed the data. PC wrote the manuscript.

ACKNOWLEDGMENTS

The French-American Fulbright Program and the French Ministry of Higher Education, Research and Innovation supported PC. This work was supported by the French Ligue contre le cancer (committees 71 and 42). We thank Dr. B. Manship for critical reading of the manuscript.

REFERENCES

- Kotorashvili, A., Ramnauth, A., Liu, C., Lin, J., Ye, K., Kim, R., et al. (2012). Effective DNA/RNA co-extraction for analysis of microRNAs, mRNAs, and genomic DNA from formalin-fixed paraffin-embedded specimens. *PLoS ONE* 7:e34683. doi: 10.1371/journal.pone.0034683
- Loudig, O., Milova, E., Brandwein-Gensler, M., Massimi, A., Belbin, T. J., Childs, G., et al. (2007). Molecular restoration of archived transcriptional profiles by complementary-template reverse-transcription (CT-RT). *Nucleic Acids Res.* 35:e94. doi: 10.1093/nar/gkm510
- Nguyen, N. T., Vendrell, J. A., Poulard, C., Gyorffy, B., Goddard-Leon, S., Bieche, I., et al. (2014). A functional interplay between *ZNF217* and estrogen receptor alpha exists in luminal breast cancers. *Mol. Oncol.* 8, 1441–1457. doi: 10.1016/j.molonc.2014.05.013
- Paik, S., Shak, S., Tang, G., Kim, C., Baker, J., Cronin, M., et al. (2004). A multigene assay to predict recurrence of tamoxifen-treated, node-negative breast cancer. *N. Engl. J. Med.* 351, 2817–2826. doi: 10.1056/NEJMoa041588
- Vendrell, J. A., Solassol, J., Gyorffy, B., Vilquin, P., Jarlier, M., Donini, C. F., et al. (2018). Evaluating *ZNF217* mRNA expression levels as a predictor of response to endocrine therapy in ER+ breast cancer. *Front. Pharmacol.* 9:1581. doi: 10.3389/fphar.2018.01581
- Vendrell, J. A., Thollet, A., Nguyen, N. T., Ghayad, S. E., Vinot, S., Bieche, I., et al. (2012). *ZNF217* is a marker of poor prognosis in breast cancer that drives epithelial-mesenchymal transition and invasion. *Cancer Res.* 72, 3593–3606. doi: 10.1158/0008-5472.CAN-11-3095

Conflict of Interest Statement: SF served in an expert advisory panel for Genomic Health.

The remaining authors declare that the research was conducted in the absence of any commercial or financial relationships that could be construed as a potential conflict of interest.

Copyright © 2019 Cohen, Loudig, Liu, Albanese and Fineberg. This is an open-access article distributed under the terms of the Creative Commons Attribution License (CC BY). The use, distribution or reproduction in other forums is permitted, provided the original author(s) and the copyright owner(s) are credited and that the original publication in this journal is cited, in accordance with accepted academic practice. No use, distribution or reproduction is permitted which does not comply with these terms.



The Bone Morphogenetic Protein Signaling Inhibitor LDN-193189 Enhances Metastasis Development in Mice

Julien Vollaire¹, Irma Machuca-Gayet^{2,3}, Jonathan Lavaud¹, Aurélie Bellanger^{3,4}, Lamia Bouazza^{2,3}, Soumaya El Moghrabi^{2,3}, Isabelle Treilleux⁵, Jean-Luc Coll¹, Olivier Peyruchaud^{2,3†}, Véronique Josserand^{1†} and Pascale A. Cohen^{3,4*†}

¹ INSERM U1209, CNRS UMR5309, Univ. Grenoble Alpes, Institute for Advanced Biosciences, Grenoble, France,

² INSERM UMR1033 LYOS, Lyon, France, ³ University of Lyon 1, Lyon, France, ⁴ INSERM U1052, CNRS 5286, Centre de Recherche en Cancérologie de Lyon, Lyon, France, ⁵ Department of Biopathology, Centre Léon Bérard, Lyon, France

OPEN ACCESS

Edited by:

Chiranjib Chakraborty,
Galgotias University, India

Reviewed by:

John M. Chirgwin,
Indiana University, United States
Martin R. Berger,
German Cancer Research Center
(DKFZ), Germany

*Correspondence:

Pascale A. Cohen
pascale.cohen@univ-lyon1.fr

[†]These authors have contributed
equally to this work.

Specialty section:

This article was submitted to
Experimental Pharmacology
and Drug Discovery,
a section of the journal
Frontiers in Pharmacology

Received: 18 November 2018

Accepted: 23 May 2019

Published: 19 June 2019

Citation:

Vollaire J, Machuca-Gayet I,
Lavaud J, Bellanger A,
Bouazza L, El Moghrabi S,
Treilleux I, Coll J-L, Peyruchaud O,
Josserand V and Cohen PA (2019)
The Bone Morphogenetic
Protein Signaling Inhibitor
LDN-193189 Enhances Metastasis
Development in Mice.
Front. Pharmacol. 10:667.
doi: 10.3389/fphar.2019.00667

Breast cancer with bone metastasis is essentially incurable with current anticancer therapies. The bone morphogenetic protein (BMP) pathway is an attractive therapeutic candidate, as it is involved in the bone turnover and in cancer cell formation and their colonization of distant organs such as the bone. We previously reported that in breast cancer cells, the ZNF217 oncogene drives BMP pathway activation, increases the metastatic growth rate in the bone, and accelerates the development of severe osteolytic lesions in mice. In the present study, we aimed at investigating the impact of the LDN-193189 compound, a potent inhibitor of the BMP type I receptor, on metastasis development *in vivo*. ZNF217-revLuc cells were injected into the left ventricle of nude mice ($n = 16$) while control mice ($n = 13$) were inoculated with control pcDNA6-revLuc cells. Mice from each group were treated or not with LDN-193189 for 35 days. We found that systemic LDN-193189 treatment of mice significantly enhanced metastasis development, by increasing both the number and the size of metastases. In pcDNA6-revLuc-injected mice, LDN-193189 also affected the kinetics of metastasis emergence. Altogether, these data suggest that *in vivo*, LDN-193189 might affect the interaction between breast cancer cells and the bone environment, favoring the emergence and development of multiple metastases. Hence, our report highlights the importance of the choice of drugs and therapeutic strategies used in the management of bone metastases.

Keywords: breast cancer, ZNF217, bone metastasis, bone morphogenetic protein pathway inhibitor, LDN-193189

INTRODUCTION

Breast cancer is the most frequent cancer among women (Ferlay et al., 2015). More than two-thirds of breast cancer patients are expected to die after the development of bone metastases (BM), primarily osteolytic lesions (Coleman, 2006). Breast cancers with BM are currently mostly incurable; therefore, the identification of suitable therapeutic candidates is of utmost importance.

Abbreviations: BM, bone metastases; BMP, Bone Morphogenetic Protein; IP, intra-peritoneal

Previous data strongly suggest that the bone morphogenetic protein (BMP) pathway, a critical regulator of bone homeostasis, may be a promising therapeutic target in tumorigenesis and BM (Bach et al., 2018). Indeed, this pathway is involved in cell-autonomous functions in tumor cells, as well as tumor–stroma interactions in the bone environment (Keller et al., 2001; Barnes et al., 2004; Javed et al., 2005; Alarmo and Kallioniemi, 2010; Sethi and Kang, 2011). The BMP pathway has been ascribed both tumor-promoting or -suppressing activities, according to the context (Bach et al., 2018), though its activation is mainly associated with tumor progression and metastasis development. For instance, in human breast cancer cells, BMP-Smad signaling stimulates development of BM (Katsuno et al., 2008). BMP inhibitors (Jiramongkolchai et al., 2016) thus constitute a promising approach for managing tumorigenesis and breast cancer-derived BM.

We previously reported that ectopic expression of the *ZNF217* oncogene in MDA-MB-231 breast cancer cells leads to the constitutive activation of the BMP pathway, indicating that *ZNF217* is a novel upstream BMP signaling activator (Bellanger et al., 2017). A series of *in vitro* experiments showed that BMP signaling is strongly involved in *ZNF217*-mediated breast cancer cell aggressiveness. Indeed, treatment of MDA-MB-231 breast cancer cells overexpressing *ZNF217* with specific BMP inhibitors (one of which being LDN-193189) led to impaired *ZNF217*-dependent cell migration and cell invasion and impeded chemotaxis to the bone (Bellanger et al., 2017). In mice, experiments conducted by intracardiac injection of *ZNF217*-positive breast cancer cells revealed that these latter rapidly colonize the bone, leading to the development of severe multiple BM detectable as early as 7 days post-injection (Bellanger et al., 2017). In this well-described and well-characterized *in vivo* model, mice injected with *ZNF217*-positive breast cancer cells developed osteolytic lesions validated by microCT, and only in extremely rare cases were concomitant metastases at other locations observed (Bellanger et al., 2017). This novel *in vivo* model of BM thus represents an attractive model for testing candidate drugs.

LDN-193189 is a potent inhibitor of the BMP type I receptor (Cuny et al., 2008) and was chosen in our study as its efficacy and toxicity in mice are well characterized (Yu et al., 2008; Boergermann et al., 2010; Lee et al., 2011; Balboni et al., 2013). Furthermore, among the different BMP inhibitors, LDN-193189 has scarcely been tested in the prevention of metastasis development. To our knowledge, only one *in vivo* study reported that LDN-193189 prevents prostate tumor growth rate in the bone and development of osteoblastic lesions (Lee et al., 2011). Based on our novel *in vivo* murine model of osteolytic lesions (Bellanger et al., 2017), we aimed at investigating whether systemic inhibition of the BMP pathway by LDN-193189 could influence metastasis development.

MATERIALS AND METHODS

Cell Culture and Treatments

MDA-MB-231-pcDNA6, MDA-MB-231-*ZNF217*, and their stable luciferase-transfected derived cell lines pcDNA6-*revLuc* and

*ZNF217-*revLuc** were previously established and described (Thollet et al., 2010; Vendrell et al., 2012). We previously validated in our cell lines the inhibitory action of 10^{-7} M LDN-193189 (Sigma, France) on the BMP pathway (Bellanger et al., 2017). Before injection into mice, pcDNA6-*revLuc* and *ZNF217-*revLuc** cells were treated for 4 h with 10^{-7} M of LDN-193189 or vehicle (distilled water).

Animal Models

Experiments were conducted following the European Union guidelines and approved by the ethics committee of Grenoble, France (C2EA-12 ComEth Grenoble). As previously described (Bellanger et al., 2017), pcDNA6-*revLuc* or *ZNF217-*revLuc** cells (2.5×10^5) were injected into the cardiac left ventricle of $n = 18$ or $n = 20$ 6-week-old athymic NMRI nude female mice (Janvier Labs, France), respectively. Cell implantation was immediately controlled by *in vivo* bioluminescence imaging (IVIS Kinetic, PerkinElmer). Only mice, the bioluminescent signal of which was diffused throughout the whole body, were considered to be correctly implanted (13/18 and 16/20, respectively, **Supplementary Figure 1A**) and were included in the following experimental groups: pcDNA6-*revLuc* ($n = 5$), pcDNA6-*revLuc* + LDN-193189 ($n = 8$), *ZNF217-*revLuc** ($n = 8$), and *ZNF217-*revLuc** + LDN-193189 ($n = 8$). Subsequently, from day 0 to day 35, pcDNA6-*revLuc* mice or *ZNF217-*revLuc** mice received daily intra-peritoneal (IP) injections of LDN-193189 (3 mg/kg body weight in distilled water) or vehicle (distilled water). The LDN-193189 experimental setup was based on previous *in vivo* studies (Yu et al., 2008; Lee et al., 2011; Balboni et al., 2013). LDN-193189-treated mice did not exhibit any loss in their body weight, demonstrating that the inhibitor had no severe toxic side effects. Bioluminescence imaging (IVIS Kinetic, Caliper), was performed weekly as previously described (Bellanger et al., 2017). A p value of <0.05 was considered statistically significant (Mann–Whitney, StatView™ Software).

Whole-Body Bioluminescence and X-Ray Microtomography (microCT) Imaging

Five minutes before imaging, vigil mice received an IP injection of 150 µg/g of D-luciferin (Promega) and were then anesthetized (isoflurane 4% for induction and 1.5% thereafter) and placed in the IVIS Kinetic imaging system (PerkinElmer). MicroCT was then performed using the vivaCT40 (ScancoMedical) at 45 keV with a 177-mA intensity, a 200-ms integration time, and an 80-mm isotropic voxel size.

Histology

Hind limbs and spines from animals were fixed, decalcified in 16% EDTA, and embedded in paraffin. Five-micrometer tissue sections were stained with Goldner's Trichrome and processed for histological analysis.

RESULTS

Figure 1A and **B** illustrates the kinetics and amplitude of metastasis development in mice implanted with pcDNA6-*revLuc*

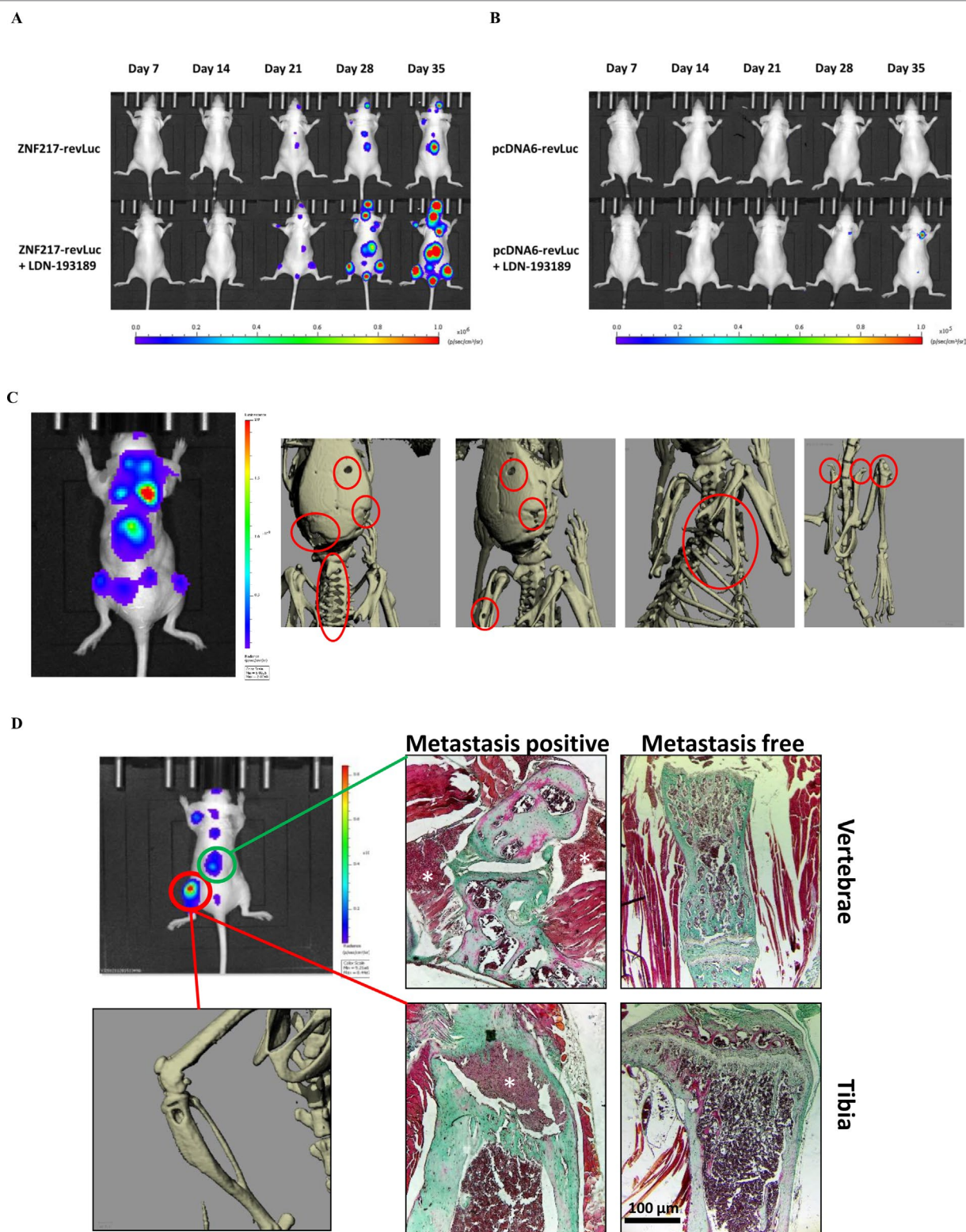


FIGURE 1 | Kinetics and development of metastases *in vivo*. The kinetics of metastases development were followed by bioluminescence in mice injected with **(A)** ZNF217-revLuc cells or **(B)** pcDNA6-revLuc cells, and treated or not with LDN-193189 (representation of one mouse per group representative of the entire group). **(C)** Whole-body bioluminescence and microCT imaging between 35 and 42 days after intracardiac injection of ZNF217-revLuc cells. **(D)** Representative bioluminescence image of an entire mouse exhibiting multiple metastasis foci including an osteolytic BM detected by microCT scan at the left tibia and by histological examination both at the vertebrae and the tibia from bone tissue sections stained with Goldner's trichrome. Mineralized bone is stained in green and cells are stained in dark red. White stars identify metastasis foci. Histological examination of similar areas from a metastasis-free mouse is also shown in vertebrae and tibia. Scale bars: 100 µm.

or ZNF217-revLuc cells, treated or not with LDN-193189. The pattern of metastases distribution observed in ZNF217-revLuc cell-injected mice, treated or not with LDN-193189, was totally superimposed with those previously observed in our well-characterized *in vivo* model of osteolytic lesions (Bellanger et al., 2017) (**Supplementary Figure 1B**). MicroCT images are capable of highlighting osteolytic lesions following a longer bone remodeling period, i.e., once the cells had sufficiently colonized the tissue (Sanches et al., 2015). **Figure 1C** illustrates representative microCT images, highlighting osteolytic bone lesions following intracardiac injection of ZNF217-revLuc cells. Histological investigations validated osteolytic lesions and the presence of breast metastatic tumor cells inside and in close contact with bone (**Figure 1D**).

Intracardiac injection of ZNF217-revLuc cells into mice ($n = 16$) led to the rapid development of multiple bioluminescent metastases (**Figure 2A**). After 7 and 21 days post-injection, 38% and 100% of the untreated injected mice ($n = 8$) developed metastases, respectively, corroborating our previous observation (Bellanger et al., 2017). In the group of ZNF217-revLuc-injected mice treated with LDN-193189 ($n = 8$), the kinetics of metastasis development was very rapid, similarly to that observed in the ZNF217-revLuc-injected mice ($n = 8$) (**Figure 2A**). Strikingly, the total metastases load and the average number of metastases per mouse were higher in the LDN-193189-treated group compared to the non-treated group, and this increase reached significance ($P = 0.017$) at days 28 and 35 post-implantation (**Figure 2B and C**).

All ZNF217-revLuc-injected mice developed multiple metastases, but those who were treated with LDN-193189 displayed much more metastases per mouse compared to the non-treated group (11.0 ± 5.0 vs. 6.1 ± 2.5) at 28 days post-injection (**Figure 2C**). Furthermore, the average bioluminescent signal per metastasis tended to be higher in the LDN-193189-treated group compared to the non-treated group, suggesting that in the presence of this BMP inhibitor, individual metastases are larger (**Figure 2D**).

Unlike ZNF217-revLuc-injected mice, and consistent with our previous report (Bellanger et al., 2017), only 1 out of 5 non-treated pcDNA6-revLuc-injected mice developed a single metastasis, detectable only at 35 days post-injection (**Figure 2E**). The LDN-193189 treatment of pcDNA6-revLuc-injected mice ($n = 8$) affected both the incidence of metastases development (**Figure 2E**), the total metastases load (**Figure 2F**), and the average number of metastases per mouse (**Figure 2G**). Indeed, 50% of LDN-193189-treated pcDNA6-revLuc-injected mice (4 of 8 mice) developed one to four metastases detectable as early as day 28 post-injection, while none were detectable in the non-treated group (**Figure 2E**). Additionally, the bioluminescent signal observed in the LDN-193189-treated pcDNA6-revLuc-injected group, though weaker than ZNF217-induced metastases, was significantly higher than that in the non-treated group at day 35 post-injection (**Figure 2F**, $P = 0.029$). **Figure 2H** illustrates and summarizes the number of bioluminescent metastases in mice injected with pcDNA6-revLuc or ZNF217-revLuc cells, and treated or not with LDN-193189.

DISCUSSION

Therapeutic BM strategies aiming at targeting the BMP pathway are very attractive, firstly because the latter is involved in the physiology and pathology of bone turnover (Rosen, 2006) and secondly because it might be dysregulated in cancer cells leading to metastases, in particular to the bone (Katsuno et al., 2008). Previous studies reported that i) the DMH1 BMP inhibitor prevents tumor burden in breast cancer and lung metastatic growth (Owens et al., 2015); ii) halofuginone, a dual BMP and TGF β inhibitor, reduces breast cancer osteolytic lesions (Juarez et al., 2017); and iii) the BMP antagonist noggin prevents development of osteolytic lesions of prostate cancer cells (Feeley et al., 2006).

However, the BMP pathway has paradoxical effects in tumorigenesis and metastasis development, owing possibly to the fine balance between members belonging to this pathway, or between BMP signaling and other pathways, in specific cellular contexts or genetic backgrounds (Jiramongkolchai et al., 2016; Bach et al., 2018). Such complexity is highlighted by apparently conflicting data using BMP inhibitors. Indeed, the BMP antagonist noggin has also been described to contribute to the development of osteolytic BM (Secondini et al., 2011). Moreover, LDN-193189, while inducing decreased tumor burden of colorectal cancer cells (Yokoyama et al., 2017), preventing the growth of pancreatic or breast cancer cells *in vivo*, and increasing survival of mice with ovarian cancer (Lee et al., 2011; Balboni et al., 2013; Ali et al., 2015), was also shown to increase the risk of intestinal carcinogenesis (Whissell et al., 2014).

Using a well-described *in vivo* model of BM metastases in breast cancer (Bellanger et al., 2017), the present report originally investigates the impact of LDN-193189 on metastasis development. Our unexpected and major finding is that systemic treatment with the LDN-193189 molecule has a pro-metastatic effect and stimulates the development of metastases, both in pcDNA6-revLuc-injected mice and in ZNF217-revLuc-injected mice. The impact was significantly greater with ZNF217-positive breast cancer cells displaying aggressiveness and with the ability to develop severe osteolytic lesions. This unexpected result might reflect the impact of this BMP inhibitor on the soil (the bone microenvironment) and/or on the seed (MDA-MB-231 breast cancer cells). Consistently, previous studies suggested that LDN-193189 facilitates bone resorption, represses bone formation, or reduces heterotopic ossification (Yu et al., 2008; Lee et al., 2011; Inubushi et al., 2017). Alternatively, LDN-193189 treatment may induce in both control and ZNF217-positive MDA-MB-231 cells yet uncharacterized molecular events favoring their *in vivo* interaction with the bone environment for osteolytic BM development. Consistently, LDN-193189 displays BMP signaling inhibitory activities on both ZNF217-overexpressing cells and control cells, suggesting that this compound is able to block the activation of both ZNF217-dependent and -independent BMP signaling (Bellanger et al., 2017). Regardless of the context, LDN-193189 treatment seems to accelerate BM development, independently of the level of activation of BMP signaling in breast cancer cells. The concomitant development of metastases to locations other than bone is very rarely obtained in the *in vivo*

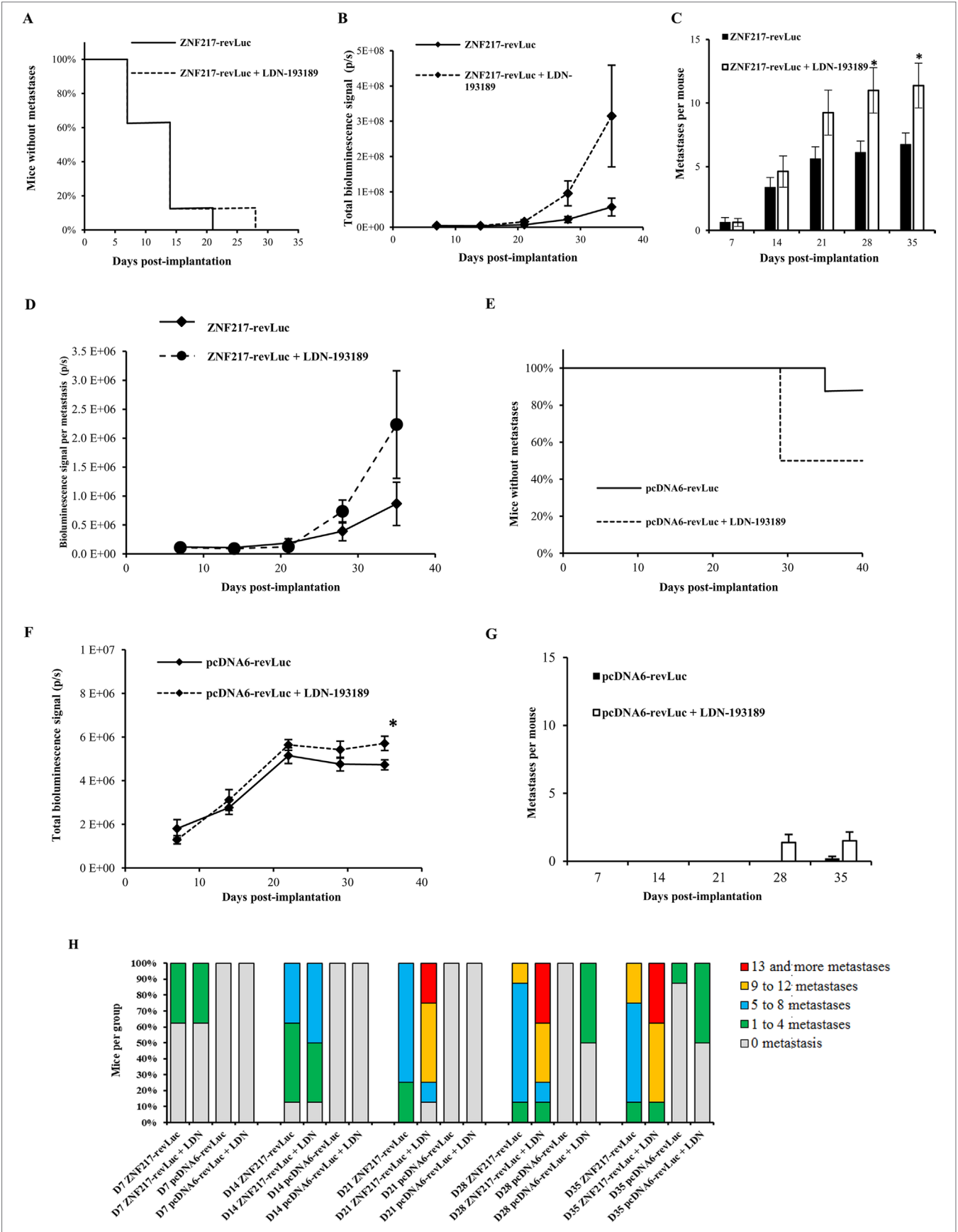


FIGURE 2 | The LDN-193189 BMP inhibitor enhances metastases development *in vivo*. ZNF217-revLuc or pcDNA6-revLuc cells were delivered *via* intracardiac injection into the bloodstream of nude mice. **(A)** Kaplan–Meier analysis of metastasis-free mice in LDN-193189-treated ($n = 8$) and non-treated ($n = 8$) ZNF217-revLuc-injected mice. **(B)** Total metastases load measured by *in vivo* bioluminescence imaging in LDN-193189-treated ($n = 8$) and non-treated ($n = 8$) ZNF217-revLuc-injected mice. **(C)** Average number of metastases per ZNF217-revLuc-injected mouse. **(D)** Total bioluminescent signal per metastasis in LDN-193189-treated and non-treated ZNF217-revLuc-injected mice. **(E)** Kaplan–Meier analysis of metastasis-free mice in LDN-193189-treated ($n = 8$) and non-treated ($n = 5$) pcDNA6-revLuc-injected mice. **(F)** Total metastases load measured by *in vivo* bioluminescence imaging in LDN-193189-treated ($n = 8$) and non-treated ($n = 5$) pcDNA6-revLuc-injected mice. **(G)** Average number of metastases per pcDNA6-revLuc-injected mouse. Results are presented as mean \pm standard error of the mean (SEM) in **(B)**, **(C)**, **(D)**, **(F)**, and **(G)**. * $P < 0.05$ (Mann–Whitney test). **(H)** Distribution of the number of metastases developed by each group of mice.

model used in this study (Bellanger et al., 2017). However, future work investigating whether LDN-193189 treatment impacts metastases development other than in the BM is much needed. Finally, one cannot preclude possible off-target effects of LDN-193189, destabilizing the balance between this pathway and other signaling pathways in the environment or in breast cancer cells (Yu et al., 2008; Vogt et al., 2011).

In conclusion, using an *in vivo* model of breast cancer BM, we found that the LDN-193189 BMP inhibitor displays pro-metastatic properties. Although this study does not refute the use of BMP inhibitors in oncology and in the prevention of metastases, it highlights the necessity to gain further insight into the fine balance governed by the BMP signaling pathway between tumor cells and the environment to improve the development of future drugs.

ETHICS STATEMENT

In vivo experiments (mice) were conducted following the European Union guidelines and approved by the ethics committee of Grenoble, France (C2EA-12 ComEth Grenoble).

AUTHOR CONTRIBUTIONS

VJ, J-LC, OP, and PC participated in the design of the study. VJ, JL, and JV performed and analyzed the *in vivo* data. IM-G, LB, SE-M, IT, and OP performed and analyzed the histological experiments. AB participated in previous *in vitro* validation of the LDN-193189 compound and in scientific discussions. JV, AB, VJ, OP, and PC wrote the manuscript.

REFERENCES

- Alarmo, E. L., and Kallioniemi, A. (2010). Bone morphogenetic proteins in breast cancer: dual role in tumorigenesis? *Endocr. Relat. Cancer* 17 (2), R123–R139. doi: 10.1677/ERC-09-0273
- Ali, J. L., Lagasse, B. J., Minuk, A. J., Love, A. J., Moraya, A. I., Lam, L., et al. (2015). Differential cellular responses induced by dorsomorphin and LDN-193189 in chemotherapy-sensitive and chemotherapy-resistant human epithelial ovarian cancer cells. *Int. J. Cancer* 136 (5), E455–E469. doi: 10.1002/ijc.29220
- Bach, D. H., Park, H. J., and Lee, S. K. (2018). The dual role of bone morphogenetic proteins in cancer. *Mol. Ther. Oncolytics* 8, 1–13. doi: 10.1016/j.omto.2017.10.002
- Balboni, A. L., Hutchinson, J. A., DeCastro, A. J., Cherukuri, P., Liby, K., Sporn, M. B., et al. (2013). DeltaNp63alpha-mediated activation of bone morphogenetic protein signaling governs stem cell activity and plasticity in normal and malignant mammary epithelial cells. *Cancer Res.* 73 (2), 1020–1030. doi: 10.1158/0008-5472.CAN-12-2862

FUNDING

This research program (PAC) was supported by grants from by the French Ligue Contre le Cancer (committees 42 and 71) and Agence Nationale de la Recherche, France (2011 ANR-CESA-018-01). Imaging systems were acquired thanks to France Life Imaging (French program “Investissement d’Avenir” grant; “Infrastructure d’avenir en Biologie Santé”, ANR-11-INBS-0006). OP was supported by grants from INSERM and the University Claude Bernard Lyon-1, the Comité Départemental de la Loire de la Ligue Contre le Cancer, the French Foundation pour la Recherche sur le Cancer (ARC, Grant n°.PJA20151203151), the ANR grant LYSBONE (Grant n°. ANR-15-CE14-0010-01). AB was supported by a PhD grant from the Ligue Nationale Contre le Cancer (LNCC).

ACKNOWLEDGMENTS

We thank L. Odeyer, A. Colombe-Vermorel, S. Leon-Goddard for technical support and Dr. B. Manship for critical reading of the manuscript.

SUPPLEMENTARY MATERIAL

The Supplementary Material for this article can be found online at: <https://www.frontiersin.org/articles/10.3389/fphar.2019.00667/full#supplementary-material>

FIGURE S1 | **(A)** Bioluminescence imaging performed immediately after intracardiac injection of cells expressing luciferase for validation of mice included in the experiments. **(B)** Distribution pattern of the bioluminescent metastases detected in the ZNF217-revLuc injected mice treated with LDN-193189 and ZNF217-revLuc injected mice treated with vehicle.

- Barnes, G. L., Hebert, K. E., Kamal, M., Javed, A., Einhorn, T. A., Lian, J. B., et al. (2004). Fidelity of Runx2 activity in breast cancer cells is required for the generation of metastases-associated osteolytic disease. *Cancer Res.* 64 (13), 4506–4513. doi: 10.1158/0008-5472.CAN-03-3851
- Bellanger, A., Donini, C. F., Vendrell, J. A., Lavaud, J., Machuca-Gayet, I., Ruel, M., et al. (2017). The critical role of the ZNF217 oncogene in promoting breast cancer metastasis to the bone. *J. Pathol.* 242 (1), 73–89. doi: 10.1002/path.4882
- Boergermann, J. H., Kopf, J., Yu, P. B., and Knaus, P. (2010). Dorsomorphin and LDN-193189 inhibit BMP-mediated Smad, p38 and Akt signalling in C2C12 cells. *Int. J. Biochem. Cell Biol.* 42 (11), 1802–1807. doi: 10.1016/j.biocel.2010.07.018
- Coleman, R. E. (2006). Clinical features of metastatic bone disease and risk of skeletal morbidity. *Clin. Cancer Res.* 12 (20 Pt 2), 6243s–6249s. doi: 10.1158/1078-0432.CCR-06-0931
- Cuny, G. D., Yu, P. B., Laha, J. K., Xing, X., Liu, J. F., Lai, C. S., et al. (2008). Structure–activity relationship study of bone morphogenetic protein (BMP)

- signaling inhibitors. *Bioorg. Med. Chem. Lett.* 18 (15), 4388–4392. doi: 10.1016/j.bmcl.2008.06.052
- Feeley, B. T., Krennek, L., Liu, N., Hsu, W. K., Gamradt, S. C., Schwarz, E. M., et al. (2006). Overexpression of noggin inhibits BMP-mediated growth of osteolytic prostate cancer lesions. *Bone* 38 (2), 154–166. doi: 10.1016/j.bone.2005.07.015
- Ferlay, J., Soerjomataram, I., Dikshit, R., Eser, S., Mathers, C., Rebelo, M., et al. (2015). Cancer incidence and mortality worldwide: sources, methods and major patterns in GLOBOCAN 2012. *Int. J. Cancer* 136 (5), E359–E386. doi: 10.1002/ijc.29210
- Inubushi, T., Nozawa, S., Matsumoto, K., Irie, F., and Yamaguchi, Y. (2017). Aberrant perichondrial BMP signaling mediates multiple osteochondromagenesis in mice. *JCI Insight* 2 (15), 1–14. doi: 10.1172/jci.insight.90049
- Javed, A., Barnes, G. L., Pratap, J., Antkowiak, T., Gerstenfeld, L. C., van Wijnen, A. J., et al. (2005). Impaired intranuclear trafficking of Runx2 (AML3/CBFA1) transcription factors in breast cancer cells inhibits osteolysis in vivo. *Proc. Natl. Acad. Sci. U. S. A.* 102 (5), 1454–1459. doi: 10.1073/pnas.0409121102
- Jiramongkolchai, P., Owens, P., and Hong, C. C. (2016). Emerging roles of the bone morphogenetic protein signaling pathway in cancer: potential therapeutic target for kinase inhibition. *Biochem. Soc. Trans.* 44 (4), 1117–1134. doi: 10.1042/BST20160069
- Juarez, P., Fournier, P. G. J., Mohammad, K. S., McKenna, R. C., Davis, H. W., Peng, X. H., et al. (2017). Halofuginone inhibits TGF-beta/BMP signaling and in combination with zoledronic acid enhances inhibition of breast cancer bone metastasis. *Oncotarget* 8 (49), 86447–86462. doi: 10.18632/oncotarget.21200
- Katsuno, Y., Hanyu, A., Kanda, H., Ishikawa, Y., Akiyama, F., Iwase, T., et al. (2008). Bone morphogenetic protein signaling enhances invasion and bone metastasis of breast cancer cells through Smad pathway. *Oncogene* 27 (49), 6322–6333. doi: 10.1038/nc.2008.232
- Keller, E. T., Zhang, J., Cooper, C. R., Smith, P. C., McCauley, L. K., Pienta, K. J., et al. (2001). Prostate carcinoma skeletal metastases: cross-talk between tumor and bone. *Cancer Metastasis Rev.* 20 (3–4), 333–349. doi: 10.1023/A:1015599831232
- Lee, Y. C., Cheng, C. J., Bilen, M. A., Lu, J. F., Satcher, R. L., Yu-Lee, L. Y., et al. (2011). BMP4 promotes prostate tumor growth in bone through osteogenesis. *Cancer Res.* 71 (15), 5194–5203. doi: 10.1158/0008-5472.CAN-10-4374
- Owens, P., Pickup, M. W., Novitskiy, S. V., Giltman, J. M., Gorska, A. E., Hopkins, C. R., et al. (2015). Inhibition of BMP signaling suppresses metastasis in mammary cancer. *Oncogene* 34 (19), 2437–2449. doi: 10.1038/nc.2014.189
- Rosen, V. (2006). BMP and BMP inhibitors in bone. *Ann. N. Y. Acad. Sci.* 1068, 19–25. doi: 10.1196/annals.1346.005
- Sanches, P. G., Peters, S., Rossin, R., Kaijzel, E. L., Que, I., Lowik, C. W., et al. (2015). Bone metastasis imaging with SPECT/CT/MRI: a preclinical toolbox for therapy studies. *Bone* 75, 62–71. doi: 10.1016/j.bone.2015.02.002
- Secondini, C., Wetterwald, A., Schwaninger, R., Thalmann, G. N., and Cecchini, M. G. (2011). The role of the BMP signaling antagonist noggin in the development of prostate cancer osteolytic bone metastasis. *PLoS One* 6 (1), e16078. doi: 10.1371/journal.pone.0016078
- Sethi, N., and Kang, Y. (2011). Dysregulation of developmental pathways in bone metastasis. *Bone* 48 (1), 16–22. doi: 10.1016/j.bone.2010.07.005
- Thollet, A., Vendrell, J. A., Payen, L., Ghayad, S. E., Ben Larbi, S., Grisard, E., et al. (2010). ZNF217 confers resistance to the pro-apoptotic signals of paclitaxel and aberrant expression of Aurora-A in breast cancer cells. *Mol. Cancer* 9, 291. doi: 10.1186/1476-4598-9-291
- Vendrell, J. A., Thollet, A., Nguyen, N. T., Ghayad, S. E., Vinot, S., Bieche, I., et al. (2012). ZNF217 is a marker of poor prognosis in breast cancer that drives epithelial–mesenchymal transition and invasion. *Cancer Res.* 72 (14), 3593–3606. doi: 10.1158/0008-5472.CAN-11-3095
- Vogt, J., Traynor, R., and Sapkota, G. P. (2011). The specificities of small molecule inhibitors of the TGFβ and BMP pathways. *Cell. Signal.* 23 (11), 1831–1842. doi: 10.1016/j.cellsig.2011.06.019
- Whissell, G., Montagni, E., Martinelli, P., Hernando-Momblona, X., Sevillano, M., Jung, P., et al. (2014). The transcription factor GATA6 enables self-renewal of colon adenoma stem cells by repressing BMP gene expression. *Nat. Cell Biol.* 16 (7), 695–707. doi: 10.1038/ncb2992
- Yokoyama, Y., Watanabe, T., Tamura, Y., Hashizume, Y., Miyazono, K., and Ehata, S. (2017). Autocrine BMP-4 signaling is a therapeutic target in colorectal cancer. *Cancer Res.* 77 (15), 4026–4038. doi: 10.1158/0008-5472.CAN-17-0112
- Yu, P. B., Deng, D. Y., Lai, C. S., Hong, C. C., Cuny, G. D., Bouxsein, M. L., et al. (2008). BMP type I receptor inhibition reduces heterotopic [corrected] ossification. *Nat. Med.* 14 (12), 1363–1369. doi: 10.1038/nm.1888

Conflict of Interest Statement: The authors declare that the research was conducted in the absence of any commercial or financial relationships that could be construed as a potential conflict of interest.

Copyright © 2019 Vollaire, Machuca-Gayet, Lavaud, Bellanger, Bouazza, El Moghrabi, Treilleux, Coll, Peyruchaud, Jossierand and Cohen. This is an open-access article distributed under the terms of the Creative Commons Attribution License (CC BY). The use, distribution or reproduction in other forums is permitted, provided the original author(s) and the copyright owner(s) are credited and that the original publication in this journal is cited, in accordance with accepted academic practice. No use, distribution or reproduction is permitted which does not comply with these terms.

Advantages of publishing in Frontiers



OPEN ACCESS

Articles are free to read
for greatest visibility
and readership



FAST PUBLICATION

Around 90 days
from submission
to decision



HIGH QUALITY PEER-REVIEW

Rigorous, collaborative,
and constructive
peer-review



TRANSPARENT PEER-REVIEW

Editors and reviewers
acknowledged by name
on published articles

Frontiers

Avenue du Tribunal-Fédéral 34
1005 Lausanne | Switzerland

Visit us: www.frontiersin.org

Contact us: info@frontiersin.org | +41 21 510 17 00



REPRODUCIBILITY OF RESEARCH

Support open data
and methods to enhance
research reproducibility



DIGITAL PUBLISHING

Articles designed
for optimal readership
across devices



FOLLOW US

@frontiersin



IMPACT METRICS

Advanced article metrics
track visibility across
digital media



EXTENSIVE PROMOTION

Marketing
and promotion
of impactful research



LOOP RESEARCH NETWORK

Our network
increases your
article's readership